Imran Ahmad Siddiqui

Hyperfine Structure Studies of Praseodymium Atoms and Ions

DISSERTATION

zur Erlangung des akademischen Grades
Doktor/in der technischen Wissenschaften

Doktoratsstudium der technischen Wissenschaften
Technische Physik

Technische Universität Graz

Betreuer:

Univ.-Prof. Dipl.-Ing. Dr.techn. Laurentius Windholz

Institut für Experimentalphysik

Graz, Mai 2010

Beschluss der Curricula-Kommission für Bachelor-, Master- und Diplomstudien vom 10.11.2008
Genehmigung des Senates am 1.12.2008

EIDESSTATTLICHE ERKLÄRUNG

Ich erkläre an Eides statt, dass ich die vorliegende Arbeit selbstständig verfasst, andere als die angegebenen Quellen/Hilfsmittel nicht benutzt, und die den benutzten Quellen wörtlich und inhaltlich entnommenen Stellen als solche kenntlich gemacht habe.

Graz, am ………………………   ……………………………..
                                                              (Unterschrift)

Englische Fassung:

STATUTORY DECLARATION

I declare that I have authored this thesis independently, that I have not used other than the declared sources / resources, and that I have explicitly marked all material which has been quoted either literally or by content from the used sources.

…………………………   ……………………………
        date   (signature)

Dedicated
To
My teachers
Prof. Dr. L. Windholz,
Prof. Dr. G. Guthöhrlein
And
My Beloved
Mother, Father and Family

Thesis Advisor   Author
Prof. Dr. L. Windholz   Imran Ahmad Siddiqui

Hyperfine structure studies
of Praseodymium atoms and ions

Abstract

The interaction between electromagnetic multipole nuclear moments and magnetic and electric field produced by spinning and orbiting electrons at the site of nucleus give rise to hyperfine splitting of fine structure levels. This dissertation is mainly devoted to the experimental investigation of fine and hyperfine structure of Praseodymium-I and -II using Laser Induced Fluorescence (LIF) spectroscopy in a hollow cathode discharge.

Praseodymium has an open 4f shell structure, as is common with the entire rare earths group. The spectroscopic properties of Pr are determined by the fact that the binding energies of 4f, 5d, 6s and 6p electrons are of same magnitude. This give rise to overlapping electron configurations with regions of high energy level density and consequently, a complex rich line spectra.

During the course of this dissertation more than 2000 spectral lines of Praseodymium in the spectral range 5000 Å to 6500 Å were investigated with laser spectroscopic methods. The excitation wavelengths were taken from already available Fourier Transform Spectra (FTS). As a result of these investigations more than 300 new, up to now unknown, energy levels both in even and odd configurations were discovered.

The excitation source is a ring-dye laser system pumped by a diode-pumped, frequency doubled Nd:Vanadate-crystal solid state laser system or by a Krypton ion laser. Rhodamine 6G, Sulforhodamine B (Keton Red), DCM and Courmarine dyes were used. Free praseodymium atoms were generated by cathode sputtering in a hollow cathode lamp and are excited by laser light. From the experimentally recorded data, using Lock-in detection technique, magnetic hyperfine interaction constant **"A"** and angular momenta **"J"** were determined for the involved energy levels. Praseodymium has a small value of electric quadrupole moment, so the constant **"B"** in most cases is small but could be determined in some cases.

A large number of spectral lines in praseodymium are still not classified, it means that the involved levels are not known. This classification could be done with the help of experimental observations if the energy levels are already known.

In cases where observed hyperfine structure could not be explained we have to assume that upto now unknown level is involved. With the help of the determined angular momentum J and hyperfine interaction A constant, one of the involved level is identified and the energy of the second new level could be determined by the addition of excitation wave number. The level found in this way must explain fluorescence wavelengths and if fluorescence lines show up in FT-Spectra the hyperfine structure must be identical with the predicted pattern.

For some of the already known levels the level energies and values of hyperfine interaction constants A and B were also improved.

The main aim of this work is to extend the on going search for finding new levels in Pr-I and Pr-II, in order to enhance the understanding of the electron shell of this element.

Betreuer der Dissertation   Autor
Prof. Dr. L. Windholz   Imran Ahmad Siddiqui

Untersuchung der Hyperfeinstruktur von Praseodym Atomen und Ionen

Die Wechselwirkung zwischen den elektromagnetischen Multipol-Momenten des Atomkerns und den magnetischen und elektrischen Feldern, die durch die Elektronenhülle des Atoms am Kernort erzeugt werden, verursacht die Hyperfein-Aufspaltung der Feinstrukturniveaus.

Diese Dissertation ist hauptsächlich der experimentellen Untersuchung der Fein- und Hyperfeinstruktur von Praseodym I und II - Spektrallinien gewidmet, wobei als experimentelle Methode Laserspektroskopie in einer Hohlkathodenentladung angewandt wurde.

Praseodym hat eine offene 4f-Schalenstruktur, wie bei allen Seltenen Erden. Die spektroskopischen Eigenschaften von Pr werden vor allem durch die Tatsache bestimmt, dass die Bindungsenergien der 4f-, 5d-, 6s- und 6p-Elektronen von derselben Größenordnung sind.

Dies führt zu überlappenden Energiebereichen der Elektronenkonfigurationen und zu hoher Energieniveaudichte und infolgedessen zu einem sehr linienreichen Spektrum.

Im Laufe dieser Arbeit wurden mehr als 2000 Spektrallinien des Praseodyms im Spektralbereich 5000 A bis 6500 A mit laserspektroskopischen Methoden untersucht. Die Anregungswellenlängen konnten bereits verfügbaren Fourier-Spektren (FTS) entnommen werden. Im Lauf der Arbeit wurden mehr als 300 neue, bisher unbekannte Energieniveaus entdeckt, sowohl in Konfiguration gerader als auch in ungerader Parität.

Als Anregungslichtquelle diente ein Ring-Farbstoff-Laser-System, gepumpt von einem diodengepumpten, frequenzverdoppelten Nd:Vanadat-Kristall Festkörper-Laser System oder von einem Krypton-Ionen-Laser. Als Laserfarbstoffe wurden Rhodamin 6G, Sulforhodamin B (Keton Red), DCM and Courmarin verwendet. Freie Pr-Atome wurden durch Kathoden-Sputtern in einer Hohlkathodenlampe erzeugt und mit Laserlicht angeregt. Aus den mittels Lock-in-Nachweisverfahren experimentell aufgenommenen Daten wurden für die untersuchten Linien die Hyperfeinwechselwirkungs-Konstanten "A" und der Drehimpuls "J" der am Übergang beteiligten Energieniveaus bestimmt. Da Praseodym einen kleinen Wert des elektrischen Quadrupolmoments besitzt, ist die Konstante "B" bei den meisten Niveaus sehr klein, konnte aber in einigen Fällen trotzdem bestimmt werden.

Viele Spektrallinien im Pr-Spektrum noch nicht klassifiziert, d.h., die am Übergang beteiligten Energieniveaus sind nicht bekannt. Diese Klassifizierung konnte mit Hilfe der experimentellen Beobachtungen ebenfalls durchgeführt werden, soferne diese Energieniveaus bereits bekannt waren.

In Fällen, wo die beobachtete Hyperfeinstruktur durch bekannte Niveaus nicht erklärt werden konnte, ist mit hoher Wahrscheinlichkeit ein bislang unbekanntes Niveau involviert. Mit Hilfe der ermittelten Drehimpulse und Hyperfeinwechselwirkungskonstanten konnte in den meisten Fällen ein am Übergang beteiligtes Niveau identifiziert werden und die Energie des zweiten, neuen Niveaus durch

Addition der Anregungswellenzahl ermittelt werden. Das so gefundene neue Niveau muss dann die beobachteten Fluoreszenz-Wellenlängen erklären. Sind die Fluoreszenzlinien im FTS sichtbar, muss außerdem ihre Hyperfeinstruktur mit dem erwarteten Muster übereinstimmen.

Zusätzlich wurden für einige der bereits bekannten Niveaus die Energiewerte und die Werte der Hyperfeinwechselwirkungskonstanten A und B verbessert.

Das wichtigste Ziel dieser Arbeit ist es, die Kenntnisse über die Energieniveaus in Pr I und Pr II zu erweitern, um das Verständnis des Aufbaus der Elektronenhülle dieses Elements zu verbessern.

Declaration

This dissertation is submitted to the Institute of Experimental Physics, Graz University of Technology, Graz Austria, in partial fulfillment of the requirement for the degree of Doctor of Technical Sciences.
The thesis is entitled:

<div align="center">

Hyperfine Structure Studies
of
Praseodymium Atoms and Ions

</div>

written by Imran Ahmad Siddiqui and has been approved by the Institute of Experimental Physics, Graz University of Technology, Graz Austria.

The final copy of this thesis has been examined by the under signed authority, and find that both the content and the form meet acceptable presentation standards of scholarly work in the above mentioned discipline.

_____
Univ. Prof. Dip.-Ing. Dr. tech. Laurentius Windholz

Date _____

Acknowledgments

Imran Ahmad Siddiqui

Contents

Chapter 1
Introduction

1.1 Preface

Hyperfine splitting of fine structure levels arise due to the interaction between electric and magnetic multipole nuclear moments and electromagnetic field produced by the electrons as the nucleus and is 3 orders of magnitude smaller than fine structure. Nucleus has a compound structure comprising protons and neutrons each with ½ intrinsic spin, giving the nucleus net angular momentum with nuclear spin quantum number I. In analogy with LS coupling, nuclear spin quantum number I and total electronic angular momentum quantum number J couple together to produce total angular momentum quantum number F for the atom. As a consequence of this interaction, the fine level splits into 2I +1 or 2J + 1 hyperfine levels for J > I or J < I.

The goal of this thesis is to experimentally investigate the fine structure of praseodymium using the hyperfine structure of the investigated transitions and since praseodymium has a very high line density so it serves as a rich testing ground for hyperfine structure studies. Apart from the applications in other branches of physics, the hyperfine studies and complete mapping of energy levels in praseodymium is of special significance for the theoretical understanding of the interactions inside the atom. The method of investigation is based on laser induced fluorescence technique in a hollow cathode discharge lamp containing praseodymium atoms and ions in ground and excited states.

1.2 Praseodymium

Praseodymium is a rare earth element (these consist of lanthanides and actinides), has the symbol Pr and atomic number 59 in the periodic table. Its atomic weight is 140.9077 and its electronic ground state configuration is [Xe] $4f^3\, 6s^2$. It is soft, silvery, malleable, and ductile. It belongs to the Lanthanide group (The lanthanide group contains rare earth elements from atomic number 57 to 71). It reacts with oxygen and makes green oxide (Pr_6O_{11}). To avoid exposure to air it is stored in oil or sealed in plastic or glass. The name Praseodymium comes from the Greek prasios, meaning green and didymous, meaning twin. It occurs along with other rare-earth elements in a variety of minerals. In 1885, the Austrian chemist C. F. Auer von Welsbach separated didmium into two elements, Praseodymium and Neodymium. Praseodymium is primarily obtained through an ion exchange process from Monazite sand, a material rich in rare earth elements. Naturally occurring Pr has only one isotope, Pr^{141}. Two of the radioisotopes of Pr are relatively stable being Pr^{143} with a half life of 13.57 hours and Pr^{142} with a half life of about 19 hours. Majority of the radioisotopes of Pr have half life time 40 seconds. The isotopes of Pr range in atomic weight from 120.955 u (Pr^{121}) to 158.955 u (Pr^{159}). The primary decay mode before the stable isotope, Pr^{141}, is electron capture and the primary mode after it is negative beta decay. The primary decay products before Pr^{141} are element 58 (Cerium) isotopes and the primary products after are element 60 (Neodymium) isotopes.

Some of the chemical and physical properties of Pr^{141} are given below:

Table 1.1: Physical and chemical properties of Praseodymium.

Atomic number	59	Atomic weight	140.9077
Chemical symbol	Pr	Specific heat	0.19 J/g K
Electro negativity	1.13	Density	6.77 g/cm^3
Color	Silvery white	Phase at Room Temperature	Solid
Ionization Potential	7.89V	Crystal Structure	Hexagonal
Thermal Conductivity	12.5 W/mk	Electronic Configuration	[Xe] 4f^{3}6s^2
Atomic Radius	182 pm	Electrical Resistivity	0.7 x 10^{-4} Ohm cm
Melting Point	935 ^{o}C	Boiling Point	3520 ^{o}C
First Ionization Energy	523.2 kJ/mol		

Praseodymium's primary use is as an alloying agent with magnesium to create high-strength metals that are used in aircraft engines. Praseodymium also makes up about 5% of Misch metal, a material that is used to make flints for lighters. Praseodymium forms the core of carbon arc lights which are used in the motion picture industry for studio lighting and projector lights. Praseodymium is added to fiber optic cables as a doping agent where it is used as a signal amplifier. Praseodymium salts are used to give glasses and enamels a yellow color. Praseodymium is also a component of didymium glass, which is used to make certain types of welder's and glass blower's goggles.

1.3 History of Spectral and Hyperfine Investigation of Pr I

In 1929 H. E.White studied the wavelength and frequency separation of fine structure components of 173 spectral lines in Pr II ion [1]. He assigned I = 2.5 to the nucleus of the Pr atom. In 1941 N. Rosen et al. studied the Zeeman effect of Pr lines in the wide range 2400 to 7100 Å. They determined g and J values for 74 Pr II levels from Zeeman patterns of 141 lines. They also found f^3(4I^o).s $-^5$I^o $_4$ as the lowest term of Pr II, and observed that the most strong lines showing hyperfine structure arise from the f^{3}s configuration [2]. In 1953 H. Lew investigated the hyperfine structure of the ground state of Pr I by the atomic magnetic resonance method [3]. He determined nuclear spin, total electronic angular momentum and g$_J$ value of ground state. He found ^{4}I$_{3/2}$ being the atomic ground state of Pr I and realized that Russel Saunders coupling also leads to this state, which is according to Hund's rules - the most probable ground state of the configuration 4f ^{3}6s^2.

In 1953 P. Brix [4] evaluated the magnetic hyperfine interaction constant for the 6s electron in the configuration 4f ^{3}(4I)6s. He also calculated the magnetic moment (μ(Pr^{141}) = 3.9±0.3 nuclear magnetons) of Pr. In 1955 J. M. Baker and B. Bleany [5] investigated the hyperfine structure of Pr lines and calculated the hyperfine structure constants of the levels involved. In 1960 K. Murakawa [6] investigated the spectrum of Pr I, classified 3

lines and measured their hyperfine structure. He also calculated the magnetic moment of Pr. In 1961 Judd and Lindgren [7] made a number of corrections to the simple Lande formula for the g values of levels belonging to the configuration of the type 4f. Their measurements were based on existing experimental data and theoretical calculations based on the processes of interpolation and extrapolation. They found that the ground states of some atoms including Pr I are of the type 4f. In 1962 B. G. Wybourne [8] examined the effect of intermediate coupling on the calculation of nuclear moments of the rare earth elements from the analysis of hyperfine structure. He found that the interaction of the electron spin moments of 4f electrons with the nuclear magnetic moment is very sensitive to the form of the coupling. He presented calculations for Pr^{141} and Ho^{165}. In 1962 Y. C. Amado et al. [9] studied the hyperfine structure of the short living (19 hours) isotope (Pr^{142}) of praseodymium in the ground state $^4I_{9/2}$ by atomic beam magnetic resonance method. They calculated the splitting factor, nuclear spin, electric quadrupole and magnetic dipole hyperfine constants, and nuclear moment and quadrupole moment for this isotope of Pr. In 1964 N. J. Spector [10] calculated energy parameters for the $4f^2 6s$ and $4f^2 6p$ electronic configurations of Pr ions. J. Reader and J. Sugar [11] in 1964, studied the nuclear moment of Pr^{141} from the hyperfine structure of doubly ionized Pr. They calculated the probability density of the 6s electron at the nucleus and the quantum difference for the configurations $4f^2 6s$ and $4f^2 7s$. By the application of the Goudsmit-Fermi-Segrè formula they calculated a value 4.09±.06 nm for nuclear moment of Pr^{141}.

In 1980 A. Ginibre [12] studied the fine and hyperfine structures in the configuration $4f^2 5d6s^2$ and 4f25d26s of neutral praseodymium based on the analysis of high resolution recordings in the IR and visible ranges. During this work she has calculated the wave numbers for 54 new fine structure levels and also calculated the hyperfine interaction constant. In 1982 R. M. Macfarlane, D. P. Burum, and R. M. Shelby also studied the magnetic moment of Pr^{141} [13] and in 1985 K.T. Cheng and W. J. Childs [14] determined the electric quadrupole moment of Pr and found a value Q = 0.066 b. In 1987 M. N. Reddy and G. N. Rao [15] performed hyperfine structure studies in neutral praseodymium using laser optogalvanic spectroscopy in a hollow cathode discharge. They identified about 78 atomic transitions of Pr I and 43 transitions of Pr II and tabulated their visual estimates of relative intensities in the spectral range 576-625 nm. They also recorded the hyperfine structure for the lines 6055.13, 5874.72, 5821.36 and 5779.28 Å. In 1988 A. Ginibre, in addition to her published work [12, 20, 21], discovered lot of new lines both in Pr I and Pr II which were never published. This work is now part of her PhD thesis [16].

In 1997 A. Krzykowski et al. [17] using the method of laser induced fluorescence on an atomic beam accurately determined the values of the hyperfine structure constants of the lower levels belonging to the configuration $4f^3 5d6s$ and for the upper levels in Pr I. Extending the work of previous experimental results in 2003 J. Ruczkowski et al. [18] performed the hyperfine structure analysis in the even configuration system $4f^2 5d6s^2$ + $4f^2 5d^2 6s$ + $4f^3 6s6p$ + $4f^3 5d6p$ + $4f^2 5d^3$ of Pr I by applying semi-empirical method. In 2006 B. Furmann et al. [19] investigated the hyperfine structure of neutral praseodymium using laser induced fluorescence (LIF) spectroscopy. In their investigation they

discovered 57 new electron levels with odd parity in Pr-I in the spectral range 560-590 nm and determined their magnetic dipole interaction constants A.

1.4 History of Spectral and Hyperfine Investigation of Pr II and Pr III

The spectra of signally ionized atom or of atom in higher states of ionization are comparatively difficult to produce and it might happen that more strong lines are found in regions of spectrum where high dispersion apparatus cannot be readily utilized. The initial account of the investigation of fine and hyperfine structure of signally ionized Praseodymium atom was performed by H.E. White in 1929 as mentioned in previous section and was able to determine spin quantum number for this element. During his investigation of the spectral region from 390-500 nm [1] he identified 200 lines exhibiting complex structure and measured component separation for 33 of those lines. But insufficient resolution prevented the accurate determination of wavenumbers of the involved energy levels. Therefore only in 1941 Rosen et al. [2] relying on their Zeeman effect data for praseodymium in the spectral range 240-710 nm could determine the energy levels of Pr II. They calculated the g and J values for 74 Pr II levels from the resolved Zeeman pattern of 141 lines.

In 1988 A. Ginibre [20], based on the analysis of high resolution data in the range 2783-27920 cm^{-1}, calculated new energy levels in the odd configuration $4f^2 5d6p$ and in the mixed even configurations $4f^2 5d^2 + 4f^2 5d6s + 4f^3 6p$ for singly ionized praseodymium. Furthermore in this work she determined or revised a number of experimental characteristics such as energy, J and hyperfine splitting of already known 105 odd levels and 187 even levels. As an extension of this work [21] she further determined new experimental even levels in the range 5854-31654 cm^{-1} of singly ionized praseodymium on the basis of the 3 mixed configurations $4f^2 5d^2 + 4f^2 5d6s + 4f^3 6p$.

In 1990 H. Iimura, Y. Nakahara, S. Ichikawa, K. Kotani, M. Wakasugi and T. Horiguchi [22] studied the hyperfine structure of Pr ion (Pr II) by means of collinear laser ion beam spectroscopy. They measured the magnetic dipole and electric quadrupole constants for the transition involved in their studies. In 1991 Kim studied the hyperfine structure of doubly ionized Pr III [23]. In 1994 H. Iimura, Y. Nakahara, S. Ichikawa, M. Kubota and T. Horiguchi [24] measured the magnetic moment and electric quadrupole moment of a Pr isotope (Pr[143]) by means laser ion beam spectroscopy. In 2000 Maosheng Li et al. [25] investigated the atomic spectra of singly ionized Pr and neodymium by means of collinear laser ion beam spectroscopy. They measured the hyperfine structure of atomic transition in the wavelength range 560 to 590 nm.

In 2001 S. Ivarsson et al. [26] recorded a high resolution fourier transform spectra in the region 280-800 nm for singly and doubly ionised praseodymium. Wavelengths of 49 lines were improved and for 31 lines gf-values were determined by means of branching fractions and lifetimes data. Furthermore for 44 levels hyperfine structure pattern was analyzed and magnetic hyperfine constants A were determined for 8 odd and 18 even levels. In 2001 B. Furmann et al. [27] using the method of laser induced fluorescence spectroscopy in a hollow cathode discharge found three new low-lying levels in singly

ionised praseodymium. This work also include the investigation of already known level in the spectral range 562-602 nm with the determination of J-quantum numbers and A-values for the ionic levels.

In 2002 Ma Hong-Liang [28] measured the hyperfine structure of singly ionized lanthanum and praseodymium using collinear fast-ion-beam laser spectroscopy. The magnetic dipole and electric quadruple coupling constants were determined for already known levels.

In 2006 B. Furmann et al. [29] investigated hyperfine structure of singly ionized praseodymium and hyperfine structure constants A and B were determined for each new level using the method of laser induced fluorescence in a hollow cathode discharge. Classification of 75 spectral lines in singly ionized praseodymium using 31 new electron levels belonging to odd configurations $4f^3 5d$ and $4f^3 6s$ and 14 new levels belonging to even configurations was then performed.

1.5 Nonlinear Optics and Second Harmonic Generation

Nonlinear optics [30] is a field of study that deals with various new optical effects arising from the interaction of intense coherent optical radiation with matter. Compared to various ordinary light sources, laser devices can provide intense coherent light beams with high directionality, high monochromaticity, high brightness and high photon degeneracy. Based on the nonlinear interaction of laser radiation with matter, various optical effects have been discovered.

1.5.1 History of Nonlinear Optics

The formation of nonlinear optics originated with the advent of maser and laser in the early 1960's. The discovery of the optical second-harmonic generation (1961) can be considered as the first step in the formation of nonlinear optics. Shortly after that, several other frequency-mixing effects were sequentially discovered based on the use of laser radiation. These include the optical sum-frequency generation (1962) [31], optical third harmonic generation (1962) [32], optical rectification (1962) [33], optical difference frequency generation (1963) [34, 35], and optical parametric amplification and oscillation (1965) [36, 37]. These experimental demonstrations not only verified the validity of nonlinear polarization theories [38] but also paved the way for an alternative approach to generate coherent optical radiation.

During the same period, the discovery of stimulated Raman scattering [39, 40] in 1962 can be considered as a second step in the history of nonlinear optics. This was the first time in history that the 'stimulated' nature of light scattering excited by an intense laser beam was reveal. The stimulated scattering is an alternative physical approach to generate coherent optical radiation without the need of population inversion. Another major nonlinear optical effect was the discovery of stimulated Brillouin scattering [41] in 1964, which arose from the interaction of an intense monochromatic optical field with the induced hypersonic field in a scattering medium through the so-called optical

electrostriction mechanism. Since then, the stimulated Brillouin scattering has become an efficient technique to generate or amplify the coherent optical radiation with a small frequency-shift or fine tunability.

Another important nonlinear effect is the change in refractive index of the medium induced by an intense laser beam and as well as the impact of this change on the laser beam itself. An important article focusing on this issue was published in 1964 with a conceptual discussion and a semi-quantitative description of the self-focusing (self-trapping) behavior of an intense optical beam propagating in a nonlinear medium [42]. Although the similar concept of the self-trapping was mentioned in an earlier paper [43]. Immediately, studies of self-focusing effect attracted a great deal of attention because (i) this effect was often related to the optical damage occurring in solid-state lasing media or optical elements and (ii) it was responsible for the observed 'anomalous' threshold decrease of some nonlinear processes, such as stimulated Raman scattering, owing to the dramatic increase of the local beam intensity inside a nonlinear medium. Further studies of dynamic self-focusing processes for short laser pulses revealed special properties of the moving focus as well as new phenomena, self-phase modulation and spectral self-broadening [44-48]. Now it is well known that self-phase modulation and spectral self-broadening effects are among the basic mechanisms for generating ultra-short laser pulses and the continuum radiation with a super-broad spectral band.

The so-called transient coherent optical effects were also reported in 1960's, these include photon echoes (1964) [49], self-induced transparency (1965, 1967) [50,51], and optical nutation (1966, 1968) [52, 53]. These effects are related to transient-response behavior of a resonant optical medium interaction with short optical pulses or a fast-switched optical field. The studies of transient optical effects can provide a new approach to investigate the relaxation behavior of resonant transitions in absorptive media.

Two other fundamental nonlinear optical effects are saturable absorption effect observed in radio-frequency spectroscopy. The logical inspiration from these observations was the idea of population inversion that led to the invention of masers and lasers [54, 55]. Shortly after the invention of first laser device, the optical saturable absorption in organic dye solutions and other materials were well studied and soon applied to the Q-switching and mode-locking of laser devices [56-59]. The other effect is two-photon absorption (TPA). Although the theoretical description of this effect was reported in the early 1930's [60], the earliest experimental demonstrations of TPA-induced fluorescence were achieved with the use of laser radiation [61, 62] in 1961.

During the period of 1970's numerous new nonlinear optical effects and novel techniques were further reported and could be summarized in three main areas. The first area was related to the invention of various novel nonlinear spectroscopic techniques, such as coherent anti-Stokes Raman spectroscopy (CARS) [63-66], Doppler-free saturation spectroscopy (1971) [67, 68], Doppler-free two-photon absorption (TPA) Spectroscopy (1970, 1974) [69-73], inverse Raman Spectroscopy [74-76], Raman gain Spectroscopy [77-79], and laser polarization spectroscopy (1976) [80-84]. All these nonlinear spectroscopy techniques require two laser beams and at least one of them should be

tunable. In general, one laser beam, referred to as pump beam, is used to excite a selected group of atoms or molecules, and the second laser beam, referred to as probe beam, is used to detect the specific change of optical properties of samples owing to selective excitation.

The second area was related to the studies of optical phase conjugation. In 1972, Russian researchers reported the experimental observation of the wave-front reversal property of backward stimulated Brillouin scattering [85, 86]. Although this understanding of this observed effect was not very clear for quite a long time. Therefore this observation did not attract enough attention until the theoretical suggestions of using special three-wave mixing and four-wave mixing to generate phase-conjugate waves were proposed (1976, 1977) [87, 88]. These two proposed methods were soon experimentally accomplished (1977) [89, 90].

The third area is related to the studies of optical bistable effects. Although the original idea of an optical bistable device was reported in 1969 based on a saturable absorber in a Fabry-Perot (FP) etalon [91], researchers attention really started to focus on this subject only after the first experimental demonstration of a real optical bistable device reported in 1975 [92]. In this case, the mechanism of optical bistability was the optical field-induced refractive-index change of a nonlinear medium inside a FP etalon [93], which is called nonlinear dispersion type of intrinsic optical bistable device. Another type of device, the so-called hybrid type of optical bistable device was demonstrated in 1977 [94]. It was based on a second-order nonlinear electro-optical crystal placed inside an FP cavity; the refractive index change of the crystal was controlled by an external electric field that was proportional to the optical feedback from the FP cavity. The significance of optical bistable studies is to explore possible ways to control light with light. The principles of optical bistability can be employed to accomplish a variety of vital functions such as optical switching, transistors, limiter, stabilizer, clipper, etc. In short, optical bistable devices may be the key elements for optical fiber telecommunications, optical logical circuits, and optical computers in future.

1.6 Thesis Layout

Including this chapter the whole thesis is divided in 8 chapters. Chapter 2 gives the theoretical background of atomic structure which is followed by theoretical mathematical background of hyperfine structure in chapter 3. Chapter 4 Laser Spectroscopy discusses the modern spectroscopic techniques for the investigation of atomic systems. Chapter 5 is about experimental setup and data analysis procedures and programs. Experimental results are divided in to two chapters i.e. chapter 6 and 7 are mainly dedicated to the discussion of experimental results. Chapter 8 gives the conclusion.

Chapter 2
Atomic Structure

Spectroscopy is concerned with the experimental and theoretical investigation of atomic and molecular structure on the basis of the absorbed or emitted electromagnetic radiation. Much of our understanding about the physical nature of the things around us and generally in the universe is mainly due to the progress in this field. In 1666, Sir Issac Newton discovered, in a simple experiment, that ordinary sunlight spreads into a band of colors when allowed to pass through a prism. It was explained by Newton that colors did not originate in the prism but were the necessary ingredients that go to make up sunlight. This could rightly be regarded as the first experimental observation in spectroscopy. Newton used the word 'Spectrum' for the band of colors. More than one hundred years later, William Hyde Wollaston and Joseph Fraunhofer independently discovered hundreds of dark absorption lines in the sun's spectrum using narrow slits as secondary sources of light. Fraunhofer while studying the sun's spectrum discovered around 700 lines which are now called Fraunhofer lines. Fraunhofer labeled eight of the most prominent lines by the first eight capital letters of alphabet. The lines in the spectrum arise when an atom in ground state make a transition to an excited state by absorption of electromagnetic radiation. After these initial accounts of experimental observations, scientist began to investigate the structure and properties of atoms and molecules. To name the few very well known physicists like J. J. Thomson, Rutherford, Bohr, Sommerfeld, Schrödinger, Dirac contributed in understanding the structure of atoms and molecules. Bohr in his semi classical theory gave for the first time the concept of stable orbits and discrete energy states by combining the concept of Rutherford's nuclear atom, Planck's quanta and Einstein's photons to explain the observed spectrum of atomic hydrogen.

Hydrogen was known to emit few series of lines (Lyman, Balmer, Paschen, Brackett and Pfund series). The most probable lines belong to the Lyman series but the Balmer series was discovered first because of its appearance in the visible region. Exact explanation of emission and absorption of electromagnetic radiations remained a bit ambiguous until quantum mechanics came into its full swing. The reason was very obvious that the emission and absorption of electromagnetic radiation are quantum mechanical phenomena. With the development of high resolution apparatus it is now possible to investigate finer details of emission and absorption spectra.

2.1 Fine Structure:

In order to remove the discrepancies in the Bohr-Sommerfeld model and to explain the finer details of the internal structure of one-electron as well as many electron atoms, quantum mechanics is used which was developed by E. Schrödinger, W. Heisenberg and others, following the ideas of L. de Broglie. The first quantum mechanical treatment that gave the explanation of the discrete spectra of atomic emission was based on the equation proposed by Schrödinger in 1926. For calculations of the energy state of one-electron

atoms such as neutral hydrogen, or He$^+$, Li^{++}, Be^{3+} etc., the time independent Schrödinger equation is used:

$$\hat{H}\psi(r,\theta,\phi) = E\psi(r,\theta,\phi) \qquad\qquad 2.1$$

The above equation is also known as eigenvalue equation. The operator $\hat{H}$ is called energy operator or Hamiltonian, and the function $\psi(r,\theta,\phi)$ is known as an eigenfunction or wave function. It contains the detailed knowledge of the quantum mechanical system. In quantum mechanics each dynamical variable (such as position, momentum, energy,…) can be represented by a linear operator and the result of a precise measurement of the variable can only be one of the eigenvalues of this operator. For example the Hamiltonian operator $\hat{H}$ operating on eigenfunction $\psi(r,\theta,\phi)$ gives energy eigenvalue E and the eigenfunction $\psi(r,\theta,\phi)$. If more than one eigenfunction corresponds to a given eigenvalue, this eigenvalue is said to be degenerate. The set of all eigenvalues of the Hamiltonian is called the energy spectrum. It may consist of discrete values or a continuous range, or both. The discrete eigenvalues are associated with bound states and the continuum to unbound states. The Hamiltonian $\hat{H}$ is also called total energy operator; in simple systems it is the sum of kinetic energy and potential energy operators. For a one particle system it is given by

$$\hat{H} = \left[-\frac{\hbar^2}{2m}\nabla^2 + V(r) \right] \qquad\qquad 2.2$$

The first term on the right is the kinetic energy operator and the second term is the potential energy operator. The time-independent Schrödinger equation can be used to study the characteristics of any quantum mechanical system with periodic time behavior. In case of atomic and molecular systems the spherical symmetry allows one to use spherical coordinates in this equation, i.e. equation 2.2 in spherical coordinates reads

$$H = -\frac{\hbar^2}{2m}\left[\frac{1}{r}\frac{\partial^2}{\partial r^2}r + \frac{1}{r^2\sin\theta}\left(\frac{\partial}{\partial\theta}\sin\theta\frac{\partial}{\partial\theta} \right) + \frac{1}{r^2\sin^2\theta}\frac{\partial^2}{\partial\phi^2} \right] + V(r) \qquad 2.3$$

Using the relation for the total orbital angular momentum operator squared L^2 and radial component of momentum operator squared p_r^2, viz.

$$L^2 = -\hbar^2\left[\frac{1}{\sin\theta}\frac{\partial}{\partial\theta}\left(\sin\theta\frac{\partial}{\partial\theta} \right) + \frac{1}{\sin^2\theta}\frac{\partial^2}{\partial\phi^2} \right]$$

$$\left(-i\hbar\frac{1}{r}\frac{\partial}{\partial r}r \right)^2 = -\hbar^2\frac{1}{r}\frac{\partial^2}{\partial r^2}r$$

In terms of r the Schrodinger equation becomes

$$\frac{\hbar^2}{2ma_o^2}\left[-\frac{1}{r}\frac{\partial^2}{\partial r^2}r\psi+\frac{L^2}{r^2}\psi\right]+V(r)\psi=E\psi \qquad 2.4$$

distances measured in Bohr radius,

$$a_o=\frac{\hbar^2}{me^2}=0.529177\,\overset{o}{A}$$

energies in unit of the rydberg,

$$1\text{ Rydberg}=\frac{\hbar^2}{2ma_o^2}=\frac{e^2}{2a_o}=13.6058eV$$

angular momenta in $\hbar$ and L^2 measured in $\hbar^2$, with V(r) and E measured in rydbergs, equation 2.4 can be written as

$$\left[-\frac{1}{r}\frac{\partial^2}{\partial r^2}r+\frac{1}{r^2}L^2+V(r)\right]\psi=E\psi \qquad 2.5$$

The exact solution of the Schrödinger equation for arbitrary atoms is very difficult because of the complex nature of this second order differential equation. However, for some simple systems exact solutions are possible. Otherwise numerical solutions or some approximations are used. One of such approximation is variable separation technique; here one can assume that various motions associated with the systems can be decoupled (like in Born Openheimer approximation applied to molecules). Using this approximation to the atomic system the eigenfunction can be written as the product of a radial part associated with the radial motion and an angular part associated with its angular momentum, i.e.

$$\psi_{nlm}(r,\theta,\phi)=R_{nl}(r)\,Y_{lm}(\theta,\phi) \qquad 2.6$$

Using this approximation the Schrödinger equation can be written in two parts i.e the radial part

$$\left[-\frac{1}{r}\frac{\partial^2}{\partial r^2}r+\frac{l(l+1)}{r^2}+\frac{Ze^2}{r}\right]R(r)=E\,R(r) \qquad 2.7$$

and the angular part

$$L^2Y(\theta,\phi)=l(l+1)\,Y(\theta,\phi) \qquad 2.8$$

where L^2 is the total orbital angular momentum operator squared and $Y(\theta,\Phi)$ is the angular part of the wavefunction. Mathematically, the solution for $Y(\theta,\Phi)$ are spherical harmonics. Equation 2.8 can further be separated into two equations, one in θ, the other in Φ. The solutions of these equations give an energy spectrum for the one electron atom.

When the number of electrons in an atom increases the exact solution of the Schrödinger equation and consequently the calculations of the energy eigenvalues and the corresponding eigenfunctions, becomes much more difficult. The non-relativistic energy contributions are the kinetic energy of the electrons and their potential energy in the electrostatic attractive field of the nucleus, assuming nucleus to be point like and the electrostatic repulsion between the electrons, i.e. electron-electron interactions. The relativistic contributions include the relativistic kinetic energy of electrons, the magnetic interactions of the electronic spins with their orbital motion, i.e. spin-orbit interactions, Darwin term, electron spin-spin interactions, radiative interactions i.e. Lamb shift corrections and nuclear contributions. The relativistic corrections are also known as fine structure corrections. Therefore the N-electron relativistic Hamiltonian can be written as,

$$H = \sum_{i=1}^{N}\left(-\nabla_i^2 - \frac{2Z}{r_i}\right) + H_{ee} + \textbf{Relativistic Corrections} \qquad 2.9$$

Or the total Hamiltonian becomes

$$H = H_o + H_{ee} + H_r + H_{so} + H_D \qquad 2.10$$

where

N is the number of electrons and Z is the atomic number, the distances are measured in Bohr unit (a_o) and energies in rydbergs.

H_o is the core Hamiltonian representing the attractive electrostatic field of the nucleus, $r_i = |\textbf{r}_i|$ is the distance of the ith electron from the nucleus

H_{ee} is the Hamiltonian compensating for the electrostatic repulsion between electrons

H_r is the relativistic Hamiltonian

H_{so} is the Hamiltonian representing the spin-orbit interaction

H_D is the Darwin Hamiltonian

The relativistic corrections in Hamiltonian comes out as a consequence of Dirac equation in an expansion of $(v/c)^2$. The estimated value of v/c is approximately Zα, α is the coupling constant named Sommerfeld's fine-structure constant and gives the strength of electromagnetic interaction i.e. how strongly a charge particle interacts with electromagnetic field, viz.

$$\alpha = \frac{e^2}{\hbar c} = \frac{1}{137.035999679}$$

These relativistic corrections are smaller than non-relativistic electrostatic coulomb interactions by a factor of $(Z\alpha)^2$.

2.2 The Central Field Approximation

The most important and fundamental aspect of a multielectron atom is the electron-electron non-symmetrical interactions and fermionc nature of electrons as indistinguishable particles. In this case the Schrödinger equation cannot be separated into radial and angular part as is possible in one-electron atom. Calculations of energy eigenvalues and eigenfunctions become much more difficult and mathematically complicated. Even for a simplest case of a multielectron atom, namely the two-electron He atom, an exact theoretical treatment is not possible.

To circumvent these difficulties either numerical methods or approximate models are used for such calculations. One such approximation is the Central Field Approximation in which all electron-electron and electron-nucleus interactions are averaged together to produce an effective field and any arbitrarily chosen electron e_i moves in this effective field, that is independent of the momentary location of the other electrons. The effective field is different for each of the electrons and the field must be computed self-consistently for all the electrons. This approximation reduces the multielectron problem to a one electron problem which could be solved relatively with less complexity. In order to compute effective field V_c Hartree-Fock methods or self-consistent field approach is used. The method is based on a supposition of a trial centrally symmetric field which then could be plugged into Schrödinger equation. The solution of Schrödinger equation results in energy eigenvalues and eigenfunctions.

Further improvements in this approximation can be done by taking into account the non-spherical nature of electron-electron interaction. The effect of this residual electrostatic interaction can be estimated using the so-called Slater determinant. This determinantal function or Slater determinant is a total wave function ψ_c describing an atom in which one electron is in a state α, another electron is in a state β, so on and then writing as an N x N determinant. The eigenvalue E_c of the central field Hamiltonian H_c corresponding to a given Slater determinant is just the sum of the energies of the N individual states present in the determinant. The total wave function must be anti-symmetric with respect to the exchange of any two arbitrary electrons. This requirement is fulfilled by interchanging two columns of the determinant which implies the exchange of two electrons, resulting in an inversion of the sign of the determinant. This satisfies the requirement of the Pauli Exclusion Principle which states that for electrons, only the functions which are totally anti-symmetric with respect to exchange in coordinate and spin are allowed.

2.2.1 Electron-electron interaction Hamiltonian (H_{ee})

Each electron in a multielectron atom moves, assuming independently, in the electrostatic attractive field of the nucleus and in the repulsive field produced by the remaining electrons. Thus the state of each electron is determined by the coulomb field of the nucleus and the screening field of the remaining electrons shielding the nucleus. The Hamiltonian for electron-electron interactions can be written as

$$H_{ee} = \sum_{i<j} \frac{Ze^2}{r_{ij}} \qquad \qquad 2.11$$

where r_{ij} represent the relative coordinate between pair of electrons.

A lengthy mathematical treatment is required for the evaluation of the matrix element of the above operator. The total wave function of the atom is the product of orbital wavefunction $\psi(r,\theta,\phi)$ and spin wavefunction $\chi(m_s)$.

$$\psi = \psi_{n,l,s,m_l,m_s}(r,\theta,\phi,m_s) = R_{n,l}(r) Y_{l,m_l}(\theta,\phi)\chi(m_s) \qquad 2.12$$

where n,l,s are principal, orbital and spin quantum numbers of an electron respectively, m_l and m_s are the projections of l and s. The operator in equation 2.11 is a two electron operator; therefore the matrix element of H_{ee} for a pair of electrons is given by

$$E_{ee} = \left\langle \psi(1)\psi(2) \left| \frac{Ze^2}{r_{ij}} \right| \psi(1)\psi(2) \right\rangle \qquad 2.13$$

The matrix elements in equation 2.13 can be expressed in terms of two more integrals known as Coulomb or direct Integral **J(i,j)** and an Exchange Integral **K(i,j)**. The Coulomb Integral represents coulomb energy of interaction due to the charge distribution of two electrons. The Exchange Integral has no classical analogue and represents the exchange part of the energy of interaction between pair of electrons. The presence of two integrals i.e. coulomb and the exchange integrals in the expression for energy of interaction between two electrons is due to the fact that description of an atom by Schrödinger equation is not accurate as it does not contain spin term in the electron-electron interaction part of the Hamiltonian. So in addition to the electrostatic coulomb integral which does not operate on the electron spin, the exchange integral must also be incorporated to account for the splitting of configurations into terms. The exchange integral is much stronger than the spin-dependent terms arising from relativistic effects, such as spin-orbit interactions and this makes the exchange part purely quantum mechanical in nature.

The $\frac{1}{r_{ij}}$ term can be expanded in a series of Legendre polynomials and then using the product of matrix elements of spherical harmonics, the integrals J and K can be computed. The coulomb integral can be written as

$$J(i,j) = \sum_k a^k(i,j) F^k(i,j) \qquad 2.14$$

where $\mathbf{a^k(i,j)}$ is the product of matrix elements of spherical harmonics and $\mathbf{F^k(i,j)}$ contains the expansion of $\dfrac{1}{r_{ij}}$ terms and is given by

$$\mathbf{F^k(i,j)} \equiv \mathbf{R^k(ij,ij)} = \int\limits_0^\infty \int\limits_0^\infty \frac{e^2 r_<^k}{r_>^{k+1}} \left| P_i(r_1) \right|^2 \left| P_j(r_2) \right|^2 dr_1 dr_2 \qquad\qquad 2.15$$

similarly the exchange integral can be written as

$$\mathbf{K(i,j)} = \sum_k \mathbf{b^k(i,j)} \mathbf{G^k(i,j)} \qquad\qquad 2.16$$

where $\mathbf{b^k(i,j)}$ is same as $\mathbf{a^k(i,j)}$ and $\mathbf{G^k(i,j)}$ is given by

$$\mathbf{G^k(i,j)} \equiv \mathbf{R^k(ij,ji)} = \int\limits_0^\infty \int\limits_0^\infty \frac{e^2 r_<^k}{r_>^{k+1}} P_i(r_1) P_j(r_2) P_i(r_2) P_j(r_1) dr_1 dr_2 \qquad\qquad 2.17$$

where $r_<$ and $r_>$ are respectively the lesser and greater of the distances r_1 and r_2 of the electrons from the nucleus.

Properties of $\mathbf{F^k(i,j)}$ and $\mathbf{G^k(i,j)}$

- The radial integral $\mathbf{F^k}$ and $\mathbf{G^k}$ are known as **Slater integrals** and are both positive.

- For equivalent electrons $\mathbf{F^k = G^k}$

- Coefficients $\mathbf{a^k}$ and $\mathbf{b^k}$ are non-vanishing only for few small values of k. Therefore the infinite sums (2.14) and (2.16) in case of practical interest contains not more than two or three terms.

2.2.2 Relativistic Kinetic Energy Correction (H_r)

The relativistic relationship between the energy and momentum of an orbiting electron of mass m is given by

$$\mathbf{E} = \left(p^2 c^2 + m^2 c^4 \right)^{1/2} = mc^2 + \frac{p^2}{2m} - \frac{1}{8}\frac{\left(p^2\right)^2}{m^3 c^2} + \cdots \qquad\qquad 2.18$$

In the expansion above the third term on right is the first order perturbation representing relativistic kinetic energy correction $\mathbf{H_r}$ viz.

$$H_r = -\frac{1}{8}\frac{(p^2)^2}{m^3c^2} \qquad 2.19$$

In comparison to $p^2 / 2m$, H_r is smaller by a factor of $p^2 / m^2c^2 = v^2 / c^2 \approx (Z\alpha)^2$. It is of the order of 0.1 cm^{-1}.

2.2.3 Spin-orbit Interaction H_{so}

In multielectron atoms as well as in single electron atoms, the magnetic moment of the electron(s) interacts with magnetic field produced by the orbiting electron(s). This interaction is known as spin-orbit interaction and is largest relativistic effect. Due to this interaction each term splits into levels whose separations are of the order of 1-1000 cm^{-1}, depending strongly on the atomic number Z.

The spin-orbit interaction Hamiltonian for one electron system can be extended to a multi-electron system. For N-electron system the spin-orbit Hamiltonian is written as

$$H_{SO} = \sum_i^N \xi(r_i)\, \vec{l}_i \cdot \vec{s}_i \qquad 2.20$$

or

$$H_{so} = \xi(r)\vec{L} \cdot \vec{S}$$

where $\xi(r)$ is the "fine-structure parameter". Assuming LS coupling which implies that the electronic repulsion energy is much greater than the spin-orbit energy. The wave functions for the various terms whose energies differ from one another due to Coulomb repulsion can be written as $|\psi(LSMLMS)\rangle$. Total angular momentum operator $\vec{J}$ can be constructed as a sum of orbital angular momentum $\vec{L}$ and spin angular momentum $\vec{S}$, i.e.

$$\vec{J} = \vec{L} + \vec{S} \qquad 2.21$$

squaring this vector sum gives

$$J^2 = \vec{J}.\vec{J} = (\vec{L}+\vec{S}).(\vec{L}+\vec{S}) \qquad 2.22$$

$$J^2 = L^2 + S^2 + 2\vec{L}.\vec{S} \qquad 2.23$$

$$\vec{L}.\vec{S} = \frac{(J^2 - L^2 - S^2)}{2} \qquad 2.24$$

so the spin-orbit Hamiltonian equation 2.20 becomes

$$H_{so} = \xi(r)\frac{(J^2 - L^2 - S^2)}{2} \qquad 2.25$$

Equation 2.21 permits a change of representation of wave functions from $|\psi(\mathbf{LSMLMS})\rangle$ to $|\psi(\mathbf{LSJM_J})\rangle$. Using irreducible tensor notation for the coupling of angular momenta, the matrix elements of the operator (equation 2.20) gives the energies associated with the spin-orbit interaction i.e.

$$\langle \mathbf{j_1 j_2 jm} | \mathbf{T}^{(k)} . \mathbf{U}^{(k)} | \mathbf{j_1' j_2' j'm'} \rangle$$

$$= (-1)^{j+j_2+j_1'} \, \delta_{jj'} \delta_{mm'} \begin{Bmatrix} \mathbf{j_1'} & \mathbf{j_2'} & \mathbf{j} \\ \mathbf{j_2} & \mathbf{j_1} & \mathbf{k} \end{Bmatrix} \langle \mathbf{j_1} | \mathbf{T}^{(k)} | \mathbf{j_1'} \rangle \langle \mathbf{j_2} | \mathbf{U}^{(k)} | \mathbf{j_2'} \rangle \qquad 2.26$$

taking k = 1, i.e. $\mathbf{l_i}$ and $\mathbf{s_i}$ are irreducible tensors of rank 1 and changing the notations

$$\langle \mathbf{LSJM_J} | l_i . s_i | \mathbf{L'S'J'M_J'} \rangle$$

$$= (-1)^{J+S+L'} \, \delta(\mathbf{J,J'}) \delta(\mathbf{M_J, M_J'}) \begin{Bmatrix} \mathbf{L'} & \mathbf{S'} & \mathbf{J} \\ \mathbf{S} & \mathbf{L} & \mathbf{1} \end{Bmatrix} \langle \mathbf{L} | l_i | \mathbf{L'} \rangle \langle \mathbf{S} | s_i | \mathbf{S'} \rangle \qquad 2.27$$

The 6j symbols vanishes unless the triangle conditions are satisfied i.e. matrix elements of $\mathbf{l_i} . \mathbf{s_i}$ vanishes unless

$$\Delta S = 0, \pm 1, \quad S' + S \geq 1$$
$$\Delta L = 0, \pm 1, \quad L' + L \geq 1 \qquad 2.28$$

and

$$\Delta J = 0, \pm 1 \quad \Delta M_J = 0 \qquad 2.29$$

Spin-orbit interaction has nonvanishing matrix elements between states which differ in spin by one unit. Thus, for example, spin-orbit interaction can produce an admixture of singlet and triplet states. With L′ = L and S′ = S the 6j symbol has the form

$$\begin{Bmatrix} \mathbf{L} & \mathbf{S} & \mathbf{J} \\ \mathbf{S} & \mathbf{L} & \mathbf{1} \end{Bmatrix} = (-1)^{L+S+J} \frac{J(J+1) - L(L+1) - S(S+1)}{\sqrt{L(2L+1)(2L+2)S(2S+1)(2S+2)}} \qquad 2.30$$

so the first order energy splitting arising from spin-orbit interaction is written as

$$\Delta \mathbf{E_{SO}} = \langle \alpha \mathbf{LSJM_J} | \mathbf{H_{SO}} | \alpha \mathbf{LSJM_J} \rangle$$

$$= \left\langle \alpha \mathbf{LSJM_J} \left| \sum_i \xi(r_i) l_i . s_i \right| \alpha \mathbf{LSJM_J} \right\rangle$$

$$= \frac{1}{2} \mathbf{A}(\alpha \mathbf{LS}) [J(J+1) - L(L+1) - S(S+1)] \qquad 2.31$$

Here α represents the dependence of the wave function on radial coordinate and A(αLS) is the proportionality factor depending on α, L and S but not on J. The reduced matrix elements, phase factor and the dependence on $\xi(r_i)$ are all contained in the factor A(αLS)

called the fine structure splitting constant. Writing the matrix elements in the form as given in equation 2.31 has an advantage that matrix element can also be written as

$$\langle \alpha LSJM_J | L \cdot S | \alpha LSJM_J \rangle = \frac{1}{2} \langle \alpha LSJM_J | J^2 - L^2 - S^2 | \alpha LSJM_J \rangle$$

$$= \frac{1}{2} [J(J+1) - L(L+1) - S(S+1)] \qquad 2.32$$

Thus within the manifold of states comprising a given LS term the matrix element of H_{SO} is proportional to the matrix element of $L \cdot S$. The fine-structure parameter can be written by introducing a quantity

$$\xi(r) = \frac{1}{2m^2c^2} \frac{1}{r} \frac{dV}{dr} \qquad 2.33$$

in this case

$$V(r) = -\frac{Ze^2}{(4\pi\varepsilon_o)r} \qquad 2.34$$

so that

$$\xi(r) = \frac{1}{2m^2c^2} \frac{Ze^2}{4\pi\varepsilon_o} \frac{1}{r^3} \qquad 2.35$$

and the expectation value of $\xi(r)$

$$\langle \xi(r) \rangle = \frac{1}{2m^2c^2} \left(\frac{Ze^2}{4\pi\varepsilon_o} \right) \left\langle \frac{1}{r^3} \right\rangle \qquad 2.36$$

- The possible values of J are $|L - S|$, $|L - S| + 1$, ...$L + S$.
- The selection rules for dipole transition is $\Delta J = 0, \pm 1$.
- Each term splits into (2s +1) term if S < L or into (2L +1) is S > L.
- The total width of splitting between L+S and L−S for L > S is 2 < $\xi(r)$ > S(2L + 1) and for S > L it is 2 < $\xi(r)$ > L(2S + 1).
- Depending on the sign of fine structure splitting constant A(αLS) i.e. positive or negative, the resulting fine structure multiplets are termed as normal or inverted repetively.

The energy difference between adjacent levels in a fine structure multiplet is given by

$$\Delta E(J) = E(J) - E(J-1) = A(\alpha LS)J \qquad 2.37$$

Equation 2.37 is known as Lande interval rule in LS coupling i.e. the energy difference between adjacent levels in a multiplet is proportional to the larger value of J. Also the energy difference does not depend on M_J; this means that the energy of an isolated atom

can not depend on orientation of its total angular momentum J in space. Departure from interval rule indicate the presence of interactions other than the spin-orbit interaction, or a break down of spin-orbit coupling approximation because the spin-orbit interaction cannot be considered as small compared with the residual electrostatic interaction. The spin-orbit interaction can have matrix elements off-diagonal in L and S, but diagonal in J, so it can mix together states of different L and S and not of the same J. In general, levels of the same J in different terms of a configuration repel each other in energy as a result of second order perturbation.

Each level has (2J + 1)-fold degeneracy therefore energy of a configuration in terms of mean value can be written as

$$\langle \mathbf{E} \rangle = \frac{\sum_{J}(2J+1)E_{J}}{\sum_{J}(2J+1)} \qquad \qquad 2.38$$

This quantity is called center-of-gravity of the levels of configuration. Its value is significant if the configuration interaction perturbations are small.

2.2.4 Darwin Term H_D

This terms applies to a special case of angular momentum $l = 0$ i.e. results in a shift of s states, viz.

$$\mathbf{H_D} = \left(\frac{e\hbar^2}{8m^2c^2} \right) \nabla . \mathbf{E} \qquad \qquad 2.39$$

This term can be understood from the "Zitterbewegung" of the electron. According to the relativistic theory, the position of a localized electron fluctuates with

$$\delta \mathbf{r} = \frac{\hbar}{mc} = \hat{\lambda}_c \qquad \qquad 2.40$$

The shift is of the order of less than 0.1 cm^{-1}.

2.2.5 The Lamb Shift (Radiative Correction)

The Lamb shift or radiative correction is similar in nature as Darwin term and results due to vacuum or zero-point fluctuations of the quantized electromagnetic field. Due to these fluctuations a shift in the position of electrons occurs. The shift in the position of electron is given by

$$\langle (\delta x)^2 \rangle \approx \frac{2\alpha}{\pi} \left(\frac{\hbar}{mc} \right)^2 \log \frac{1}{\alpha Z} \qquad \qquad 2.41$$

and the Lamb shift in energy is given by

$$\Delta E_{Lamb} \approx \frac{4}{3\pi} \frac{mc^2 Z^4 \alpha^5}{n^3} \log \frac{1}{\alpha Z} \delta_{l,0} \qquad 2.42$$

For hydrogen the Lamb shift $\Delta \approx 660$ MHz from $2S_{1/2}$ towards $2P_{1/2}$. As compared to Darwin term the radiative corrections are smaller by a factor of $\alpha \log (1/\alpha)$.

2.3 Fine Structure Splitting

The non-relativistic energy levels $\mathbf{E_n}$ are $2n^2$ times degenerate, the factor of 2 arises due to spin. This degeneracy is partly removed by Dirac theory of relativistic treatment of electronic levels. According to Dirac theory, the non-relativistic levels $\mathbf{E_n}$ depending on the principal quantum number n splits into n sublevels, one for each value of total angular momentum (j = l + s) quantum number j = 1/2, 3/2,……n-1/2. This splitting is called 'fine structure splitting', and n levels j = 1/2, 3/2,…….n-1/2 are said to form a 'fine structure multiplet'. All three relativistic corrections, i.e. $\mathbf{H_r}$, $\mathbf{H_{so}}$, $\mathbf{H_D}$, contribute to the fine structure splitting but for the most part the dominant is the spin-orbit correction. Contributions due relativistic and Darwin terms are not very significant as compared to other non-relativistic and spin-orbit interactions, therefore the total Hamiltonian for a system of N electron atom is given by

$$H = H_o + H_1 + H_2 \qquad 2.43$$

where H_1 represents electron-electron interaction Hamiltonian and H_2 is the spin-orbit interaction Hamiltonian.

2.4 Parity

The electrons are indistinguishable particles, this means the Hamiltonian must be invariant under the interchange of spatial and spin coordinates of any two electrons. Since the electrons are Fermions the eigen function of a system of N electrons must be antisymmetric or the electrons in an atom obey Pauli's exclusion principle. Since the general Hamiltonian is invariant under inversion, so the eigen function must have a definite parity or in other words, the parity is a good quantum number for an atomic state. Eigenfunctions with even values of $\sum l_i$ do not change sign. These states, also function are called even or gerade (in german). For odd $\sum l_i$, the functions change sign on an inversion of transformation. In this case the state is called odd or ungerade. The parity of state is entirely dependent on the value of $\sum l_i$.

2.5 Electron Configurations, Shell and Subshells

In the central field approximation the total energy of the atom is specified by the number of electrons occupying each of the individual energy levels E_{nl}. This distribution of electrons with respect to the quantum numbers n and l is called electron configuration. The configuration of ground state is called ground configuration and that of excited

states, excited configurations. The states with the same n and *l* form a subshell, the subshells with the same n form a shell. Thus the assignment of an electron configuration requires the enumeration of the values of n and *l*. In spectroscopic notations value of n is given as a number and that of *l* as letter. The number of electrons in a configuration is given as a numerical superscript, e.g. $(2s)^2$ or $2s^2$.

There are $2(2l + 1)$ states having same value of n and *l* but differing in m_l and m_s such states are called 'equivalent' and electrons are called 'equivalent electrons'. In filling states Pauli Exclusion Principle must be satisfied which says that there cannot be more than one electron in each individual state labeled by the quantum numbers (n,l,m_l,m_s). Thus the maximum number of electrons in each subshell is $2(2l + 1)$. An assembly of $2(2l + 1)$ equivalent electrons is called a closed or filled subshell. The maximum number of electrons in a shell is $2n^2$ and such assembly is called closed or filled shell.

2.6 Configurations with open subshells

The electron configurations of successive atoms in periodic table are determined according to a principle known as Aufbau principle or Building-up principle. Electrons fill orbitals starting at the lowest available energy state before filling higher states. The order in which these orbitals are filled is based on a rule known as Madelung rule, after Erwin Madelung, which says "orbitals with a lower value of n+*l* are filled before those with higher value of n+*l*". The number of electrons each orbital can occupy is limited by Pauli Exclusion Principle.

Many configurations of atoms especially ground state configuration contain one or more open, i.e. unfilled, subshells, for example, configurations of lanthanide and actinide elements (Z = 57 – 70), for example ground state configuration of Praseodymium (Pr) :

$$(1s^2\, 2s^2\, 2p^6\, 3s^2\, 3p^6\, 3d^{10}\, 4s^2\, 4p^6\, 4d^{10}\, 5s^2\, 5p^6)\, 4f^3\, 5d\, 6s^2\ {}^4I^o_{9/2}$$
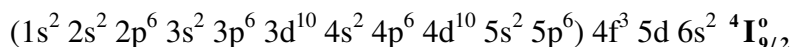
For such a ground state configuration the number of LS terms and corresponding number of energy levels, can be very large. Consequently the spectrum is exceedingly complex, as is observed in case of Praseodymium. Further more highly excited states overlap each other, in such cases the configuration is given by the mixture of all overlapping configurations. This situation is called configuration mixing or configuration interaction. In explaining resulting spectra due to such interaction, it is necessary to consider several configurations simultaneously. Since the parity is a good quantum number, configuration mixing takes place only within configuration of same parity.

2.7 Coupling Schemes for Electronic Angular Momenta

In a many electron atom various angular momenta (orbital and spin) couople to give a total angular momentum for the atom. Generally, the coupling scheme depends on several features but two distinct interactions between the electrons are (i) electrostatic interaction (ii) spin-orbit interaction. If electrostatic interaction between electrons is larger than spin-orbit interaction, then electrons couple according to LS-coupling scheme. If spin-orbit interactions are larger than electrostatic interactions between electrons then electrons

couple according to jj-coupling scheme. When neither of the two dominates, an intermediate coupling scheme must be employed, which can occur for low-lying excited states of heavy systems.

i) LS Coupling

In cases where the electrostatic Coulomb repulsion between electrons is larger than spin-orbit interaction of either electron, LS-coupling or Russell-Saunders [95] coupling is a good approximation. In this scheme the orbital angular momenta of the individual electrons couple to give a total $\vec{L}$ and the individual spins couple to give a total $\vec{S}$. The coupling of the total orbital angular momentum, $\vec{L}$ and the total spin, $\vec{S}$ gives $\vec{J}$. The maximum and minimum value of J are $|\mathbf{J}+\mathbf{S}|$ and $|\mathbf{J}-\mathbf{S}|$, respectively. The electrostatic interaction usually dominates in low-lying states of light atoms where the electron(s) in the outer shell interact strongly with electrons in the inner shells known as the core. This coupling scheme is often appropriate for the ground states of atoms as well.

The electrostatic Coulomb repulsions affect only the orbital angular momenta and not the spins. Therefore it is appropriate first to couple together all the individual orbital angular momenta and the spin momenta. This gives the total orbital angular momentum i.e.,

$$\mathbf{L}=\sum_i l_i \quad \text{with } |\mathbf{L}|=\sqrt{\mathbf{L(L+1)}}\ \hbar \qquad 2.44$$

and the individual spins add together to give the total spin momentum i.e.,

$$\mathbf{S}=\sum_i s_i \quad \text{with } |\mathbf{S}|=\sqrt{\mathbf{S(S+1)}}\ \hbar \qquad 2.45$$

of the atomic states. Therefore the total angular momentum of the electron shell is given by

$$\mathbf{J}=\mathbf{L}+\mathbf{S} \quad \text{with } |\mathbf{J}|=\sqrt{\mathbf{J(J+1)}}\ \hbar \qquad 2.46$$

This coupling scheme is called LS coupling or Russell Sunders coupling and is usually observed for light atoms. If in an atom the physical conditions closely approximate the LS coupling conditions then the individual l_i are thought to precess rapidly about the resultant $\mathbf{L}$, and the individual s_i similarly as precessing about their resultant $\mathbf{S}$. Neglecting all other interactions except the Coulomb interaction, then $\mathbf{L}$ and $\mathbf{S}$ are constants of motion and the wave functions and the quantum states can be decribed in terms of four good quantum numbers $\mathbf{L}$, $\mathbf{S}$, $\mathbf{M_L}$ and $\mathbf{M_S}$. Physically, however, the vectors $\mathbf{L}$ and $\mathbf{S}$ are always coupled together by weak spin-orbit interactions and the vectors $\mathbf{L}$ and $\mathbf{S}$ precess about their resultant $\mathbf{J}$. Precession is taking place sufficiently slowly such that the magnitudes of $\mathbf{L}$ and $\mathbf{S}$ are well-defined and sum of the z-components ($\mathbf{M_J} = \mathbf{M_L} + \mathbf{M_S}$) is defined. Now the quantum states are described in terms of four quantum numbers $\mathbf{L}$, $\mathbf{S}$, $\mathbf{J}$ and $\mathbf{M_J}$.

ii) jj Coupling

When the spin–orbit interaction of electrons is stronger than the electrostatic interaction between the electrons, *jj* coupling is most appropriate scheme. In other words, for example, the two electrons are sufficiently far from each other that the electrostatic interaction between them is weak and thus only their total angular momenta, *j*, are constants of the motion. This is most often the case when the excited electron is in a high-*n* state and thus spends most of its time far from the others confined to the core near the nucleus. This coupling is appropriate for heavier atoms with large value of Z.

In this case the residual electrostatic interaction between electrons is neglected, the electrons move quite independently of each other in a central field, each electron separately being subject to a spin-orbit interaction. Initially l_i and s_i of individual electrons couple to form the resultant angular momentum

$$\vec{j}_i = \vec{l}_i + \vec{s}_i \qquad\qquad 2.47$$

Then the vectors $\mathbf{j}_i$ of different electrons couple together to give total angular momentum J of the atomic state, given by,

$$\vec{J} = \sum_i \vec{j}_i \qquad\qquad 2.48$$

For example for two electron system $\vec{j_1} + \vec{j_2} = \vec{J}$. The possible values of j lie between $\left| \vec{j_1} + \vec{j_2} \right|$ and $\left| \vec{j_1} - \vec{j_2} \right|$.

In vector atom model each l_i and s_i precess rapidly about their resultant $\mathbf{j}_i$ and afterwards application of the residual electrostatic interaction acting as a small perturbation causes a slower precession of $\mathbf{j}_i$ about their resultant $\mathbf{J}$ which is a constant of motion in both LS- and jj-coupling schemes. But in the jj-coupling scheme L and S have no meaning.

The manifold of J values and the total number of quantum states are the same in all coupling scheme. There are many situations for which neither LS- nor jj-coupling scheme are valid approximations. In such cases the Coulomb repulsion and the spin-orbit interaction for each value of J is diagonalized. The coupling is then said to be intermediate.

Chapter 3
Hyperfine Interaction

3.1 Hyperfine Structure

Up till now in discussing the atomic structure of an atom, we were mainly concerned, starting from the gross interaction, the radial distribution of electrons in shells around the nucleus. This is due to the electrostatic Coulomb interaction between the nucleus considered only as a massive point charge and charged electrons. Further more we discussed other smaller electrodynamic interactions such as spin-orbit interactions leading to fine structure levels. In this chapter hyperfine structure of atoms is discussed. The hyperfine spectra of atoms or molecules result due to the interaction between electronic degrees of freedom and nuclear properties other than the dominant nuclear Coulomb field.

Apart from the fundamental properties of nucleus that is its charge and mass, the nucleus has other observable characteristics such as its spin, electromagnetic multipole moments of higher order other than electric monopole moment. The interactions between these moments and the electromagnetic field produced at the nucleus by spinning and orbiting electrons give rise to further splitting of fine structure levels. Such interactions are classified as **hyperfine interactions** and resulting structure is called **hyperfine structure (hfs)**. The order of magnitude of splitting of fine structure levels range from 10^{-3} cm^{-1} to 1 cm^{-1} depending on the atomic number Z of the element.

The nucleus has a compound structure of nucleons that is positively charged protons and neutrons (without charge). Each of these nuclear particles has an intrinsic spin ½ and may take part in the orbital motion within the nucleus. This gives the nucleus a resultant spin I and a magnetic dipole moment **μ** in the direction of **I**. The major contribution in splitting of fine structure levels is due to the interaction between the magnetic dipole moment of the nucleus and magnetic moment of electrons. The magnitude or strength of splitting of the fine structure levels is given by a constant known as **magnetic dipole interaction constant A**. Another weak interaction is the nuclear electric quadrupole moment **Q** interacting with the electron structure of the atom. The electric quadrupole moment arise as a result of non-spherical distribution of the charges inside the nucleus. The quadrupole interaction causes a shift in hyperfine structure levels and does not contribute to splitting of levels. This shifting is given by a constant known as **electric quadrupole interaction constant B**.

Apart from the hyperfine interactions the mass and size of the nucleus also affect the atomic energy levels and is reflected in **isotopic shifts**. Although the affect is very small but is accessible through high resolution spectroscopy. Due to the finite nuclear mass, the nucleus possesses a small nuclear recoil energy which is observed as a "mass shift" between the atomic transition frequencies of different isotopes of an element. Isotope shifts can also be due to the nucleus not being a point charge but have an extended charge distribution which is different for different isotopes. This is known as "**nuclear volume**

shift" or "**field shift**". The quantity which governs the isotope shift is the second radial moment of the nuclear charge distribution. This quantity is called "nuclear mean square charge radius", and can be considered as a monopole moment of the nucleus.

3.2 Nuclear Angular Momentum

The nuclear constitutents protons and neutrons are composite particles belonging to the group of particles known as baryons which are strongly interacting heavy particles with half-integer spins (1/2, 3/2, ...). Protons and neutrons are the lightest members of the group and are most stable.

The structure of nucleons i.e. protons and neutrons is successfully explained by quark theory. This theory postulates that composite heavier particles are made up of six types of quarks known as up, down, charm, strange, top, and bottom quarks which are termed as flavours of quarks. According to this theory protons and neutrons contain only up quarks (u) and down quarks (d). A proton is composed of two up quarks and one down quark (uud) whereas a neutron has two down quarks and one up quark (ddu). These quarks are bound by a fundamental strong field called "gluon field". The charge on an up quarks is (2/3)e and on down a quark it is (-1/3)e. Thus the charge on a proton (uud) is equal to e and on a neutron is equal to zero. Each quark has an intrinsic spin and can be represented by a vector whose length is measured in units of $\hbar$. Measurement of spin vector components along a given axis yield values $+(1/2)\hbar$ or $-(1/2)\hbar$. In a proton or neutron the up and down quarks are combined in such a way that net spin s of a proton or a neutron is equal to 1/2.

The quarks which are charged particles inside a proton or a neutron are bound together by a strong interacting field. This gives a proton and a neutron magnetic moments μ_p, μ_n and a quantized angular momentum l. For each nucleon the orbital angular momentum l and spin s couple to give total angular momentum j. In an approximation that nuclear potential is central l, s and j are constant of motion. For a nucleus containing A nucleons the total angular momentum is the vector sum **I** of the angular momenta of all the nucleons, i.e.

$$\vec{I} = \sum_{i=1}^{A} (\vec{l}_i + \vec{s}_i) \qquad\qquad 3.1$$

$$\vec{I} = \vec{L} + \vec{S} \qquad\qquad 3.2$$

$$\vec{I} = \sum_{i=1}^{A} \vec{j}_i \qquad\qquad 3.3$$

The nuclear angular momentum I has similar quantum menchanical properties as seen for the atomic case $I^2 = \hbar^2 I(I + 1)$ and $I_z = m_I\hbar$ (m_I = -I, ... , +I). In ordinary external magnetic fields, nuclear Zeeman effect can be observed, since state I splits up in to (2I +1) individual equal spaced substates m = -I, -I +1, ... I − 1, I. If very large magnetic field is applied enough to break the coupling between the nucleons, then each individual j splits up in to (2j + 1) substates. The nucleus is treated as an elementary particle with

single spin quantum number representing the intrinsic angular momentum of the particle. This is only possible because for conventional spectroscopic investigations the nucleus is subjected to such static electromagnetic field which is not sufficiently strong to change the internal structure or break the coupling of nucleons that is responsible for equation 3.1. Finally to deal with the total angular momentum of the atom that is, the sum of nuclear and electronic angular momentum, a total angular momentum vector **F** of the atom is introduced which is given by

$$\vec{F} = \vec{I} + \vec{J} \qquad\qquad 3.4$$

The quantum numbers **I** and **J** may be integral or half-integral as the number of nucleons or electrons are even or odd respectively.

3.3 Nuclear Electromagnetic Moments

The strong nuclear interaction establishes the distribution and motion of nucleons inside the nucleus. This distribution of electric charges and currents produce electric and magnetic fields that change in a characteristic manner. To these charge and current distributions electromagnetic multipole moment can be assigned depending up on their characteristic spatial dependence. For example $1/r^2$ electric field arises from the net charge and is the zeroth or monopole moment, $1/r^3$ field arises from the first or dipole moment, $1/r^4$ field arises from the second or quadrupole moment and so on. With the exception of monopole magnetic moment the magnetic multipole moments also behave in a similar manner.

The multipole moments (2^k pole moments) which do not vanish are (1) the magnetic moments for odd k and (2) the electric moments for even k. where k > 0. A nucleus of spin quantum number I can not have a multipole moment of order 2k where k > 2I. Usually we deal with the two lowest orders of interaction, i.e. for k = 1 and 2. k = 1 corresponds to magnetic dipole interaction and k = 2 corresponds to electric quadrupole interaction. Magnetic dipole moment gives information about the structure of individual nucleons where as electric quadrupole moment gives the shape and charge distribution within the nucleus. In the investigations of hyperfine structure of fine structure levels the major contribution is from the magnetic dipole nuclear moment and a smaller contribution from electric quadrupole nuclear moment.

3.4 Magnetic Dipole Interaction

At the most fundamental level the circular loop carrying current i and enclosing an area A has a magnetic moment of magnitude $|\mu| = iA$. If the current is caused by a charge e, moving with speed v in a circle of radius r with period of rotation $2\pi r / v$, then the magnitude of magnetic moment is given by

$$|\mu| = \frac{e}{2\pi r / v}\pi r^2 = \frac{evr}{2} \qquad\qquad 3.5$$

Classically magnitude of angular momentum $|l|$ = mvr, equation 3.5 can be written as

$$|\mu| = \frac{e}{2m}|l|$$ 3.6

Quantum mechanically the magnetic moment corresponds to the direction of greatest component of l. Therefore expectation value of l relative to axis where it has maximum projection is $m_l\hbar$ with m_l = +l. Thus equation 3.6 becomes

$$\mu = \frac{e\hbar}{2m}l$$ 3.7

where l is the angular momentum quantum number of the orbit. The quantity **eħ / 2m** is called a **magneton**. For atomic motion this quantity is known as Bohr magneton μ_B = 5.7884 x 10^{-5} eV/T. Putting the proton mass changes to nuclear magneton μ_N = 3.1525 x 10^{-8} eV/T which is much smaller than Bohr magneton owing to the difference in masses. Thus normally atomic magnetism has much larger effects as compared to nuclear magnetism. Equation 3.7 can also be written as

$$\mu = g_l\,l\,\mu_N$$ 3.8

where g_l is the **g-factor** associated with the orbital angular momentum l. For proton g_l = 1 and because neutrons have no electric charge, so equation 3.8 can be used to describe the orbital motion of neutrons by putting g_l = 0. Considering the intrinsic spin which is a quantum mechanical characteristic, so the spin magnetic moment is given by

$$\mu = g_s\,s\,\mu_N$$ 3.9

where s = 1/2 for protons, neutrons and electrons. The quantity g_s is called the spin g factor and is obtained by calculating the relativistic quantum mechanical equation. For electron which is a spin-1/2 particle the Dirac equation gives g_s = 2 which is quite consistent with the experimentally measured value of 2.0023 for electron. For free nucleons the experimental values are far from expected value for point particles:

proton: g_s = 5.5856912 ± 0.0000022

neutron: g_s = -3.8260837 ± 0.0000018

Not only the experimental value for proton is far from the expected value but the uncharged neutron has a nonzero magnetic moment. This is evidence that nucleons are not elementary point like particles like electrons, but have an internal structure. The internal structure is due to charge particles in motion whose resulting current give the observed magnetic moment.

Therefore the nuclear magnetic dipole moment due to both contributions is written as

$$\mu = (g_l \, l + g_s \, s)\mu_N \qquad\qquad 3.10$$

the g-factors g_l and g_s account for the orbital and intrinsic contributions to μ. Their values can be adjusted for individual particles i.e. $g_l = 1$ for protons and $g_s = 5.5856912$ as measured experimentally for free protons in which l does not contribute to μ. For neutrons which are uncharged $g_l = 0$ and experimentally measured value $g_s = -3.8260837$. Modifying equation 3.10 for all nucleons, gives the magnetic dipole moment of a nucleus with total angular momentum I

$$\mu_I = \sum_{i=1}^{A} \left[g_{l,i} l_i + g_{s,i} s_i \right] \mu_N / \hbar \qquad\qquad 3.11$$

Therefore the interaction energy between nuclear magnetic moment μ_I and magnetic field B_{el} produced by orbiting and spinning electrons is given by the Hamiltonian H_μ

$$\widehat{H}_\mu = -\vec{\mu}_I \cdot \vec{B}_{el} \qquad\qquad 3.12$$

Using central field approximation, the interaction of magnetic moment is with an isolated J electronic level. Thus one can call this coupling as IJ coupling approximation, similar to LS coupling. Therefore I and J are good quantum numbers with corresponding matrix element which are diagonal in I and J. Using this approximation B_{el} is proportional to J and taking $B_{el} = B_J$, the interaction Hamiltonian becomes

$$\widehat{H}_\mu \propto -\vec{I} \cdot \vec{J} \qquad\qquad 3.13$$

or

$$\widehat{H}_\mu = A \vec{I} \cdot \vec{J} \qquad\qquad 3.14$$

where 'A' is the magnetic hyperfine interaction constant and is the product of nuclear and electronic quantities.
The interaction energy can be obtained using the matrix elements of the operator $\widehat{H}_\mu$

$$E_\mu = \left\langle \psi(r,\theta,\phi) \middle| \widehat{H}_\mu \middle| \psi(r,\theta,\phi) \right\rangle \qquad\qquad 3.15$$

or

$$E_\mu = \left\langle \psi(r,\theta,\phi) \middle| A \, I \cdot J \middle| \psi(r,\theta,\phi) \right\rangle \qquad\qquad 3.16$$

This interaction energy which leads to hyperfine splitting is extremely small. The contribution to B_J is zero for closed subshells since the magnetic effects are cancelled due to pairing of electrons. Magnetic effect is largest for those electrons which approach the

nucleus more closely, therefore the value of magnetic hyperfine interaction constant A would be greatest for levels belonging to configurations containing half-filled s subshell.

For a given atomic level characterized by resultant electronic angular momentum quantum number **J** coupling with nuclear angular momentum quantum number **I** gives the total angular momentum quantum number **F** of the atom i.e.,

$$\vec{F} = \vec{I} + \vec{J} \qquad\qquad 3.17$$

$$F^2 = I^2 + J^2 + 2\vec{I}.\vec{J} \qquad\qquad 3.18$$

$$\vec{I}.\vec{J} = \frac{F^2 - I^2 - J^2}{2} \qquad\qquad 3.19$$

Substituting this product in equation 3.16 we get expression for the hyperfine structure energies of all F levels of a hyperfine structure multiplet with respect to the atomic fine structure level J, viz.,

$$E_\mu = \frac{A}{2}\left[F(F+1) - I(I+1) - J(J+1)\right] \qquad\qquad 3.20$$

$$E_\mu = \frac{AC}{2} \qquad\qquad 3.21$$

where

$$C = F(F+1) - I(I+1) - J(J+1) \qquad\qquad 3.22$$

The relative spacing of hyperfine levels obeys Landé interval rule which states that "the energy spacing between successive hyperfine levels F – 1 and F is proportional to F" i.e.,

$$\Delta E_\mu(F, F-1) = E_\mu(F) - E_\mu(F-1)$$

$$\Delta E_\mu(F, F-1) = \frac{A}{2}\left[F(F+1) - (F-1)F\right] = A(J)F \qquad\qquad 3.23$$

the center of gravity of the hyperfine structure levels lies at the position of un-split level J.

where

$$A(J) = \frac{\mu_I < \vec{B} >}{IJ}$$

$$A(J) = \frac{g_I \mu_B < \vec{B} >}{1836\, J} \qquad\qquad 3.24$$

Characteristics of Hyperfine Structure Multiplet for Magnetic Dipole Interactions:

- The possible values of F levels are | I - J |, | I - J | + 1, ... I + J.
- Due to magnetic and electric interaction between the nucleus and orbital electrons, the fine-structure level splits into hyperfine-structure multiplet. The number of hyperfine-structure levels of a given J depends on the number of possible orientations of angular momentum vectors **I** and **J**, i.e. fine level splits into 2I + 1 if J ≥ I or 2J + 1 if I ≥ J hyperfine-structure levels.
- The total width of splitting between level J+I and | J - I | is
$$\Delta W = AI(2J + 1) \text{ for } J > I$$
and it is $\quad \Delta W = AJ(2I + 1) \text{ for } J < I$
Hyperfine structure splitting is in the range 10^{-3} to 1 cm^{-1} and is smaller than fine structure splitting due to stronger interaction between **S** and **L** as compared to interaction with **I**.
- The total width of splitting is largest for an unpaired 's' electron.
- The electric dipole selection rule for F is $\Delta F = 0, \pm 1$
- The transition form F = 0 to F = 0 is forbidden.
- The separation between two adjacent hf levels is proportional to the larger F value of the two levels.
- As for fine structure multiplets for hyperfine structure when A > 0 the hyperfine level having smallest possible value of F has the lowest energy value, and known as normal hyperfine multiplet. When A < 0 then the level having largest possible value of F has the lowest energy value. Such hyperfine multiplet is known as inverted multiplet. Physically it can be explained in the following manner: If the spinning electron and nucleus are considered as small magnets which influence each other at a certain distance, then the most stable position would be one for which their magnetic moments are in opposite directions and the mechanical moments are in the same direction. This leads to normal hfs splitting of fine level such that smallest F lies deepest. In the reverse case the highest F value lies deepest i.e. inverted hfs levels.

3.5 Electric Quadrupole Interaction

The quadrupole moment Q of a nucleus is a measure of the departure of the mean distribution of the nuclear charge from spherical symmetry. The existence of a non-zero electric quadrupole moment implies that the charge distribution of the nuclear state is no longer spherical and the nucleus is said to be deformed.

The simplest distributions of charges in the nucleus give only lowest order electric multipole moment. A spherical charge distribution gives only an electric monopole moment which results in an electrostatic Coulomb interaction between nucleus considered as a point charge ($r_n \ll r_e$) and electrons. This is given by

$$H = \frac{-e^2}{4\pi\varepsilon_o |r_e - r_n|} \qquad\qquad 3.25$$

With departures from spherical symmetry higher order electric multipole moments need to be considered. In order to calculate higher order electric moments expanding the factor $(r_e - r_n)^{-1}$ in powers of r_n / r_e and in Legendre polynomials $P_k (\cos \theta_{en})$ where θ_{en} is the angle between r_e and r_n:

$$H = - \frac{e^2}{4\pi\varepsilon_o} \left[r_e^2 + r_n^2 - 2r_e r_n \cos \theta_{en} \right]^{-1/2}$$

$$H = - \frac{e^2}{4\pi\varepsilon_o} \sum_k \frac{r_n^k}{r_e^{k+1}} P_k (\cos \theta_{en})$$

Expanding the Legendre polynomials

$$H = - \frac{e^2}{4\pi\varepsilon_o r_e} - \frac{e^2 r_n}{4\pi\varepsilon_o r_e^2} P_1 (\cos \theta_{en}) - \frac{e^2 r_n^2}{4\pi\varepsilon_o r_e^3} P_2 (\cos \theta_{en}) \text{ ...} \qquad 3.26$$

The first term is the monopole interaction, second term is electric dipole interaction and third term is electric quadrupole interaction, etc., and higher order terms need not be considered as the series converges sufficiently rapidly. Applying spherical harmonic addition theorem i.e.,

$$P_k (\cos \theta_{en}) = \frac{4\pi}{2k+1} \sum_{q=-k} (-1)^q Y_k^{-q} (\theta_n, \phi_n) Y_k^q (\theta_e, \phi_e) \qquad 3.27$$

where the Y_k^q are spherical harmonics of rank k, projection q similar to l and m_l respectively. Therefore using equation 3.27 and standard form of spherical harmonics, equation 3.26 becomes

$$H = 1 \qquad + r \cos (\theta) \qquad + r^2 (3\cos^2 \theta - 1) \qquad 3.28$$
$$\quad \text{Monopole} \qquad \text{Dipole} \qquad \quad \text{Quadrupole}$$
$$\quad \text{Term} \qquad \quad \text{Term} \qquad \qquad \text{Term}$$

Nucleus has a definite spin **I** and direction of **I** establishes an axis of cylindrical symmetry. Only matrix elements diagonal in I are used and direction of **I** of is the principle axis for the quadrupole tensor. The nuclear electric quadrupole moment Q in terms of expectation value, in a state $|\mathbf{I},\mathbf{I}\rangle$ can be written as

$$Q = \langle \mathbf{I},\mathbf{I} | \sum_i r_{ni}^2 (3\cos^2 \theta_{ni} - 1) | \mathbf{I},\mathbf{I} \rangle \qquad 3.29$$

where sum is over the protons in the nucleus. According to symmetry property "no quantum system can have an electric dipole moment if its wave function has definite parity". Therefore second term in equation 3.28 is zero.

The average gradient of the electric field produced by the electrons at the nucleus is defined by

$$W_Q = \frac{1}{e}\left\langle J,J \left| \frac{\partial^2 V_e}{\partial z^2} \right| J,J \right\rangle \qquad 3.30$$

In terms of angular momentum operator, the Hamiltonian for the interaction between nuclear electric quadrupole moment and the gradient of the electric field produced by electron is written as

$$H_Q = eQ\left\langle \frac{\partial^2 V_e}{\partial z^2} \right\rangle \frac{\left[3(I.J)^2 + \frac{3}{2}I.J - I(I+1)J(J+1) \right]}{2I(2I-1)J(2J-1)} \qquad 3.31$$

The classical analogue of equation 3.31 is

$$W = \frac{1}{4}eQ\frac{\partial^2 V_e}{\partial z^2}\frac{1}{2}(3\cos^2\theta_{IJ} - 1) \qquad 3.32$$

where the angle θ_{IJ} is the angle between the directions of **I** and **J** which are the principle axes of the nuclear and electronic systems.

- If nuclear charge distribution is elongated along the direction of **I** i.e. prolate then Q is positive.
- If nuclear charge distribution is flattened i.e. oblate then Q is negative.
- The magnitude of Q is determined by $<r_n^2>$.
- The magnitude of $\frac{\partial^2 V_e}{\partial z^2}$ is determined by $<1/r_e^3>$ and is measured experimentally and is the product of

$$B = eQ\left\langle \frac{\partial^2 V_e}{\partial z^2} \right\rangle$$

  where B is 'electric quadrupole hyperfine interaction constant'.
- The unit of Q is 'barn' and is equal to 10^{-24} cm^2.

The quadrupole interaction causes a shift in hyperfine structure levels and do not produce splitting. The shift in energy is given by

$$\Delta E_Q = \left\langle \psi(I,J,F) \left| H_Q \right| \psi(I,J,F) \right\rangle$$

$$\Delta E_Q = \frac{B}{4}\frac{\frac{3}{2}C(C+1) - 2I(I+1)J(J+1)}{I(2I-1)J(2J-1)} \qquad 3.33$$

where

$$C = F(F + 1) - J(J + 1) - I(I + 1) \qquad 3.34$$

- For 's' terms electron charge distribution is spherically symmetric and it makes $\left\langle \dfrac{\partial^2 V_e}{\partial z^2} \right\rangle = 0$. Hence for 's' terms the electric hyperfine constant "B" is zero.
- The electric hyperfine constant is zero for $I < 1$ and for $J < 1$.
- B is zero for atoms having even number of protons and even number of neutrons.

Combining magnetic hyperfine interaction which causes splitting and electric quadrupole interaction producing shifts in energy, then from equations 3.20 and 3.33

$$\Delta E = \frac{C}{2} A + \frac{B}{4} \frac{\frac{3}{2} C(C + 1) - 2I(I + 1)J(J + 1)}{I(2I - 1)J(2J - 1)} \qquad 3.35$$

From the above equation it is clear that the quadrupole interaction gives rise to a departure from the interval rule because of its dependence on F which is different from that of the magnetic dipole interaction. Also deviation from the interval rule is more prominent whenever the quadrupole constant B is comparable in magnitude with the magnetic constant A.

The interaction of the total electronic magnetic moment μ_J and of the nuclear magnetic moment μ_I with a steady magnetic field along the z-axis produces Zeeman Effect of hyperfine structure and removes $(2I + 1)(2J + 1)$-fold degeneracy of the hyperfine structure energy levels.

3.6 Tensor Operator Formalism of Hyperfine Structure

Electromagnetic interaction between atomic nucleus and orbiting and spinning electron is expressed in terms of tensor operator and therefore hyperfine interaction Hamiltonian for single particle becomes

$$h_{hfs}(r_i) = \sum_k T^k(N) . t^k(e)$$

$$h_{hfs}(r_i) = \sum_{kq} (-1)^i T_q^k(N) t_{-q}^k(e) \qquad 3.36$$

where $T^k(N)$ is an irreducible tensor operator of rank k acting on nuclear coordinates and spin and $t^k(e)$ is an irreducible tensor operator of rank k acting on electron coordinates and spin. Here, $k = 1$ for the magnetic dipole interaction and $k = 2$ for the electric-quadrupole interaction. For a collection of N electrons

$$H_{hfs} = \sum_{i=1}^{N} h_{hfs}(r_i) = \sum_q (-1)^q T_q^k(N) T_{-q}^k(e) \qquad 3.37$$

Using the Wigner-Eckart theorem, the matrix elements for the hyperfine interaction operator H_{hfs}

$$E_{hfs} = \langle JIF | H_{hfs} | JIF \rangle \qquad 3.38$$

$$E_{hfs} = \sum_k (-1)^{I+J+F} \begin{Bmatrix} I & J & F \\ J & I & k \end{Bmatrix} \langle J \| T^k(e) \| J \rangle \langle I \| T^k(N) \| I \rangle \qquad 3.39$$

9j symbol can be written as

$$(-1)^{I+J+F} \begin{Bmatrix} I & J & F \\ J & I & k \end{Bmatrix}$$

$$= \frac{(2I)!(2J)!}{\sqrt{(2I-k)!(2I+k+1)!(2J-k)!(2J+k+1)!}} M(IJ,Fk) \qquad 3.40$$

where

$$M(IJ,Fk) = \begin{cases} \dfrac{C}{2IJ} & \text{for } k = 1 \\ \dfrac{6C(C+1) - 8J(J+1)I(I+1)}{2I(2I-1)\,2J(2J-1)} & \text{for } k = 2 \end{cases}$$

$$C = F(F+1) - I(I+1) - J(J+1)$$

Defining the product of the matrix elements of electromagnetic interaction operators between electrons and spins and between nucleus and spin, viz.,

$$A_k(J) = \langle JJ | T^k(e) | JJ \rangle \langle II | T^k(N) | II \rangle \qquad 3.41$$

or

$$A_k(J) = \begin{pmatrix} J & k & J \\ -J & 0 & J \end{pmatrix} \begin{pmatrix} I & k & I \\ -I & 0 & I \end{pmatrix} \langle J | T^k(e) | J \rangle \langle I | T^k(N) | I \rangle \qquad 3.42$$

Substituting in equation 3.39 the splitting in energy due to hyperfine interaction becomes

$$E_{hfs} = (-1)^{I+J+F} \sum_k \begin{Bmatrix} I & J & F \\ J & I & k \end{Bmatrix} \cdot \begin{pmatrix} J & k & J \\ -J & 0 & J \end{pmatrix}^{-1} \cdot \begin{pmatrix} I & k & I \\ -I & 0 & I \end{pmatrix}^{-1} \cdot A_k(J) \quad 3.43$$

constants $A_1(J)$ and $A_2(J)$ are related to hyperfine constants $A(J)$ and $B(J)$ through the following relationships

$$A_1(J) = h \cdot J \cdot I \cdot A(J) \qquad 3.44$$

$$A_2(J) = \frac{1}{4} \cdot h \cdot B(J) \qquad\qquad 3.45$$

using the definition of 3j- and 6j-symbols [96], the equation obtained for energy splitting due to hyperfine interactions is same as obtained in equation 3.35, i.e.,

$$\Delta E = \frac{C}{2} h A(J) + \frac{\frac{3}{4} C(C+1) - 2I(I+1)J(J+1)}{2I(2I-1)J(2J-1)} h B(J) \qquad\qquad 3.46$$

3.7 Experimental Determination of Hyperfine Constants

The hyperfine interaction energy has two contributions, (i) magnetic moment of the nucleus interacting with the magnetic field produced by the spinning and orbiting electrons, (ii) electrostatic interaction of electrons with asymmetric charge distribution inside the nucleus. Equation 3.46 can be written as

$$\Delta E = \alpha \cdot h \cdot A(J) + \beta \cdot h \cdot B(J) \qquad\qquad 3.47$$

where α and β are Casimir Factors and are function of total orbital angular momentum of electrons J and total angular momentum F of atom with spin I, viz.

$$\alpha = \frac{1}{2} [F(F+1) - I(I+1) - J(J+1)] = \frac{C}{2} \qquad\qquad 3.48$$

and

$$\beta = \frac{\frac{3}{4} C(C+1) - I(I+1)J(J+1)}{2I \, J(2I-1)(2J-1)} \qquad\qquad 3.49$$

The electric dipole transition between two different fine structure levels having hyperfine splitting ΔE follows selection rules $\Delta J = 0, \pm 1$ and $\Delta F = 0, \pm 1$. As photon carries angular momentum therefore transition between two hyperfine levels each having $F = 0$ is forbidden. For electric dipole transitions parities of the combining fine structure levels must be different. The parities of both levels should be different. Each allowed transition represents a component of the hyperfine structure pattern of a spectral line with component positions given by

$$\nu = \nu_c + \alpha_o(F_o, J_o, I) A_o + \beta_o(F_o, J_o, I) B_o - \alpha_u(F_u, J_u, I) A_u - \beta_u(F_u, J_u, I) B_u \quad 3.50$$

ν_c is the energy difference between fine structure levels and experimentally it is the excitation energy for the combining lower and upper fine structure levels. The upper level is labelled by the letter 'o' (German word 'oben', means upper) and lower level is labelled by the letter 'u' (German word 'unten', means lower). Apart from ν_c, equation

3.50 contains Ao, Bo, Au and Bu as unknown quantities. Thus, for experimental determination of hyperfine constants from a given spectrum, it is necessary to identify the quantum numbers of at least 5 hyperfine components and to measure their (absolute or relative) positions. If one can identify more than 5 components, a least square method has to be used.

3.8 Line Strengths

For a dipole transition the connecting atomic states with total electronic orbital angular momentum J_o and J_u and with nuclear spin I, the line strength $S(F_o \rightarrow F_u)$ of the hyperfine components connecting F_o and F_u is given by the expression

$$S(F_o \rightarrow F_u) = \frac{(2F_o + 1)(2F_u + 1)}{2I + 1} \begin{Bmatrix} J_o & F_o & I \\ F_u & J_u & 1 \end{Bmatrix}^2 \qquad 3.51$$

Above equation is applicable in cases where interactions between neighboring levels are weak, so that J_o and J_u are good quantum numbers. The strongest components of hyperfine structure multiplet are those for which F and J change in the same direction and are called **diagonal lines or components**, i.e.

$$\Delta F = \Delta J \qquad 3.52$$

and the line strength of diagonal lines increases with increasing **F**. The other weaker lines are called **off-diagonal lines**. Physical interpretation of equality 3.52 is that since the nuclear spin is so weakly coupled to the electronic system that it does not affect the total radiation of the atom with a given **J**. But by forcing **J** into a certain orientation with regard to **F** it affects the statistical weight of the level and causes a certain distribution of radiation over the hyperfine structure components.

3.9 Intensity Rule or Sum Rule for Hyperfine Components

The hyperfine structure term with a given F has a statistical weight (2F + 1). In hyperfine multiplets, this statistical weight is important for the determination of intensity ratios between hyperfine structure components. The relative intensities within a hyperfine multiplet is found to obey the intensity or sum rule discovered empirically by Ornstein, Burger and Dorgelo [97]. It can be stated as
"within a hyperfine multiplet, the ratio of the sums of the intensities of all transitions from two states with quantum numbers F and F' are in the ratio of their statistical weights (2F + 1) : (2F' + 1)"

3.10 Anomalous Intensity of Hyperfine Components

The regular structures of series and multiplets are explained by theoretical approximations in terms of certain interactions expressed for every level by a definite set of quantum numbers. These approximations may break down completely or partially

when two energy levels happen to be very close together and irregularities appear as perturbations. Two levels can perturb each other when following conditions are fulfilled [80]:

- The levels have the same parity
- They have the same value of F
- Their values of J differ by 0 or ±1.

The perturbation appears as a mutual "repulsion" of the energy levels and in changes of the transition probabilities. Transitions with $\Delta J = \pm 2$ may also occur. It is also observed that for very light atoms or for complex or highly excited configurations where levels lie very close to each other or in cases where hyperfine interactions are large, the hyperfine splitting is comparable to fine structure separation. This leads to appreciable mixing of basis states with different J value and so that J is not a good quantum number. In situations like these the interactions among various basis states of given F belonging to different levels produce distortion in hfs pattern. In order to account for such distortions the approximate Hamiltonian (equation 3.8) must be replaced by a more exact form involving individual r_i, l_i and s_i to compute off-diagonal as well as diagonal matrix elements for each value of F.

Chapter 4
Laser Spectroscopy

4.1 Introduction

The invention of Lasers brought unprecedented progress in all fields of science and technology in general and especially in Spectroscopy. Lasers are intense coherent light sources with spectral energy density several orders of magnitude higher than conventional incoherent light sources. Furthermore, better resolution can be obtained using single mode laser due to their extremely narrow bandwidth as compared to conventional spectrometers. Combined, these two most obvious attributes, i.e. high intensity and sufficiently high resolution, paved the way for the investigation of structure of atoms and molecules in much more detail.

Lasers as coherent and monochromatic light sources for excitation, have the following characteristic properties which show their superiority and preference over conventional light sources:

- High spectral power density, which significantly improve the signal-to-noise ratio, furthermore nonlinear spectroscopic techniques can be explored.
- The small divergence of the collimated laser beams provides long path lengths through the absorbing sample.
- Small spectral linewidth of lasers is particularly suited for high resolution spectroscopy. In laser spectroscopy usually the spectral linewidth of the absorbing or emitting atoms or molecules determines the resolution of the spectroscopic technique.
- In addition to being an intense light source, the ability of continuous tunability over wide range of frequencies has made lasers an alternative to conventional intense light sources and ultrahigh resolution spectrometers.

Laser basically consists of three components (a) active medium, where population inversion takes place, (b) energy pump (for example flash lamp or electrical discharges) that generates population inversion, (c) optical resonator which stores the light emitted by active medium in few modes of the radiation field.

Different frequencies at which the laser resonator oscillates are determined by two factors:

- the gain profile of the amplifying medium
- eigenfrequency spectrum of the resonator

Without any wavelength selective elements inside the laser cavity, laser oscillation on all resonator modes are possible with wavelengths within the gain profile above threshold because for all modes gain exceeds the total losses. This is true for resonators which has completely inhomogeneous gain profile such that no gain competition occurs between different modes. On the basis of the width of the gain profile lasers can be classified as:

(i) *Fixed wavelength or fixed frequency lasers* where laser wavelength is restricted to a narrow gain region such as in gas lasers, for example He-Ne lasers, or in solid-state lasers, for example Nd:YAG lasers.

(ii) *Multiline fixed wavelength lasers*. In this case the active medium shows gain on several transitions and the laser can oscillate simultaneously on many lines. In this case also the wavelength of each line is restricted to its narrow gain range. For example Argon-ion laser or Krypton-ion laser with multiline operation.

(iii) *Tunable lasers*. Here the gain profile extends over a broad spectral range of laser wavelength that can be tuned continuously over a wide range. For example dye-lasers, where stimulated emission from the excited state to many vibronic levels of the electronic ground state is possible.

The difference between fixed wavelength lasers and tunable lasers lies in the width of the tuning range which is narrow for the "fixed wavelength" lasers and broader for the so called "tunable" lasers.

4.2 A Typical Energy Level Diagram of a Dye Molecule

In the visible part of electromagnetic spectrum dye lasers are by far most widely used excitation sources for doing laser spectroscopy. The main advantage is their continuous tunability over a wide range of frequencies.

Active media in dye lasers are organic dye molecules dissolved in liquid solvents and, upon irradiation by visible or UV light, show a strong broad-band fluorescence spectra. Figure 4.1 is an energy level scheme of an organic dye molecule showing rovibronic singlet (S) and triplet (T) states.

Dye molecules are pumped from rovibronic levels of the ground singlet state S_0 to higher rovibronic levels of excited singlet state S_1. Collisions with the solvent molecules induce a fast radiationless transition to the lowest rovibronic level of S_1 state with relaxation times of 10^{-11} to 10^{-12} s. This level is depopulated either by spontaneous emission into different rovibronic levels of ground state S_0 or by radiationless transition into the lower triplet state T_1. Transition to ground state S_0 determines the laser frequency. Due to strong interaction of dye molecules with the solvent the fluorescence spectra of dye molecules is continuous rather than discrete, in essence this gives a continuous tunability over wide range of frequencies.

High pump intensity ensures a population inversion between the rovibronic level v_0 of S_1 and higher rovibronic levels v_k of S_0 which have negligible population at room temperature, due to its small Boltzmann factor $\exp[-E(v_k) / kT]$. As soon as the gain on the transition $v_0(S_1) \rightarrow v_k(S_0)$ exceeds the total losses, laser oscillation starts. The lower level $v_k(S_0)$ which now is populated by stimulated emission, is depleted rapidly by collisions with the solvent molecules to the lowest vibrational level v_o of the ground singlet state S_0.

The population inversion between S_0 and S_1 is strongly affected by transitions from S_1 into the long-living triplet state T_1. Furthermore, transitions from lower triplet state T_1 into higher triplet states can also take place. To minimize these effects, molecules with populated state T_1 should be removed from the laser active zone in a time scale much shorter than the life-time of T_1. One way of doing this is by forming a flat stream of dye solution (dye jet) in a nozzle and inserting this free jet in the cavity, where the path inside the cavity and the focused pump beam overlap. At high enough pressure, the time of flight of the dye through the active region satisfies the condition above.
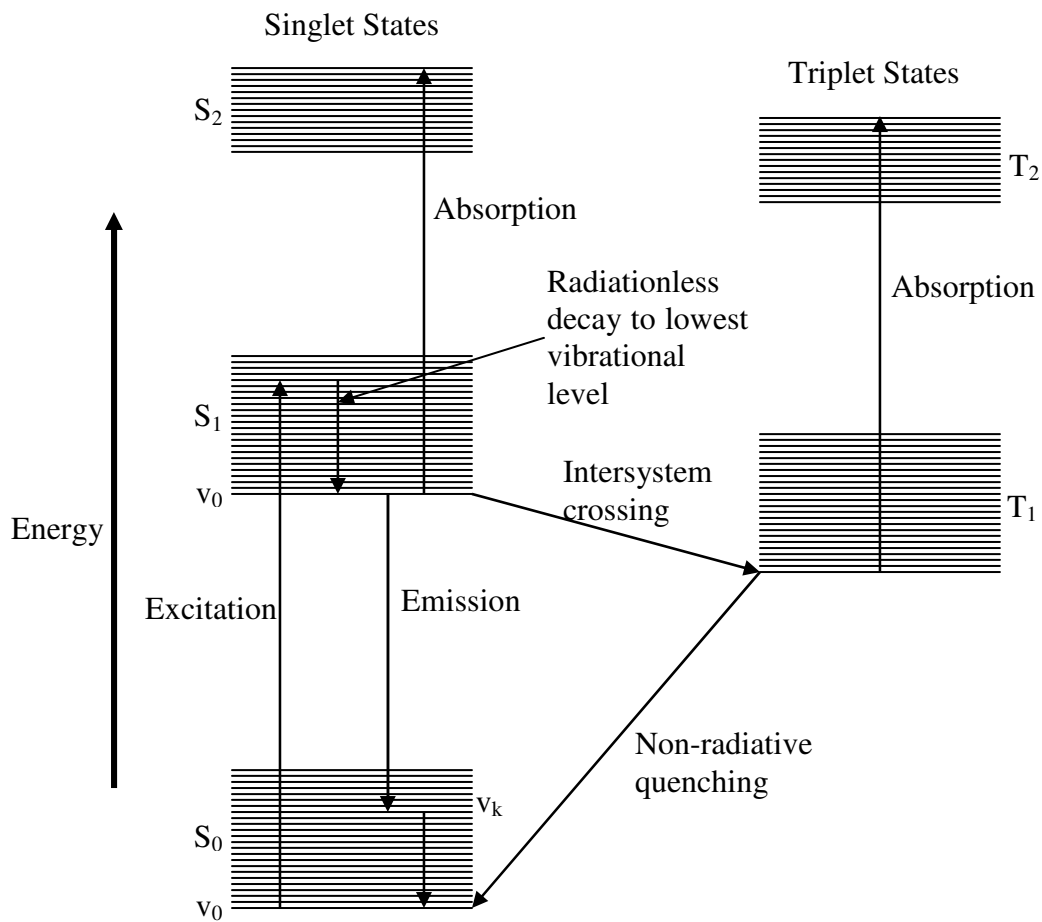
Figure 4.1: Energy level diagram of an organic dye molecule

4.3 Ring Dye Laser

Active medium in a ring-dye laser system (see figure 2) is a thin liquid jet of the dye solution oriented at Brewster angle for avoiding reflection losses. A pump beam which is focused by a spherical mirror onto the dye jet excites the dye molecules in the jet. Four mirrors M1, M2, M3 and M4 are used which closes the laser beam path on to itself forming a ring resonator arrangement with a running laser wave only in one direction. Transmissivity of M4, which is the output coupler, depends on the dye being used. In contrast in a linear dye laser system a standing wave is established in the cavity. The advantage of ring-cavity scheme over linear scheme is that no nodes within the jet are present and whole inversion of the active medium can contribute to the laser amplification. Unidirectional propagation of laser wave is achieved by inducing more losses for one direction as compared to the other. This can be achieved by a unidirectional device known as optical diode. An optical diode consists of a Faraday glass in a longitudinal magnetic field and a Faraday polarization rotator, which turns the birefringent rotation back to the input polarization for the wave incident in one direction, but increases the rotation for the other direction. Waves with incorrect polarization direction suffers large losses at the many Brewster surfaces in the resonator cavity and therefore do not reach the threshold. Mirror M2 is mounted on a Piezo-Electric Transducer (PZT) also known as tweeter mirror and a Galvo or Brewster Plate is inserted in front of the output coupler M4 inside the laser cavity. Both these elements work in conjunction with each other for tuning the laser wavelength. To select one of the modes of laser cavity, a number of mode selection elements with different finesse and free spectral range (FSR) are inserted. These include birefringent filter and two Fabry-Perot etalons, i.e. a thick etalon and a thin etalon.

A Birefringent filter is a Lyot type filter consisting of more than one quartz plate each plate being four times the thickness of the previous one and inserted at Brewster angle in the cavity. The Birefringent filter has low finesse and an FSR of the order of THz.

Due to its low finesse the birefringent filter alone cannot select a single mode of the laser cavity. Therefore thin and thick Fabry-Perot etalons are also placed inside the cavity. Thin etalon is a glass plate of 0.5 mm thickness with a reflectivity of R ≈ 20 % and is inserted at close-to-normal incidence. Last of the mode selection elements is the thick etalon which is a 10 mm solid prism etalon and is divided into two parts. It is piezo driven and is also inserted at nearly normal incidence. Thick etalon also has a reflectivity of R ≈ 20 % and is most effective in selecting one mode of laser cavity. The FSR of both thin (200 GHz) and thick (15 GHz) etalons is in GHz.

Proper alignment of etalons and laser cavity avoids any sudden jumps in laser frequency. This sudden jump in laser frequency is known as "mode hopping". In addition to miss-aligned etalons and laser cavity, mode hopping may also be due to thermal fluctuations, turbulence in the dye jet, presence of microbubbles in the dye jet etc. In order to avoid mode hopping and to perform frequency stabilization, thick etalon and laser cavity each need an electronic feedback loop. This feedback signal or the "error signal" is generated by a temperature stabilized confocal external reference cavity. With the help of a beam

splitter mounted outside the laser cavity, a fraction of the linearly polarized laser beam is passing through the reference cavity and detected by a photodiode known as reference diode. Another fraction of the main laser beam is directly reflected to a second photodiode known as power diode which is used to detect the total power level. A side-locking technique is used in which laser wavelength is directly locked to one side of a transmission peak of the confocal reference cavity. Therefore the signal from reference photodiode acts as an error signal for the feedback loop. To avoid intensity fluctuations the signal from the reference photodiode is divided by the total power level using the signal from the power diode. The error signal generated is then divided into a low-frequncy and high-frequency parts. The high-frequency part is feedback to the tweeter mirror M2 whereas low-frequency part is used to drive the Galvo plate. Both these tuning elements allow changing the length of the cavity for stabilizing the frequency of laser.

130 mm
pump beam input

140 mm
dye laser beam output
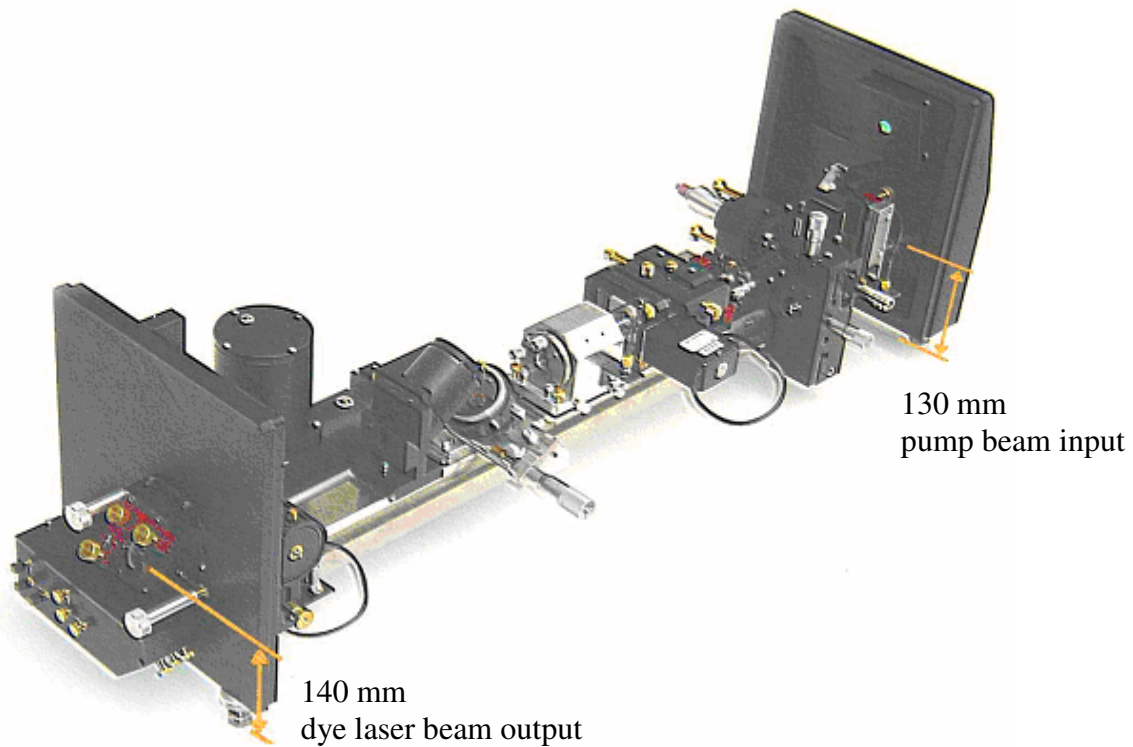
Figure 4.2: Ring Dye laser system
      Optical layout : Coherent Inc.
      Mechanical Layout: Institute of Experimental Physics, TU Graz

If transmission peaks of all these elements are tuned to same wavelength λ, the laser will oscillate at this wavelength as a single mode laser. Laser wavelength can be scanned continuously without mode hopping if all the elements are synchronously tuned using this electronic feedback control system.
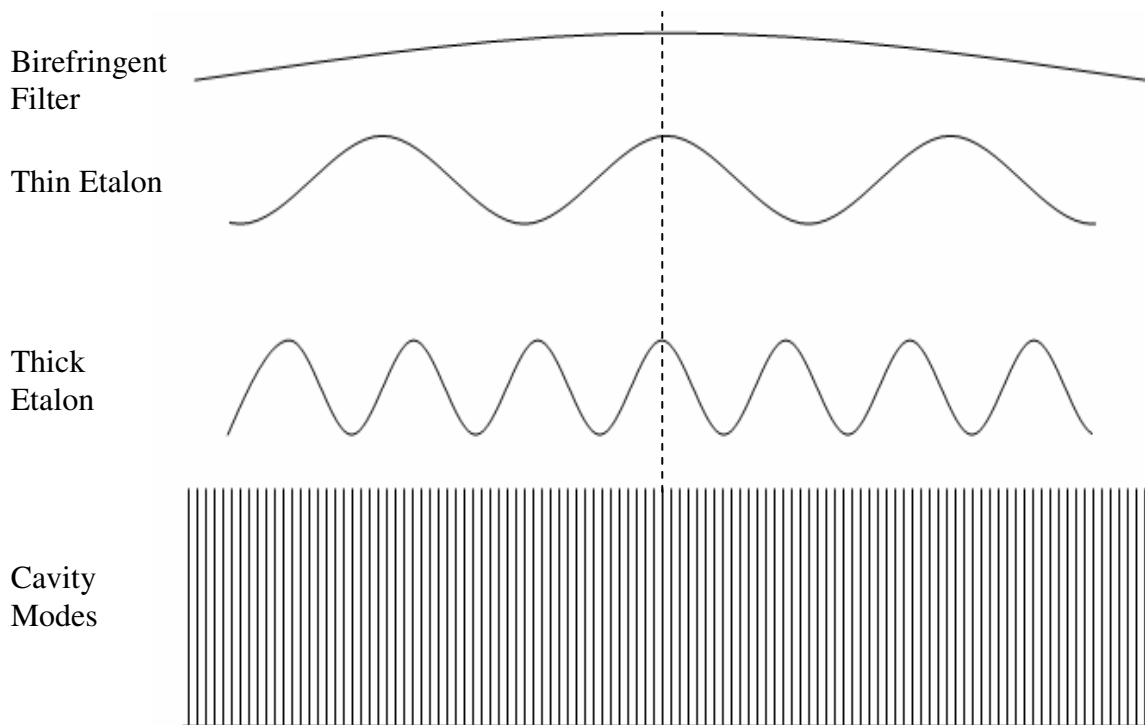
Figure 4.3: Transmission curves for Birefringent filter, thin etalon and thick etalon.

4.4 Line Profile and Line Broadening Mechanisms of Spectral Lines

In an atomic or molecular transition the spectral lines observed due to absorption or emission of radiation are never strictly monochromatic. Even with interferometers with high resolving power one observes a spectral distribution $I(v)$ of the absorbed or emitted intensity around the center frequency $v_o = (E_i - E_f) / h$ corresponding to a transition between upper and lower levels. The spectral distribution function $I(v)$ of absorbed or emitted radiation in the vicinity of v_o is called the **line profile** as shown in figure 4.5.
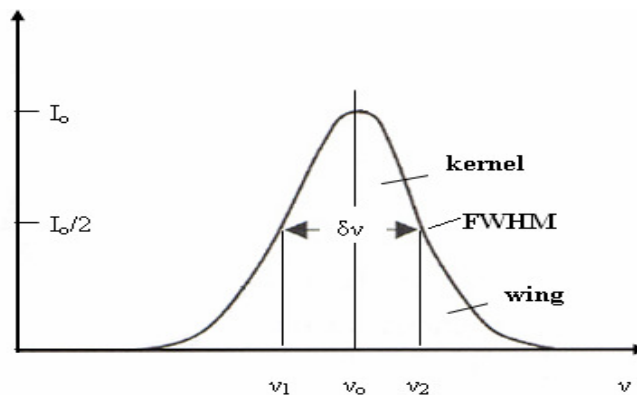
Figure 4.5: Line profile, halfwidth, kernel and wings of spectral line.

The frequency interval $\delta\nu = |\nu_2 - \nu_1|$ between the two frequencies ν_1 and ν_2 for which $I(\nu_1) = I(\nu_2) = I(\nu_o)/2$ is the **full width at half maximum** of the line abbreviated as FWHM or in short **linewidth** or **halfwidth** of the spectral line. The line profile or broadening of spectral line not only depends on the spectral resolution of the measuring instrument but also on certain basic physical properties such as finite life time of the atomic states involved in the transition, velocity distribution of the moving atoms and pressure of the gaseous ensemble. These broadening mechanisms are respectively called natural, Doppler, and collision or pressure broadenings. Broadening mechanisms can also be classified as homogenous and inhomogeneous broadening mechanisms. If the probability of absorption or emission of radiations with frequency ν for a certain transition is equal for all atoms in a gaseous ensemble, then the spectral line profile is homogenously broadened. Natural broadening and pressure broadenings are examples of homogeneous broadening. If the probability of absorption or emission of radiations is not the same for all atoms, then the spectral line is said to be inhomogeneously broadened. Doppler broadening is an example of inhomogeneous broadening, in which different atoms contribute to different parts of the line profile. In the following discussion angular frequency $\boldsymbol{\omega = 2\pi\nu}$ is used in order to avoid factors of 2π in equations.

4.4.1 Natural Linewidth

Heisenberg's uncertainty principle in the form $\Delta E \, \Delta t > \hbar / 2$ requires that the spectral line cannot be arbitrarily sharp. Because if the spectral line is arbitrarily sharp then from uncertainty principle it would mean perfect knowledge of E which is not possible unless an atom spend infinite amount of time in a state before decaying into a lower state. Instead the lifetime is finite say τ_{decay}, then approximately the linewidth is $\Delta E \sim \hbar / \tau_{decay}$. This type of broadening which is due to the finite lifetime of one or both levels involved in a transition is called *natural broadening*, and represents the limit on how sharp a spectral line can be. Natural broadening belongs to the homogenous class of broadenings. The population N_i of excited state $|i\rangle$ at any time is given by

$$N_i(t) = N_i(0)\,e^{-t/\tau_i} \qquad\qquad 4.1$$

where τ_i is the mean natural life time of the state and it depends on the total spontaneous transition probability to all levels with $E_j < E_i$. The life time τ_i in the state $|i\rangle$ is given by

$$\tau_i = \sum_j \frac{1}{A_{ij}} \qquad\qquad 4.2$$

where A_{ij} is spontaneous transition probability from state with energy E_i to state with energy E_j. Using uncertainty principle the uncertainty or spread in energy ΔE is given by

$$\Delta E \approx \frac{\hbar}{\Delta t} = \frac{\hbar}{\tau_i} \qquad\qquad 4.3$$

where Δt is the uncertainty in time associated with finding the atom in that particular state and is given by mean life time τ_i of the state. The frequency $\omega_{ij} = (E_i - E_j) / \hbar$ of a transition terminating in the stable ground state with energy E_j has therefore corresponding uncertainty or frequency spread, which is given by

$$\Delta\omega_i = \frac{\Delta E}{\hbar} = \frac{1}{\tau_i} \qquad 4.4$$

If the lower state E_j is not the ground state but also an excited state with a life time τ_j, the uncertainties ΔE_i and ΔE_j of the two levels both contribute to the linewidth. This yield the total uncertainty

$$\Delta E = \Delta E_i + \Delta E_j \qquad 4.5$$

$$\Delta\omega = \left(\frac{1}{\tau_i} + \frac{1}{\tau_j} \right) \qquad 4.6$$

The normalized line profile of the intensity of a transition is a Lorentzian profile and is determined by the equation

$$g(\omega - \omega_o) = \frac{\frac{1}{2\pi}\gamma}{(\omega - \omega_o)^2 + \left(\frac{\gamma}{2} \right)^2} \qquad 4.7$$

where γ is the damping or decay constant characterizing the radiative energy loss. The intensity reduces to half of its peak value at

$$\delta\omega = \omega - \omega_o = \pm\frac{\gamma}{2} \qquad 4.8$$

The full width at half (FWHM) i.e. $2\delta\omega$ which is the "natural linewidth" $\delta\omega_n$ is given by:

$$\delta\omega_n = \gamma$$

or

$$\delta\nu_n = \frac{\gamma}{2\pi} \qquad 4.9$$

The mean lifetime of an atomic state E_i which decays exponentially by spontaneous emission is related to Einstein Coefficient A_i by $\tau_i = 1/A_i$. If classical damping constant γ is replaced by spontaneous transition probability A_i for a transition from excited state E_i to ground state then halfwidth of the spectral line is given by

$$\delta\omega_n = A_i$$

or

$$\delta\nu_n = \frac{A_i}{2\pi} = \frac{1}{2\pi\tau_i} \qquad\qquad 4.10$$

Above equations can also be derived from Heisenberg's uncertainty relationship. In general the decay from excited state is not only by spontaneous emission but also by nonradiative relaxation. Therefore the line profile function is determined by total decay constants γ_i and γ_j, so the normalized line profile function is given by

$$g(\omega - \omega_{ij}) = \frac{\frac{1}{2\pi}(\gamma_i + \gamma_j)}{(\omega - \omega_{ij})^2 + [(\gamma_i + \gamma_j)/2]^2} \qquad\qquad 4.11$$

where both γ_i and γ_j are the sum ($\gamma = \gamma_R + \gamma_{NR}$) of radiative and nonradiative contributions.

Life times of higher lying excited states are in general longer than lower lying states. Ground state has infinitely long life time and metastable states have life times of the order of 10^{-3} sec, therefore for these states the frequency spread is negligible. The life time of excited states is of the order 10^{-6} to 10^{-9} sec. Hence a transition from such state to the ground state will have a line width of 0.1 to 100 MHz. A similar situation exists in absorption; the absorption line is broadened due to finite life time of the excited state. The line width is small in infrared and micro wave regions ($A_{ij} \propto \nu^3$).

4.4.2 Doppler Broadening

In gases at low pressure the dominant contribution to the spectral linewidth is the Doppler width which is due to the thermal motion of the absorbing or emitting atoms. Generally the Lorentzian line shape which is due to natural linewidth is completely masked by *Doppler broadening effect*. Doppler broadening is an example of inhomogeneous broadening, in which different atoms contribute to different parts of the line profile. Due to Doppler Effect the emitted or absorbed radiation by a single atom appears to be shifted relative to the central frequency of transition. Nevertheless, for an ensemble the Doppler profile becomes symmetric, since all directions and velocities are appearing.

Consider an atom in an excited state moving with velocity $\vec{v} = \{v_x, v_y, v_z\}$ relative to the rest frame of an observer. For the observer at rest the central frequency ω_o of the emitted radiation with the propagation wave vector **k** in the direction of the observer appears to be Doppler shifted and is given by

$$\omega_e = \omega_o + \vec{k} \cdot \vec{v} \qquad\qquad 4.12$$

$$\text{with } \left|\vec{k}\right| = \frac{2\pi}{\lambda}$$

The apparent frequency is increased if the atom while emitting is moving towards the stationary observer i.e. $\vec{k}.\vec{v} > 0$ and is decreased if the atom is moving away from the observer i.e. $\vec{k}.\vec{v} < 0$.

Similarly absorption frequency ω_a is also shifted for an atom moving with velocity v. If a plane wave with wave vector $\mathbf{k}$ and frequency ω interacts with a moving atom, then the frequency ω appears to be shifted in the moving frame of the atom. The shift in frequency is given by

$$\omega' = \omega - \vec{k}.\vec{v} \qquad\qquad 4.13$$

The moving atom can only absorb if ω' coincides with the eigenfrequency ω_o i.e. $\omega' = \omega_o$, then absorption frequency $\omega_a = \omega$, therefore equation 4.13 can be written as

$$\omega = \omega_o + \vec{k}.\vec{v} \qquad\qquad 4.14$$

If the atom moves parallel to the wave propagation then the absorption ω_a increases with $\vec{k}.\vec{v} > 0$ and it decreases if the atom moves opposite to the propagating wave with $\vec{k}.\vec{v} < 0$. If the incident wave moves along z-axis then the wave vector $\mathbf{k} = \{0,0,v_z\} \Rightarrow \mathbf{k}.\mathbf{v} = \mathbf{k}_z \mathbf{v}_z$ absorption frequency becomes

$$\omega_a = \omega_o + k_z v_z \qquad\qquad 4.15$$

Since $\omega_o = 2\pi\nu_o$ and $k = 2\pi / \lambda$, equation 4.15 becomes

$$\omega_a = \omega = \omega_o \left(1 + \frac{v_z}{c} \right) \qquad\qquad 4.16$$

At thermal equilibrium with temperature T the velocity of atoms follow Maxwell-Boltzmann statistics. The number density $n_i(v_z)\, dv_z$ of atoms in absorbing state $|i\rangle$ with velocity component v_z within the interval v_z to $v_z + dv_z$ is given by

$$n_i(v_z)dv_z = \frac{N_i}{v_p \sqrt{\pi}} e^{-\left(\frac{v_z}{v_p}\right)^2} dv_z \qquad\qquad 4.17$$

where $v_p = (2k_BT / m)^{1/2}$ is the most probable velocity of atoms and k_B is the Boltzmann constant. N_i is the total number of all atoms in state $|i\rangle$.

By using equation 4.16, v_z and dv_z can be expressed in terms of frequency ω and frequency shift $d\omega$ to obtain $v_z = (c/\omega_o) (\omega - \omega_o)$ and $dv_z = (c/\omega_o) d\omega$. Substituting these values in equation 4.17, the relationship for the number of atoms with absorption frequency shifted from ω_o in the interval ω and $\omega + d\omega$ is given by

$$n_i(\omega)\,d\omega = \frac{cN_i}{\omega_o v_p \sqrt{\pi}}\,e^{-\left(\frac{c(\omega-\omega_o)}{\omega_o v_p}\right)^2}\,d\omega \qquad\qquad 4.18$$

Since the spectral power density of absorbed or emitted line is proportional to n(ω) dω, the intensity profile of Doppler-broadened absorbed or emitted line becomes

$$P_\omega(\omega) = P_\omega(\omega_o)\,e^{-\left(\frac{c(\omega-\omega_o)}{\omega_o v_p}\right)^2} \qquad\qquad 4.19$$

This is a Gaussian function which is symmetric about the center frequency ω_o.
Now full half-width is written as

$$\delta\omega_D = |\omega_1 - \omega_2| \qquad\qquad 4.20$$

$$\text{with } P_\omega(\omega_1) = P_\omega(\omega_2) = \frac{1}{2}P_\omega(\omega_o)$$

Using equation 4.19 the half intensity point is given as

$$P_\omega(\omega) = \frac{1}{2}P_\omega(\omega_o) = P_\omega(\omega_o)e^{-\left(\frac{c(\omega-\omega_o)}{\omega_o v_p}\right)^2} \qquad\qquad 4.21$$

or
$$\sqrt{\ln 2} = \frac{c}{v_p}\left(\frac{(\omega-\omega_o)}{\omega_o}\right) \qquad\qquad 4.22$$

Substituting the value of the most probable velocity v_p

$$\sqrt{\ln 2} = \sqrt{\frac{mc^2}{2k_B T}}\left(\frac{(\omega-\omega_o)}{\omega_o}\right), \qquad\qquad 4.23$$

the Doppler width is given by

$$\delta\omega_D = 2(\omega-\omega_o) = \frac{\omega_o}{c}\sqrt{\frac{8k_B T \ln 2}{m}} \qquad\qquad 4.24$$

Using Avogadro number N_A, molar mass $M = N_A m$ and gas constant $R = N_A k_B$, the convenient form of above equation can be written as:

$$\delta\nu_D = 7.16 \times 10^{-7}\,\nu_o\sqrt{\frac{T}{M}}\quad \text{sec}^{-1} \qquad\qquad 4.25$$

where T is measured in K and M in g/mol.

- The Doppler width $\delta\nu_D$ increases proportionally with central frequency ν_o, i.e. Doppler width is larger in visible or ultraviolet regions as compared to IR region.
- The Doppler width increases with the square root of temperature, i.e. Doppler width is smaller at lower temperature. Therefore for example by cooling the hollow cathode discharge with liquid Nitrogen, the Doppler width, which is the dominating source of broadening, can be reduced in order to observe the hyperfine structure of a spectral line.
- Doppler width decreases with increasing atomic or molecular mass M as $M^{-1/2}$.

The Doppler width can be reduced by many orders of magnitude by using atomic and ion beam experiments, where a well collimated atomic or ionic beam interacts at right angle with the laser beam.

The Gaussian line profile of a Doppler Broadened line decreases exponentially with increasing distance $|\omega - \omega_o|$ from central frequency ω_o, whereas the Lorentzian line profile for natural line width only decreases quadratically i.e. $(\omega - \omega_o)^{-2}$. This suggests that it is possible to extract from the extreme line wings information on the natural line profile in spite of the much larger Doppler-width.

4.4.3 Collisional or Pressure Broadening

In addition to radiative relaxation processes, an atom in an excited state can also decay to a lower state by nonradiative processes such as collisions with other atoms. Collision of the atom in excited states with another atom results in a release of excitation energy to the colliding partner. This reduces the lifetime of the excited states resulting in the broadening of line. Since with increasing pressure the atoms under investigation undergo more frequent collisions, this type of broadening is also known as *pressure broadening*. Pressure broadening can be categorized as *Lorentzian Broadening* which occur due to collisions between different kinds of atoms and *Holtsmark Boradening* which is due to collisions between the same kinds of atoms. Both types of broadenings are treated together as pressure broadening. The collisional broadening is actually the result of inelastic collision between atoms. It is prominent in plasmas and gas discharges because of the long range Coulomb interaction between charged particles.

The collisional broadening produces a Lorentzian profile, the same as that of natural broadening. But it is of increased width. In order to avoid pressure broadening, the pressure in the spectral source should be kept low. By changing the pressure and observing the corresponding change in line width the information about the collisions occurring in the gas can also be obtained. The collisions which have large impact parameter cause noticeable line broadening but can also shift the line center.

4.4.4 Stark Broadening

The levels of atoms or molecules in the presence of electric field split into (2J + 1) stark components where J is the total angular momentum quantum number. This splitting of levels and corresponding splitting of spectral lines is called Stark effect named after J. Stark who first studied this effect in 1913 for hydrogen atom. In gas discharges due to

strong electrical fields experienced by atoms collisions with electrons and ions can also occur. This also contributes to total line broadening and is known as *Stark Broadening*.

4.4.5 Saturation Broadening

A laser of sufficiently high intensity operating at near resonant frequency can significantly change the population densities N_1 and N_2 of an atomic system by induced absorption and emission. This saturation of population densities also causes additional line broadening and is known as *Saturation Broadening*. Saturation broadening is also called *power broadening*. The spectral line profiles for saturation broadening are different for homogeneously and for inhomogenously broadened lines. For a homogeneously broadened spectral line the line profile is Lorentzian and for inhomogeneouly broadened spectral line the line shape is Gaussian.

4.4.6 Self-Absorption Broadening

Photons emitted in one region of a source may partly be absorbed when they pass other regions, of the source. These photons may be lost as a contribution to the original spectrum line either as a result of radiative decay to a different lower level or through collisional de-excitation of the absorbing atom. This process of re-absorption is known as self-absorption. Since the *absorption profile* is of the same shape as the *emission profile*, therefore energy is selectively absorbed from the emission line, i.e., the *absorption coefficient* is a maximum at the centre of the line or central wavelength. This means that the intensity of spectral line is reduced proportionately more in the center then elsewhere altering the line shape and making the line appear broader. This is termed as *self-absorption broadening*.

4.4.7 Combined Line Profile or Voigt Profile

In any experiment the different line broadening mechanisms contribute to the total line width of the emitted or absorbed spectral line. One can reduce a specific line width contribution by modifying experimental parameters, e.g. Doppler broadening can be reduced by cooling the ensemble of atoms by using liquid Nitrogen or water, pressure or collisional broadening is reduced by reducing pressure, by reducing the intensity of laser light saturation broadening can be minimized. Ultimately it comes down to natural line width which is limited by the finite lifetime of the energy state.

A spectral line profile $\mathbf{I(\omega)}$ can be obtained which include contributions from all the broadening mechanisms i.e.,

$$\mathbf{I(\omega) = I_N(\omega) * I_D(\omega) * I_P(\omega) * I_S(\omega)} \qquad 4.26$$

where

$\mathbf{I_N(\omega)} \equiv$ Natural line profile
$\mathbf{I_D(\omega)} \equiv$ Doppler line profile
$\mathbf{I_P(\omega)} \equiv$ Pressure or Collisional line profile
$\mathbf{I_S(\omega)} \equiv$ Saturation line profile

Natural and Collisional line broadening mechanisms have Lorentzian line shape, Doppler broadening has Gaussian Line shape, whereas Saturation broadening depending on homogeneous or inhomogeneous class give Lorentzian or Gaussian line shape. Therefore depending on line shape all the broadening mechanisms can be grouped into two classes i.e. Lorentzian and Gaussian types. So the combined line profile of a spectral line is a convolution of Lorentzian and Gaussian line profiles and is known as *Voigt Profile*, i.e.

$$\mathbf{I_V(\omega) = I_L(\omega) * I_G(\omega)} \qquad\qquad 4.27$$

where $\mathbf{I_L(\omega)}$ is the Lorentzian line profile due to broadening mechanisms which give Lorentzian line shape, $\mathbf{I_G(\omega)}$ is the Gaussian line profile due to broadening mechanisms which give Gaussian line shape and $\mathbf{I_V(\omega)}$ is the Voigt line profile.

In our investigations of hyperfine structure of atoms and ions we mainly observe Gaussian line profile and no saturation broadening is observed as excitation probability is less then what is needed for saturation effect. However, in cases where excitation probability is high, saturation effects leads to saturation broadening and we observe Voigt line profiles. In the investigation of hyperfine structure of Praseodymium using laser spectroscopy the observed Doppler width is around 800 MHz.

4.5 Laser Spectroscopy

Electromagnetic radiation interacting with matter is scattered, absorbed or even cause stimulated emission. This classify the subject of spectroscopy into three main branches, i.e. Emission Spectroscopy which is used to observe light emitted by atoms excited by radiation/matter interactions, Raman Spectroscopy measures light scattered from molecules and Absorption Spectroscopy studies radiation absorbed by atoms or molecules at different frequencies or wavelengths.

Classical absorption spectroscopy utilizes radiation sources with a broad emission continuum such Xe flash lamps. A collimated beam of light is passing through an absorption cell and by using a dispersing device the intensity $I_T(\lambda)$ of transmitted light is measured as a function of wavelength λ. By comparison with the intensity of reference beam $I_R(\lambda)$ the absorption spectrum can be obtained. Here the spectral resolution is limited by the resolving power of the dispersing device. The detection sensitivity defined as minimum detectable absorbed power is limited by the detector noise and fluctuations in radiation source.

In laser absorption spectroscopy the radiation sources with broad emission continuum are replaced by tunable lasers. Tunable lasers offer a wide spectral region extending from UV to IR with extremely narrow bandwidths and with power densities much greater than conventional incoherent light sources. Some of the advantages of using lasers as radiation sources are listed below:

(i)   The absorption coefficient $\alpha(\omega)$ and its frequency dependence can be measured directly from the difference $\Delta I(\omega) = aI_R(\omega) - I_T(\omega)$ ('a' represent reflection losses) between the intensities of the reference beam and transmitted beam. A monochromator is not required. With the use of tunable single-mode lasers the

spectral resolution is much higher than in conventional spectroscopy and is only limited by the line width of the absorbing transition.

(ii)   Due to high power density achievable with lasers, the detector noise is generally negligible. This increases signal-to-noise ratio and enhances sensitivity.

(iii) Because of low divergence long absorption paths are possible by multiple reflections back and forth through the absorption cell. Such long absorption paths facilitate the measurements of transitions with small absorption coefficients.

(iv)   By allowing a small fraction of main laser beam to pass through a Fabry-Perot interferometer with a separation d of the mirrors, a photodetector receives intensity peaks each time the laser frequency v_L is tuned to a transmission maximum of interferometer at $v = mc/2d$. These equal spaced intensity peaks serves as accurate wavelength markers which allow measurement of adjacent absorption lines. The separation between two adjacent transmission maxima or this wavelength interval is called free spectral range of interferometer (FSR).

(v)   The laser frequency may be stabilized onto the center of an absorption line. The need for frequency stabilization can be relaxed if the frequency jitter is small compared to absorption line width.

(vi)   It is possible to tune the laser frequency over the spectral region of interest. For example the transitions between hyperfine levels of two fine structure levels can be observed in a single scan of laser.

(vii) With high intensity and small laser line width appreciable population in selectively excited states can be achieved. This is advantageous for doing absorption and fluorescence spectroscopy of excited states.

With all the advantages mentioned above the achievable resolution is finally limited by finite line width of the absorption line. On one hand this maybe due to the natural line width of the atomic or molecular levels as energy levels have an energy uncertainty related to their finite life time and on the other hand it maybe due to the Doppler broadening of the absorption line which is caused by the thermal motion of atoms or molecules. Spectroscopic techniques in which Doppler broadening limits the achievable resolution are known as Doppler limited techniques. In these techniques primarily the level structures are determined with any regard to their finer details such as their hyperfine structure. Two photon absorption spectroscopy, optogalvanic spectroscopy, optical double resonance and level crossing spectroscopy are few examples of Doppler limited laser absorption spectroscopy.

In Doppler free high resolution spectroscopy extremely narrow band single mode lasers are utilized. The collimated atomic beam spectroscopy and saturation spectroscopy are the examples of the Doppler free absorption spectroscopy. The saturation spectroscopy is based on nonlinear spectroscopic techniques.

4.5.1 Two-Photon Spectroscopy

Two-photon excitation can be interpreted as two successive one-photon excitations. Excited levels with same parity can be reached via two-photon excitation. Two-photon excitation can be distinguished either as a step-wise excitation with intermediate real level where two photons are in resonance with the successive excitations, or it is a

simultaneous absorption of two photons with an intermediate virtual level, undergoing a transition from $E_i \rightarrow E_f$. Two photons may either come from a single laser beam passing through the absorbing sample or they may come from two separate lasers.

In an atom or molecule at rest, two photons with energy $\hbar\omega_1$ and $\hbar\omega_2$ either coming from two laser beams, or two photons with energy $\hbar\omega$ from the same laser, induce a transition from an initial level $\langle i |$ to the final level $\langle f |$, using conservation of energy; viz.

$$E_f - E_i = \hbar(\omega_1 + \omega_2) \qquad\qquad 4.28$$

For an atom or molecule moving with velocity v, the frequency ω of the light wave is shifted in the atomic or molecular frame to

$$\omega' = \omega - \vec{k}.\vec{v} \qquad\qquad 4.29$$

Therefore the resonance condition given in equation 1 becomes

$$E_f - E_i = \hbar(\omega_1 + \omega_2) - \hbar\vec{v}(\vec{k_1} + \vec{k_2}) \qquad\qquad 4.30$$

Now if the two photons come from the two beams of the same laser but traveling in opposite direction, i.e. $\omega_1 = \omega_2$ and $\vec{k_1} = -\vec{k_2}$ then as a consequence the last term in equation 4.30 vanishes. This implies that the absorption of two photons becomes independent of the velocity of atoms or molecules. This means that all atoms or molecules independent of their velocity group contribute to the two photon absorption, making two-photon absorption Doppler-free. Experimentally the two-photon absorption is monitored by laser-induced fluorescence emitted from the upper level E_f by an allowed one-photon dipole transition into a lower level E_m.

As the laser frequency ω is tuned over the two-photon resonance, the resulting signal consists of a narrow peak produced by two photons with opposite $\vec{k}$ vectors and a Doppler-broadened background produced by two photons coming from the same beam with parallel $\vec{k}$ vectors.

The main characteristics of two photon spectroscopy:
- Optical transitions which are parity forbidden by a single photon excitation can be excited via a two photon transitions.
- The final state may have an excitation energy in the far UV, while the incident light beam has a frequency in the near UV or visible region,
- By proper combination of participating photons, it is possible to eliminate momentum transfer between electromagnetic fields and atoms or molecules, this allows one to get Doppler free spectrum. However the cross section of two photon absorption is usually very small compared to that of a direct transition, this make this process not of general use.

4.5.2 Saturation Spectroscopy

The hyperfine splitting which is in the range 10^{-3} to 1 cm^{-1} is sometimes not observable using traditional excitation sources. This is due to the fact that thermal motion of atoms or molecules will give rise to Doppler-broadening which is larger than the hyperfine splitting to be investigated. One of the ways of addressing such problems is to use saturation spectroscopy. The first saturation spectroscopy experiments using a tunable narrow-band laser were performed by Hänsch, Schawlow and co-workers [98, 99] and by Borde [100].

Consider a monochromatic laser beam with frequency ω passing in the x direction through an ensemble of atoms or molecules in gas phase. Since the atoms are in thermal motion with velocity distribution determined by Maxwell-Boltzmann statistics so the Doppler-broadened absorption profile is of Gaussian line shape with center frequency ω_o. Atoms which are Doppler-shifted into resonance with the laser frequency can absorb the laser photons with Doppler shift given by $\Delta\omega = \mathbf{k}\mathbf{v}_x$ and inducing a transition from an initial level $\langle\mathbf{i}|$ to the final level $\langle\mathbf{f}|$. The population N_i of these atoms in the initial level decreases whereas population N_f in the final level increases accordingly. Therefore a narrow dip is burnt in the velocity distribution $N_i(v_x)$ of these atoms in initial level and correspondingly a narrow peak appears in the distribution $N_f(v_x)$ of atoms in the upper level.

In saturation spectroscopy instead of a single laser beam two counter propagating beams with frequency ω_L are allowed to interact with the ensemble of atoms. The experimental arrangement is as shown in figure 4.6. A laser beam from a tunable laser source is split by a beam splitter BS into a strong pump beam and a weak probe beam that passes through the absorption cell in opposite direction. The probe and pump beams have a good overlap inside the absorption cell. The pump beam is intensity modulated by a mechanical chopper and the modulation frequency is fed into the lock-in amplifier as reference frequency. A detector sees the transmitted probe beam intensity as a function of the laser frequency ω_L whose output goes to the lock-in amplifier as second input.
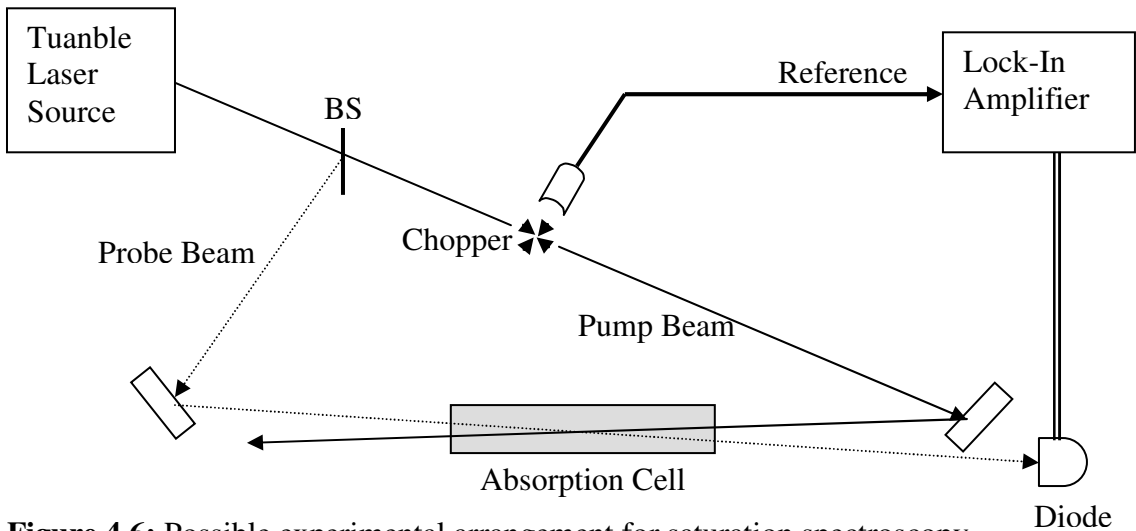
Figure 4.6: Possible experimental arrangement for saturation spectroscopy

Laser frequency is tuned over the Doppler-broadened absorption profile of the ensemble of atoms moving with different velocities. When the laser frequency ω_L coincides with the center of absorption line ω_0, only one velocity class in the interval dv_x around $v_x=0$ interacts with the laser beam. The pump beam is strongly absorbed, depleting the population in the initial level $\langle i |$ with corresponding increase in the population of the final level $\langle f |$. A narrow hole or dip is burnt in the velocity distribution $N_i(x)$ of the initial level and a corresponding narrow peak appears in the distribution $N_f(x)$ of atoms in final level. The absorption coefficient $\alpha(\omega)$ with a Doppler-broadened profile has a dip around the center frequency ω_0. The counter propagating weak probe beam interacts with atoms whose absorption is saturated by the strong pump beam, resulting in a sharp decrease of absorption of the weak probe beam at the center of the line. The intensity of the probe beam is modulated only when the probe beam is responsive to the hole burnt in the Doppler profile by the strong modulated pump beam. The modulated part of the probe beam intensity recorded by a phase sensitive lock-in amplifier depends only on the saturated absorption and is not sensitive to the unsaturated part of the Doppler profile.

The dip at the center of Doppler-broadened absorption profile caused by the saturation of the population, which is probed by the second weak probe beam is called Lamb Dip named after Willis Lamb who first explained this effect quantitatively. Since the detector measure the intensity of the transmitted probe beam so each time Laser frequency coincides with the center frequency of atomic transition, a Lamb peak appears in the transmitted intensity, because the absorption exhibits a dip at this frequency.

For monitoring laser induced fluorescence (LIF) signal two counter propagating laser beams must be of equal intensity and the Lamp dips can seen easily. The total LIF intensity is proportional to

- Laser intensity
- Number density in the initial sate
- Einstein coefficient for absorption, and
- Quantum yield (ratio of the number of photons to the number of photons absorbed)

Obviously the Lamb dip is much narrower than the Doppler width. If the intrinsic frequency width or linewidth of the laser used in the experiment is small enough, the observed width of the Lamb dip is always limited by saturation broadening. The Doppler-broadened background can be eliminated when the pump beam is periodically chopped. A lock-in detector measures the difference of the transmitted probe intensity with the pump beam on and off. The result is a Doppler-free spectrum with a better signal-to-noise ratio.

4.5.3 Collimated Atomic Beam Spectroscopy

High resolution spectroscopy can be performed by irradiating a well collimated atomic beam at right angles with a narrow-band, single-mode laser. In this case the Doppler

width is reduced by the collimation ratio C and very small absorption width of atoms is formed.
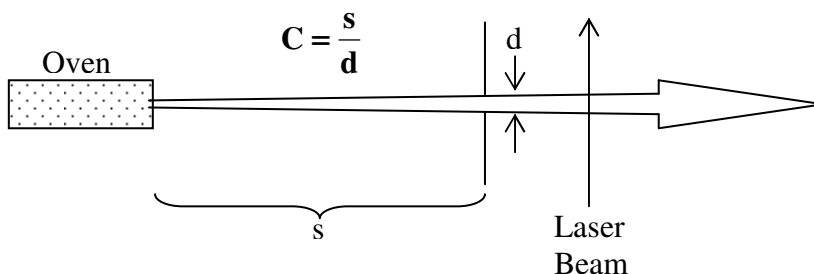
Figure 4.7: Definition of Collimation Ratio.

Utility of this technique comes from the fact that the atoms in the collimated beam do not have velocity components in the direction of laser beam.
D. A. Jackson and H. Kuhn [101] had used atomic beams long before the invention of lasers. In their work the absorption was analyzed by means of a high resolution Fabry Perot interferometer. The first application of atomic or molecular beams in laser spectroscopy was described S. Ezekiel and R. Weiss [102].
Main characteristics of atomic beam spectroscopy:
- An atomic beam can be produced essentially for any element.
- The Doppler width is reduced by a factor of sinε which is equal to the collimation ratio.
- The number of collisions are small subsequently collisional broadening is reduced. This is because all atoms have almost same velocity so fewer collisions occur as compared to a gas at equivalent pressure.
- Fluorescence light radiates in 4π steradians and very few of them reach the photodetector.

Detection techniques:

Detection by fluorescence: The most direct way to study the optical resonance is to observe fluorescence light, released after excitation.

Detection by photoionization: Here the atomic beam interacts simultaneously with a narrow band laser and an intense laser. The narrow band laser brings the atoms to an excited state and an intense laser, having sufficient energy, ionizes the atoms in excited states. The photoelectrons or the ions are detected in an electron detector [103]. This process has also been demonstrated for isotopes separation [104].

Detection of recoil atoms: When an atom absorbs a photon, the momentum of the photon is transferred to the atom. As a result the atom is deflected from the beam. In the de-excitation process the recoil the momentum transferred either is cancelled (stimulated emission) or is transferred to the atomic beam (spontaneous emission). The latter results in spread and broadening of atomic

beam. The deflection of an atomic beam was first demonstrated by R. Frish in 1933 [105]. A. Ashkin [106] proposed to use this technique for isotope separation. P. Jacquinet et al. [107] first time recorded the hyperfine structure by beam deflection for the sodium D lines.

Detection of change in magnetic sublevels in an atomic beam deflected by an inhomogenous magnetic field: The first application of the magnetic resonance principle was made with the introduction of atomic beam magnetic resonance technique by I. I. Rabi, J. R. Zacharias, S. Millman, and P. Kusch in 1938 [108]. They discovered that any change in magnetic sub levels of an atom in the atomic beam can be detected by a change in the deflection of the beam in an inhomogeneous magnetic field. In 1952 I. I. Rabi [109] suggested that this technique could be used in the study excited states if atoms are illuminated resonantly in the interaction region. He also suggested that this method could be used to study isotope shifts. In 1965 Marrus [110] used Rabi's arrangement and by using the change in magnetic sub levels of ground state he detected and measured optical transitions.

4.5.4 Laser-Induced Fluorescence (LIF) Spectroscopy

In laser induced fluorescence (LIF) atoms or molecules are excited from a lower energy state to a higher energy state by means of radiation from a laser source. The atoms or molecules thus excited can relax or de-excite in a number of ways for example by spontaneously emitting light or by collisional de-excitation. The spontaneous emission of light constitutes the fluorescence signal. Since the fluorescence signal is laser induced so such spectroscopic investigations of atoms and molecules is known as laser induced fluorescence spectroscopy.

LIF measurements can be made by tuning the laser frequency across the atomic or molecular resonances and capturing the resulting fluorescence signals. The spectrum obtained mimics an absorption spectrum of the investigated species. This is a specific form of absorption spectroscopy known as **excitation spectroscopy,** in which the fluorescence intensity of a certain spectral line is monitored as a function of laser wavelength. Thus, the observed fluorescence intensity reflects the change of population of the upper excited state. The signal strengths depend on laser intensity, species concentration and temperature but also very much on the collisional environment the investigated species reside in. LIF signal is monitored by a phase-sensitive detector i.e. lock-in amplifier which is tuned to the modulation frequency (reference frequency) while chopping the excitation light.

Our research is mainly concerned with the investigation of hyperfine structure of fine energy levels which are characterized by a number of parameters such as level energy, parity, total electronic orbital angular momentum J and nuclear spin I. Besides these other parameters of interest are the hyperfine constants and Lande 'g' factor. These parameters characterize a specific energy level.

An atom in the ground or in one of the excited state E_i absorbs a laser photon of suitable wavelength, undergoes a transition to an upper energy state E_f. The population of upper state increases, and subsequently it decays via several relaxation processes. Fluorescence signal is one of these processes and is monitored as a function of laser wavelength. In exciting sufficiently higher lying states, a number of fluorescence wavelengths are observed due to the decay to lower states according to allowed dipole transitions (figure 4.8). The strength of a LIF signal is determined by the branching ratio of the upper excited level. The hyperfine transition of the LIF lines does not play any role, since the monochromator selecting one LIF line does not resolve the hfs of this line, but acts only as a filter to suppress other lines of the discharge.

Quantitative analysis of LIF signal **[111]:**

LIF detection is a very sensitive version of absorption spectroscopy which can be appreciated by following estimation:
Consider the laser wavelength λ_L tuned to an absorbing transition $E_i \rightarrow E_f$, the number of photons n_a absorbed per second (s) for an absorption path length Δx is given by

$$\mathbf{n_a = N_i \, \sigma_{if} \, n_L \, \Delta x} \qquad\qquad 4.31$$

where
$n_L \equiv$ Number of incident laser photons
$\sigma_{if} \equiv$ the absorption cross-section per molecule or atom. Absorption cross-section determines the absorption probability and is also related to absorption coefficient α_{if} by

$$\mathbf{\alpha_{if} = \sigma_{if} \left(N_i - N_f \, \frac{g_i}{g_f} \right)} \qquad\qquad 4.32$$

Absorption cross-section is terms of Einstein coefficient B_{if}

$$\mathbf{\sigma_{if} = \frac{h\nu}{c} \, I(\nu - \nu_o) \, B_{if}} \qquad\qquad 4.33$$

$g(\nu - \nu_o)$ is the line profile function.
$N_i \equiv$ Density of atoms in absorbing state E_i.

The number of fluorescence photons emitted per second from the excited state E_f is

$$\mathbf{n_{flu} = N_f \, A_f = n_a \, \eta_f} \qquad\qquad 4.34$$

where
$A_f = \sum A_{fm}$ represents the total spontaneous transition probability in case of several transition paths from E_f to different lower states E_m.
η_f is the quantum efficiency of excited state.

The Quantum efficiency η_f is the ratio of the spontaneous transition rate to the total deactivation rate which may also include radiation-less transitions, viz.

$$\eta_f = \frac{A_f}{A_f + R_f} \qquad 4.35$$

For $\eta_f = 1$ the number n_A of the fluorescence photons emitted per second equals the number n_a of the photons absorbed per second under stationary conditions.

The quantum efficiency of photocathode η_{ph} is defined as the ratio of the rate of production of photoelectrons, n_{pe}, to the rate of incidence of photons, n_{ph}, i.e.

$$\eta_{ph} = \frac{n_{pe}}{n_{ph}} \qquad 4.36$$

One must take into account of the fact that only fraction δ of the fluorescence photons emitted into all directions, can be collected on the photomultiplier cathode which is a geometrical factor and only fraction of these photons produce on the average n_{pe} photoelectrons. The number n_{PE} of the photoelectrons counted per second is then

$$n_{PE} = n_a \, \eta_f \, \eta_{ph} \, \delta \qquad 4.37$$

Substituting the value of n_a we get

$$n_{PE} = N_i \, \sigma_{if} \, n_L \, \Delta x \, \eta_f \, \eta_{ph} \, \delta \qquad 4.38$$

Therefore total fluorescence intensity monitored as a function of wavelength λ_L is given by the relation

$$I_{Fl}(\lambda) \propto n_L \, \sigma_{if} \, N_i \qquad 4.39$$

Above relation contains n_{PE}, the number of photoelectrons counted per second, in terms of ($N_i \, \sigma_{if}$) and the proportionality factor depends on the quantum efficiency η_{ph} of the photomultiplier cathode and on the collection factor δ of the fluorescence photons.

Main characteristics of LIF:
- For all excited states E_f, quantum efficiency η_f must be same. At sufficiently low pressure the excited state atom radiate before it can collide with another atom and $\eta_f = 1$ for all excited states.
- At higher pressures the quantum efficiency η_f of the excited state E_f is decreased due to collisional deactivation processes which compete with radiative transitions.
- The quantum efficiency η_{ph} of photomultiplier cathode should be constant over the whole spectral range of the emitted fluorescence.
- The geometrical collection efficiency δ of the detector system should be identical for the total fluorescence from different excited states.

- With increasing wavelength λ the sensitivity decreases for two reasons (i) the detected photoelectron rate n_{PE} decreases with η_f, η_{ph}, and δ as these numbers generally decrease with increasing wavelength and (ii) the quantum efficiency of photomultipler cathode η_{ph} and the attainable signal-to-noise ratio are much lower for infrared than for visible photodetectors.

Detection of LIF signal and types of decay mechanisms:

Detection of LIF signal is carried out in the following manner: Laser frequency is tuned across hyperfine components of a line and those atoms which are in resonance with the laser light are excited. This modulates the population of the levels involved in the transition which results in the modulation of fluorescence intensity only those fluorescence lines originating from the levels involved in the excited transition. These modulated fluorescence lines are selected by tuning the transmission wavelength of a monochromator across the spectrum. Finally phase sensitive detection is carried out by a phase sensitive lock-in amplifier which has two input signals (i) modulated fluorescence intensity (ii) modulation or chopping frequency of the laser beam. Combining the two signals has an advantage of detecting: only those fluorescence lines which are in-phase with the modulation frequency of the laser beam are detected. Thus discrimination between modulated and non-modulated fluorescence lines is easy. One other advantage of phase sensitive detection by lock-in amplifier is the differentiation between fluorescence lines originating from the upper and lower transition levels accordingly as the modulation phase of the fluorescence lines are in phase or out of phase with respect to intensity modulation phase of the laser beam. This can be understood as follows. The intensity of a fluorescence line is proportional to the population of the upper level of the fluorescence line. Laser induced absorption increases the population of the upper level of the excited transition in phase with the modulation frequency of the laser beam therefore the fluorescence lines originating from the upper level are also in phase. At the same time laser induced absorption also diminishes the population of the lower level of the excited transition and thus the corresponding fluorescence lines originating from lower level are antiphase modulated i.e are 180 degrees out of phase compared with the intensity modulation phase of the laser beam.

Figure 4.8 shows a simple scheme of transitions between various levels. The observed fluorescence lines can be categorize in the following manner:

(i)   *Fluorescence with positive LIF Signal:* Due to the resonant transition from lower level E_2 to the upper level E_3, the population of excited level E_3 increases and at the same time population of lower level E_2 decreases. A subsequent decay occurs to more than one lower levels i.e. E_4 and E_5 by emitting fluorescence light of wavelengths λ_{34} and λ_{35}. Laser frequency is modulated at a chopping frequency 'f' which act as a reference frequency for phase-sensitive detection (Lock-in amplifier). If LIF signal and reference frequency are in phase, maximum LIF signal is observed. Since the LIF signal intensity increases with laser light on, this type of fluorescence is called a **positive phase** or a **positive fluorescence**. This

type of fluorescence which is observed as a result of decay from the upper level of excited transition is also termed as direct fluorescence.

(ii) **Impact or Collisional Coupling:** If other level energies lie close to a level populated or depopulated by laser light, the probability of impact or collisional transfer of population is high. In such a situation through impact or collision an excited state atom transfers its energy to another atom whose excited level energy happens to lie close by which subsequently decays to lower level by emitting fluorescence light. This type of fluorescence is also positive phase fluorescence. As shown in figure 3 due to an impact a population transfer occurs from E_3 to E_6 which decays to E_7 by emitting a fluorescence wavelength λ_{67}. This is an indirect fluorescence as it is observed due to decay from an upper level which is not directly excited in original transition. Population transfer between lower levels, E_2, E_8 is also possible.

(iii) *Negative Fluorescence:* In situations where the lower level of a certain transition is high lying as compared to very low lying levels, this lower level decays to the further low lying levels by emitting fluorescence light. Such LIF signal is negative in phase and is known as **negative fluorescence**. In figure 4.8 for the resonance excitation from E_2 to E_3 some of the atoms in lower level E_2 decay to level E_1 by emitting a fluorescence wavelength λ_{12}. The population of level E_2 decreases when the laser light is on and the fluorescence observed has 180° phase shift as compared to a positive fluorescence. Negative fluorescence wavelengths are useful in identifying the lower level of an excitation transition. Furthermore if exact fluorescence wavelengths are determined the lower level of fluorescence decay can also be identified.

(iv) *Self-absorption:* Usually in optically thin light sources the photon emitted by spontaneous emission has a little chance of being re-absorbed. For spectral lines involving ground state of the atom this assumption in most cases breaks down. Especially true for spectral lines arising due to combination between ground state and lowest excited states. These are very strong lines and are called resonance lines. For such lines it may happen that a photon emitted by an atom at one point in a light source may be re-absorbed by a different atom before it has a chance to escape from the source. This phenomenon is known as self-absorption. It can happen if the photon which is being re-absorbed has an energy coincidence with the energy difference of the two levels involved in the re-absorption excitation. Due to self-absorption line shape changes, making it appear broader. Since the probability of emission was greatest at the center of the line, the probability of absorption is also greatest at the center. Thus as a result of re-absorption within the light source, the intensity of the spectral line decreases proportionately more in the center of the line than elsewhere. If the self-absorption is strong, then an intensity minimum develops in the center of the spectral line and the line is said to be self-reversed. Self-absorption is by no means restricted to lines involving ground state, it can also happen for lines arising from the combination of two excited states.

Advantages of LIF Spectroscopy:

- *Blend situation:* In elements like praseodymium where there are regions of high energy level density, more than one level is excited simultaneously in a single range of laser. So the observed LIF patterns corresponding to all excited levels show a complex structure caused by this blend situation. LIF spectroscopy has the advantage that individual transition lines can be separated by searching for fluorescence channels corresponding to one particular upper level. In this way hyperfine structure of each line can be recorded and level energy is determined by using the information from the recorded structure, wave number of excitation line and energy of lower level.

- *LIF signal of free atoms:* In a hollow cathode discharge it is easier to produce free atoms than free ions, therefore LIF signal of an atomic line of comparable intensity should be stronger than that of an ionic line.

61
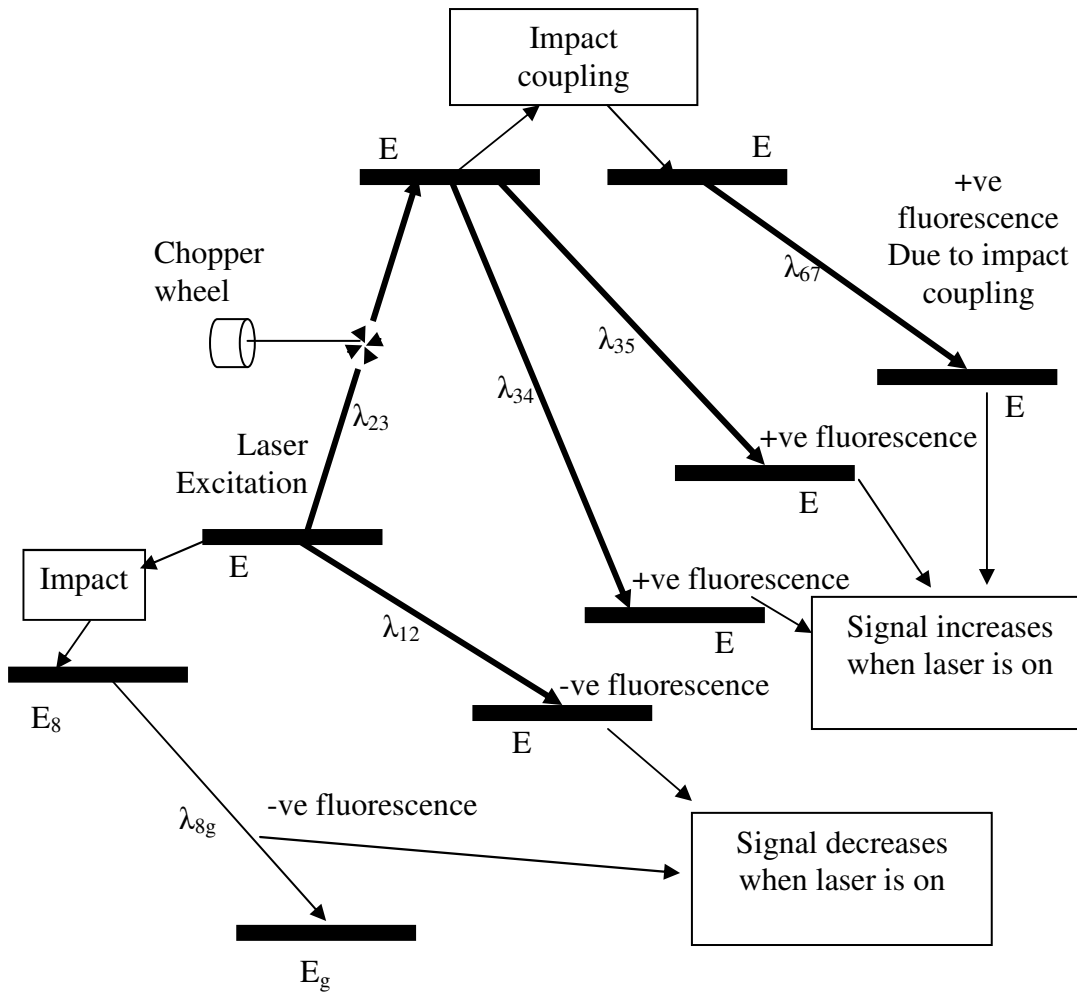
Figure 4.8: Positive and negative fluorescence signals and impact coupling

- *Large laser intensity:* Availability of lasers with high intensities makes it possible to achieve of large population densities in the excited states, yielding high intensities of fluorescence lines even for transitions with low transition probabilities.

- *Higher sensitivity for Fluorescence Signal:* Using Lock-in techniques higher sensitivity is achievable for fluorescence signal as compared to absorption measurements.

4.5.5 Optogalvanic Spectroscopy

Light induced changes in electrical properties of a plasma were first discovered by F. M. Penning [112] in 1928. He observed a perturbation of a gas discharge caused by the light of a second discharge. This effect as a spectroscopic tool had to await till the invention of tunable dye laser. The first spectroscopic account of this effect, named as 'optogalvanic effect', was published by Green et al. [113] in 1976. They used a commercially available hollow cathode lamp as a gas discharge tube which they irradiated with laser light tuned to wavelength of a transition of one of the species present in the discharge. The effect was apparent as a change in the tube voltage. The use of this effect opened a new branch of spectroscopy know as Optogalvanic Spectroscopy which is a very sensitive and simple technique of performing laser spectroscopy in a hollow cathode gas discharge. The standard experimental setup is shown in figure 4.9.
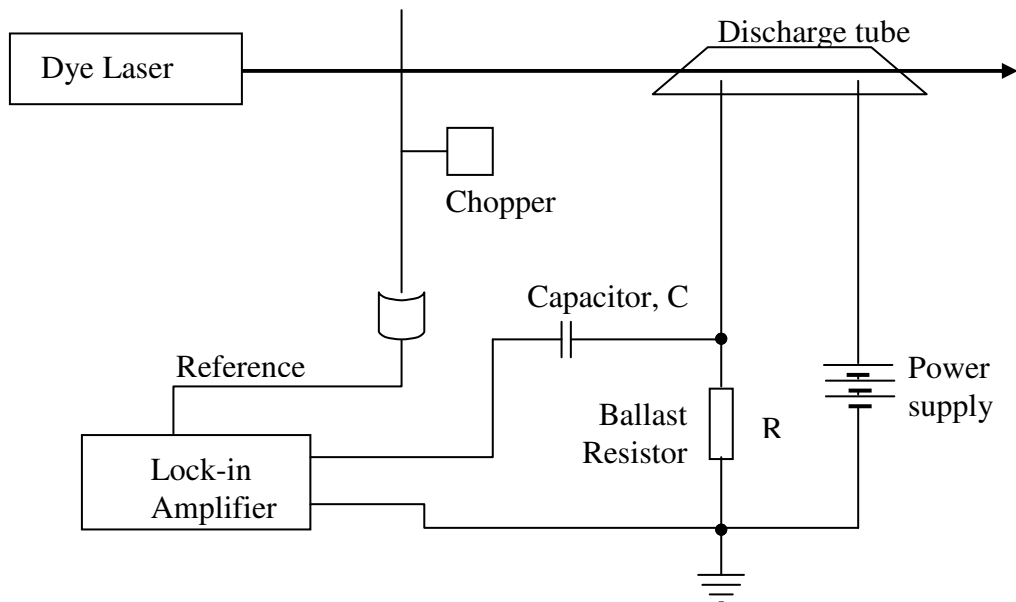
Figure 4.9: Possible experimental setup for optogalvanic spectroscopy

A laser beam is passed through a hollow cathode discharge. The wavelength is tuned to a resonance transition $E_i \rightarrow E_f$ between levels of atoms or ions in the discharge which subsequently changes the population densities $n_i(E_i)$ and $n_f(E_f)$ of the combing levels. Since atoms in different stationary states E_i and E_f have different ionization probabilities this change in population results in a change of discharge current ΔI which could be detected as a voltage change $\Delta V = R\Delta I$ across the ballast resistor R. In order to achieve a good signal-to-noise ratio, the excitation must be done by chopping the laser beam and use of a lock-in amplifier for phase-sensitive detection. Periodic changes in tube voltage can be detected by connecting one of the electrodes via a capacitor C to the input of the lock-in amplifier. The effect is more pronounced for high lying levels as they have a reasonable probability of collisions and ionization compared to low lying levels. Both positive and negative signals are observed, depending on the levels E_i and E_f involved in the laser-induced transition $E_i \rightarrow E_f$. Since the absorbed laser photons are detected by optically induced current change of discharge, therefore this sensitive technique for doing spectroscopy is so named as Optogalvanic Spectroscopy.

Several competing processes may contribute to ionization of an atom in level E_i. Some of them are discussed below:
(i)   Direct ionization by electron impact

$$A + e^- \rightarrow A^+ + 2e^- \qquad\qquad 4.42$$

       This process dominates at low pressure.
(ii)   Two step ionization or multi step ionization:

$$A + e^- \rightarrow A^* + e^-, \; A^* + e^- \rightarrow A^+ + 2e^- \qquad\qquad 4.43$$
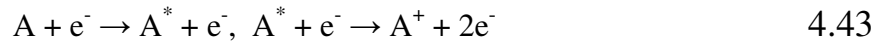
       In noble gases this process is particularly important if excited states are metastable states.

(iii)   Collisional ionization by metastable atoms:
       Two atoms in metastable states collide with one another; one of the atom absorbs sufficient energy and becomes ionized

$$A^* + B^* \rightarrow A^+ + B + e^- \qquad\qquad 4.44$$
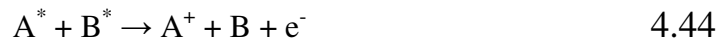
Advantages/Disadvantages of Optogalvanic Spectroscopy:

(i)   The experimental setup is very simple since it does not require a monochromator and a detector such as photomultiplier tube or photodiode detector to obtain the investigated spectra. This is because the discharge itself acts as a detector.
(ii)   Only excitation wavelength is required no need to monitor fluorescence signal.
(iii)   The substantial disadvantage of this type of spectroscopy is unstable discharge condition. For recording optogalvanic signal the discharge must be burning very calmly.

(iv) The optogalvanic signal has nothing to do with the fluorescence light, hence nothing can be said about the levels involved in the transition. Of course the excitation probability and thus the hf structure of the excited transition are mirrored in the OG signal.

Application of Optogalvanic effect

(i) Determination of the hyperfine constants by exciting classified lines.
(ii) When exciting an unclassified line, OG signal can help in recording the hf structure of the line, and to place the laser frequency when later searching for LIF lines.
(iii) To study the collision process and ionization probabilities in a gas discharge.
(iv) This technique can be used for wavelength calibration in laser spectroscopy [114].
(v) The study of Rydberg states is also possible by optogalvanic spectroscopy [115].
(vi) It is very efficient for the investigation of Autoionizing levels [116].
(vii) The optogalvanic signals may be used for laser frequency stabilization [117, 118].

Chapter 5
Experimental Setup and Data Analysis Programs

5.1 Experimental Setup

LIF method in a hollow cathode discharge for the investigation of atomic or ionic transitions and subsequent identification of new electronic levels proves to be advantageous since in addition to the information about the hyperfine structure of spectral line under investigation, one also obtains information on the fluorescence wavelengths by a monochromator in selected channels. This information is useful in cases where more than one-identification possibility exist. Praseodymium has only one stable isotope therefore LIF method in a hollow cathode discharge is particularly efficient since with even large Doppler width the hfs spectra are quite legible. Furthermore if hfs splitting of a fine structure level is large, which is quite frequent in praseodymium, then there is no need for Doppler-reduced methods. The experimental setup is illustrated in figure 5.1.
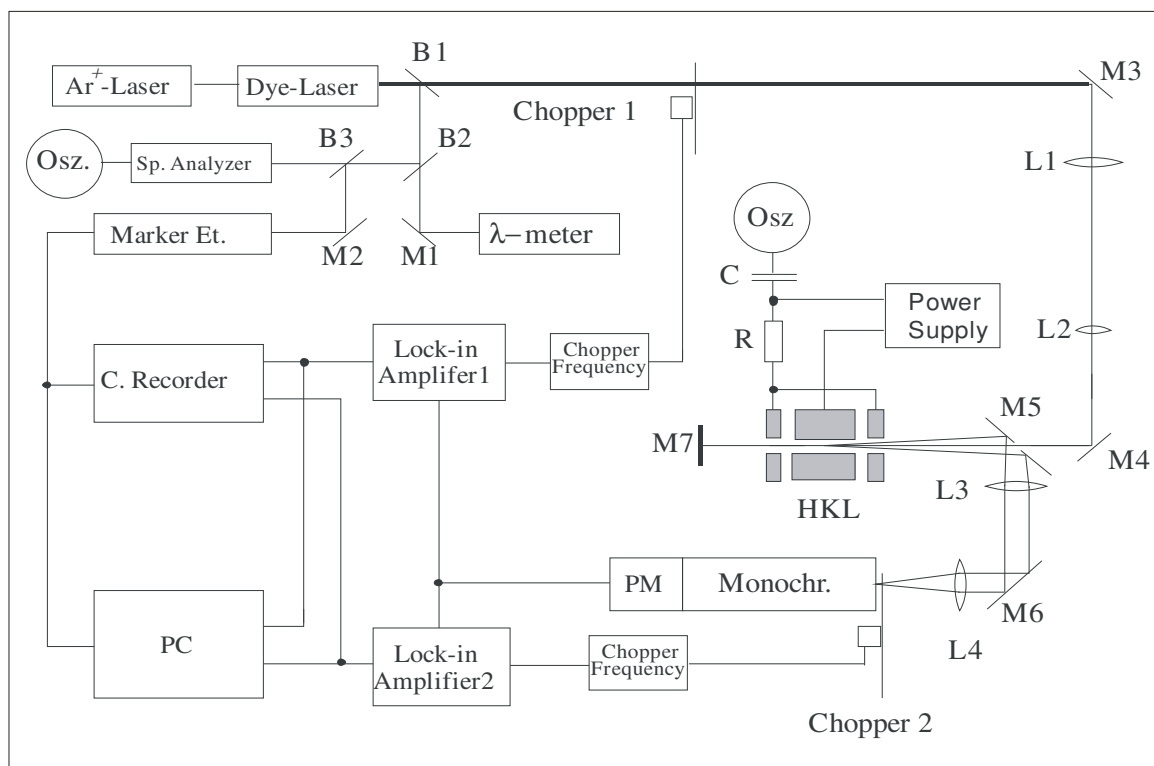
Figure 5.1: Schematic diagram of Experimental setup
HKL...Hollow Cathode Lamp, M1-M4, M6, M7...Mirrors, M5...Mirror with central hole, L1-L4 lenses, B,B1,B2...Beam splitters, Ar⁺Laser...Pumplaser, Dye-Laser...Ring Dye Laser, Osz...Oscilloscope, Sp. Analyzer...Spectrum-Analyzer, Marker Et…Marker etalon for measuring frequency markers, λ–meter...Wavemeter, Monochr...Monochromator, PM…Photomultiplier tube, C. Recorder….Strip Chart Recorder, HKL….Hollow Cathode Lamp, R...Ohmic resistance, C...Capacitive reactance

The setup can be divided into three parts:

i.   A source of exciting radiation,
ii.   A discharge lamp containing the sample to be investigated,
iii. Measurement and fluorescence detection system.

5.1.1 Excitation Source

In the investigations of hyperfine structure of praseodymium the source of exciting radiation is a cw single-mode tunable ring-dye laser optically pumped by an argon-ion, krypton-ion or by diode-pumped, frequency doubled Nd:Vanadate (Nd:YVO$_4$) Verdi V-18 laser system. Noble ion lasers such as argon-ion or krypton-ion laser are not very efficient due to high energy requirement for first ionizing the atoms and only after ionization can a population inversion be established in the ion population. As pump laser argon-ion laser utilize ionized argon as lasing medium. A number of different wavelengths may be emitted simultaneously but the strongest are at 488 and 514.5 nm. The relevant energy levels are those of singly ionized argon gas. The lowest energy level is the ground state of the argon ion, which lies 16 eV above the ground state of the neutral argon atom. In addition, the upper energy levels lie about 20 eV above the ionic ground state. Therefore for laser operation, a considerable amount of energy must be supplied to the neutral argon atom to first ionize and then raise it to the upper laser level. Krypton-ion laser as pumping laser produces about nine lines in the range 476-800 nm, with the 647.1 nm line being the most intense. The Verdi laser produces single frequency light at 532 nm. For pumping the ring-dye laser system, the pumped power range from 4 to 7.5 watts.
Depending on the region of investigation following laser dyes were used as lasing medium in ring-dye laser system:

Pump laser	Pumping region
Argon-ion Ar$^+$	Visible or 532 nm
Krypton-ion Kr$^+$	Violet
Verdi V-18	532 nm

Laser dyes	range / nm
Rhodamine 6G	560 - 595
Sulforhodamine B (Kiton Red)	598 – 650
DCM	630 - 690
Coumarin 102	463 – 515

The lasing action in dye laser produces laser light which has a certain range of wavelength depending on the type of dye used for lasing. To obtain a stable single mode laser light within the spectral range of dye various mode selective elements in ring-dye

laser cavity are tuned synchronously. Frequency stabilization is achieved by locking the laser wavelength to a very stable external reference cavity.

5.1.2 Hollow cathode lamp

Hollow cathode lamp is a discharge lamp and is an efficient light source producing comparatively narrow spectral lines. The first hollow cathode lamp was used by Schüler [119, 120], it however had one anode. Paschen made a hollow cathode with the cathode inside two anodes [121]. Feldmann was the first who introduced a discharge with a clear path through the electrodes [122], Miyazaki et al. modified his discharge assembly by placing the hollow cathode between two hollow anodes [123]. A similar lamp was developed by Behrens and Guthöhrlein et al. [124, 125].

If the material to be investigated is metal then the cathode as a whole is made up of it on the other hand in case it is non-metallic then a hollow cylindrical piece of the material is well inserted into a copper or aluminum hollow cylinder. The cathode itself should not or only very little contribute to the discharge. Since the discharge is wholly confined inside the cathode, the efficiency of excitation is high.

In the present work of investigation of hyperfine structure of praseodymium hollow cathode consists of a copper cylinder with a wide axial hole. The material to be spectroscopically investigated, in this case is Praseodymium in the form of a well-fitted axially hollowed cylinder placed inside the copper cathode cylinder. Thus the inner wall of the copper hollow cathode is covered with a thick layer of Praseodymium. The complete hollow cathode lamp is shown in the figure 5.2. The length of copper cathode with praseodymium cylinder inserted inside is $\approx$ 19 mm with inner bore diameter 3 mm. On both sides of the cathode two aluminum anodes are placed. The anodes are mounted on a ceramic holder to avoid their contact with the cathode. The separation between anode and cathode is approximately 0.75 mm. The anodes, the cathode and the ceramic parts had coaxial hole of almost same diameter. The whole arrangement is screwed in a brass tube, which is soldered in a glass tube that extended to both ends, forming the actual discharge container. The anodes are provided with conducting pins, led to the outside of the device through a feedthrough. The ends of glass tube are sealed by the two circular quartz glass plates acting as windows of hollow cathode lamp. The quartz windows are used in order to allow UV fluorescence light to pass that would emerge from the cathode lamp.

The whole device is evacuated by a rotary vacuum pump and is then filled with argon gas as buffer gas. The pressure maintained range from 0.5 to 0.8 mbar depending on the type of specie to be investigated i.e. neutral atom or ions, region of investigation and discharge conditions. The current used in the experiments with praseodymium is typically between 50 and 60 mA. The DC voltage varies from 350 to 650 V. Before the discharge is switched on it is normally evacuated for 10-12 hours. Hollow cathode lamp with vacuum system is shown in figure 5.3.
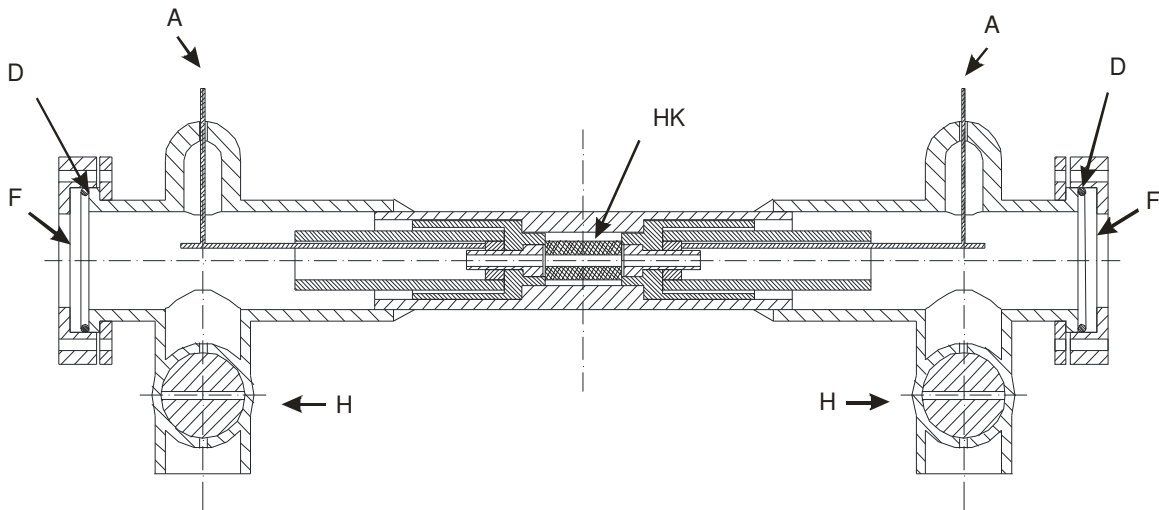
Figure 5.2: Hollow cathode lamp. HK...Hollow Cathode, A…Anode current feedthrough F…Quartz windows, D…O rings, H…Glass stop cocks
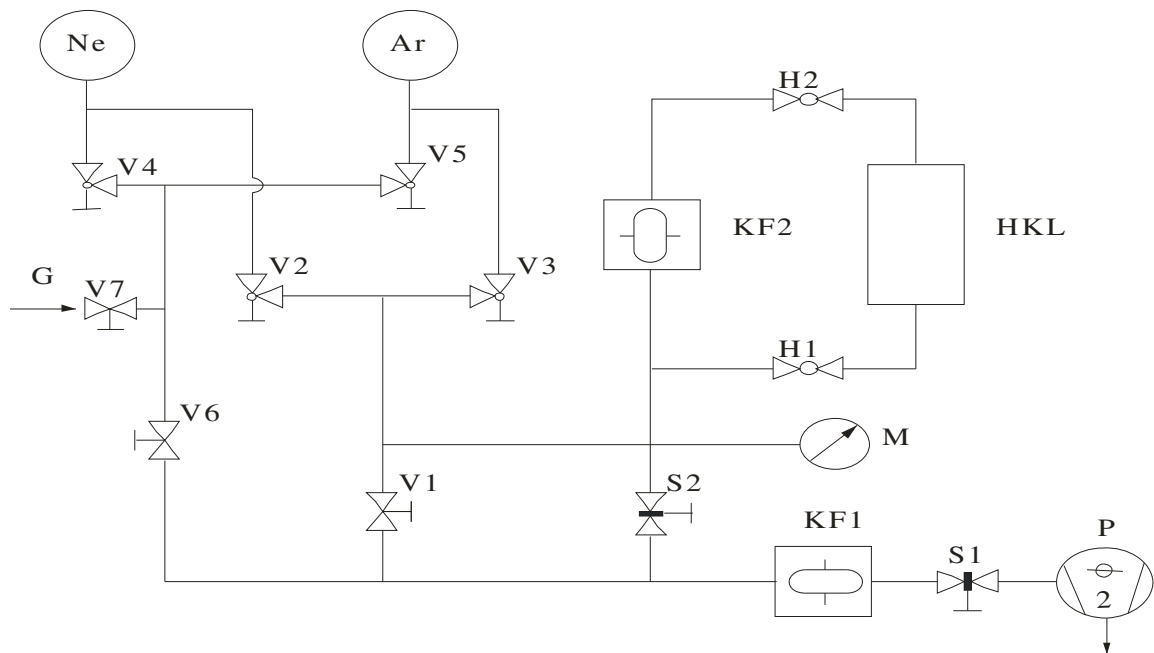
Figure 5.3: Schematic design of the vacuum system. HKL...hollow cathode lamp, H1 H2…Glass stop cocks, S1-S2...Slide valves, V1-V7...Shut-off and gauge valves, KF1, KF2...Cold traps, M...Manometer, P...Two-stage rotary vacuum pump, G...Gas inlet, Ne...Reservoir for Neon, Ar...Reservoir for argon.

Application of DC voltage across the discharge lamp ionizes the buffer gas into ions and electrons. Due to the field distribution around the coaxial hole the discharge runs down into the hole. The ionized gas is accelerated and hits the cathode material which in our case is praseodymium. If these ionized gas particles have energy significantly in excess of the binding energy of the atoms of cathode material then atoms and ions can be released with a probability known as the ***sputtering yield*** and the process is known as ***cathode sputtering***. Sputtering yield is the number of sputtered particles per incident particle as a function of energy and identity of the incident particle. Sputtering yield depend on the mass of the incident particle as well as energy, with heavy atoms such as xenon being more effective than light atoms such as helium. For example for incident Ar ion the sputtering yield is higher with lower energy threshold as compared to Ne which has low sputtering yield with higher energy threshold for same kind of sputtered material. Cathode sputtering and interaction of the sputtered species with the carrier gas of the discharge produces a cloud of neutral atoms and ions in ground and excited states, with considerable population of neutral atoms in ground and excited states whereas ionic levels occupy a smaller part of population. An intense light emission is obtained from the hole.

In a hollow cathode discharge the population of excited states is in accordance with the kinetic energy of electrons i.e. the electron temperature. This is due to the fact that the probability of electron impact excitation is higher. At much higher electron temperatures such as in sparks as compared to arcs, identification of ion lines is also possible. Conventionally these ionic lines are called spark lines in contrast to atomic arc lines. The dominant relaxation process is spontaneous emission although collision deactivation processes are also possible. The Doppler width of the hyperfine components is reduced by cooling the discharge surroundings with liquid nitrogen.

5.1.3 Measurement and Fluorescence Detection

The optical layout of the experimental setup is shown in figure 5.1. A laser beam from tunable dye laser falls on beam splitter B1 which splits the incoming light into two beams, one of the beam falls on another beam splitter B2 which further divides it into two parts. One part of the beam after reflection from mirror M1 goes into wavemeter for reading wavelength and the other part falls on another beam splitter B3 which splits it into two beams. One goes to the spectrum analyzer and the other after reflection from mirror M2 goes to Marker etalon for producing equidistant frequency markers.

The major part of the beam from beam splitter B1 passes through a mechanical chopper-1 and falls on the mirror M3. The intensity of the laser beam is modulated by chopper-1 and the modulation or chopping frequency is fed into the Lock-in Amplifier-1 as a reference frequency. The laser beam from mirror M3 passes through a telescope arrangement of lenses L1 and L2, making it into a parallel beam. This parallel beam passes through a hole in mirror M5 and into the hollow cathode discharge lamp. The laser beam entering the hollow cathode discharge lamp interacts with plasma which contain atoms and ions in ground or excited states. The excited state atom or ion relaxes in a number of relaxation processes such as relaxation by collisions with other atoms or ions

or by spontaneous emission of light. Laser induced fluorescence (LIF) occurs upon the excitation of atoms and ions from a lower energy level to a higher energy level by means of laser radiation. The atoms or ions thus excited give up their acquired energy by spontaneous emission of light and this constitutes the fluorescence signal. The fluorescence light is reflected by the mirror M5 and in combination with lenses L3, L4 and mirror M6 goes into the monochromator. (grating monochromator with 1200 lines/mm). A photomultiplier tube mounted at the exit slit of the monochromator detects the fluorescence signal and converts it into a photocurrent, which is then fed to a **lock-in-amplifier**, whose reference frequency is the chopping frequency. Lock-in amplifier is tuned to laser chopping frequency via the triggering signal provided by the beam chopper. Lock-in amplifier does not amplify DC signals (e.g. photomultiplier tube dark current) but only the AC signal at the reference frequency. In addition to frequency sensitivity, lock-in amplifier also has the feature of being phase sensitive. In fluorescence measurements the phase of the signal is tuned such that lock-in amplifier output is maximum. This would correspond to signals that are in phase with the chopped laser excitation wavelength.

In order to investigate the hyperfine structure of a line, the frequency distances between different hyperfine components must be measured exactly. This is done by directing a part of laser beam into a marker etalon which is a temperature stabilized Fabry Perot interferometer. This gives equidistant frequency marks parallel to the hyperfine structure signal. The distance between successive frequency markers is known as **free spectral range (FSR)** and its magnitude depends on a particular interferometer i.e. our interferometer working in blue region has an FSR of 149.6 MHz, in red region it is 197.6 MHz and in yellow region it is 367.33 MHz. For further evaluation and documentation of the excited transition, both signals i.e. marker signal and hyperfine structure signal are recorded simultaneously on a computer as well as on strip chart recorder.

Monochromator gives the reading precision of the detected wavelength of fluorescence signal with an uncertainty of ±2 Å. It is sometimes necessary to determine the wavelength of LIF signal with higher accuracy. This especially desirable and advantageous in situations where the detected fluorescence wavelength(s) lie in the accessible region of laser dye for second or more excitations of the identified upper level. In order to modulate the whole emitted radiation from hollow cathode lamp, a second chopper is placed in front of the entrance slit of the monochromator. Laser light is tuned to the highest hyperfine component of the excited transition, and the grating monochromator is scanned over region of 10 Å containing the laser induced fluorescence wavelength signal. The whole fluorescence light from the discharge as well as the LIF signal is recorded simultaneously on separate traces. Comparison with FT spectra gives the wavelength of LIF line with an accuracy of ±0.05 Å. Accurate measure of fluorescence wavelengths is also beneficial in situations where the excited transition could not be identified meaning in the involved transition both lower and upper levels are unknown. In such cases precise fluorescence wavelength information gives indication to the identification of upper level.

5.2 Experimental Investigation of Spectral Lines

The determination of energy levels of atoms and ions can be accurately done by experimentally investigating their spectral lines. In a hollow cathode discharge atoms and ions are produced in ground and excited states. These atoms and ions are excited to higher states by laser light interaction. Atoms or ions in excited states upon subsequent decay to lower states emit of light which is recorded as fluorescence signal. This leads to further knowledge of the electron shell structure of atoms and ions. The energy needed to excite an atom or ion can be supplied either thermally i.e. by heating, or electrically i.e. through electrical discharge or by impact with another energetic particle. Excitation can also take place by direct absorption of electromagnetic radiation, for this the resonance condition **ΔE = hν** must be fulfilled. Apart from the metastable states the lifetime of excited states is of the order of 10^{-7} sec. so the excited states decay spontaneously by emitting electromagnetic radiation at discrete frequencies. The emitted radiation passes through a dispersing device which resolves it into components or discrete lines. The observed spectra which characterizes an element is in the form of distribution of intensity as a function of frequency or wavelength and is known as finger print of specific element. Provided the spectral line has sufficient intensity then by using high resolution techniques even the hyperfine structure of a spectral line can be seen. Complete and reliable knowledge of the electron structure demands that numerous spectral lines have been experimentally investigated. Experimental investigation of wide spectral region, requires a high resolution spectra from UV to far infrared. Such a high resolution spectra is a Fourier Transform Spectra (FTS) which is being used in our research group for the investigation of spectral lines of praseodymium, tantalum, lanthanum and neodymium.

5.2.1 Fourier Transform Spectra (FTS)

Fourier transform spectrometry is the spectroscopic technique used in research areas which require high accuracy, sensitivity and resolution. A Fourier transform spectrometer which is just a Michelson interferometer with a movable mirror is used to measure the coherence of a radiative source using space or time domain measurements of electromagnetic radiation. The intensity plot recorded in space or time domain is called **interferogram** which is converted into **spectrum** i.e. plot of intensity in inverse space (wavenumber) or inverse time (Frequency) domain by using a mathematical function known as Fourier transform.

In laser induced fluorescence (LIF) spectroscopy, FT-spectra is particularly advantageous since with help of FT-Spectra one can very precisely set the excitation wavelength for a spectral line. Further more by using the center of gravity wavelength of a spectral line and by comparing its hyperfine structure with the FT-spectra one can very easily and precisely classify the spectral line to a specific transition without the need of LIF spectroscopy. The FT-spectra for praseodymium [126] was recorded in the **Institute of Quantum Optics at University of Hannover** using FT-spectrometer model number IFS 120 HR with resolution that could be set between 0.0015 and 16 cm^{-1}. The Fourier transformed spectra recorded cover the region from 3173 Å to 11761 Å. A small portion of these spectra is shown in figure 5.4.
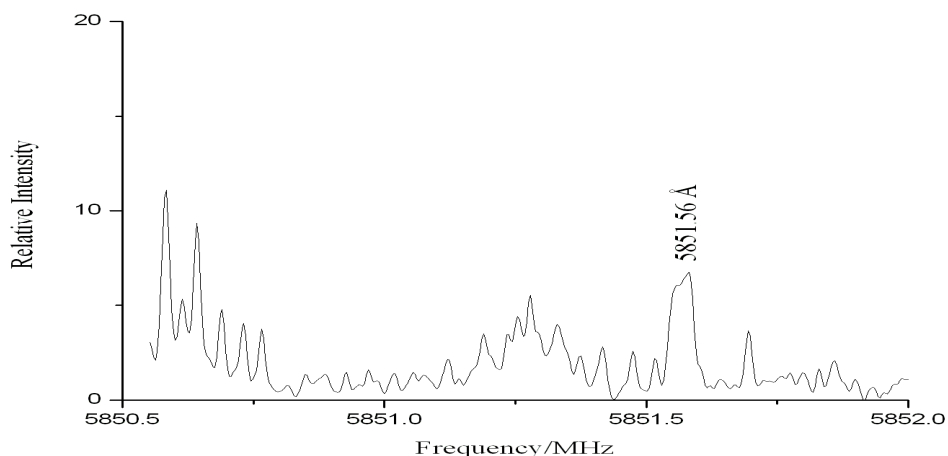
Figure 5.4: Fourier Transform Spectra in the region 5850.5 Å to 5852.0 Å.

The resolution is limited by the Doppler width of the lines and the apparatus profile of the FT spectrometer and for majority of spectral lines the hyperfine structure is only partially resolved. Since the wave number of a line is equal to the difference between the term values of the levels involved in its formation the classification of these lines is possible only if the hyperfine constants of levels are known. Hyperfine structure of some of the lines in FT-Spectra is fully resolved so for these lines hyperfine constants can be determined by fitting the line profile obtained from FT-Spectra and for others LIF signal must be recorded in order to classify the line to a specific transition involving lower and upper levels.

Advantages and Disadvantages of FT-Spectra:

1. FT-spectra is available in electronic form for further analysis and fitting hyperfine structure to mathematical function.
2. Resolution is high i.e. in some cases hyperfine structure is fully resolved.
3. Large spectral range can be covered.
4. FT-spectra are characterized by accurately assigning the wavenumbers to the observed lines.
5. The disadvantage of FT spectra maybe that it is hard to find a light source that emits weak lines with sufficient intensity.

5.3 Data Analysis Computer Programs

Different computer programs for data analysis were used during the completion of this dissertation. The main program which manages the data related to spectral lines in Praseodymium is the **Classification Program**. A data fitting program known as **Fitter** is used to fit the experimentally recorded hyperfine structures to mathematical functions in order to get the best fit spectroscopic parameters. This program is also used to fit hyperfine structures extracted from FT-spectra.

5.3.1 Classification Program

A Classification program is a set of computer programs used for managing large number of spectral lines and allows the classification of known and unknown lines via their expected hyperfine structure. This program was written by L. Windholz (Institute of Experimental Physics, TU Graz Austria) [127]. The viewer version of the program is available on internet. The program is written in such a way that it can be used for any element. In our laser spectroscopy group we are using this program for the classification of spectral lines in Praseodymium, Tantalum, Lanthanum and Neodymium. Program works simultaneously for both atomic and ionic lines and has also the option to suppress any type and showing only the other. The program uses three data files for any specific element:

(i)   The wavelength file or table, containing all the known spectral lines whether classified or unclassified. The Pr wavelength table has presently more than 23000 entries in the following format:

5873.095, , , , , 30149.869, 2.5 ,o, 966.36   ,   ,*Sq080, 13127.787,2.5 ,e, 156(1), -2(3), YS03s/,(Pr I) Sq080124 a5873.095 f5009 f5249 f5606

The first entry is line wavelength in Å in air, next four entries are intensities from different sources. If the line is classified the next entries are the energy, angular momentum, parity, A and B values and comment about the upper level. Then the next entries are for lower levels in the same order as for the upper level. Finally, it is possible to comment the lines, for example to give excitation wavelengths, fluorescence wavelengths and so on.

(ii)   A data file containing all the known neutral atom levels, e.g. in case of praseodymium this file is named Level_pr.dat, for example,

1.5 , o, 25849.518, 876.12 ,   , *Sq081214 pr292003 a5842.21 pr479013 a6655.71 f+5154 f4992 f6194 f6655 f6780

(iii)   A data file containing all known ionic levels, e.g. lev_prii.dat, for example,

4, o, 12431.364   , 860.73   ,   , *Sq080205 pr054009 pr502025 a5722.61 f3773 pr112001 a5908.69 f+3852 pr410041 a6687.53 f+3885   (New Lower Level from upper level=29901.053 cm-1 confirmed by FT-spectra)

The main window of the newest version of classification program is divided into three sections. Middle window containing the list of suggestions for the spectral line selected, leftmost window displays the classification of the spectral line and rightmost graphical window for a fast graphical overview of all suggestions.

The center of gravity wavelength of a spectral line is entered by either selecting the button "GoTo Lambda" for already known line or "Insert Line" for an unknown line. The program first calculates and searches for all possible transitions (number of possible suggestions depends on the selectable bandwidth) by comparing the wavenumber of the line with the difference of energies of pairs of levels which fulfill selections rules. The classification suggestions are then displayed in the middle section of the main window. Both atomic and ionic suggested transitions are displayed, one can suppress any one of them using an option in the menu bar. This section also contains a graphic field which displays the expected hyperfine pattern of the selected suggestion.
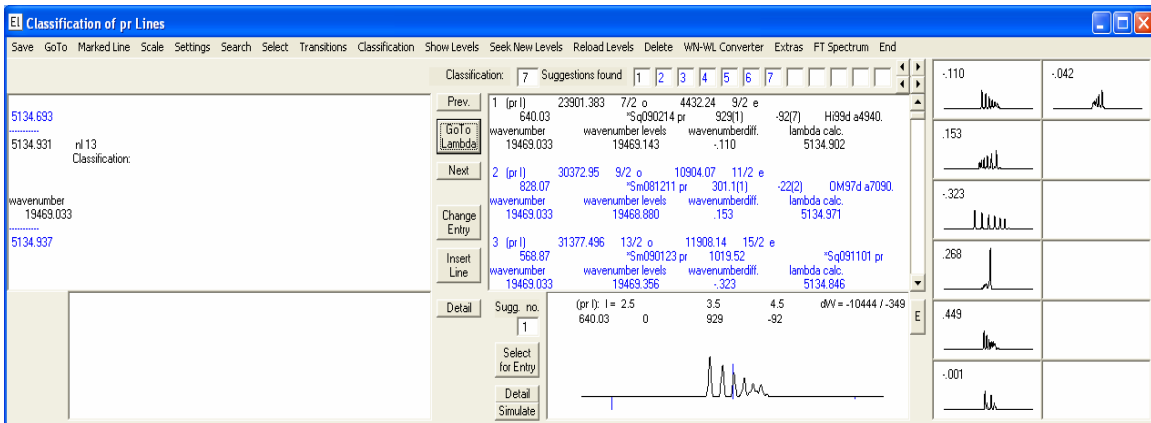
Figure 5.6: Main window of classification program with line inserted at 5134.931 Å.

If the spectral line is classified then the leftmost section displays energy, angular momenta, parity and hyperfine interaction constants for both upper and lower levels and remarks against both upper and lower levels display the name(s) of person(s) or group who discovered the level. The center of gravity wavelength is converted in the wave number by using the dispersion formula of Peck and Reeder [128]. The difference of upper and lower wave numbers is also displayed, which is again converted into wavelength by the Peck and Reeder formula. The difference of calculated wave number and center of gravity wave number is also displayed, which helps to understand how accurately the wave numbers of upper or lower levels are known. This window also displays the wavelengths of previous and next lines. It contains a graphic field as well which displays the hyperfine structure of the transition only if A and B of both levels are known. The width of the structure is shown MHz and milliKayser (mK). On the other hand if the line is not classified this section remains blank. In case the line is not classified then by selecting "Select for Entry" button the line is classified with one of the list suggestion. For classifying the spectral line with correct suggestion requires either laser excitation of the line resulting in a hyperfine structure which matches with one of the list suggestion or by comparing the list suggestions with hyperfine structure profile of the spectral line in FT-Spectra.

The third section displays graphically the hyperfine structures for all the suggestions in the middle section to give a fast overview. The difference in wavenumber of a specific suggestion with the center of gravity wavenumber of line is displayed at the top left most corner of each graphic field. Figure 5.5 shows the main window of classification program with the classification of line at 5134.931 Å. This line is correctly classified by suggestion 5 as shown in middle window (Figure 5.6).
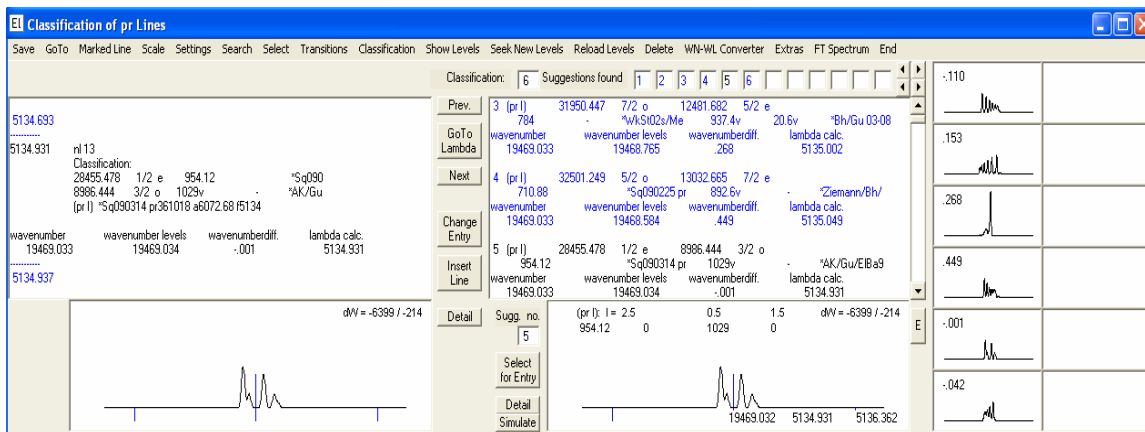
Figure 5.6: Main window of classification program with classification of line 5134.931 Å.

Important features of classification program:

i. Easy navigation through different spectral lines using **prev.** and **next** buttons.

ii. Out of thousands of spectral line any lines can be selected using **Goto Lambda** button.

iii. A new line can be inserted in the wavelength table without opening the wavelength file using **Insert Line** button. A window appears in which important information related to the line can be entered such as intensity of the line. In the comment field one can enter whether the line is atomic or ionic, when and who discovered the level connected to this line, the excitation and fluorescence wavelengths etc.

iv. For an already selected suggestion one can edit the parameters related to the line using the **Change Entry** button. Insert line and Change line buttons are convenient way of inserting and changing spectral line information in the wavelength table without actually opening the wavelength file manually.

v. The **Detail** button displays graphically the hyperfine structure of the selected suggestion related to the current spectral line. The display contains the level scheme showing transitions between hyperfine levels of upper and lower levels. Also shown are the spectroscopic parameters of the two combining levels.

vi. The **Select for Entry** button selects a particular suggestion from the suggestion list for classification of the spectral line and adds the selected transition to the line in the wavelength table. Thus its possible to classify a line as a selected transition between two levels.

vii. The **Simulation** button displays the simulation of the selected suggestion from the suggestion list for classified or unclassified line. It automatically takes the angular momenta and hyperfine interaction constants for upper and lower levels and displays the hyperfine structure of the combination.

viii. **Save** option in the menu bar saves the modified wavelength file.

ix. Navigation through different lines and to beginning and end of file can also be done by using **Goto** option in menu bar.

x. Two lines can be marked for later on movement to these lines using **Markline** option in menu bar.

xi. Hyperfine structure displayed in graphic fields can be expanded or shrinked using **Scale** option in menu bar.

xii. The **Setting** option in menu bar sets certain parameters for the classification program such as Wavelength/Wavenumber difference limit, Wavelength limit for fluorescence lines, Doppler width, Nuclear spin quantum no. Ionization limts.

xiii. The Search options in the menu bar sets the search criterion for searching transitions connected to a spectral line and include atomic levels, ionic levels, both, transitions with certain ΔJ i.e. +1, -1 or 0, or transitions with any arbitrary ΔJ (sometimes the J value of a level is not known or is doubtful).

xiv. **Select** option in menu bar either select all lines in wavelength list or selects lines based on specific comments, energy of level and intensity of line.

xv. **Transition** option in menu bar has options which display all positive fluorescence and negative fluorescence lines, transitions list to upper level, transition list to lower level.

xvi. **Classification** option in menu bar either activates or suppresses the classification routine.

xvii. **Show levels** option in menu bar displays the list of all atomic or ionic levels sorted either according to level energy or by J values and parity.

xviii. **Seek New Levels** option in menu bar seeks a suggested new level based on current line, on some special level, on fluorescence lines and on A and J values.

xix. **Reload Levels** in menu bar reloads the atomic and ionic levels from the updated level files.

xx. **Delete** option in menu bar deletes a classification or the current line.

xxi. **WN-WL Converter** option in menu bar contains a sub program window that can be activated, which converts the wavelength into wave number, or wave number into wavelength automatically using Peck and Reeder dispersion formula. It also displays the difference between two wavelengths in wave number or difference between two wave numbers in terms of wavelength.

xxii. **FT Spectrum** option in menu bar displays FT Spectrum in a separate window. This window displays the FT Spectra graphically, if mouse pointer is clicked at a particular point wavelength in air and in vacuum is displayed.
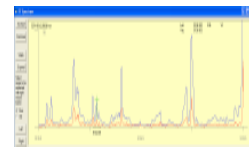
5.3.1.1 Simulation Program

The simulation program is part of the classification program and is used to simulate and display the hyperfine structure of the selected transition for classified or unclassified line. Since it is activated from classification program therefore it automatically takes the angular momenta values and hyperfine interactions constants for both upper and lower levels. Nevertheless, it allows changing all these values. Simulation program has the ability to overlap the experimentally recorded linearized hyperfine pattern or the hyperfine structure in FT spectra on to the simulated hyperfine structure. Simulation can

be accepted and the line can be classified if the simulation matches with the experimentally recorded hyperfine structure or it matches with the well resolved hyperfine structure in FT spectra. For analysis angular momenta values, hyperfine interactions constant, nuclear spin and Doppler width can be changed in the simulation program. An unclassified line can be classified by simulating the hyperfine structure to either an experimentally recorded structure or to a well resolved hyperfine structure in FT spectra. If the simulation matches then simulated spectroscopic parameters of the transition i.e. J values and A and B values can be used as starting point for further fitting the experimentally recorded structure and subsequently identifying the levels involved in the transition. Figure 5.7 show the simulation of line at 5134.931 Å, the simulated curve overlaps the hyperfine structure extracted from FT spectra.
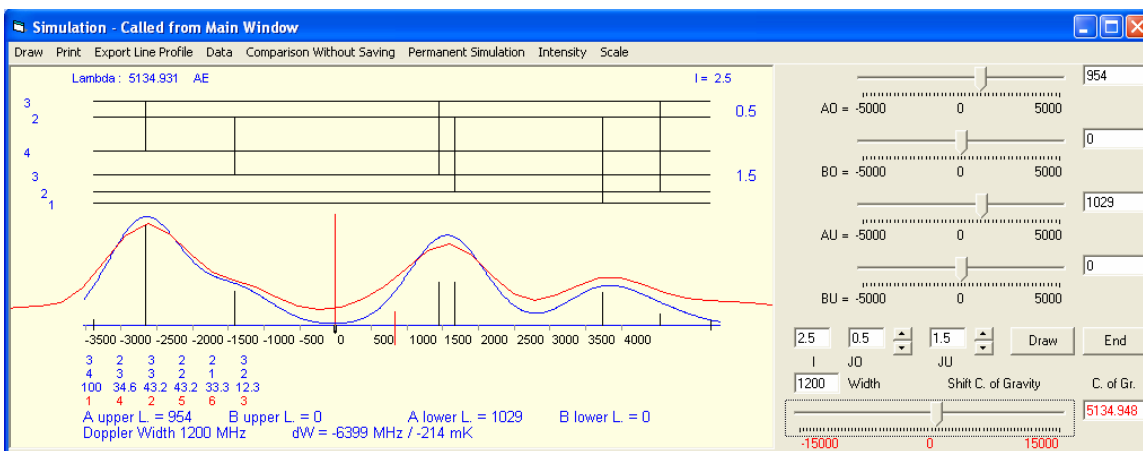
Figure 5.7: Simulation of line at 5134.931 Å with overlap from FT spectra.

5.3.1.2 Classification of a Line by its Hyperfine Structure
        (Already known levels)

For any spectral line in FT-Spectra, classification program shows a large number of suggestions indicating the transition between two levels with their corresponding hyperfine structure in graphic field. This is particularly true for Praseodymium which has large number of levels with high line density. A line can be classified if the hyperfine structure of a specific transition in the listed suggestion not only matches in shape but the peak positions are also coincident with hyperfine structure shown in FT-Spectra. This can only be done if the hyperfine structure of a line in FT has good S/N ratio and does not involve in a blend. A line at 5783.964 Å has S/N ratio of 53 and was not classified. After inserting this line in classification program, one of the suggested transition has a similar shape and peak positions as displayed in FT-Spectra. The suggestion is selected as the classification of this line by pressing the button "**Select for Entry**". The line is classified as a transition between 22150.902 cm^{-1}, odd parity, J_o = 13/2, A_o = 322.56 MHz and 4866.53 cm^{-1}, even parity, J_u = 11/2 and A_u = 867.997 MHz, B_u = -50.319 MHz and is stored in the wavelength table. Finally by selecting "**Save**" option, the modified wavelength file is saved. Figure 5.8 show the classification program with FT-Spectra for

the classification of line 5783.964 Å. In this way hundreds of lines were classified by our group.
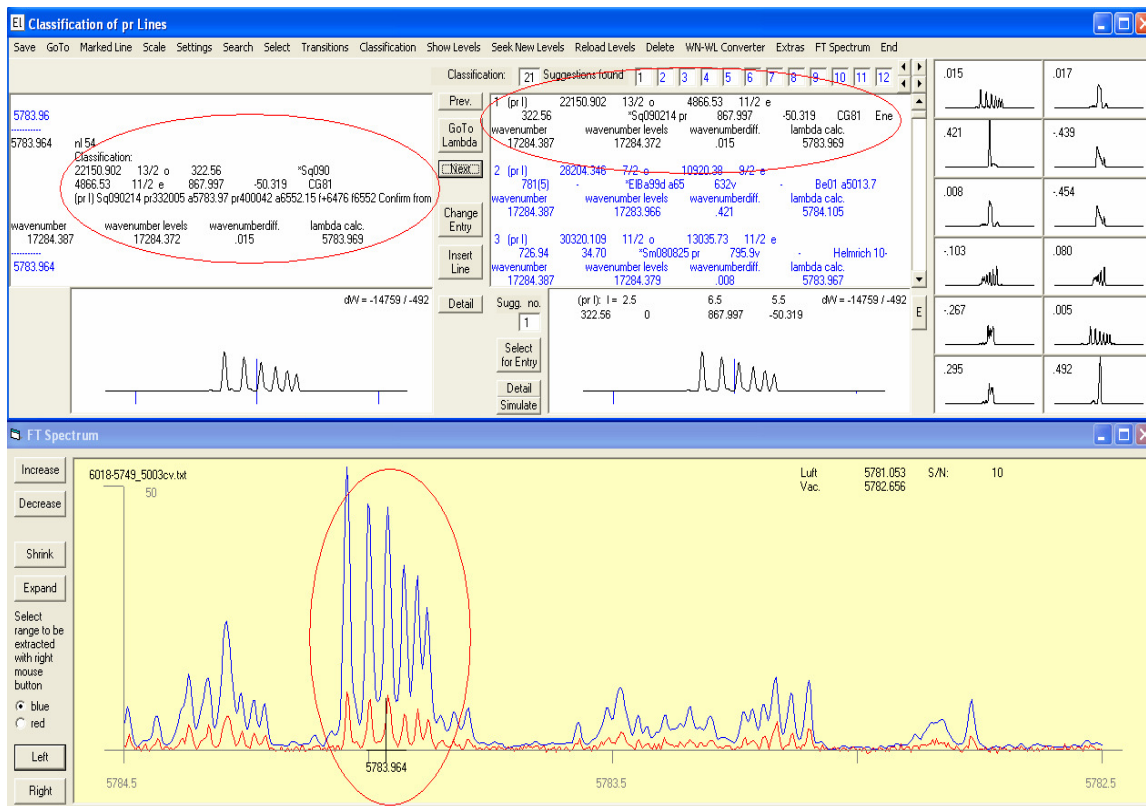
Figure 5.8: Classification of line at $\lambda = 5783.964$ Å by a transition between $\mathbf{22150.902^o_{13/2}}$ **cm^{-1}** and $\mathbf{4866.53^e_{11/2}}$ **cm^{-1}**.

5.3.1.3 Determination of a New Level by Combination of Wave Numbers

It is evident from the inspection of FT-Spectra for praseodymium that large number of lines were/are yet to be classified. Furthermore both for unclassified and classified lines large number of new energy levels were/are not accounted for. In view of this complexity one can make use of several of the search strategies present in the classification program for finding new levels.

When inserting the wavelength of a line in the classification program, the program calculates the wave number of the line and then search for differences of level energies which fit (within some limit) the wave number. These transitions are called suggestion. If the hfs constants of a combining level are known, also the expected hfs pattern is shown and can be compared with the pattern in the FT-Spectra (or with the recorded LIF pattern). If the hyperfine structure displayed in the FT-Spectra or the hyperfine structure resulting from the experimental excitation of line does not match any of the suggestions listed, then one can safely assume that at least one of the combining level is unknown.

One of the search strategies is to use the wave number of the unclassified line and making use of Ritz combination principle [129]. The new point in this procedure is just that the verification of classification becomes possible by the introduction of a new level including its hyperfine structure parameters.

The search procedure is based on the parity assumption of new level, for example taking the parity of the new level to be ***odd***. Now from the list of known even levels, the level with lowest energy is taken and the wave number of the unclassified line is added to the energy of this level giving the energy of the predicted new odd parity level in wave numbers. In the next step the wave number of all other lines in the line list are added to other even level energies. If the energy obtained in this way coincides, within a certain margin of uncertainty, with the energy of the predicted new odd parity level then for such additions the even parity levels with wavelengths are listed. The whole procedure is repeated again but now taking the next higher even level in the list. Completing the process for all even parity levels give a number of possible new odd parity levels. The J-value for these levels can easily be determined by using selection rules for the combination of levels. For each of these transitions it is possible to simulate the hyperfine structure by varying the A- and B-values of the new odd parity level keeping fixed the A- and B-values of the combining even parity level. If for this combination the simulation is not possible then it is excluded. But if the simulation is possible then one gets an estimate of the A- and B- values of the new odd parity level using the known A- and B- values of the known even parity level. By introducing this new level the hyperfine patterns of other lines can be calculated and compared with the structures in the FT-spectra. If such comparisons with FT-spectra are positive the existence of new level is confirmed.

If none of the odd levels listed in this way conforms to the conditions mentioned above then the new level is searched with ***even*** parity. This strategy, developed while investigating the spectra of Ta, is not useful for Pr since there are too many lines in the wavelength list, thus too many coincidences just by accident appear.

5.3.1.4 Determination of a New Level by Fluorescence Lines

A possible new energy level involved in an excitation of an unclassified line by laser light can also be determined by making use of the exact wavelengths of the observed fluorescence lines. When seeking a new level, the center-of-gravity wavelength (in air) of the excitation line is inserted in the classification program as the current line. The program works in the following steps:

(i) The measured exact fluorescence wavelengths $\lambda_{F,i}$ are inserted in the classification program using the option "**Search for New Levels based on Fluorescence Lines**", as shown above.
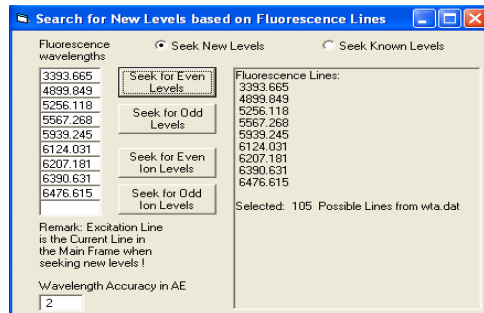
(ii) Program calculates the wave number of the line, takes the lower levels from the list of known levels and add the wave number of the line. This gives the wave number of the hypothetical new upper level.

(iii) Program now calculates the fluorescence transition wavelengths from the new hypothetical upper level. The calculated fluorescence lines which corresponds to the observed fluorescence wavelengths $\lambda_{F,I}$ with in some limit are displayed in the list, as shown in figure 5.9.

(iv) The hypothetical level which explains most of the fluorescence lines $\lambda_{F,I}$ can be treated as the level which is being searched.
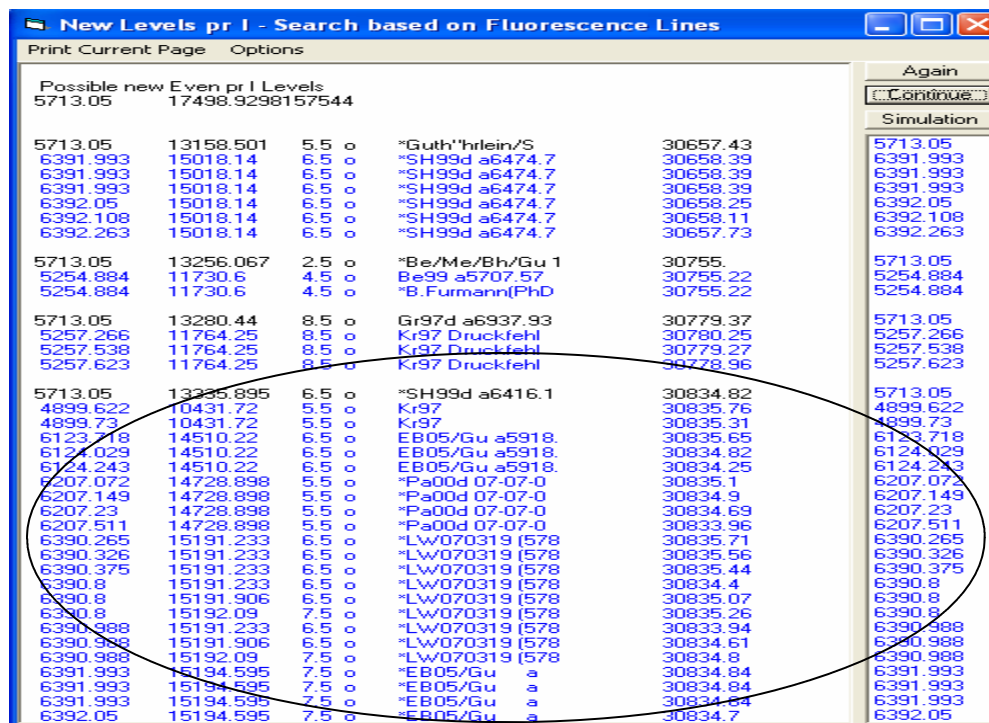
Figure 5.9: Determination of energy level $30834.815^{e}_{13/2}$ $\mathbf{cm^{-1}}$ at an unclassified line 5713.05 Å

5.3.1.5 Determination of a New Level by Analysis of the Hyperfine Structure

A possible new level in an excited transition can be identified if the pair of angular momenta and pair of hyperfine constants for lower and upper levels are known. These spectroscopic parameters are determined by simulating the recorded hyperfine structure. The method works as follows:

(i)   Simulation or fitting procedure (to be discussed later) of the recorded hyperfine pattern of the line gives angular momentum values and hyperfine interaction constants for combining levels i.e. J_o, J_u, A_o, B_o, A_u, B_u.

(ii) Using the simulated or fit parameters lower or upper level is searched in the data base of known levels.

(iii)   Unknown lower or upper level is calculated using the wave number of the investigated line.

(iv)   New found levels is introduced in the classification which generates a transition list. For correct identification of the unknown level the fluorescence line observed should appear in the transition list.

As an example consider an excitation of line at $\lambda = 5785.34$ Å where a new upper level was discovered. A widely splitted hyperfine structure was recorded on fluorescence wavelengths 5321 Å, 5361 Å, 5675 Å, 5693 Å, 5883 Å. Fitting the recorded hyperfine structure of the line gave $J_o = 17/2$, $J_u = 17/2$, $A_o = 452.1$ MHz, $B_o = 34.90$ MHz, $A_u = 208.1$ MHz and $B_u = 20$ MHz. Based on these fitted parameters, initially an unknown upper level was searched using the search routine *"Seek New Levels Based on A and J"* in classification program. The classification program displays possible new upper levels both in even and odd configurations along with transition list as shown in figure 5.10.
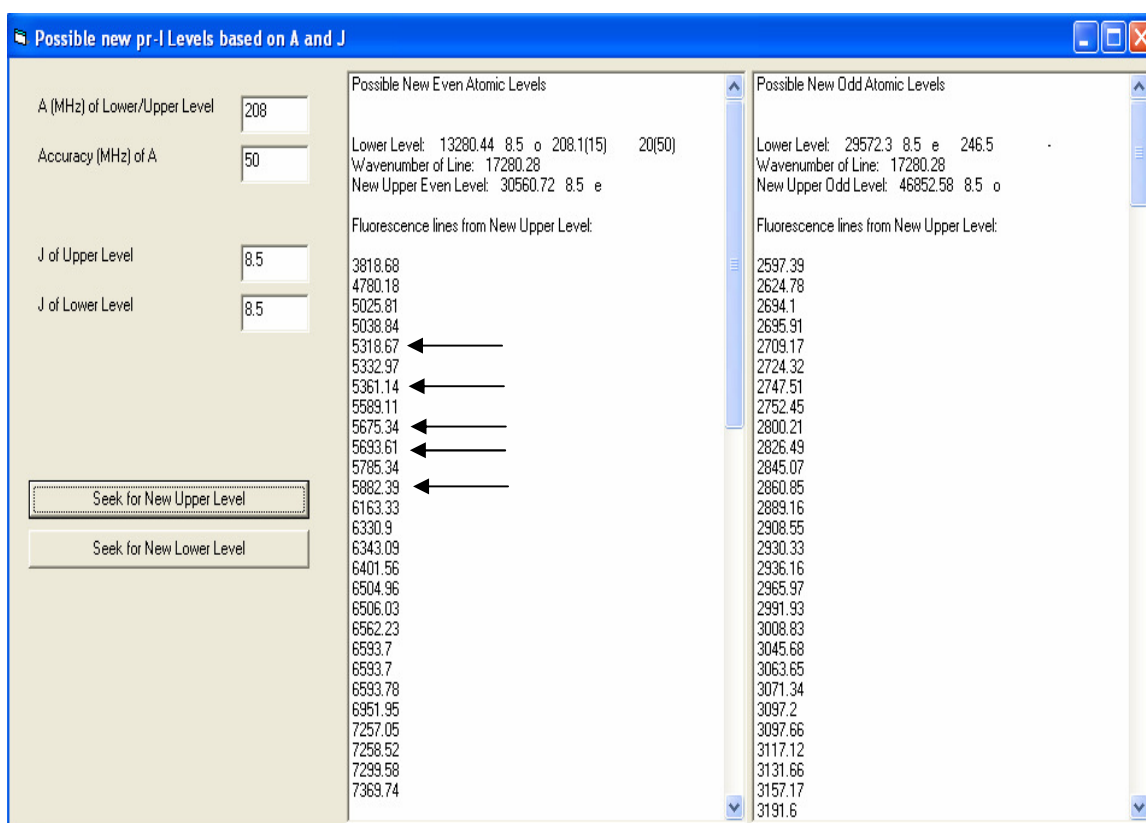
Figure 5.10: Possible new upper levels for the excitation of line at 5785.34 Å

In the even configuration first listed suggestion explained all the observed fluorescence lines. The excitation is explained as a transition from a lower level $\mathbf{13280.44^{o}_{17/2}\,cm^{-1}}$ to a new upper level $\mathbf{30560.725^{e}_{17/2}\,cm^{-1}}$. The level scheme for this newly found level is given figure 5.11.

17/2, e, 30560.725, 452.3 MHz, 34.94

5883 Å

5785.34 Å

5693.56 Å

5318 Å

5675 Å

15/2, o, 13565.52, 916.6 MHz
12 MHz

17/2, o, 13280.44, 208.1
MHz

5361 Å

15/2, o, 13002.05, 316.6 MHz
29 MHz

19/2, o, 12945.51, 837.1 MHz, -7
MHz

19/2, o, 11913.16, 829.9 MHz, 2 MHz

17/2, o, 11764.25, 892.5 MHz, -10 MHz
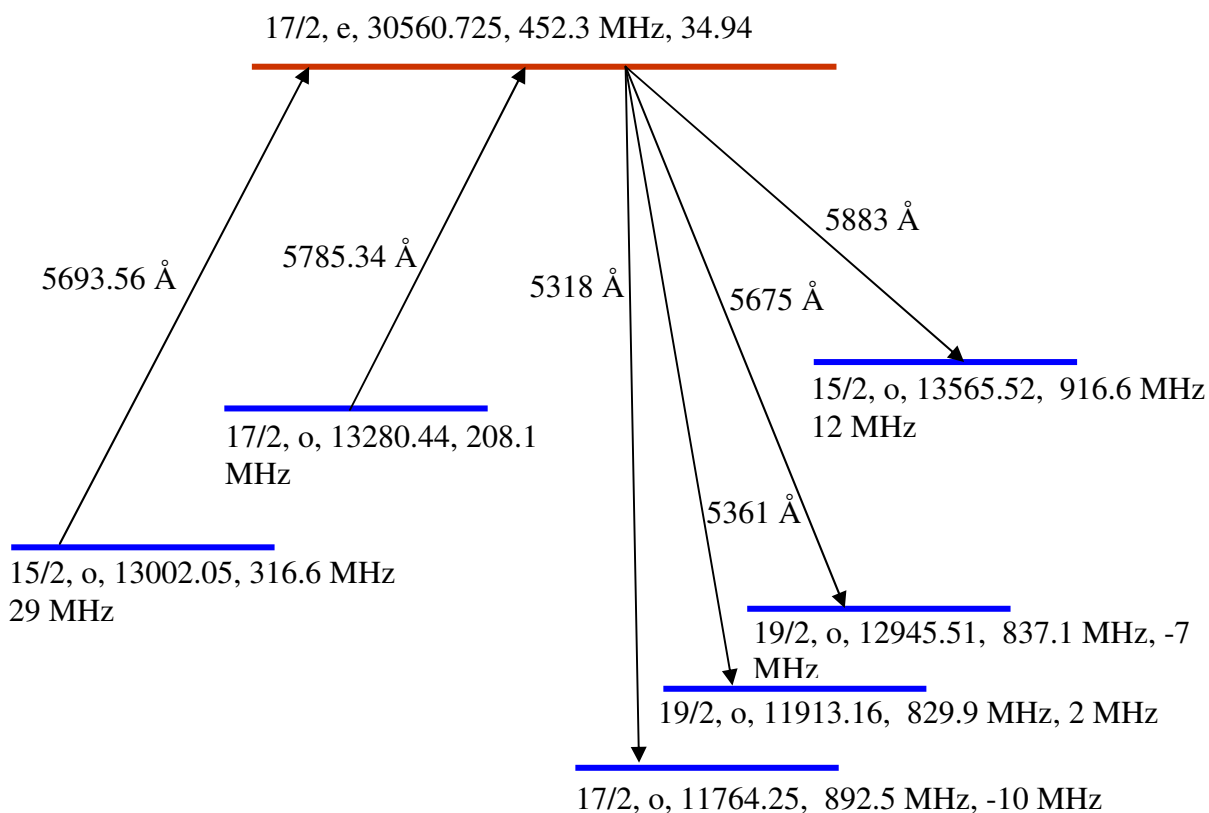
Figure 5.11: Level scheme for new level $\mathbf{30560.725^{e}_{17/2}}$ **cm^{-1}** at line $\lambda = 5785.34$ Å.

5.3.1.6 Determination of Both New Lower and Upper Levels

All the above methods are based on the assumption that one of combining level is already known. In situations where both lower and upper levels are unknown, one relies on the observed fluorescence wavelengths. For the method to work at least three or more fluorescence lines from the unknown upper level have been observed to decay to known lower levels. The basic idea behind this procedure is to look for known lower levels to which fluorescence lines from the unknown upper level decay.

As a first step the exact values of fluorescence wavelengths are measured. Then the wave number differences i.e. $\Delta_{ij} = |\sigma_i - \sigma_j|$ for each pair of fluorescence lines are determined. Now from the data base of known levels, lower levels with same parity are search based on the criteria that the differences between the wave numbers of these levels are within some margin of error equal to the wave number differences Δ_{ij} of fluorescence lines. Once all the wave number differences are accounted for, meaning that all the lower levels are found with the difference of wave numbers any pair of levels corresponds to the wave number difference for any pair of fluorescence lines. If such a set of lower levels is found then by using their wave numbers and the wave numbers of the fluorescence lines, the level energy of the unknown upper level can be estimated. Parity of the estimated upper can be set opposite to that of the set of lower levels. Now the level energy of the

excitation lower level is determined using the energy of the upper level. Hyperfine constants and J-values of the unknown lower and upper levels can be determined by the fit of the structure. This procedure was adopted while solving one of the problems involving both unknown lower and upper levels. This is discussed in section 6.2

5.3.2 Mathematical Fitting of hyperfine structure pattern

The recorded hyperfine structure profile can be best fitted to an appropriate mathematical function using the "method of least squares". The method is an iterative process in which a curve is fitted to data points so as to minimize the sum of the squares of the deviation of the points from the curve. A pre-fit analysis of the recorded hyperfine structure profile is usually helpful in evaluating spectroscopic parameters. The hyperfine splittings of fine structure levels are characterized by a number of spectroscopic parameters such as nuclear spin quantum number I, angular momentum J values of upper and lower levels and hyperfine interaction constants A, B.

The amount of splitting of a fine structure level into hyperfine structure levels depends in most cases on the magnitude of the hyperfine interaction constant. So by inspecting the recorded hyperfine structure one can roughly suggest the magnitudes of hyperfine constants. Assuming both and A_o and A_u are positive (which is mostly the case with praseodymium), then from relative intensities of diagonal ($\Delta F = \Delta J$) components it can be decided whether $A_o > A_u$ or $A_o < A_u$ accordingly if the relative intensities of diagonal components are decreasing towards shorter or longer wavelength. From the relative intensities and positions of diagonal components one can suggest the J values of the combining levels with an error of ±1. The change in J values of fine structure levels for transition from lower to upper level can also be suggested. If the off-diagonal ($\Delta F \neq \Delta J$) components appear on both sides of diagonal components then there is no change in J value in going from lower to upper level i.e. $\Delta J = 0$. If off-diagonal components appear either on the longer or on the shorter wavelength side then the J value changes by +1 or -1 respectively. The recorded hyperfine structure profile can also be simulated using the simulation program (see section 5.3.1.1).

Using preliminary values of the spectroscopic parameters and the center of gravity wavelength of experimentally recorded data, the hfs patterns must be fitted with an appropriate mathematical profile function. Depending on the intensity profile of the recorded structure one can choose between **Gaussian** or **Lorentzian** functions. If the recorded hyperfine pattern show the characteristics of both Gaussian and Lorentzian profiles then a convolution or mixture of both functions is used. Such a function is known as the **Voigt** function. A especially designed computer program for this purpose known as **Fitter** is used which fits the recorded structure to a function. The program evaluates the hyperfine constants and center of gravity wavelength for the fitted structure of a laser excited hyperfine structure profile or of the hyperfine structure profile of a line extracted from FT spectra.

5.3.3 Fitter

Fitter program was developed in University of Bundeswehr Hamburg, Germany [130] and is used for the calculation of spectral intensity distributions associated with various hyperfine structures recorded using laser induced fluorescence spectroscopy. These hyperfine structures are electronically recorded in digital form as a function of changing laser frequency. In order to extract the physical information contained in the recorded hyperfine structure of an excited line or a profile from FT-Spectra. The fitter program fits the recorded structure to a function using the method of least squares and calculates the hyperfine constants and center of gravity wavelength. Before the structure can be fitted the recorded file containing the data points must be converted in a form acceptable to the fitter program.

The intensity distribution of an excited transition is recorded in time domain i.e. as a function of equidistant time intervals. Due to scanning behavior of laser the data points representing the intensity distribution are not equally spaced in frequency. Therefore by a process known as linearization the recorded spectrum which is in time domain I(t) must be converted into frequency domain I(ν) using equal marker etalon signal which is simultaneously recorded with the LIF spectrum. Practically speaking the linearization process starts by supplying to the electronically recorded data file the start wavelength of the laser scan and free-spectral range (FSR) of the marker etalon.

The requirement for data points to be equally spaced stems from the fact that mathematical least square routine has a faster and better convergence towards best fit situation for data points. Program calculates the position of individual components and hyperfine constants by the following relation

$$\nu = \nu_c + \alpha_o \cdot A_o + \beta_o \cdot B_o - \alpha_u \cdot A_u - \beta_u \cdot B_u \qquad 5.1$$

where α_o, β_o, α_u, β_u are the Casimir factors for upper and lower energy levels respectively (see section 3.6). Intensity of each component is taken from the theoretical intensity formula using 6j symbols (see section 3.7). A suitable mathematical model (see section 4.3.7) is used with physical boundary conditions as input parameters. By gradually varying the values of these parameters, the model progressively evolve and adjusted according to the method of least squares or Gauss-Newton method to the series of experimentally recorded data points, i.e. minimizing squared error sum given by the function ESS,

$$ESS = \sum_{k=1}^{n} [I_\nu(k) - I_\nu(\nu_k, \vec{a})]^2 \qquad 5.2$$

where $I_\nu(k)$ is the measured intensity at a given frequency point ν_k, $I_\nu(\nu_k, \vec{a})$ is the calculated intensity at the corresponding position and the vector $\vec{a}$ is a set of fit parameters. Using Tayler series the expansion of above equation gives a system of nonlinear, inhomogeneous equations. The number of such equations in the system equals

the number of parameters in vector $\vec{a}$. The method of least square is an iterative process so a solution of these equations is obtained in such a way that the deviation from measured intensity becomes less and less and a new set of parameters values are obtained for next iteration. The procedure is repeated until termination criterion is reached. Important input parameters are hyperfine constants of lower and upper levels, the frequency of a certain hyperfine component, the half width of the components, the underground intensity and center of gravity wavelength.

This iterative procedure is complicated and the program runs only in pure mathematical sense with only objective of minimizing the squared error sum. This pure mathematical evaluation sometimes leads to unreasonable values of the physical parameters such as negative intensities or negative frequencies. One way of avoiding this is to reduce the number of input parameters. This can be done by fixing certain parameters according to a specific situation. For example if one of the levels involved in a transition is known then by fixing the hyperfine constants of this level the number of parameters are reduced by 2. If half-width is known then the number of parameters is reduced by 1. Furthermore this can also be done by coupling the intensities of various components together. So by coupling the coupling parameters are reduced by 1. Coupling of components can also be done in situations where saturation effects change the relative intensity of hyperfine components.

In addition to single line fit, fitter program can also be used for multi-line fitting. In cases where simultaneously more than one hyperfine structure patterns are overlapped such as in a blend situation or more than one isotope are involved in a transition multi-line fitting procedure is adopted. Figures 5.13, 5.14 and 5.15 show a single line, two line and a multi-line best fit situations respectively.
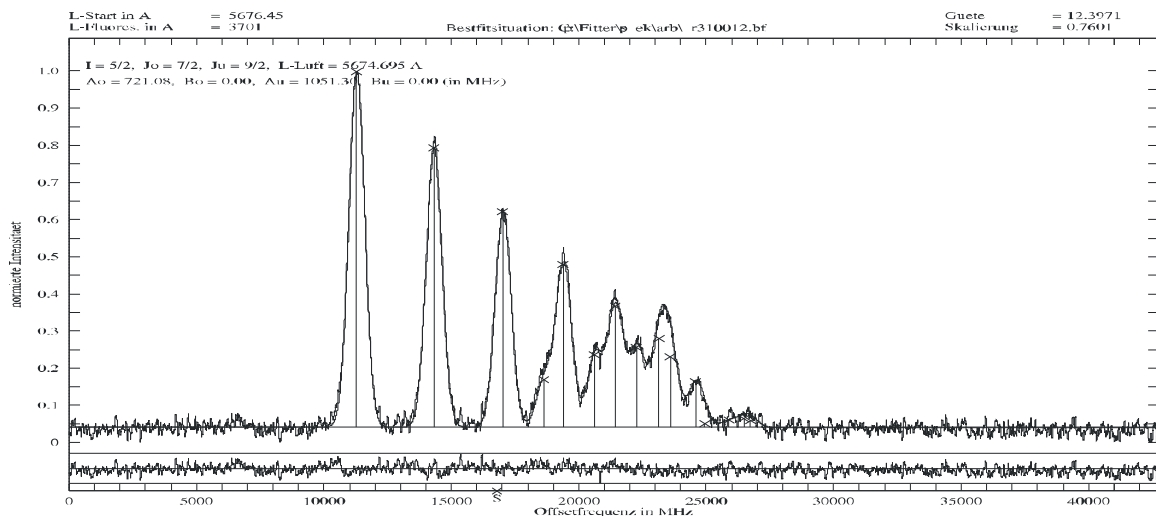
Figure 5.13: Best fit situation for single line fit of Pr-I line at λ = 5674.69 Å
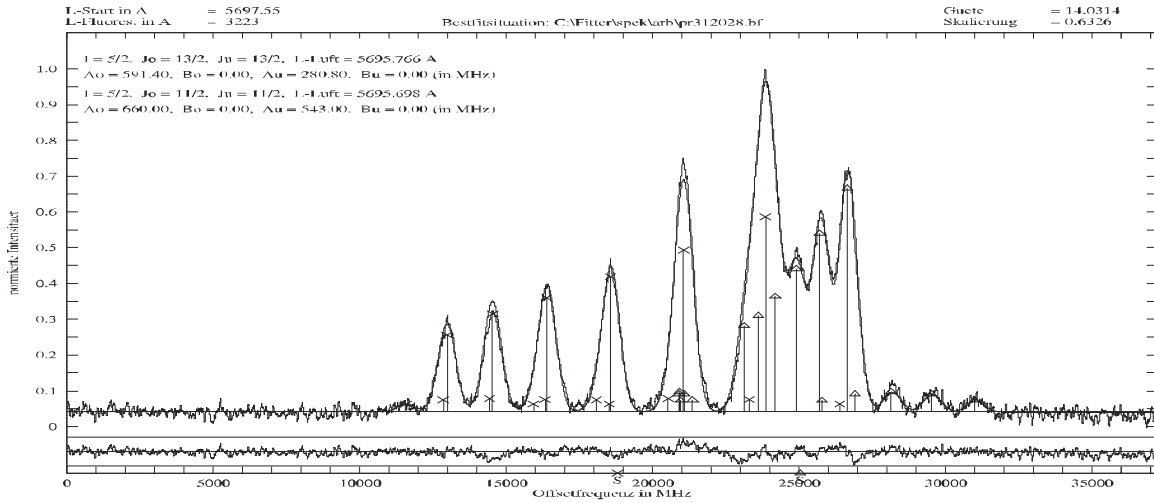
Figure 5.14: Best fit situation for two line fit of Pr-I lines at λ = 5695.77 Å and 5695.69 Å
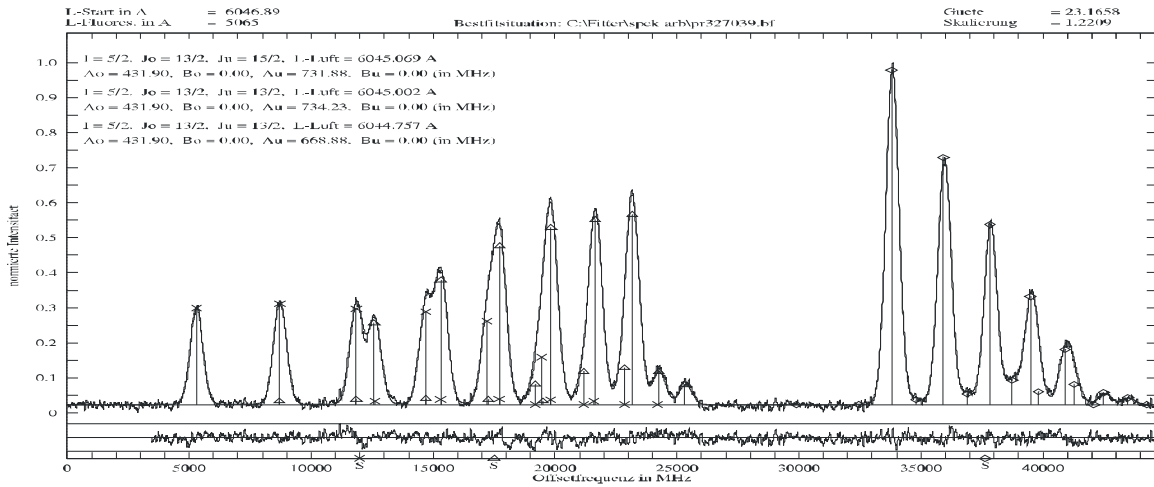
Figure 5.15: Best fit situation for three line fit of Pr-I with transition from three lower levels to a single upper level at lines 6045.069 Å, 6045.002 Å and 6044.757 Å.

5.4 Selection Rules

The optical transitions between hyperfine structure levels of fine structure levels are governed by following selection rules:

Only those transitions are allowed for which the total electronic angular momentum quantum number J obeys the selection rule

$$\Delta J = 0, \pm 1$$

but

$$J = 0 \rightarrow J = 0 \text{ is forbidden}$$

Parity:

Even (gerade) levels solely combine with odd (ungerade) levels

For transitions between hyperfine structure levels of two fine structure levels (assuming that transition between fine levels is allowed), the total angular momentum quantum number F of the atom obeys the selection rule

$$\Delta F = 0, \pm 1$$

but

$$F = 0 \rightarrow F = 0 \text{ is forbidden}$$

For a transition from an initial level $\left|\mathbf{i}\right\rangle$ to final level $\left|\mathbf{f}\right\rangle$, the selection $\Delta J = +1$ imply

J(initial level) < J(final level)

for $\Delta J = -1$

J(initial level) > J(final level)
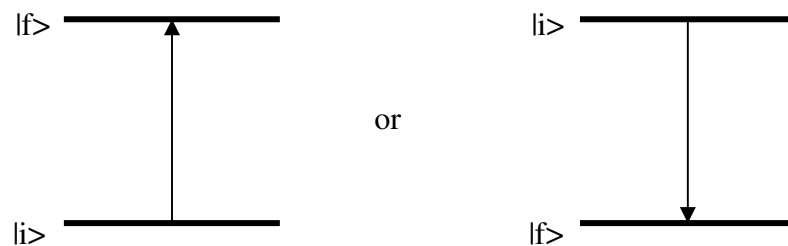
CHAPTER 6
EXPERIMENTAL RESULTS AND DISCUSSION (PART I)

ANOMALOUS INTENSITY DISTRIBUTION OF THE HYPERFINE COMPONENTS OF PRASEODYMIUM-I LINES
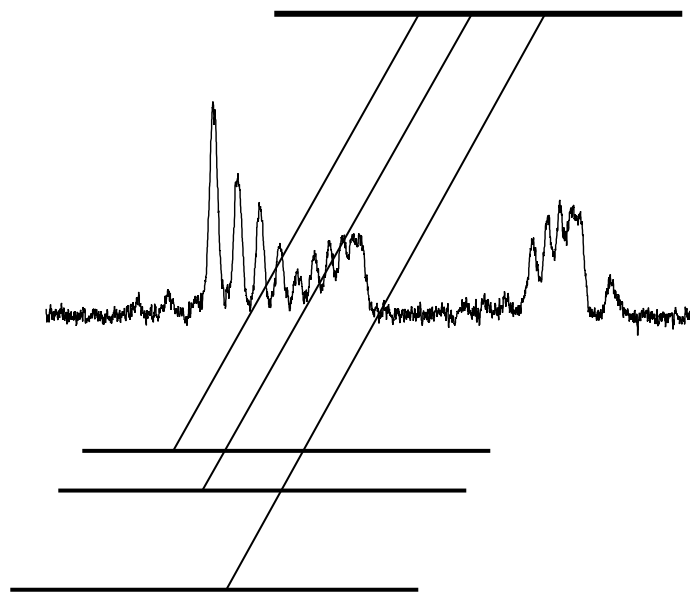
6.1 Anomalies in Line Strengths and Shapes

According to central field approximation the states of atoms are classified as belonging to various electron configurations. These configurations satisfactorily explain the marked regularities either in the spacing of levels or in the strength and shape of transitions. Breakdowns in such regularities occur in various forms such as in displacement of energy levels from their expected positions, line strengths and line shapes anomalies. All such anomalies are explained in terms of configuration mixing or configuration interactions according to which energy levels of the same parity and J-value arising from two or more configurations either overlap or are very close to each other. In such multi-configuration scheme the basis set includes functions from two or more configurations and total electronic angular momentum J is no longer a good quantum number, rather F is a good quantum number. Experimentally effects of such multi-configuration behavior, energy levels exert influences on each other and are usually termed as perturbations which manifest themselves as shifts in energy levels or changes in transitions probabilities or line intensities and shape anomalies. These effects are expected and are more pronounced in spectra of elements having high density of energy levels. Praseodymium is one such element belonging to Lanthanide group having elements with very large number of energy level. During our investigation of the spectra of Praseodymium we excited a line which revealed unusual behavior in the distribution of intensities of hyperfine components.

6.2 Anomalous Intensity Profile of Hyperfine Components for the Excitation of Line at 5780.51 Å

The praseodymium has a very high spectral line density and correspondingly large number of energy level. Therefore most of the lines appear in a blend situation, as can be seen in FT-Spectra. The hyperfine structure of lines is either not resolved at all or is partially resolved. While investigating the spectral region from 5780.55 Å to 5780.25 Å, the hyperfine pattern for several lines were recorded. Some of these lines were classified using existing levels (see Table 6.1) and for the rest laser excitation for recording their hyperfine structure must be performed.

Table 6.1: List of lines investigated in the region 5780.55 Å to 5780.25 Å with their explanation

Excitation Wavelength λ_{air} (Å)	Lower level	Upper Level	Fluorescence wavelengths λ_{air} (Å)
5780.34	$9464.45^e_{13/2}$	$26759.707^o_{15/2}$	5315, 5556, 5875.78 6644.643
5780.40	$13727.48^e_{11/2}$	$31022.55^o_{11/2}$	4637, 4966, 5110, 5175 5403
5780.41	$15006.707^e_{5/2}$	$32301.715^o_{7/2}$	3774, 4242, 4717, 5302
5780.42	$11361.817^e_{3/2}$	$28656.732^o_{3/2}$	4503

The lines at 5780.51 Å and 5780.27 Å could not be explained using any of the existing levels by comparing their predicted hyperfine structure pattern with the line profiles of these two lines in FT-Spectra. Lines have good signal-to-noise ratio with relative intensity of 14 as can be seen in FT-spectra (see figure 6.1). Experimental investigation of lines was performed by setting the laser excitation frequency to the wavelengths of these lines and searching for fluorescence lines. LIF signal was observed on a number of fluorescence wavelengths i.e. 6182 Å, 5205 Å, 4836 Å, 4820 Å, 3372 Å with one very peculiar and interesting observation that at both excitation positions i.e. 5780.51 Å and 5780.27 Å same set of fluorescence wavelengths were seen. At one of the observed fluorescence wavelength i.e. 6182 Å, its LIF signal was recorded by scanning the laser wavelength from 5780.67 Å down to 5780.16 Å. A very broad hyperfine structure having approximately a width of 40 GHz with anomalous intensity distribution of the hyperfine components was recorded (see figure 6.2).

While investigating the atomic and ionic spectra of praseodymium blend situations are commonly observed, this is due to its high line density. The recorded structure (figure 6.2) could be associated with such a blend situation which means that the laser may have excited two or three transitions to two or three different levels which by chance have almost the same wave number difference. The recorded structure would then be a convolution of two or three hyperfine structures apparently depicting an excitation and fluorescence blend situation. In such a situation a same hyperfine structure pattern would not be observed on all observed fluorescence wavelengths. But contrary to this situation same hyperfine structure was recorded on all observed fluorescence wavelengths i.e. 6182 Å, 5205 Å, 4836 Å, 4820 Å, 3372 Å.
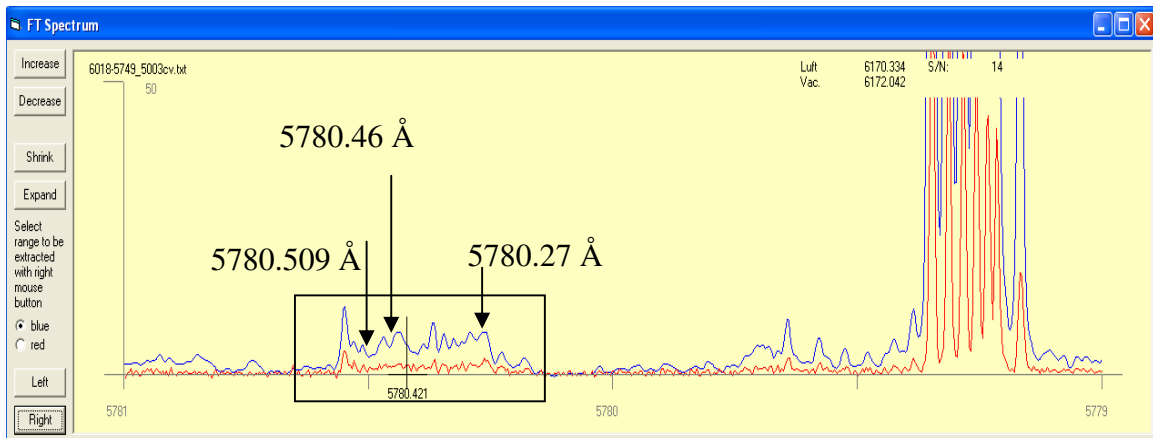
Figure 6.1: FT-spectra showing the line at 5780.51 Å.

The unusual behaviour of intensities of hyperfine components in the recorded structure could not be explained because normally for praseodymium which has a nuclear spin quantum number $I = 5/2$, six large or diagonal hyperfine components (valid for $J > I$) should be seen. Contrary to this if the whole structure is divided into three parts then in each part four or five large components are observed, see figure 6.2. Furthermore a sharp decrease in the intensities of the diagonal hyperfine components is also seen which is in

contradiction with the intensity rules for normal hyperfine structure patterns. Also, by carefully inspecting the recorded structure, it seems that the interval rule is not violated.
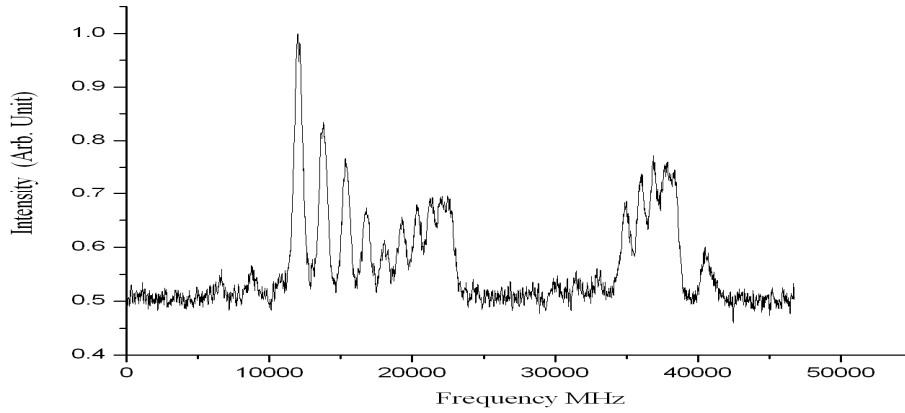
Figure 6.2: Excitation of Pr-I line with start wavelength 5780.67 Å at fluorescence wavelength 6182 Å. Clearly the intensity distribution of the recorded line is anomalous.

Therefore from these experimental observations, it was conclude that more than two levels combine in the excitation of this line. So two level schemes can be suggested, see figure 6.3. In one scheme three narrow spaced lower levels combine with a single upper level, this model is consistent with the observations that on all observed fluorescence wavelengths same hyperfine structure is seen. In the other scheme a single lower level combines with three narrow spaced upper levels so all three upper levels narrowly separated from each other may have same all fluorescence wavelengths. Nevertheless considering different J values of levels in triplet and J values of lower levels of fluorescence channels then it is highly unlikely that the same structure is seen on all observed fluorescence lines because of ΔJ rules.
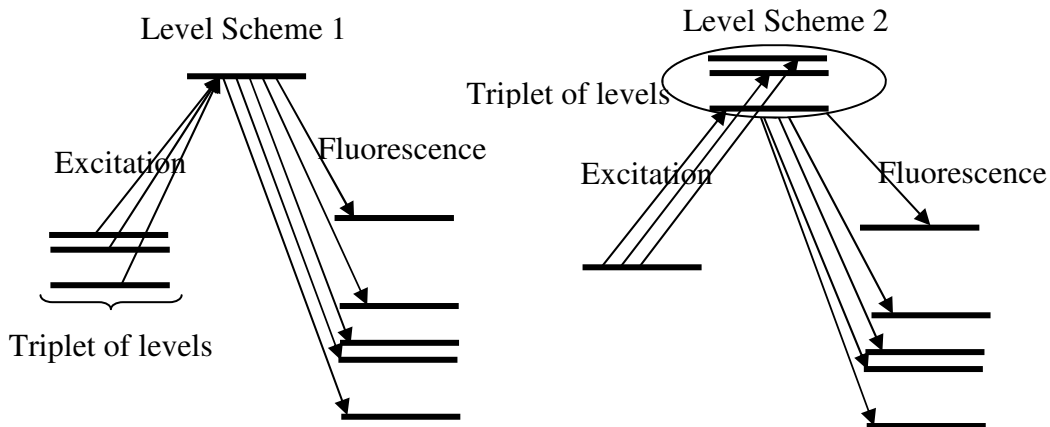
Figure 6.3: Suggested level schemes

Careful analysis of the recorded spectrum revealed following points:

i. Clearly an anomaly exists in the excited transition with start wavelength 5780.67 Å.
ii. Three closely spaced lower levels are involved (level scheme 1) in the excited transition.
iii. Structure at longer wavelength side with center of gravity excitation wavelength 5780.51 Å, has small components on both side of diagonal components, suggesting no change in angular momentum values in a transition between lower and upper levels i.e. $\Delta J = 0$.
iv. The spacing between diagonal components is same indicating high angular momentum, while the strong decrease of the intensity of diagonal components indicated small J-values.
v. The shorter wavelength side of the spectrum indicates a transition from another closely lying lower level with again disturbed intensity distribution of hyperfine components.
vi. At a little shorter wavelength i.e. 5780.26 Å another structure always appear on all fluorescence lines.
vii. The total width of the recorded structure is approximately 40 GHz.
viii. All wavelengths, excitation and fluorescence are measured in air.

In order to explain the anomalous behaviour of the excited transition we made use of the following assumptions:

i. Three closely spaced lower levels simultaneously excite a single upper level; hence the set of lower levels was termed as ***lower triplet***.
ii. Interval rule is not violated and the spacing between the components is given by Casimir formulas.
iii. By carefully inspecting the recorded hyperfine pattern, for the left most transition ΔJ is taken as '0', for the two right structures ΔJ is taken as '+1'.
iv. High values of angular momenta are involved i.e. $15/2_o - 15/2_u$ and/or $15/2_o - 13/2_u$.
v. In almost all transitions from level triplet to upper level three groups of hyperfine structures are observed, hereafter will be referred to as first, second and third group in order of decreasing center of gravity wavelength.
vi. Approximate center-of-gravity (cog) wavelengths for the three structures were estimated as 5780.509 Å, 5780.46 Å and 5780.27 Å.

With the above assumptions in mind the recorded structure was fitted using multiline fitting procedure taking different values of angular momenta for upper and lower set of levels. A reasonably good fit was obtained with the exception of the last group of hyperfine components, as shown in figure 6.4. Table 6.2 gives the best fit J and A values of the combining levels in the investigated line.
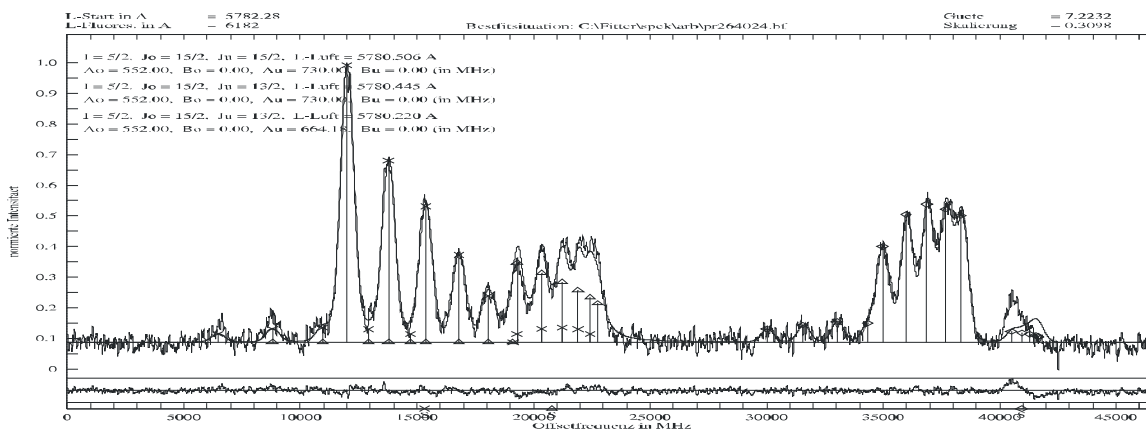
Figure 6.4: Multiline fit of the recorded hyperfine pattern for the excitation with start wavelength 5780.67 Å

Figure 6.2: Best fit values of structure recorded at 5780.51 Å
(For Pr B is taken as zero due to small value of Quadrupole moment)

Lower level			Upper level		
J_u	A_u (MHz)	B_u (MHz)	J_o	A_o (MHz)	B_o (MHz)
15/2	730	-			
13/2	730	-	15/2	552	-
13/2	664.18	-			

The data base of known levels is then searched using J and A values from the fitter program. No level was found whose J and A values are in agreement with the fitted values. It was then conclude that in the excited transition both lower and upper levels are up till now unknown.

6.2.1 Identification of Fluorescence Lower Levels Using Observed Fluorescence Lines

Since both the upper level and lower set of levels are unknown, the procedure outlined in section 5.3.1.6 is used. For the method to give reliable results all the observed fluorescence wavelengths from the unknown upper level are determined as accurately as possible. In order to measure the exact fluorescence wavelengths for all the decay lines of the unknown upper level, the discharge spectrum using in addition to the first, a second lock-in amplifier is also used. Then by using a computer program Comparison which works by comparing the LIF signal and recorded discharge emission spectrum with the high resolution Fourier transform spectra. This is done by shifting the recorded discharge spectrum over the fix FT-spectra such that peak positions in discharge spectrum matches with that of FT-Spectra. The exact fluorescence wavelength is then read by locating the position of LIF signal (see figure 6.5). This gives an accuracy of 0.005 Å much better than the resolution of monochromator which is 1 Å.
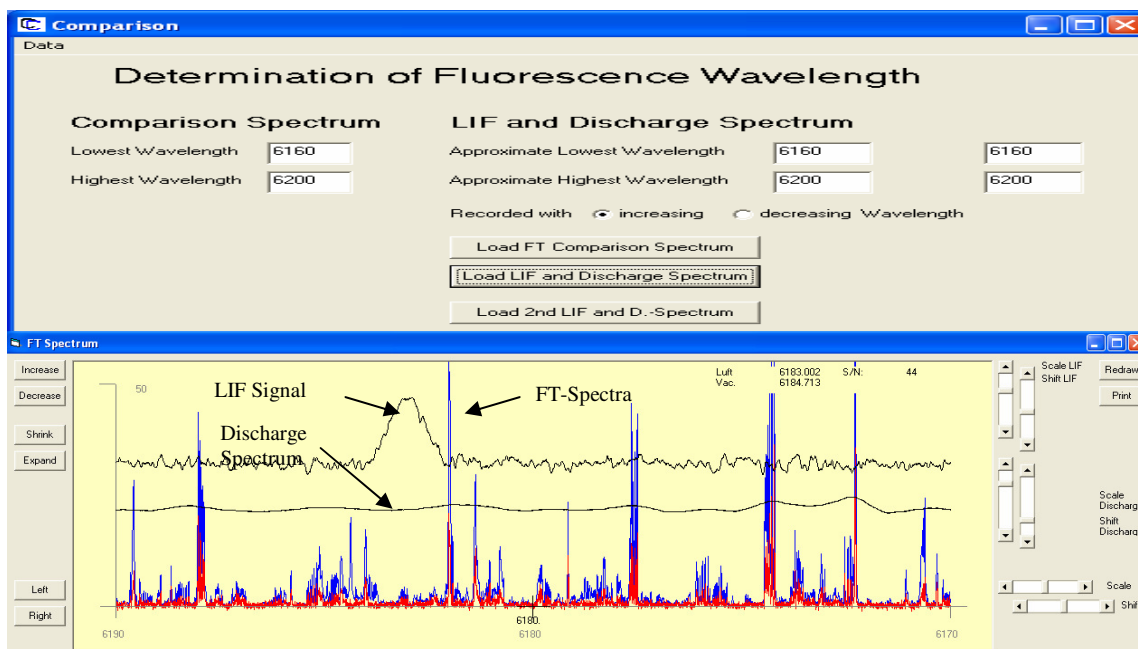
Figure 6.5: Determination of precise wavelength of the fluorescence line at 6183 Å using a computer program

The exact measure of fluorescence wavelengths for all the observed decay lines from the unknown upper level are given in Table 6.3 with their wave numbers and wave number differences in cm^{-1}. Now by using the method outlined in section 5.3.1.6 for the determination of both lower and upper levels in an excitation, the lower set of levels corresponding to fluorescence decay lines from the unknown upper level are searched in the list of known levels. The search within the same parity group is based on the criteria that the wave number differences of the observed fluorescence lines are comparable to the wave number difference of a pair of levels. For the found levels the wave number differences of each pair of lower levels are calculated, see figure 6.6 and Table 6.4. Within a certain margin of error the two differences are good in agreement, Table 6.3 and Table 6.4.

Table 6.3: Exact Fluorescence wavelengths & wave numbers for the excitation of line at 5780.51 Å

Observed Fluorescence wavelength λ_{air} (Å)	Determined Fluorescence wavelength λ_{air} (Å)	wavenumber (cm^{-1})	Difference in wave numbers of fluorescence lines (cm^{-1})
6183	6183.093	16168.661	
5205	5205.159	19206.360	3037.699
4836	4836.077	20672.140	1465.78
4820	4820.146	20740.463	68.323
3372	3372.846	29640.037	8899.574
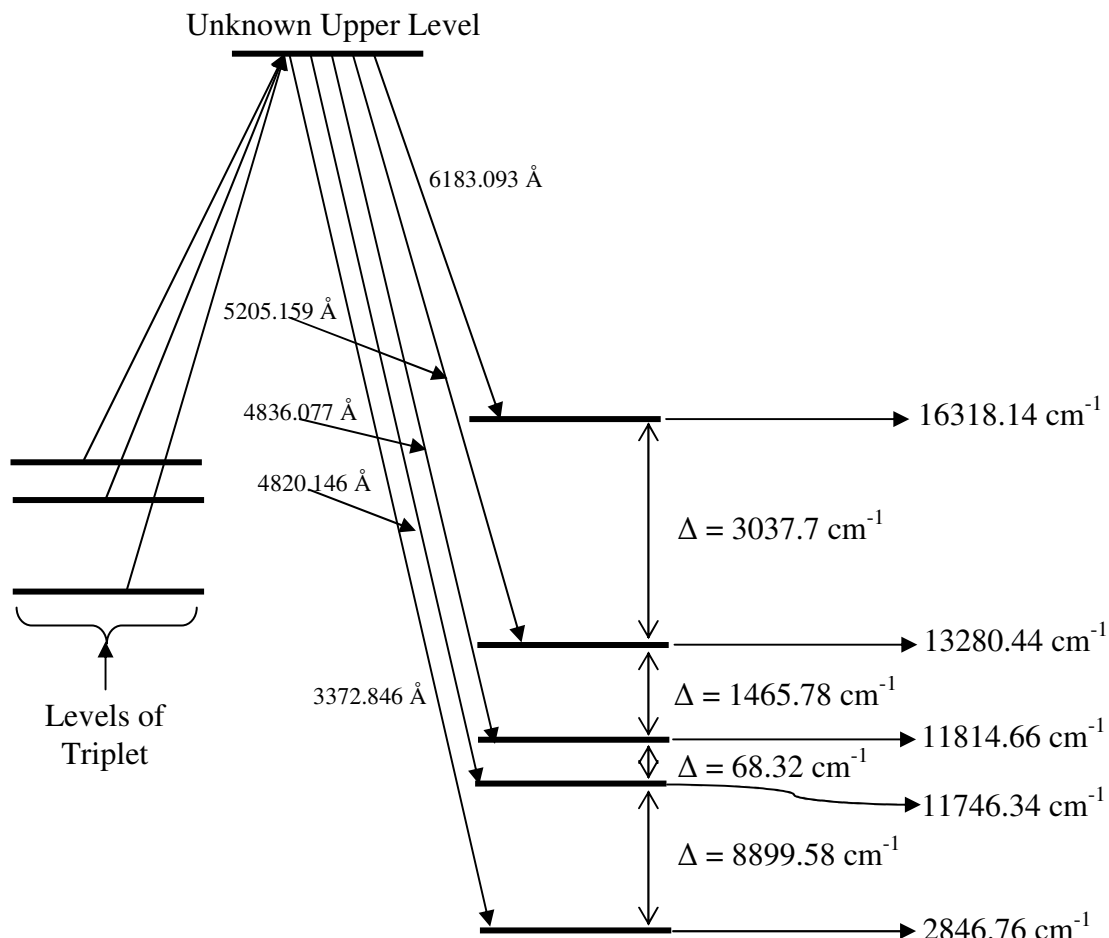
Figure 6.6: Level scheme for transition from level triplet and wave number differences between fluorescence decay levels

Table 6.4: Lower decay levels from unknown upper level

Possible Lower decay levels	Difference in wave numbers cm^{-1}
16318.14 cm^{-1}, o, 13/2, 280.8 MHz	
13280.44 cm^{-1}, o, 17/2, 208.1 MHz, 20 MHz	3037.7
11814.66 cm^{-1}, o, 15/2, 354.5 MHz, -1 MHz	1465.78
11746.34cm^{-1}, o, 13/2, 401 MHz, 55 MHz	68.32
2846.76 cm^{-1}, o, 13/2, 613.24 MHz, -11.877 MHz	8899.58

6.2.2 Determination of New Upper and Lower Triplet Levels

Assuming the levels listed in Table 6.4 as a correct set of lower levels where the fluorescence lines decay, the wave number of the unknown upper level is estimated by adding the wave number of fluorescence lines to the corresponding wave numbers of lower levels listed in Table 6.4. Table 6.5 list the results of calculations for the unknown upper level with parity assigned as even compared to odd parity lower levels.

Table 6.5: Lower decay levels from unknown upper level

Possible Lower decay levels	Wave number of unknown upper even level cm^{-1}
16318.14 cm^{-1}, o, 13/2, 280.8 MHz	32486.801
13280.44 cm^{-1}, o, 17/2, 208.1 MHz, 20 MHz	32486.8
11814.66 cm^{-1}, o, 15/2, 354.5 MHz, -1 MHz	32486.8
11746.34cm^{-1}, o, 13/2, 401 MHz, 55 MHz	32486.803
2846.76 cm^{-1}, o, 13/2, 613.24 MHz, -11.877 MHz	32486.797

One of the fluorescence line i.e. line at 6183 Å lie in the wavelength range of our dye laser (Kiton Red), this line was experimentally investigated by recording its LIF signal. The recorded hyperfine pattern and corresponding best fit situation for the recorded LIF signal is show in figure 6.7 and 6.8. The fitter gave the center of gravity wavelength as 6183.09 Å. This pattern shows regular intensities of the hyperfine components and then the irregularities in intensities of the hyperfine components in the excitation of line 5780.509 Å are due to the lower triplet levels.
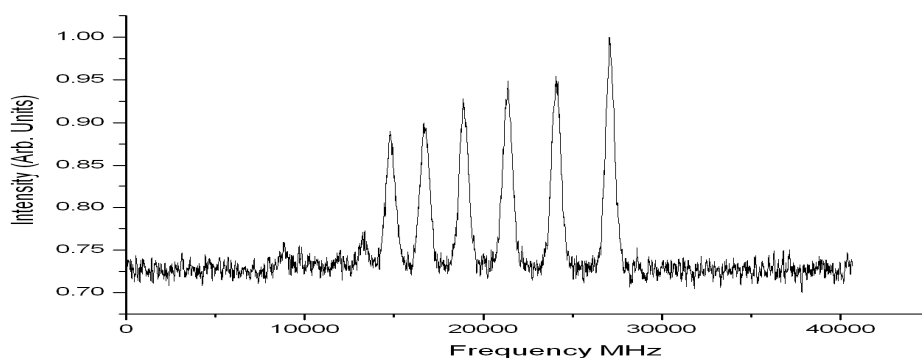
Figure 6.7: Hyperfine pattern of the recorded line at 6183 Å
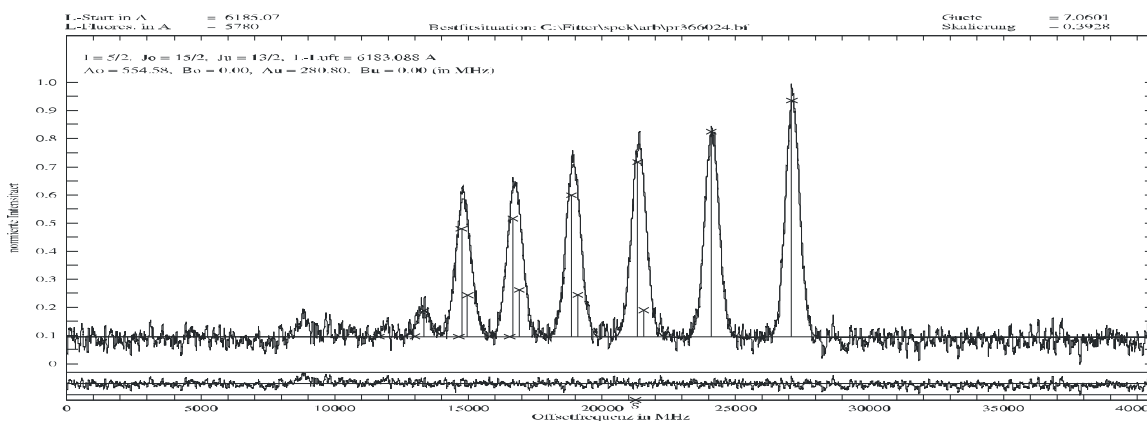
Figure 6.8: Best fit situation of the recorded line at 6183 Å

The experimental investigation of the line at 6183.93 Å further confirmed our estimate of energy of the unknown upper level. The best fit of the recorded line gave $J_o = 15/2$ and $A_o = 552.5$ MHz. So the line 6183.09 Å was classified as a transition between

$$32486.80^e_{15/2} \text{ cm}^{-1} - 16318.18^o_{13/2} \text{ cm}^{-1}$$

Using center of gravity wavelengths 5780.509 Å, 5780.46 Å and 5780.27 Å in the initial excitation and using the energy of upper level 32486.80 cm^{-1}, the wave numbers for the lower triplet levels were calculated with odd parity as the newly found upper level is an even parity level. Since the angular momentum for the upper level 32486.80 cm^{-1} is now known beyond doubt therefore angular momentum values for lower triplet levels could be suggested as 17/2, 15/2 or 13/2. We suggested based on experimental observations that upper most level of triplet has an angular momentum of 15/2 and the two of the lower levels of triplet have angular momenta of 13/2. Estimated wave numbers of the levels in triplet are given in table 6.6.

Table 6.6: Wave numbers for the triplet levels for excitation 5780.51 Å

cog λ_{air} (Å)	Lower Level Triplet				Upper Level
	J	P	Energy (cm^{-1})	A (MHz)	
5780.509	15/2	o	15192.090	730	
5780.46	13/2	o	15191.906	730	15/2, e, 32486.80, 552.5
5780.27	13/2	o	15191.233	666	

In order to justify the angular momentum values of levels in triplet, further investigations were performed and a level $31402.87^e_{15/2} \text{ cm}^{-1}$ in our database of known levels was found which has decay channels to two lower levels triplet with fluorescence wavelengths 6166.95 Å and 6166.69 Å. This was experimentally verified (figure 6.9) by exciting a line at 5918.088 Å which is classified as a transition between

$$31402.87^e_{15/2} \text{ cm}^{-1}, A_o = 630.4\,\text{MHz} - 14510.22^o_{13/2} \text{ cm}^{-1}, A_u = 1085.4\,\text{MHz}$$

with just two very closely lying fluorescence lines at around 6166 Å.
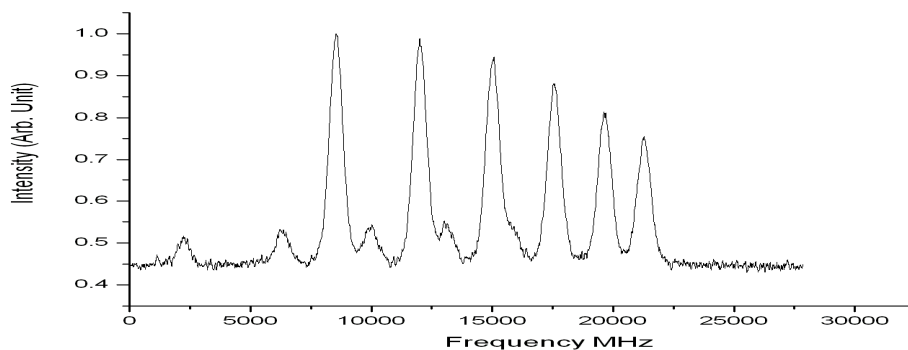
Figure 6.9: Hyperfine structure pattern for the excitation of line 5918.088 Å.

Measuring the exact fluorescence wavelengths two lines were identified at 6166.95 Å and 6166.693 Å with S/N ratio of 14 in FT-Spectra, figure 6.10. As is obvious in FT-Spectra the hyperfine structure of these lines is almost resolved.

An excitation with start wavelength 6167.25 Å, revealed almost a normal behaviour of relative intensities of hyperfine components, even though the excitation is from the level triplet. The hyperfine structure was recorded on two fluorescence lines i.e. at 5918 Å and 5742 Å. Plot of the recorded hyperfine structure pattern is shown in figure 6.11.
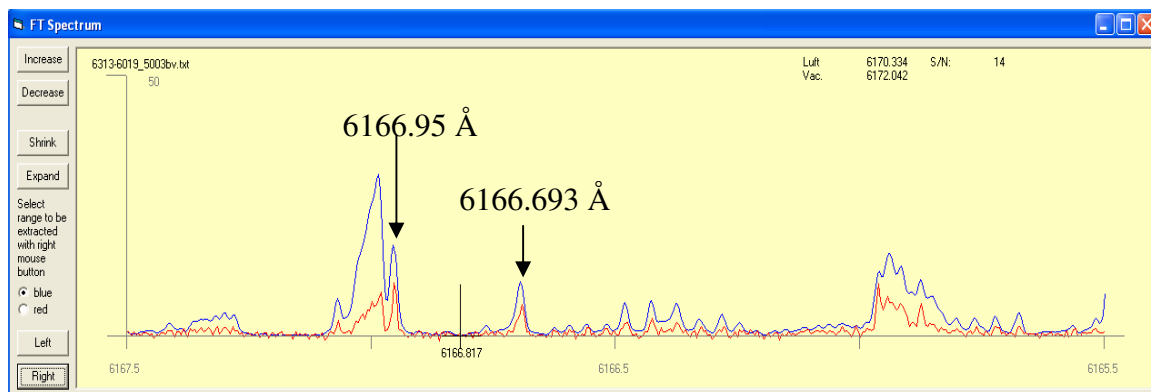
Figure 6.10: FT-Spectra show the lines at 6166.95 Å and 6166.693 Å.
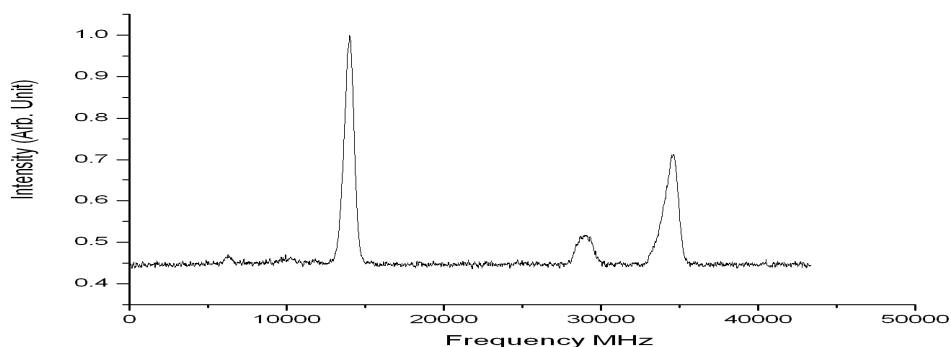
Figure 6.11: Hyperfine pattern detected at 5918 Å and 5742 Å with excitation start wavelength 6167.25 Å.

Fit of the recorded hyperfine structure pattern (see figure 6.12) for the excitation at 6166.95 Å and 6166.67 Å confirmed the angular momentum values for the two lower triplet levels. The values of hyperfine A constants for the lower triplet levels are also in accordance with earlier best fit values.

From the fluorescence information it was confirmed that this excitation belongs to a transition from two lower levels of triplet to a different upper level i.e. 31402.87 cm^{-1}. Transition scheme involving all the levels is shown in figure 6.13.

This was the first confirmation that an anomaly exist and that the anomaly is among the lower levels rather than in upper level of original excitation at 5780.509 Å as was hypothesized at the start of the investigations. The striking feature for this excitation is that there is no excitation from the upper most level of the lower triplet to the upper level 31402.87 cm^{-1}.
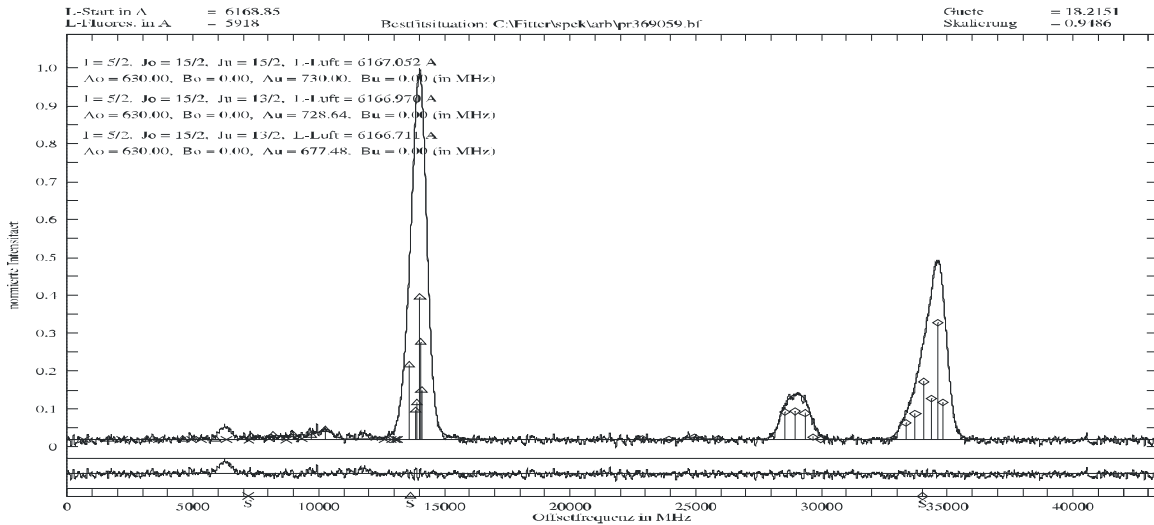
Figure 6.12: Multiline fit of recorded hyperfine structure for the excitation with start wavelength 6167.25 Å.
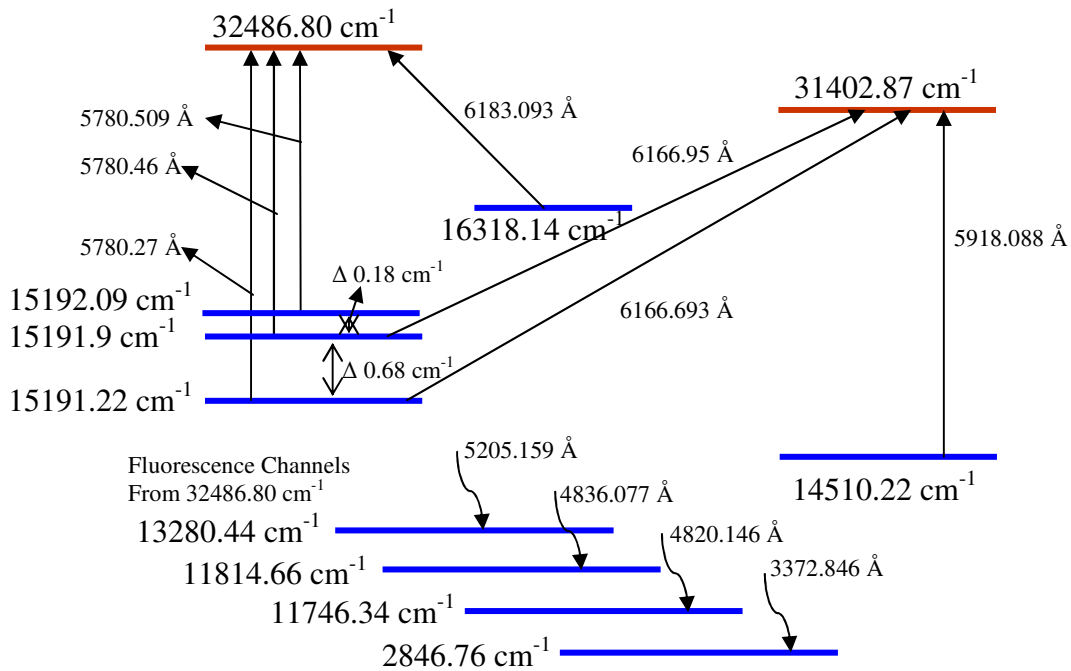
Figure 6.13: Level scheme for the investigated transition from level triplet upper levels 32486.80 cm^{-1} and 31402.87 cm^{-1}

6.2.3 Relative Intensities of Hyperfine Components

The recorded hyperfine structure pattern involving the transition from triplet show a marked deviation of relative intensities of hyperfine components from the relative intensities predicted by intensity rules (see section 3.9). This deviation could be seen in comparison to the relative intensities in the absence of any perturbing effect as shown in figure 6.14. The component positions are almost unchanged indicating that interval rule is not violated with positions of hfs components given by Casimir Formulas. The transition from the upper most level of triplet i.e. 15192.09 cm^{-1} to the upper level show a sharp decrease in relative intensities of diagonal hyperfine components. Also, the relative intensities of diagonal components resulting from the transition between 15191.906 cm^{-1} and upper level also show deviation in relative intensities. The most pronounced deviation in intensities of diagonal components is observed with a transition between lower most triplet level i.e. from 15191.233 cm^{-1} to upper level. Here it is observed that the intensities of diagonal components ($\Delta F = +1$) are much less than the intensities of off-diagonal components ($\Delta F = 0$) show pronounced anomalous behaviour.
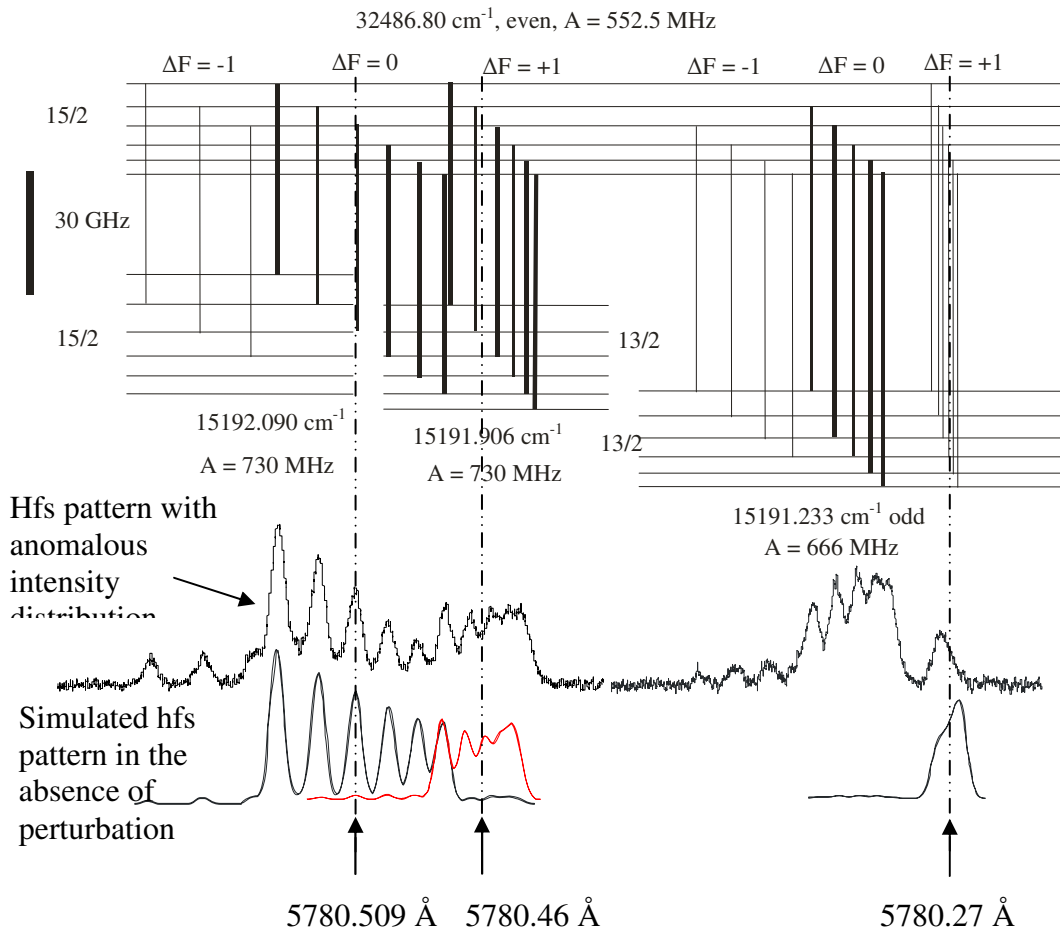
Figure 6.14: Levels scheme for transition from triplet system to 32486.80 cm^{-1}, center-of-gravity positions marked by broken lines.

Almost a normal behaviour of relative intensities of hyperfine components is observed for this transition from two lower levels of triplet to the upper level 31402.87 cm^{-1}, as seen in comparison with FT-Spectra and with simulated hyperfine patterns, figure 6.15. The most striking feature in this transition is the absence of transition from upper most level of triplet i.e. 15192.09 cm^{-1} to upper level. One sees, that for this transition the intensity distribution follows nearly the prediction i.e. having a weak perturbation.

31402.87 cm^{-1} even

A = 630.4 MHz

$\Delta F = -1$ $\quad$ $\Delta F = 0$ $\Delta F = +1$ $\quad$ $\Delta F = -1$ $\quad$ $\Delta F = 0$ $\quad$ $\Delta F = +1$

15/2

30 GHz

15/2 $\qquad$ 13/2

15192.090 cm^{-1} $\qquad$ 15191.906 cm^{-1} $\qquad$ 13/2

A = 730 MHz $\qquad$ A = 730 MHz

15191.233 cm^{-1} odd

A = 666 MHz

Fourier-Spectra $\qquad$ Recorded hfs pattern

Simulated hfs

6166.95 Å $\qquad$ 6166.67 Å
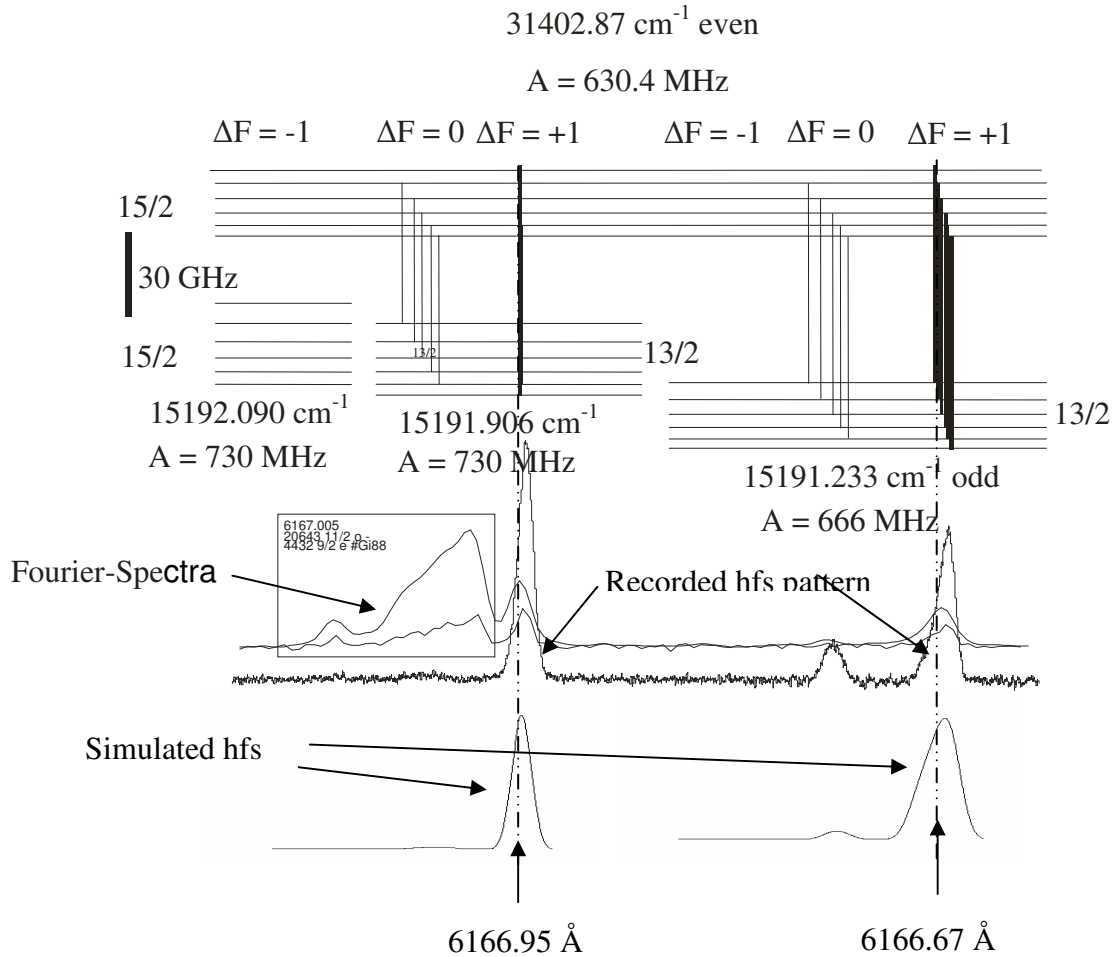
Figure 6.15: Levels scheme for transition from triplet system to 31402.87 cm^{-1}, center-of-gravity positions marked by broken lines.

In the absence of any perturbing behaviour of levels in the triplet the simulated hyperfine structure patterns for transitions from the three lower levels to the levels 32486.80 cm^{-1} and 31402.87 cm^{-1} with normal intensity distribution and hyperfine components positions is shown in figure 6.16 a,b,c,e.

32486.80 cm^{-1} ⟷ 15192.09 cm^{-1} 32486.80 cm^{-1} ⟷ 15191.9 cm^{-1}

(a)   (b)

32486.80 cm^{-1} ⟷ 15191.233 cm^{-1} 31402.87 cm^{-1} ⟷ 15191.9 cm^{-1}

(c)   (d)

31402.87 cm^{-1} ⟷ 15191.233 cm^{-1}

(e)
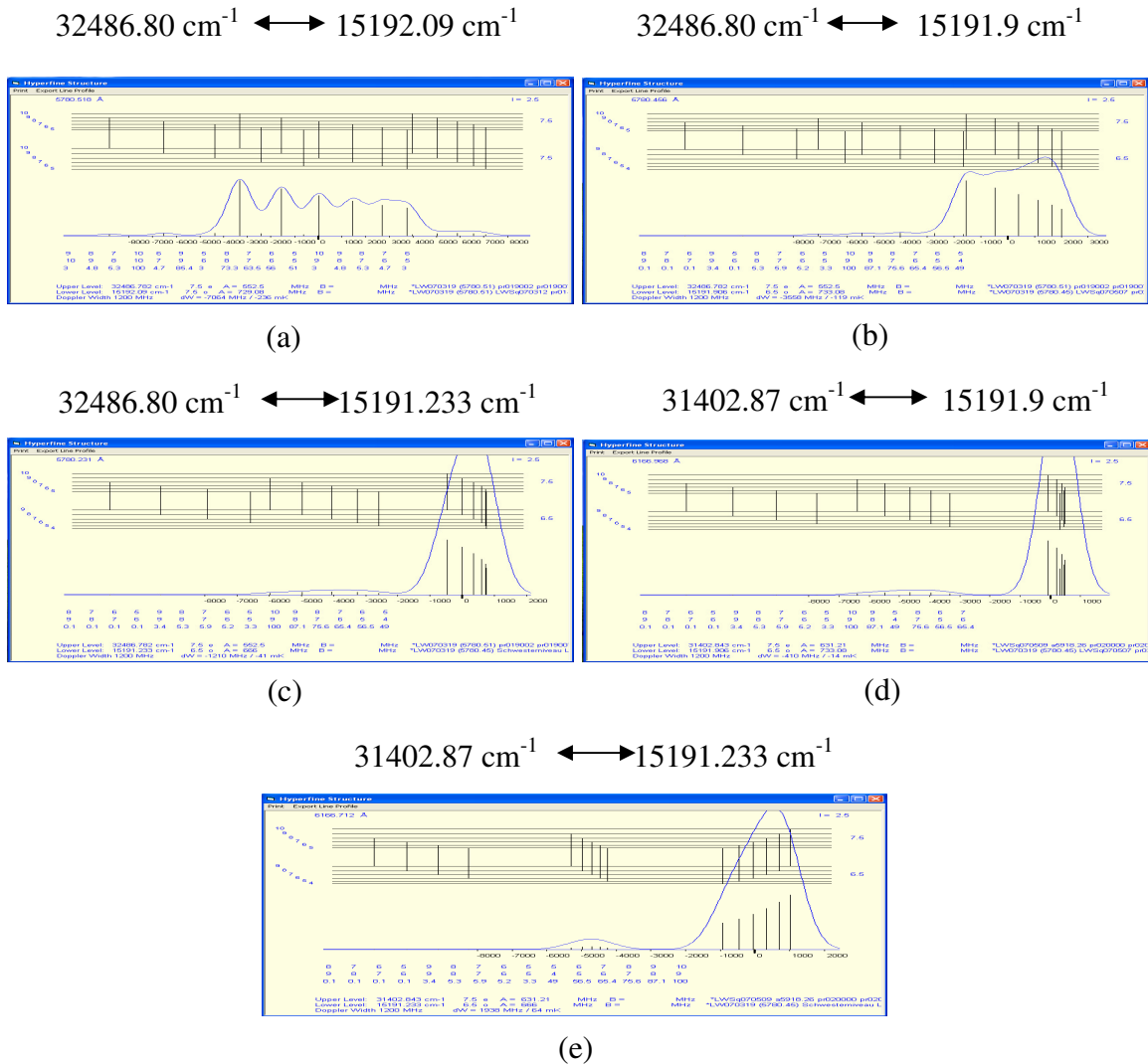
Figure 6.16: Simulated hyperfine structure pattern for transitions from levels in triplet to upper levels 32486.80 cm^{-1} and 31402.87 cm^{-1} without perturbation.

During our systematic investigations up till now around 44 transitions were discovered from level triplet to unknown or known upper levels. In all these transitions anomalous intensity distribution of hyperfine components was observed. Some of these transitions are discussed in the following sections.

6.3 Excitation of level $32166.51^{e}_{15/2}$ from Level Triplet

The experimental investigation of a line in the neighborhood of 5889.58 Å again reveal anomalous intensity distribution of hyperfine components. The line profile in FT-Spectra (see figure 6.17) shows a blend situation and apart from the investigated line other lines are also present. Generally the hyperfine structure of a line in FT-Spectra is not always fully resolved showing all its hyperfine components but rather in most cases what is seen in FT-Spectra is a convolution of hyperfine structures of several lines lying very close to each other.

Laser frequency was set to a position 5889.58 Å where a strong LIF signal was observed on a fluorescence wavelength in UV i.e. 3411 Å. Several other fluorescence lines were also found i.e. 4899 Å, 5293 Å, 5308 Å, 5374 Å, 5502 Å, 5662 Å, 5747 Å, 5962 Å and 6309 Å. Now by continuously scanning the laser excitation wavelength starting from 5889.71 Å, LIF signal was recorded at the strongest fluorescence wavelength i.e. 3411 Å showing perturbed intensity distribution of hyperfine components (see figure 6.18). LIF signal was recorded on all observed fluorescence wavelengths showing in each case anomalous intensity distribution of hyperfine components.
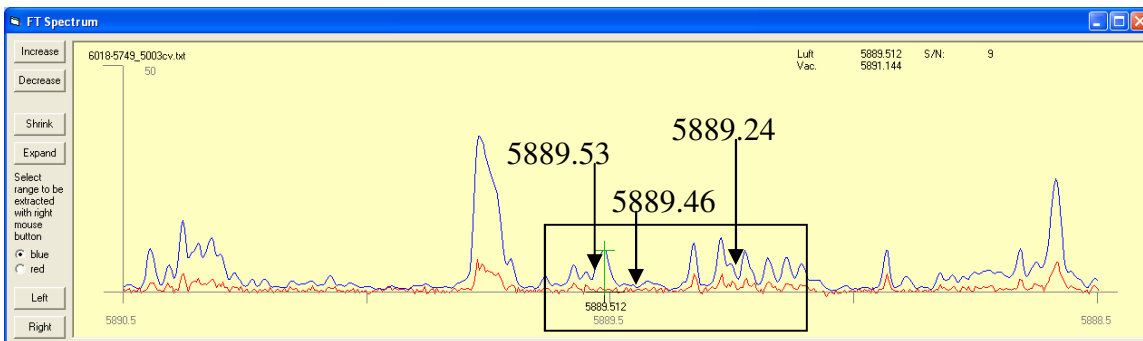
Figure 6.17: FT-spectra for the line 5889.51 Å.

As can be seen in figure 6.18 all three groups of hyperfine structure pattern are appearing in the recorded structure with more or less the same perturbation in relative intensities of hyperfine components as observed in the last excitation. Again a deviation from intensity rule is clearly observed.
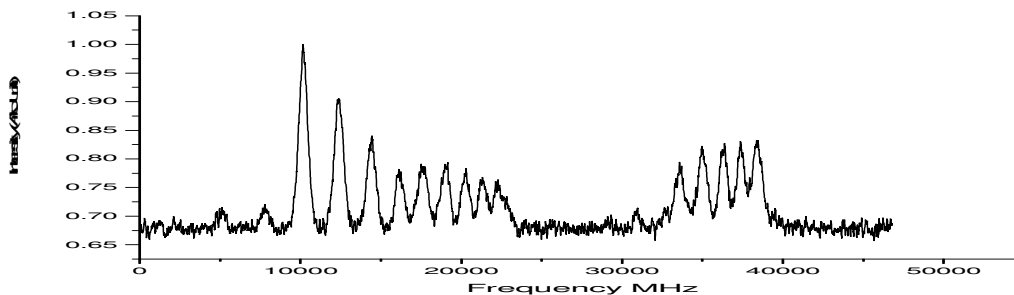
Figure 6.18: Hyperfine structure pattern of the recorded line with start wavelength 5889.71 Å.

Assuming that level triplet is involved in the excitation to an unknown upper level, the intensity profile of the recorded perturbed structure is simulated (see figure 6.19). A good agreement in terms of the positions of hyperfine components is obtained for J-value of 15/2 and A-value of around 510 MHz for the upper level. The strange behaviour which is noted from this simulation is that the diagonal components ($\Delta F = +1$) in the third group are completely missing and with increased intensity of the off-diagonal components ($\Delta F = 0$). In the first and second group the diagonal components appear with changed intensity profile. Using this preliminary information the recorded structure was fitted using a multiline fitting routine in fitter program; best fit (see figure 6.20) of the structure gave the center of gravity wavelengths, J-values and A-values for the level triplet and upper level.

Figure 6.19: Simulation of the perturbed recorded structure (red line profile) recorded with start wavelength 5889.71 Å

Figure 6.20: Best fit situation of the recorded hyperfine pattern using multiline fit with start wavelength 5889.71 Å

Using the center-of-gravity wave number and wave number of each of the levels in triplet, the wave number for upper level is determined. These values are given in table 6.7.

Table 6.7: Best fit values and wave numbers upper and lower levels for the excitation with start wavelength 5889.71 Å.

cog λ_{air} (Å)	Lower Level				Upper Level	
	J_u	Parity	Energy (cm^{-1})	A_u (MHz)	$J_o = 15/2$, Parity = e, $A_o = 510$ MHz	
					Energy (cm^{-1})	Average Energy (cm^{-1})
5889.53	15/2	o	15192.09	732.01	32166.663	
5889.46	13/2	o	15191.9	733	32166.694	32166.673
5889.24	13/2	o	15191.233	668.21	32166.663	

In order to confirm the existence and J value of the upper level a second excitation was performed at one of the observed fluorescence lines i.e. 5962.23 Å. The hyperfine structure of the line is not clearly seen in FT-Spectra due to a mixture of two or more lines (see FT-spectra in figure 6.21). Apart from the line 5962.23 Å, the other prominent line at center-of-gravity wavelength 5962.19 Å can be explained as a known transition from $9268.741^e_{11/2}$ to $26036.419^o_{13/2}$ with strong fluorescence observed at 5144.50 Å.
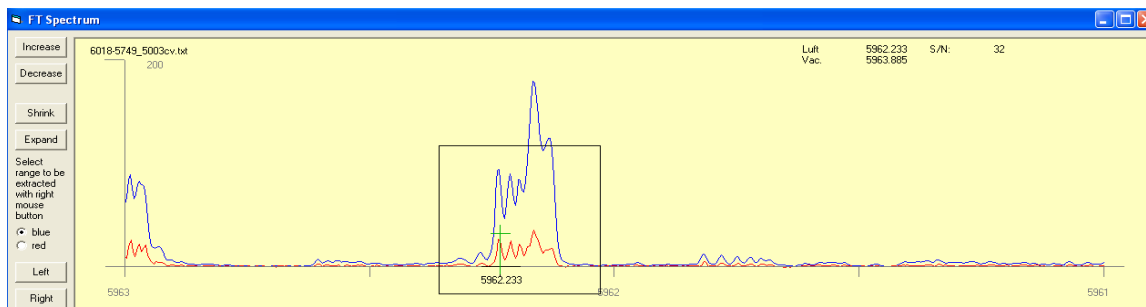
Figure 6.21: FT-Spectra of the line 5962.23 Å

The transition list generated by the classification program indicates a combination of upper level with 15398.916 cm^{-1}, odd parity, J_u = 15/2 and A_u = 889.5 MHz at the investigated line i.e. 5962.23 Å. The hyperfine structure of the line at 5962.23 Å was recorded using laser induced fluorescence at 5890 Å and 6309 Å. The recorded structure has a good signal-to-noise ratio as shown in figure 6.22.
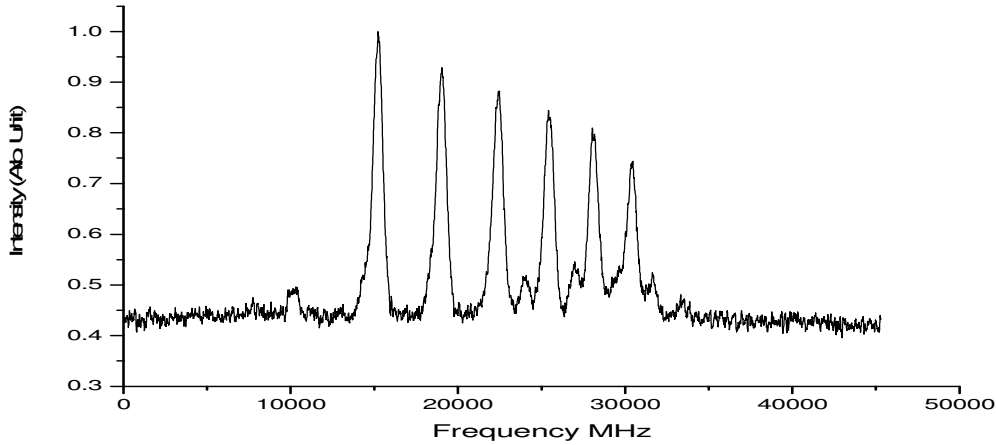
Figure 6.22: Hyperfine structure of the line at 5962.23 Å.

The recorded hyperfine structure is in good agreement in terms of shape and position of hyperfine components with respect to the predicted hyperfine structure of the line. This confirmed the existence of the upper level and furthermore the J-value and parity of the upper level as determined in first excitation were also confirmed. The recorded structure was also fitted (see figure 6.23) which gave J and A values of lower and upper level in conformity with the previous excitation and predictions.
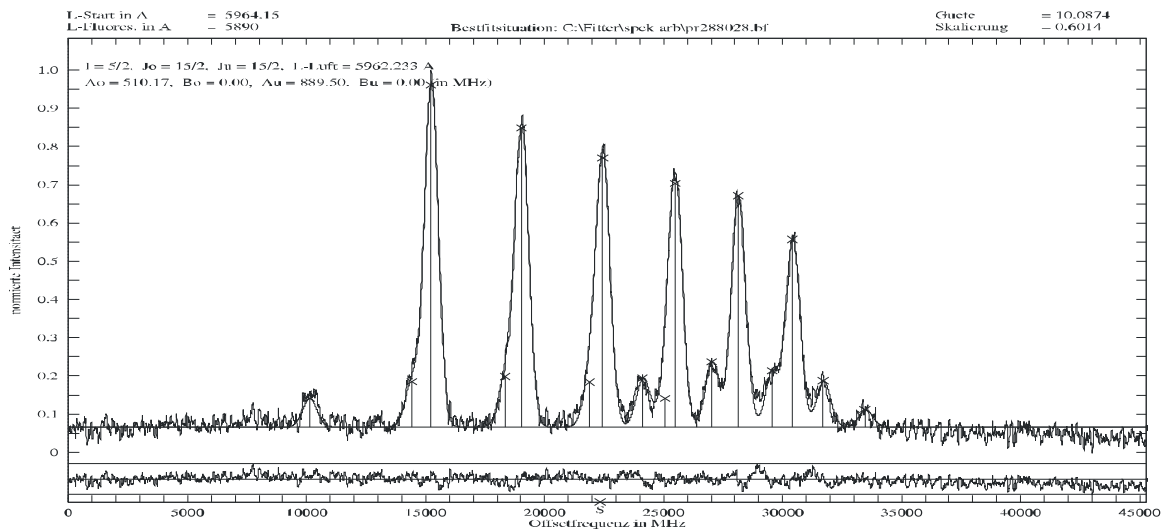
Figure 6.23: Best fit situation of hfs pattern for the line recorded at λ = 5962.23 Å.

106

Addition of the wave number of the line to the energy of lower level i.e. 15398.916 cm^{-1}, the energy of upper level was determined as 32166.51 cm^{-1}. A difference of 0.163 cm^{-1} was noticed in the wave number of upper level as calculated in the first and second excitations, i.e. at excitation lines 5889.51 Å and 5962.23 Å. Considering the difference of energies of levels in triplet (i.e. 0.185 cm^{-1} and 0.68 cm^{-1}), this difference is quite large. After careful analysis of the lower level involved in the excitation of this line i.e. 5962.23 Å, a slight discrepancy in energy of the lower level 15398.916 cm^{-1} was found. Using already known upper level 33114.42 cm^{-1} excited at 5643.25 Å, the energy of the lower level was corrected to 15399.08 cm^{-1}. The wave number and hyperfine structure A constant for the upper level were then again calculated. Incorporating all these corrections the line is identified as a transition

$$\mathbf{32166.674^e_{15/2}\ ,\ A_o = 510.2\,MHz \longleftrightarrow 15399.08^o_{15/2}\ ,\ A_u = 889.5\,MHz}$$

The wave numbers of levels in triplet were then again computed by using the center of gravity wave number from the first excitation involving transition from triplet and wave number of upper level computed from second excitation. Improvements in the wave numbers of levels in triplet are given in Table 6.8. The level scheme with a comparison between experimentally recorded perturbed and simulated unperturbed hyperfine structure pattern is presented in figure 6.24.

Table 6.8: Improved values of wave numbers of levels in triplet, computed from the upper level 32166.674 cm^{-1}.

cog λ_{air} (Å)	Lower Level				Upper Level
	J_u	Parity	Energy (cm^{-1})	A_u (MHz)	$J_o = 15/2$, Parity = e, $A_o = 510$ MHz
					Energy (cm^{-1})
5889.53	15/2	o	15192.095	732.01	
5889.46	13/2	o	15191.894	733	32166.674
5889.24	13/2	o	15191.259	668.23	
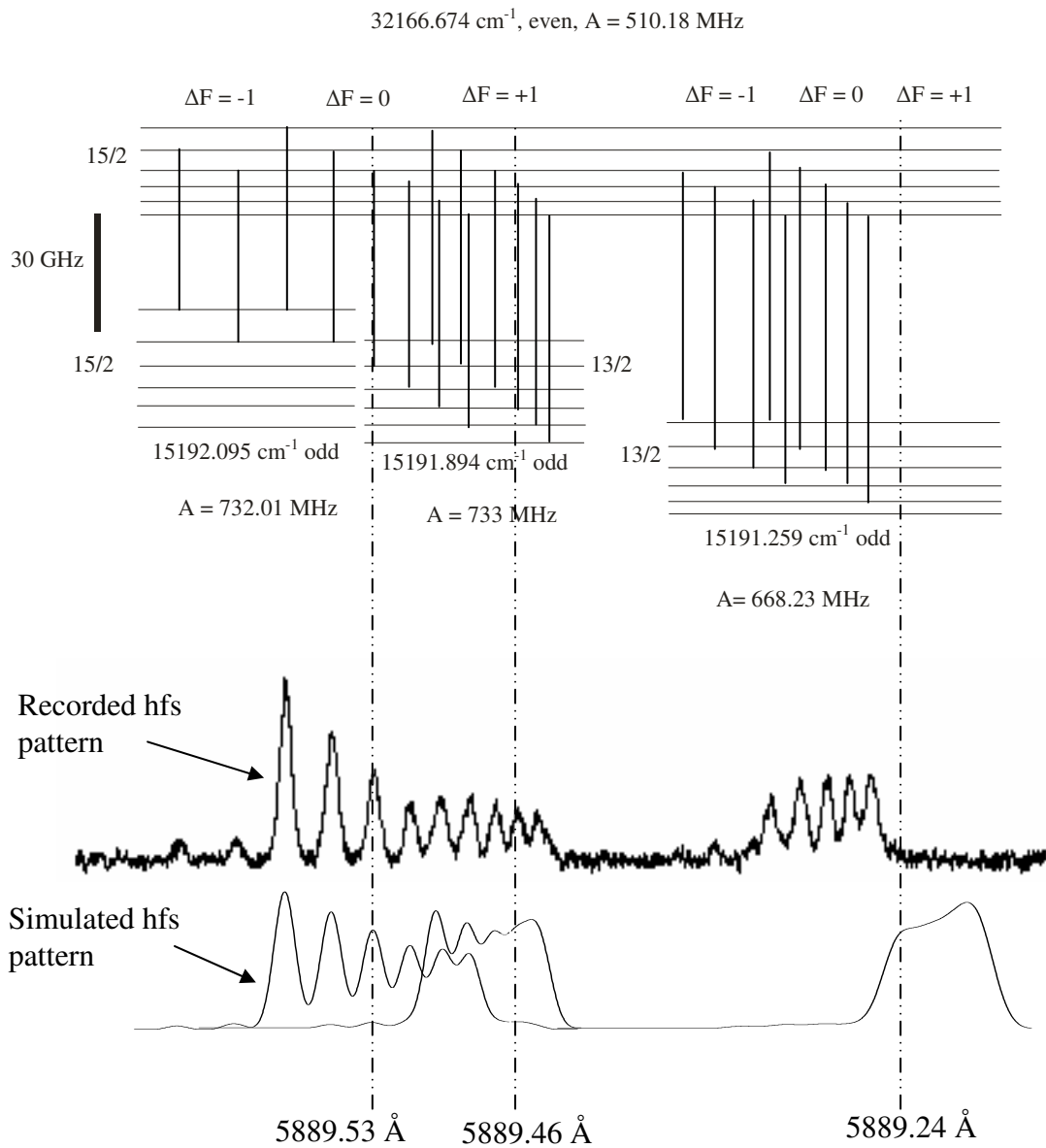
Figure 6.24: Levels scheme for transition from triplet system to 32166.51 cm^{-1}, center-of-gravity positions marked by broken lines

6.4 Excitation of level $32206.775^e_{15/2}$ from Level Triplet

An unclassified line at 6572.23 Å with a relative intensity of 2 in FT-spectra (see figure 6.25) could not be classified by using any of the list suggestion for the line in classification program. The LIF signal was then recorded which gave a widely spread hyperfine structure (see figure 6.26) at fluorescence wavelengths 3405 Å, 5281 Å, 5875 Å, 5948 Å. The relative intensities and separation between diagonal components suggested a high angular momentum values for upper and lower levels of transition.
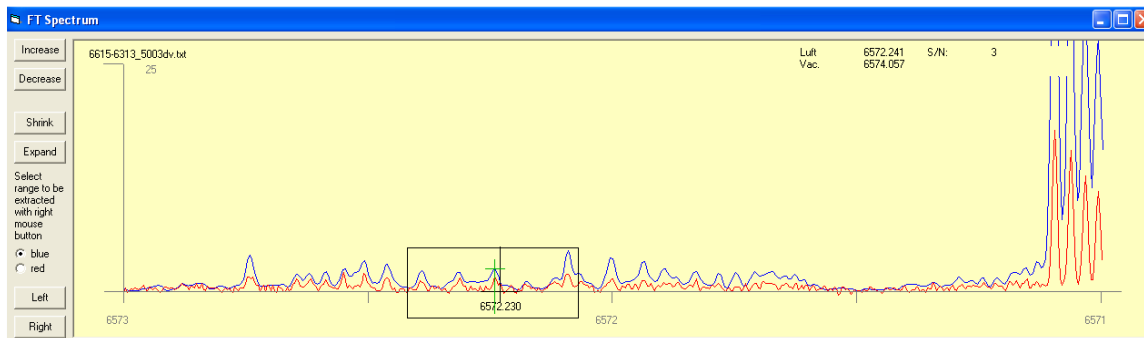
Figure 6.25: FT-Spectra for the line at 6572.24 Å.
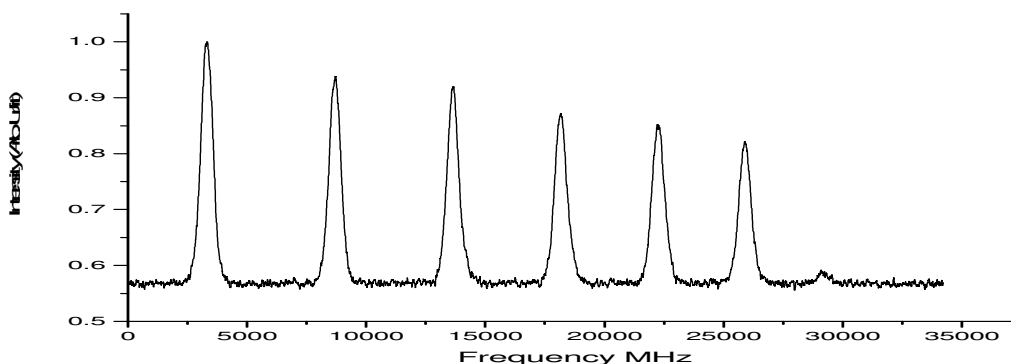
Figure 6.26: LIF signal of a line at 6572.23 Å with large spacing between diagonal components.

A best of the recorded structure was obtained (see figure 6.27) for J-values upper and lower levels as $J_o = 15/2$ and $J_u = 17/2$. The resulting hyperfine constants are $A_o = 559.62$ MHz and $A_u = 998.61$ MHz. Searching a lower level in the data base of known levels having J value as given by the fitter program and A value comparable to the fitted value. An odd parity lower level was found having $A_u = 992.60$ MHz and with energy 16995.46 cm^{-1}. The structure was again fitted by taking these values of known lower level. Using center-of-gravity wave number of the line and wave number of lower level the wave number of upper level was determined as 32206.794 cm^{-1} with even parity and $A_o = 552.5(2)$ MHz. The energy of the upper level was corrected to 32206.775 cm^{-1} using one of its fluorescence line i.e. 5282.173 Å from FT-Spectra. The line was thus classified as a transition between

$$32206.775^e_{15/2}, A_o = 552.5(2)\,\text{MHz} \longleftrightarrow 16995.46^o_{17/2}, A_u = 992.60\,\text{MHz}$$
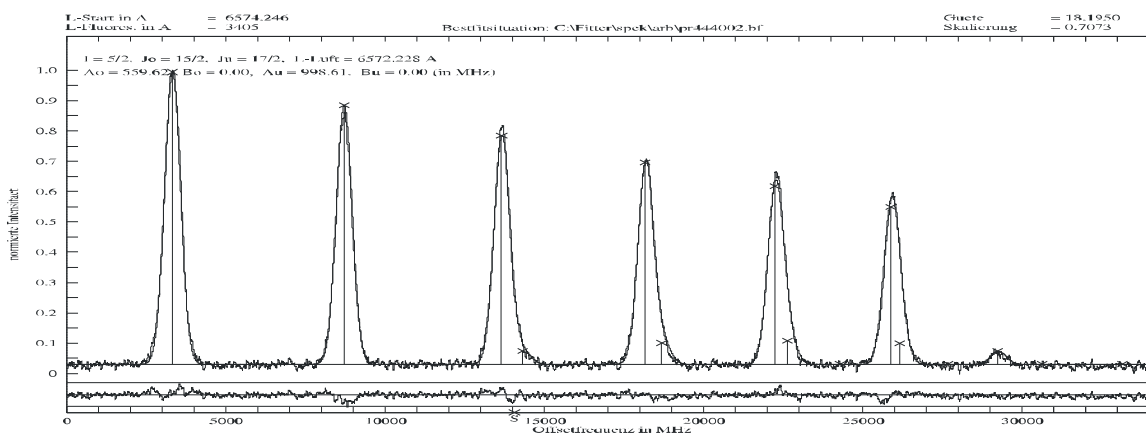
Figure 6.27: Best situation of the recorded hyperfine structure of line 6572.23 Å

In order to confirm the existence of upper level a second excitation at the line 5875.65 Å in FT-Spectra (see figure 6.28), which is one of the fluorescence wavelengths in the first excitation, was performed. Furthermore the excitation of this is motivated by the fact that the transition list generated by the classification program for the newly found upper level indicated a combination with level triplet for this line. Contrary to the predictions of the classification program about the line at 5875.65 Å, the FT-Spectra show almost no profile at the indicated positions.
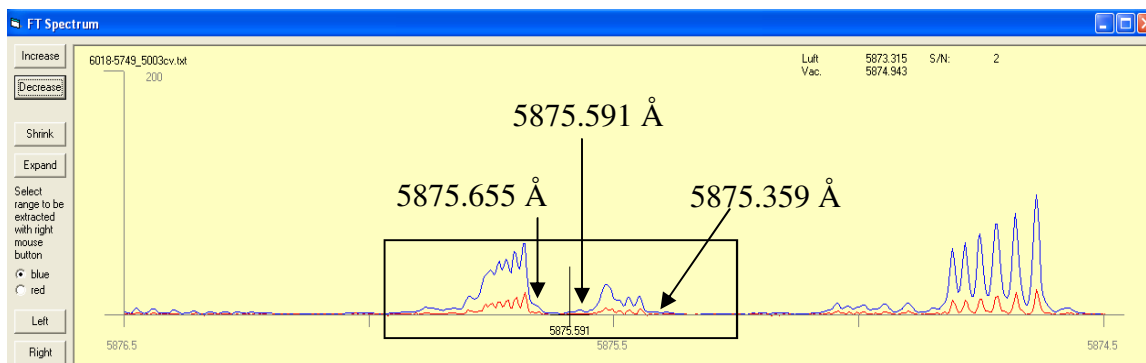
Figure 6.28: FT-Spectra for the line at 5875.65 Å.

So contrary to this a structure with anomalous intensity distribution of hyperfine components was experimentally recorded on all previously observed fluorescence wavelengths i.e. 3405 Å, 5281 Å, 5948 Å, 6572 Å (see figure 6.29).

Assuming that the level triplet is involved in the excitation to the known upper level, a good agreement (see figure 6.30) is obtained in terms of the positions of hyperfine components when the recorded structure is simulated with predicted hyperfine pattern for the transition involving upper level 32206.775 cm^{-1}.
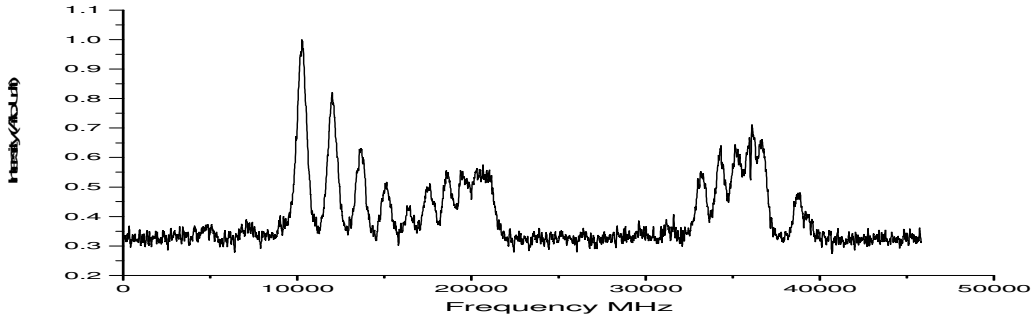
Figure 6.29: Anomalous intensity distribution of the line at 5875.65 Å
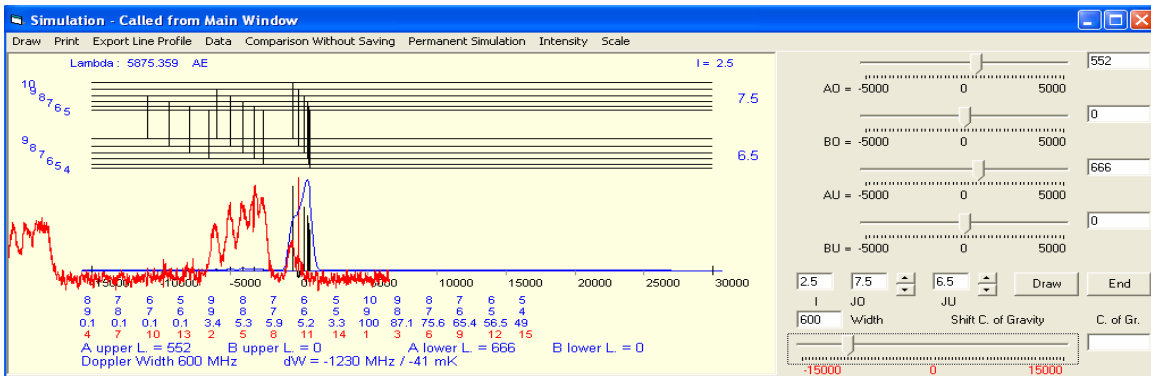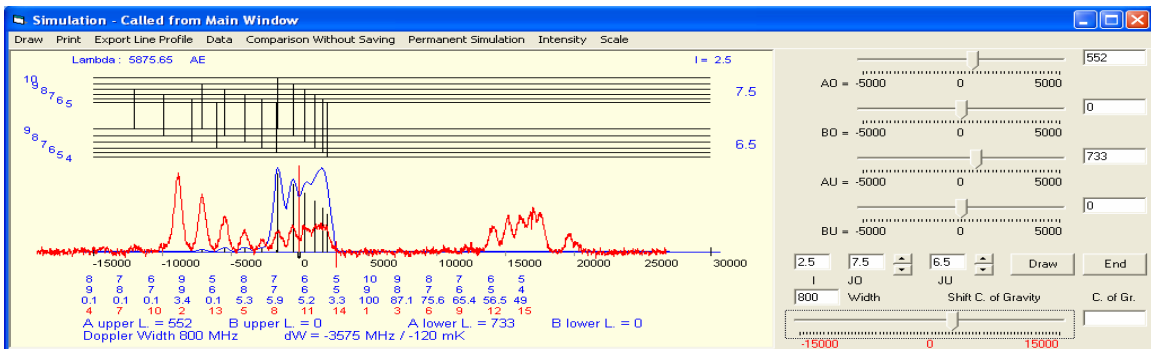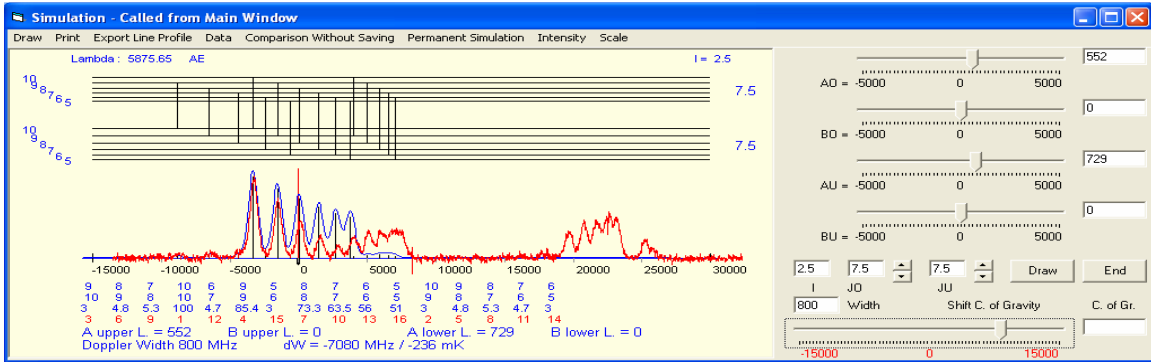
Figure 6.30: Simulation of the perturbed recorded structure (red line profile) recorded with start wavelength 5875.81 Å

Again the abnormality appears as the change in relative intensities of hyperfine components. For the transition from lowest level of triplet to upper the relative intensities of diagonal ($\Delta F = +1$) components are completely changed whereas the relative intensities of off-diagonal ($\Delta F = 0$) components are increased. Similarly in the first and second group the diagonal components appear with changed relative intensities of hyperfine components. Now using the J-value and A-value of the upper level which were determined in first excitation, the recorded perturbed structure was fitted using multiline fit. A value of upper level was kept fixed letting free the A values of levels in triplet. Best fit situation (figure 6.31) was obtained giving nearly the same J- and A-values of levels in triplet and upper already known level.
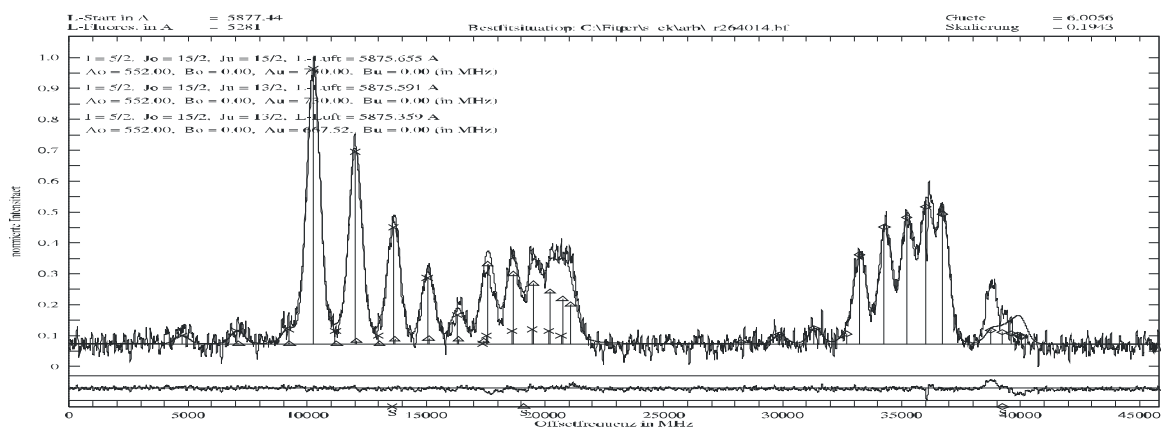
Figure 6.31: Best fit situation of the recorded structure for the excitation from level triplet to upper level with start wavelength 5875.81 Å

Wave numbers of the levels in triplet are computed by subtracting from the wave number of upper level the center-of-gravity wave number of the excitation from level triplet to upper level (Table 6.9). The level scheme with a comparison between experimentally recorded perturbed and simulated unperturbed hyperfine structure pattern is presented in figure 6.32.

Table 6.9: Improved values of wave numbers of levels in triplet, computed from the upper level 32206.775 cm^{-1}.

cog λ_{air} (Å)	Lower Level				Upper Level
	J_u	Parity	Energy (cm^{-1})	A_u (MHz)	$J_o = 15/2$, Parity = e, $A_o = 552.5(2)$ MHz
					Energy (cm^{-1})
5875.657	15/2	o	15192.117	730	
5875.595	13/2	o	15191.938	730	32206.775
5875.36	13/2	o	15191.258	667.52	

32206.775 cm^{-1}, even, A = 552.5 MHz

$\Delta F = -1$ $\Delta F = 0$ $\Delta F = +1$ $\Delta F = -1$ $\Delta F = 0$ $\Delta F = +1$

15/2

30 GHz

15/2

13/2

15192.117 cm^{-1} odd

15191.938 cm^{-1} odd

13/2

A = 730 MHz

A = 730 MHz

15191.258 cm^{-1} odd

A = 667 MHz

Perturbed

Simulated hfs

5875.655 Å

5875.591 Å

5875.359 Å
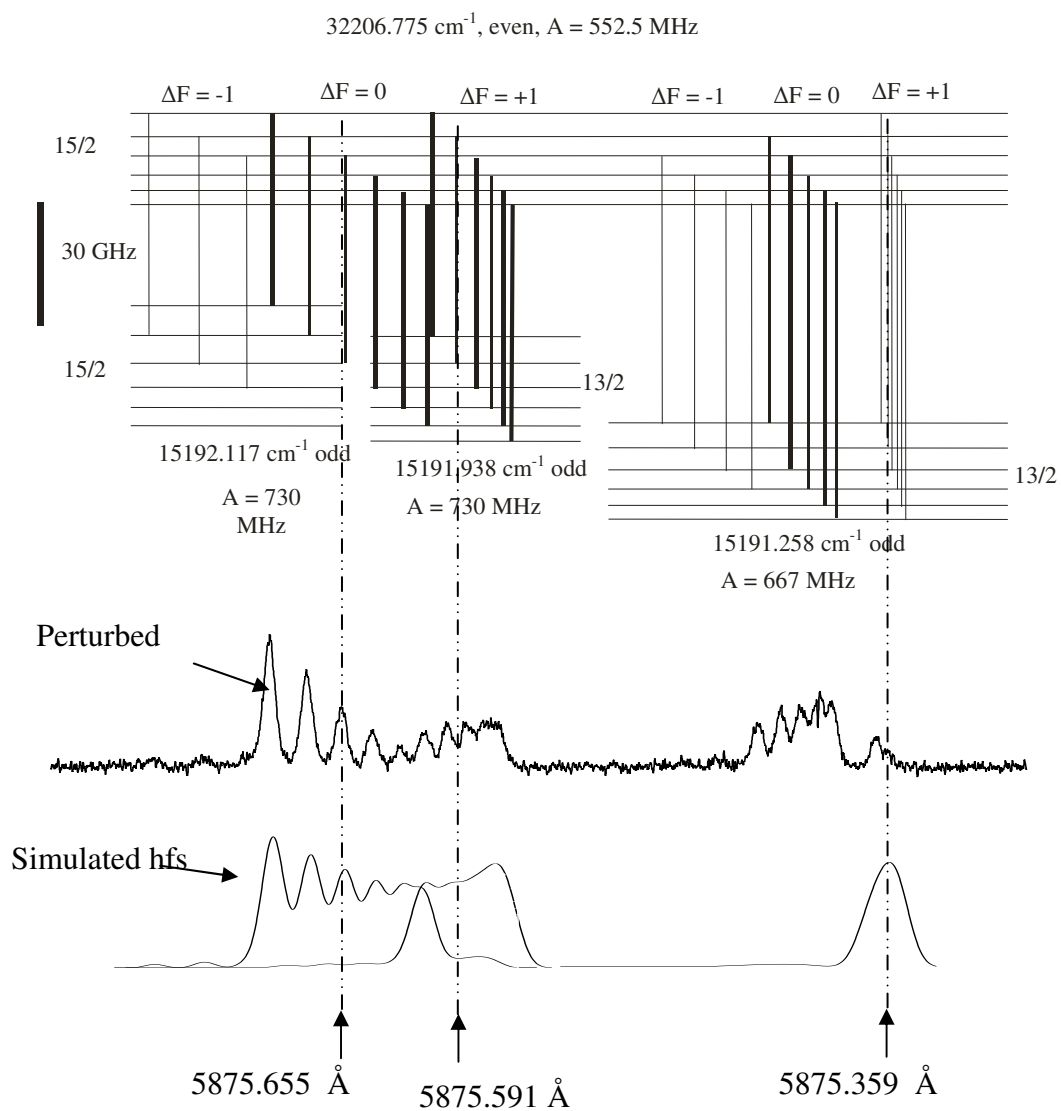
Figure 6.32: Level scheme for the transition from triplet system to upper level 32206.775 cm^{-1}, center-of-gravity positions marked by broken lines.

6.5 Excitation of level $31729.933^e_{13/2}$ from Level Triplet

The level with energy 31729.933 cm^{-1} was discovered via laser excitation of the line at 5639.362 Å which has a good signal to noise ratio with a relative intensity of 12 in FT-spectra (see figure 6.33). The investigated line appears in a blend and its hyperfine structure not clearly seen in FT-Spectra. The other prominent line appearing in the blend is at 5639.41 Å and can be explained as transition between $14780.939^e_{15/2}$ and $32508.36^o_{17/2}$ with strong fluorescence at 4209 Å.
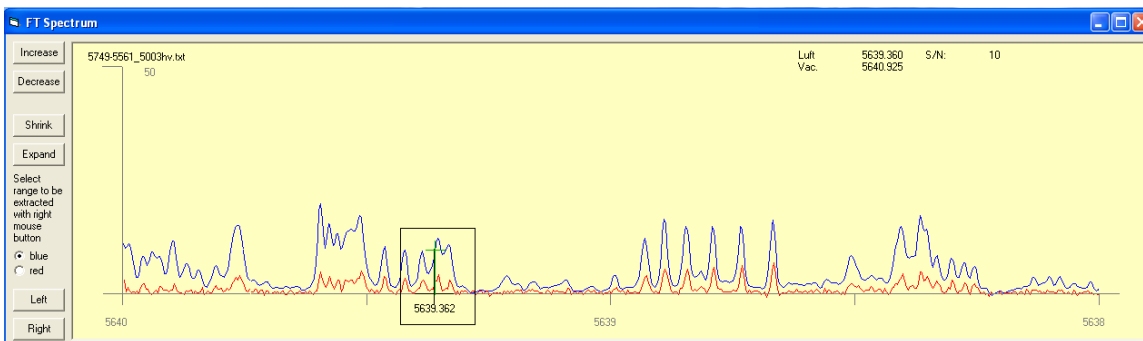
Figure 6.33: FT-Spectra for the line at 5639.362 Å

The recorded spectrum shows a narrow spaced hyperfine structure which was observed at fluorescence wavelengths 3292 Å, 5065 Å, 5711 Å, 6044 Å (see figure 6.33).
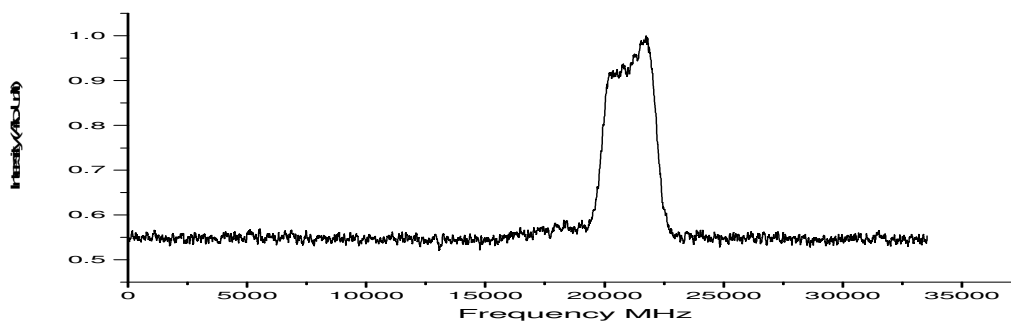
Figure 6.33: Observed hyperfine structure of the line 5639.362 Å.

A best fit of the recorded structure was obtained J_o = 13/2, J_u = 11/2, A_o = 418 MHz and A_u = 549 MHz and with a quality factor of 14 (see figure 6.34). Assuming an unknown upper level known, a lower level was search based on A and J values. A lower level with energy 14002.322 cm^{-1} with odd parity and A_u = 566.4 MHz and B_u = -125 MHz was found. The recorded structure was again fitted keeping fix the A and B values of lower level, the hyperfine constant of upper level was determined as 432.86 MHz. Using the center of gravity wave number and the wave number of lower level the wave number of the upper level was computed as 31729.933 cm^{-1}. The parity of upper level was set as even with respect to the odd parity lower level. The line was then classified as a transition between

$$31729.933^e_{13/2}\ \mathrm{cm^{-1}}, A_o = 432.86\ \mathrm{MHz} \longleftrightarrow$$

$$14002.323^o_{11/2}\ ,\ A_u = 566.4\ \ \mathrm{and}\ B_u = -125\,\mathrm{MHz}$$
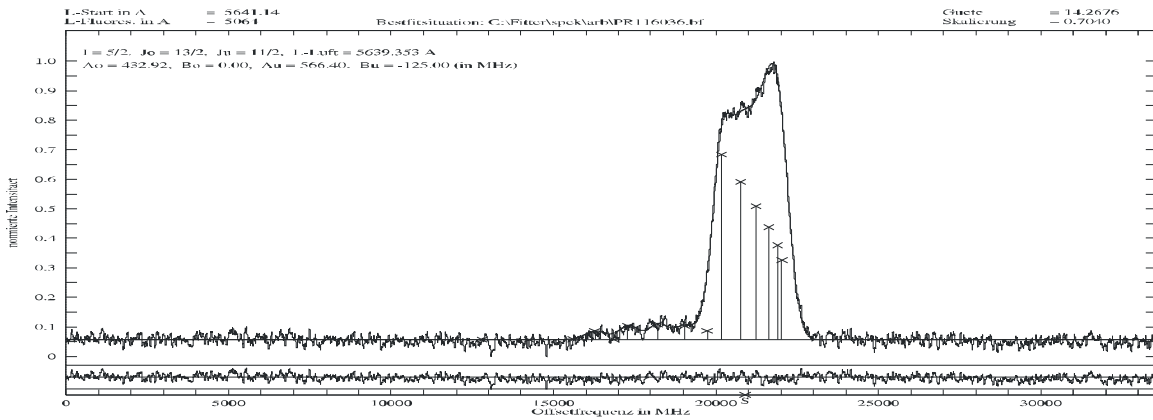
Figure 6.34: Best fit situation of the recorded hyperfine structure of line 5639.36 Å

In order to confirm the existence of this upper level an excitation of line at 6045.096 Å which is the also the fluorescence wavelength in the above excitation was performed. The line has a good signal to noise ratio but seems to be lying in a mixture of more than one line in FT-Spectra (see figure 6.35). In the suggestion list of the line the computed upper level was combining with the level triplet.
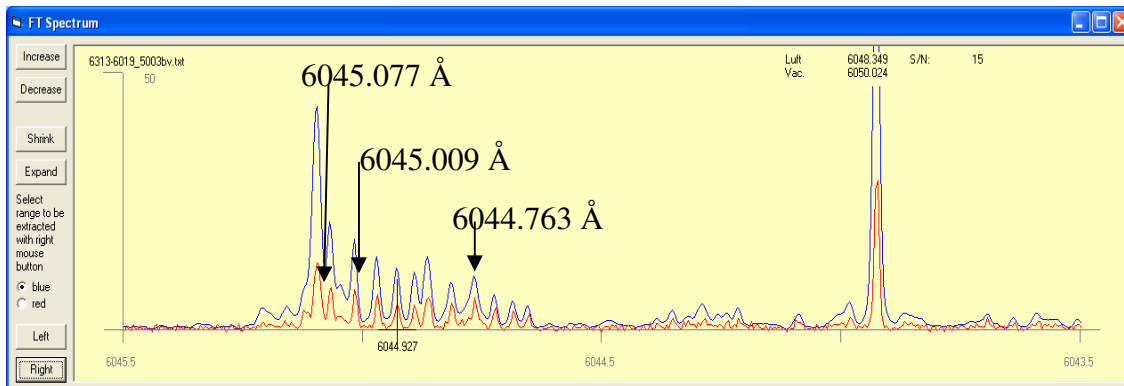
Figure 6.35: FT-Spectra for the lines 6045.077 Å, 6045.009 Å and 6044.763 Å.

Laser excitation of this line with start wavelength 6045.22 Å reveal a hyperfine structure pattern with anomalous intensity distribution of hyperfine components (see figure 6.36). As before three groups of intensity profile are clearly seen, but unlike the last two transitions from level triplet the structure recorded in this excitation shows a comparatively wider separation between hyperfine components, and a different shape of the intensity profile for the three groups is also observed. Furthermore in the third group the diagonal components ($\Delta F = 0$) are more pronounced whereas one set of off-diagonal components ($\Delta F = -1$) is not seen. In the second group the intensity profile of diagonal components ($\Delta F = 0$) appears to be inverted. The first group show more of less normal

intensity profile of diagonal components ($\Delta F = -1$). The same structure with disturbed intensity profile was recorded on all previously observed fluorescence wavelengths i.e. 3292 Å, 5065 Å, 5639 Å, 5711 Å.
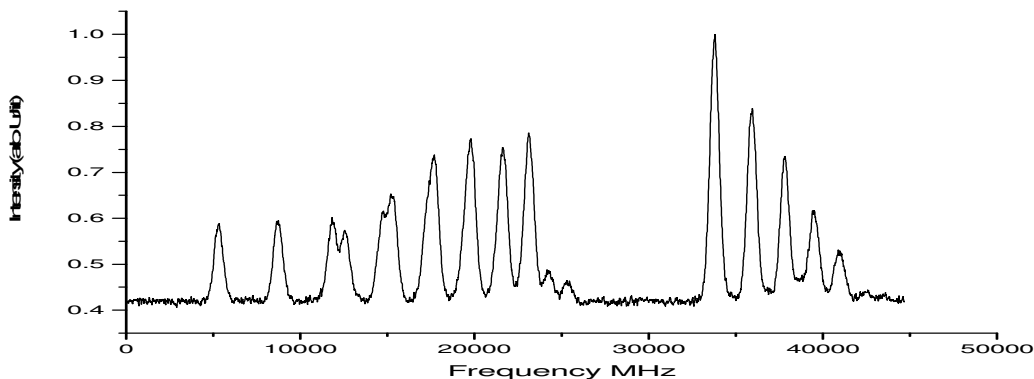
Figure 6.36: Excitation with start wavelength 6045.22 Å showing anomalous behaviour in intensity distribution of diagonal components in all three groups.

Again assuming the transition from level triplet the disturbed intensity profile of the recorded structure was simulated (see figure 6.37) with the theoretically predicted structure involving the upper level 31729.933 cm^{-1} from the first excitation and the triplet levels as lower levels. A good agreement is observed in terms of the positions of the diagonal hyperfine components for all the three groups in recorded structure. This confirmed that the recorded structure is due to the transition from level triplet to upper level 31729.933 cm^{-1}. In this transition from levels of triplet to the upper the diagonal components in all three groups are more resolved as compared to previous transitions.

The J- and A-values of upper level through simulation came out to be 13/2 and 430 MHz, respectively, which are in conformity with first excitation of level 31729.933 cm^{-1}. Using J and A values of the triplet levels and of the upper level, the recorded structure was fitted using a multiline fit. Best fit was obtained (see figure 6.38) for J and A values within good agreement with the previously determined values. Fitting of such structures with perturbed relative intensities of hyperfine components is only possible, if the intensity ratios between components are not locked to the normal (theoretically predicted) ratios. Thus, each component has its own intensity parameter, but the distances follow Casimir formula.

Wave numbers of the levels in triplet are improved using the center of gravity wave number for transition from triplet and wave number of upper level (Table 6.10). The level scheme with a comparison between experimentally recorded perturbed and simulated unperturbed hyperfine structure pattern is presented in figure 6.39.
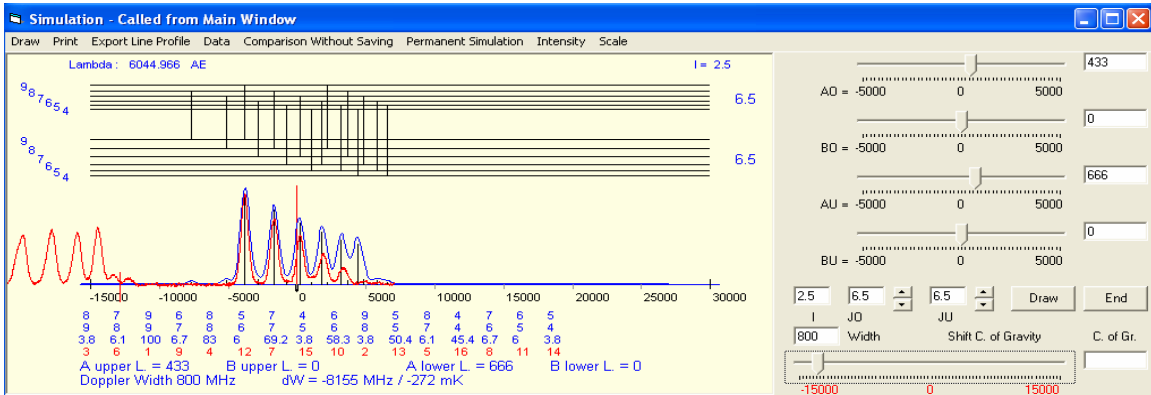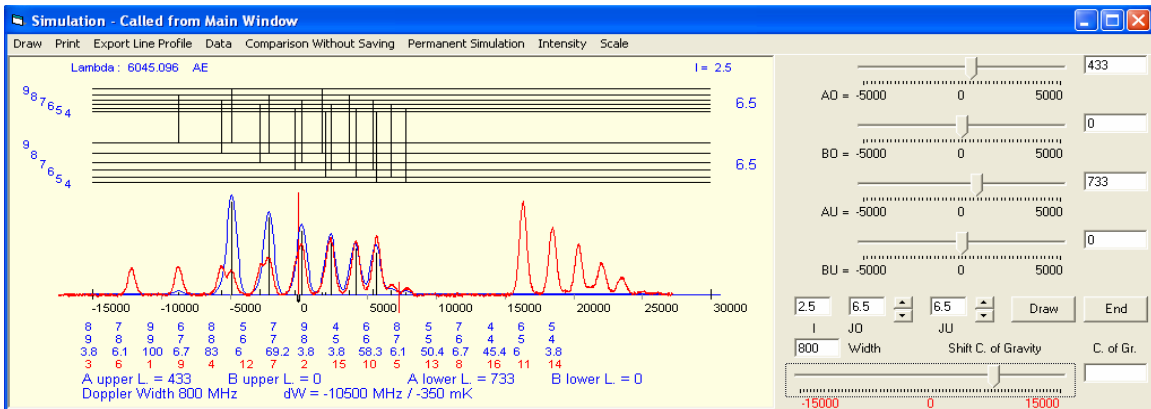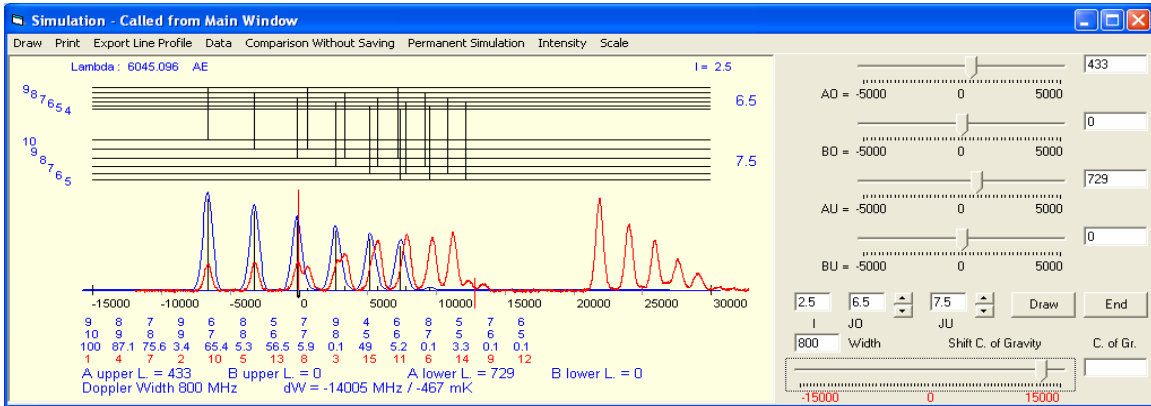
Figure 6.37: Simulation of the perturbed structure (red line profile) recorded with start wavelength 6045.22 Å
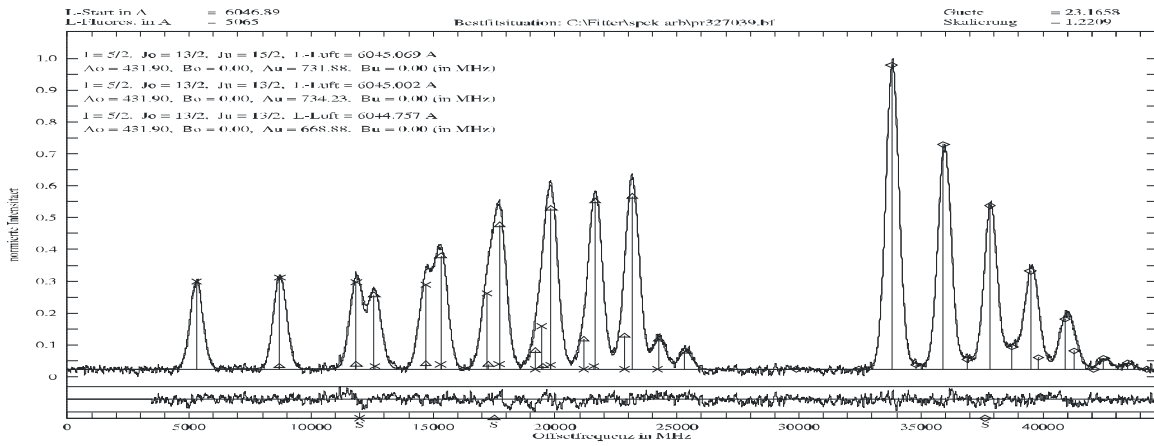
Figure 6.38: Best fit situation of the recorded structure for the excitation from level triplet to upper level with start wavelength 6045.22 Å

Table 6.11: Improved values of wave numbers of levels in triplet, computed from the upper level 31729.933 cm^{-1}

| cog λ_{air} (Å) | Lower Level | | | | Upper Level | |
| | J_u | Parity | Energy (cm^{-1}) | A_u (MHz) | J_o = 13/2, Parity = e, A_o = 432.8(1) MHz | |
					Energy (cm^{-1})	
6045.069	15/2	o	15192.106	731.88		
6045.002	13/2	o	15191.922	734.23	31729.933	
6044.757	13/2	o	15191.251	668.88		

118
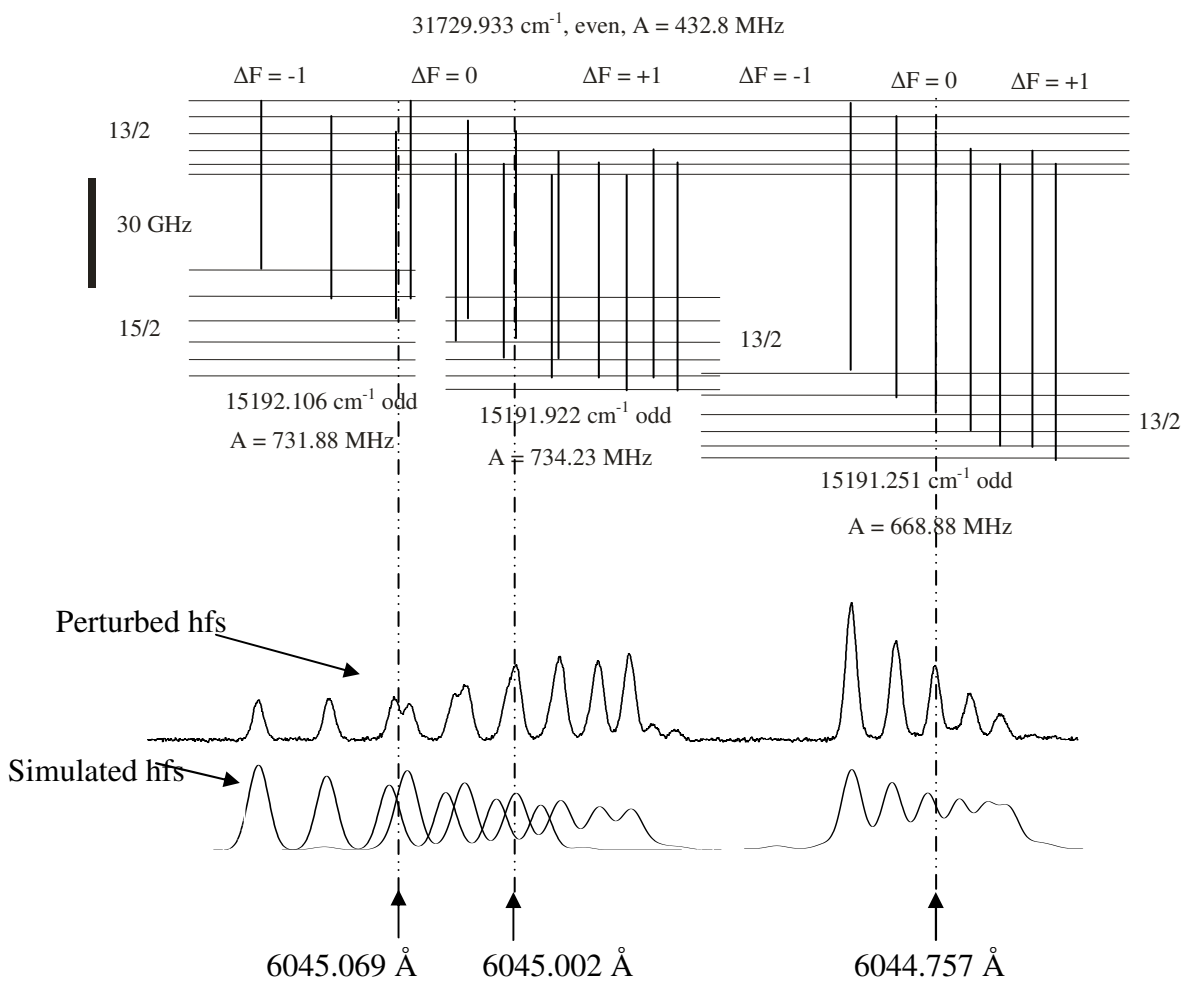
Figure 6.39: Level scheme for transition from triplet to upper level 31729.933 cm^{-1}, center-of-gravity positions marked by broken lines.

6.6 Excitation of level $\mathbf{31629.427^{e}_{17/2}}$ from Level Triplet

The line in FT-Spectra at 6082.04 Å with relative intensity of 13 has a good signal-to-noise ratio and the hyperfine components are partially resolved (see figure 6.40).
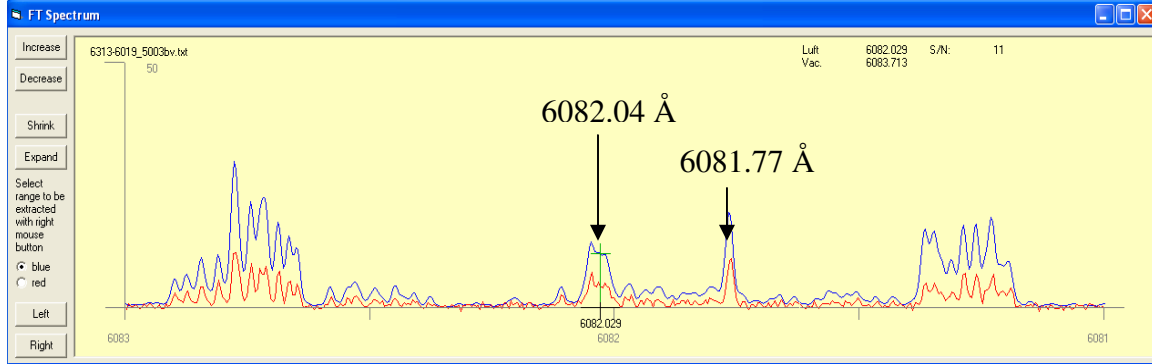
Figure 6.40: FT-Spectra for the lines 6082.04 Å and 6081.77 Å

The line was not classified and none of the suggestions list in the classification program could classify the line. Therefore laser excitation with start wavelength 6082.19 Å of the line was performed. The intensity distribution of hyperfine components in the recorded structure show anomalous behaviour at all observed fluorescence wavelengths i.e. 3669 Å, 3735 Å, 4865 Å, 5350 Å, 5940 Å, 5990 Å, 6159 Å (see figure 6.41).
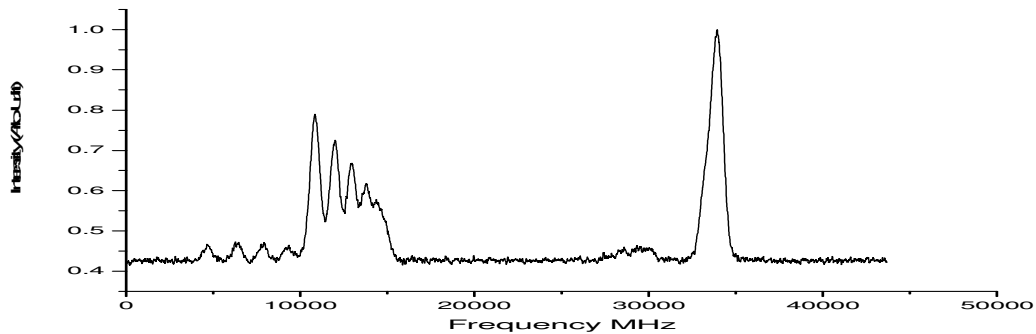
Figure 6.41: Excitation with start wavelength 6082.19 Å showing anomalous behaviour of intensity distribution of hyperfine components

Since the recorded hyperfine structure pattern appears quite normal with almost normal relative intensities of hyperfine components. So at first glance it seemed as if two separate transitions have occurred which happen to lie in the same scan width of laser. But contrary to this the same line profile appeared on all observed decay wavelength and furthermore it would be highly unlikely that two levels have more than one same decay wavelengths. After this preliminary analysis it was again assumed that level triplet might be involved in the excitation to the upper level. Assuming the transition from level triplet, simulation can only be performed for the first group of hyperfine structure by taking the J and A values of upper most level of triplet i.e. $J_u = 15/2$ and $A_u = 730$ MHz.

A good agreement (see figure 6.42) between recorded line profile and simulation was only obtained when J of upper level was taken as 17/2 with A of 560 MHz.
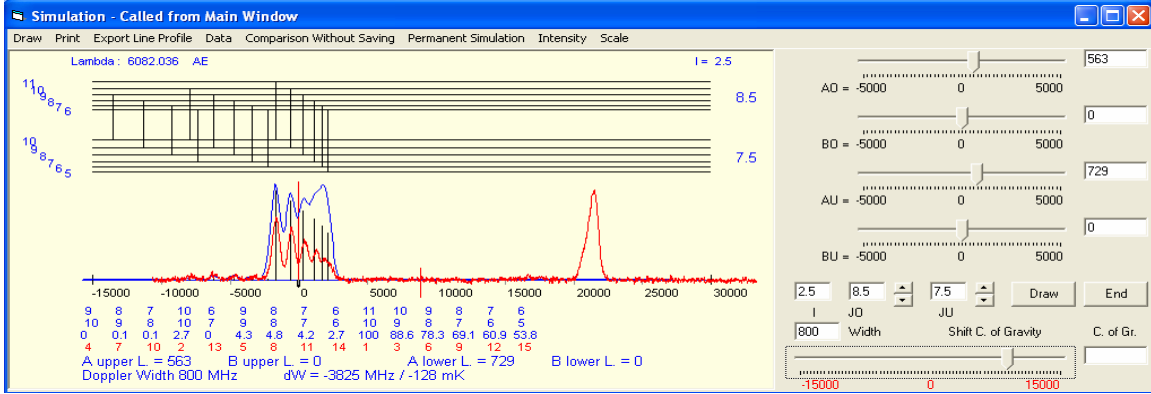
Figure 6.42: Simulation of the perturbed recorded structure (red line profile) recorded with start wavelength 6082.19 Å

The first group of hyperfine structure for a transition between J_o=17/2 - J_u=15/2 is allowed i.e. from the uppermost level of triplet to upper level. The transition from middle level of triplet to the upper level is completely missing and the last group of hyperfine structure components appears as a narrow spaced single peak structure corresponding to a transition from lowest level of triplet with J = 13/2 to upper level with J = 17/2 which is electric dipole forbidden transition. Simulation with J_o = 17/2 has a very serious implication i.e. assuming the simulation is correct then perturbation has caused a transition to become allowed which would be forbidden in an unperturbed transition i.e. ΔJ = +2 occurs as dipole transition from the lowest triplet level (J_u = 13/2) with changed intensity distribution of hyperfine components as evident from the appearance of third group. This means that J is no longer a good quantum number for the lowest triplet level with angular momentum appears as an admixture of 13/2 and 15/2. In order to prove this grossly perturbed behaviour a second excitation to the upper level is needed.

Recorded structure is fitted using single line fit procedure taking into account only the group i.e. for transition from uppermost level of triplet to upper level. Best fit (see figure 6.43) is obtained for J_o = 17/2 - J_u = 15/2 and giving A_o = 560.53 MHz and A_u = 729.01 MHz. The wave number of the upper level is calculated by using the center of gravity wave number of the fitted first group and the wave number of the upper most level of triplet, this gives the following

$$31629.417^e_{17/2} \, cm^{-1} \, , A = 560.53 \, MHz$$

The level is introduced and second excitation at 6159.59 Å is performed. The line 6159.59 Å is contained in an admixture of several lines in FT-Spectra (see figure 6.44) so in a narrow region all peaks are excited to look for LIF signal on all previously observed fluorescence channels.
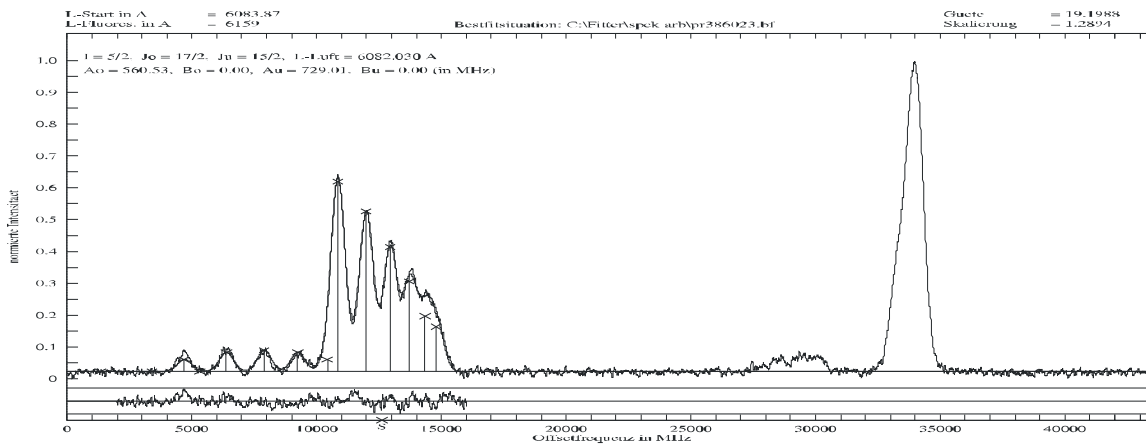
Figure 6.43: Best fit of the perturbed structure recorded with start wavelength 6082.19 Å
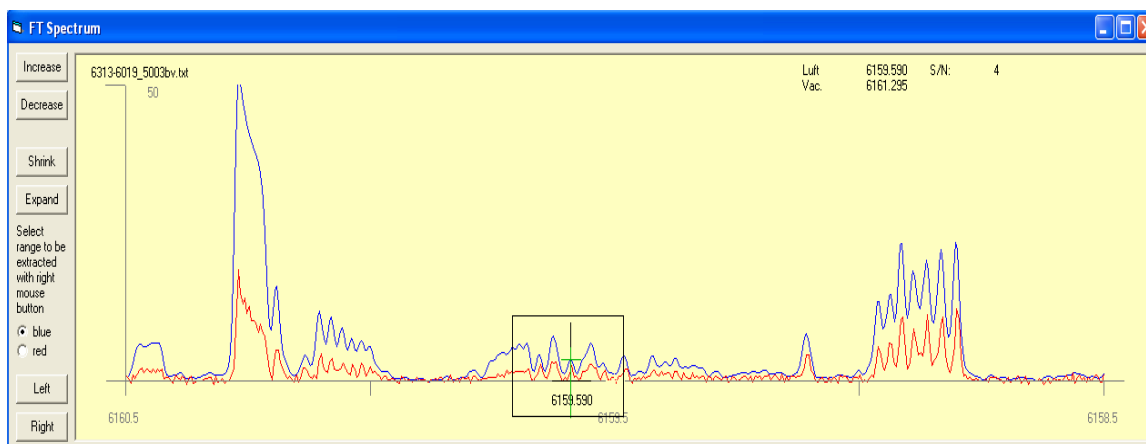
Figure 6.44: FT-Spectra for the line at 6159.59 Å

LIF signal with very good signal to noise ratio was recorded (see figure 6.45 a) on all previously observed fluorescence wavelengths. In terms of positions and shape of the hyperfine components a good a agreement is observed between recorded structure and theoretically predicted transition (see figure 6.45 b) from a known lower level to the upper level 31629.417 cm^{-1} as shown in the suggestion list of the classification program.

In order to further confirm the existence of upper level and the J-value the recorded structure was fitted independently i.e. by trying different sets of J-values of upper and lower level and letting free the A-values. The best fit of the recorded structure (see figure 6.46) was obtained with $J_o = 17/2 - J_u = 15/2$ and with $A_o = 560.93$ MHz, $A_u = 887.16$ MHz. These values are in full agreement with the predicted values and now keeping fix hyperfine constant of known combining lower level at this line as $A_u = 889.50$ MHz the structure is again fitted. The fit gave the hyperfine constant of upper level as $A_o = 563.08$ MHz. The wave number of the upper level is corrected using this excitation resulting in a value 31629.427 cm^{-1}. This proved beyond doubt the existence of upper level in terms of energy and J value.
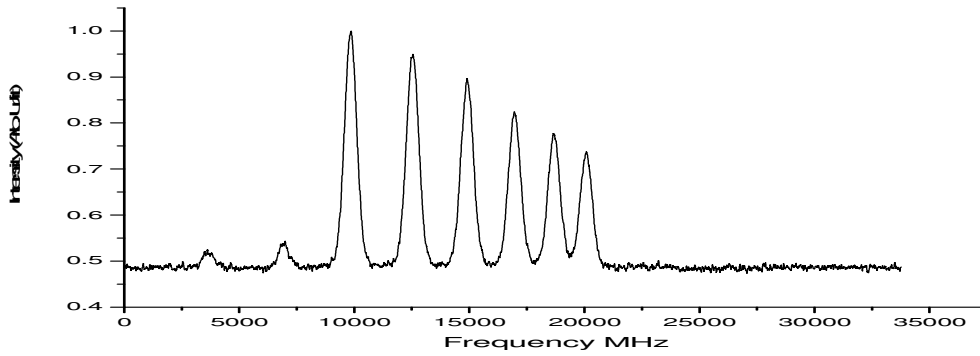
(a)
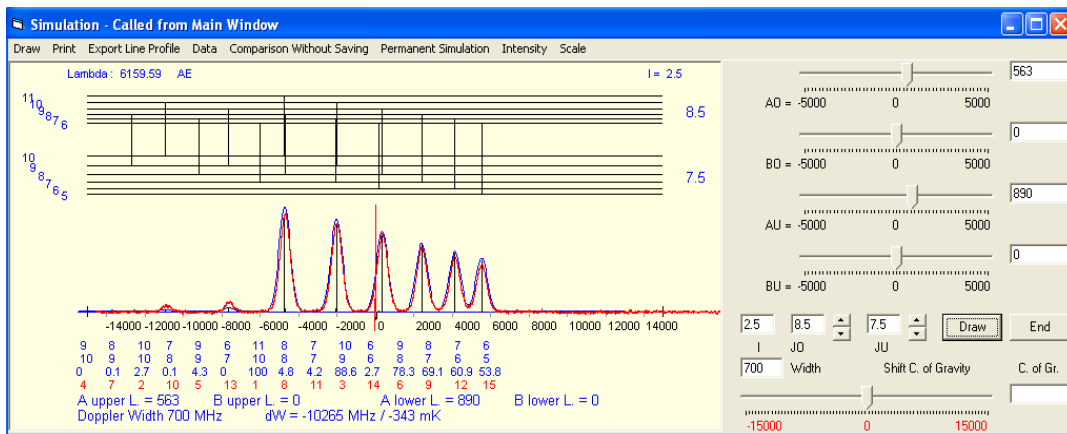
(b)

Figure 6.45: (a) LIF signal of line at 6159.59 Å (b) simulation with theoretical prediction
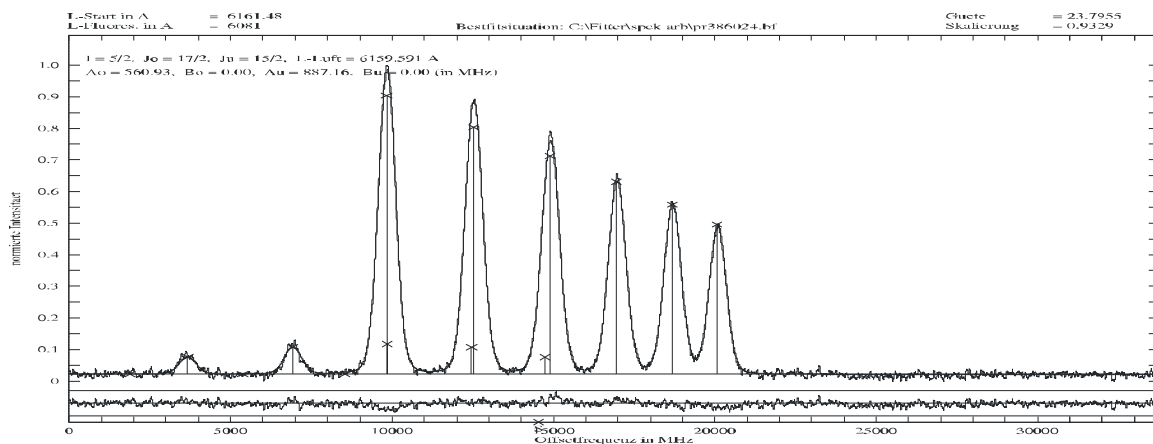
Figure 6.46: Best situation of the recorded hyperfine structure of line 6159.59 Å

Wave number of the upper most level of triplet can now be improved by using the corrected wave number of upper level from second excitation and center of gravity wave number from first excitation involving perturbed structure and is listed in table 6.12.

Table 6.12: Improved values of wave number of upper most level of triplet, computed from the wave number of upper level 31629.427 cm^{-1}.

cog λ_{air} (Å)	J_u	Parity	Energy (cm^{-1})	A_u (MHz)	$J_o = 17/2$, Parity = e, $A_o = 563.08$ MHz
					Energy (cm^{-1})
6082.034	15/2	o	15192.085	729.01	
---	---	---	---	---	31629.427
---	---	---	---	---	

This transition from level triplet to upper level 31629.266 cm^{-1} is of particular importance due to the appearance of third group of hyperfine components which corresponds to a transition from the lowest triplet level which has J = 13/2 to the upper level with J = 17/2. Such a transition is electric dipole forbidden ($\Delta J = +2$). Furthermore there is no transition from the middle triplet level to upper level. Hyperfine structure resulting from the transition from the upper most triplet level to upper level 31629.427 cm^{-1} has almost the normal relative intensities showing almost no deviation from the predicted structure. As the transition from lowest level of triplet to upper level is electric dipole forbidden ($\Delta J = +2$), the frequency positions for transitions between their F-sublevels responsible for third group are calculated manually using Casimir formula (see section 3.7). For this taking $J_o = 17/2$, $J_u = 13/2$, $A_o = 560.53$ MHz, $A_u = 666$ MHz and the wave number difference of lowest triplet level and upper level. Also, B_o and B_u are set equal to zero (in most cases in praseodymium value of B is taken equal to zero due to its small nuclear quadrupole moment Q). The results of calculations are summarized in Table 6.13. Transition scheme between triplet levels and upper level 31629.427 cm^{-1} is shown in figure 6.47. Frequency positions for the third group are drawn taking the values from Table 6.13.

Table 6.13: Frequency positions of hyperfine components in third group of perturbed structure.

F_o - F_u	Casimir Factors		Frequency positions of hfs components ν / cm^{-1}
	α_o	α_u	
11 - 9	21.25	16.25	16438.220
10 - 8	10.25	7.25	16438.214
9 - 7	0.25	-0.75	16438.205
8 - 6	-8.75	-7.75	16438.192
7 - 5	-16.75	-13.75	16438.176
6 - 4	-23.75	-18.75	16438.156
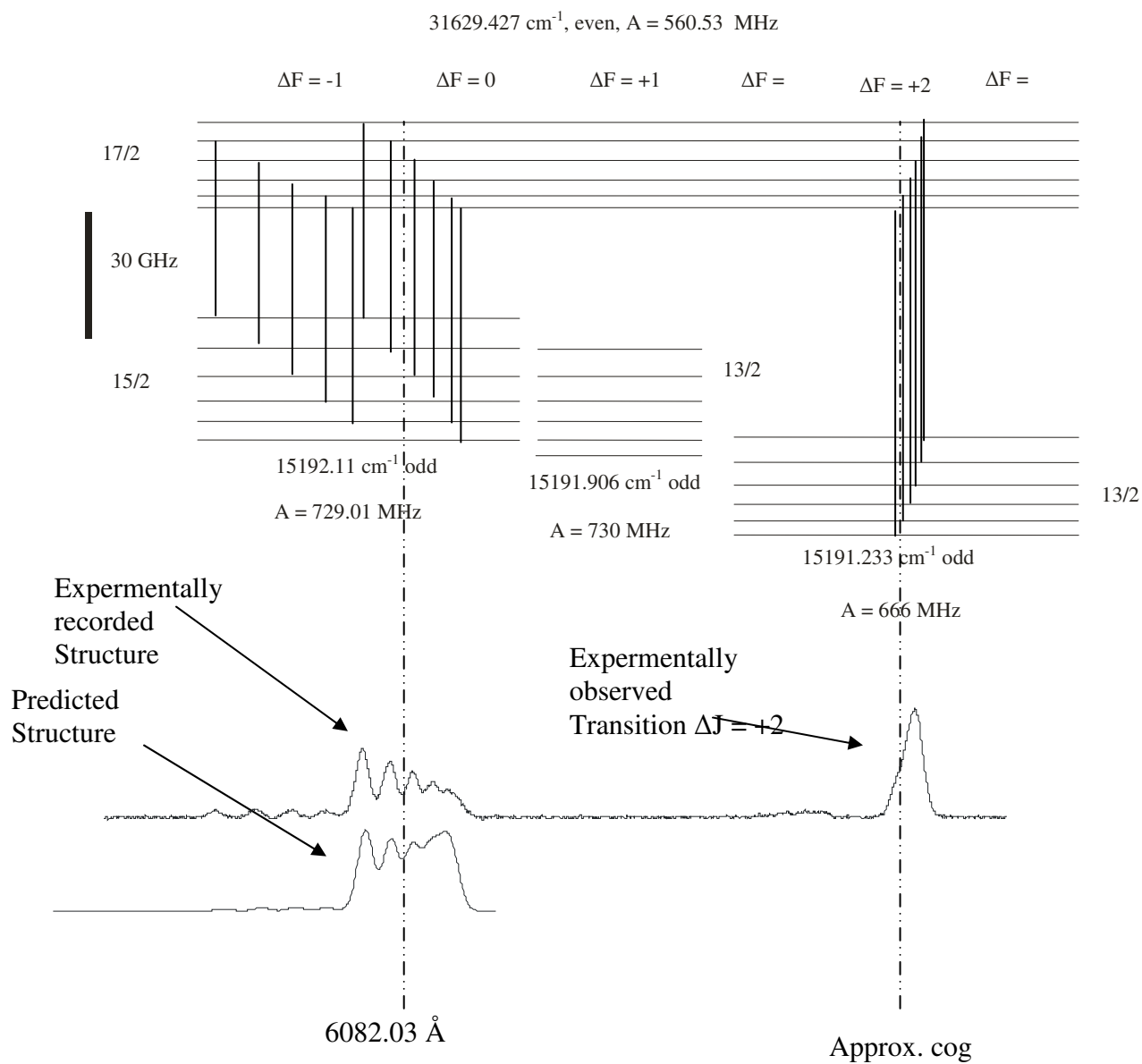
Figure 6.47: Level scheme for transition from triplet to upper level 31629.427 cm^{-1}, center-of-gravity positions marked by broken lines.

6.7 Excitation of level $31437.408^{e}_{17/2}$ cm^{-1} from Level Triplet

The spectral line at 6153.93 Å has a good signal to noise ratio in FT-Spectra (see figure 6.48) with a relative intensity of 8. Although hyperfine components of the line in FT-Spectra are not fully resolved, nevertheless the line was experimentally investigated with an expectation that the shape of the line will be reproduced.
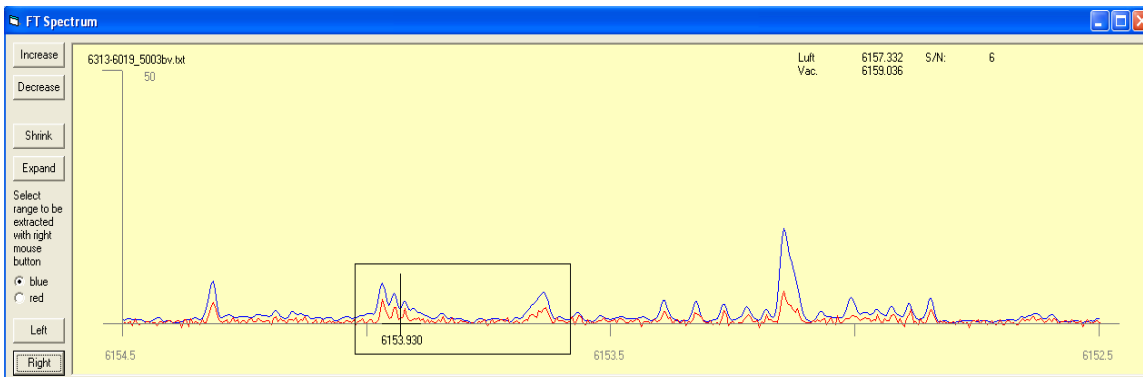
Figure 6.48: FT-Spectra of the line at 6153.93 Å

By setting the laser frequency to the highest component position, LIF signal is detected on 3695 Å, 5405 Å, 5997 Å, 6007 Å, 6061 Å, 6233 Å, 6823 Å and 6930 Å fluorescence wavelengths with strongest appearing on 6232 Å. Now by continuous scanning the laser frequency LIF signal of the line was recorded at fluorescence wavelength 6232 Å. The recorded hyperfine structure of the line indicated anomalous intensity distribution of hyperfine components as shown in figure 6.49. A similar behaviour is seen on the observed fluorescence wavelengths.
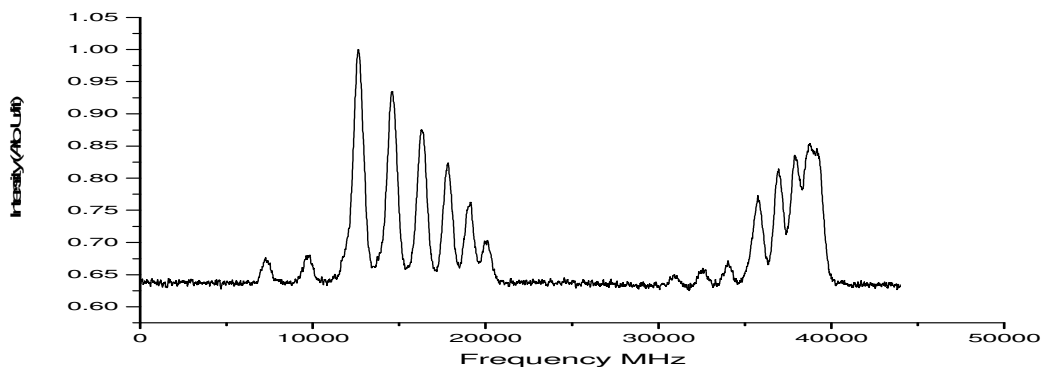
Figure 6.49: LIF Signal of the line with start wavelength 6154.12 Å

It is assumed that the level triplet is involved in the excitation of the line. In the recorded spectrum the relative intensities of hyperfine structure components for transition from uppermost level of triplet to upper level are not severely disturbed, suggesting a weak perturbation. The transitions from the middle level of triplet to upper level are completely missing. The last group of hyperfine structure components as transition from the lowest level of triplet to upper level appears with deformed hyperfine structure pattern. In the

126

recorded spectrum hyperfine structure appearing at longer wavelength was simulated and the best result of the simulation (see figure 6.50) was observed for J of upper level as 17/2 with A = 486 MHz. Similar to the transition from level triplet discussed in section 6.6, this means a transition from the upper most level of triplet to upper level with J_o = 17/2 and J_u = 15/2. For the last group of hyperfine structure components a similar interpretation as given earlier in section 6.6., that due to perturbation J of the lowest level of triplet is no longer a good quantum number having a value which is an admixture of 13/2 and 15/2.
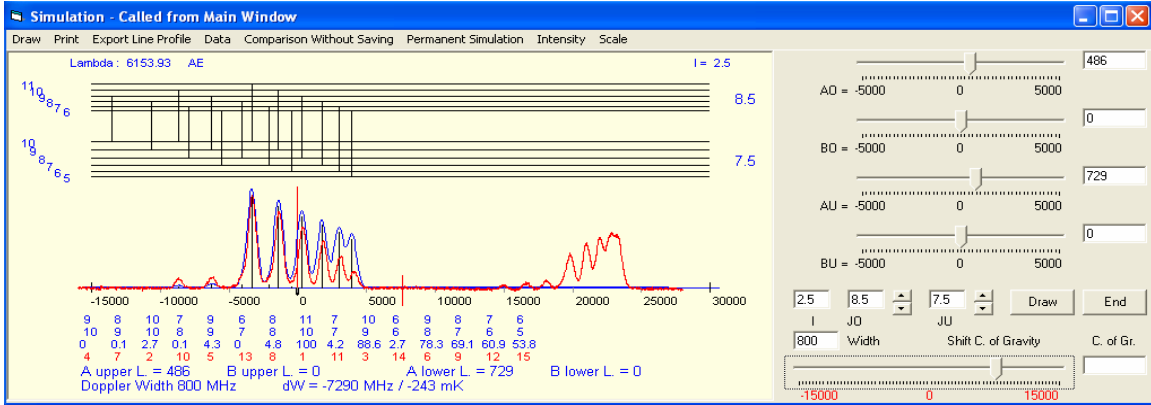
Figure 6.50: Simulation of the perturbed recorded structure (red line profile) recorded with start wavelength 6154.12 Å

The recorded perturbed structure is fitted using single line fit procedure taking into account only the first group of hyperfine components i.e. for transition from uppermost level of triplet to upper level. Best fit (see figure 6.51) is obtained for J_o = 17/2 - J_u = 15/2 and giving A_o = 488.54 MHz and A_u = 733.54 MHz. The wave number of the upper level is calculated by using the center of gravity wave number of the fitted first group and the wave number of the upper most level of triplet. The computation gave the wave number of the expected new upper level as 31437.414 cm^{-1}. The newly found upper level was introduced in the classification program which generated its transition list.
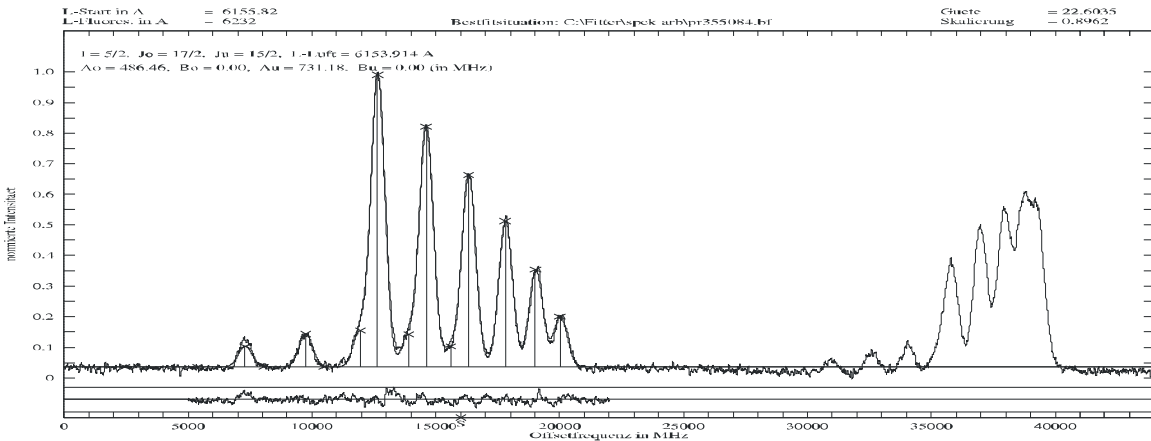
Figure 6.51: Best fit of perturbed structure recorded with start wavelength 6154.12 Å

In order to prove the existence of upper level with an angular momentum of 17/2, more excitations to the upper level are required. Two more excitations to the upper level i.e. at center of gravity wavelengths 6061.30 Å and 6233.34 Å which were also the fluorescence lines for this level, were performed. The line at 6061.30 Å has a good signal-to-noise ratio in FT-spectra (see figure 6.52) with a relative intensity of 8. The hyperfine components are partially resolved.
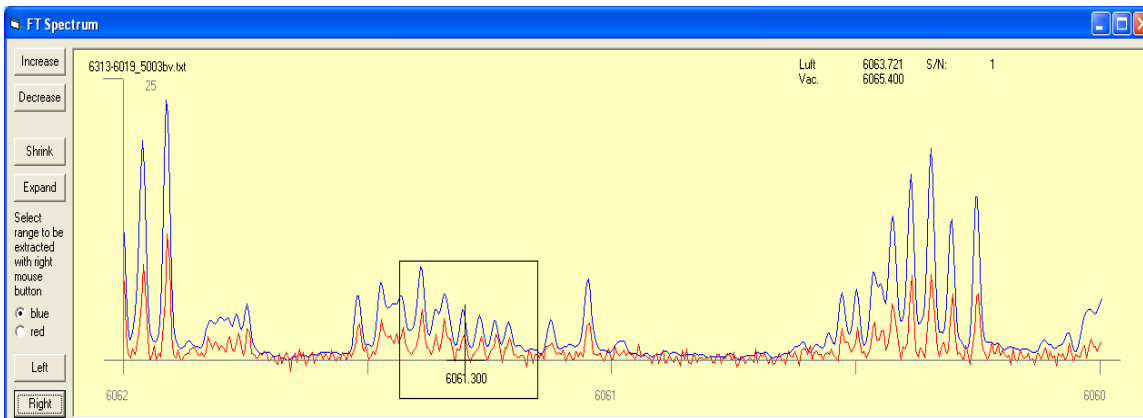
Figure 6.52: FT-Spectra for the line at 6061.30 Å

At this line the upper level 31437.414 cm^{-1} is combining with an odd parity level with level energy 14943.85 cm^{-1} having J = 17/2 and A = 808.1 MHz. By scanning the laser frequency, the LIF signal of the line was recorded on fluorescence wavelength 6154 Å. The recorded hyperfine structure (see figure 6.53) indicated off-diagonal components on both sides of well resolved diagonal components. In order to improve the A value determined from first excitation, the recorded structure at this line 6061.29 Å was fitted keeping fix the A value of lower level as 808.1 MHz. The best fit (see figure 6.54) gave the A value of upper level as 486.46 MHz. Level energy for the upper level was corrected i.e. 31437.408 cm^{-1} (assuming that energy of lower level is correct within some margin of error). Furthermore this excitation also confirmed the J value of upper level as 17/2.
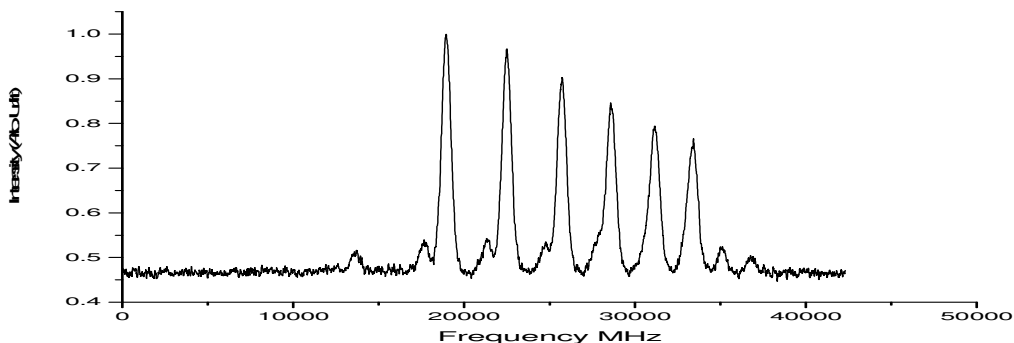
Figure 6.53: Recorded hyperfine structure of line at 6061.29 Å

Another confirmation of the upper level was done by the excitation of the line at 6233.34 Å. The recorded hyperfine structure for this line is shown in figure 6.55. The line is explained as a combination $\mathbf{31437.408^e_{17/2} - 15398.916^o_{15/2}}$. These two excitations are

sufficient proof of the J-value and wave number of the upper level excited from triplet. Wave number of the upper most level of triplet can now be re-calculated by using the corrected wave number of upper level from second excitation and center of gravity wave number from first excitation involving perturbed structure and is listed in table 6.14.
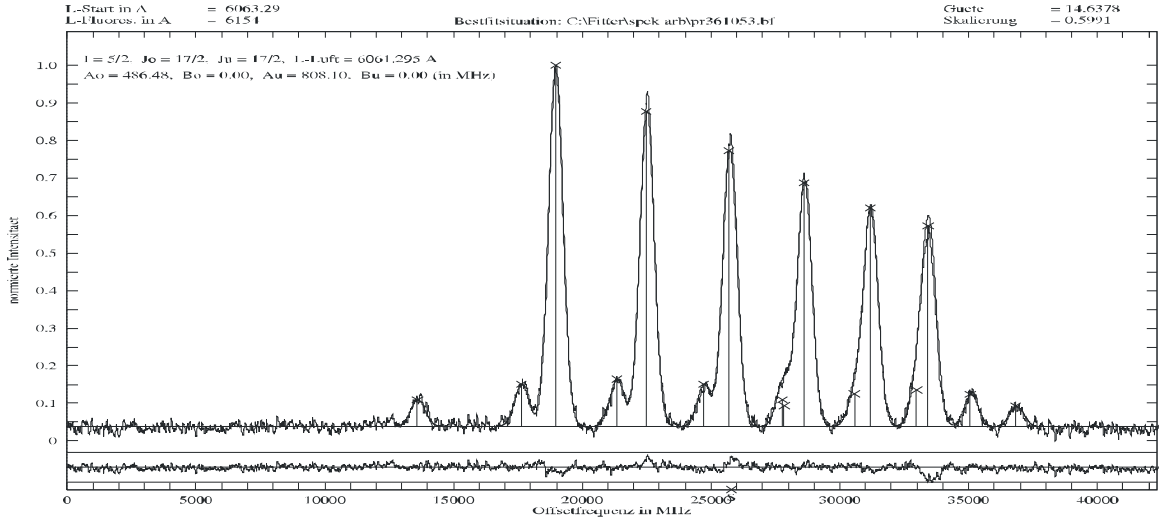
Figure 6.54: Best fit situation of the line at 6061.29 Å
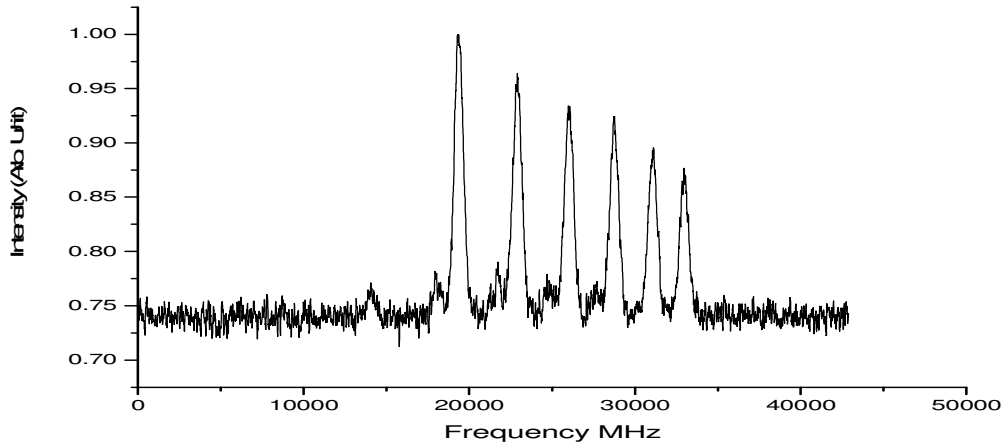
Figure 6.55: Recorded hyperfine structure of line at 6233.34 Å

Table 6.14: Improved values of wave number of upper most level of triplet, computed from the wave number of upper level 31437.408 cm^{-1}.

cog λ_{air} (Å)	Lower Level				Upper Level
	J_u	Parity	Energy (cm^{-1})	A_u (MHz)	J_o = 17/2, Parity = e, A_o = 486.463 MHz
					Average Energy (cm^{-1})
6153.91	15/2	o	15192.084	731.18	31437.408
---	---	---	---	---	
---	---	---	---	---	

Similar to the transition discussed in section 6.6, an excitation from the upper most level of triplet to upper level is dipole allowed but from lowest level of triplet to upper level with $J = 17/2$ is electric dipole forbidden ($\Delta J = +2$). Even then the third group of hyperfine structure components (see figure 6.47) is observed. So the frequency positions for transitions between the F-sublevels of lowest level of triplet and upper level are calculated manually using Casimir formula (see section 3.7), taking $J_o = 17/2$, $J_u = 13/2$, $A_o = 486.463$ MHz, $A_u = 666$ MHz and the wave number difference of lowest triplet level and upper level. B_o and B_u are set equal to zero. The results of calculations are summarized in Table 6.15. Transition scheme between triplet levels and upper level 31437.408 cm^{-1} is shown in figure 6.56. Frequency positions for the third group are drawn taking the values from Table 6.15.

Table 6.16: Frequency positions of hyperfine components in third group of perturbed structure.

F_o - F_u	Casimir Factors		Frequency positions of hfs components ν / cm^{-1}
	α_o	α_u	
11 - 9	21.25	16.25	16246.158
10 - 8	10.25	7.25	16246.180
9 – 7	0.25	-0.75	16246.195
8 – 6	-8.75	-7.75	16246.205
7 – 5	-16.75	-13.75	16246.208
6 – 4	-23.75	-18.75	16246.206

31437.408 cm^{-1} , even, A = 486.463 MHz

$\Delta F = -1$ $\Delta F = 0$ $\Delta F = +1$ $\Delta F =$ $\Delta F = +2$ $\Delta F =$

17/2

30 GHz

15/2

13/2

15192.084 cm^{-1} odd

15191.906 cm^{-1} odd

13/2

A = 731.18 MHz

A = 730 MHz

15191.233 cm^{-1} odd

Perturbed Structure

A = 666 MHz

Observed
Transition $\Delta J = +2$

Predicted
structure

6153.91 Å

Approx. cog
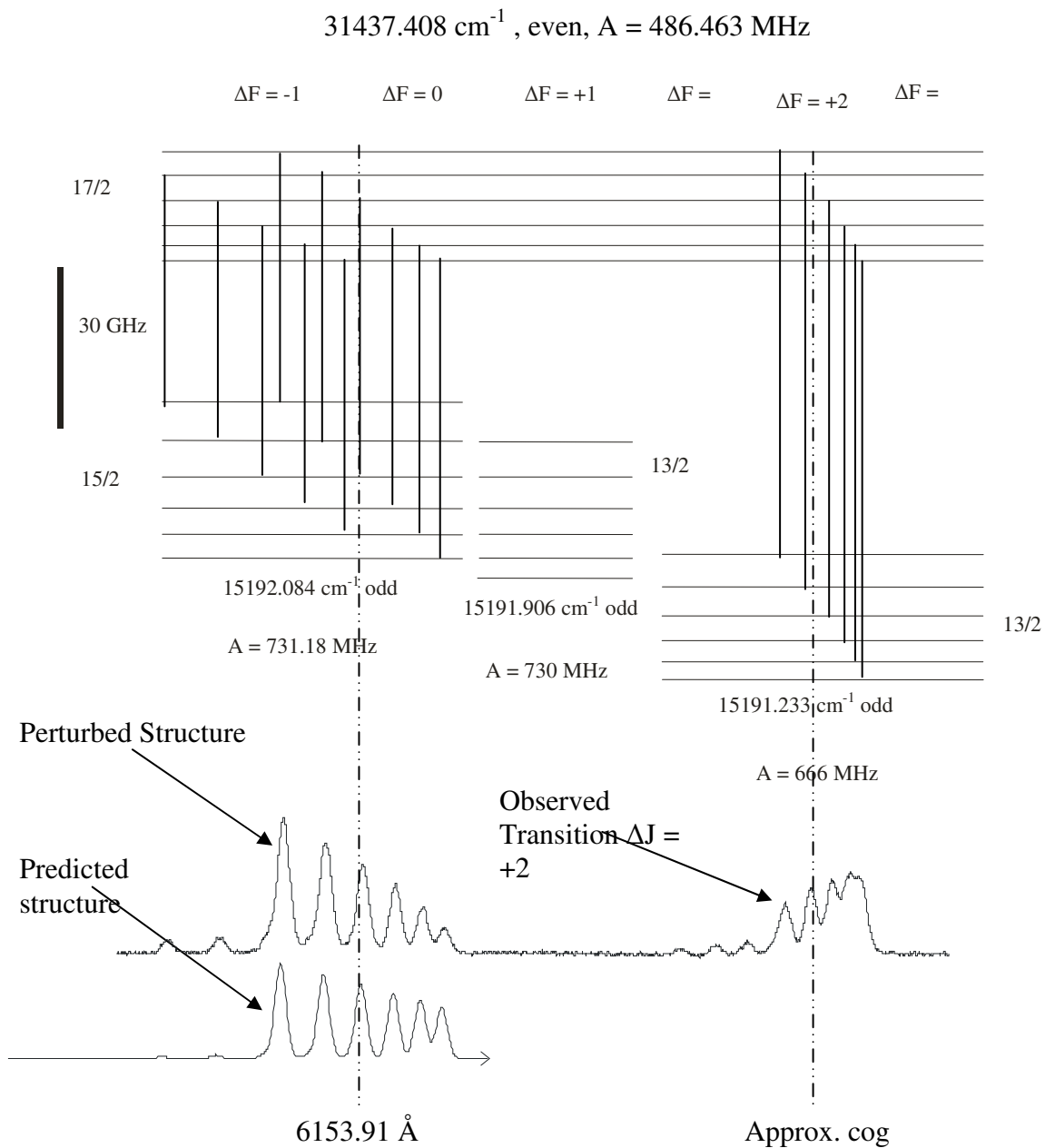
Figure 6.56: Level scheme for transition from triplet to upper level 31437.408 cm^{-1}, center-of-gravity positions marked by broken lines.

131

6.8 Excitation of level $31642.946^e_{13/2}$ cm^{-1} from Level Triplet

The level with energy 31642.946 cm^{-1} was discovered via laser excitation of the line at 5835.15 Å. Only through laser excitation the hyperfine structure for the line reveals itself since in FT-Spectra (see figure 6.57) hyperfine structure of the recorded line is not clearly seen and the stronger line completely hides its hyperfine structure.
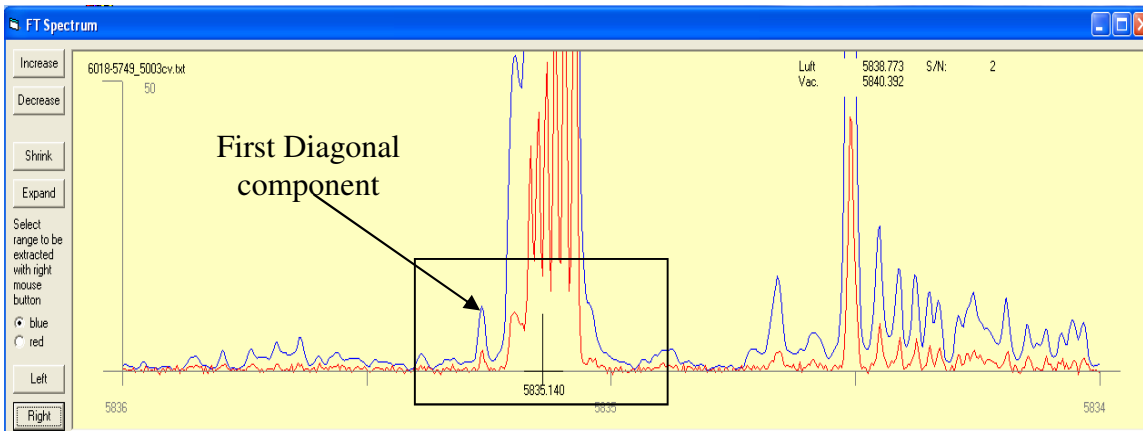
Figure 6.57: FT-Spectra of the line at 5835.15 Å

Nevertheless the hyperfine structure of the line was experimentally recorded on 10 different fluorescence channels i.e. 3304 Å, 3668 Å, 4919 Å, 5090 Å, 5329 Å, 5364 Å, 5530 Å, 6076 Å, 6136 Å and 6568 Å. The recorded spectrum is shown in figure 6.58.
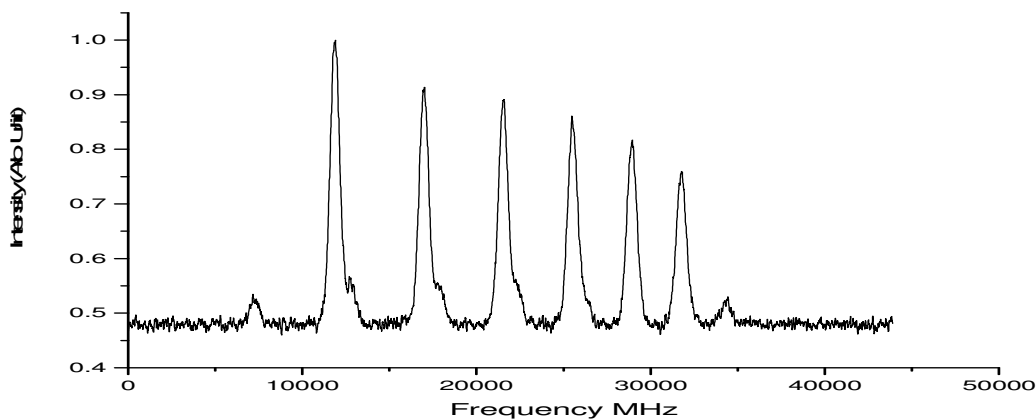
Figure 6.58: Hyperfine structure of recorded line at 5835.15 Å

A best fit of the recorded structure was obtained with J_o = 13/2, J_u = 13/2, A_o = 518.65 MHz and A_u = 1086.42 MHz and with a quality factor of 16 (see figure 6.59). Assuming an unknown upper level, a known lower level was searched based on A and J values in the data base of known levels. A level with energy 14510.22 cm^{-1} with odd parity and A_u = 1085.4 MHz was found. The recorded structure was again fitted keeping fix the A value of lower level. With this assumption, the hyperfine constant of upper level was determined to be 518.7 MHz. Using the center of gravity wave number and the wave

number of lower level the wave number of the upper level was computed as 31642.946 cm^{-1}. The parity of upper level was set as even with respect to the odd parity lower level. The line was then classified as a transition between

$$31642.946^{e}_{13/2}\,cm^{-1}\,,A_{o}=518.7\,MHz \longleftrightarrow 14510.22^{o}_{13/2}\,,A_{u}=1085.4\,MHz$$
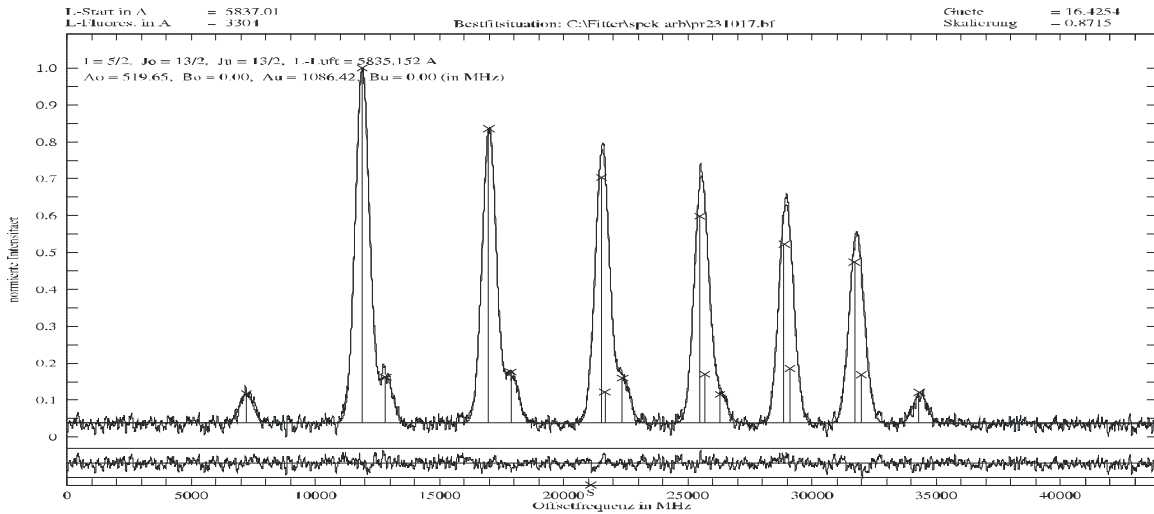
Figure 6.59: Best fit situation for the line recorded at 5835.15 Å

In order to confirm the existence of upper level a second excitation at the line 6077.02 Å was performed. The suggestion list for the line predicts a combination of the upper level 31642.946 cm^{-1} with the level triplet, although with normal intensity distribution of hyperfine structure components. This is because the classification program uses normal intensity ratios. FT-Spectra (figure 6.60) indicate a mixture of several lines possibly embedding the lines responsible for transition from level triplet to upper level.
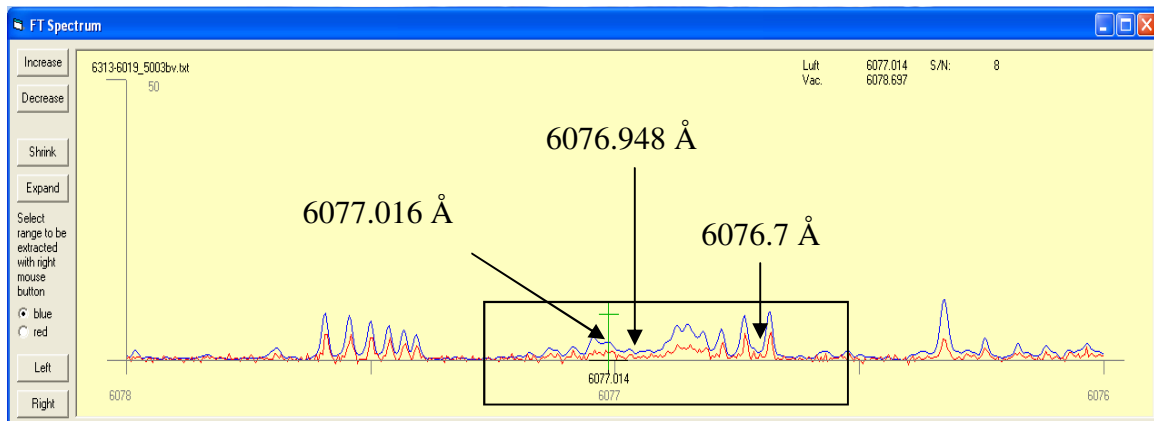
Figure 6.60: FT-Spectra showing the positions of lines for expected transition from level triplet

Setting the laser frequency at 6077.016 Å, a strong LIF signal was seen on one of the previously recorded fluorescence wavelength i.e. 3304 Å. Furthermore LIF was also seen on all other previously observed fluorescence wavelengths. Now by continuously scanning the laser frequency from start wavelength 6077.17 Å and setting the monochromator to 3304 Å, LIF signal was recorded. As is usual for transitions from level triplet the intensity profile of the recorded spectrum is disturbed (see figure 6.61). The three groups of intensity profile are clearly seen with wider separation between hyperfine components. Furthermore in the third group the diagonal components ($\Delta F = 0$) are more pronounced whereas one set of off-diagonal components ($\Delta F = -1$) is not seen. The diagonal components ($\Delta F = 0$) of second group and diagonal components ($\Delta F = -1$) of first group perturb each shows a changed intensity profile. LIF signal was recorded on all previously observed fluorescence channels, i.e. 3304 Å, 3668 Å, 4919 Å, 5090 Å, 5329 Å, 5364 Å, 5530 Å, 6076 Å, 6136 Å and 6568 Å and each case same perturbed behaviour was seen.
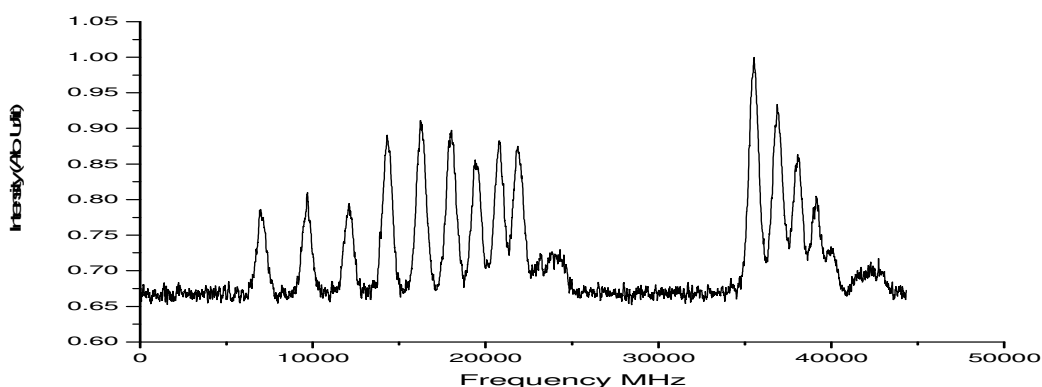
Figure 6.61: Perturbed hyperfine structure for lines with start wavelength 6077.17 Å

Simulation of the recorded structure (see figure 6.62) with the predicted hyperfine structure patterns involving the known upper level from the first excitation and levels in triplet as lower levels gave a good agreement in terms of the positions of the diagonal hyperfine components.

This confirmed that the recorded structure is due to the transition from level triplet to upper level 31642.946 cm^{-1} with diagonal components appearing in all three groups (see figure 6.61). The J- and A-values of upper level as a result of simulation are 13/2 and 519 MHz respectively in conformity with first excitation to the upper level. Using J and A values of levels in triplet and of upper level, the recorded structure was fitted using a multiline fit. Best fit was obtained (see figure 6.63) for J and A values within good agreement with the previously determined values.
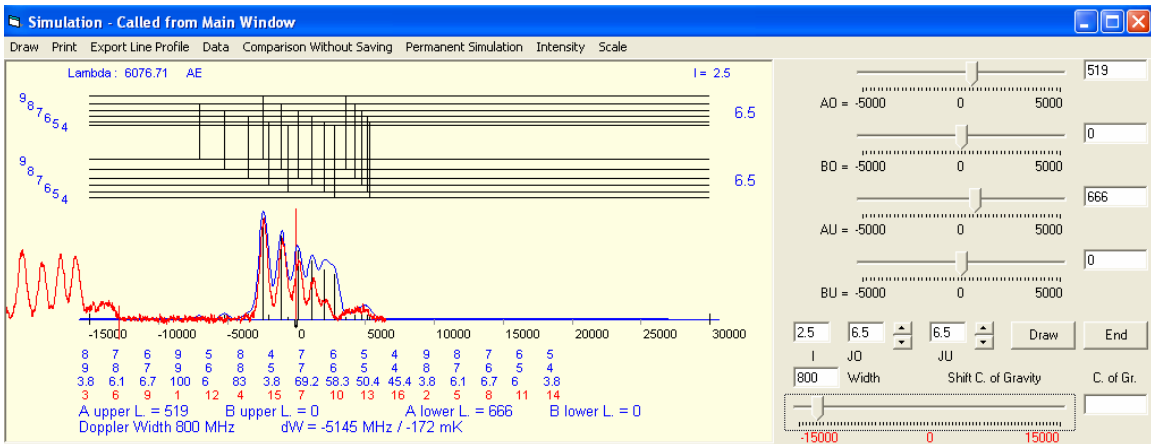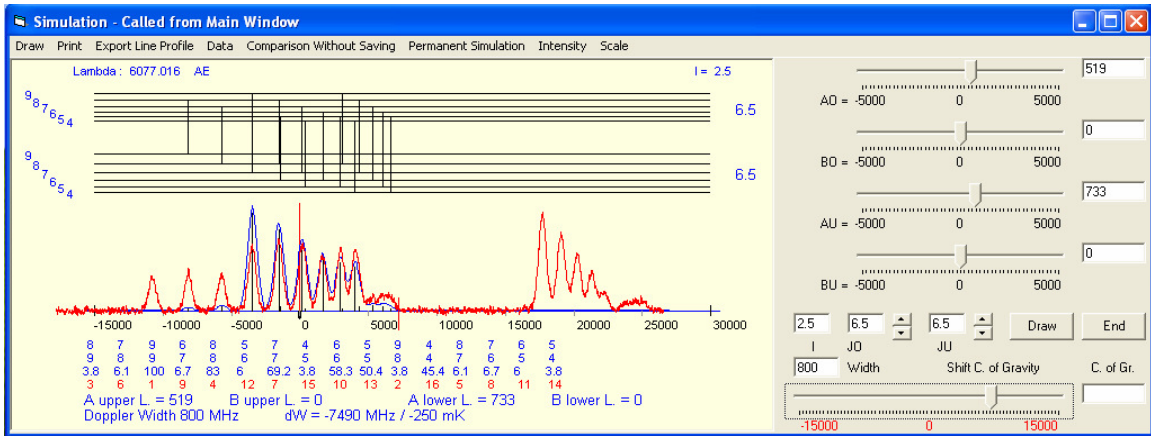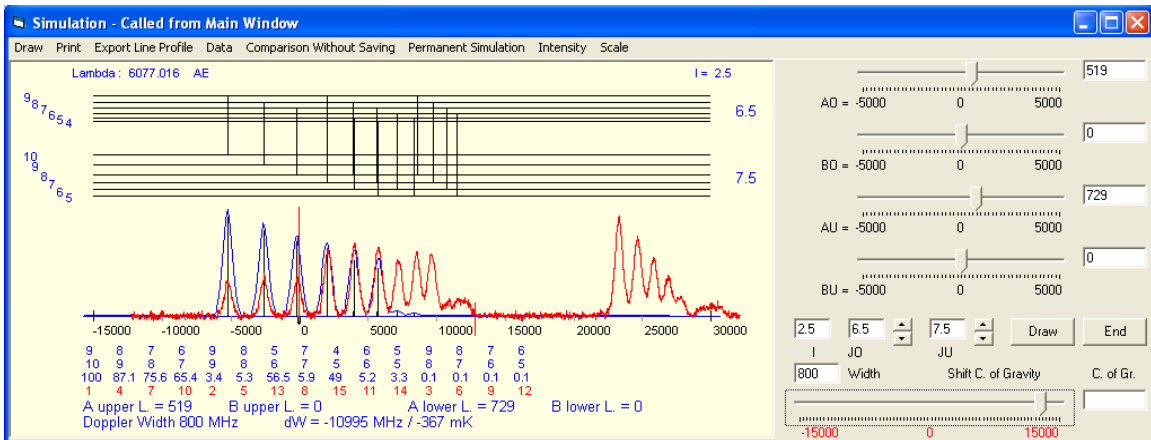
Figure 6.62: Simulation of the perturbed recorded structure (red line profile) recorded with start wavelength 6077.17 Å
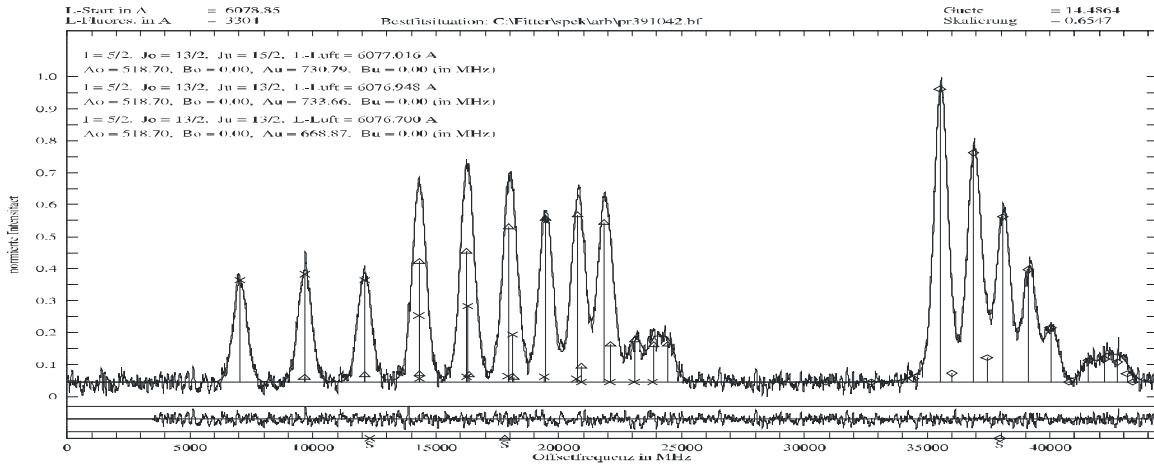
Figure 6.63: Best fit situation of the recorded perturbed structure with start wavelength 6077.17 Å

Wave numbers of the levels in triplet are improved using wave number of the upper level and the center of gravity wave numbers from best fit situation for transition from triplet and wave number of upper level (Table 6.16). The level scheme with a comparison between experimentally recorded perturbed and simulated unperturbed hyperfine structure pattern is presented in figure 6.64.

Table 6.16: Improved values of wave numbers of levels in triplet, computed from the wave number of upper level 31642.946 cm^{-1}.

cog λ_{air} (Å)	Lower Level				Upper Level
	J_u	Parity	Energy (cm^{-1})	A_u (MHz)	J_o = 13/2, Parity = e, A_o = 518.7 MHz
					Energy (cm^{-1})
6077.016	15/2	o	15192.056	730.79	
6076.948	13/2	o	15191.872	733.66	31642.946
6076.700	13/2	o	15191.200	668.87	

136
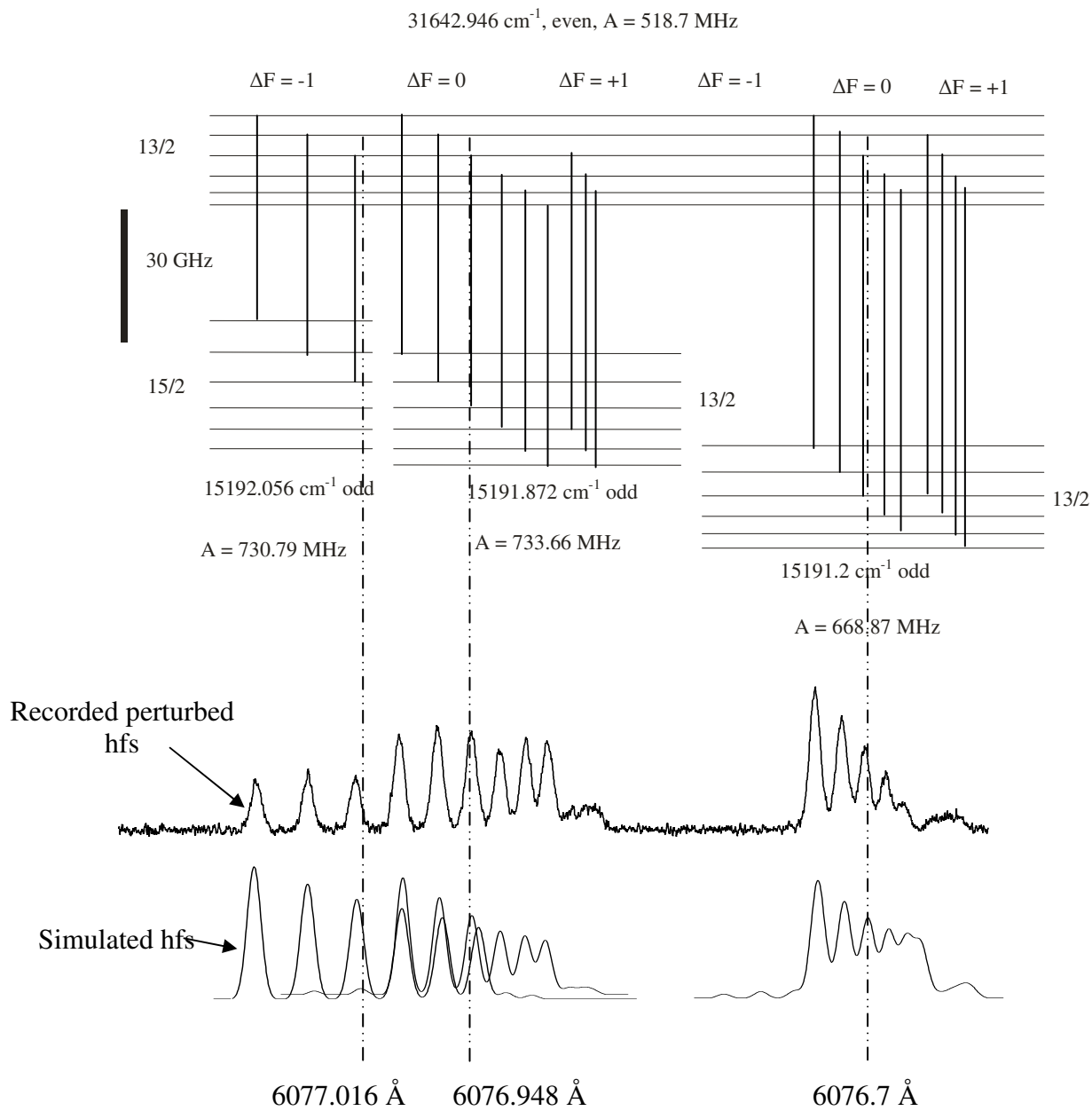
Figure 6.64: Level scheme for transition from triplet to upper level 31642.946 cm^{-1}, center-of-gravity positions marked by broken lines.

6.9 Excitation of level $31688.137^{e}_{15/2} \, \mathbf{cm^{-1}}$ from Level Triplet

The level with energy 31688.137 cm^{-1} was discovered via a laser excitation of line at 6137.39 Å. The line has a very poor signal-to-noise ratio in FT-Spectra (see figure 6.65) with a relative intensity of only 2.
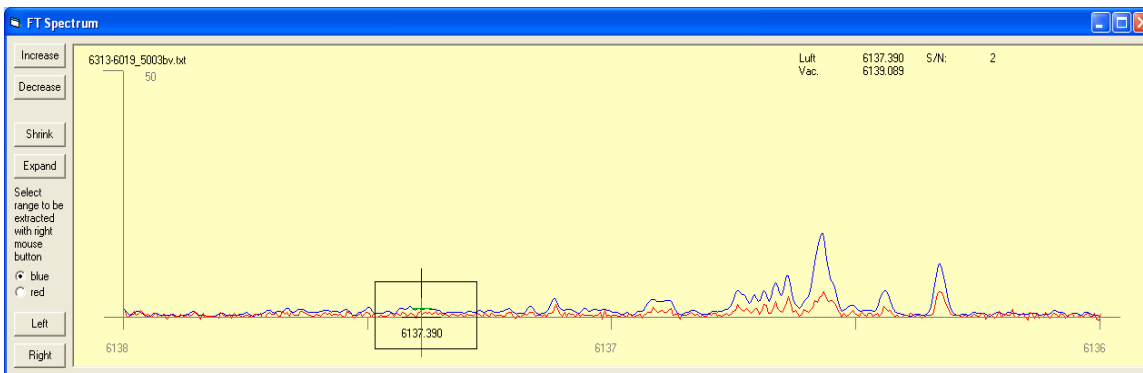
Figure 6.65: FT-Spectra for the line at 6137.39 Å

Contrary to this the LIF signal of line has a much better signal to noise ratio (see figure 6.66) and was recorded on 4 fluorescence channels i.e. 3467 Å, 5432 Å, 6060 Å, 6117 Å. The recorded hyperfine structure appears to have a transition with ΔJ = 0 i.e. with off-diagonal components on both sides of diagonal components.
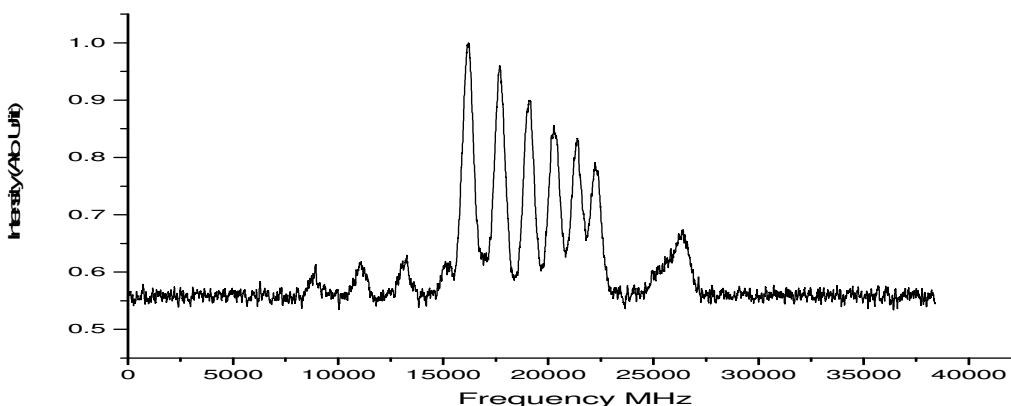
Figure 6.66: LIF signal of the line at 6137.39 Å

The recorded structure was fitted with best fit obtained for a transition with J = 15/2 – 15/2 and with A_o = 734.22 MHz and A_u = 886.31 MHz. The line could not be classified with any of the suggestions listed in classification program so by assuming a known lower level an upper level was search based on A and J values. A lower level with energy 15399.08 cm^{-1}, J_u = 15/2 and A_u = 889.50 MHz was found. Addition of the wave number of the excitation line gave the upper level as 31688.137 cm^{-1}, which explained all the observed fluorescence lines i.e. 3467 Å, 5432 Å, 6060 Å, 6117 Å. The structure was again fitted keeping fix A_u = 889.50 MHz and the hyperfine constant for upper level was

determined as 737.25 MHz (see figure 6.67). The wave number of upper level was determined by using the center of gravity wave number of the line and the wave number of the lower level and the line was then identified as a transition

$$31688.137^e_{15/2}, A_o = 737.28\,\text{MHz} \longleftrightarrow 15399.08^o_{15/2}, A_u = 889.50\,\text{MHz}$$
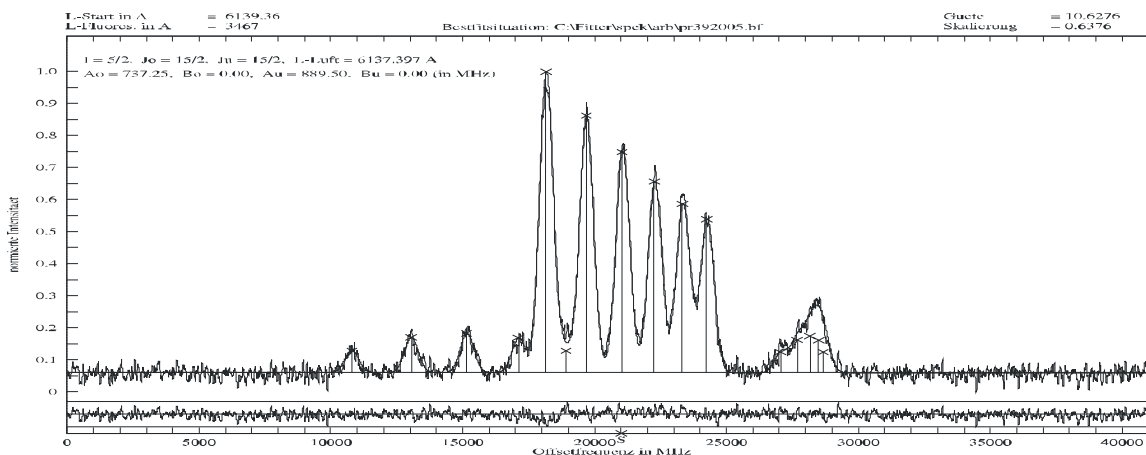
Figure 6.67: Best fit of the line at 6137.39 Å

Distinct feature of this transition is that the hyperfine splitting of upper level as determined from this excitation is large, comparable to the hyperfine splitting of levels in triplet. The newly discovered level was introduced and a transition list was generated by the classification program. At one of the observed fluorescence line i.e. 6060.38 Å the level appears to be combining with the level triplet. The FT-Spectrum shows an admixture of several lines (see figure 6.68) and has a good signal- to-noise ratio.
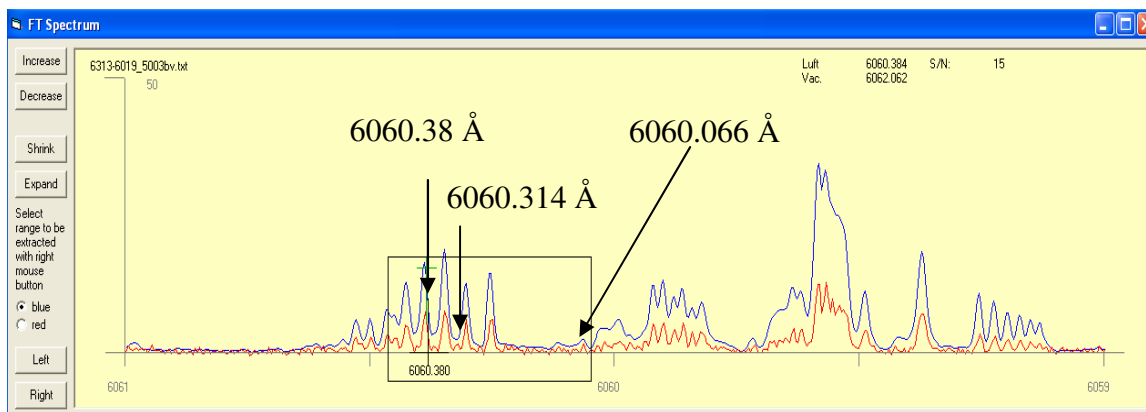
Figure 6.68: FT-Spectra showing the lines for transition from level triplet to upper level 31688.137 cm^{-1}

In order to confirm the energy of the newly discovered upper level a second excitation was performed on one of its fluorescence line i.e. 6060.38 Å. One of the listed suggestions for the line shows the combination of the upper level with level triplet. Although the predicted hyperfine structure pattern has normal intensity distribution of its

components this is because the classification program uses normal intensity ratios. Nevertheless laser excitation was performed by scanning the laser wavelength from 6060.42 Å and a hyperfine structure with abnormal intensity distribution of hyperfine components (see figure 6.69) was recorded at all the previously observed fluorescence wavelengths i.e. 3467 Å, 5432 Å, 6060 Å, 6117 Å.
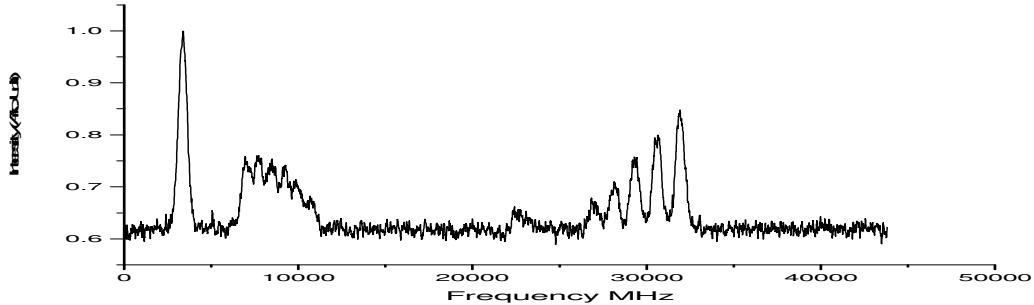
Figure 6.69: Anomalous intensity distribution of hyperfine components for the line recorded with start wavelength 6060.42 Å

Simulations of the recorded perturbed structure with the predicted transitions from levels of triplet to upper level 31688.137 cm^{-1} are presented in figure 6.70 a and b.
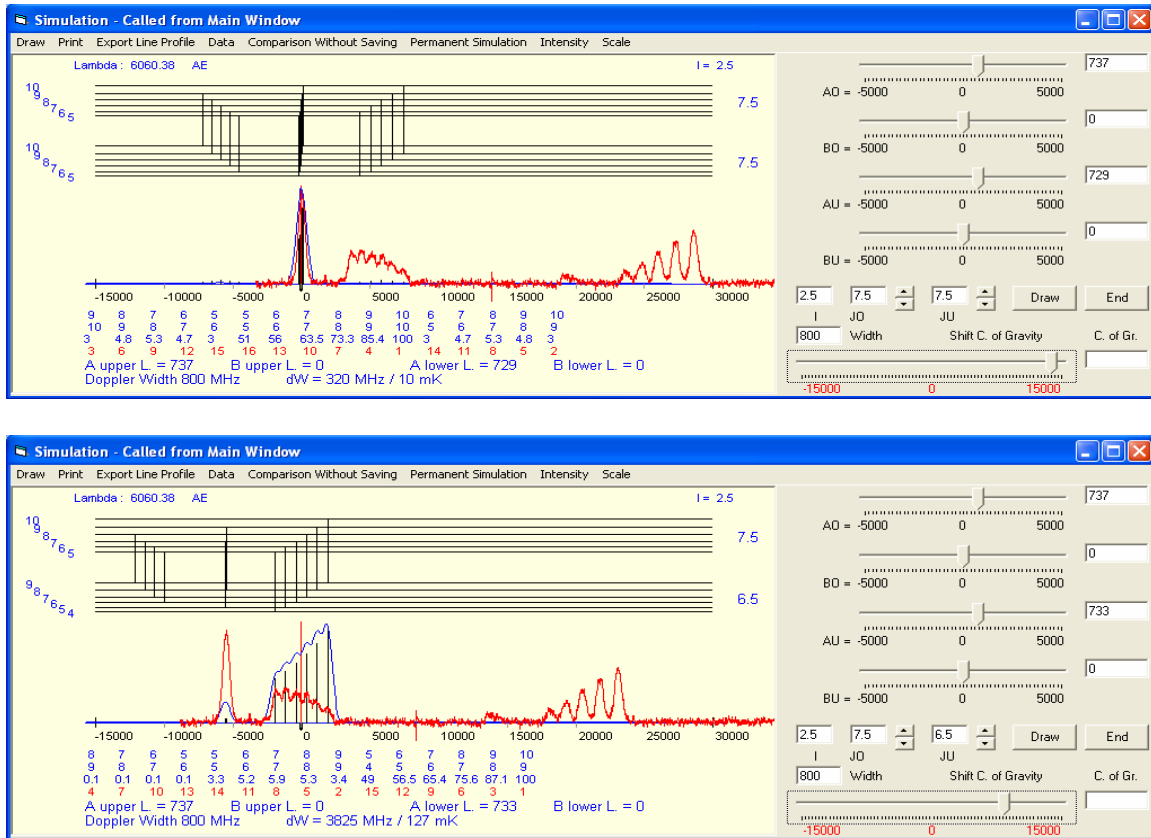
Figure 6.70 a: Simulations of the perturbed structure (red line profile) recorded with start wavelength 6060.42 Å

140
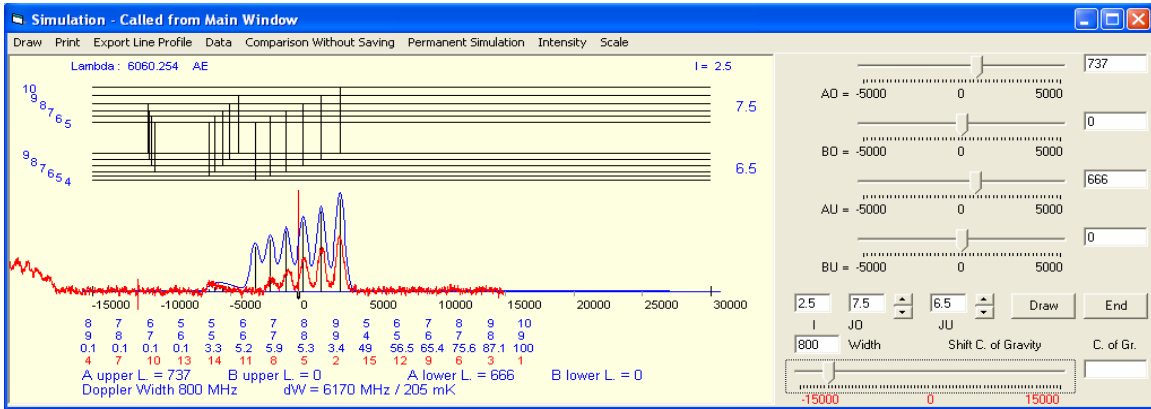
Figure 6.70 b: Simulations of the perturbed structure (red line profile) recorded with start wavelength 6060.42 Å

Simulations proved that the excited transition involve level triplet as a set of lower levels. Furthermore in comparison with the predicted pattern the character of the recorded hyperfine structure for the transition from the middle level to the upper level is changed whereas it remains almost the same for the transitions from uppermost level and the lowest level of triplet to upper level. The J- and A-values of upper level as a result of simulation are 15/2 and 737 MHz respectively in conformity with first excitation to the upper level.

Using J and A values of levels in triplet and of upper level, the recorded structure was fitted using a multiline fit. Best fit was obtained (see figure 6.71) for J and A values within good agreement with the previously determined values.
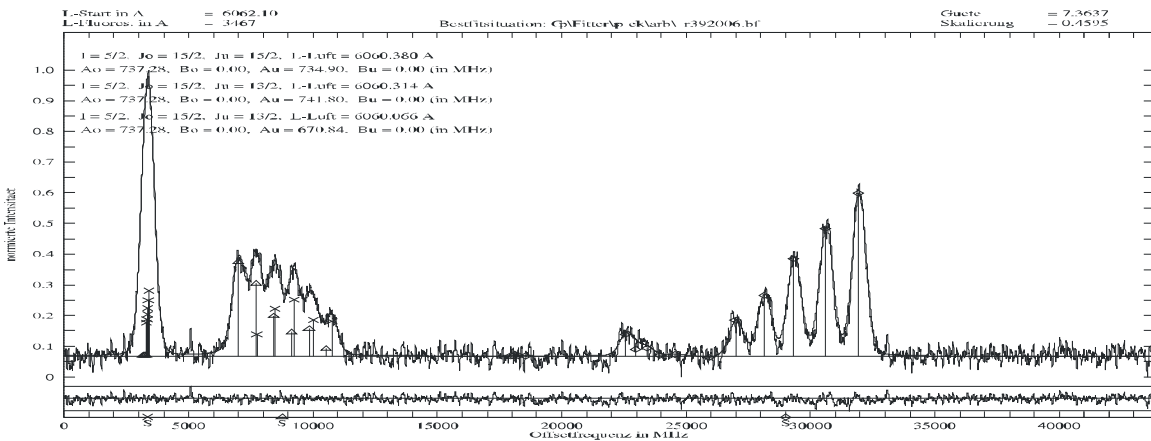
Figure 6.71: Best situation of the perturbed structure recorded with start wavelength 6060.42 Å

Using the center of gravity wave numbers from the fitted structure and the wave number of upper level as determined from first excitation, the wave number of the levels in triplet are improved (Table 6.17). The level scheme with a comparison between experimentally

recorded perturbed and simulated unperturbed hyperfine structure pattern is presented in figure 6.72.

Table 6.17: Improved values of wave numbers of levels in triplet, computed from the wave number of upper level 31688.137 cm^{-1}.

cog λ_{air} (Å)	\multicolumn{4}{c}{Lower Level}	Upper Level
	J_u	Parity	Energy (cm^{-1})	A_u (MHz)	$J_o = 15/2$, Parity = e, $A_o = 737.28$ MHz
					Energy (cm^{-1})
6060.380	15/2	o	15191.09	734.900	
6060.314	13/2	o	15191.91	741.800	31688.137
6060.066	13/2	o	15191.235	670.066	

31688.137 cm^{-1} even, A = 737.28 MHz

$\Delta F = 0$ $\Delta F = +1$ $\Delta F = -1$ $\Delta F = 0$

15/2

30 GHz

15/2

13/2

15191.09 cm^{-1} odd 15191.91 cm^{-1} odd 13/2

A = 734.90 MHz A = 741.80 MHz 15191.235 cm^{-1} odd

Perturbed Recorded hfs A = 670.84 MHz

Simulated hfs

6060.380 Å 6060.314 Å 6060.066 Å
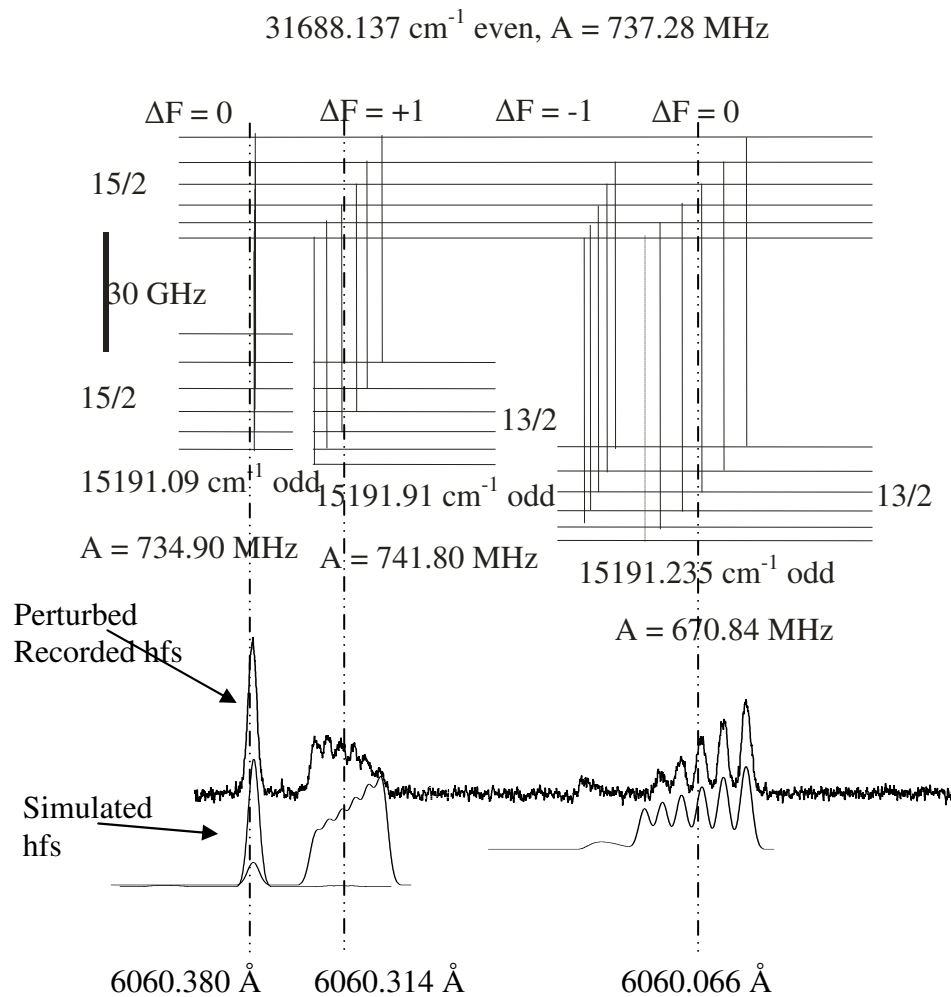
Figure 6.72: Level scheme for transition from triplet to upper level 31688.137 cm^{-1}, center-of-gravity positions marked by broken lines.

In addition to the excitation above from level triplet to the upper level, an excitation from level triplet to a known upper level with angular momenta J = 15/2 was also observed.

Laser excitation of line at 6340.33 Å to an already known upper level **$30959.778^{e}_{15/2}$ cm^{-1}** (Shamim 19-09-09 private communication) resulted in a recorded hyperfine structure pattern with an anomalous intensity distribution of hyperfine components (see figure 6.73). The structure was seen on more than one fluorescence wavelengths i.e. 5747 Å, 6077 Å, 6242 Å, 6425 Å, 6533 Å. Analysis of the recorded perturbed structure confirmed the combination of known upper level with level triplet at this line. Initially the upper level was discovered by laser excitation of line at 6075.25 Å showing normal intensity distribution of its hyperfine components. The result of the analysis is given in Table 6.31.
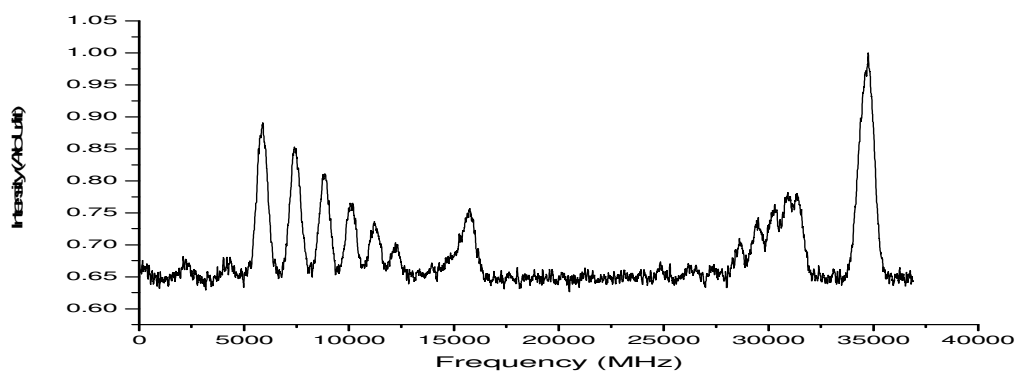
Figure 6.73: Anomalous intensity distribution of hyperfine components for the line recorded with start wavelength 6340.44 Å

6.10 Excitation of Level $31744.873^{e}_{15/2}$ cm^{-1} from Level Triplet

The level with energy 31744.873 cm^{-1} was discovered via a laser excitation of line at 6116.09 Å. The line has a good signal to noise ratio in FT-Spectra (see figure 6.74) and the hyperfine components are partially resolved with a relative intensity of 4.
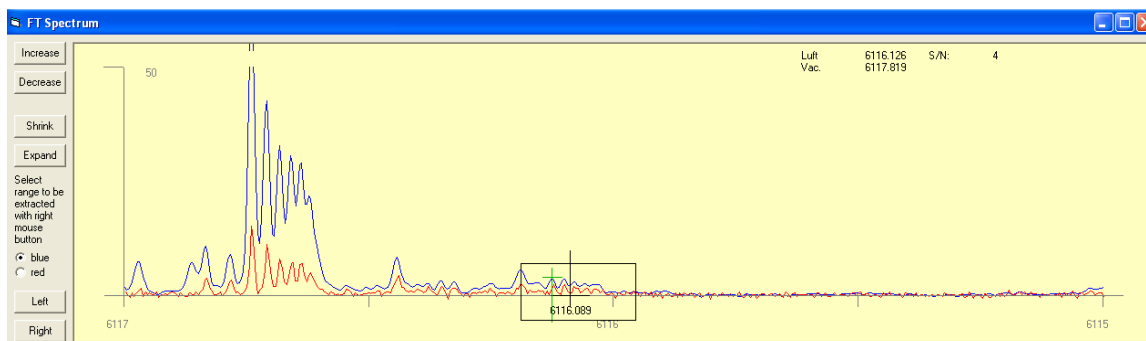
Figure 6.74: FT-Spectra of the line at 6116.09 Å

The laser excitation of the line resulted in a well resolved hyperfine structure recorded on 7 observed fluorescence channels i.e. 3460 Å, 5414 Å, 5633 Å, 5800 Å, 5947 Å, 6040 Å, 6478 Å. The recorded structure appears to have a transition with $\Delta J = 0$ i.e. with off-diagonal components on both sides of diagonal components (see figure 6.75).
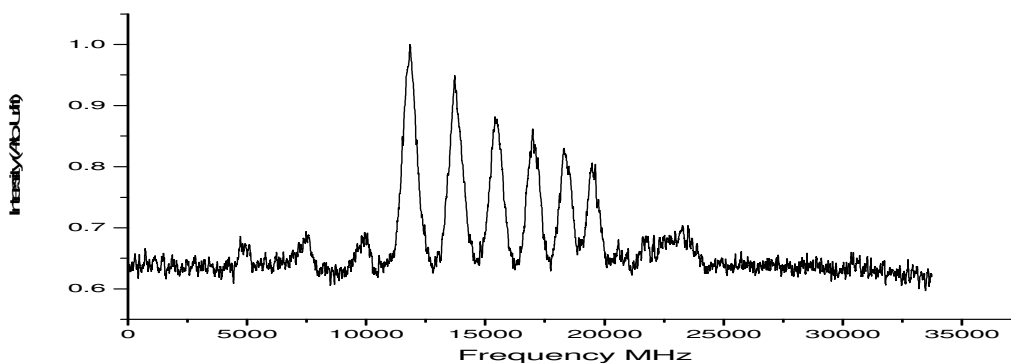
Figure 6.75: LIF signal of the line at 6116.09 Å on fluorescence wavelength 6040 Å

The best fit situation was obtained for a transition with J = 15/2 – 15/2 and with A_o = 695.68 MHz and A_u = 888.70 MHz. The line could not be classified with any of the suggestions listed in classification program. Assuming an unknown upper level involved in the excitation of line, a known lower level was search based on A and J values in the data base of known levels. A lower level with energy 15399.08 cm^{-1}, J_u = 15/2 and A_u = 889.50 MHz was found. Addition of the wave number of the excitation line gave the upper level as 31744.873 cm^{-1} which explained all the observed fluorescence lines i.e. 3460 Å, 5414 Å, 5633 Å, 5800 Å, 5947 Å, 6040 Å, 6478 Å.

The structure was again fitted keeping fix A_u = 889.50 MHz, the hyperfine constant for upper level was determined as 696.54 MHz (see figure 6.76). The wave number of upper level was determined by using the center of gravity wave number of the line and the wave number of the lower level and the line was then identified as a transition

$$31744.873^e_{15/2}, A_o = 696.54 \text{ MHz} \longleftrightarrow 15399.08^o_{15/2}, A_u = 889.50 \text{ MHz}$$
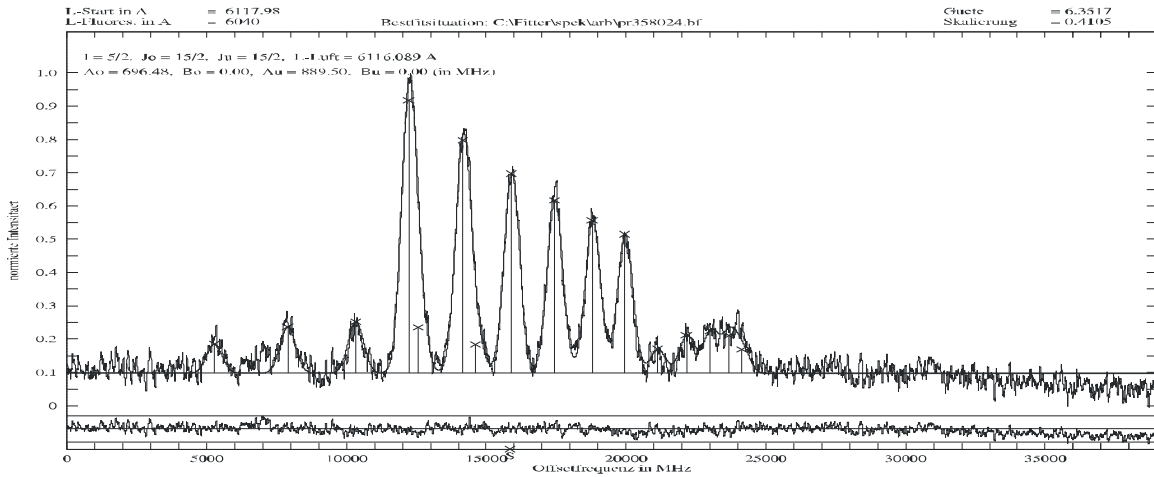
Figure 6.76: Best fit of the line at 6116.09 Å

The level was introduced and a transition list was generated by the classification program. At one of the observed fluorescence line i.e. 6040 Å the newly discovered upper level is combining with the level triplet. FT-Spectrum of the line is a mixture of several lines with not so good signal-to-noise ratio (see figure 6.77). In FT-Spectra the line seems to be hidden and nothing could be said about the expected transition.
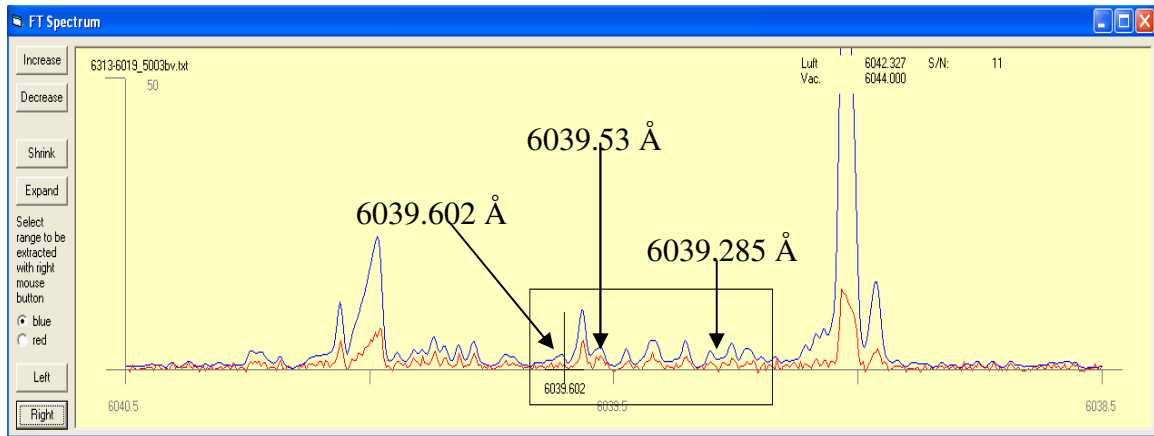
Figure 6.77: FT-Spectra showing the lines for transition from level triplet to upper level 31744.873 cm^{-1}

A laser excitation with start wavelength 6039.71 Å was performed and a hyperfine structure with abnormal intensity distribution of hyperfine components (see figure 6.78)

was recorded at all the previously observed fluorescence wavelengths i.e. 3460 Å, 5414 Å, 5633 Å, 5800 Å, 5947 Å, 6040 Å, 6478 Å.
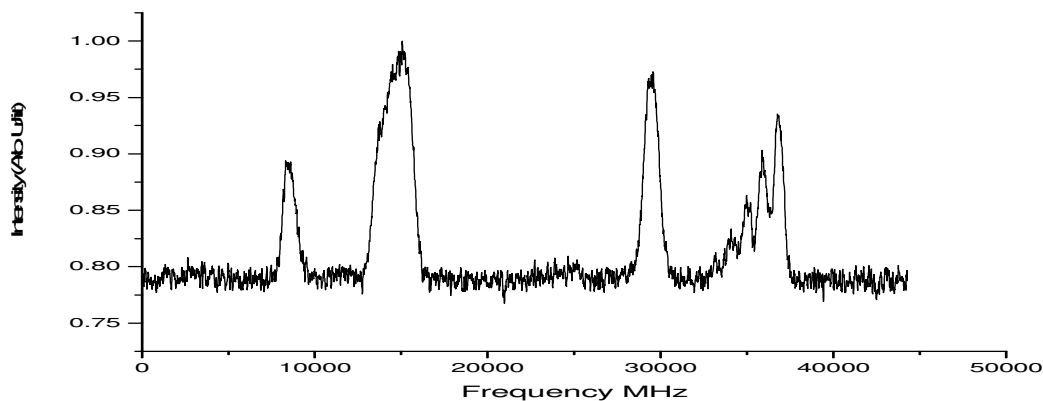
Figure 6.78: Hyperfine structure of the line recorded with start wavelength 6039.71 Å

Simulations of the recorded perturbed structure with predicted hyperfine structure patterns of line are presented in following figure 6.79a and 6.79b.
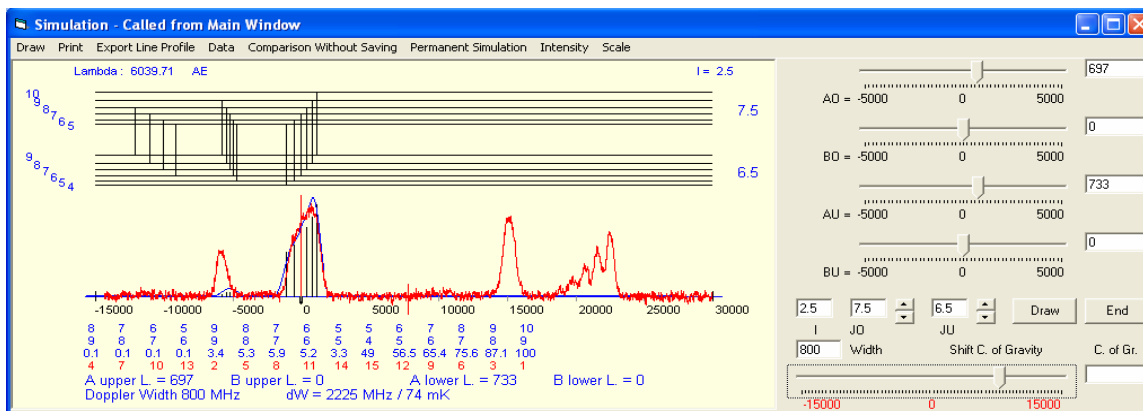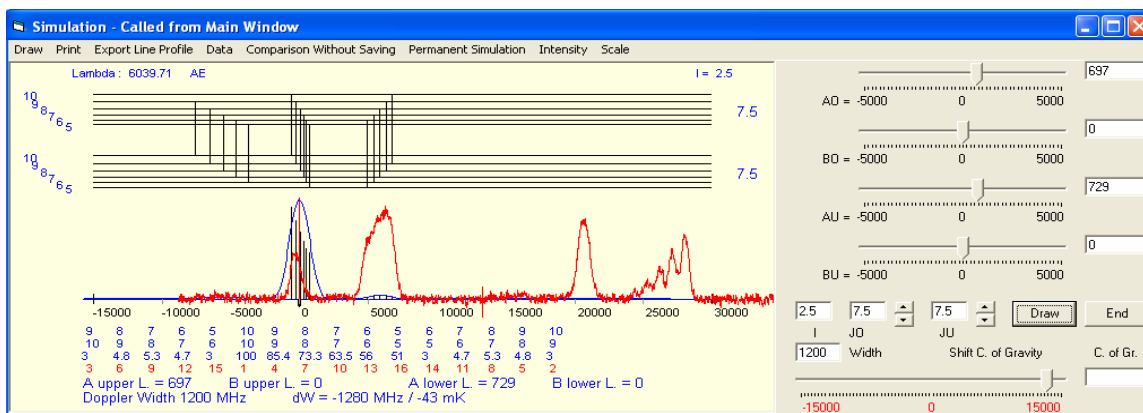
Figure 6.79 a: Simulations of the perturbed structure (red line profile) recorded with start wavelength 6039.71 Å
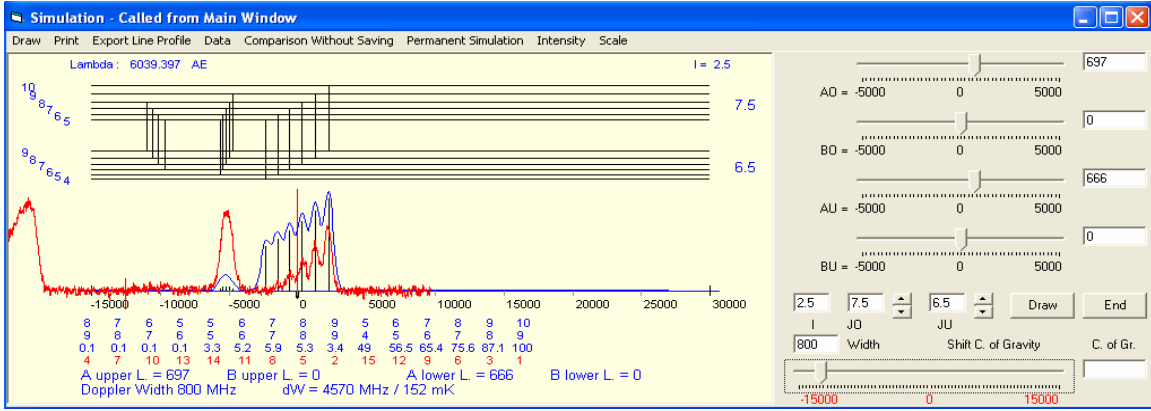
Figure 6.79 b: Simulations of the perturbed structure (red line profile) recorded with start wavelength 6039.71 Å

Simulations proved that the excited transition involve level triplet as a set of lower levels. Simulations further show that the character of recorded hyperfine structure of the said transition remains almost the same as the predicted transitions from all three levels of triplet to upper level. In can be noted here that the intensity of hyperfine components of the first group, which corresponds to a transition from upper most level of triplet, is small as compared to the intensities of hyperfine components in second and third groups corresponding to transitions from middle and lowest levels of triplet.

The J- and A-values of upper level as a result of simulation are 15/2 and 697 MHz respectively in conformity with first excitation to the upper level. Using J and A values of levels in triplet and of upper level, the recorded structure was fitted using a multiline fit. Best fit was obtained (see figure 6.80) for J and A values within good agreement with the previously determined values.
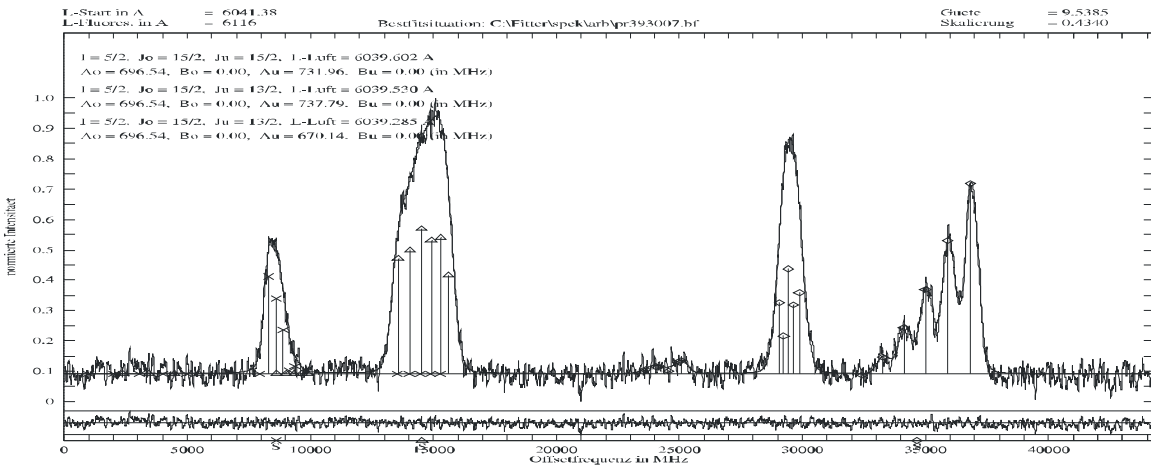
Figure 6.80: Best fit situation for perturbed hyperfine structure recorded with start wavelength 6039.71 Å

Using the center of gravity wave numbers from the fitted structure and the wave number of upper level as determined from the first excitation, the wave numbers of the levels in triplet are improved (Table 6.18). The level scheme with a comparison between experimentally recorded perturbed and simulated unperturbed hyperfine structure pattern is presented in figure 6.81.

Table 6.18: Improved values of wave numbers of levels in triplet, computed from the wave number of upper level 31744.873 cm^{-1}.

cog λ_{air} (Å)	Lower Level				Upper Level
	J_u	Parity	Energy (cm^{-1})	A_u (MHz)	$J_o = 15/2$, Parity = e, $A_o = 696.54$ MHz
					Energy (cm^{-1})
6039.605	15/2	o	15192.080	731.960	
6039.537	13/2	o	15191.898	737.790	31744.873
6039.289	13/2	o	15191.218	670.140	
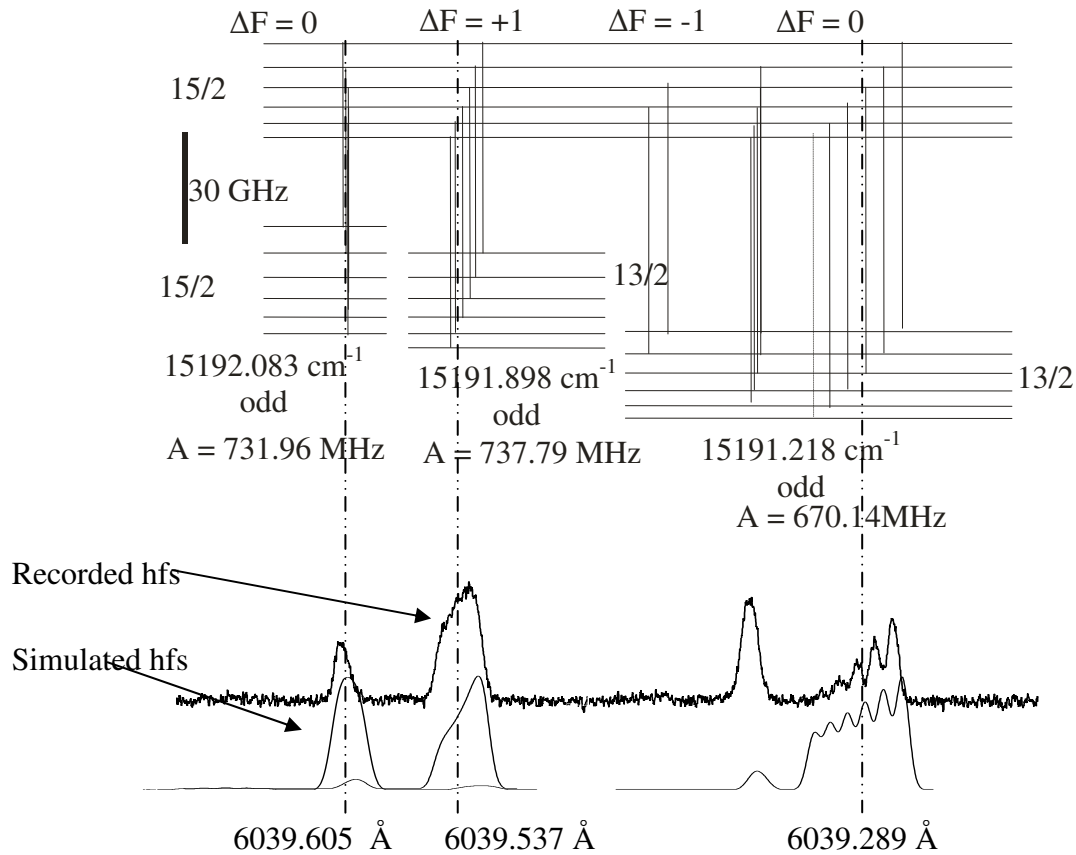
Figure 6.81: Level scheme for transition from triplet to upper level 31744.873 cm^{-1}, center-of-gravity positions marked by broken lines.

6.11 Excitation of Level $31619.982^e_{15/2}$ cm^{-1} from Level Triplet

This level was discovered via a laser excitation of line at 5785.51 Å. The line has a poor signal to noise ratio in FT-Spectra (see figure 6.82) with a relative intensity of 2.
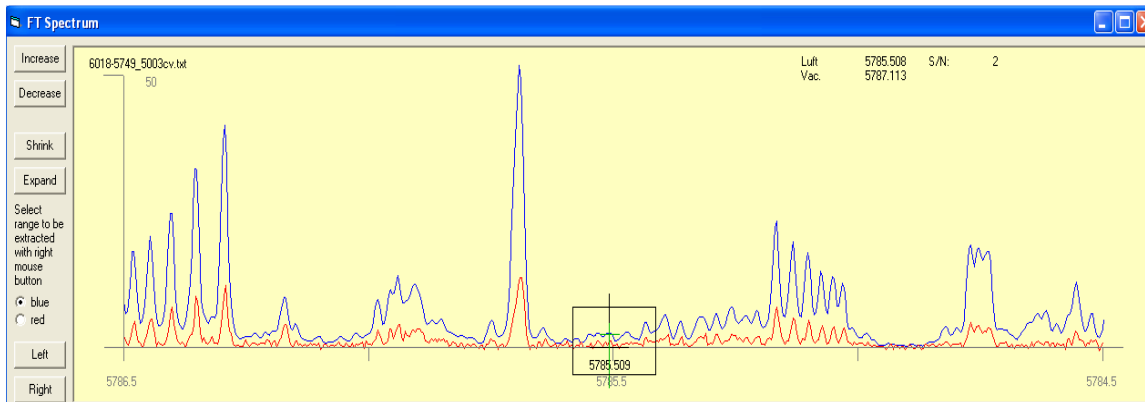
Figure 6.82: FT-Spectra for line at 5785.51 Å

Laser excitation of the line at 5785.51 Å was performed which gave a very strong LIF signal at a fluorescence wavelength 3475 Å. LIF signal was also seen on other fluorescence wavelengths i.e. 5452 Å, 5538 Å, 5672 Å, 6085 Å. LIF signal for the line 5785.51 Å is then recorded (see figure 6.83).on all observed fluorescence wavelengths by continuously scanning the laser wavelength starting from 5785.73 Å. The recorded structure has a good S/N ratio with resolved diagonal components.
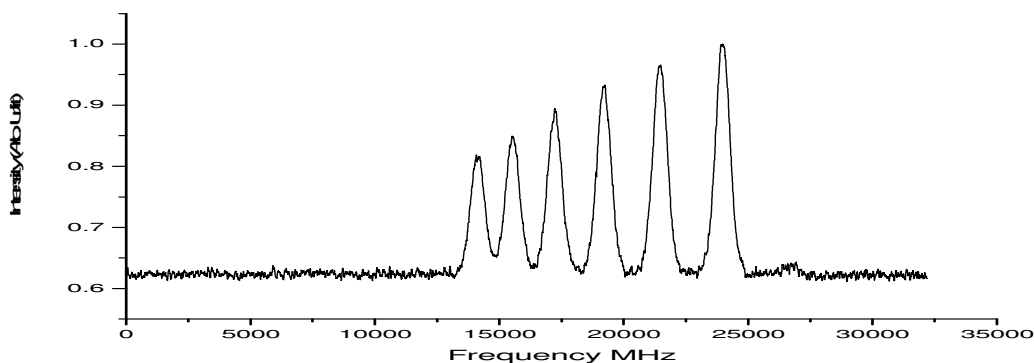
Figure 6.83: Hyperfine structure pattern recorded for the excitation of line at 5785.51 Å

The best fit situation was obtained for a transition with J = 15/2 – 17/2 and with A_o = 524.94 MHz and A_u = 247.51 MHz. The line could not be classified with any of the suggestions listed in classification program so by assuming a known lower level an upper level was search based on A and J values. A lower level with energy 14340.21 cm^{-1}, J_u = 17/2 and A_u = 244.7(3) MHz, B_u = -20(5) MHz was found. Addition of wave number of excitation line gave the wave number of upper level as 31619.982 cm^{-1} which explained all the observed fluorescence lines i.e. 3474 Å, 5452 Å, 5538 Å, 5672 Å, 6085 Å. The

structure was again fitted keeping fix A_u = 244.7 MHz, B_u = -20 MHz the hyperfine constant for upper level was determined as 521.53 MHz (see figure 6.84).

The wave number of upper level was determined by using the center of gravity wave number of the line and the wave number of the lower level and the line was then identified as a transition

$$31619.982^e_{15/2}, A_o = 521.53 \text{ MHz} \longleftrightarrow$$

$$14340.21^o_{17/2}, A_u = 244.7(3), B_u = -20(5) \text{ MHz}$$
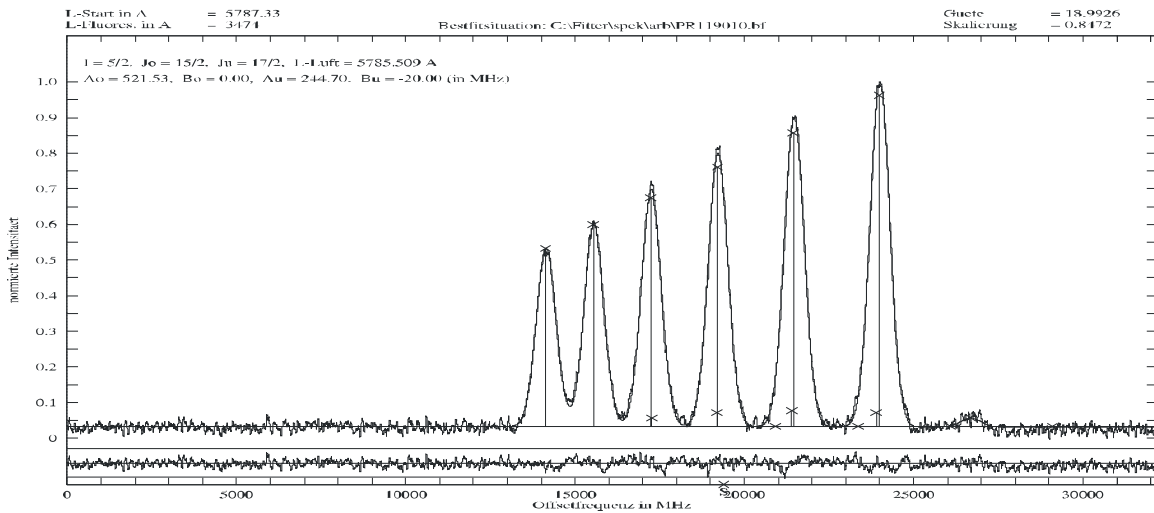
Figure 6.84: Best fit situation of the line recorded at 5785.51 Å

The level is introduced in classification program and a transition list is generated. The existence of the upper level and angular momentum was confirmed by second excitation to the level at one of the observed fluorescence line with center of gravity wavelength 5672.50 Å. FT-Spectra (figure 6.85) show a blend of several lines in the vicinity of each other and the hyperfine structure of the line at 5672.50 Å is not obvious.
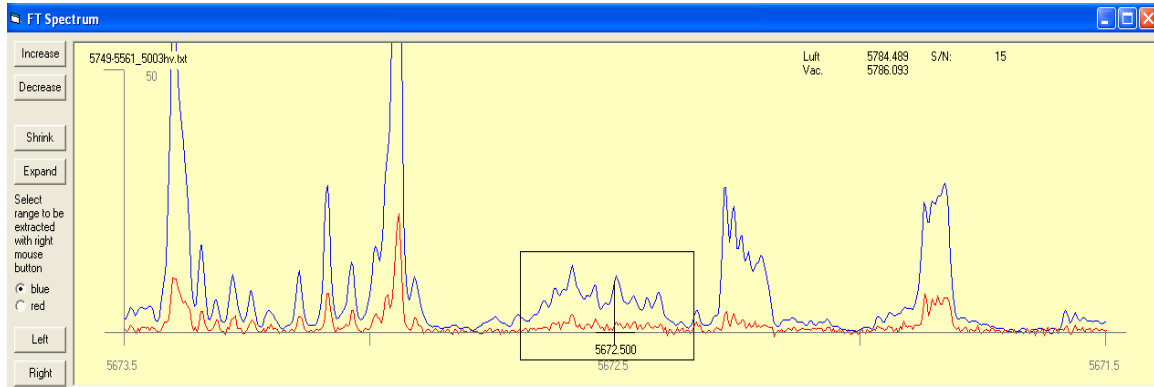
Figure 6.85: FT-Spectra of the line at 5672.50 Å

A very strong LIF signal was observed at the fluorescence line 3475 Å and by scanning the laser frequency the hyperfine structure of the line was recorded see figure 6.86. The fit of the structure (see figure 6.87) confirmed the J and A values of the upper level. The transition was identified as an excitation from lower level with energy 13996.091 cm^{-1}, J_u = 13/2 and A_u = 1067 MHz, B_u = 200 MHz to the upper level 31619.982 cm^{-1}.
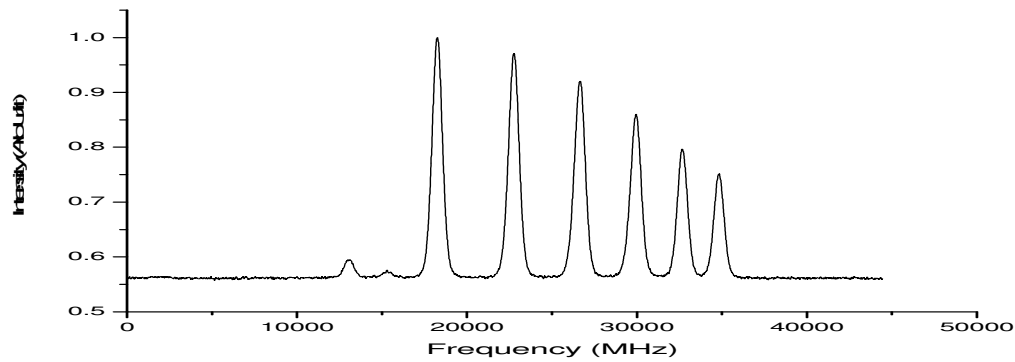
Figure 6.86: Hyperfine structure pattern recorded for the excitation of line at 5672.50 Å
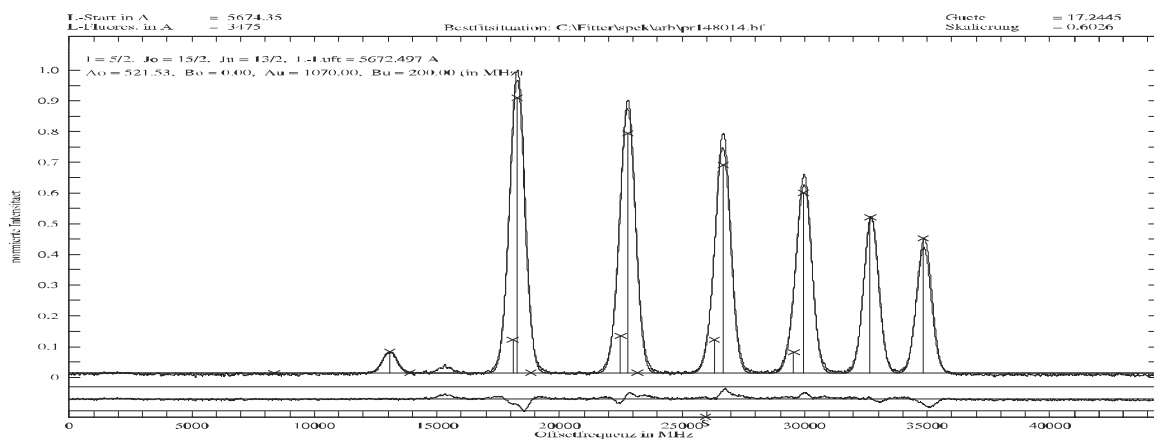
Figure 6.87: Best fit of the recorded hyperfine structure of line at 5672.50 Å

The transition list of the upper level 31619.982 cm^{-1} explains one of the observed fluorescence line i.e. 6085 Å as a combination with level triplet. The suggestion list displays hyperfine structure of line(s) connecting level triplet to upper level with normal intensity distribution of hyperfine components. FT-Spectra for the line at 6085 Å has a poor signal to noise ratio (see figure 6.88) and having a relative intensity of only 3. Furthermore from FT-Spectra nothing could be said about the hyperfine structure of the line as several lines are in close vicinity of each other, hiding each others hyperfine structure.

151
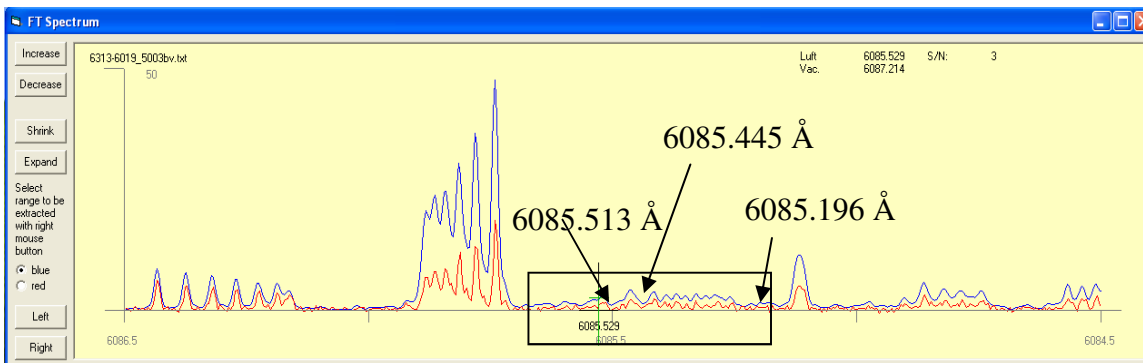
Figure 6.88: FT-Spectra of the lines where transition is expected from level triplet to upper level 31619.982 cm^{-1}

LIF signal was detected at one of the previously observed fluorescence wavelength i.e. 3475 Å. LIF signal was then recorded by scanning the laser excitation wavelength from 6085.66 Å and by setting the monochromator at 3475 Å. A perturbed intensity distribution of hyperfine components (see figure 6.89) was recorded and is seen on all previously observed fluorescence wavelengths.
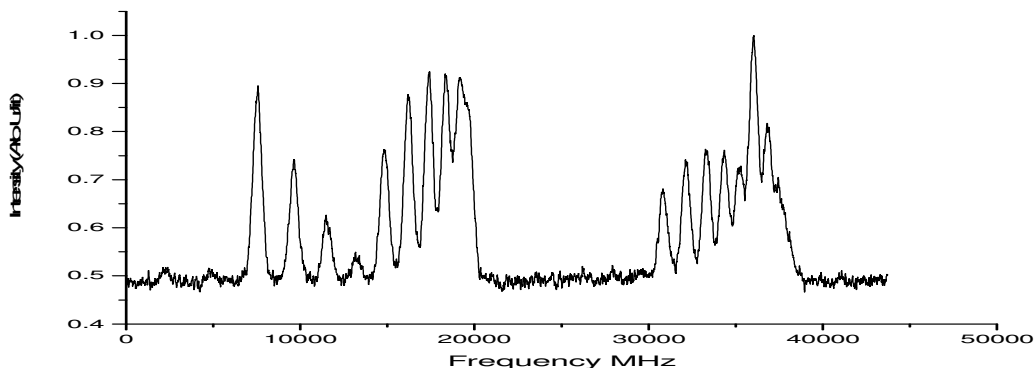
Figure 6.89: Hyperfine structure of the line recorded with start wavelength 6085.66 Å

Simulations of the recorded perturbed structure with predicted hyperfine pattern for the transitions from level triplet to upper level 31619.982 cm^{-1} are presented in figure 6.90. For all three transitions from the three levels of triplet to upper level the hyperfine structure component positions of the recorded structure are in good agreement with the predictions suggesting again that interval rule is not violated. But the intensity distribution of diagonal hyperfine components in all three groups is different from the predicted structures with large deviation is seen for the last group. Also, in the last group the intensities of off-diagonal ($\Delta F = 0$) components has increased.

152
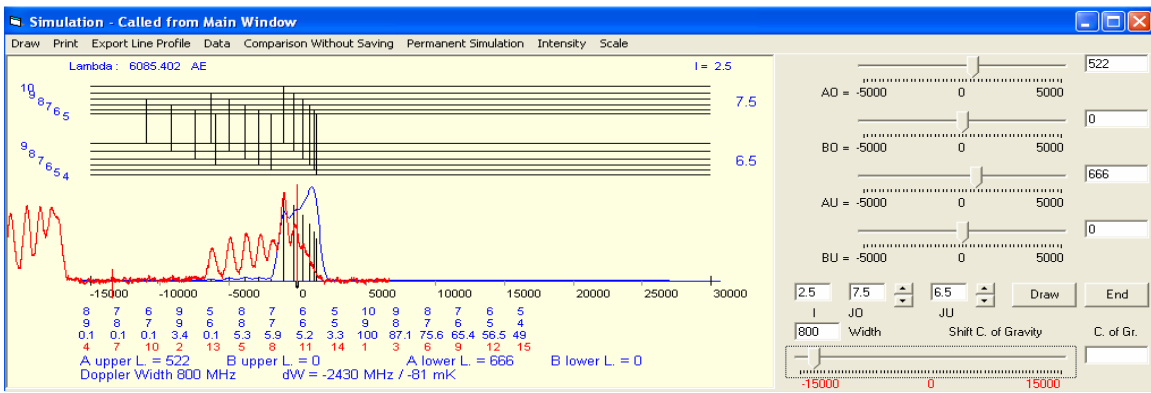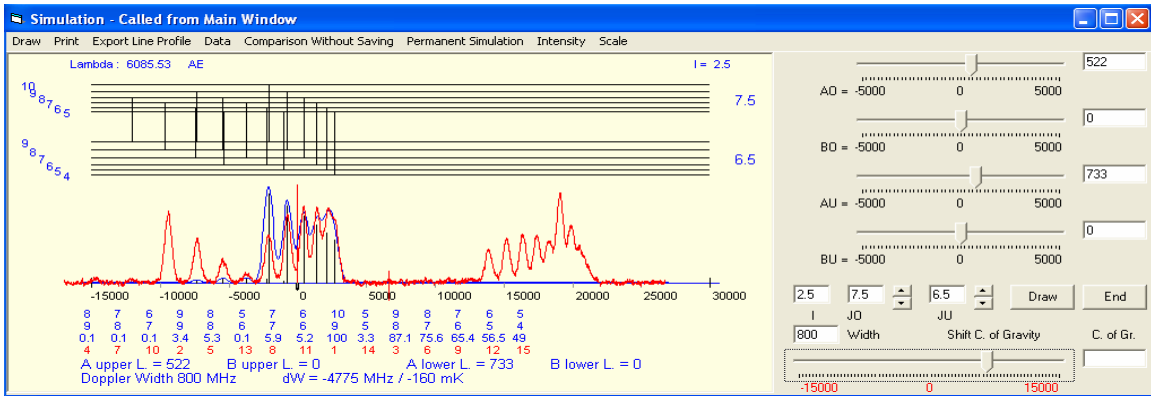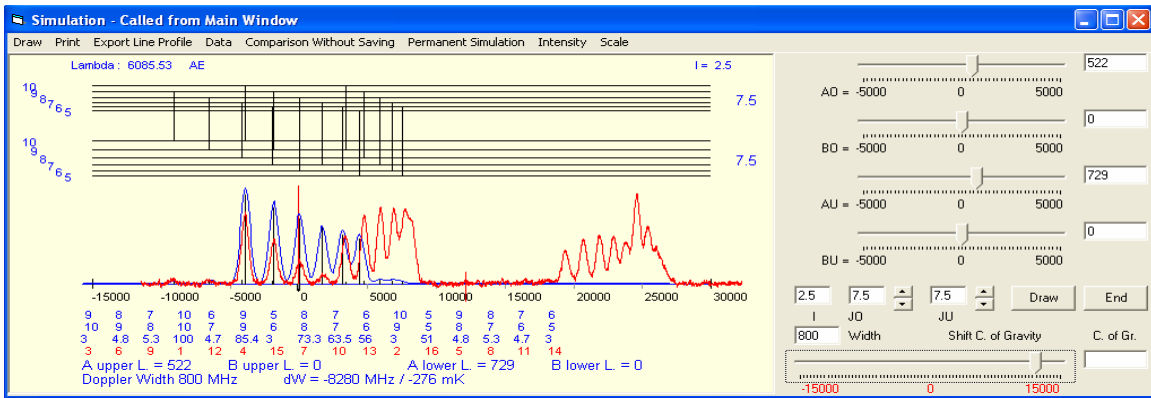
Figure 6.90: Simulations of the perturbed structure (red line profile) recorded with start wavelength 6085.66 Å

Using the J- and A-values of upper level and of levels in triplet, the perturbed structure is fitted using a multiline fit. Best fit was obtained (see figure 6.91) for J and A values within good agreement with the already determined values.
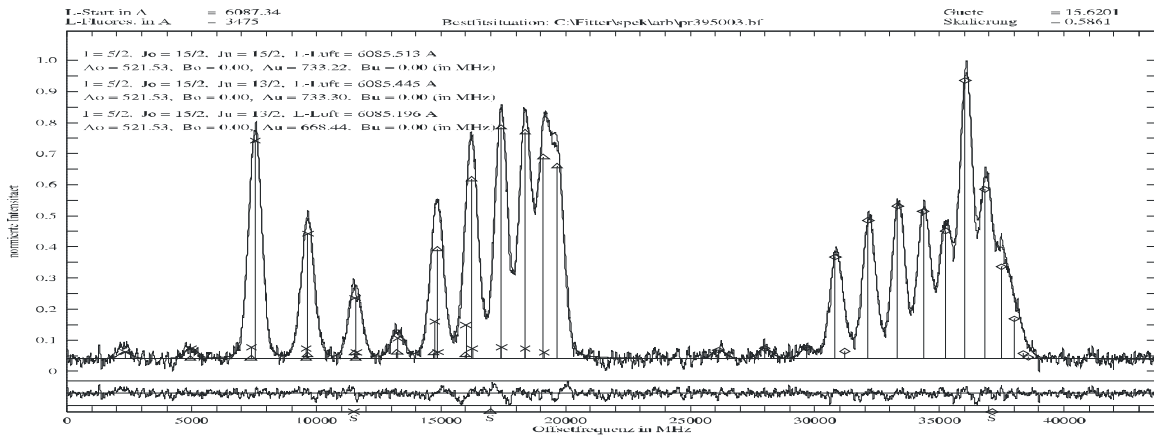
Figure 6.91: Best fit situation for the line recorded with start wavelength 6085.66 Å

Using the center of gravity wave numbers from the fitted structure and the wave number of upper level as determined from first excitation, the wave numbers of the levels in triplet are improved (Table 6.19). The level scheme with a comparison between experimentally recorded perturbed and simulated unperturbed hyperfine structure pattern is presented in figure 6.92.

Table 6.19: Improved values of wave numbers of levels in triplet, computed from the wave number of upper level 31619.982 cm^{-1}.

cog λ_{air} (Å)	J_u	Parity	Energy (cm^{-1})	A_u (MHz)	$J_o = 15/2$, Parity = e, $A_o = 521.53$ MHz
					Average Energy (cm^{-1})
6085.513	15/2	o	15192.062	733.22	
6085.445	13/2	o	15191.879	733.30	31619.982
6085.196	13/2	o	15191.206	668.44	
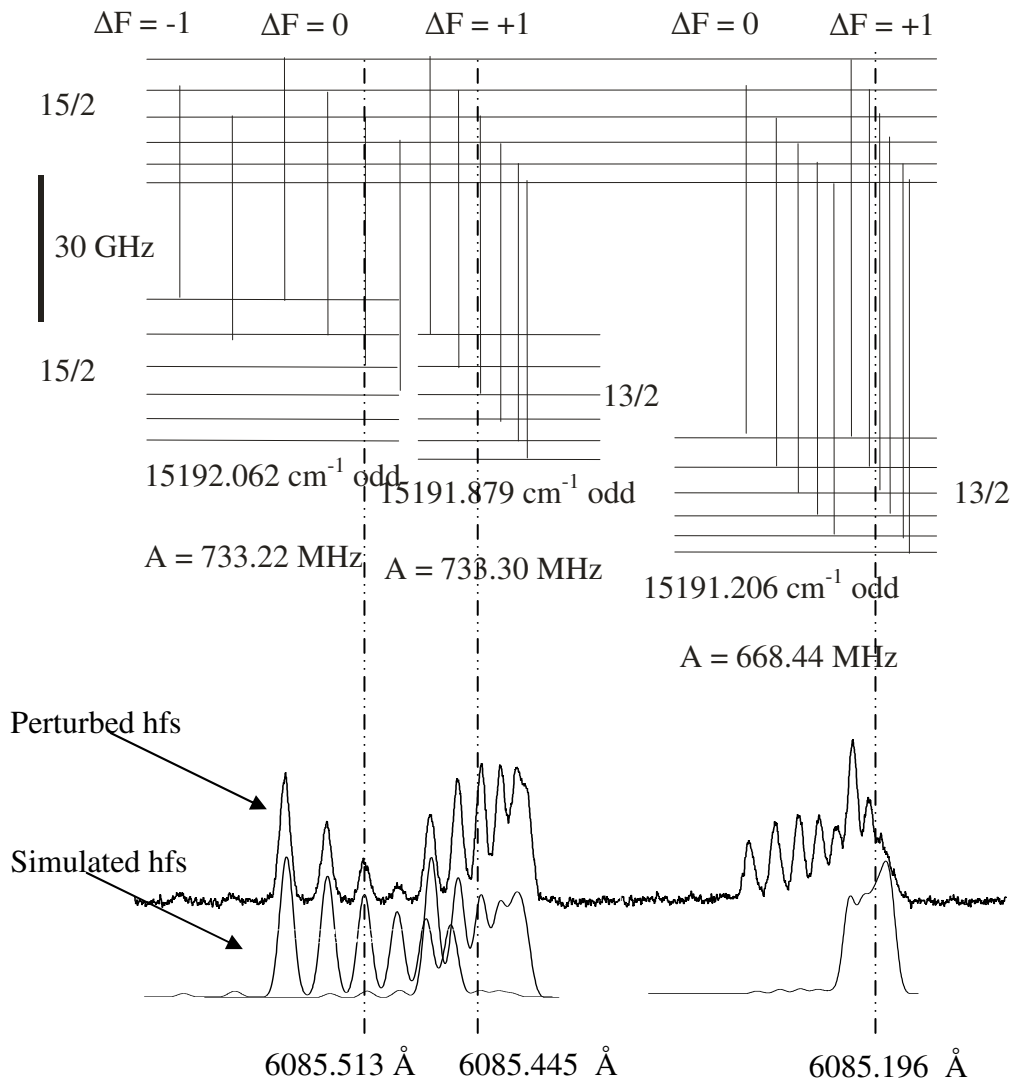
Figure 6.92: Level scheme for transition from triplet to upper level 31619.982 cm^{-1}, center-of-gravity positions marked by broken lines.

6.12 Excitation of level $\mathbf{32773.833^e_{13/2}}$ from Level Triplet

The level 32773.833 cm^{-1} was discovered via laser excitation of the line at 5686.15 Å. The FT-Spectra of the line has a good signal to noise ratio with a relative intensity of 31 (see figure 6.93) and it was expected that the excitation would result in a transition involving a narrow spaced single peak hyperfine structure.
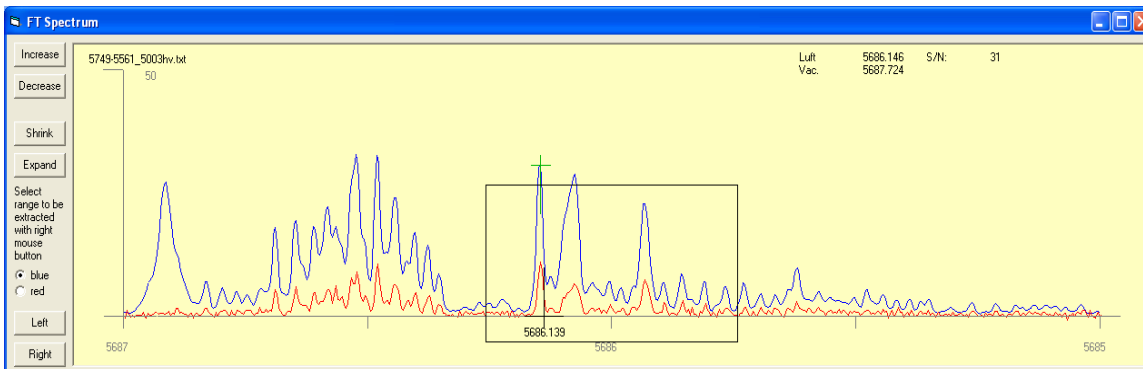
Figure 6.93: FT-Spectra for the line at 5685.15 Å

Contrary to the initial supposition the excitation with start wavelength 5686.22 Å resulted in a structure with anomalous intensity distribution of hyperfine components (see figure 6.94) and was observed on more than one fluorescence channels i.e. 3185 Å, 4471 Å, 5155 Å, 5476 Å, 5540 Å, 5552 Å, 5570 Å and 5952 Å. Apparently three largely separated groups of hyperfine structure can be seen.
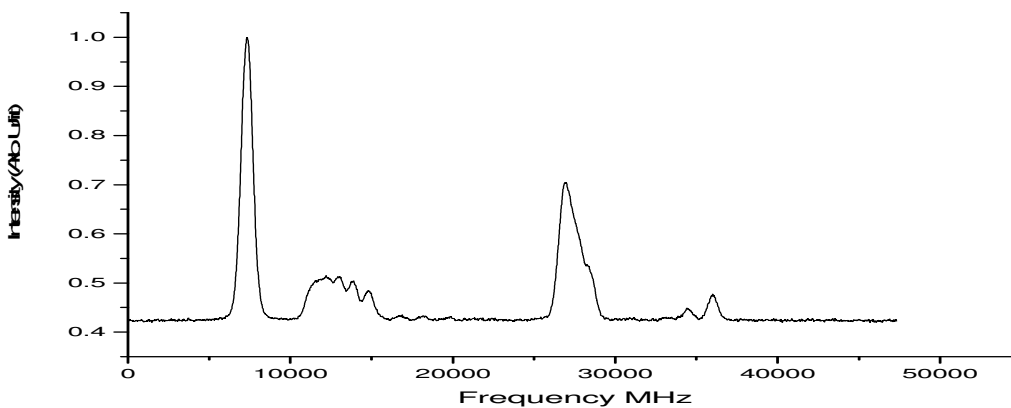
Figure 6.94: Hyperfine structure recorded with perturbed intensity distribution for the excitation with start wavelength 5686.22 Å

Furthermore, none of the suggestions listed for the line gave any clue for the identification of the levels (upper and lower involved) involved in the excitation of the line. Assuming the excitation as a transition taking place from the level triplet, the first group of hyperfine components of the recorded structure which is less perturbed was simulated taking J and A values of levels in triplet for the lower level and varying J and A

156

values for the upper level. Good simulation results were obtained for simulated J and A values of upper level as 13/2 and 834 MHz.

Furthermore with these J and A values of upper level and J and A values of levels in triplet, the recorded hyperfine structure was fitted using a multiline fit. While fitting the J and A values for the lower levels were kept fixed. Best fit was obtained for J value of upper level as 13/2 and A values 835.45 MHz, 838.81 MHz, 839.67 MHz with an average value of 837.97 MHz (see figure 6.95), giving a quality factor of 51. It was to some extent a sufficient proof that indeed the recorded perturbed structure belongs to a transition from the level triplet.
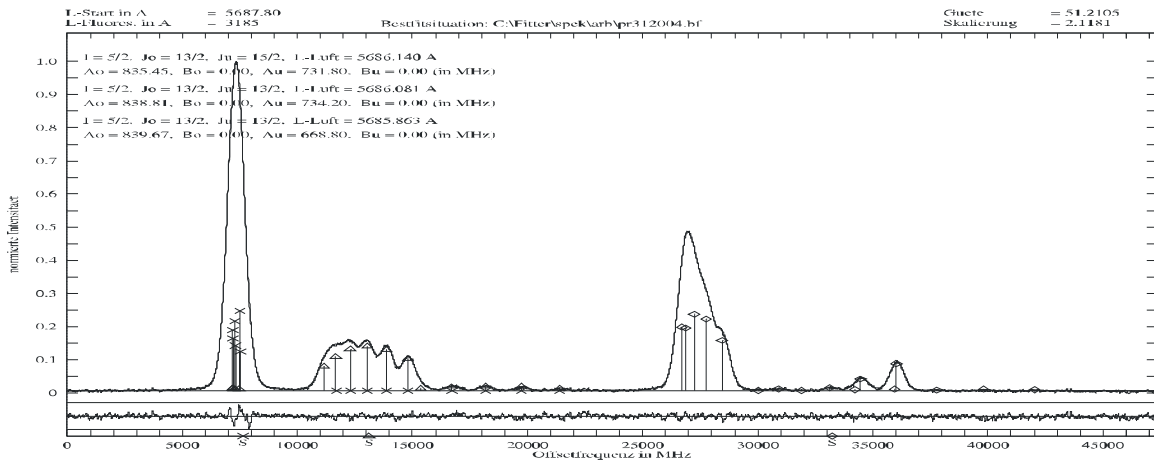
Figure 6.95: Best fit situation for the line recorded with start wavelength 5686.22 Å

The wave number of the upper level was determined using the center of gravity wave numbers as obtained from the fit and wave numbers of each of the levels in triplet. Average value of the wave number of upper level is also computed, see Table 6.20. The newly found upper level was introduced in the classification program which generated a transition list for the upper level which explained the observed fluorescence lines. Classification program using A and J values and using normal intensity ratios for the hyperfine components also generated the hyperfine structures for the transitions from the three levels of triplet to the upper level.

Further analysis of the recorded perturbed hyperfine structure can be done by comparing the recorded structure with hyperfine structures predicted by classification program, see figure 6.96. For the first group that is for transition from upper most level of triplet to upper level, both the shape and intensities of diagonal and off-diagonal hyperfine components are in good agreement with the predictions. In case of second group i.e. transition from middle level of triplet to upper level; intensities of diagonal hyperfine components are much lower than the predicted intensities. In case of third group i.e. for transition from lowest level of triplet to upper level, the intensities of diagonal components are almost missing whereas the intensities of off-diagonal ($\Delta F = -1$) are

157

much higher than predicted intensities. In all three groups the positions of hyperfine components are not changed and follow interval rule.
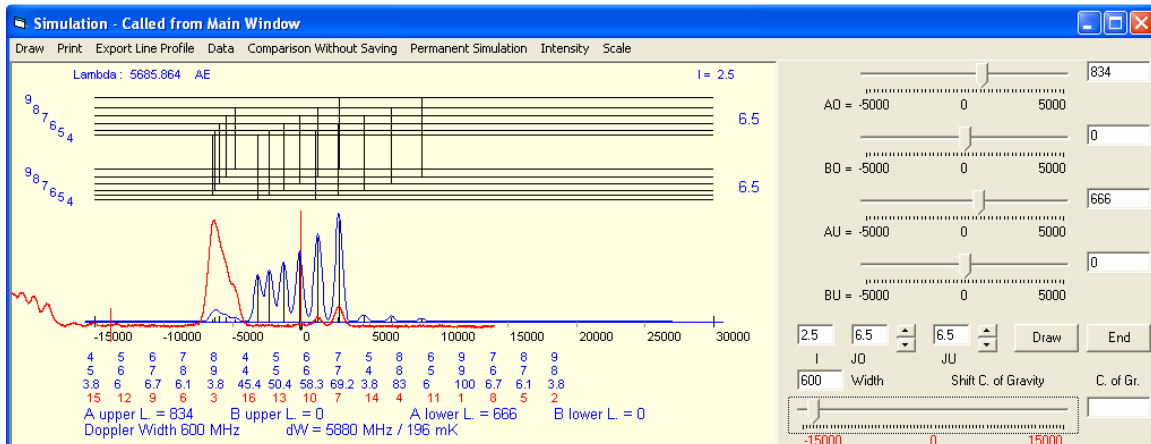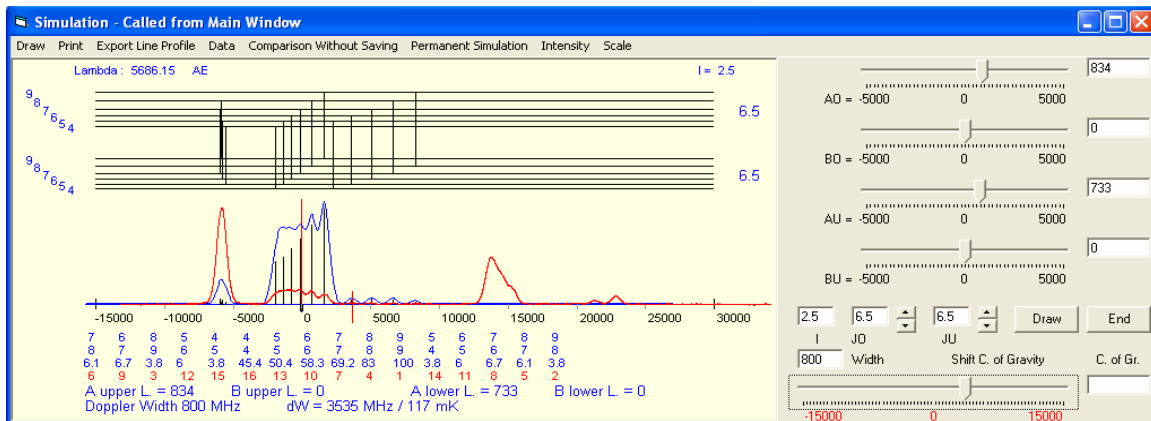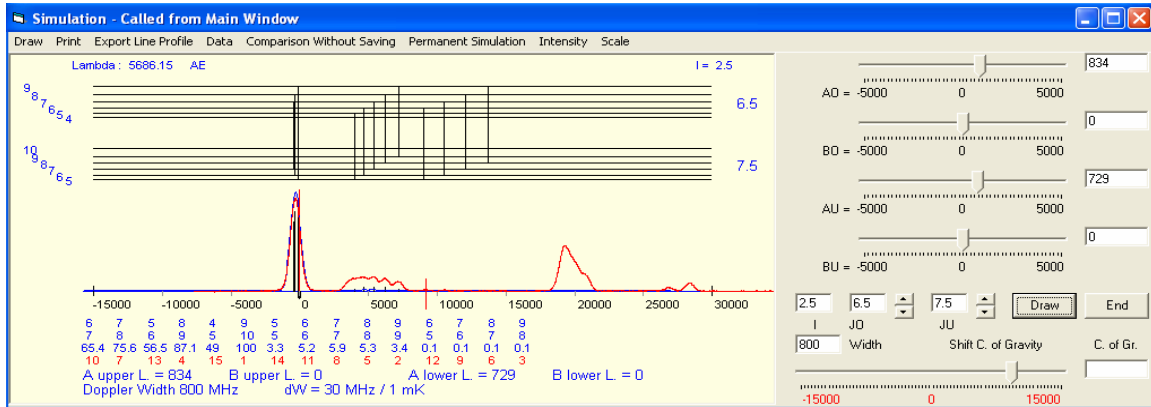
Figure 6.96: Simulations of the perturbed structure (red line profile) recorded with start wavelength 5686.22 Å

Table 6.20: Best fit values for the transition from level triplet with start wavelength 5686.22 Å, also calculated wave number for upper level.

cog λ_{air} (Å)	J_u	Parity	Energy (cm⁻¹)	A_u (MHz)	$J_o = 13/2$, Parity = e, $A_o = 834$ MHz	
					Energy (cm⁻¹)	Average Energy (cm⁻¹)
5686.14	15/2	o	15192.09	731.02	32773.835	
5686.08	13/2	o	15191.9	729.96	32773.834	32773.833
5685.864	13/2	o	15191.233	663.94	32773.832	

A second excitation for the existence and J value of upper level was performed at one of the observed fluorescence wavelengths i.e. 5952.02 Å. The FT-spectra (see figure 6.97) has a poor signal to noise ratio but since this is the only observed fluorescence wavelength lying in our laser range so in any case the excitation was performed. Hyperfine structure of the line (see figure 6.98a) was recorded at fluorescence wavelengths 5686 Å with not a good signal to noise ratio. A good agreement is seen (see figure 6.98b) while simulating the recorded hyperfine structure with predicted hyperfine pattern. Furthermore, in order to be sure that the transition belongs to the upper level determined previously in combination with the level triplet, the recorded hyperfine structure of the line at 5952.02 Å was fitted independently. The best fit was obtained for $J_o = 13/2$, $J_u = 11/2$, $A_o = 837.03$ MHz and $A_u = 68.83$ MHz.

Using the fitted J and A values as 11/2 and 68.83 MHz respectively, the data base of known levels was search for an already know lower level.
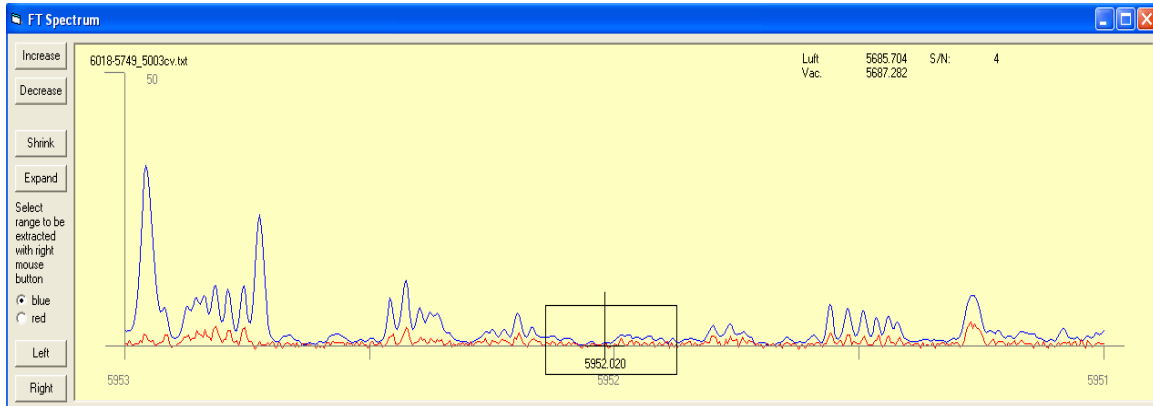
Figure 6.97: FT-Spectra of line at 5952.02 Å

A level was found with energy 15977.6 cm⁻¹, odd parity, $J_u = 11/2$ and $A_u = 65.8$ MHz in the data base. The structure was again fitted keeping fix the A value of lower level i.e. 65.8 MHz and a best fit (see figure 6.99) was obtained for A-value of upper level as 834.44 MHz which is in agreement (with in an error of 3 MHz) with the previously determined A-value of upper level by simulation and fitting procedure. The wave number of upper level is again calculated using the wave number of lower level for this line and the center of gravity wave number of the line i.e. 16796.382 cm⁻¹. The resulting wave number of upper level is 32773.972 cm⁻¹ which 0.139 cm⁻¹ different from the previous

calculations. This difference may be attributed to the error in wave number of lower level involved in this excitation. So the previous value of upper level is retained.
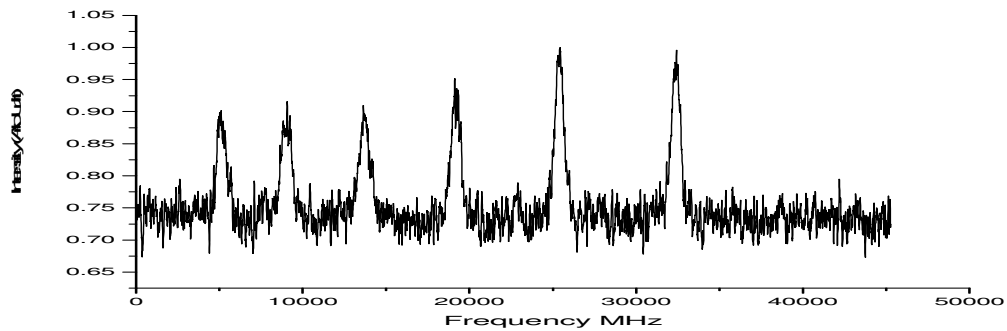
(a)
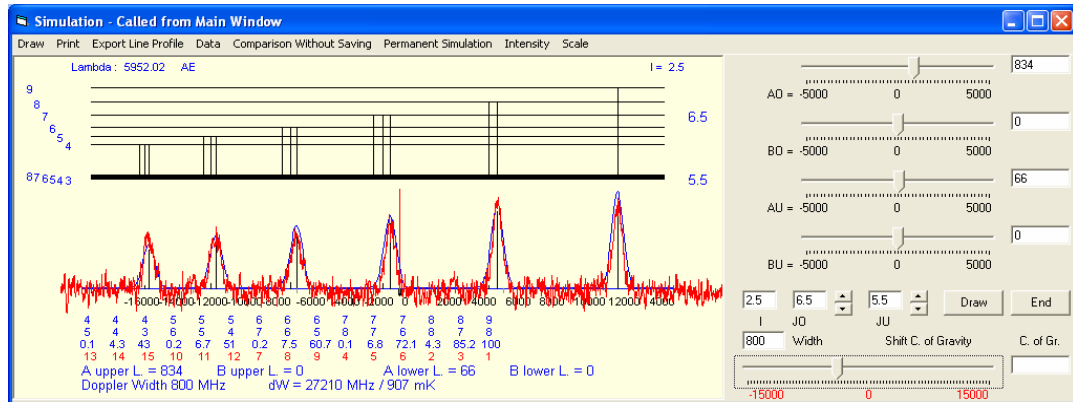
(b)

Figure 6.98: (a) Hyperfine structure recorded at the center of gravity wavelength 5952.02 Å (b) Simulation with the prediction hyperfine structure
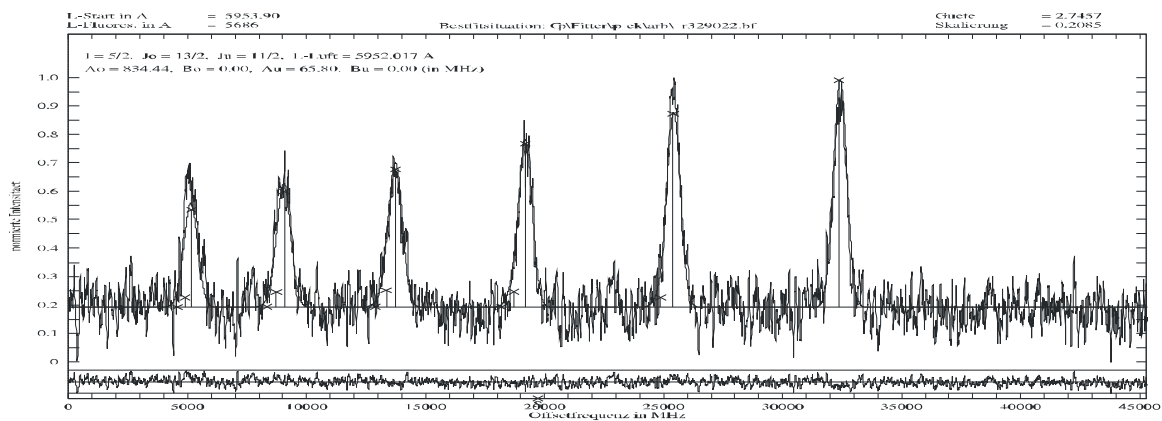
Figure 6.99: Best fit of the hyperfine structure of the line excited at center of gravity wavelength 5952.02 Å

The level scheme with a comparison between experimentally recorded perturbed and simulated unperturbed hyperfine structure pattern is presented in figure 6.100.
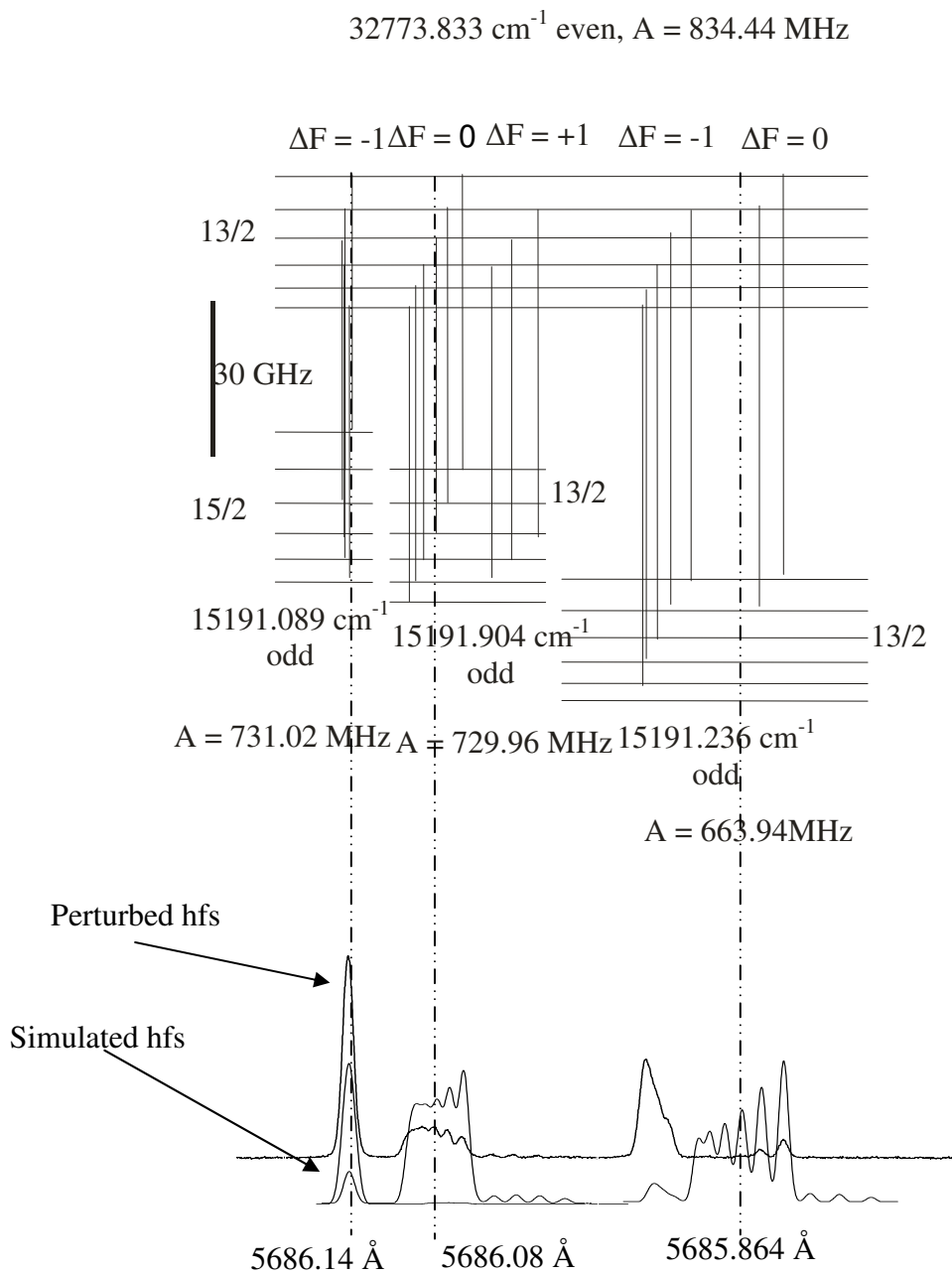
Figure 6.100: Level scheme for transition from triplet to upper level 32773.833 cm^{-1}, center-of-gravity positions marked by broken lines.

6.13 Excitation of level $\mathbf{32658.325^{e}_{15/2}}$ from Level Triplet

The level 32658.325 cm^{-1} was discovered via a laser excitation of the line with start wavelength 5723.89 Å. The indicated portion in FT-Spectra (see figure 6.101) show a blend of several lines in a close proximity of each other. So the hyperfine structure pattern of the investigated line is not clearly visible in FT-Spectra.
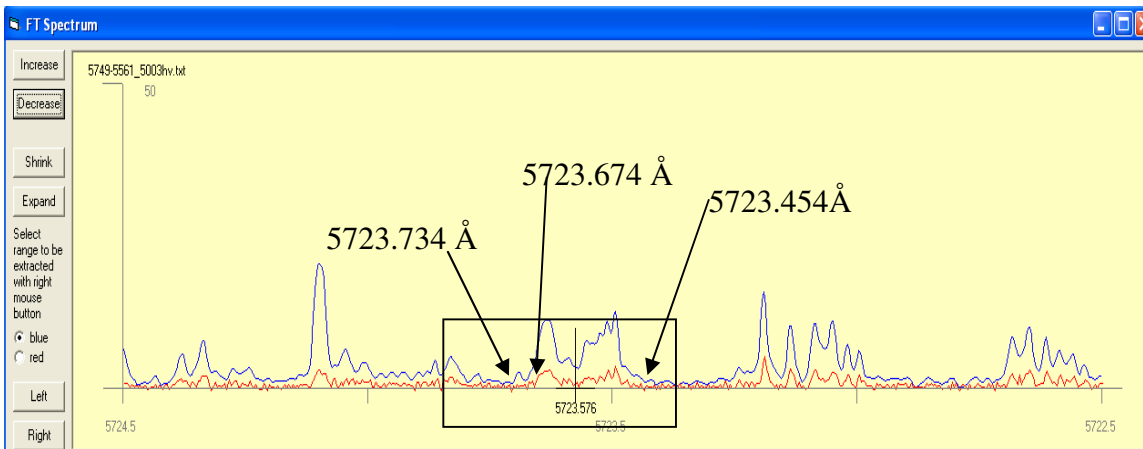
Figure 6.101: FT-Spectra showing center of gravity wavelengths of the recorded structure

The LIF signal was recorded at fluorescence wavelengths 3354 Å, 5157 Å, 5801 Å, 6118 Å revealing a perturbed behaviour of hyperfine components (see figure 6.102).
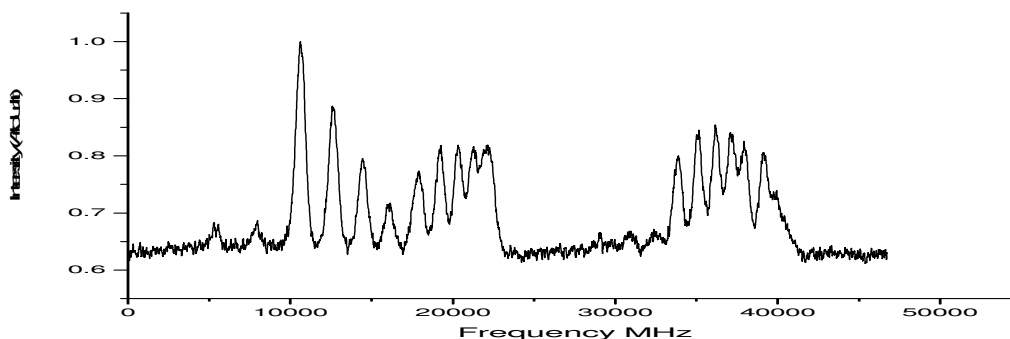
Figure 6.102: LIF Signal recorded with start wavelength 5723.89 Å showing perturbed intensity distribution of hyperfine components

The recorded perturbed structure was simulated under the assumption that the transition is from the levels in triplet to an unknown upper level. With this assumption simulation of the recorded hyperfine structure is done such that the J and A values of the lower levels are kept fixed as shown in figure 6.103. Simulations are sufficient proof of the combination of unknown upper level with levels in triplet, this gave values for J and A of upper level as 15/2 and 531 MHz respectively. Furthermore simulations show that for the transition from upper most level of triplet is in a good agreement in terms of positions

and character of diagonal hyperfine components between recorded perturbed structure and predicted hyperfine structure patterns but for transitions from lower two levels of triplet the relative intensities of hyperfine components are vastly deviated from the predictions.
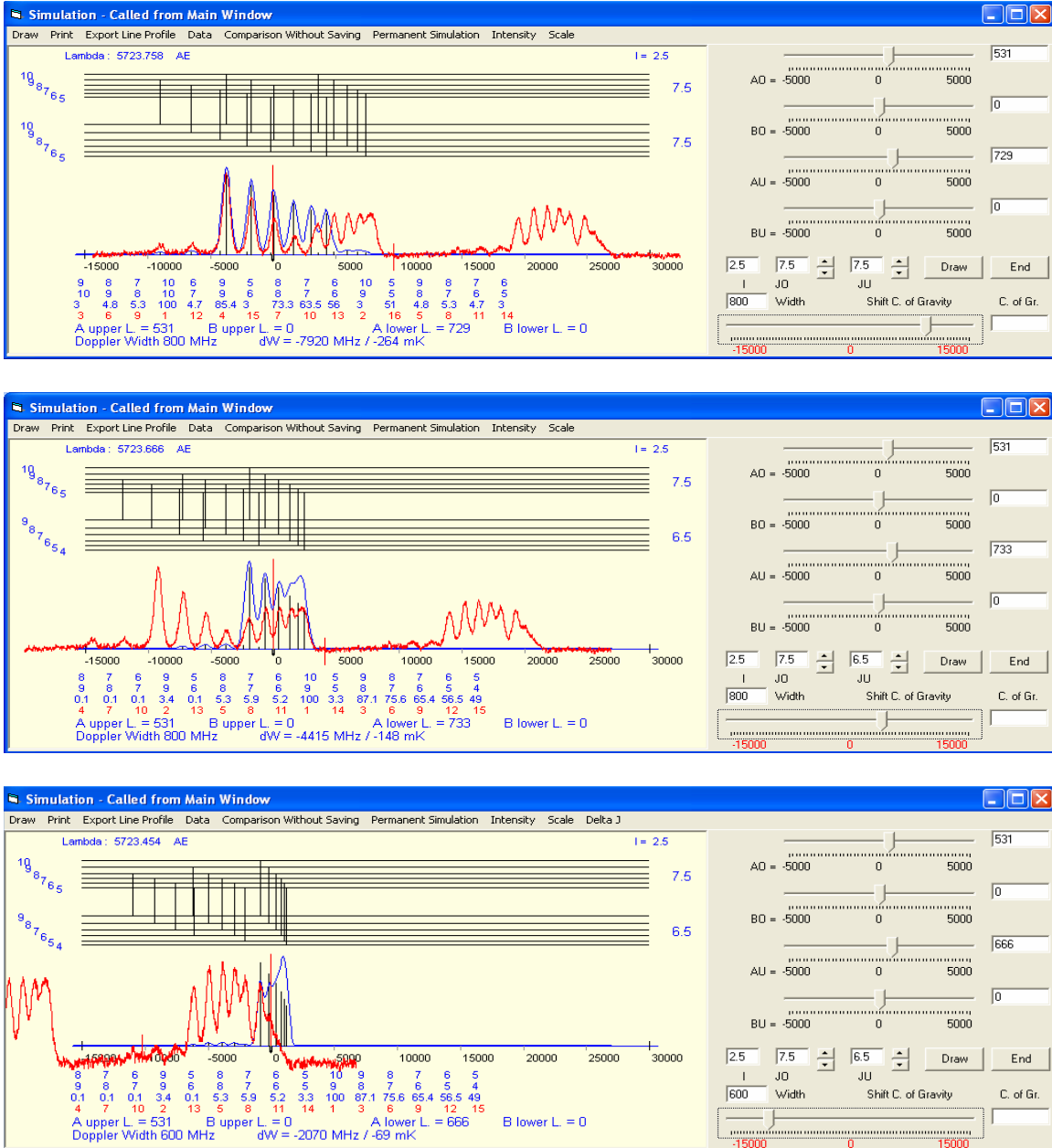
Figure 6.103: Simulations of the perturbed structure (red line profile) recorded from start wavelength 5723.89 Å

Using the J and A values of the upper from simulation and already known J and A values of levels in triplet, the perturbed structure was fitted using a multiline fit. Best fit was

obtained (see figure 6.104) for J and A values within good agreement with the simulated values of upper level and already determined values of levels in triplet.
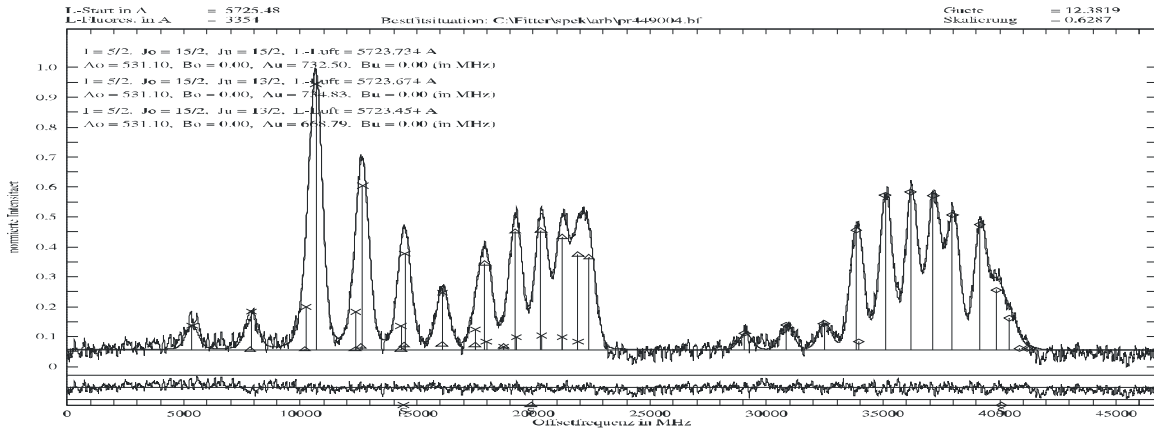
Figure 6.104: Best of the perturbed structure recorded from start wavelength 5723.89 Å

Wave number of the upper level was determined by using the wave numbers of the levels in triplet and the center of gravity wave numbers from the fit (Table 6.21). The upper level with energy 32658.353 cm^{-1}, J = 15/2 and A = 531 is introduced in the classification program and a transition list for the upper level is generated explaining all the observed fluorescence lines. In order to confirm the existence and J-value of upper level a second excitation at one of the observed fluorescence line i.e. 5801.58 Å was performed. FT-Spectra of the line has a relative intensity of 7 but hyperfine components are not resolved (see figure 6.105) with investigated line appearing in a blend.

Table 6.21: Best fit values for the transition from level triplet with start wavelength 5723.89 Å, also calculated wave number for upper level.

cog λ_{air} (Å)	Lower Level				Upper Level	
					J_o = 15/2, Parity = e, A_o = 531 MHz	
	J_u	Parity	Energy (cm^{-1})	A_u (MHz)	Energy (cm^{-1})	Average Energy (cm^{-1})
5723.738	15/2	o	15192.09	732.50	32658.345	
5723.677	13/2	o	15191.9	734.83	32658.34	32658.346
5723.454	13/2	o	15191.233	668.79	32658.353	

LIF signal was recorded (see figure 6.106 a) on all the previously observed fluorescence lines i.e. 3354 Å, 5157 Å, 5801 Å, 6118 Å and is in agreement in terms of shape and position with the predicted hyperfine structure (see figure 6.106 b). To re-confirm J and A values of upper level which were determined in the first excitation for the transitions from levels in triplet to upper level, the recorded structure of the line was fitted by varying input parameters and a best fit was observed for J_o = 15/2 – J_u = 13/2 with A_o = 521 MHz and A_u = 725 MHz. Based on J and A values from the fit a known lower level was found as 15426.41 cm^{-1}, J = 13/2 and A = 737.1 MHz. Recorded structure was again

fitted now taking J and A values of lower level as fixed. A good fit was obtained (see figure 6.107) giving A_o = 531.13 MHz confirming the J and A values of upper level as determined in first excitation.
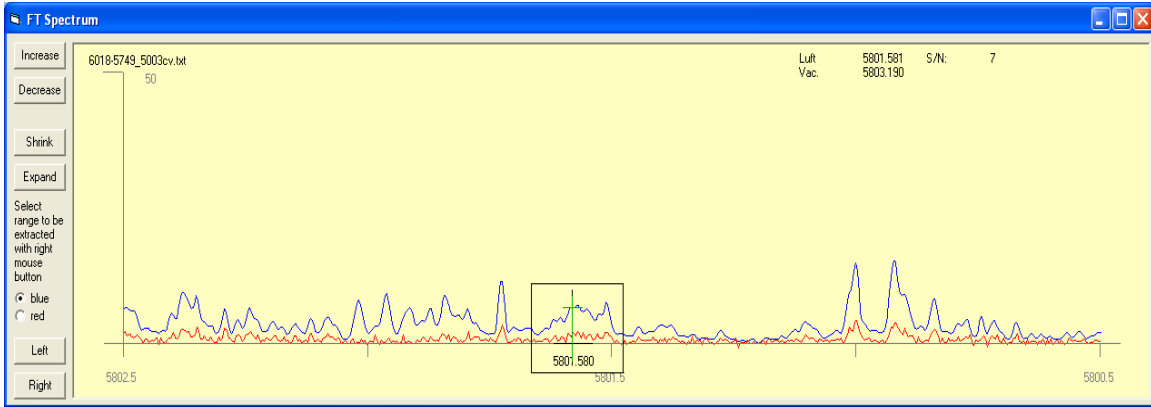
Figure 6.105: FT-Spectra of the line at 5801.58 Å
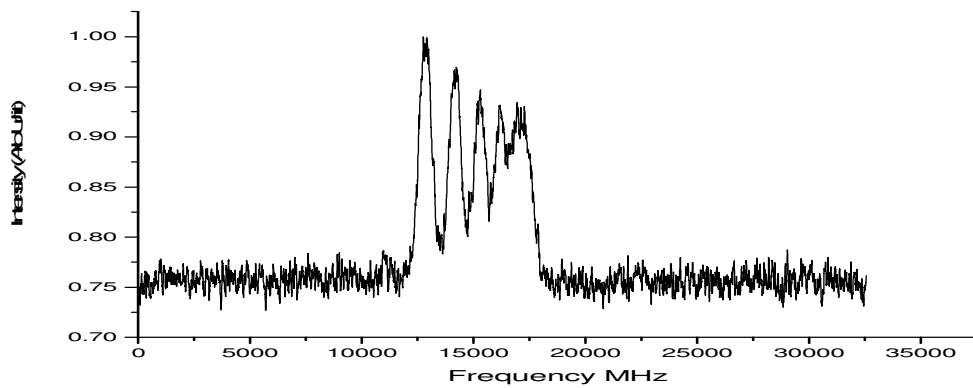
(a)
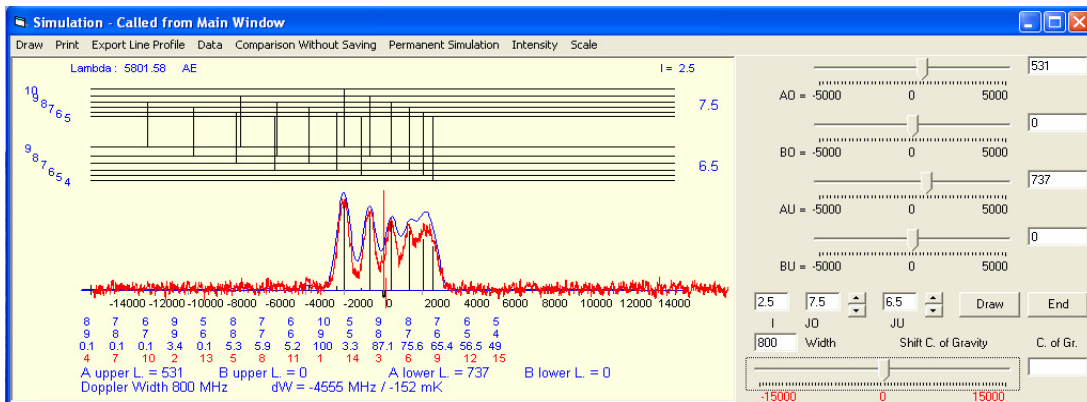
(b)

Figure 6.106: (a) Experimentally recorded hyperfine structure for line at 5801.58 Å (b) Simulation with theoretical prediction

165
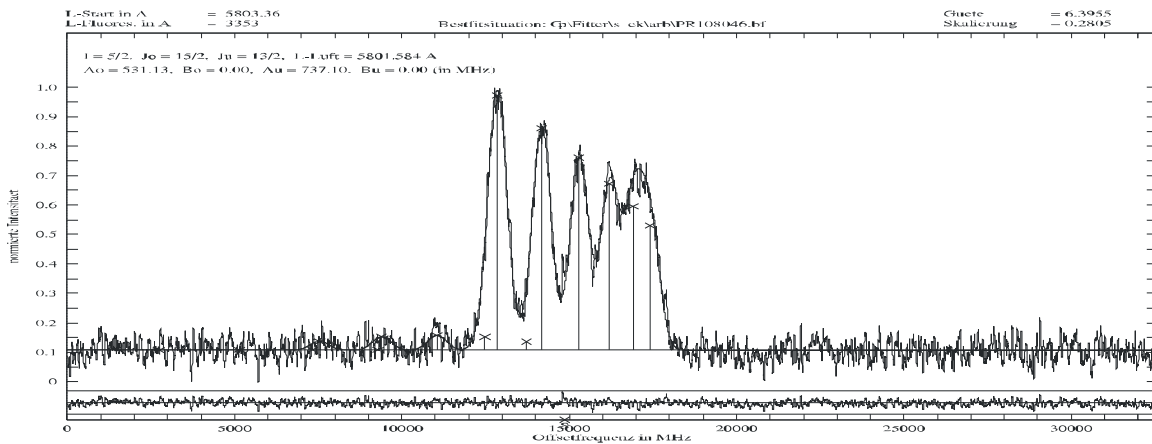
Figure 6.107: Best fit of the hyperfine structure of line recorded at 5801.58 Å

Now the wave number of the upper level was again calculated independent of the first excitation by using the center of gravity wave number from the fit of the second excitation and wave number of the lower level identified in second excitation. This resulted in a value of 32658.346 cm^{-1} for upper level which confirms its existence. The level energy of the upper level was corrected using FT-Spectra at one of its observed fluorescence lines i.e. 3354 Å which gave level energy 32658.325 cm^{-1}. An improvement in the wave numbers of levels in triplet can now be done by using the center of gravity wave number of the fitted structure in first excitation and the wave number of upper level as determined from second excitation, the wave numbers of the levels in triplet are given in Table 6.22. The level scheme with a comparison between experimentally recorded perturbed and simulated unperturbed hyperfine structure pattern is presented in figure 6.108.

Table 6.22: Improved values of wave numbers of levels in triplet, computed from the wave number of upper level 32658.325 cm^{-1}.

cog λ_{air} (Å)	Lower Level				Upper Level
	J_u	Parity	Energy (cm^{-1})	A_u (MHz)	J_o = 15/2, Parity = e, A_o = 531.13 MHz
					Energy (cm^{-1})
5723.738	15/2	o	15192.07	732.50	
5723.677	13/2	o	15191.885	734.83	32658.325
5723.454	13/2	o	15191.205	668.79	
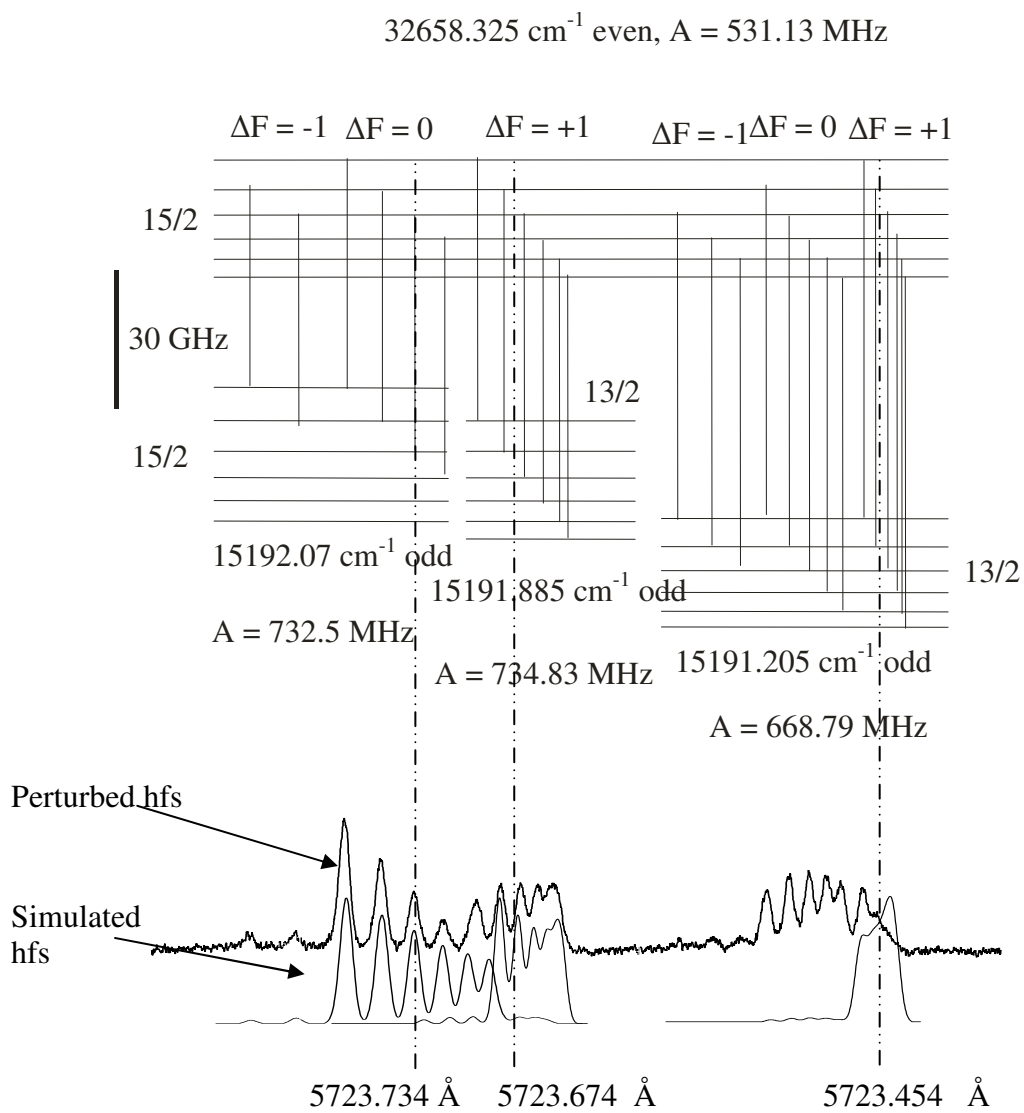
Figure 6.108: Level scheme for transition from triplet to upper level 32658.325 cm^{-1}, center-of-gravity positions marked by broken lines.

6.14 Excitation of level $31483.15^e_{13/2}$ cm^{-1} from Level Triplet

This level was discovered via a laser excitation of line at 5716.89 Å. The line has a good signal to noise ratio in FT-Spectra (see figure 6.109) with a relative intensity of 4. In the vicinity of line 5716.89 Å several lines are present and shape seen in FT-Spectra is a mixture of hyperfine structures of these lines. The single peak at 5717.00 Å can be explained as a transition $26591.843^o_{7/2} - 9105.035^e_{9/2}$. Apart from this the hyperfine components of the investigated line 5716.89 Å are seen partially resolved.
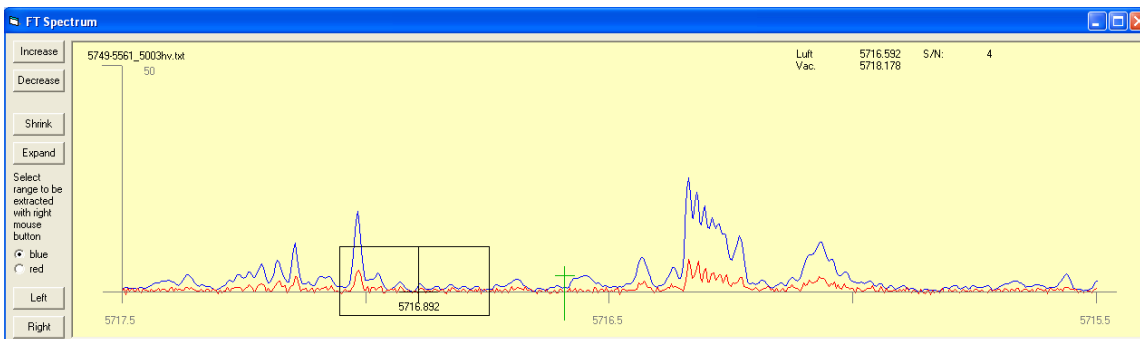
Figure 6.109: FT-Spectra of the line at 5716.89 Å

Laser excitation of the line resulted in a widely split hyperfine structure (see figure 6.110) and was observed on more than one fluorescence channels i.e. 5890 Å, 6071 Å, 6136 Å, 6226 Å.
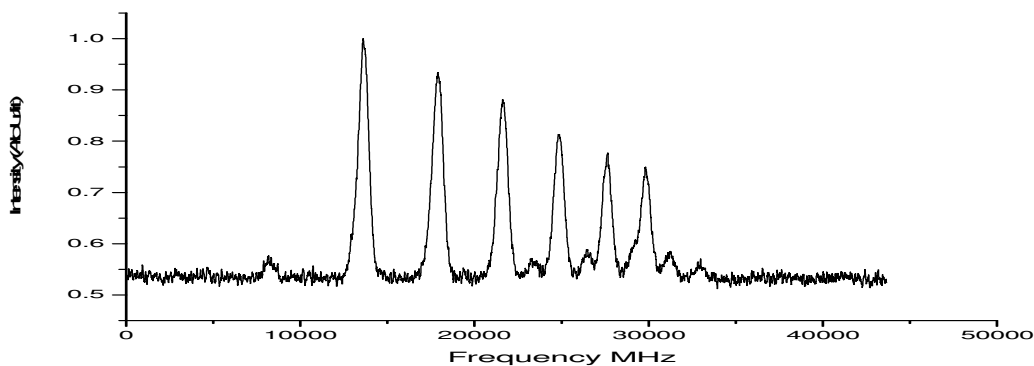
Figure 6.110: LIF Signal of the line recorded at 5716.89 Å

The best fit situation was obtained for a transition with J = 13/2 – 13/2 and with A_o = 604.67 MHz and A_u = 1068.29 MHz, B_u = 219.15 MHz. The line could not be classified with any of the suggestions listed in classification program so by assuming a known lower level an upper level was search based on A and J values. A lower level with energy 13996.096 cm^{-1}, J_u = 13/2 and A_u = 1067 MHz, B_u = 200 MHz was found. Addition of center of gravity wave number of excitation line gave the upper level 31483.252 cm^{-1}, which explained all the observed fluorescence lines i.e. 5890 Å, 6071 Å, 6136 Å, 6226 Å.

The structure was again fitted keeping fix A_u = 1067 MHz and B_u = 200 MHz the hyperfine constant for upper level was determined as 603.3 MHz (see figure 6.111). The wave number of upper level was determined by using the center of gravity wave number of the line and the wave number of the lower level and the line was then identified as a transition

$$31483.252^e_{13/2}, A_o = 603.3\,\text{MHz} \longleftrightarrow 13996.096^o_{13/2}, A_u = 1067\,\text{MHz}, B_u = 200\,\text{MHz}$$
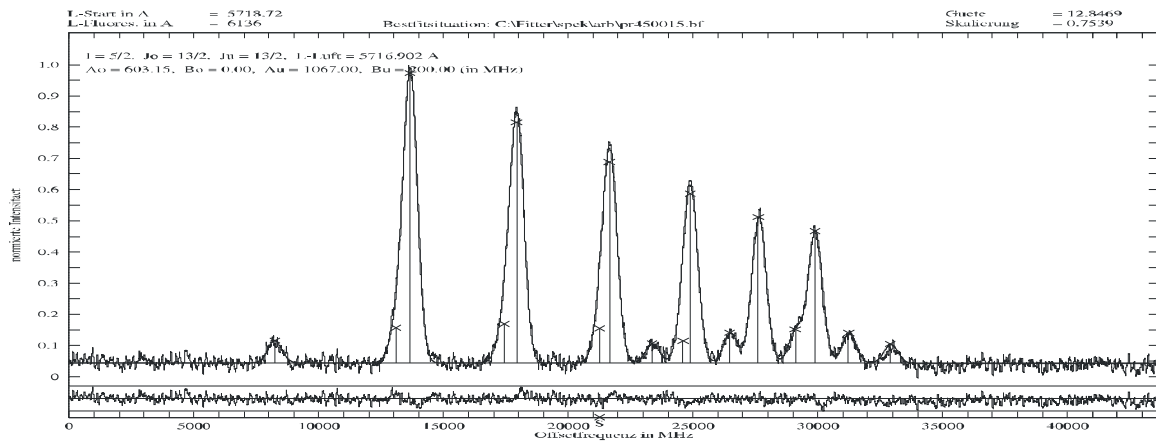
Figure 6.111: Best fit of the recorded hyperfine structure of the line at 5716.89 Å

The level is introduced in classification program and a transition list is generated. Transition list indicated a combination of this upper level with level triplet at one of the observed fluorescence line i.e. at 6136.65 Å. In FT-Spectra the line has a good signal to noise ratio but appears in an admixture of more than one line (see figure 6.112).
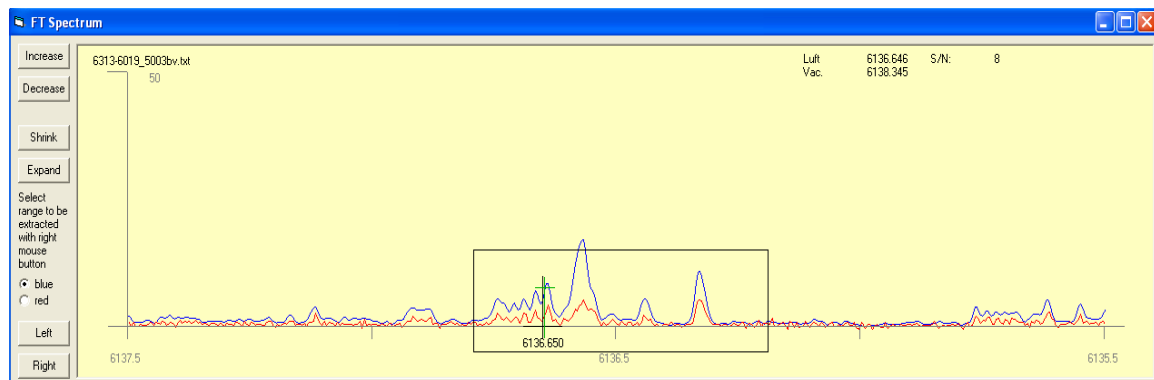
Figure 6.112: FT-Spectra of the line at 6136.65 Å

Laser excitation of the line was performed with start wavelength 6136.73 Å. Hyperfine structure with anomalous intensity distribution of hyperfine components was recorded (see figure 6.113) on all previously observed fluorescence channels i.e. 5716 Å and 6072 Å.

Simulations of the recorded hyperfine structure with predicted hyperfine structure for combination of upper level with level triplet are presented in figure 6.114.
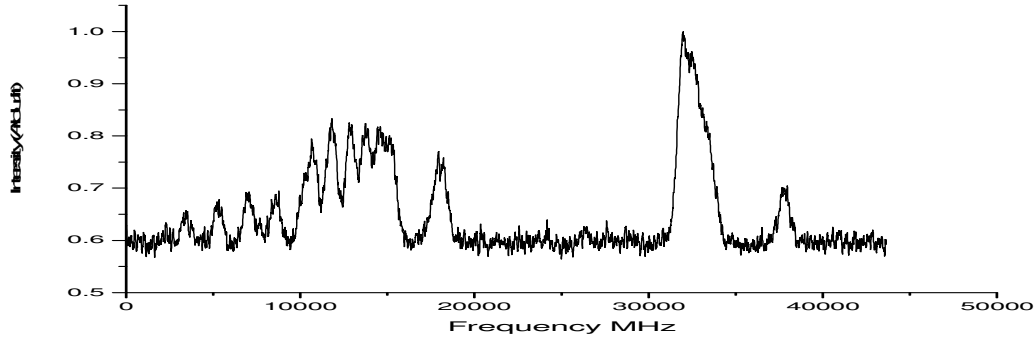
Figure 6.113: Hyperfine structure with anomalous intensity distribution of hyperfine components recorded with start wavelength 6136.73 Å

In case of excitation from the upper most level of triplet, the intensities of hyperfine components are very small as compared for excitations from middle and lowest levels of triplet. This is in contradiction to most of the lines. The excitation from the lower two levels of triplet to upper level the simulations are almost in accordance with the predictions with small variation in intensities of hyperfine components. Using the J and A values of the upper from first excitation and already known J and A values of levels in triplet, the perturbed structure was fitted using a multiline fit. Best fit was obtained (see figure 6.115) for J and A values within good agreement with the previously determined values of upper level and already known values of levels in triplet. The upper level was further confirmed and its energy was corrected by two more excitations at lines 6071.8 Å and 5890.14 Å. The corrected energy of the upper level is 31483.15 cm^{-1}. This correction in energy is made by using lines 5716.89 Å, 5890.14 Å and 6071.8 Å. Wave numbers of levels in triplet are calculated by using the corrected wave number of the upper level determined from other three excitations of lines and the center of gravity wave numbers determined from the fit of the perturbed structure. Computed wave numbers of levels in triplet are presented in Table 6.23. The level scheme with a comparison between experimentally recorded perturbed and simulated unperturbed hyperfine structure pattern is presented in figure 6.116.

Table 6.23: Improved values of wave numbers of levels in triplet, computed from the wave number of upper level 31483.15 cm^{-1}.

cog λ_{air} (Å)	Lower Level				Upper Level
	J_u	Parity	Energy (cm^{-1})	A_u (MHz)	$J_o = 13/2$, Parity = e, $A_o = 603.3$ MHz
					Energy (cm^{-1})
6136.640	15/2	o	15192.097	727.80	
6136.570	13/2	o	15191.911	731.63	31483.15
6136.316	13/2	o	15191.237	672.91	

170
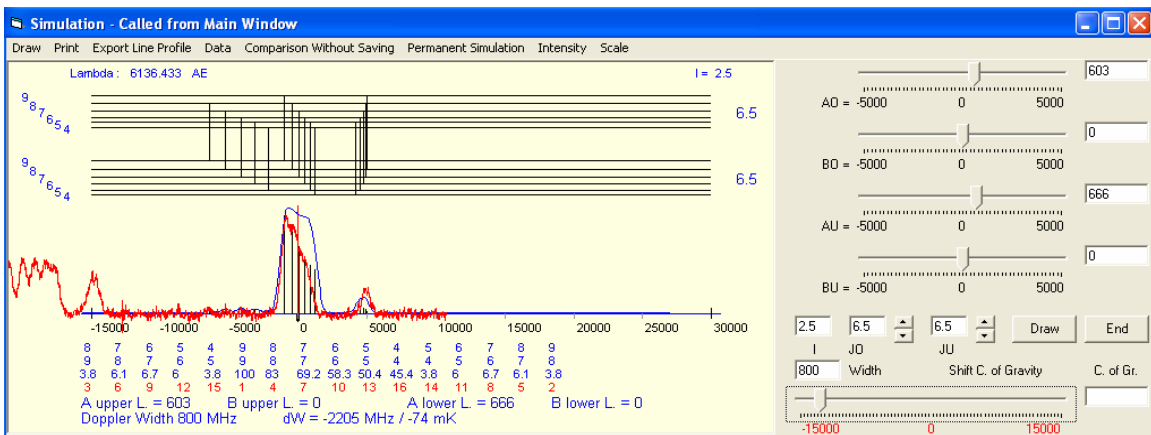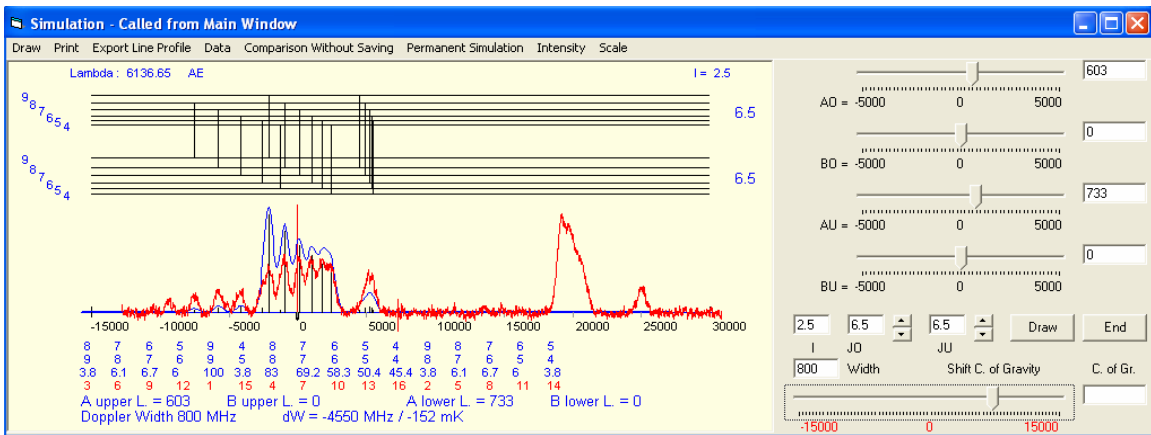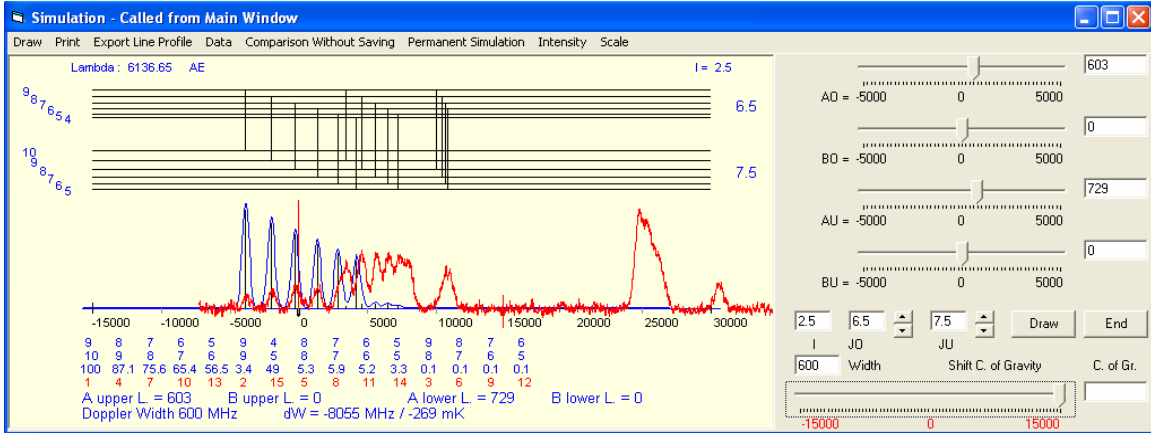
Figure 6.114: Simulations of the perturbed structure (red line profile) recorded from start wavelength 6136.73 Å
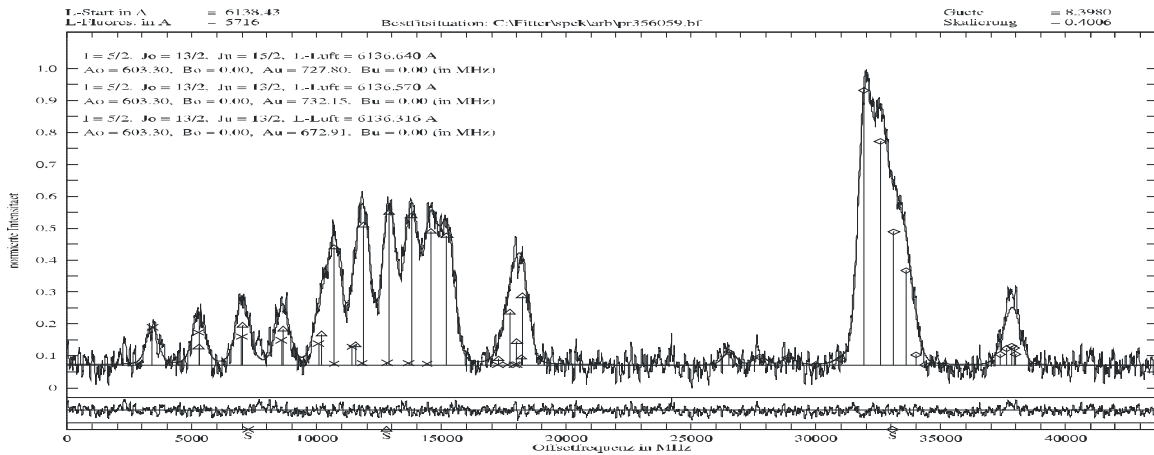
Figure 6.115: Best fit situation of the perturbed structure recorded with start wavelength 6136.73 Å

31483.15 cm^{-1} even, A = 603.3 MHz
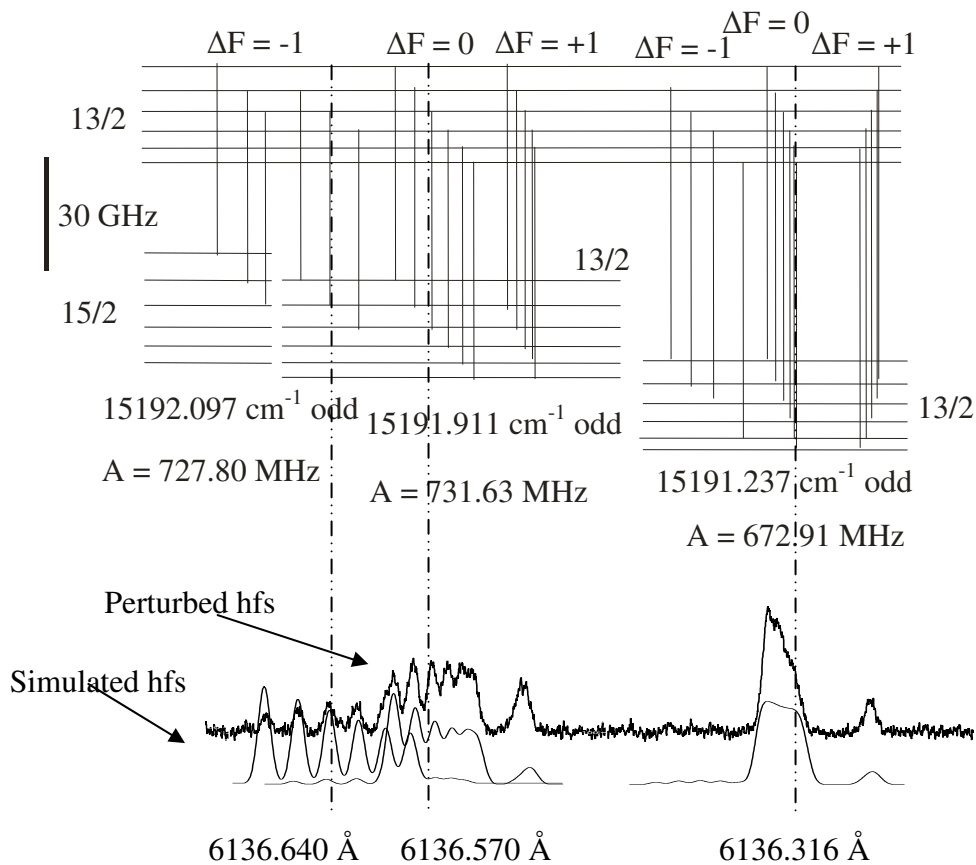
Figure 6.116: Level scheme for transition from triplet to upper level 31483.15 cm^{-1}, center-of-gravity positions marked by broken lines.

6.15 Excitation to a known upper level $32302.603^{e}_{13/2}$ cm^{-1} from Level Triplet

The level with energy 32302.603[*] cm^{-1} was discovered via a laser excitation of the line at 5783.95 Å and an LIF signal was recorded on florescence lines with wavelengths 3394 Å, 5179 Å, 5690 Å, 5701 Å, 5842 Å. After fitting procedure the line was classified as a transition from a known lower level with energy 15018.14 cm^{-1}, odd parity, J_u = 13/2 and A_u = 108(3) MHz to the upper level 32302.603 cm^{-1}, even parity, J_o = 13/2 and A_o= 568.77 MHz. Later on the level was confirmed by further excitations on the two of the observed fluorescence lines i.e. at 5688.74 Å and 5701.95 Å. So the values of angular momentum J and hyperfine constant A of the level have already been confirmed beyond any doubts. The transition list of the level generated by the classification program indicated a combination of this level with level triplet at one of the observed fluorescence lines i.e. 5842.67 Å. FT-spectra of the line (see figure 6.117) show a poor signal to noise ratio with a relative intensity of 2. So from FT-Spectra nothing could be inferred about the transition.
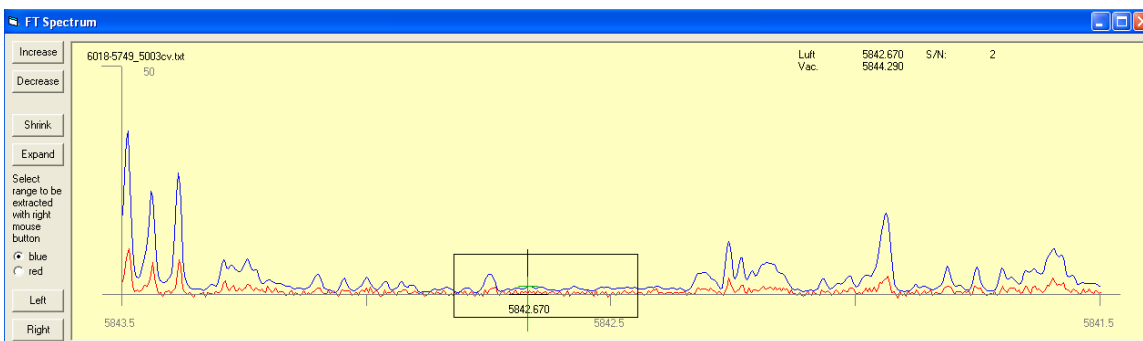
Figure 6.117: FT-Spectra of the line at 5842.67 Å.

Laser excitation of the line at 5842.67 Å was performed and LIF signal was recorded on all previously observed fluorescence channels showing anomalous intensity distribution of hyperfine components (see figure 6.118).
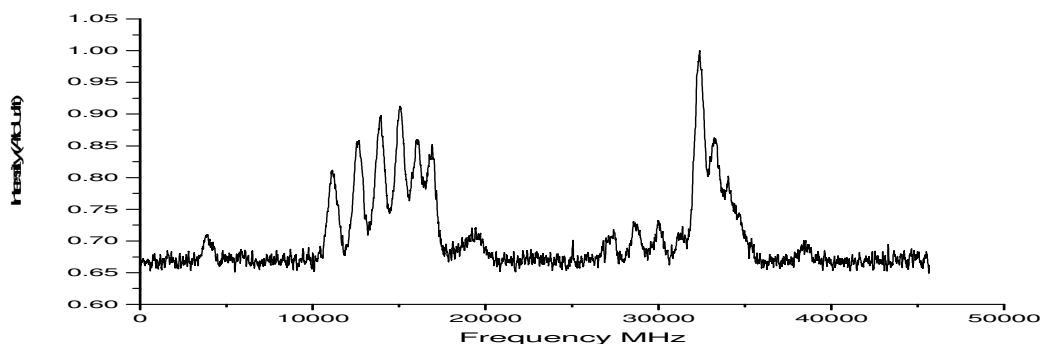
Figure 6.118: Hyperfine structure with anomalous intensity distribution of hyperfine components recorded with start wavelength 5846.07 Å

---

[*] Discovered by Shamim and Tanweer (29-06-2008) private communication

Simulations of the recorded perturbed hyperfine structure with predicted hyperfine structures for transitions from level triplet to the upper level are presented in figure 6.119. The best simulation was observed for J of upper level as 13/2 with A = 568 MHz and assuming level triplet as a lower set of levels.
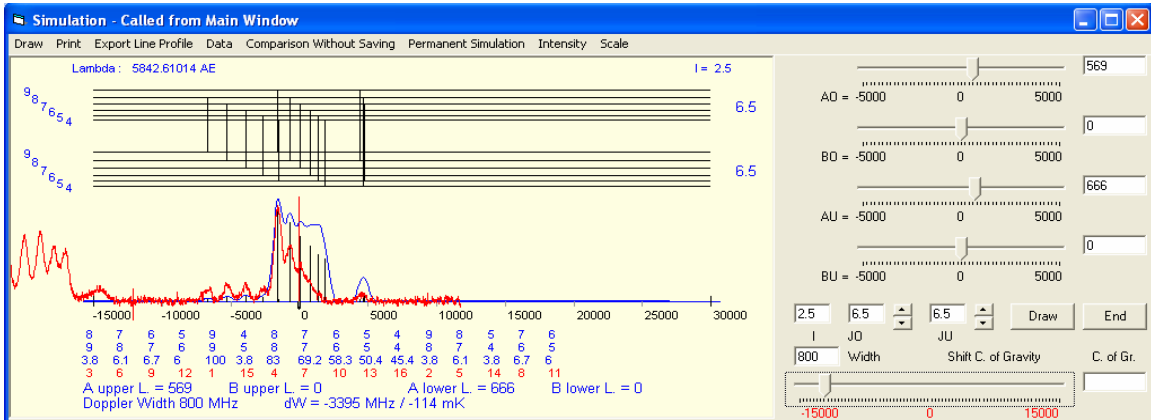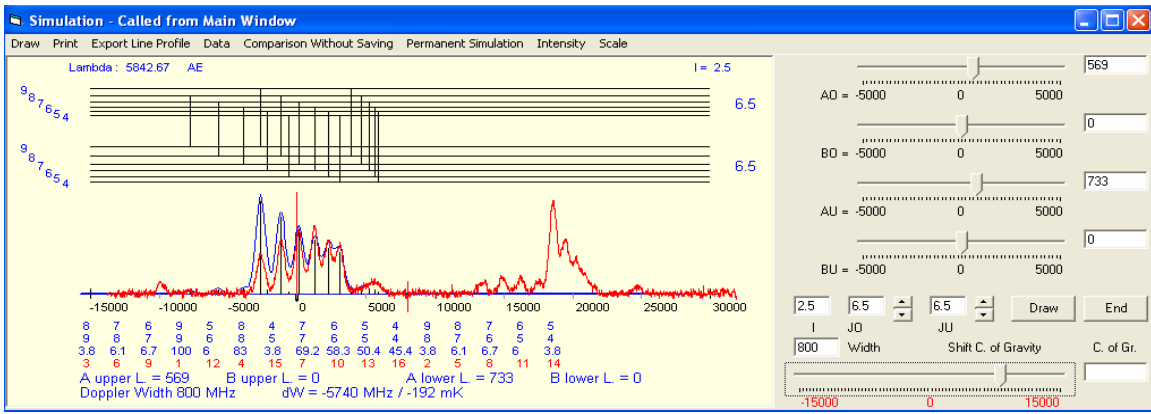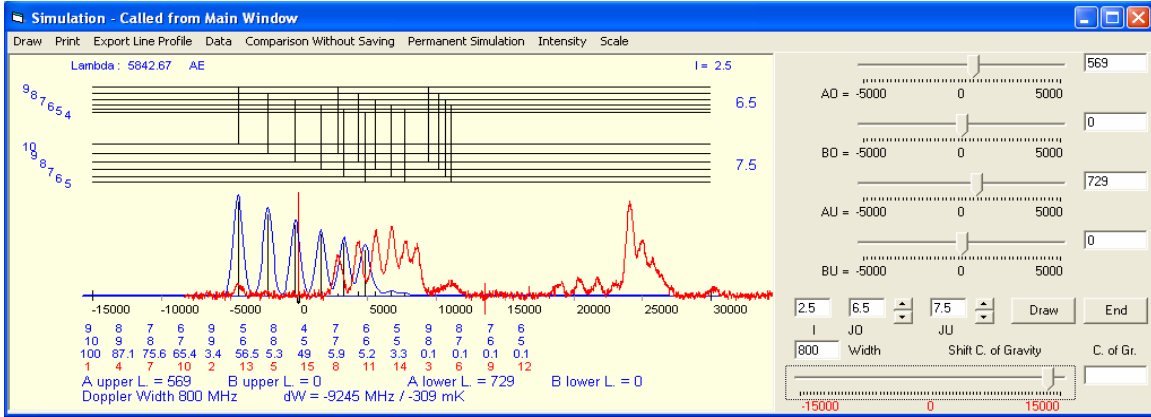
Figure 6.119: Simulations of the perturbed structure (red line profile) recorded from start wavelength 5846.07 Å

It is clear from the simulation that the first group is almost absent i.e. for transition from upper most level of triplet to upper level the intensities of hyperfine components are almost zero with the exception of the first diagonal component. For the second and third group i.e. for excitations from middle and lower most levels of triplet to upper, a good agreement is observed between experimentally recorded and predicted structures in terms of hyperfine components, although the intensity distribution is changed. Best fit of the recorded structure (see figure 6.120) is obtained for J and A values of level triplet given in table 6.16. Since the wave number of the upper level is already known with good accuracy therefore the wave numbers of levels in triplet are calculated (see table 6.24) using center of gravity wave numbers obtained from the fit of the recorded structure and the wave number of upper level. The level scheme with a comparison between experimentally recorded perturbed and simulated unperturbed hyperfine structure pattern is presented in figure 6.121.
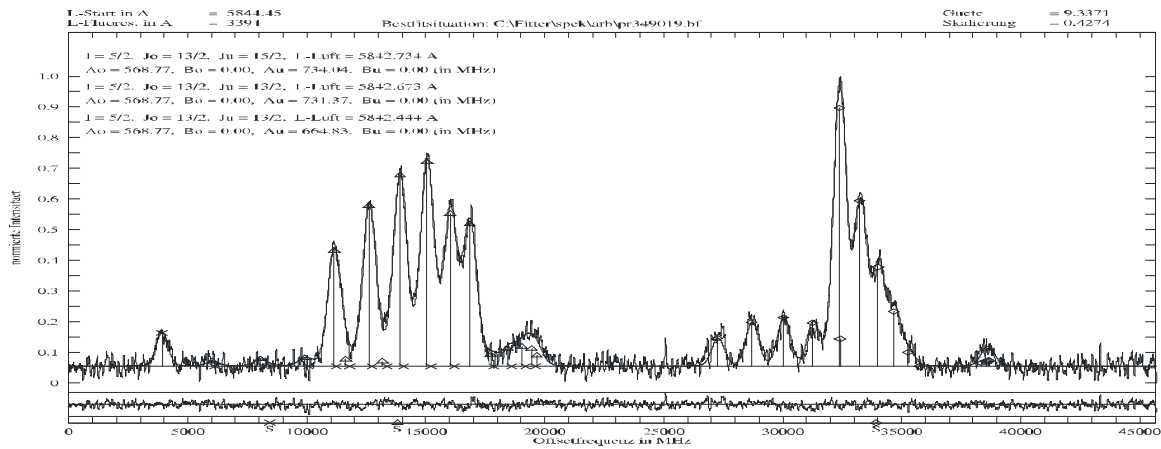
Figure 6.120: Best fit of the perturbed structure recorded with start wavelength 5846.07 Å

Table 6.24: Improved values of wave numbers of levels in triplet, computed from the wave number of upper level 32302.603 cm^{-1}.

cog λ_{air} (Å)	Lower Level				Upper Level
	J_u	Parity	Energy (cm^{-1})	A_u (MHz)	$J_o = 13/2$, Parity = e, $A_o = 568.77$ MHz
					Average Energy (cm^{-1})
5842.734	15/2	o	15192.072	734.04	
5842.673	13/2	o	15191.893	731.37	32302.603
5842.444	13/2	o	15191.222	664.83	

175

32302.56 cm^{-1} even, A = 568.77 MHz

ΔF = -1   ΔF = 0   ΔF = +1   ΔF = -1   ΔF = 0 ΔF = +1

13/2

30 GHz

13/2

15/2

$15192.029 \text{ cm}^{-1}$ odd

15191.85 cm^{-1} odd

A = 734.04 MHz

A = 731.37 MHz

13/2

$15191.178 \text{ cm}^{-1}$ odd

A = 664.83 MHz

Perturbed hfs

Simulated hfs

5842.734 Å   5842.673 Å   5842.444 Å
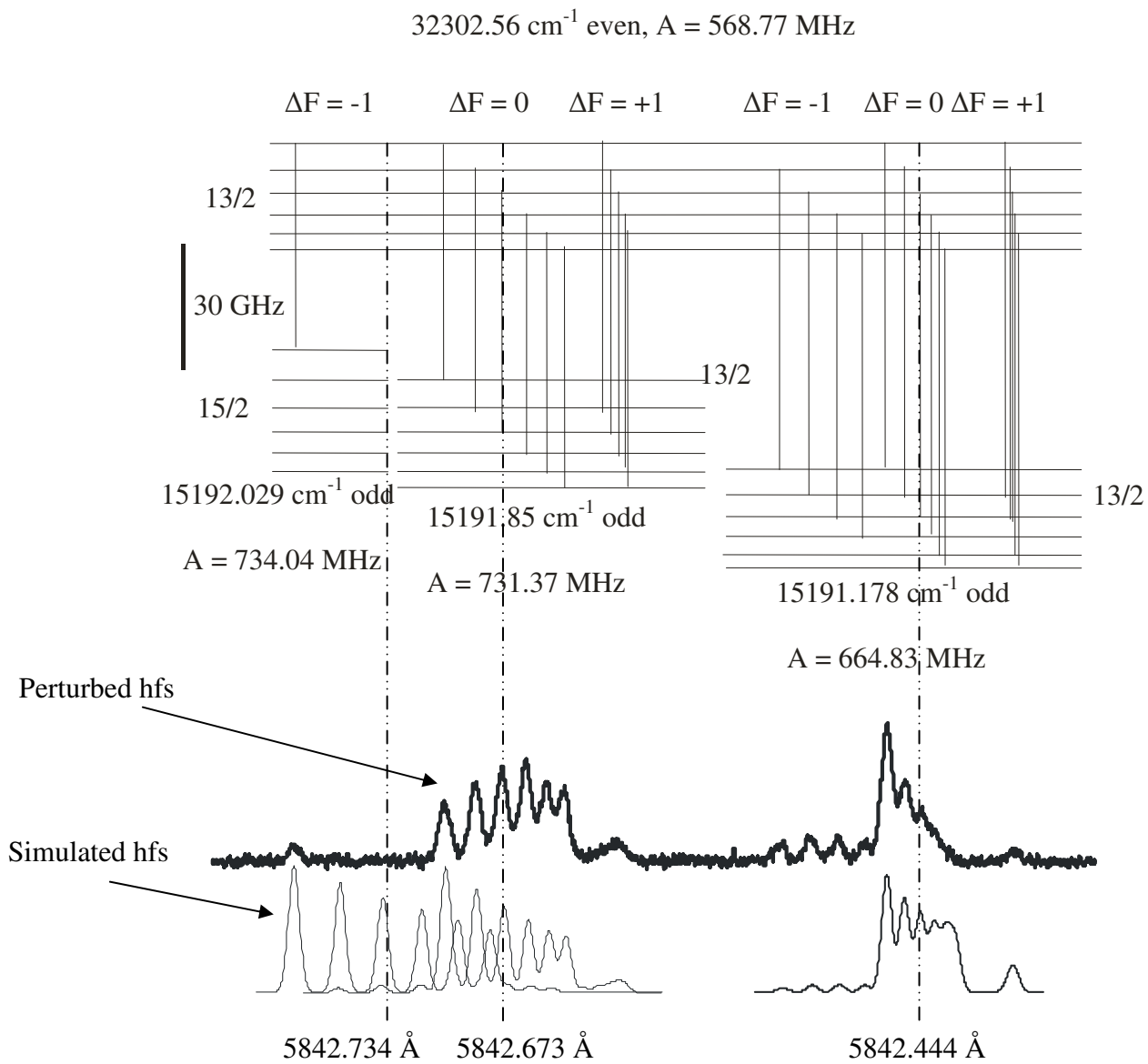
Figure 6.121: Level scheme for transition from triplet to upper level $32302.603 \text{ cm}^{-1}$, center-of-gravity positions marked by broken lines.

6.16 Excitation to a known upper level $31758.102^{e}_{13/2}$ cm^{-1} from Level Triplet

This level with energy 31758.102^{*} cm^{-1} was discovered via a excitation of the line at 6474.910 Å with LIF signal recorded on florescence lines 5059 Å, 5374 Å, 5426 Å and 7796 Å. The line was classified as transition from lower level 16318.145 cm^{-1}, odd parity, $J_u = 13/2$ and $A_u = 280.8(8)$ MHz to the upper level 31758.102, even parity, $J_o = 13/2$ and $A_o = 501$ MHz. The existence of the upper level was then confirmed by second excitation at line 7796.202 Å. So angular momentum J and hyperfine constant A of the upper level are already known with a good accuracy. The transition list of the level generated by the classification program indicated a combination of this level with level triplet at one of the listed line i.e. 6034.78 Å not mentioned as the observed fluorescence line. FT-spectra of the line (see figure 6.122) is an admixture of more than one line with a relative intensity of 4.
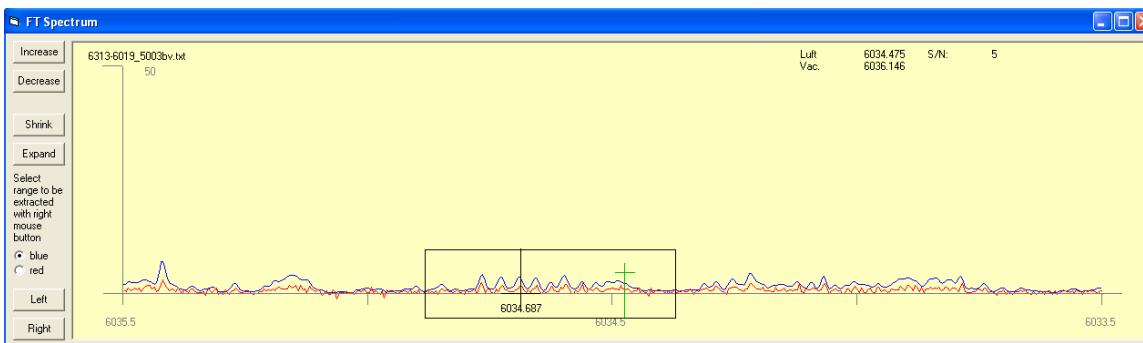
Figure 6.122: FT-Spectra of the line 6034.687 Å

Laser excitation with start wavelength 6034.88 Å was performed and a hyperfine structure with perturbed intensity distribution of hyperfine components was recorded (see figure 6.123) at fluorescence channels 5059 Å, 5374 Å, 5426 Å.
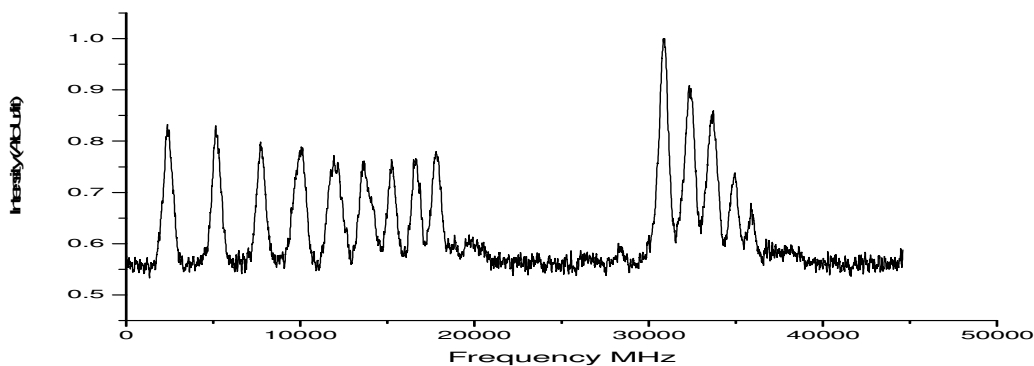
Figure 6.123: Hyperfine structure with anomalous intensity distribution of hyperfine components recorded with start wavelength 6034.88 Å

---

[*] Sc02d/ElKh99d/Gu   14-03-02

Simulations of the recorded perturbed structure with theoretically suggested transitions from level triplet to the upper level are presented in figure 6.124. The best simulation was observed for J of upper level as 13/2 with A = 501 MHz and assuming level triplet as a lower set of levels.
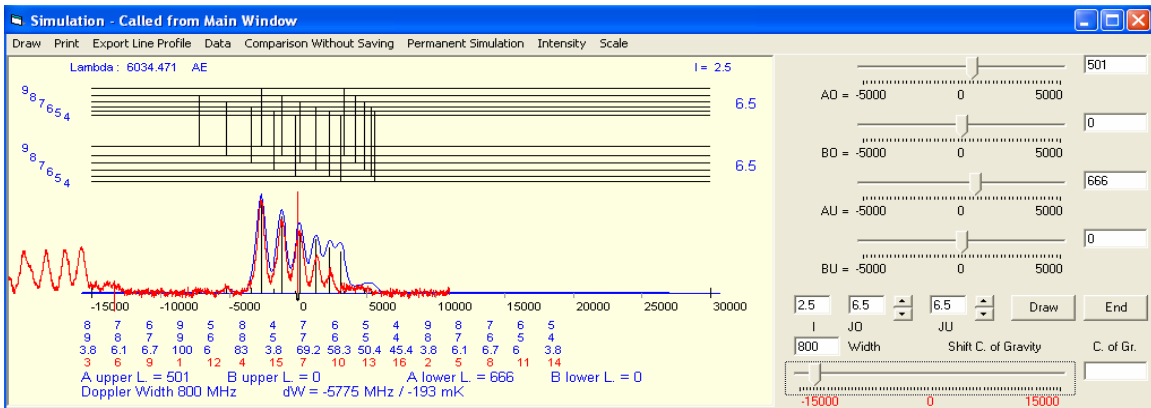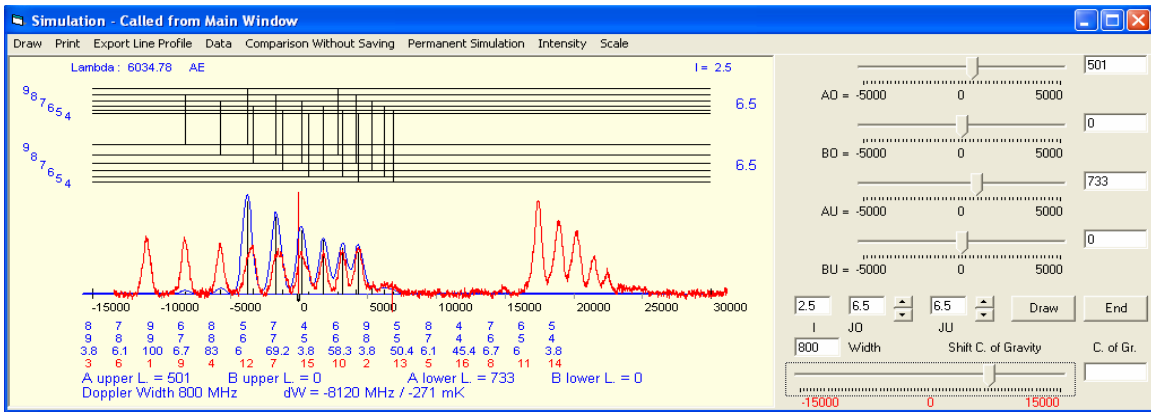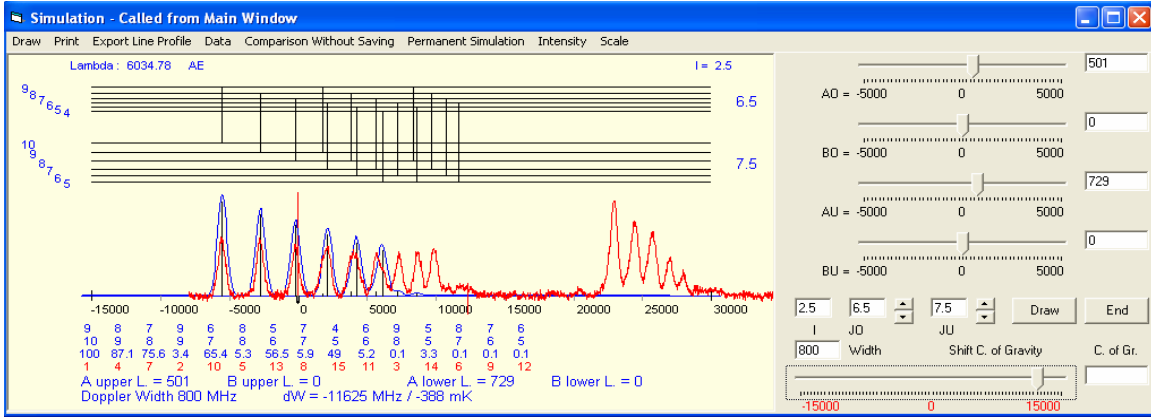
Figure 6.124: Simulations of the perturbed structure (red line profile) recorded from start wavelength 6034.88 Å

Good agreement is observed in terms of positions of hyperfine components for all three groups representing transitions from all three levels of triplet to upper level. Although the intensity distribution of hyperfine components is changed this is in accordance with the previous transitions from level triplet to upper levels. Best fit of the recorded structure (see figure 6.125) is obtained for J and A values of level triplet given in table 6.25.
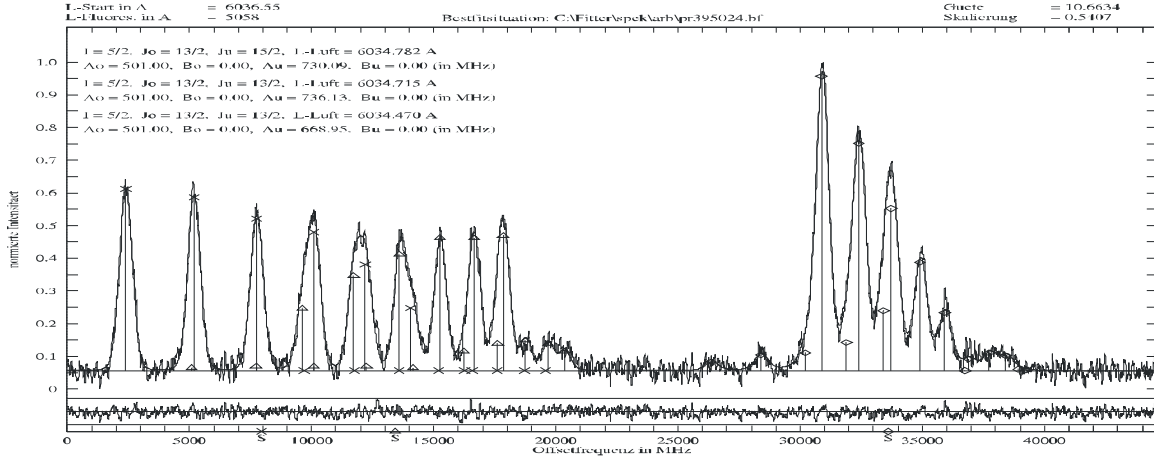
Figure 6.125: Best fit of the perturbed structure recorded with start wavelength 6034.88 Å

Since the wave number of the upper level is already known with good accuracy therefore the wave numbers of levels in triplet are calculated using center of gravity wave numbers obtained from the fit of the recorded structure and the wave number of upper level (see table 6.25). The level scheme with a comparison between experimentally recorded perturbed and simulated unperturbed hyperfine structure pattern is presented in figure 6.126.

Table 6.25: Improved values of wave numbers of levels in triplet, computed from the wave number of upper level 31758.102 cm^{-1}.

cog λ_{air} (Å)	Lower Level				Upper Level
	J_u	Parity	Energy (cm^{-1})	A_u (MHz)	J_o = 13/2, Parity = e, A_o = 501 MHz
					Energy (cm^{-1})
6034.782	15/2	o	15192.081	730.09	
6034.715	13/2	o	15191.9	736.13	31758.102
6034.470	13/2	o	15191.227	668.95	
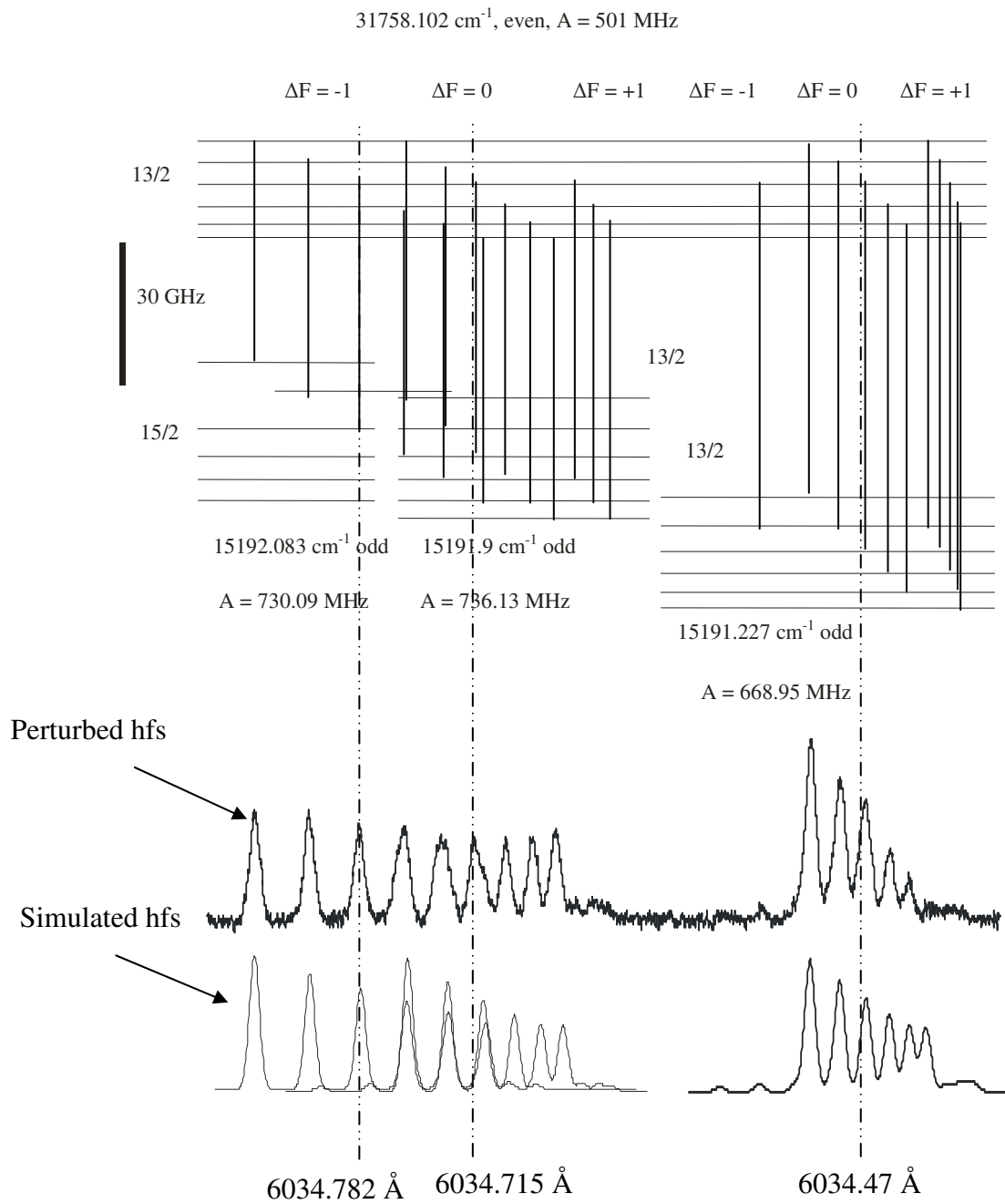
Figure 6.126: Level scheme for transition from triplet to upper level 31758.102 cm^{-1}, center-of-gravity positions marked by broken lines.

In addition to these excitations from level triplet to an upper level, few other excitations from level triplet to known or unknown upper levels with angular momenta J = 13/2 were also observed.

The laser excitation of line at 5701.38 Å gave LIF signal at fluorescence wavelengths 5555 Å, 5404 Å, 5337 Å 6050.93 Å. The hyperfine structure recorded on all observed fluorescence wavelengths indicated perturbed intensity distribution of hyperfine components (see figure 6.127). From the analysis of the recorded hyperfine structure the transition was identified as an excitation from the level triplet to an unknown upper level $32726.843^{e}_{13/2}$ **cm^{-1}** (Shamim 01-05-2008 private communication).
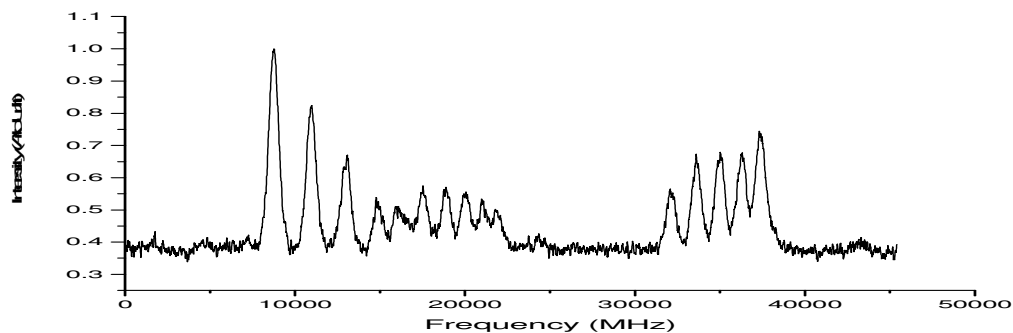
Figure 6.127: Hyperfine structure with anomalous intensity distribution of hyperfine components recorded with start wavelength 5701.53 Å

Laser excitation of line at 5771.71 Å to an already known upper level $32512.95^{e}_{13/2}$ **cm^{-1}** (Tanweer 24-09-2008 private communication) resulted in an anomalous intensity distribution of hyperfine components (see figure 6.128). The structure was recorded on more than one fluorescence wavelengths i.e. 4872 Å , 5121 Å , 5397 Å, 5465 Å, 5622 Å. Analysis of the recorded perturbed structure confirmed the combination of known upper level with level triplet at this line. Initially the upper level was discovered by laser excitation of line at 5824.04 Å showing normal intensity distribution of its hyperfine components.
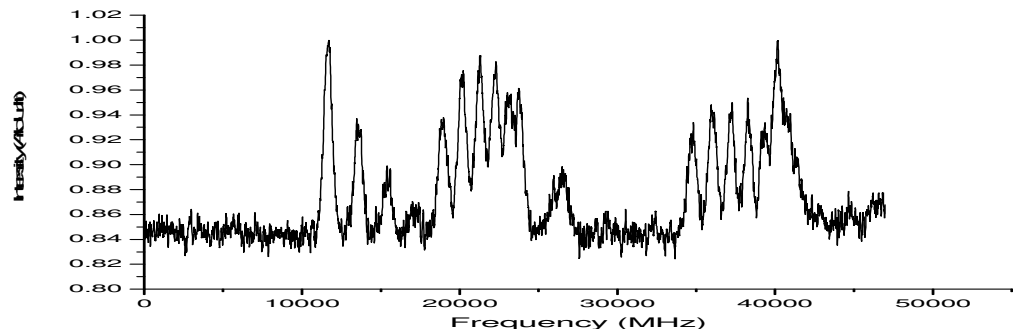
Figure 6.128: Hyperfine structure with anomalous intensity distribution of hyperfine components recorded with start wavelength 5771.96 Å

The laser excitation of line at 5907.47 Å resulted in an LIF signal at fluorescence wavelengths 3415 Å, 5847.36 Å. The recorded hyperfine structure indicated a perturbed intensity distribution of hyperfine components (see figure 6.129). The analysis of the recorded structure resulted in a new upper level $\mathbf{32115.102^e_{13/2}\,cm^{-1}}$ (Tanweer 31-10-2008 private communication) which combines with the level triplet.
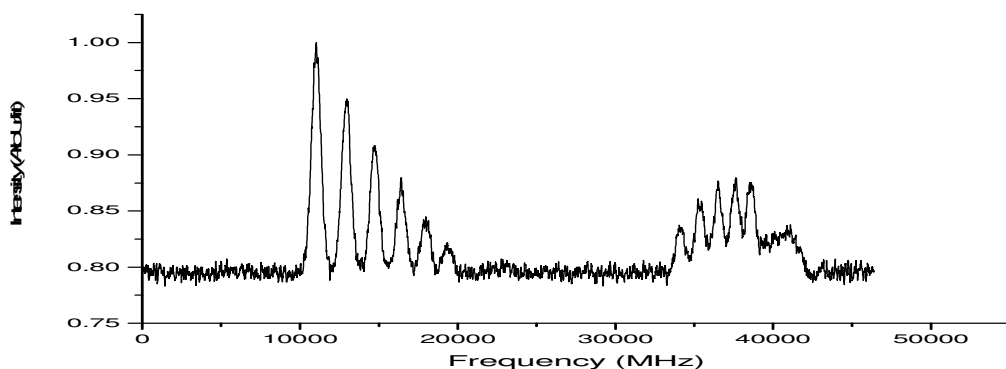
Figure 6.129: Hyperfine structure with anomalous intensity distribution of hyperfine components recorded with start wavelength 5907.68 Å

Laser excitation of line at 6058.29 Å to an already known upper level $\mathbf{31693.865^e_{13/2}\,cm^{-1}}$ (Shamim 26-11-2008 private communication) resulted in a recorded hyperfine structure pattern with an anomalous intensity distribution of hyperfine components (see figure 6.130). The structure was seen on more than one fluorescence wavelengths i.e. 5075 Å, 5892.87 Å. Analysis of the recorded perturbed structure confirmed the combination of known upper level with level triplet at this line. Initially the upper level was discovered by laser excitation of line at 5892.87 Å showing normal intensity distribution of its hyperfine components.
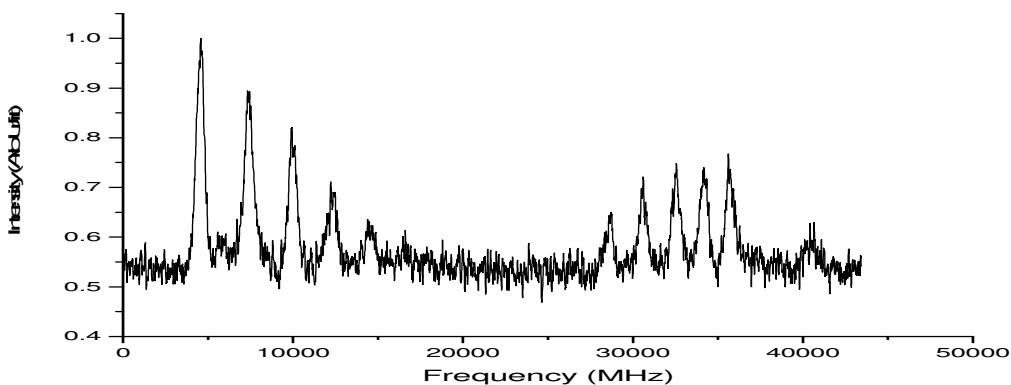
Figure 6.130: Hyperfine structure with anomalous intensity distribution of hyperfine components recorded with start wavelength 6058.42 Å

For the above transitions, the energies of the levels in triplet are computed and further improved based on the second excitations of the respective upper levels. The results of computations are given in Table 6.31.

6.17 Excitation to known Upper Levels $32631.828^{e}_{11/2}$ cm^{-1} and $32587.304^{e}_{11/2}$ cm^{-1} from Level Triplet

Levels with energies 32631.828[*] cm^{-1} and 32587.304[*] cm^{-1} were discovered via laser excitations of the lines 5693.13 Å and 5746.82 Å respectively. The LIF signal for the level 32631.828 cm^{-1} was recorded on florescence lines 3197 Å, 3800 Å, 3844 Å, 3998 Å, 4355 Å, 4589 Å, 5214 Å, 5291 Å, 5519 Å, 5615 Å, 5732 Å and for 32587.304 cm^{-1} was recorded on 3204 Å, 4702 Å, 4855 Å. The signal-to-noise ratio for the recorded hyperfine structure of the line 5693.13 Å is better as compared to the record hyperfine structure of the line 5746.82 Å. So the detailed analysis for the level 32631.828 cm^{-1} is presented in this section but the results of the analysis for level 32587.304 cm^{-1} are included in Table 6.31.

Using the best fit values the line at 5693.13 Å was identified as transition from the known lower level 15071.648 cm^{-1}, odd parity, J_u = 9/2 and A_u = 637 MHz to the upper level 32631.83 cm^{-1}, even parity, J_o = 11/2, A_o = 465 MHz. The transition list of the upper level 32631.828 cm^{-1} indicates a combination of the upper level with lower two levels of triplet at 5732.38 Å, which is one of the previously observed fluorescence line of the upper level. The transition from the upper most level of triplet is electric dipole forbidden since the angular momentum J of upper level is 11/2. Due to this reason the transition from upper most level of triplet is not shown in the transition list of the upper level. The line at 5732.38 Å has good signal to noise ratio in FT-Spectra (see figure 6.131) with a relative intensity of 5.
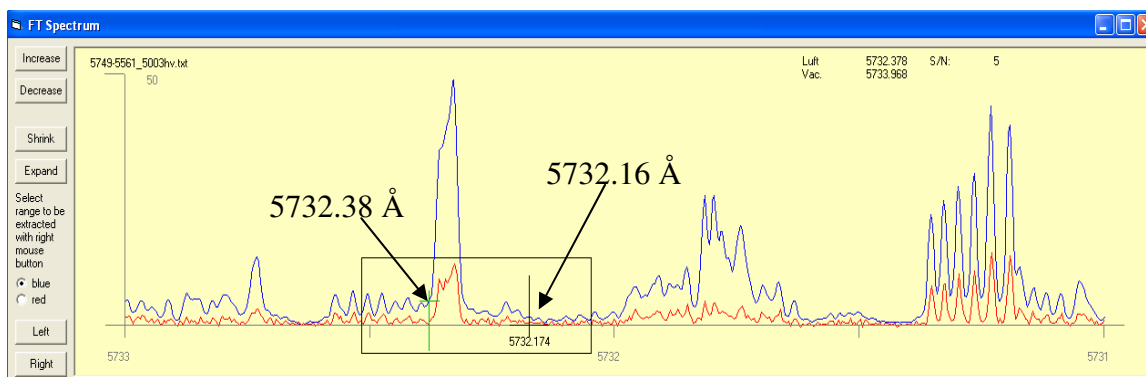
Figure 6.131: FT-Spectra of the lines where upper level is combining with level triplet.

Nevertheless laser excitation of line was performed with start wavelength 5732.58 Å and as expected the recorded LIF signal (see figure 6.132) show anomalous intensity distribution of hyperfine components on all the previously observed fluorescence wavelengths. The recorded spectrum shows two groups of hyperfine structure components corresponding to excitations from the lower two levels of triplet to the upper level. The upper level of the excited transition has an angular momentum J = 11/2. So the

---

[*] Discovered by Shamim (20-02-2009) and Tanweer (22-08-2008) private communication

excitation from the upper most level of triplet to upper level is dipole forbidden which is the reason for the first group of hyperfine structure not showing up. Simulation of the recorded perturbed structure with the predicted structure gave good agreement in terms of positions of hyperfine components but deviations in the intensities of hyperfine components can easily be seen (see figure 6.133a and 6.133b). Nevertheless, this confirms that the level triplet combines with the upper level 32631.828 cm^{-1} at the lines 5732.38 Å and 5732.16. **This transition is of special significance because only two lower levels of triplet (J = 13/2) are involved in the excitation to the upper level (J = 11/2) and provides an evidence for the existence of middle level of triplet.**
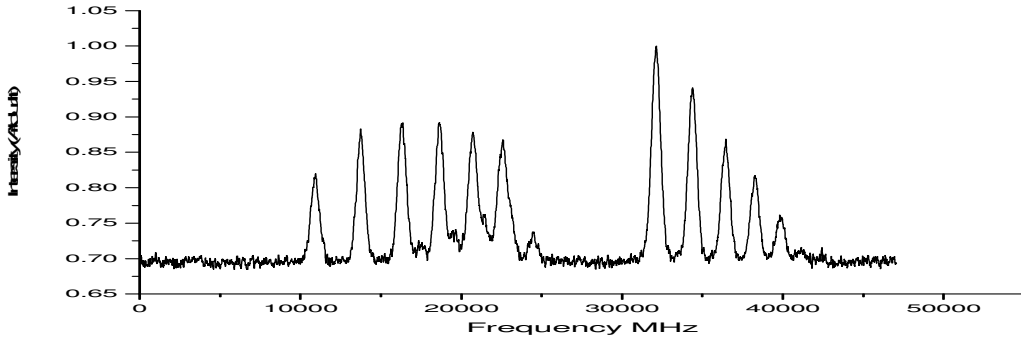
Figure 6.132: Perturbed hyperfine structure recorded with start wavelength 5732.58 Å

The recorded structure is fitted using two lines rather than three lines fit procedure and keeping fix the A-value of the already known upper level. The J value of upper level is taken as 11/2 and for the lower two levels of triplet J is taken as 13/2 and 13/2 respectively. The best fit (see figure 6.134) is obtained giving A values of lower two levels of triplet as given in table 6.26. Since the wave number of the upper level is already known with good accuracy therefore the wave numbers of the lower two levels of triplet are calculated using center of gravity wave numbers obtained from the fit of the recorded structure and the wave number of upper level (see table 6.26). The level scheme with a comparison between experimentally recorded perturbed and simulated unperturbed hyperfine structure pattern is presented in figure 6.135.
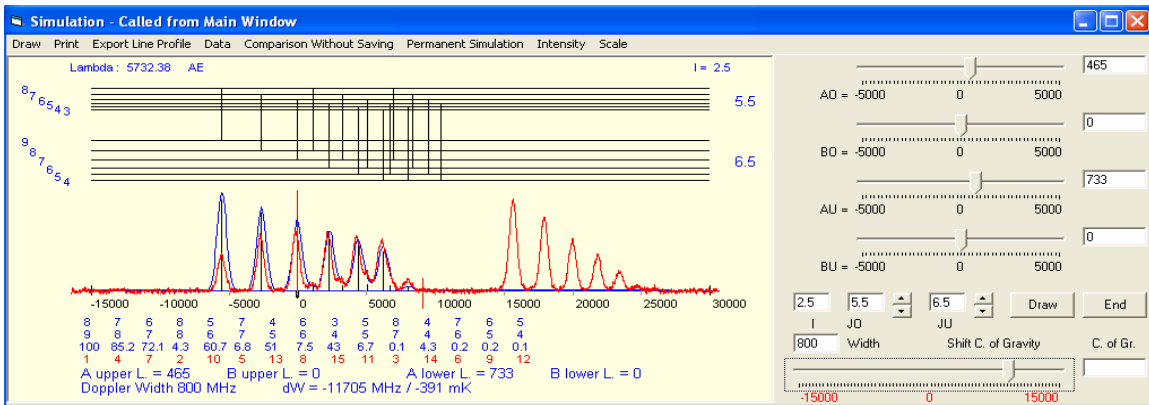
Figure 6.133a: Simulations of the perturbed structure (red line profile) recorded with start wavelength 5732.58 Å
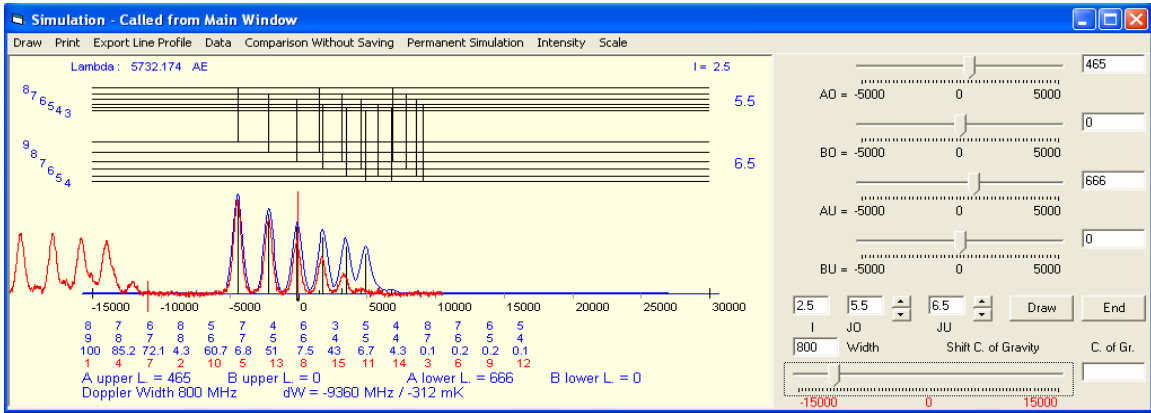
Figure 6.133b: Simulations of the perturbed structure (red line profile) recorded with start wavelength 5732.58 Å
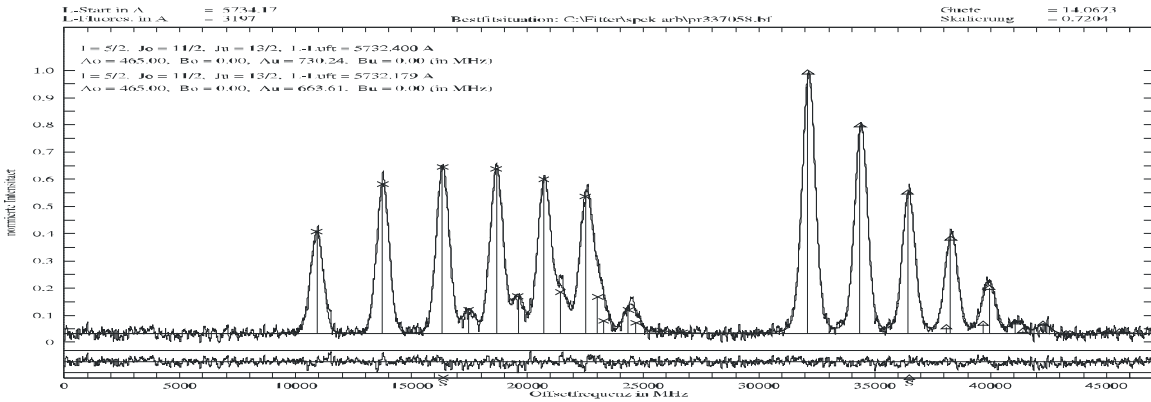
Figure 6.134: Best fit of the perturbed structure recorded with start wave length 5732.58 Å

Table 6.26: Improved values of wave numbers of levels in triplet, computed from the wave number of upper level 32631.828 cm^{-1}.

| cog λ_{air} (Å) | Lower Level | | | | Upper Level | |
| | J_u | Parity | Energy (cm^{-1}) | A_u (MHz) | $J_o = 11/2$, Parity = e, A_o = 465 MHz | |
					Energy (cm^{-1})	
---	---	---	---	---	32631.828	
5732.400	13/2	o	15191.966	730.24		
5732.179	13/2	o	15191.295	663.61		

32631.828 cm^{-1}, even, A = 465 MHz

ΔF = -1   ΔF = 0   ΔF = -1

11/2

30 GHz

13/2

15/2

13/2

15192.09 cm^{-1} odd   15191.9 cm^{-1} odd

A = 730 MHz   A = 736.13 MHz

15191.227 cm^{-1} odd

A = 668.95 MHz

Perturbed hfs

Simulated hfs

5732.40 Å   5732.179 Å
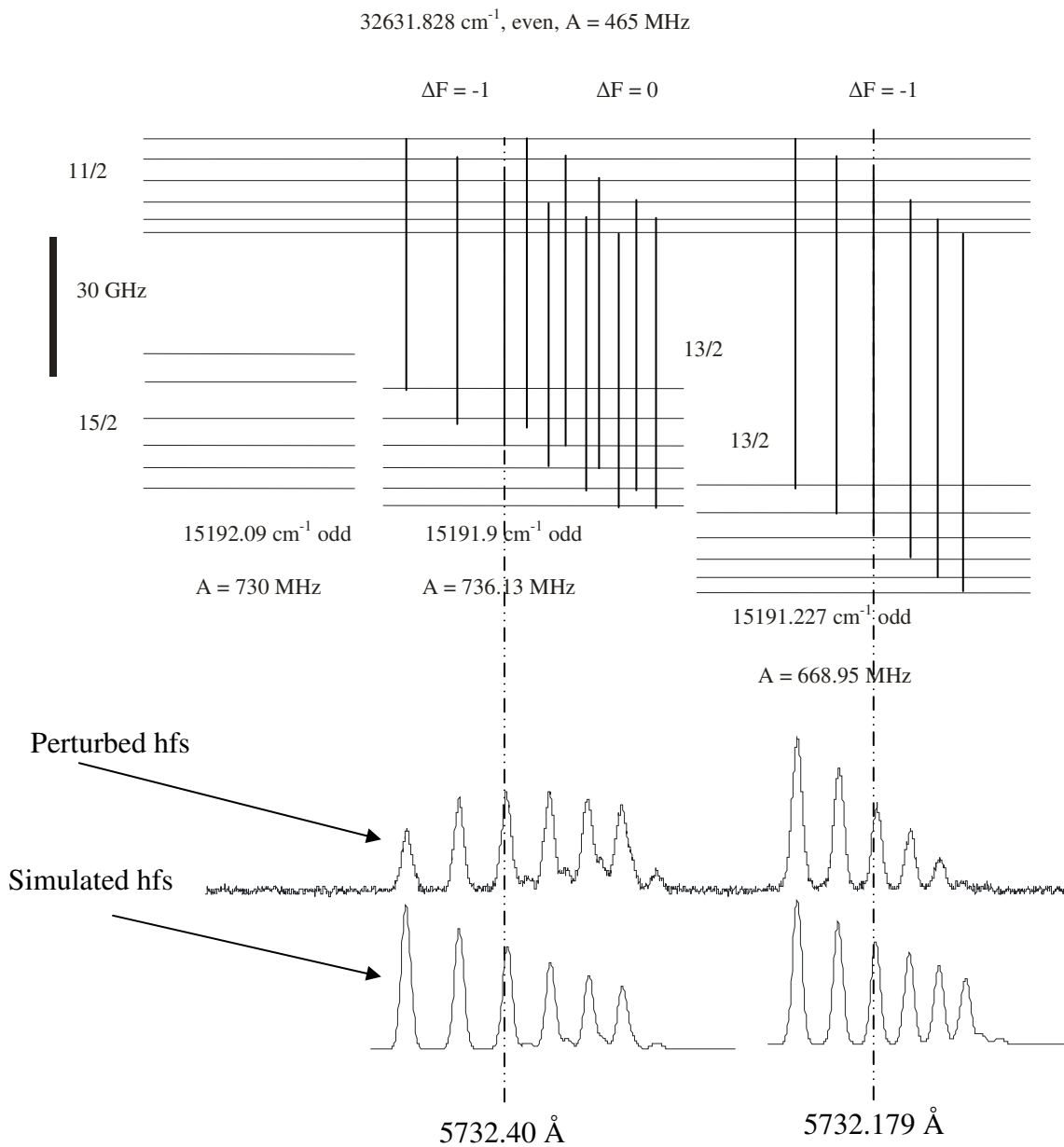
Figure 6.135: Level scheme for transition from triplet to upper level 32631.828 cm^{-1}, center-of-gravity positions marked by broken lines.

6.18 Excitation to a known upper level $30826.776^{e}_{17/2}$ cm^{-1} from Level Triplet

This level with energy 30826.706^{*} cm^{-1} was discovered via an excitation of the line at 5791.716 Å with LIF signal recorded on florescence lines 5245 Å, 5590 Å, 5608 Å, 6063 Å and 6226 Å. The line was classified as transition from lower level 13565.52 cm^{-1}, odd parity, J_u = 15/2 and A_u = 916.6(2) MHz, B_u = 12(7) MHz to the upper level 30826.706 cm^{-1}, even parity, J_o = 17/2 and A_o = 580 MHz. The existence of the upper level was confirmed by another excitation at line 5608.660 Å. So angular momentum J and hyperfine constant A of the upper level are already known with a good accuracy. The transition list of the level generated by the classification program indicated a combination of this level with level triplet at one of the listed line i.e. 6394.27 Å not mentioned as an observed fluorescence line. FT-spectra of the line (see figure 6.136) has relative intensity of 3 unresolved hyperfine components.
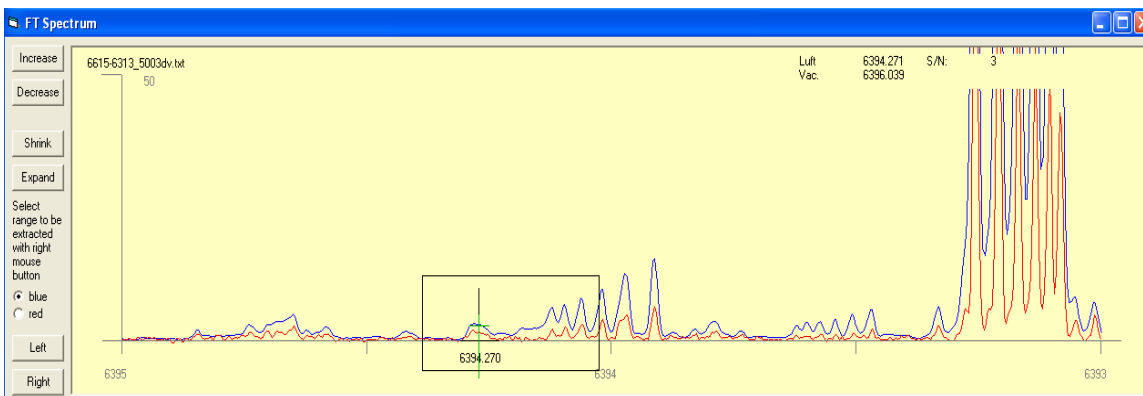
Figure 6.136: FT-Spectra of the line involving a transition from level triplet

Laser excitation with start wavelength 6394.42 Å was performed and a structure with apparently perturbed intensity distribution of hyperfine components was recorded (see figure 6.137) at fluorescence channels 5245 Å and 5791 Å.
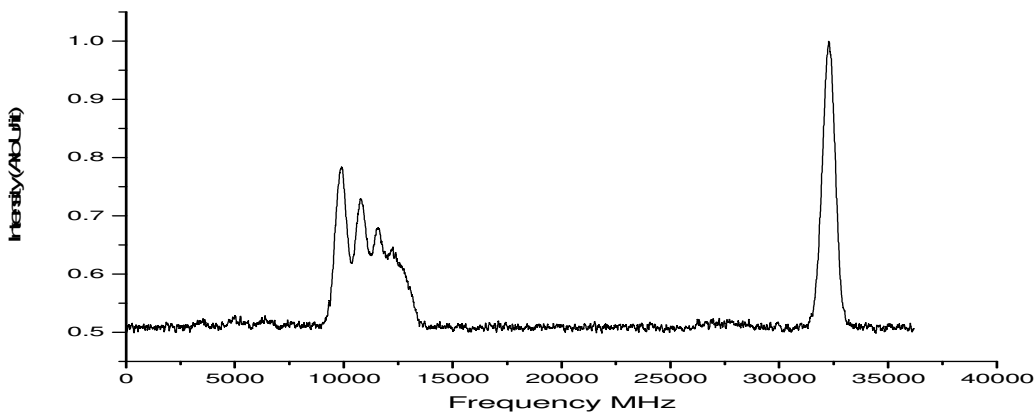
Figure 6.137: Perturbed hyperfine structure recorded with start wavelength 6394.42 Å

---

* EB05/ZaFa/Gu Private Communication

A similar behaviour is seen as observed previously for transitions from level triplet to an upper level with J = 17/2. Here again two groups of hyperfine components with anomalous intensity distribution are seen. A similar behaviour is observed on two other fluorescence lines, as a first approximation it was assumed that the excitation of line involved a transition from level triplet to the known upper level. Based on the assumption, simulation can only be performed for transitions from lower two levels of triplet to upper level. A good agreement (see figure 6.138) between recorded line profile and predicted transition is obtained use already known J and A values of upper level and taking J and A value of the first level of triplet.
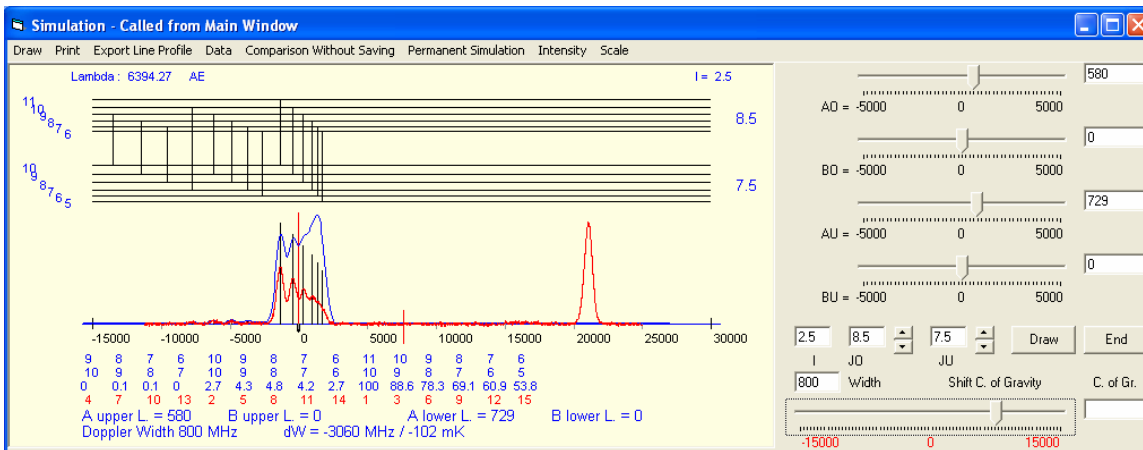
Figure 6.138: Simulation of the perturbed structure (red line profile) recorded with start wavelength 6394.42 Å

The first group of hyperfine structure for a transition between J_o=17/2 - J_u=15/2 is allowed i.e. from the uppermost level of triplet. The second group is missing and the third group appears as a narrow spaced single peak structure corresponding to a transition from lowest level of triplet with J = 13/2 to upper level with J = 17/2 which is electric dipole forbidden transition. As before the reason for the appearance of third group with unusual intensity profile is the mixing of wave functions of the lower most and upper most levels of triplet so J is no longer a good quantum number for the lower most level of triplet and is an admixture of angular momentum 13/2 and 15/2. What is recorded as a single peak structure are transitions between various F-sublevels of lowest level of triplet and upper level.

Recorded structure is fitted using single line fit procedure by only fitting the transition from uppermost level of triplet to upper level. Best fit (see figure 6.139) is obtained giving A value of uppermost level of triplet as given in table 6.27. Level energy of upper level 30826.706 cm^{-1} was corrected from FT-Spectra at 5791.715 Å (see figure 6.140). The corrected energy is now 30826.776 cm^{-1}. Since the wave number of the upper level is already known with good accuracy therefore the wave number of only uppermost level of triplet is calculated using center of gravity wave number obtained from the fit of the recorded structure and the wave number of upper level (see table 6.21).
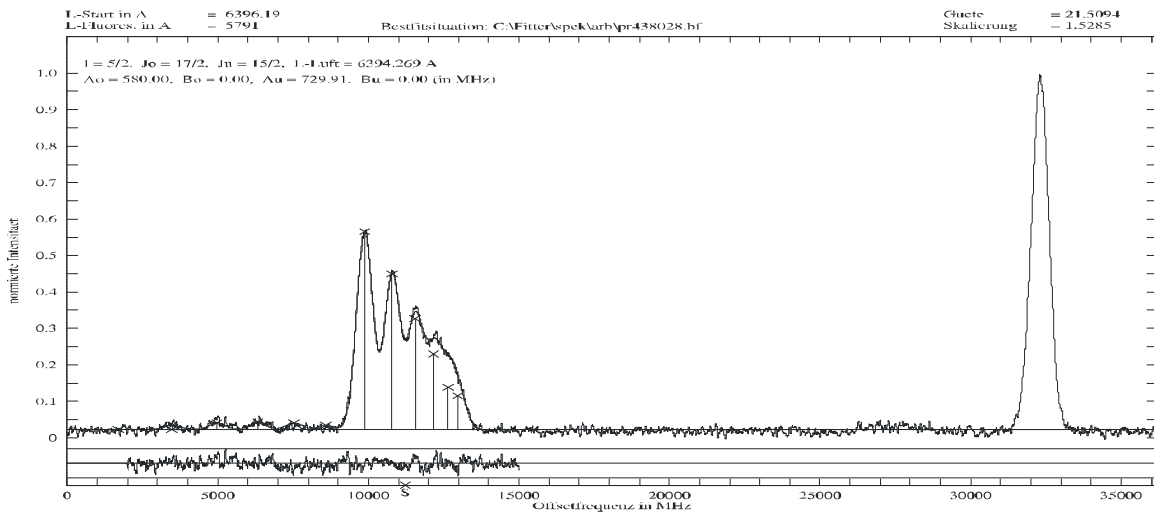
Figure 6.139: Best of the perturbed structure recorded with start wave length 6394.42 Å
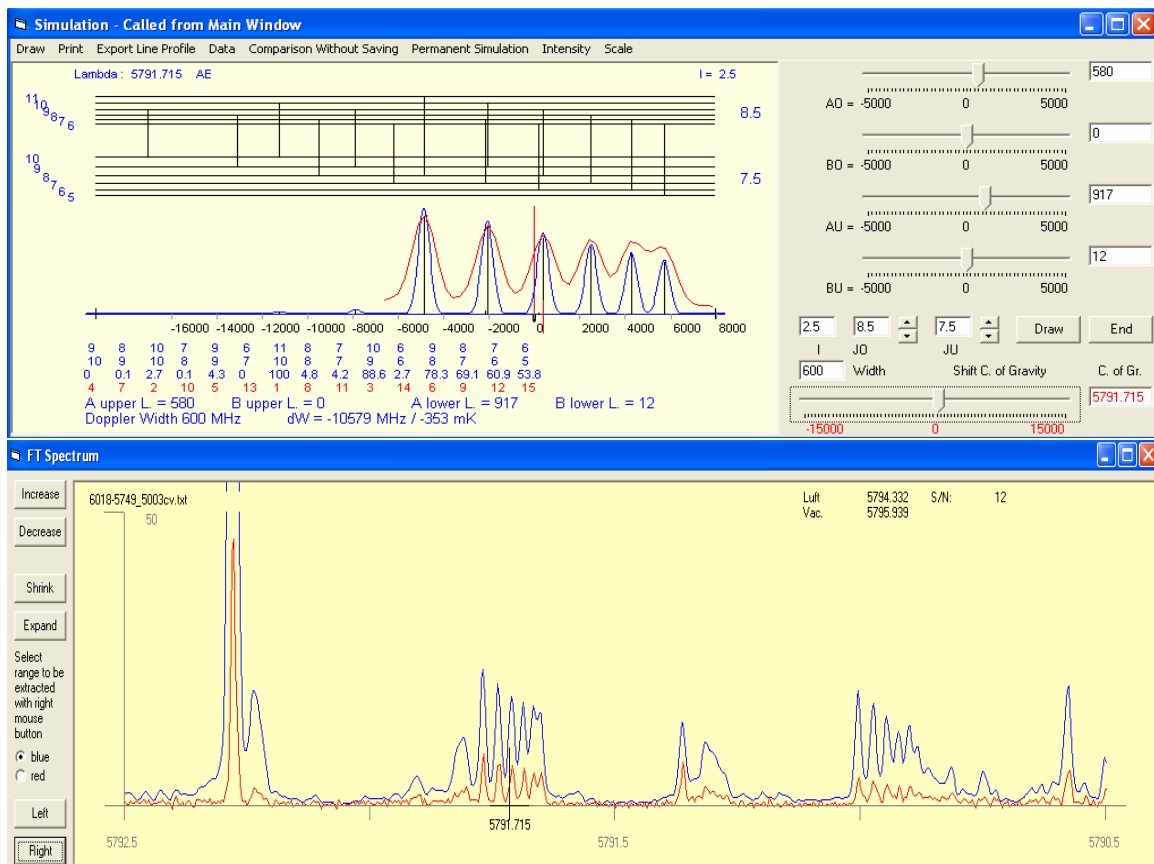
Figure 6.140: Correction in energy of the upper level at 5791.715 Å

Table 6.27: Improved values of wave numbers of levels in triplet, computed from the wave number of upper level 30826.776 cm^{-1}.

| cog λ_{air} (Å) | Lower Level | | | | Upper Level |
	J_u	Parity	Energy (cm^{-1})	A_u (MHz)	$J_o = 17/2$, Parity = e, A_o = 580 MHz
					Corrected Energy (cm^{-1})
6394.269	15/2	o	15192.094	729.98	
---	---	---	---	---	30826.776
---	---	---	---	---	

This transition is similar in character to the transition from level triplet to the upper level 31629.427 cm^{-1}. The third group of hyperfine components corresponding to a transition from the lowest level of triplet with J = 13/2 to the upper level with J = 17/2. Such a transition is electric dipole forbidden ($\Delta J = +2$). Transition from the middle level of triplet to upper level is not observed. Hyperfine structure resulting from the transition from the upper most triplet level to upper level 30826.776 cm^{-1} has almost the normal relative intensities showing almost no deviation from the predicted structure. As the transition from lowest level of triplet to upper level is electric dipole forbidden ($\Delta J = +2$), the frequency positions for transitions between their F-sublevels responsible for third group are calculated manually using Casimir formula (see section 3.7) taking $J_o = 17/2$, $J_u = 13/2$, $A_o = 580$ MHz, $A_u = 666$ MHz and wave number difference of lowest triplet level and upper level. The results of calculations are summarized in Table 6.28. Transition scheme between levels of triplet and upper level 30826.776 cm^{-1} is shown in figure 6.141. Frequency positions for the third group are drawn taking the values from Table 6.28.

Table 6.28: Frequency positions of hyperfine components in third group of perturbed structure.

| $F_o - F_u$ | Casimir Factors | | Frequency positions of hfs components ν / cm^{-1} |
	α_o	α_u	
11 - 9	21.25	16.25	15635.593
10 - 8	10.25	7.25	15635.580
9 - 7	0.25	-0.75	15635.564
8 - 6	-8.75	-7.75	15635.545
7 - 5	-16.75	-13.75	15635.524
6 - 4	-23.75	-18.75	15635.500

30826.776 cm^{-1}, even, A = 580 MHz

ΔF = -1   ΔF = 0   ΔF = +1   ΔF =   ΔF = +2   ΔF =

17/2

30 GHz

15/2

13/2

15192.094 cm^{-1} odd

15191.906 cm^{-1} odd

A = 729.98.01 MHz

A = 730 MHz

13/2

15191.233 cm^{-1} odd

Experimentally
recorded
Structure

Experimentally
observed
Transition ΔJ = +2

A = 666 MHz

Predicted
Structure

6394.269 Å

Approx. cog
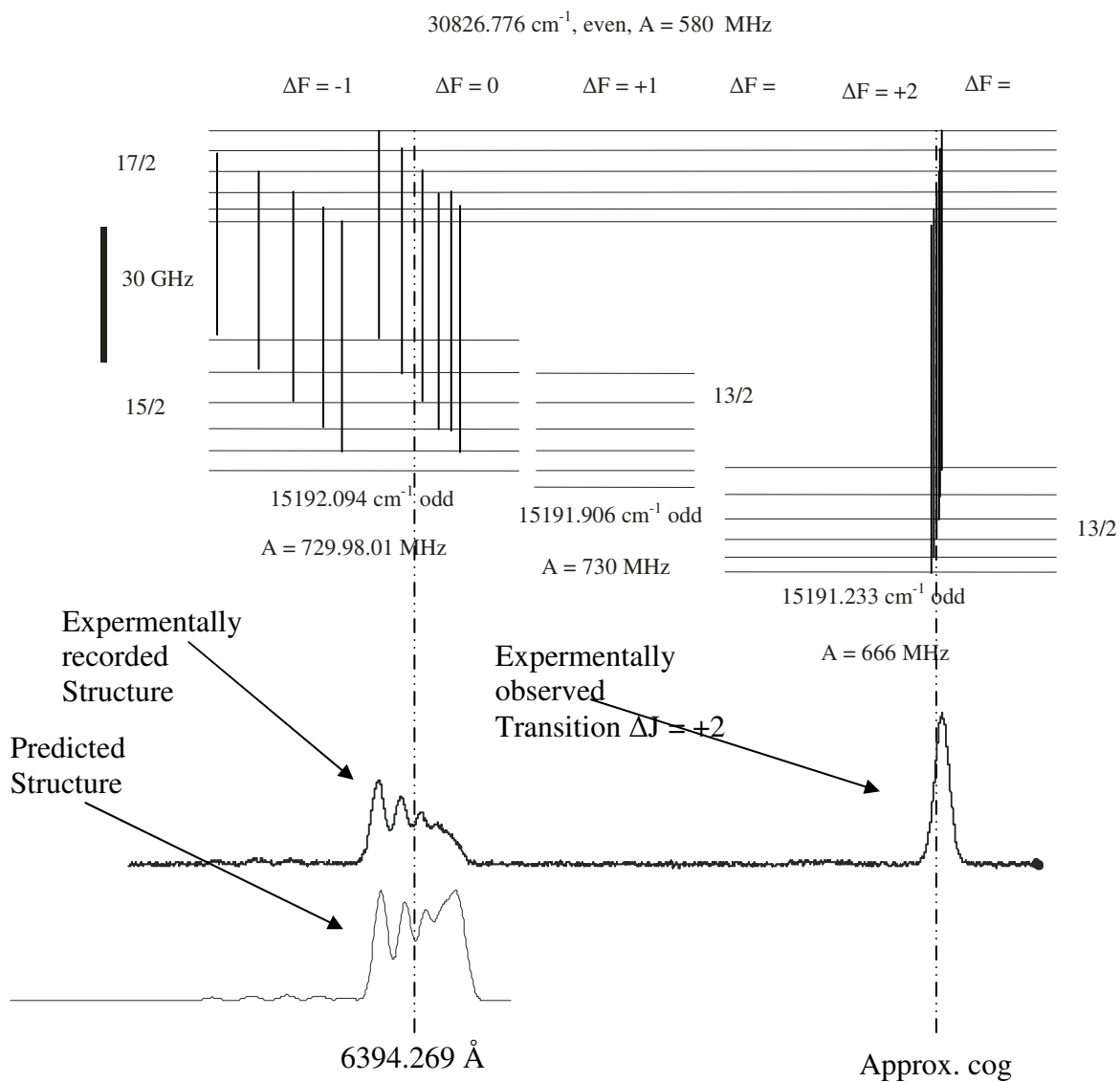
Figure 6.141: Level scheme for transition from triplet to upper level 30826.776 cm^{-1}, center-of-gravity positions marked by broken lines.

In addition to these excitations from level triplet to an upper level, few other excitations from level triplet to known or unknown upper levels with angular momenta J = 17/2 were also observed. The results of the analysis for these recorded structures are included in Table 6.31.

Laser excitation of line at 5785.35 Å to an already known upper level $\mathbf{32472.324^e_{17/2}\ cm^{-1}}$ (Discovered on 01-10-2007) resulted in a recorded hyperfine structure pattern with an anomalous intensity distribution of hyperfine components (see figure 6.142). The structure was seen on more than one fluorescence wavelengths i.e. 3558 Å, 5209 Å, 5516 Å, 5656.95 Å, 6549 Å. Analysis of the recorded perturbed structure confirmed the combination of known upper level with level triplet at this line. Initially the upper level was discovered by laser excitation of line at 5855.49 Å showing normal intensity distribution of its hyperfine components.
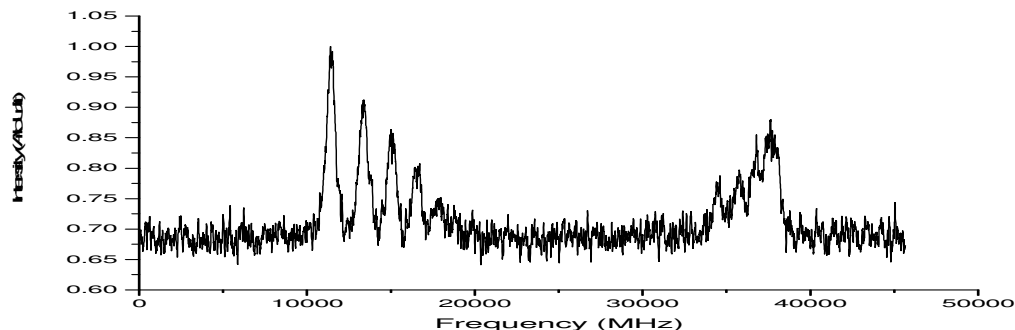
Figure 6.142: Hyperfine structure with anomalous intensity distribution of hyperfine components recorded with start wavelength 5785.52 Å

Laser excitation of line at 6385.22 Å to an already known upper level $\mathbf{30848.875^e_{17/2}\ cm^{-1}}$ (Discovered by G. H. Guthöhrlein et. al.) resulted in a recorded hyperfine structure pattern with an anomalous intensity distribution of hyperfine components (see figure 6.143). The structure was seen on more than one fluorescence wavelengths i.e. 5238 Å, 5583 Å, 5690 Å, 5784 Å. Analysis of the recorded perturbed structure confirmed the combination of known upper level with level triplet at this line. Initially the upper level was discovered by laser excitation of line at 5784.308 Å showing normal intensity distribution of its hyperfine components.
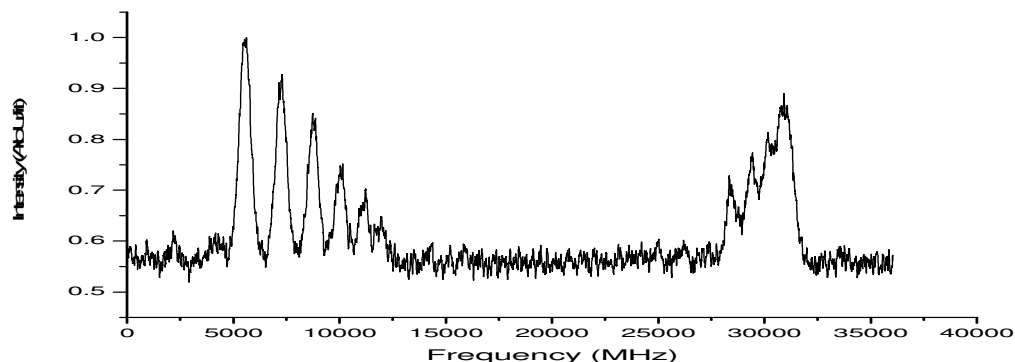
Figure 6.143: Hyperfine structure with anomalous intensity distribution of hyperfine components recorded with start wavelength 6385.34 Å

6.19 Excitation to a known upper level $31535.107^e_{13/2}$ cm^{-1} from Level Triplet

The level 31535.107[*] cm^{-1} was discovered via a laser excitation of the line at 5702.02 Å with LIF signal recorded on florescence lines 3315 Å, 3486 Å, 3683 Å, 5068 Å, 5116 Å, 5393 Å, 5873 Å, 5962 Å, 6053Å, 6116 Å and 6194 Å. Using the best fit values the line was identified as transition from known lower level 14002.323 cm^{-1}, odd parity, $J_u = 11/2$ and $A_u = 566.4$ MHz, $B_u = -125$ MHz to the upper level 31535.107 cm^{-1}, even parity, $J_o = 502.20$ MHz. The existence and J and A values of the upper level were further confirmed by two more laser excitations at lines 5872.132 Å and 5774.78 Å.

At one of the observed fluorescence line 6117.13 Å which is also present in the transition of the upper level 31535.107 cm^{-1}, the level is combining with level triplet with normal intensity distribution of hyperfine structure components as predicted by the classification program. The line at 6117.13 Å in FT-Spectra (see figure 6.144) has a relative intensity of 3.
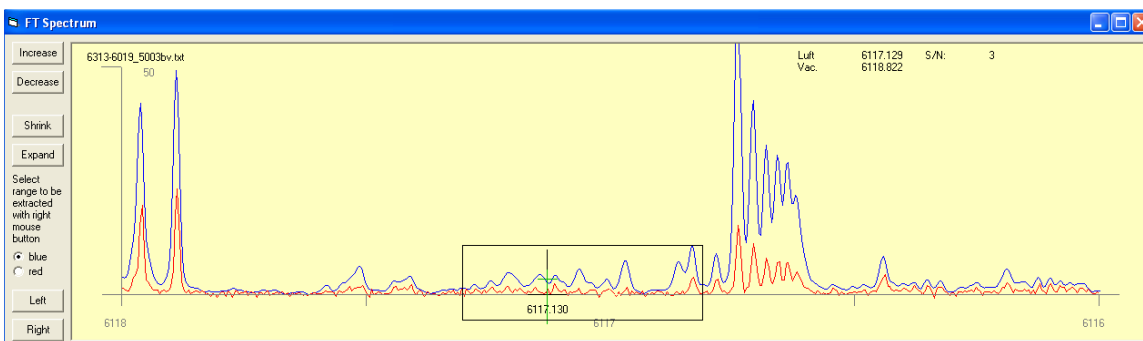
Figure 6.144: FT-Spectra of the line involving a transition from level triplet

Laser excitation with start wavelength 6117.26 Å was performed and as expected hyperfine structure was recorded with perturbed intensity distribution of hyperfine components (see figure 6.145). Wide splitting is seen with all three groups present. Same perturbed behaviour was seen on all previously observed fluorescence lines.
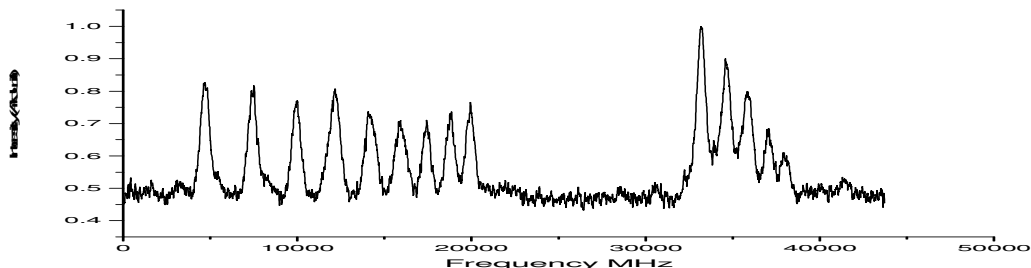
Figure 6.145: Perturbed intensity distribution of hyperfine components recorded with start wavelength 6117.26 Å

---

[*] Discovered by Shamim (04-09-2008) private communication

193

Using already known J and A values of the upper level and J and A values of levels in triplet, the recorded structure was simulated which gave a good agreement between predicted and experimentally observed hyperfine structure profile (see figure 6.146).
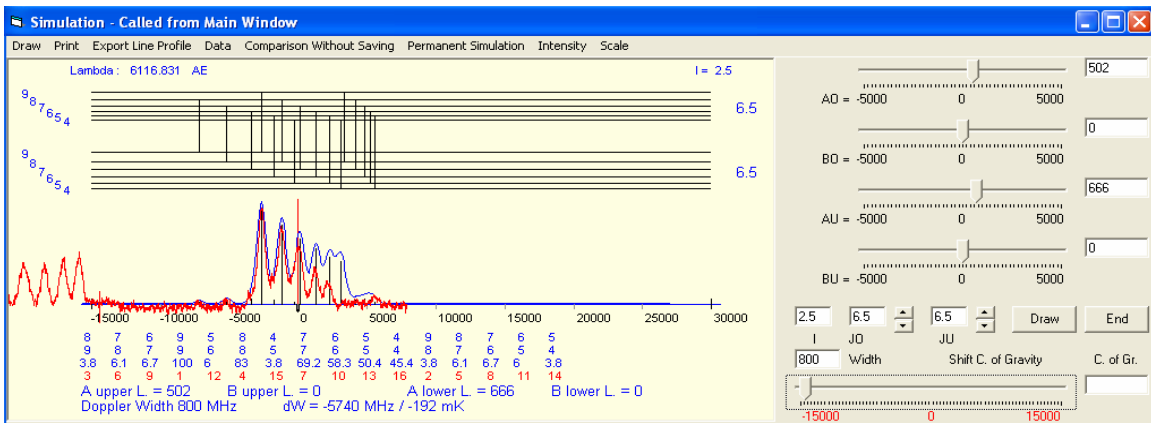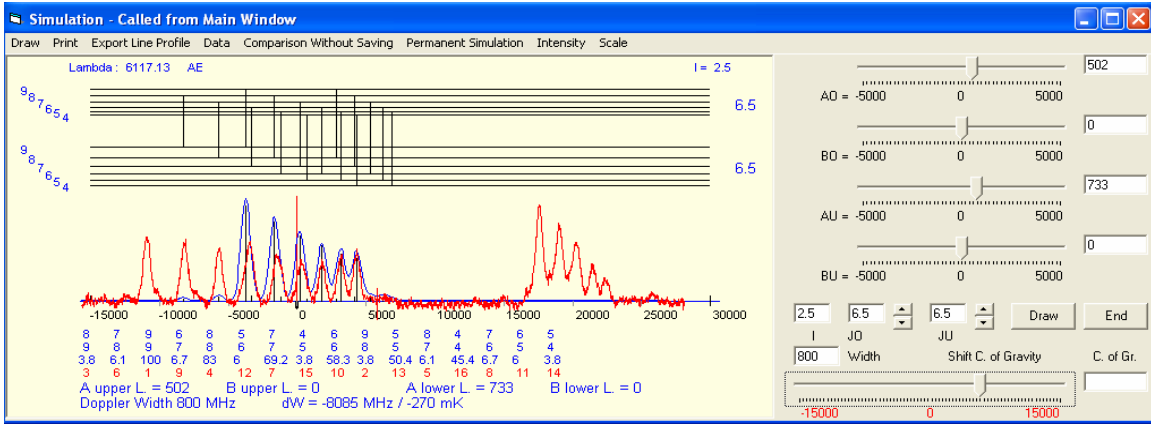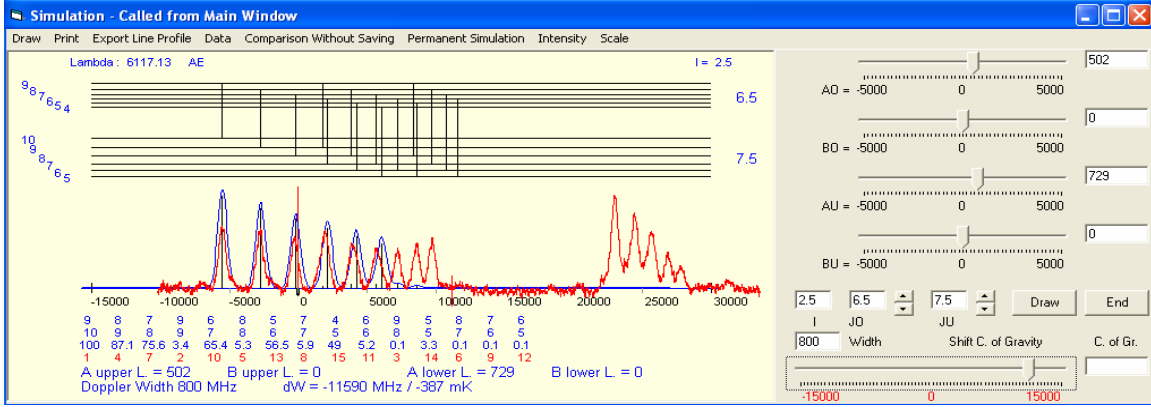
Figure 6.146: Simulation of the perturbed structure (red line profile) recorded with start wavelength 6117.26 Å

Simulations confirmed the presence of all three groups with transitions from all three levels of triplet to upper level. As usual the intensity distribution of hyperfine components is changed as compared to the normal predicted hyperfine patterns. Recorded structure is fitted using the known J and A values of upper level as being fixed and letting free the A values of lower triplet levels. Best fit is obtained (see figure 6.147) with A values of lower triplet levels nearly same as previously determined values (see table 6.29).
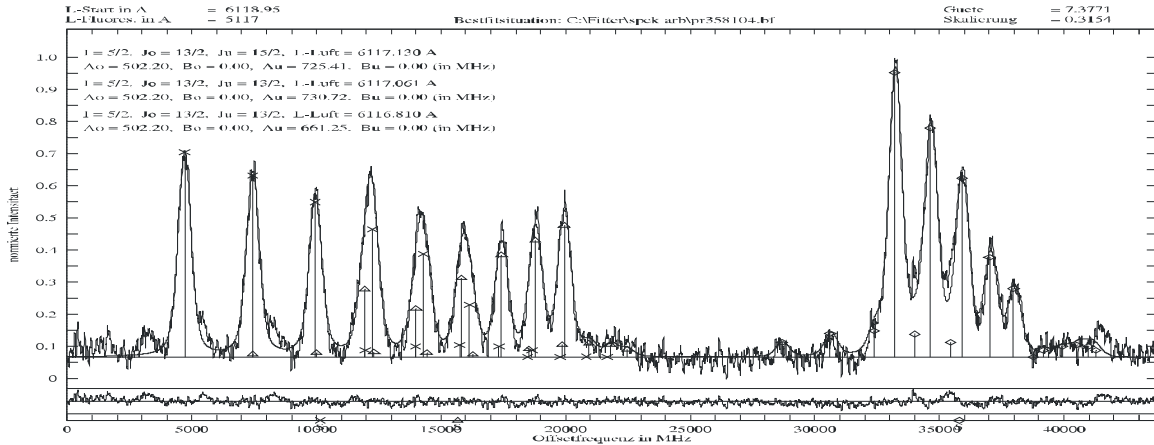
Figure 6.147: Best fit situation of the perturbed structure recorded with start wavelength 6117.26 Å

Since the wave number of the upper level is already known with good accuracy therefore the wave numbers of levels in triplet were calculated using center of gravity wave numbers obtained from the fit of the recorded structure and the wave number of upper level (see table 6.29). The level scheme with a comparison between experimentally recorded perturbed and simulated unperturbed hyperfine structure pattern is presented in figure 6.148.

Table 6.29: Improved values of wave numbers of levels in triplet, computed from the wave number of upper level 31535.107 cm^{-1}.

| cog λ_{air} (Å) | Lower Level | | | | Upper Level |
| | J_u | Parity | Energy (cm^{-1}) | A_u (MHz) | $J_o = 13/2$, Parity = e, $A_o = 502.20$ MHz |
					Energy (cm^{-1})
6117.130	15/2	o	15192.095	725.41	
6117.061	13/2	o	15191.911	730.72	31535.107
6116.810	13/2	o	15191.24	661.25	

31535.107 cm^{-1}, even, A = 502.20 MHz

$\Delta F = -1$ $\Delta F = 0$ $\Delta F = +1$ $\Delta F = -1$ $\Delta F = 0$ $\Delta F = +1$

13/2

30 GHz

13/2

15/2

13/2

15192.095 cm^{-1} odd

15191.911 cm^{-1} odd

A = 725.41 MHz

A = 730.72 MHz

15191.24 cm^{-1} odd

A = 661.25 MHz

Perturbed hfs

Simulated hfs

6117.130 Å 6117.061 Å

6116.810 Å
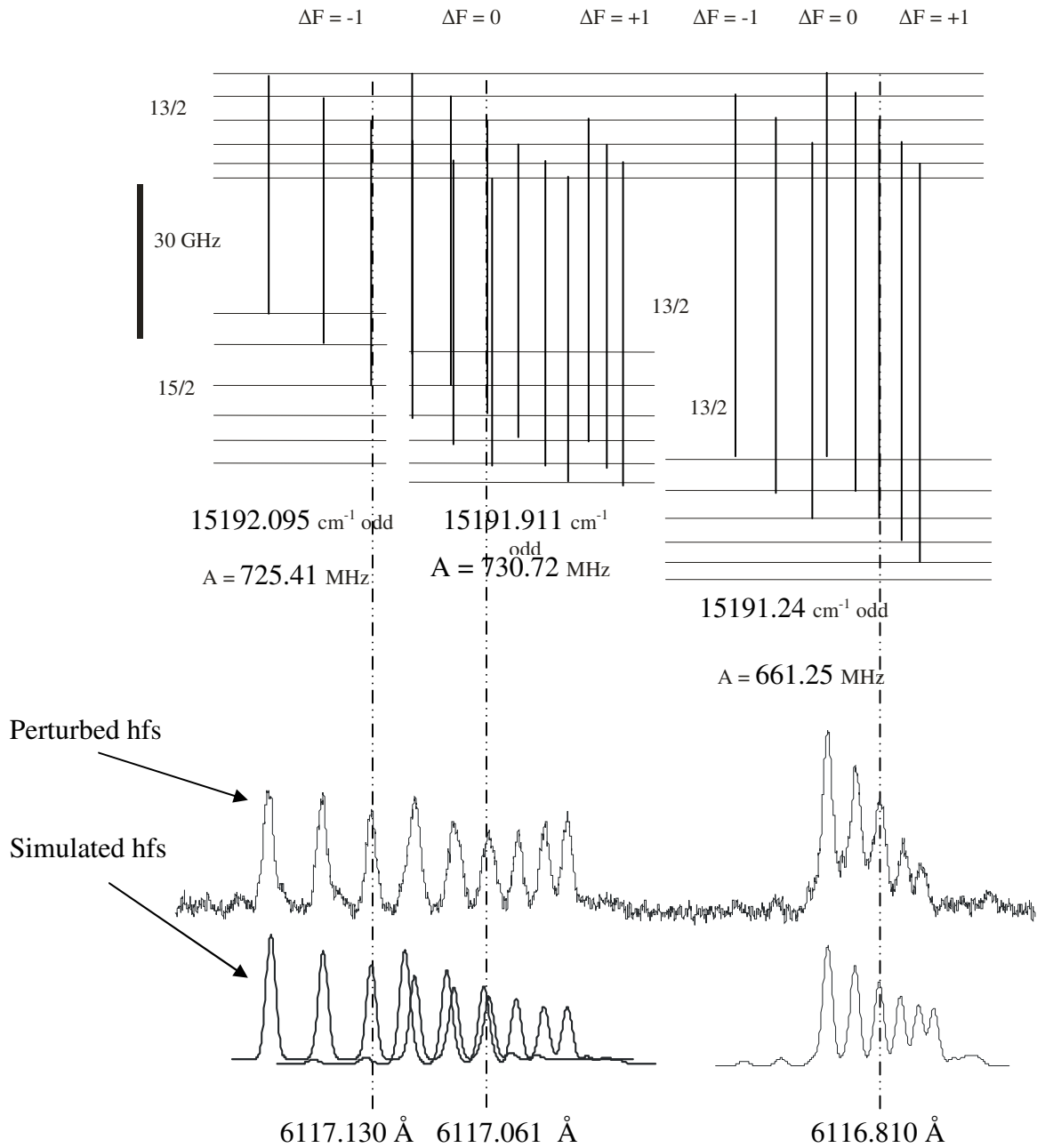
Figure 6.148: Level scheme for transition from triplet to upper level 31535.107 cm^{-1}, center-of-gravity positions marked by broken lines

196

6.20 Analysis

Up till now we have experimentally investigated 44 spectral lines in Pr I involving only transitions from level triplet to new and already known different upper levels with angular momentum values 11/2, 13/2, 15/2 or 17/2. These large number of investigations provide sufficient evidence regarding the reliability of assignment of values of angular momentum (15/2, 13/2 and 13/2), parity (odd) and the energy (15192.09 cm^{-1}, 15191.906 cm^{-1}, 15191.233 cm^{-1}) of the levels in triplet with center of gravity separations of 0.185 and 0.68 cm^{-1}. The positions of F-sublevels of the upper two fine structure levels in triplet are almost coincident except for F(15192.09) = 10 and F(15191.906) = 4. Theoretically this means that their wave functions overlap, resulting in a clearly noticeable (experimental observations) disturbance in the intensity distribution of hyperfine components for transitions from levels of triplet to various upper levels. A sketch of level scheme is shown in figure 6.149. Center of gravity of each level is marked and the energy spacing between successive F-sublevels is also shown.
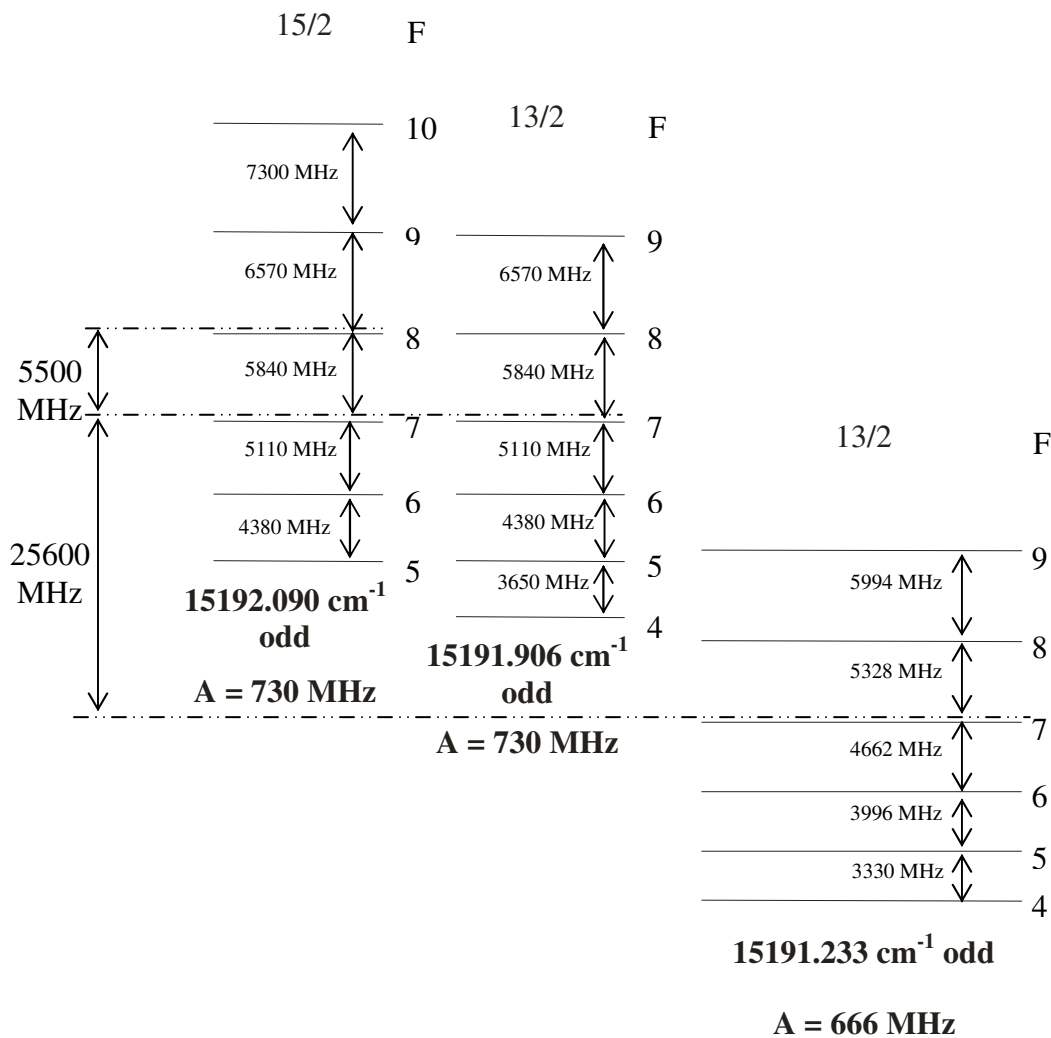
Figure 6.149: Energy level scheme for the levels in the triplet.

The key to the existence of three closely lying levels in triplet is the identification of transitions from these hyperfine levels.

Three separate sets of transitions are observed corresponding to transitions to upper levels with J_o = {15/2, 13/2}, {17/2} and {11/2}.

(a) In almost all the investigated transitions up till from levels of triplet to upper levels with angular momentum J_o = 13/2 and 15/2, all three groups of hyperfine structure with anomalous intensity distribution of hyperfine components are observed. There is one exception that is the excitation of line at 6166.95 Å, where only excitation from lower two levels of triplet to upper level is observed.

(b) For transitions to an upper level with J = 17/2 two groups of hyperfine structure are observed corresponding to transitions from upper most and lowest levels of triplet with no transition from the middle level as it is dipole forbidden. The first group of hyperfine structure corresponding to a transition from upper most level of triplet show almost normal intensity behavior whereas the other group corresponding to a transition from lowest level of triplet show large abnormal behaviour of the recorded intensity profile. Although the transition from lowest level (J = 13/2) of triplet to upper level (J = 17/2) is theoretically dipole forbidden but we argue that the angular momentum of the lowest level is an admixture of 15/2 and 13/2. In this case J is no longer a good quantum number and transitions are seen between F-sublevels. So F becomes a good quantum number. As an example see sections 6.6 and 6.7.

(c) For transitions to an upper level with J = 11/2 again two groups are observed now from lower two levels of triplet but no excitation from upper most level of triplet. Here again the intensity distribution in both groups show disturbed behavior. As an example see section 6.17.

The key to the existence of three levels in triplet lies in a proof that a transition from F_u = 10 of upper most level and F_u = 4 of middle level of triplet could be identified separately. A comparative analysis can be done for the component positions of three group of hyperfine structure (see table 6.30). For an adequate component to component comparison a transition is chosen from level triplet to an upper level with J either 15/2 or 13/2 having good signal-to-noise ratio and comparatively large hyperfine splitting. Level with energy 31729.933 cm^{-1} (see section 6.5) and J_o = 13/2 is used here for such a comparison. This level was discovered by laser excitation of the line at 5639.362 Å and was recorded on fluorescence wavelengths 3292 Å, 5065 Å, 5711 Å, 6044 Å. A second excitation for this upper level at the line 6045.22 Å reveal a hyperfine structure pattern with anomalous intensity distribution of hyperfine components on all previously observed fluorescence wavelengths. Simulation of the recorded anomalous hyperfine pattern with theoretically predicted transitions confirmed the excitation from level triplet. Figure 6.150 shows the recorded hyperfine structure with diagonal components marked by F-quantum numbers (F_o, F_u) for transitions from lower triplet to upper level. Using J_o = 13/2 of upper level and J_u = 15/2, 13/2, 13/2 for levels in triplet, the recorded structure was fitted using a multiline fit (figure 6.38).
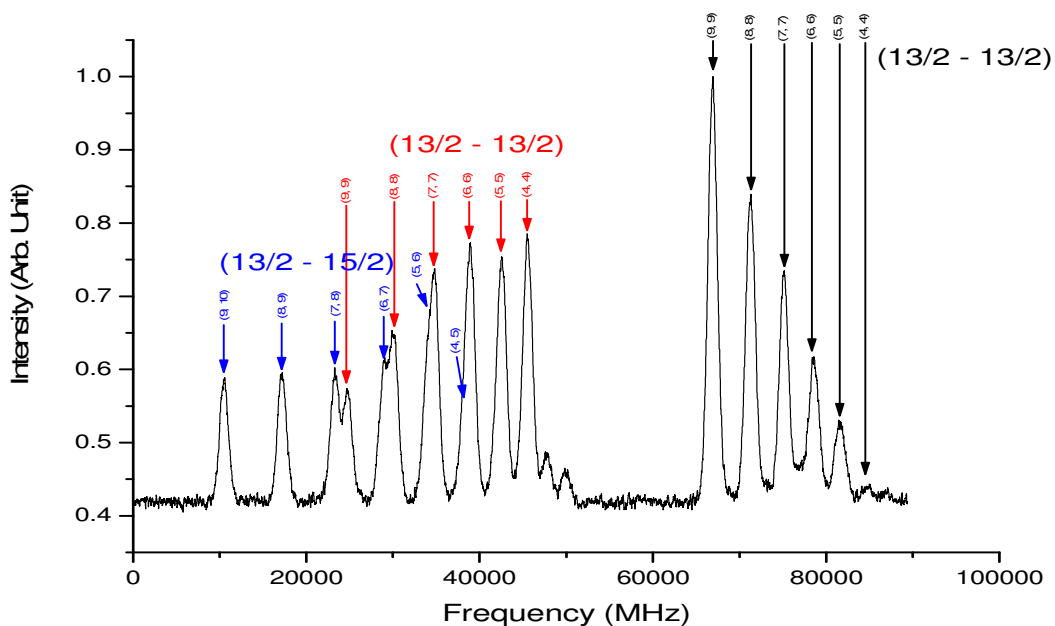
Figure 6.150: Anomalous intensity distribution of the line 6045.22 Å

Figure 6.151 shows the overlap of the predicted hyperfine structure (without perturbation) of the of the line at 6045.22 Å over its experimentally recorded perturbed hyperfine structure. Table 6.30 gives the hyperfine component positions (in MHz) calculated from multi-line fitting procedure, single component fit and calculations based on A_o, B_o, A_u, B_u of the upper level combining with the levels of triplet in the excitation of line at 6045.22 Å. For praseodymium usually value of B is taken as zero due to its small nuclear quadrupole moment.
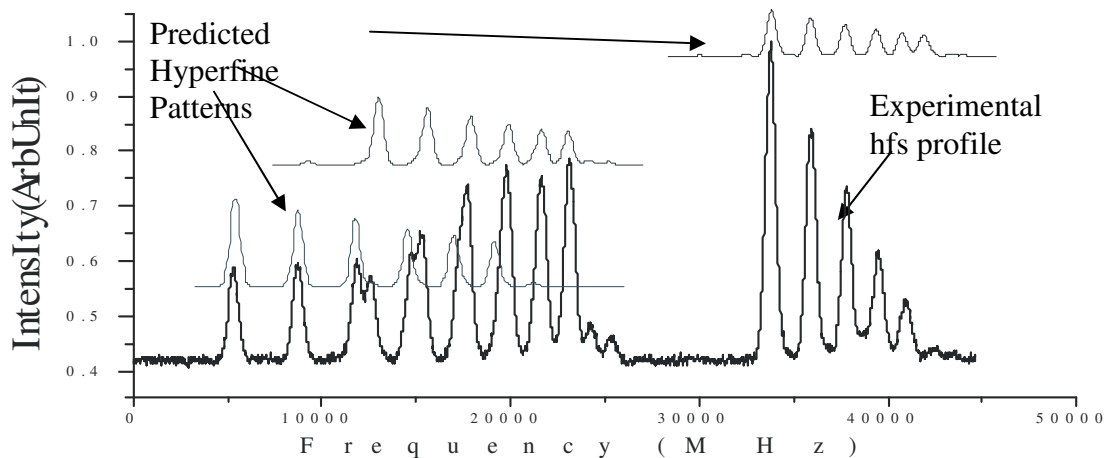
Figure 6.151: Theoretical line profiles overlapped on experimental hfs.

Table 6.30: Comparative measure of the hyperfine component positions of line 6045.22 Å (see figure 6.143).

F_o-F_u	$J_o = 13/2$ - $J_u = 15/2$, $A_o = 432.8$ MHz, $A_u = 731.23$ MHz Component Positions (MHz)			F_o-F_u	$J_o = 13/2$ - $J_u = 13/2$, $A_o = 432.8$ MHz, $A_u = 734.23$ MHz Component Positions (MHz)			$J_o = 13/2$ - $J_u = 13/2$, $A_o = 432.8$ MHz, $A_u = 668.88$ MHz Component Positions (MHz)		
	Multi line fit	Single comp* fit	Calc.[†]		Multi line fit	Single comp* fit	Calc.[†]	Multi line fit	Single comp* fit	Calc.[†]
9-10	5298.99	5314.15	5310.22	-	-	-	-	-	-	-
8-9	8730.66	8728.69	8733.84	8-9	8704.08		8756.55	29908.89		30218.49
7-8	11862.35	11866.00	11858.37	7-8	11856.97		11902.23	32473.62		32776.02
9-9	12617.76	-	12629.02	9-9	12591.18	12527.38	12651.73	33795.99	33794.15	34113.67
6-7	14694.07	14830.28	14683.83	6-7	14707.52		14746.49	34801.36		35097.48
8-8	15317.55		15320.76	8-8	15312.17	15247.05	15364.62	35928.82	35937.07	36238.41
5-6	17225.81		17210.20	5-6	17255.75		17289.31	36892.13		37182.85
7-7	17717.37		17713.41	7-7	17730.82	17618.02	17776.07	37824.66	37823.50	38127.06
9-8	19204.65		19215.94	9-8	19199.27		19259.80	39815.92		40133.59
4-5	19457.57		19437.49	4-5	19501.64		19530.70	38745.91		39032.14
6-6	19817.21		19806.99	6-6	19847.15	19753.44	19886.10	39483.53	39496.39	39779.64
8-7	21172.57		21175.80	8-7	21186.02		21238.46	41279.86		41589.45
5-5	21617.07		21601.48	5-5	21661.14	21623.53	21694.69	40905.41	40947.45	41196.13
7-6	22840.51		22836.57	7-6	22870.45		22915.68	42506.83		42809.22
6-5	24208.47		24198.27	6-5	24252.54		24291.48	43496.81		43792.92
-	-	-	-	4-4	23172.80	23139.79	23201.85	42090.32		42376.54
-	-	-	-	5-4	25332.30		25365.84	44249.82		44540.53

*Only diagonal component positions are measured
[†]Calculations based on A_o, B_o, A_u, B_u of the combining levels

Only small differences are seen between the component positions determined from the experimentally observed hyperfine structure and positions calculated based on the A_o, B_o, A_u, B_u of the combining levels. This gives sufficient proof of the existence of all three closely lying levels. In table 6.31 transitions discovered up till now with good S/N ratio from level triplet to different upper levels are tabulated. In each case energies of levels in triplet are determined using the energy of the upper level and center of gravity wave number of the excitation line producing anomalous intensity distribution of hyperfine components. Transitions from level triplet to upper levels with low S/N ratio are listed in table 6.32.

Table 6.31: Summary of level energies in triplet for transitions with good S/N ratio.
(In last column 'f' = fluorescence, '+' = strength of fluorescence)

File number	cog Excitation wavelength λ_{air} (Å)	Lower Triplet levels with odd parity (energy in cm^{-1}, hf constant in MHz)			Upper Level with fluorescence wavelengths λ_{air} (Å)
Pr312004	5686.14	15/2	15192.089	731.02	**13/2, e, 32773.833, 834**
	5686.08	13/2	15191.904	729.96	f5158 f3185 f4427 f4471 f4885 f5476 f5541 f5560
	5685.864	13/2	15191.236	663.94	f5952.02
Pr162026	5701.381	15/2	15192.1	729.20	**13/2, e, 32726.843, 571**
	5701.32	13/2	15191.911	731.34	f+5555 f5404 f5337
	5701.099	13/2	15191.231	667.34	f6050.93
Pr449004	5723.738	15/2	15192.07	732.50	**15/2, e, 32658.325, 531.13**
	5723.677	13/2	15191.885	734.83	f++5157 f++3353 f6118
	5723.454	13/2	15191.205	668.79	f5801.581
Pr337058	Forbidden				**11/2, e, 32631.828, 465**
	5732.400	13/2	15191.966	730.24	f+3200 f3800 f5693.13
	5732.179	13/2	15191.295	663.61	
Pr226006	Forbidden				**11/2, e, 32587.304, 485**
	5747.04	13/2	15191.867	730	f4702 f4855 f3204
	5746.815	13/2	15191.188	665	
Pr332007	5771.789	15/2	15192.104	729.21	**13/2, e, 32512.95, 596.14**
	5771.729	13/2	15191.924	735.09	f4872 f5121 f5397 f5465
	5771.503	13/2	15191.245	673.06	f5622 f5824.04
Pr014028 Pr264024	5780.509	15/2	15192.090	730	**15/2, e, 32486.80, 552.5**
	5780.46	13/2	15191.906	730	f6183.09 f5205 f4836
	5780.27	13/2	15191.233	666	f4820 f3372
Pr447049	5785.35	15/2	15192.078	729	**17/2, e, 32472.324, 491.14**
	Forbidden				f3558 f5209 f5516

	Observed but distored				f5656.95 f5855.48 f6459
Pr349019	5842.734	15/2	15192.072	734.04	**13/2, e, 32302.603, 568.77** f3393 f5896 f5783.953 f5701.948 f5688.736
	5842.673	13/2	15191.893	731.37	
	5842.444	13/2	15191.222	664.83	
Pr264014	5875.657	15/2	15192.117	730	**15/2, e, 32206.775, 552.5** f5281 f3406 f5876 f5948 f6291 f6572.22
	5875.595	13/2	15191.938	730	
	5875.36	13/2	15191.258	667.52	
Pr269039	5889.53	15/2	15192.095	732.01	**15/2, e, 32166.673, 510.18** f5293 f4899 f3411 f5502 f5747 f5308 f5662 f5374 f6309 f5962.23 f5746.48
	5889.46	13/2	15191.894	733	
	5889.24	13/2	15191.259	668.21	
Pr262039	5907.51	15/2	15192.19	730	**13/2, e, 32115.102, 595.62** f3415 f5847.36
	Not observed experimentally from middle level of triplet				
	5907.173	13/2	15191.221	668	
Pr395024	6034.782	15/2	15192.081	730.09	**13/2, e, 31758.102, 501** f6474.910 f7796.202 f+5059.05 f5374.51 f5426.72
	6034.715	13/2	15191.9	736.13	
	6034.470	13/2	15191.227	668.95	
Pr393007	6039.605	15/2	15192.080	731.960	**15/2, e, 31744.873, 696.54** f+6040 f6478 f5633 f+5414 f5800 f5947 f3460 f6116.09
	6039.537	13/2	15191.898	737.790	
	6039.289	13/2	15191.218	670.140	
Pr327039	6045.069	15/2	15192.106	731.88	**13/2, e, 31729.933, 432.8** f5065 f3292 f6044 f5639.362 f5711.509 f6429.62
	6045.002	13/2	15191.922	734.23	
	6044.757	13/2	15191.251	668.88	
Pr394053	6058.275	15/2	15192.087	730	**13/2, e, 31693.865,**

	Not observed experimentally from upper most triplet level			**498.22** f5075 f5892.867
	6057.958	13/2	15191.222	668	
Pr392006	6060.380	15/2	15192.09	734.900	**15/2, e, 31688.137, 737.28** f+3467 f5432 f6137.39 f6117.99
	6060.314	13/2	15191.91	741.800	
	6060.066	13/2	15191.235	670.066	
Pr391042	6077.016	15/2	15192.056	730.79	**13/2, e, 31642.946, 518.7** f+3304 f4919 f5090 f5329 f5364 f5530 f6076 f6136 f6568.20 f5835.14
	6076.948	13/2	15191.872	733.66	
	6076.700	13/2	15191.200	668.87	
Pr386023	6082.034	15/2	15192.11	729.01	**17/2, e, 31629.427, 563.08** f6151 f5350 f3669 f5990 f5940 f4865 f3735 f4270 f6159.59
	Forbidden				
	Observed but distorted				
Pr395003	6085.513	15/2	15192.062	733.22	**15/2, e, 31619.982, 521.53** f3474 f5452 f5538 f5785.509 f5672.50
	6085.445	13/2	15191.879	733.30	
	6085.196	13/2	15191.206	668.44	
Pr358104	6117.130	15/2	15192.095	725.41	**13/2, e, 31535.107, 502.20** f3315 f3486 f3683 f5068 f+5116 f+5393 f5872.132 f5962 f6053 f6116 f6195.6 f5702.019 f5774.78
	6117.061	13/2	15191.911	730.72	
	6116.810	13/2	15191.24	661.25	
Pr356059	6136.685	15/2	15192.097	727.80	**13/2, e, 31483.15, 603.3** f5716.9 f6071.8 f5890.14 f6136
	6136.570	13/2	15191.911	731.63	
	6136.316	13/2	15191.237	672.91	
Pr355084	6153.91	15/2	15192.084	731.18	**17/2, e, 31437.408, 486.463** f+6233.34 f+6061.30
	Forbidden				

	Observed but distorted				f+5997 f+5405 f3695 f6823 f6930 f6007
Pr020004 Pr369059	Not observed experimentally from upper most triplet level				**15/2, e, 31402.87, 630** f5918.26 f6167
	6166.95	13/2	15191.906	730	
	6166.693	13/2	15191.233	666	
Pr422049	6340.32	15/2	15192.064	729	**15/2, e, 30959.778, 573.24** f5747 f6077.50 f6242 f6272 f6425 f6533
	6340.25	13/2	15191.889	730	
	6339.976	13/2	15191.209	668	
Pr431044	6385.24	15/2	15192.085	730	**17/2, e, 30848.875, 507.1** f5238.361 f5583.99 f5690.427 f5784.308
	Forbidden				
	Observed but distorted				
Pr438028	6394.269	15/2	15192.094	729.91	**17/2, e, 30826.776, 580** f5791.716 f+5244.453 f5590.913 f5608.66 f6063.889 f6226.028
	Forbidden				
	Observed but distorted				

Table 6.32: List of transitions from level triplet to upper level with weak S/N ratio.

Registration number	cog excitation wavelength λ_{air} (Å)	Upper Level with fluorescence wavelengths λ_{air} (Å)
Pr209039	5802.73	15/2, e, 32420.593, 688 f+6481 f+5224 6392
Pr264005	5830.10	15/2, e, 32336.86, 475 f5847.842 f5747.842 f5772.491 f5690.815 f5884
Pr264021	5930.22	13/2, e, 32049.99, 521.29 f4985 f3425 f5785.285 f5771.71 f6583.66
Pr327010	6019.97	13/2, e, 31798.949, 556.51 f4985 f5414 f5484 f5617.48 f5957 f6095
Pr336059	5794.43	13/2, e, 32445.251, 666.80 f4889 f5656 f5847.09 f5864.80 f5954 f6071 f6155
Pr366027	6187.48	15/2, e, 31349.288, 609.85 f5761.03 f6122 f6269
Pr393009	5976.56	13/2, e, 31918.637, 519 f5018.288 f5380 f5446 5650
Pr431059	6296.08	15/2, e, 31070.645, 551(2) F3542 f3747 f5191 f+5533 f5855 f6036.83 f6227.83 f+6380 f+6485
Pr457018	5740.27	13/2, e, 32608.084, 628.61 f+5811 f5896 f5590 f5100 f3360 f6085.51 f5896.74 f5809.30
Pr440018	6585.75	13/2, e, 30371.978, 612.41 f+5008 f5388 f6107 f6191 f6303 f6584 f 5876.77 f6191.87

Pr440032	6642.30	15/2, e, 30242.931, 460.63 f+3649 f5122 f+5913 f5991 f+6153 f6285 f6457 f5798.548 f5994.459
Pr440040	6624.52	15/2, e, 30283.139, 480 f+5399 f5899 f6517.403 f6444.179
Pr468010	6390.98	13/2 , e, 30834.815, 667.86 f3393 f4899 f5255 f5567 f5938 f6020 f6125 f6207 f6390 f6477 f5713.05 f5939.24
Pr475020	5682.86	15/2, e, 32784.03, 501.11 f3340 f+6021 f5473 f6338.87 f5836.21

6.21 Conclusion

It can be concluded from the above analysis that three very closely lying fine structure levels exist in the level triplet with the upper two having their center of gravity very close to each other. For the upper two levels of triplet, their F-sublevels (with the exception of F(15192.09) = 10 and F(15191.9) = 4) have energies (see figure 6.149) which are nearly coincident within a few MHz and therefore are strongly interacting. Furthermore the upper most and lowest levels of triplet have their center of gravity positions which are further away from each other and from the experimental observations it comes out that these two levels strongly mix with each other. Angular momentum J for these two levels is not a good quantum number and lowest level of triplet assumes an angular momentum character which is a mixture 13/2 and 15/2. So for transitions from level triplet to an upper level with J = 17/2, the transition from lowest level becomes allowed even though $\Delta J = +2$, which is very rare. Based on these experimental findings, it can be concluded that the wave functions of these levels overlap resulting in a change in transition probabilities of these levels to different upper level. This means that intensity distribution of hyperfine components does not follow the normal intensity rules. As is evident in all the experimentally recorded transitions from level triplet to different upper levels where large distortion in the intensity distribution of hyperfine structure components is observed. This further suggests that these triplet levels are one group of very strongly interacting levels in the spectra of praseodymium. Energies of levels in triplet determined from excitations to different upper levels are averaged and for each excitation hyperfine constants are also determined, which are then given here in a reliable range in MHz. These are given as follows:

15/2, o, 15192.091 cm^{-1}, 730(3) MHz
13/2, o, 15191.904 cm^{-1}, 730(3) MHz
13/2, o, 15191.230 cm^{-1}, 668(4) MHz

6.22 Outlook

The spectral region so far explored for the investigation of transitions from level triplet to upper level lies between 5600 Å to 6500 Å with the identification of transitions from level triplet to upper level having J-values 11/2, 13/2, 15/2 and 17/2. The results can further be consolidated by investigating the transitions from level triplet to other new or known upper levels. It would be further beneficial to measure hyperfine level splitting by means of the direct transition in the radio frequency range. This would lead to a better estimate of separation between hyperfine levels in level triplet. It is also interesting to search for transitions from very low lying even level (as lower level) to level triplet (as upper set of levels) and see whether perturbation still appear.

Praseodymium has a very high level density which is often manifested while recording hyperfine structure in blend situations. Therefore it would be safe to say that there might be other closely lying systems of levels having similar perturbing behaviour.

Chapter 7
Experimental Results and Discussion (Part II)

In past fine and hyperfine structure investigation of praseodymium has been done already in great detail. One of the major contributors to these investigations is the work of A. Ginibre [12, 16, 20, 21] who mainly determined the energies and calculated hyperfine interaction constants of energy levels involved in excitation of lines without using the technique of laser induced fluorescence. Other contributions are from Böklen et al. [128], Reddy et al. [15], and Childs et al. [129]. The group of Prof. G. H. Guthöhrlein in Hamburg was also involved in the investigation of the spectra of praseodymium using laser spectroscopy and classified a large number of lines using already known and new energy levels.

Nevertheless, lot of work is still to be done. Large numbers of unclassified lines can be classified using already known levels. Further, laser induced fluorescence investigation of unclassified lines is required for proper identification of levels involved in the transition. Some of the lines seen in FT-Spectra are very weak and the upper levels involved have very low transition probability. In such cases laser excitation is more beneficial compared to emission spectra. Fluorescence information obtained as a result of laser excitation of an upper level also enables us to identify the fluorescence lower levels. Furthermore, large numbers of lines were never experimentally investigated and could result in the discovery of new energy levels. Experimental investigations can be categorized as:

i.   Discovery of new Pr-I and Pr-II energy levels in even and odd configurations by laser excitation.
ii.   Classification of line using known or unknown levels via laser excitation.
iii. Classification of line by position and shape of the hyperfine pattern.

A high resolution Fourier Transform Spectra from UV to Far infrared for praseodymium is available in traces. High resolution FT-Spectra are quite convenient to investigate the spectral lines of an element. FT-Spectra are useful in the determination of classification of spectral lines and the determination of transitions. It can also be used to determine or to increase the accuracy of hyperfine structure constant. Most importantly, one can use it for searching possible new lines and levels.

Generally investigation of a spectral line starts with first trying to classify the line of interest with already known transitions listed in classification program. If the line could not be classified with any of the known transitions then laser excitation of the line is needed to be performed. Initially the laser wavelength is precisely tuned to the highest hyperfine component of the line to be investigated in the FT-Spectra and then we search for fluorescence wavelengths from the excited level. The hyperfine structure is recorded on all observed fluorescence lines and for fitting purpose the fluorescence line with strongest LIF signal and good S/N ratio is recorded three times. Using the results of fitting process and fluorescence information the transition can then be identified relatively easy if one of the combining levels is already known. Alternatively, if the

transition can not be explained then it is possible that both the combining levels for the said transition are unknown. Then other methods for determination and identification are used. In case the transition is identified the level (upper/lower) energy is determined by adding/subtraction the center of gravity wave number of the excitation line to/from lower/upper level. If a new level is involved in the excitation of a line then in most cases it is the upper level of transition, although during this work new lower level have also been discovered. The level then is introduced in classification program which generates a transition list to all possible lower/upper levels. For confirming the existence and corrections of the level parameters, further excitations are performed for transitions involving the newly found level and another known level.

7.1 Interpretation of Experimental Data: Spacing and Intensities within the Hyperfine Multiplet

Hyperfine spectra of praseodymium in particular and in general the spectra of other elements show in most cases a regular decrease of spacing and intensities with in the hyperfine multiplets. This can be interpreted as a combination between two levels with one having a larger width of hyperfine splitting compared to the other and this stems from the fact that the magnitudes of hyperfine interaction A constants in such cases differ appreciably. In other situations the magnitudes of hyperfine constants are almost comparable which results in an appearance of closely spaced hyperfine diagonal components forming a single peak. All such observations can be explained using interval rules (equation 3.19) and intensity rules. The intensity rule [97] can be stated as "within a hf multiplet, the ratio of the sums of the intensities of all transitions from two states with quantum numbers F and F′ are in the ratio of their statistical weights $(2F +1) : (2F′ + 1)$".

Another very interesting aspect of experimental observations is the wideness of the hyperfine structure i.e. in a large number of situations a very wide hyperfine structure is observed. Classically this can be explained for an atom with two valence electrons in which one is in penetrating s orbit and the other is in a non-penetrating d orbit. For s-orbit electron has a greater opportunity of strengthening the coupling between the resultant electronic angular momentum J and nuclear spin I. Furthermore, for greater coupling not only the s-orbit must be deeply penetrating but it should be tightly bound meaning that it spends more time near the nucleus. As hyperfine interaction A constant is a measure of splitting so the arguments in preceding lines means larger value of A constant. Not all wide hfs patterns arise from the deeply penetrating orbital configurations having tightly bound s electron. In other situations one of the p, d or f-electrons is tightly bound which lie deep in the energy level diagram and therefore contribute equally to the coupling of J and I.

In a number of situations it is observed that intensities of the recorded diagonal hyperfine components appear to deviate from intensity rules. In a severe case it is observed that all the diagonal and off-diagonal components are of equal intensity, a miss-leading behavior in a sense that one can miss-interpret it as if the intensity of off-diagonal components has increased. This apparent deviation can be explained in terms of nonlinear absorption behaviour of laser light.

At sufficiently low incident intensity the absorption follows Beer's law of linear absorption, viz.

$$I = I_0 \exp(-\alpha z) \qquad\qquad 7.1$$

$$\text{with } \alpha = \sigma_{ik}\, \Delta N \rho$$

where I_0 is the incident intensity, $\sigma_{ik}(\nu)$ is the absorption cross-section per atom as a function of light frequency $\nu = \omega/2\pi$, $\Delta N = [N_i - (g_i / g_k) N_k]$ is the difference of population densities of states with population N_i and N_k, z is the absorption length, g_i and g_k are the statistical weights of states $|i\rangle$ and $|k\rangle$, $\rho_\nu(\nu) = I_\nu / c$ [W s^2 / m^3] is the spectral energy density of incident light and I_ν [Ws/m^2] is the spectral intensity. For a two level system the fluorescence intensity I_{fl} from the upper level is proportional to the absorbed power therefore the plot between fluorescence intensity I_{fl} and incident laser intensity I_L is linear.

The deviation from linearity occurs as the intensity of incident radiation increases, the population N_i in lower absorbing level $|i\rangle$ decreases and rate of absorption becomes faster than the relaxation processes refilling the level $|i\rangle$. Therefore the fluorescence curve deviates from straight curve until it reaches a constant saturation value. In this situation ΔN decreases and the absorption coefficient α becomes a function of incident light intensity I_0. Because of the decreasing population difference the absorption decreases non-linearly with the increasing incident intensity and so the depopulation of level $|i\rangle$ by absorption of laser photons becomes a noticeable fraction of the repopulation rate resulting in a decrease of population N_i. Now since absorbed power is measured via laser induced fluorescence (LIF) therefore the laser induced fluorescence intensity increases non-linearly with the incident laser intensity.

7.2 Discovery of New Pr-I and Pr-II Energy Levels in Even and Odd Configurations

The nucleus of praseodymium contains 59 protons and 82 neutrons i.e. it is an odd-even nucleus. The spin and magnetic moment of the nucleus are determined by the last unpaired nuclear particle. In case of praseodymium, it is the last unpaired proton which determines the spin and magnetic moment of praseodymium nucleus. The nuclear spin quantum number I is 5/2 and the magnetic moment is $\mu_I / \mu_N = 4.136$. Due to almost spherical charge distribution in the nucleus of praseodymium its quadrupole moment is small i.e. Q = -0.024 b [106].

The electronic ground state configuration of praseodymium is [Xe] $4f^3\, 6s^2$ and ground state is $^4I^o_{9/2}$. s-orbital electrons have large probability density near the nucleus which means that their wave functions have a strong penetration into the core comprising of nucleus and electrons in completely filled shells. Therefore the two s-orbital electrons in praseodymium couple strongly with the core and contribute appreciably to the hyperfine structure splitting of fine structure levels.

Praseodymium has a very high line density i.e. on the average 5 to 10 lines per Å and correspondingly the number of energy levels is also very high. Our data base of spectral lines contains around 23000 lines mainly of Pr I and Pr II and some of Ar I and Ar II. Our data base of levels contain 1000 even parity and 1400 odd parity Pr I levels and 200 even parity and 115 odd parity Pr II levels. Due to the densely populated line spectra blend situations are more frequently observed in the spectra of praseodymium as compared to the spectra of other elements, for example Tantalum. How numerous the spectral lines in praseodymium are, can be judged by the fact that quite often one observes LIF signal from two or more distinct levels at a specific excitation wavelength. This happened in situations where two very closely spaced lines involving different pairs of levels are excited simultaneously. Also an excitation of a single upper level from two closely lying lower levels lying in the same scan range of laser is possible. This can be attributed to the fact that praseodymium in most of the electronic configurations has a core of two or three 4f-electrons resulting in a large number of excited levels.

Since nuclear spin I of praseodymium is 5/2, therefore due to the interaction between electronic and nuclear magnetic moments fine structure levels are splitted into (2I + 1) or (2J + 1) hyperfine levels (for J > I or J < I, respectively). The transition between hyperfine levels of two fine structure levels results in 6 (J > I) diagonal hyperfine components with a number of non-diagonal components which depend on ΔJ. Each hyperfine component has a Doppler profile which can be described by Gaussian function and which arises from the plasma conditions within the hollow cathode discharge.

During the course of this dissertation more than 2000 spectral lines in Praseodymium were investigated using laser induced fluorescence spectroscopy. The spectral range covered is between wavelengths 5000 Å (Coumarin dye) to around 6800 Å (DCM dye). Majority of the investigated lines belong to the transition between atomic levels but some belong to transitions involving ionic levels. In large number of the investigated transitions an upper level is unknown and only in few cases lower or both lower and upper levels were found to be unknown. These investigations led to the discovery of more than 300 new previously unknown energy levels, both in even and odd configurations. Angular momentum quantum number of these newly discovered atomic energy levels range from 1/2 to 21/2. Level energies are corrected at various observed fluorescence lines using FT-Spectra. Furthermore the existence of the new level and its energy is confirmed by more than one excitation. Generally the magnetic hyperfine structure constant "A" can be positive or negative which give rise to normal or inverted hyperfine multiplets. In case of praseodymium value of constant A is mostly positive. Due to small value of quadrupole moment Q for praseodymium, the value of quadrupole constant "B" in most cases is taken to be equal to zero. In all tables the "-" in the column for B implies B = 0. All wavelengths, excitation and fluorescence are measured in air. In the following sections some of the newly discovered energy levels of Pr-I and Pr-II are discussed. A complete list of all the newly discovered levels in Pr-I and Pr-II are given in Tables 7.12, 7.13, 7.14 and 7.15.

7.2.1 Discovery of $28667.334^{o}_{21/2}$ level via Laser Excitation of Line 5707.62 Å

An unclassified line at 5707.62 is investigated. FT-Spectra of the investigated line show clearly resolved hyperfine structure with relative intensity of 126 (see figure 7.1). From the shape and position of hyperfine components, the line could not be classified using any of the known transitions suggested by the classification program.
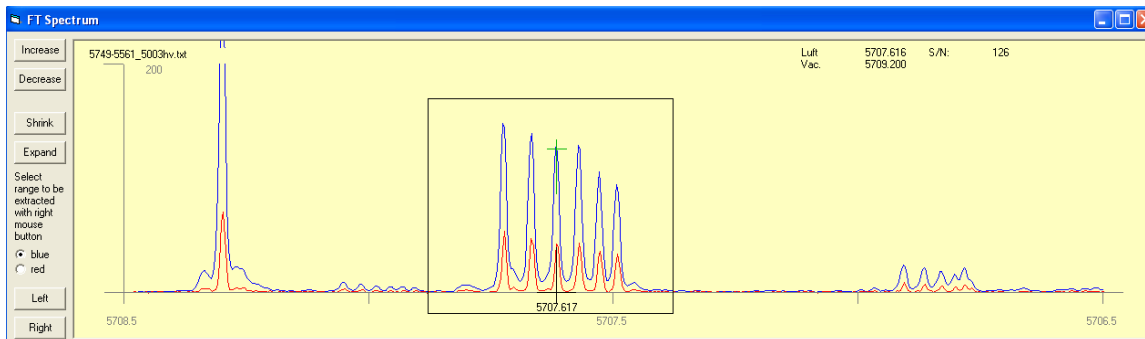
Figure 7.1: FT-Spectra of the line at 5707.62 Å

At the excitation wavelength 5707.62 Å, LIF signal is observed on fluorescence wavelengths 6247 Å, 6647 Å, 6357 Å, 5986 Å which is then recorded by scanning the laser frequency. The hyperfine structure of the line has a good S/N ratio with a wide separation between diagonal hyperfine components (see figure 7.2) as seen in FT-Spectra. A Similar hyperfine pattern is seen on all observed fluorescence lines with widely separated hyperfine components having a total width of approximately 21 GHz.
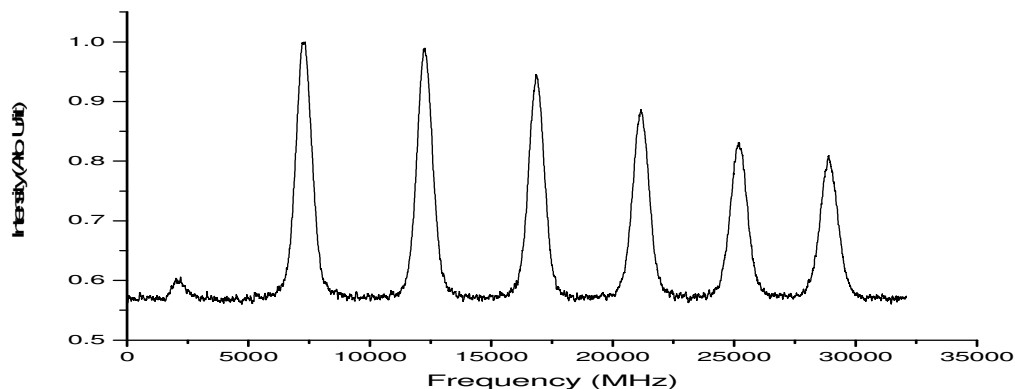
Figure 7.2: Laser excitation of line at 5707.62 Å showing widely split hyperfine structure.

The separation between diagonal hyperfine components is almost the same or decreases very slowly towards shorter wavelength and relative intensities of diagonal and off-diagonal components suggest a transition involving high angular momentum values of lower and upper level. Also one of the off-diagonal component appears on the longer wavelength side and intensities of the diagonal components degraded towards shorter

wavelength side indicating a transition with an angular momentum change of +1 and A_u > A_o (Assuming both Au and Ao positive, as is most times fulfilled for Pr Levels).

The recorded structure is fitted with angular momentum values J_o = 21/2 and J_u = 19/2. The best fit is obtained at A_o = 409.82 MHz and A_u = 877.69 MHz with quality factor of 19 (see figure 7.3). Assuming a known lower level involved in the transition, a search in the classification program is initiated for a lower level having reliable J- and A-values. A lower level with comparable A value is 11151.49 cm^{-1}, A = 876.1(3) MHz, B = -31(12) MHz, parity even. The hyperfine structure is again fitted with A = 876.1(3) MHz, B = -31(12) MHz of lower level being fixed. The energy of the upper level is determined by adding the wave number of the excitation line, 17515.586 cm^{-1}, to the wave number of lower level, 11151.49 cm^{-1}. The new upper level determined is **28667.067 cm^{-1}, J = 21/2, odd parity, A = 407.73 MHz, B = -15.56 MHz.** After introducing the level into our level data base, the classification program explained two out of four observed fluorescence lines. In order to check the authenticity of measurements and subsequent confirmation of the upper level, there is a need to perform a second excitation to this new upper level from some other lower level, conveniently from one of the lower levels of the fluorescence lines. Existence of upper level is guaranteed only if the resulting hyperfine structure is comparable to the predicted hyperfine pattern (calculated using the constants of the lower level and the new upper level) and to lines in the FT-Spectra with regard to wavelength and hyperfine pattern.
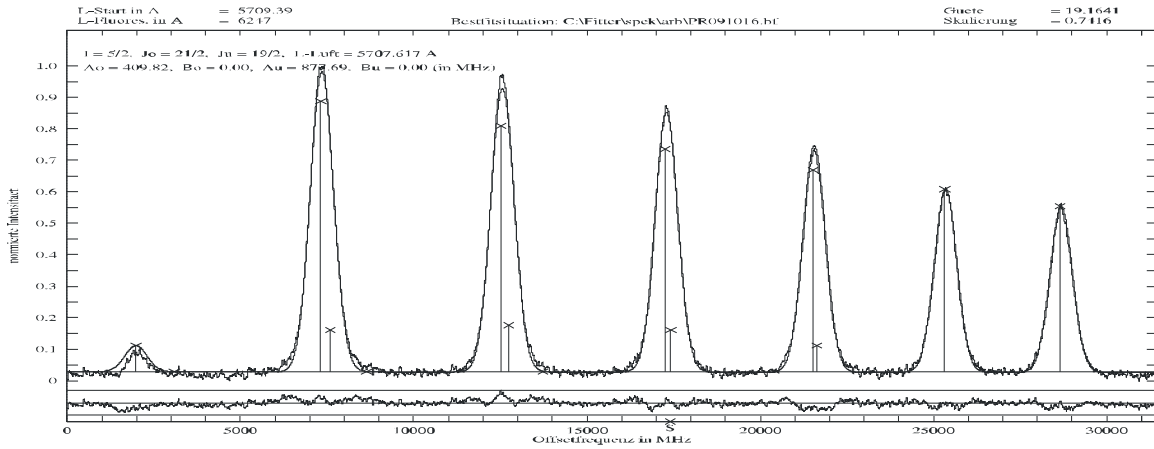
Figure 7.3: Best fit situation of the recorded hyperfine structure of the line at 5707.62 Å

A second excitation to the upper level is performed at 6247.39 Å and a hyperfine structure with good S/N ratio was recorded at the fluorescence line 5707 Å (see figure 7.4). A transition in which ΔJ = 0, i.e. J_o = 21/2 – J_u = 21/2.

Although in FT-Spectra the hyperfine structure of the line is not resolved and the transition appears in a blend situation, in contrary the LIF signal has good S/N ratio and the recorded structure is in good agreement in terms of component positions and their separation with the predicted hyperfine pattern (see figure 7.5). Furthermore, the same pattern is recorded on other previously observed fluorescence lines. This confirms the existence and energy of the newly found level.

213
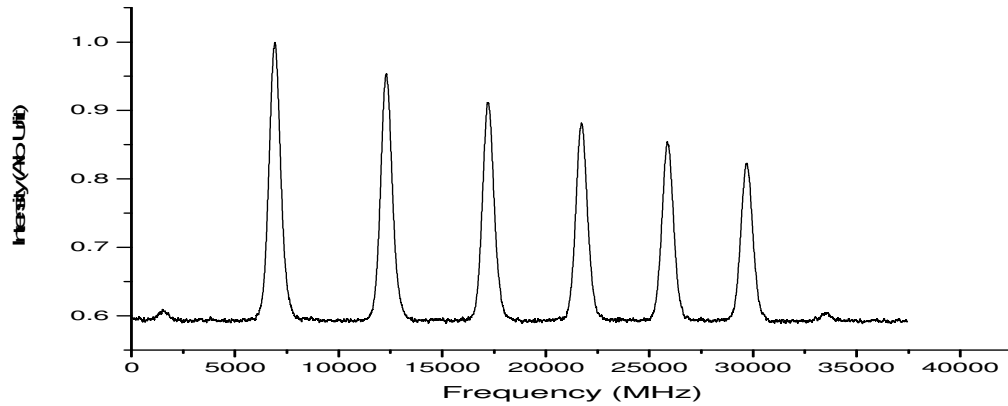
Figure 7.4: Hyperfine structure of the line at 6247.39Å with widely separated hyperfine components
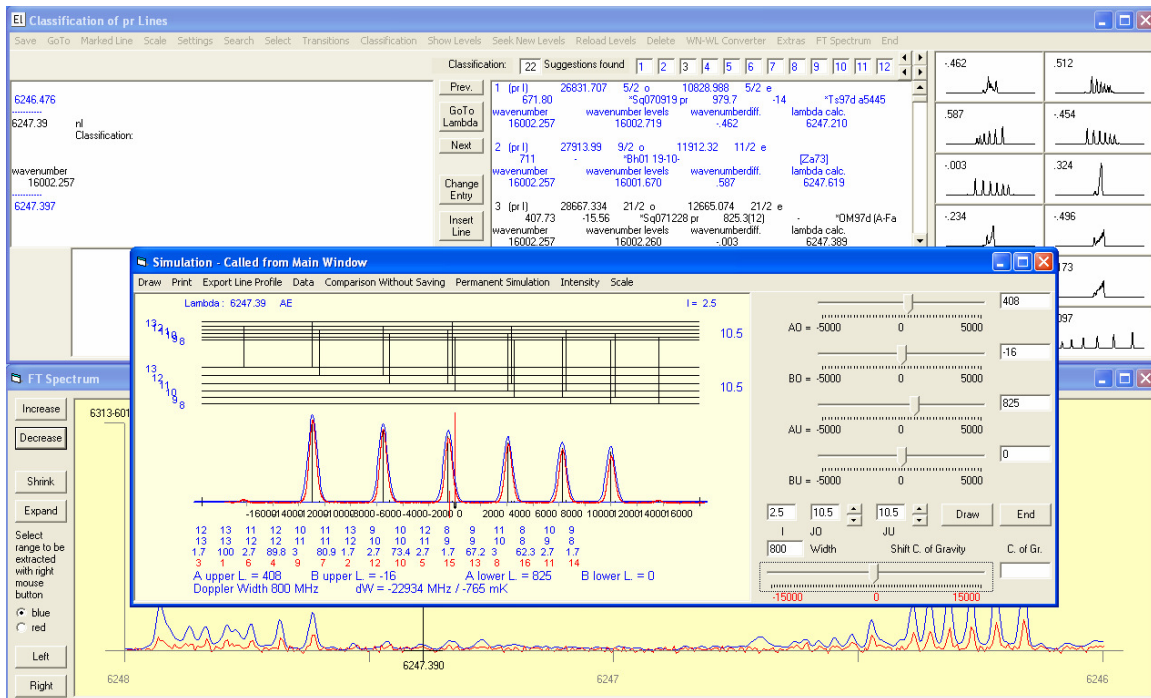
Figure 7.5: Simulation of recorded line profile with predicted hyperfine pattern of line at 6247.39 Å

In order to further consolidate the newly found level, another excitation is performed at 6646.94 Å to the newly found upper level as shown in figure 7.6. This time a transition with $\Delta J = +1$ is observed. Similar to the previous excitation FT-Spectra does not show clearly the hyperfine structure of the line but again the component positions and their separation are in good agreement with the prediction. Both these lines are now classified using the new upper level. The new level explained further two of the fluorescence lines as shown in level scheme figure 7.7. Table 7.1 lists all lower levels combining with the newly found upper level.

A weak or completely non-appearance of hyperfine pattern of this or any other line in FT-spectra, but having a very strong LIF signal, can be explained as follows. The intensity of a line in FT-Spectrum is determined by the population of the upper level of the transition and the spontaneous transition probability, i.e. FT-Spectrum is an emission spectrum. If an upper level has a low spontaneous transition probability and is weakly populated the line intensity is smaller than the S/N ratio of the FT-Spectra. The laser-induced increase of the population of the upper level is proportional to the induced transition probability times the energy density of the exciting light times the population of the lower level. Since the spectral density of laser light is quite high, the LIF signal can be recorded with comparatively better S/N ratio.
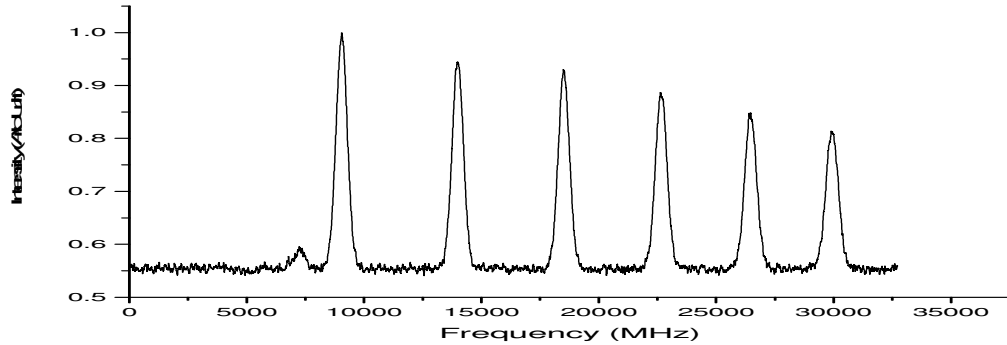
Figure 7.6: Hyperfine structure of the recorded line at 6646.94 Å

Table 7.1: Fluorescence lines explained by the new Pr I level 28667.067 cm^{-1}, J = 21/2, odd parity, A = 407.73 MHz, B = -15.56 MHz

Fluorescence Wavelength λ_{air} (Å)	Lower level				
	Energy (cm^{-1})	J	Parity	A (MHz)	B (MHz)
5707.62	11151.49	19/2	e	876.1(3)	-31(12)
6247.39	12665.074	21/2	e	825.3(12)	-
6646.94	13626.72	19/2	e	863.32	-
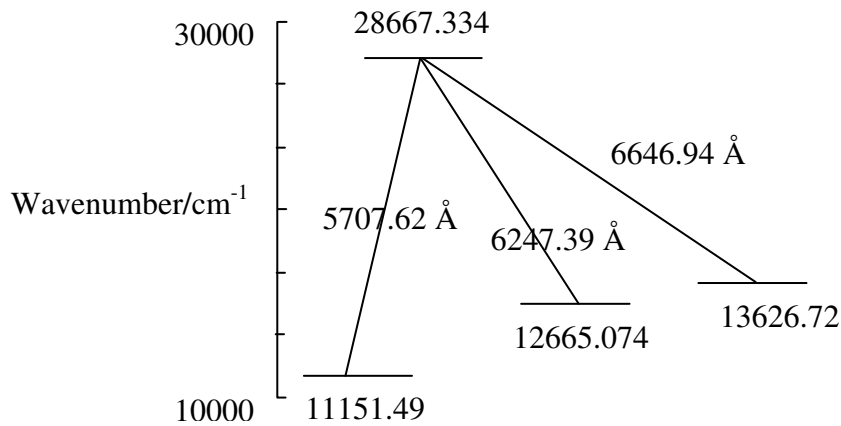
Figure 7.7: Level scheme for the excitation of upper level 28667.067 cm^{-1}

7.2.2 Discovery of $29541.534^{o}_{19/2}$ level via Laser Excitation of Line 5607.86 Å

The line in FT-Spectra at 5607.86 Å was also not classified and has a good S/N ratio with a relative intensity of 34 (see figure 7.8). The line could not be classified using any of the suggestions calculated by the classification program. Laser excitation of the line resulted in a hyperfine structure with widely separated hyperfine components as shown in figure 7.9.
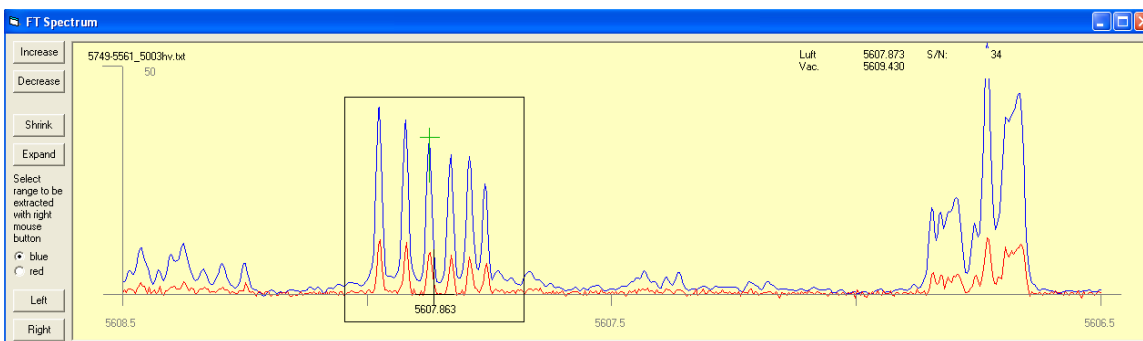
Figure 7.8: FT-Spectra of the line at 5607.863 Å

LIF signal (see figure 7.9) at excitation wavelength 5607.863 Å is observed on fluorescence wavelengths viz. 5949.01 Å, 5923.76 Å 5258 Å, 5435 Å, 6281 Å. Signal is then recorded by scanning the laser frequency on all observed fluorescence wavelengths. Again the diagonal hyperfine components are widely separated and with a gradual decrease of spacing and relative intensities towards higher frequency, which suggest a transition with high angular momenta.
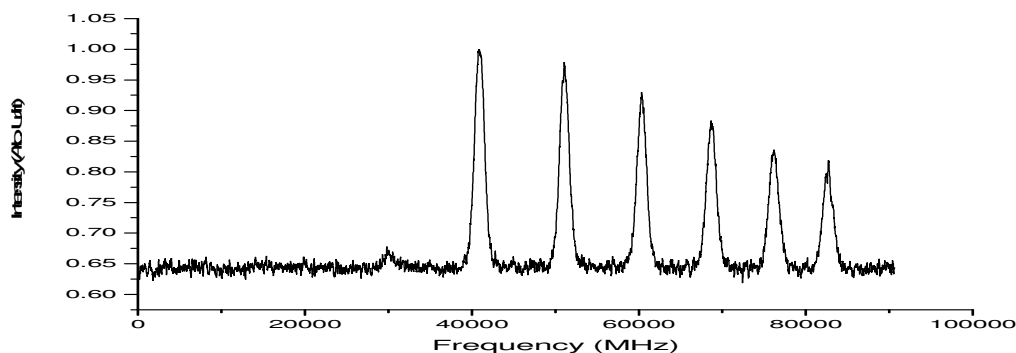
Figure 7.9: Laser excitation of the line showing six widely separated diagonal hyperfine components

The recorded structure is fitted with angular momentum values $J_o = 19/2$ and $J_u = 17/2$ and a best fit is obtained at $A_o = 459$ MHz and $A_u = 970$ MHz with quality factor of 10 (see figure 7.10). Assuming a new upper level the J and A values of lower level are searched in the data base of known levels. A lower level with level energy 11714.38 cm^{-1}, J = 17/2, even parity, A = 970.2(3) MHz, B = -16(4) MHz was found. The recorded hyperfine structure is again fitted with A = 970.2(3) MHz, B = -16(4) MHz of lower level

as being fixed. The energy of the upper level is determined by adding the wavenumber of the excitation line 17827.154 cm^{-1} to the wavenumber of lower level 11714.38 cm^{-1}. The new upper level obtained is **29541.534 cm^{-1}, J = 19/2, odd parity, A = 459.05 MHz**. The level is introduced in classification program and explains all the observed fluorescence lines from upper level in accordance with FT-Spectra. The simulations of the observed fluorescence lines in FT-Spectra with the predicted hyperfine pattern confirmed the existence and reliability of newly measured upper level.
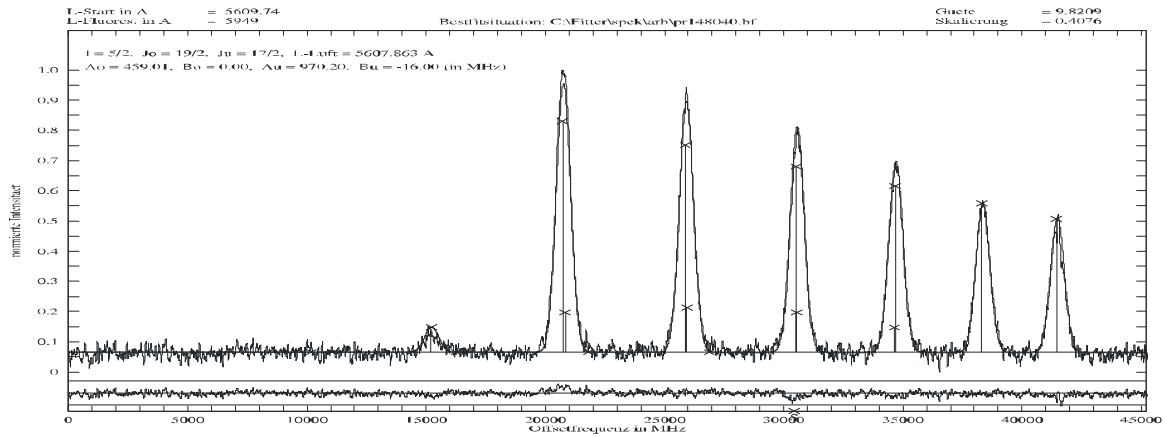
Figure 7.10: Best fit situation of the recorded hyperfine pattern of the line at 5607.863 Å

Furthermore, experimentally the upper level was confirmed by two more excitations at lines 5949.01 Å and 5923.76 Å having good S/N ratio in FT-Spectra (see figures 7.11 and 7.12). The LIF signals (see figure 7.13 and 7.14) of both the lines i.e.5949.01 Å and 5923.76 Å were recorded at one of the previously observed fluorescence wavelength 5607 Å.
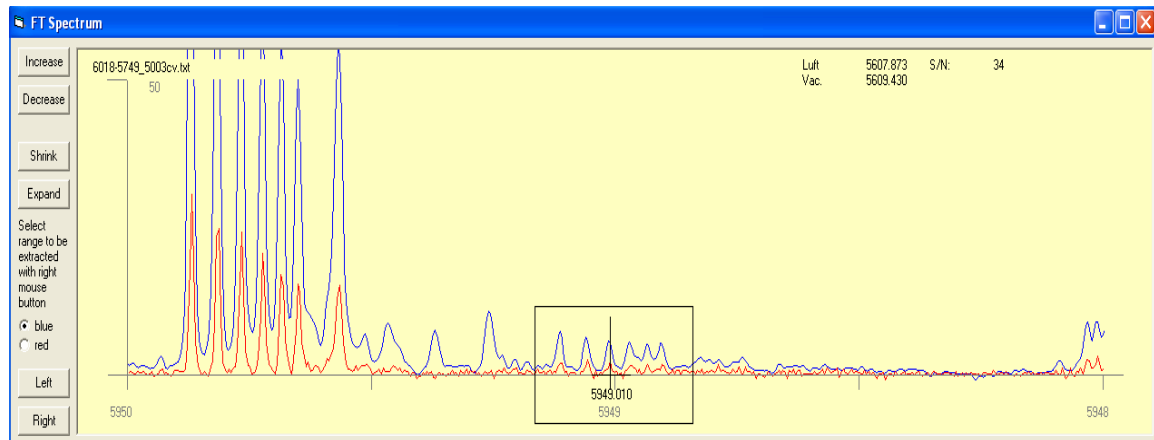
Figure 7.11: FT-Spectra of the line at 5949.01 Å

217
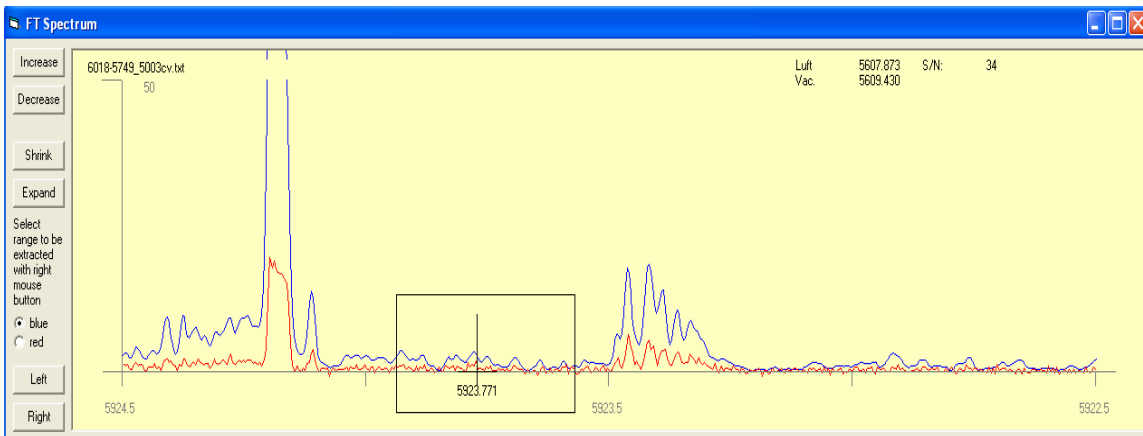
Figure 7.12: FT-Spectra of the line at 5923.76 Å
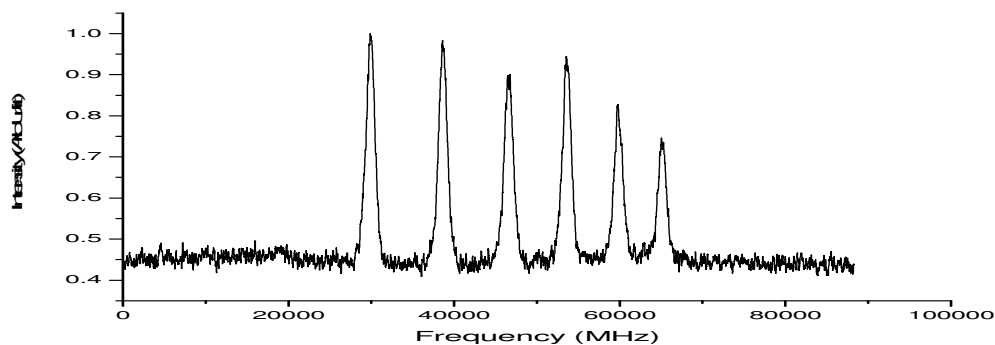
Figure 7.13: LIF signal of the line 5949.01 Å.
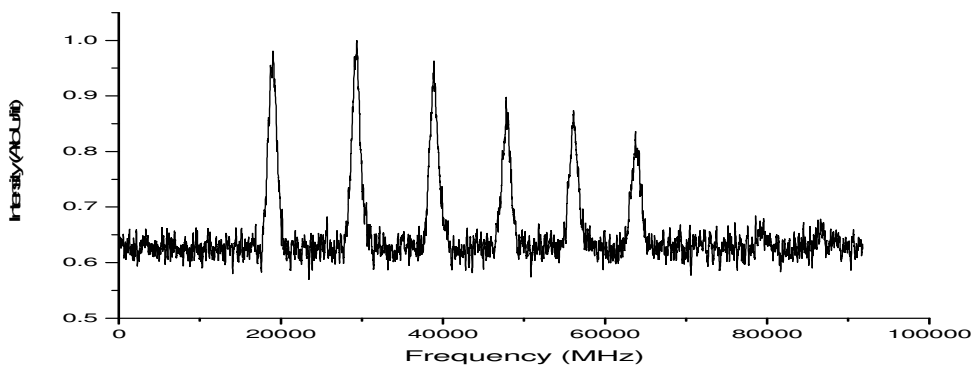
Figure 7.14: LIF signal of the line 5923.76 Å.

The recorded hyperfine patterns for both lines 5949.01 Å and 5923.76 Å are in agreement with the predicted hyperfine pattern (see figure 7.15). This further confirms the existence of the upper level. The wave number of the upper level was corrected from these transitions.
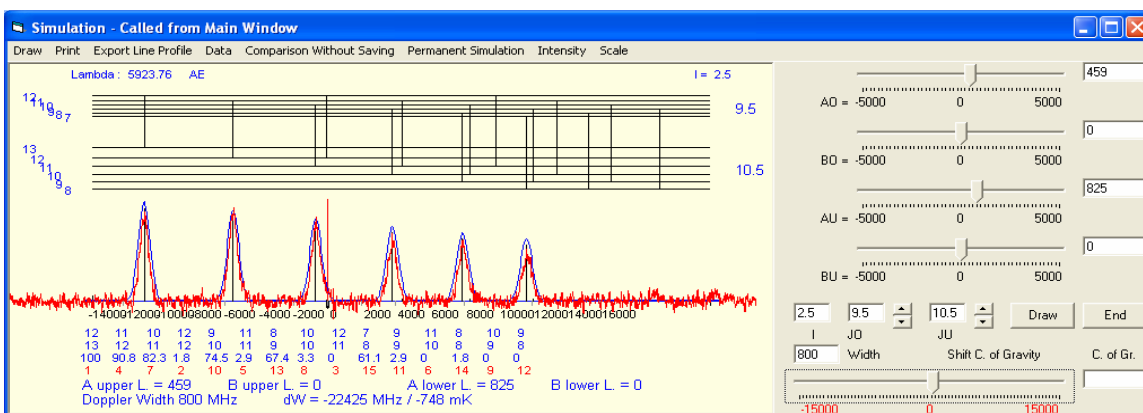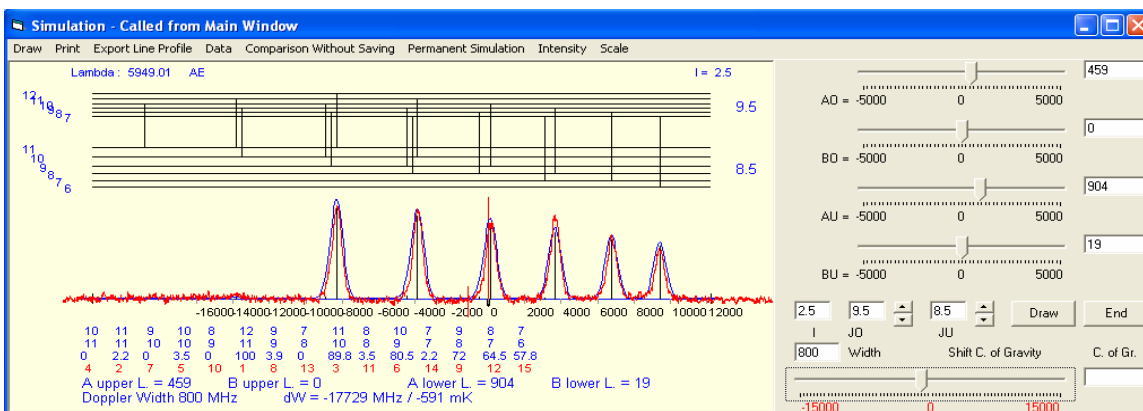
Figure 7.15: Comparison of recorded line profiles with the predicted hyperfine patterns of lines at 5949.01 Å and 5923.76 Å

The newly discovered upper level also explained the other observed fluorescence lines in accordance with FT-Spectra. Table 7.2 lists all the lower levels combining with the newly found upper level.

Table 7.2: Fluorescence lines explained by the new Pr I level 29541.534 cm^{-1}, J = 19/2, odd parity, A = 459.05 MHz

Fluorescence Wavelength λ_{air} (Å)	Lower level				
	Energy (cm^{-1})	J	Parity	A (MHz)	B (MHz)
5259.060	10532.001	17/2	e	546	-
5436.215	11151.49	19/2	e	876.1(3)	-31(12)
5607.86	11714.38	17/2	e	970.2(3)	-16(4)
5923.76	12665.074	21/2	e	825.3(12)	-
5949.01	12736.67	17/2	e	904.1	19
6281.721	13626.72	19/2	e	863.32	-

7.2.3 Discovery of $33759.75^{o}_{17/2}$ level via Laser Excitation of Line 5874.80 Å

The level 33759.75 cm^{-1} was discovered via laser excitation of an unclassified line at 5874.80 Å in FT-Spectra (see figure 7.16). The hyperfine pattern of the investigated line is not clearly seen in FT-Spectra and is partly hidden under a very strong line at 5874.728 Å. This line is explained as a transition between already known levels

$$21398.47^{e}_{15/2} - 4381.1^{o}_{15/2}$$
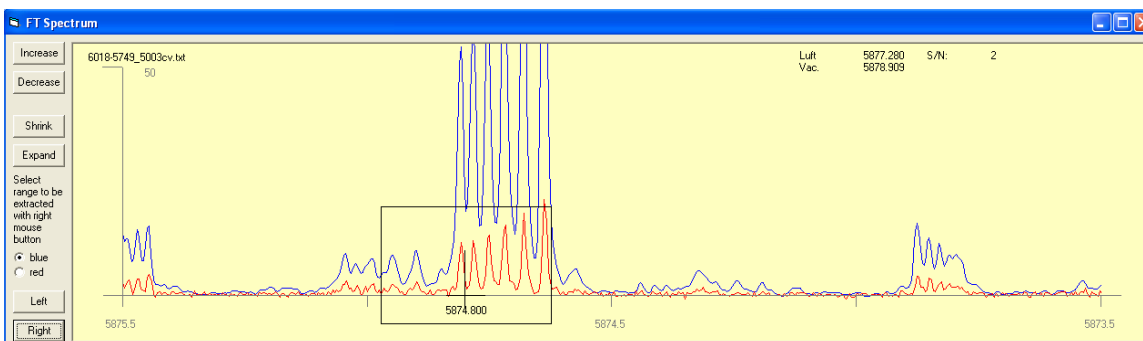
Figure 7.16: FT-Spectra of the line at 5874.80 Å in a blend

Laser excitation wavelength is set to 5874.80 Å and LIF signal was searched. The investigated line is appearing in a blend of several lines therefore several fluorescence lines were observed. By using classification program from all the observed fluorescence lines, the lines belonging to the known upper level were eliminated. The remaining fluorescence wavelengths are 4755 Å, 4965 Å, 5212 Å, 5843.14 Å. Now by scanning the laser wavelength starting from 5875.00 Å, LIF signal (see figure 7.17) is recorded at one of the strongly observed fluorescence wavelength 4965 Å. Again the distribution of relative position and intensities of diagonal components and of off-diagonal components around main components suggest a high angular momentum values for the combining levels with $\Delta J = 0$. None of the suggestions listed in classification program for the line agrees in terms of shape and component positions with the recorded structure, this implies that either one or both combining level is/are new.
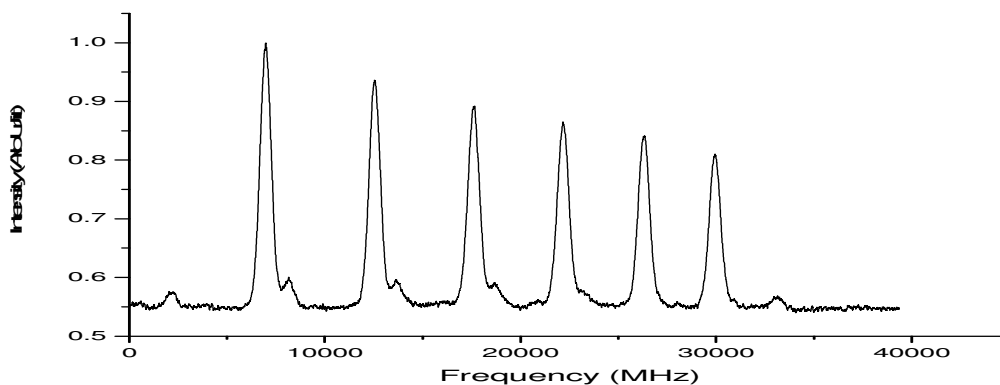
Figure 7.17: Recorded hyperfine structure pattern of the line at 5874.80 Å

The best fit of the recorded structure was obtained for $J_o = 17/2 – J_u = 17/2$ and $A_o = 440.82$ MHz and $A_u = 951.95$ MHz as shown in figure 7.18. Assuming a new upper level, the data base of known levels is search for a known lower level having $J = 17/2$ and $A = 951$ MHz. The level with energy 16742.603 cm^{-1}, even parity, $J = 17/2$ and $A = 950$ MHz was found. Using center of gravity wave number 17017.15 cm^{-1} and wave number of lower level, the level energy for upper level is determined.
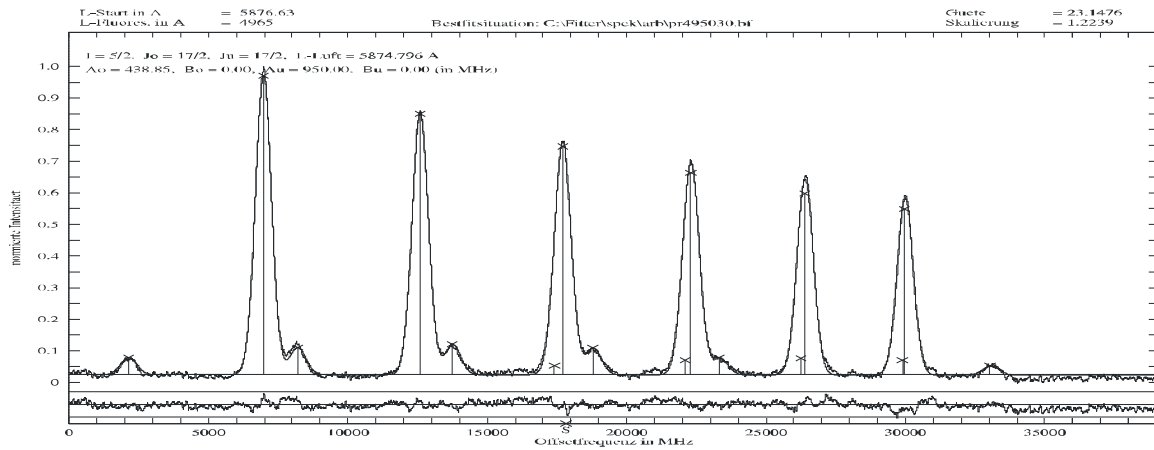
Figure 7.18: Best fit of the recorded structure for the line 5874.80 Å

The new upper level determined has the parameters **33759.75 cm^{-1}, odd parity, $J = 17/2$ and $A = 439.03$ MHz.** After introducing the level in classification program, it explained all the observed fluorescence lines in relevance to their FT-Spectra. To further consolidate the existence and energy of the newly found level a second excitation to this upper level is performed at the line 5843.14 Å. In FT-Spectra (see figure 7.19) this line seems to be hidden in a blend of more than one lines and the hyperfine structure of the line is not seen.
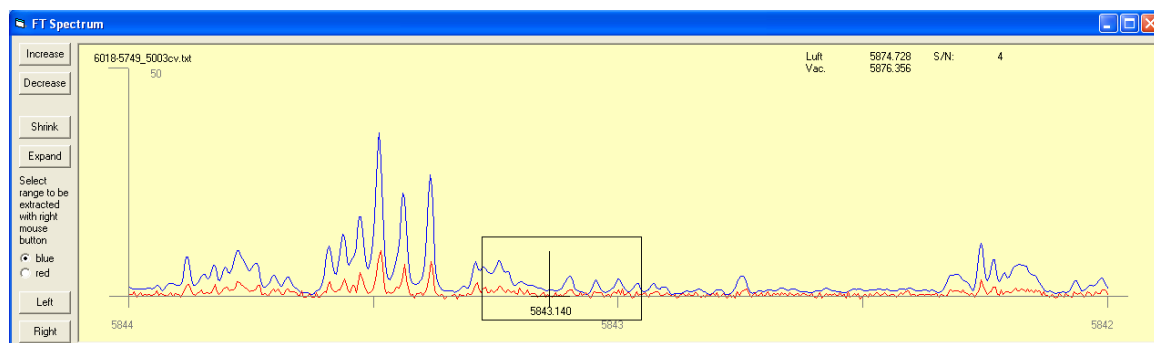
Figure 7.19: FT-Spectra of line at 5843.14 Å

The LIF signal is seen on all previously observed fluorescence lines and the recorded hyperfine pattern (see figure 7.20) is in agreement in terms of shape and component positions (see figure 7.21) with prediction. Table 7.3 lists all the lower levels combining with the newly found upper level.
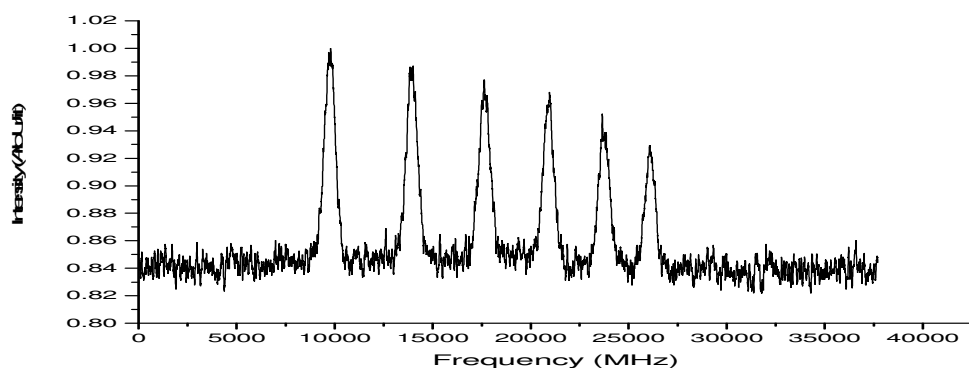
Figure 7.20: Recorded hyperfine structure pattern of the line at 5843.14 Å
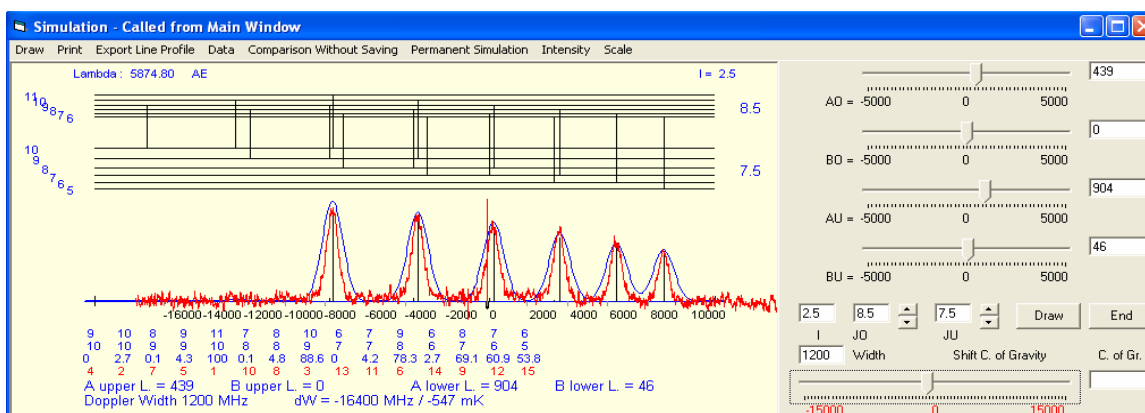
Figure 7.21: Comparison of the recorded hyperfine structure of the line with the predicted hyperfine structure pattern

Table 7.3: Fluorescence lines explained by the new Pr I level 33759.75 cm^{-1}, J = 17/2 odd parity, and A = 439.03 MHz

Fluorescence Wavelength λ_{air} (Å)	Lower level				
	Energy (cm^{-1})	J	Parity	A (MHz)	B (MHz)
4755.347	12736.67	17/2	e	904.1	19
4965.577	13626.72	19/2	e	863.32	-
5212.246	14579.504	15/2	e	872.7	-
5843.14	16650.62	15/2	e	903.7(3)	46(9)
5874.80	16742.603	17/2	e	950	-

7.2.4 Discovery of $30781.638^{e}_{15/2}$ level via Laser Excitation of Line 5622.87Å

The line in FT-Spectra (see figure 7.22) at 5622.87 Å has a good S/N ratio with a relative intensity of 23 and has a resolved hyperfine structure pattern. The line could not be classified using any of the suggestions listed in classification program. Therefore laser excitation of the line at 5622.87 Å is performed and an LIF signal is observed on fluorescence lines 3786 Å, 4971 Å, 5256 Å, 5730 Å, 6080 Å and 6341 Å. Signal is then recorded by scanning the laser frequency which resulted in a narrowly spaced hyperfine pattern with resolved diagonal components as shown in figure 7.23.
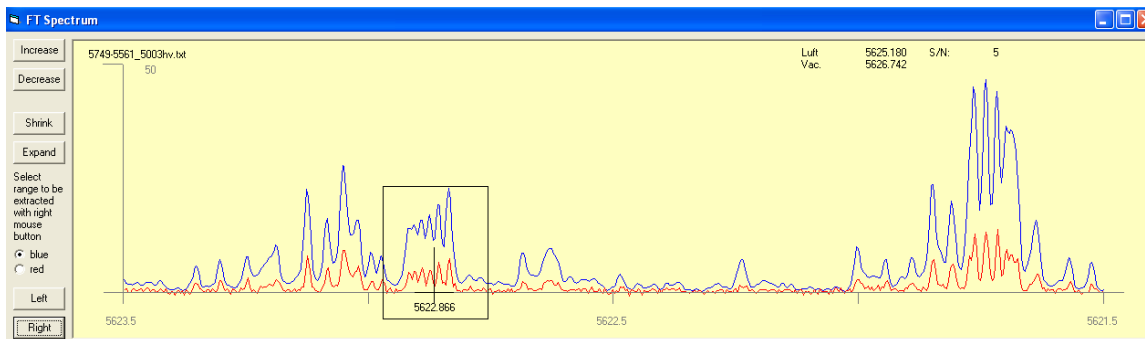
Figure 7.22: FT-Spectra of the line at 5622.87 Å

The recorded hyperfine structure pattern suggest a transition between levels with $\Delta J = 0$. The intensities of diagonal components decreases towards longer wavelength side. This implies that magnitude of hyperfine interaction constant of upper level is larger than that of the lower level. On all observed fluorescence lines the intensities of diagonal hyperfine components show a slightly abnormal behaviour. This could be attributed like to a **saturation effect** or to the fact that off-diagonal components might be lying underneath diagonal components resulting in an increase in height of the diagonal components.
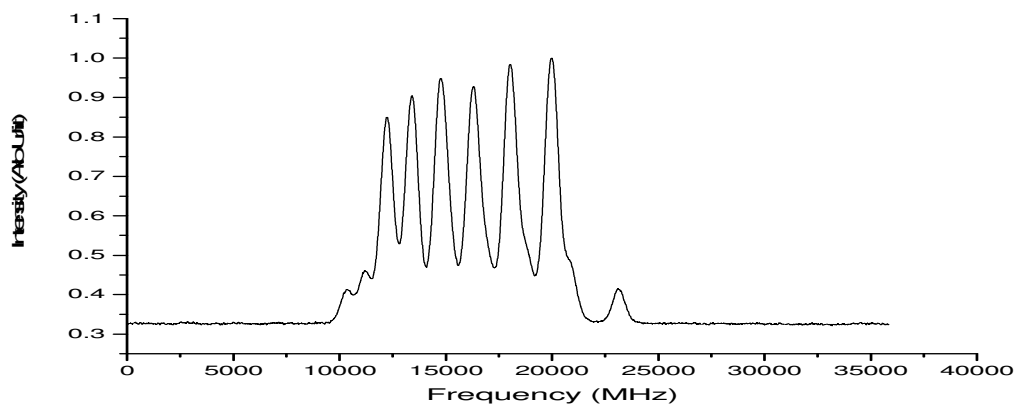
Figure 7.23: Recorded hyperfine structure of the line at 5622.87 Å

The recorded structure is fitted and a best fit (see figure 7.24) is obtained for values $J_o = 15/2 - J_u = 15/2$, $A_o = 512.61$ MHz, $A_u = 318.47$ MHz. Assuming a new upper level, a

lower level based on fitting parameters and fluorescence information is searched in the data base of known levels. A lower level with level energy 13002.05 cm^{-1}, odd parity, J = 15/2, A = 316.6(14) MHz, B = 29(33) MHz was found. The recorded structure was again fitted keeping fix the A and B values of lower level.
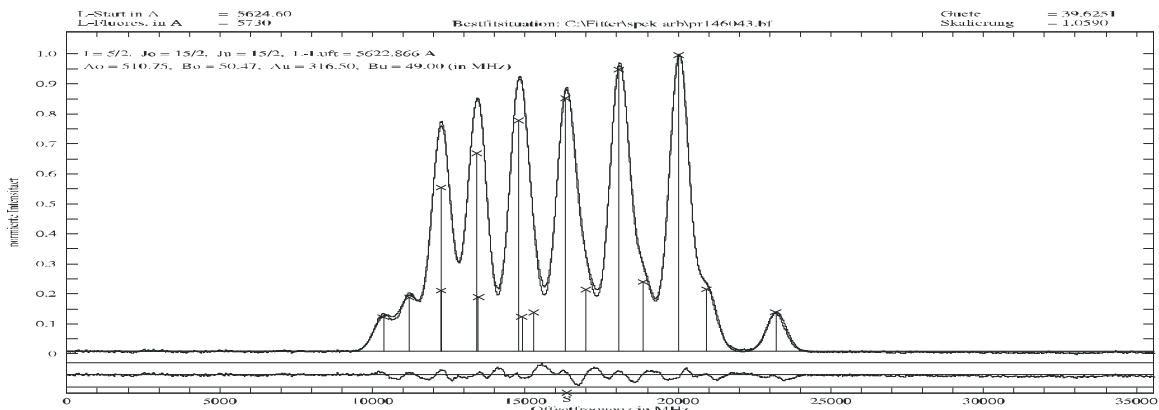
Figure 7.24: Best fit situation of the recorded hyperfine structure of line at 5622.87 Å

The quality factor increases from 29 to 39 if quadrupole constant B for the upper level is allowed to change. This implies that a slight shift of hyperfine components is compensated by a small value of quadrupole constant B. The energy of the upper level is determined by adding the center of gravity wave number of the line 17779.588 cm^{-1} and the wave number of the lower level. Therefore the new level determined is **30781.638 cm^{-1}, even parity, J = 15/2, A = 510.75 MHz, B = 50.47 MHz**. The determined new upper level is introduced in classification program and explains all the observed fluorescence lines, also in relevance to their FT-Spectra. The level is confirmed by second excitation to upper level at the line 5730.46 Å. This line has a good S/N ratio in FT-Spectra and the hyperfine components are well resolved. The recorded hyperfine pattern (see figure 7.25) is in good agreement with FT-Spectra and predicted pattern in terms of shape and component positions (see figure 7.26). Table 7.4 lists all the lower fluorescence levels.
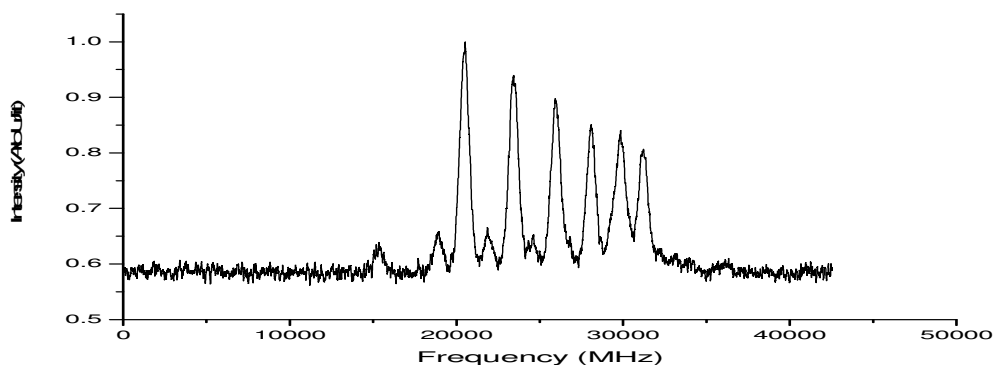
Figure 7.25: Recorded hf structure of the line at 5730.46 Å

224
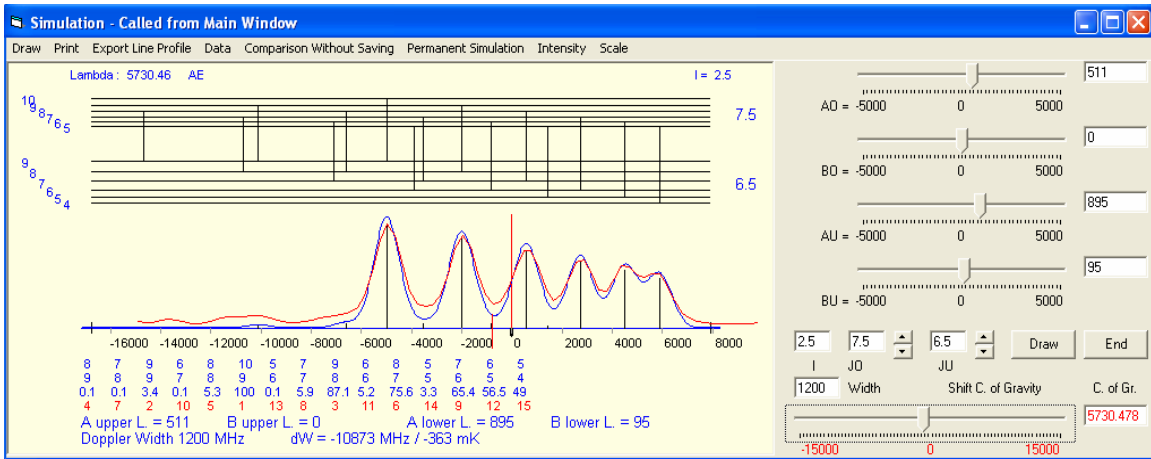
Figure 7.26: Comparison of line profile from FT-Spectra with predicted hyperfine structure pattern

Table 7.4: Fluorescence lines explained by the new Pr I level 30781.638 cm^{-1}, J = 15/2, even parity, A = 510.75 MHz, B = 50.47 MHz

Fluorescence	Lower level				
Wavelength λ_{air} (Å)	Energy (cm^{-1})	J	Parity	A (MHz)	B (MHz)
3786.726	4381.1	15/2	o	541.575	-14.558
4970.601	10668.96	15/2	o	951.310	-2.670
5256.882	11764.25	17/2	o	892.5(7)	-10(25)
5730.468	13335.895	13/2	o	895	95
6080.513	14340.21	17/2	o	244.7(3)	-20(5)
6342.016	15018.14	13/2	o	108(3)	-

7.2.5 Discovery of $27037.09^o_{13/2}$ level via Laser Excitation of Line 5626.43 Å

The line at 5626.43 Å in FT-Spectra (see figure 7.27) could not be classified using any of the suggestions listed in classification program. The relative intensity of the line in FT-Spectra is 12 and the hyperfine components are not resolved. From the appearance of line in FT-Spectra a narrowly spaced hyperfine structure is anticipated.
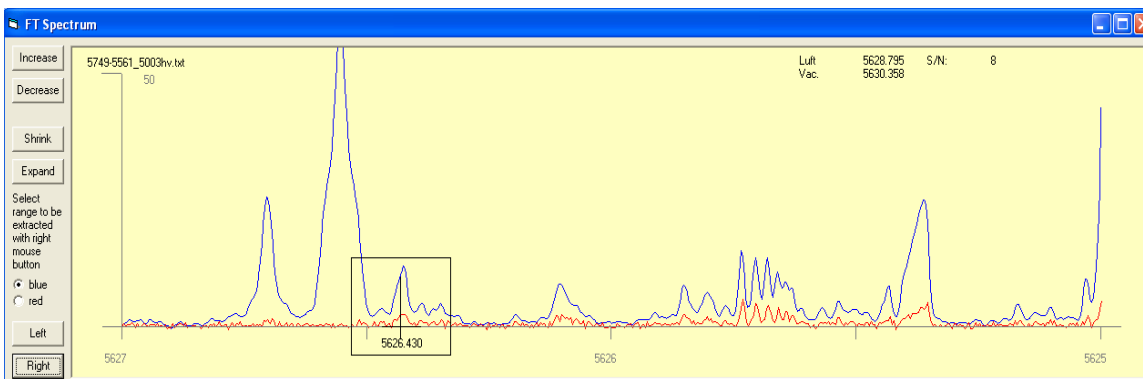
Figure 7.27: FT-Spectra for the line at 5626.43 Å

Laser excitation of line resulted in LIF signal on fluorescence wavelengths 4892 Å, 5151 Å, 5491 Å, 5688 Å and 6196 Å. The LIF pattern is subsequently recorded on all observed fluorescence wavelengths by scanning the laser frequency. As expected a closely spaced hyperfine structure is recorded with a very good S/N ratio (see figure 7.28). One of the groups of off-diagonal hyperfine components is fully separated from diagonal components and lie on the longer wavelength side, suggesting a combination between pair of levels with $\Delta J = +1$.
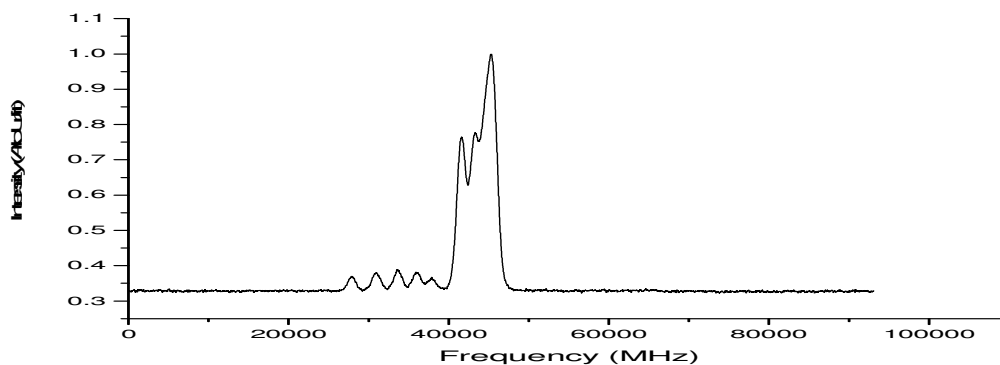
Figure 7.28: Recorded Hyperfine structure of line at 5626.43 Å

The recorded hyperfine structure was fitted best with values $J_o = 13/2$ - $J_u = 11/2$, $A_o = 776.26$ MHz, $A_u = 974.04$ MHz (see figure 7.29). Assuming an unknown upper level the data base of known levels is searched for a lower level. A lower level with level energy 9268.741 cm^{-1}, even parity, J = 11/2 and A = 976.8(2) MHz, B = -23.7(63) MHz was found. Recorded structure was again fitted keeping fix the A and B values of the lower level. Level energy for the upper level is determined by adding center of gravity wave

number 17768.465 cm^{-1} of the line and wave number of the lower level giving **27037.09 cm^{-1}, odd parity, J = 13/2 and A = 782.10 MHz**. The newly calculated upper level explained all the observed fluorescence lines in accordance with FT-Spectra. The level energy and other parameters of the newly found level are corrected and confirmed by more excitations to upper level from known lower levels.
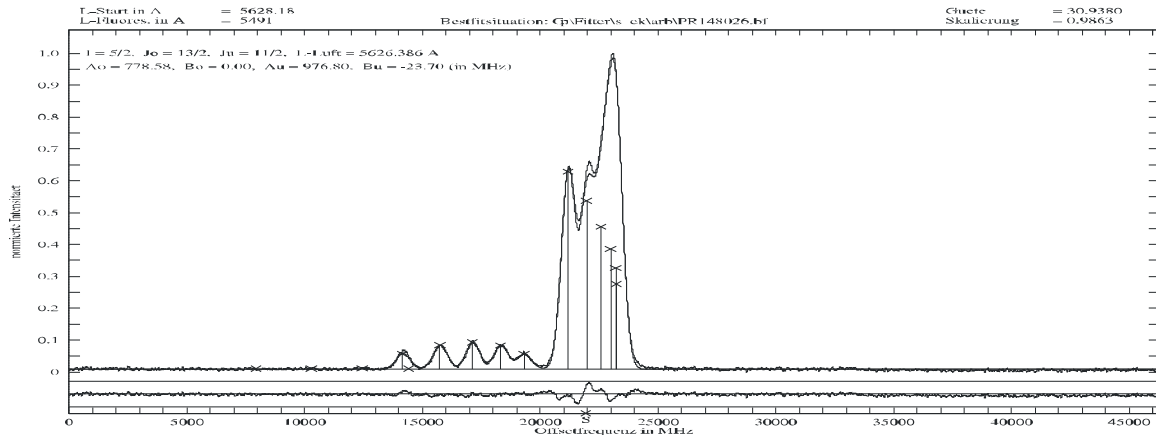
Figure 7.29: Best fit situation of the recorded hf structure of the line at 5626.43 Å

Further, laser excitations to upper level were performed at lines 5689.10 Å, 6033.20 Å 6419.12 Å and 6460.55 Å. Their hyperfine structures were recorded on previously observed fluorescence wavelengths. As an example the comparison between line profile from FT-Spectra at 5689.10 Å with predicted hyperfine structure pattern is given in figure 7.30.
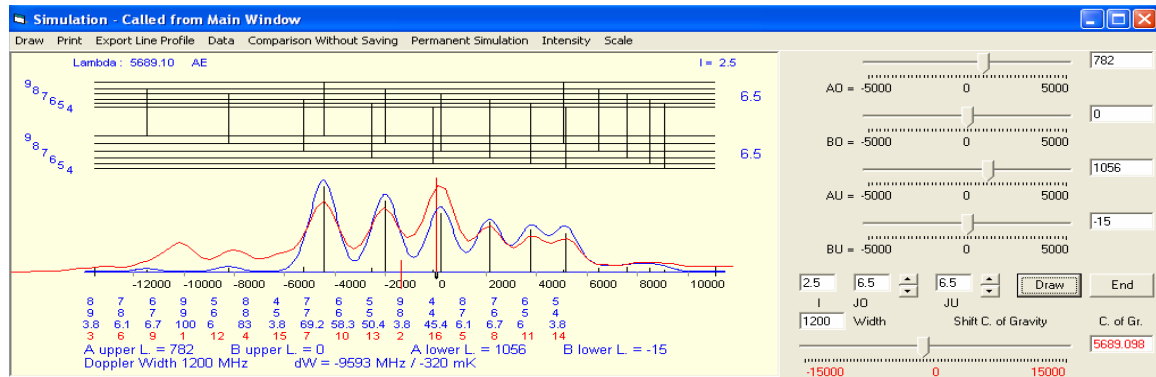
Figure 7.30: Comparison of the line profile from FT-Spectra with prediction of the hf pattern of the line at 5689.10 Å

This confirmed beyond doubt the existence of newly found level and the level parameters were improved. Table 7.5 lists all the observed fluorescence lower levels combining with the newly found upper level.

Table 7.5: Fluorescence lines explained by the new Pr I level 27037.09 cm^{-1}, J = 13/2 odd parity and A =782.10 MHz

Fluorescence Wavelength λ_{air} (Å)	Lower level				
	Energy cm^{-1}	J	Parity	A (MHz)	B (MHz)
4892.562	6603.606	13/2	e	755.456	-48.633
5151.36	7630.147	13/2	e	776.286	-43.592
5490.562	8829.078	11/2	e	769.4	-31
5689.086	9464.46	13/2	e	1056.3(1)	-14.8(52)
6033.201	10466.73	15/2	e	1041.7(15)	-19(10)
6196.753	10904.07	11/2	e	301.1(1)	-22(2)
6419.088	11462.858	13/2	e	804.1(4)	-
6460.542	11562.79	13/2	e	819(2)	-

7.2.6 Experimental Investigation of Line at 6377.79 Å Leading to the Discovery of New Pr-I Lower and Upper Levels

Laser excitation of line at 6377.79 Å is performed which has a relative intensity of 7 in FT-Spectra. Before laser excitation, a careful analysis of the line in FT-Spectra suggested that it might be due to a transition between two levels with comparable splitting (see figure 7.31) with all diagonal components bunched together in the shape of a single peak hyperfine structure. Further more none of the listed suggestions in the classification program could classify the line in FT-Spectra.
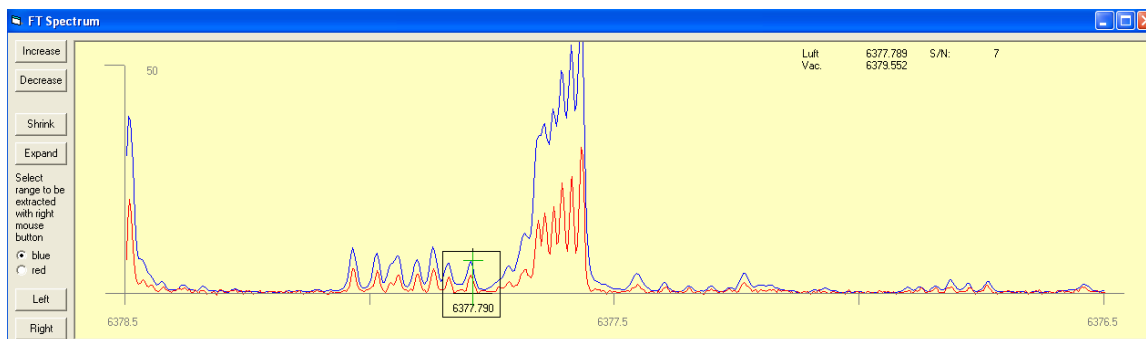
Figure 7.31: FT-Spectra of the line at 6377.79 Å

LIF signal with fluorescence wavelengths 3405 Å, 4415 Å, 4785 Å, 4942 Å, 5812 Å, 5924 Å, 6242 Å and 6915 Å is observed at excitation wavelength 6377.79 Å. Then hyperfine pattern is recorded on all observed fluorescence lines by scanning laser frequency. The recorded hyperfine structure is in the shape of a single peak with symmetrical distribution of off-diagonal components as shown in figure 7.32.
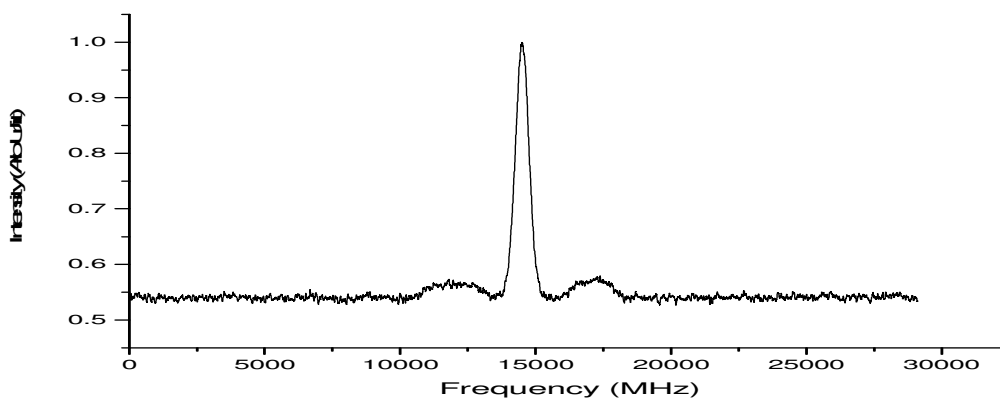
Figure 7.32: Hyperfine structure of the line 6377.79 Å

The recorded structure is fitted best with values $J_o = 11/2$ - $J_u = 11/2$, $A_o = 428.74$ MHz, $A_u = 437.79$ MHz (see figure 7.33). Using the best fit values a known lower level is searched in the data base of known levels assuming that a new upper level is involved. But after careful investigation no upper level could be introduced was found which could

explain all the fluorescence lines. In the next step a known upper level is searched assuming an unknown lower level. As before no level was found which could explain all the fluorescence lines. After reviewing the fitting process and further analysis it was concluded that this line might be a transition involving both unknown lower and upper levels.
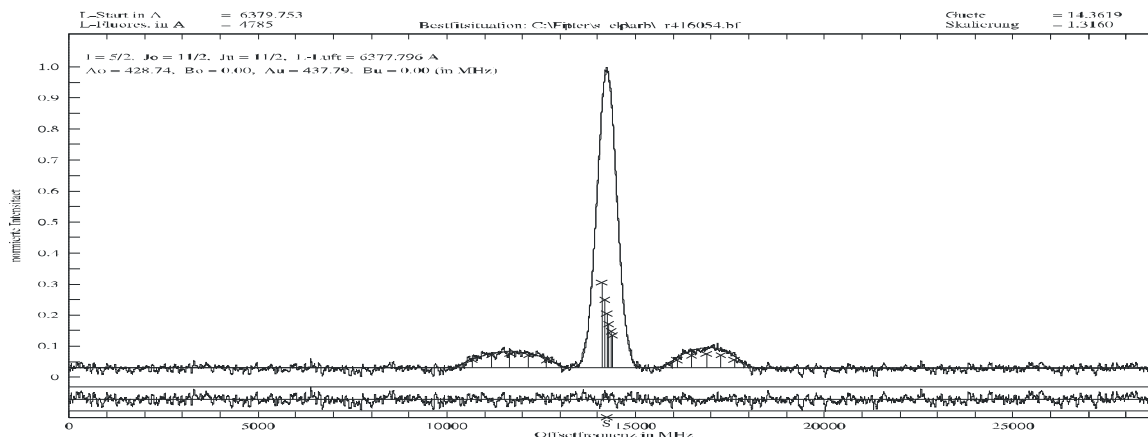
Figure 7.33: Best fit situation of line at 6377.79 Å

Fortunately two of the fluorescence lines i.e. 5812 Å and 5924 Å, lay in spectral region of Rhodamine 6G. Exact fluorescence wavelengths were measured for these lines as 5811.15 Å and 5924.55 Å. Laser excitation was then performed at these lines and LIF signal at center of gravity excitation wavelengths 5924.47 Å and 5811.06 Å was seen on all previously observed fluorescence wavelengths and in addition on the wavelength 6377 Å, the previous excitation wavelength. The hyperfine components of the line at 5924.47 Å in FT-Spectra (see figure 7.34) have low relative intensity and are not clearly resolved.
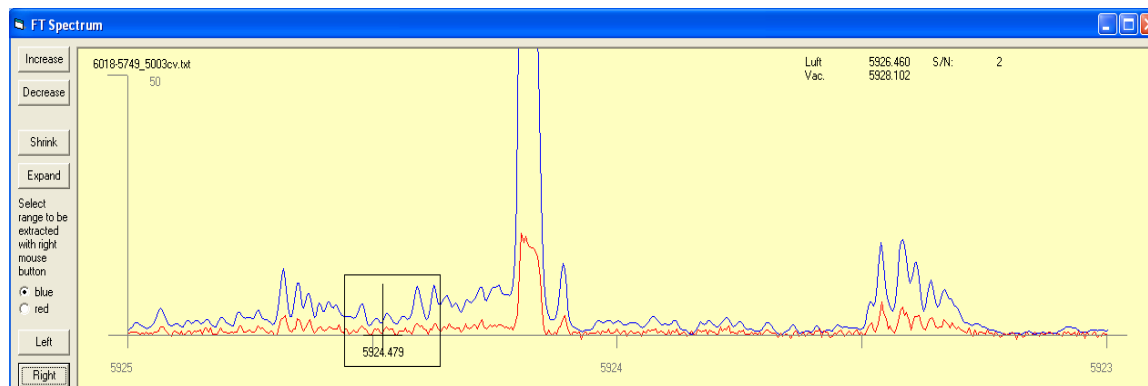
Figure 7.34: FT-Spectra of line at 5924.47 Å

LIF signal is then recorded by scanning the laser frequency at the strongest fluorescence wavelength i.e. 4785 Å (see figure 7.35). The recorded hyperfine structure of the line at 5924.47 Å is fitted taking J and A values of upper level the same as for the previous excitation at 6377.79 Å. Best fit is obtained for values $J_o = 11/2 - J_u = 13/2$, $A_o = 424.32$ MHz and $A_u = 673.25$ MHz (see figure 7.36).

230
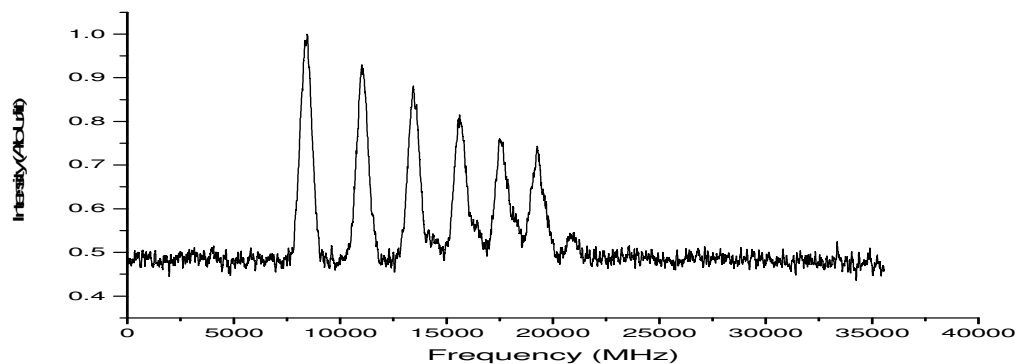
Figure 7.35: Recorded hyperfine pattern of the line at 5924.47 Å
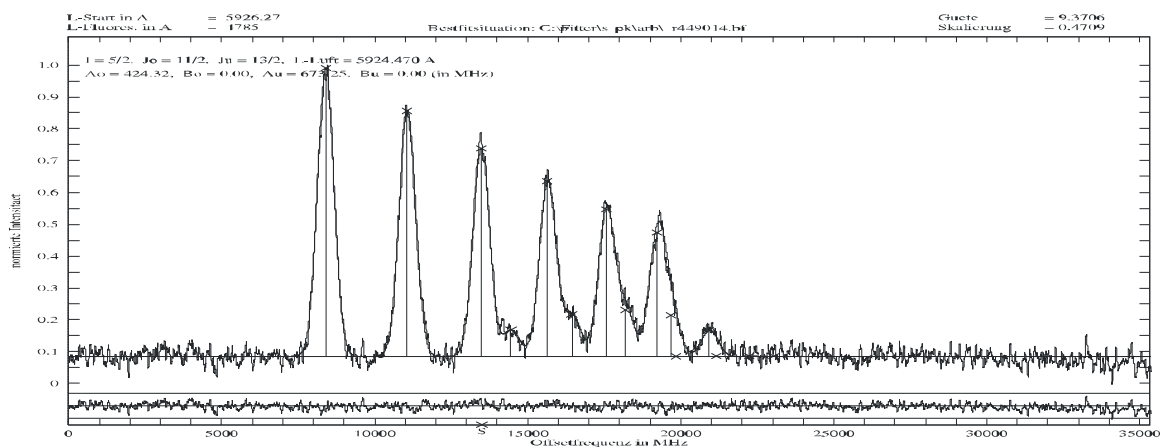
Figure 7.36: Best fit situation of the recorded line at 5924.47 Å

Now a known lower level is searched assuming an unknown upper level for this line. A level with energy 15347.433 cm^{-1}, odd parity, J = 13/2 and A = 674(2) MHz is found. Assuming that this level is involved in the transition, the recorded structure is again fitted keeping fix the A values of the lower level. Now the A value obtained for the upper level is 425.16 MHz. The upper level is then calculated by adding center of gravity wave number of the line 16874.471 cm^{-1} to the wave number of the lower level. The computed upper level is **32221.905 cm^{-1}, even parity, J = 11/2 and A = 425.16 MHz.** The level is introduced in the classification program which generated the transition list for the upper level. The newly computed level explained all the previously observed fluorescence lines with the exception of the line at 6377.79 Å. This suggests very strongly a situation where an unknown lower level is involved in the line 6377.79 Å (see figure 7.32).

A second excitation at the line 5811.06 Å is performed which appears in the transition list of the newly found upper level. The recorded hyperfine structure of the line is in agreement with the predicted hyperfine pattern of the line, confirming the existence of upper level. The level energy and other parameters of the newly found level are again calculated from this line which gave the values **32221.949 cm^{-1}, even parity, J = 11/2 and A = 420.87 MHz.** Mean values determined from the two transitions are **32221.927**

cm^{-1}, even parity, J = 11/2 and A = 423(1) MHz. Figure 7.37 show a good agreement between recorded and predicted line profile at 5811.08 Å.
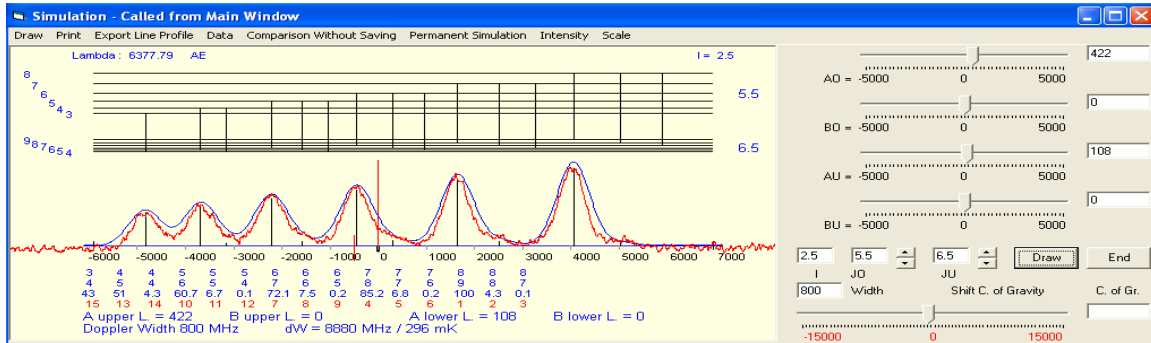
Figure 7.37: Comparison of the recorded hyperfine structure of the line 5811.08 Å with predicted hyperfine pattern.

In order to justify the argument that an unknown lower level exist at the line 6377.79 Å, the recorded hyperfine structure (see figure 7.32) of line 6377.79 Å is again fitted by keeping fix the value of magnetic hyperfine constant A = 423(1) MHz of the upper level as determined by fittings of the recorded hyperfine structure of lines 5924.47 Å and 5811.06 Å (see figure 7.36). This process resulted in a value of magnetic hyperfine A constant of probable lower level as 432.36 MHz (see figure 7.38). Subtracting the center of gravity wave number of the line i.e. 15675.064 cm^{-1} from wave number of the newly discovered upper level, the energy of the probable lower level is calculated. The newly calculated lower level is **16546.863 cm^{-1}, odd parity, 11/2 and A = 432.36 MHz.**
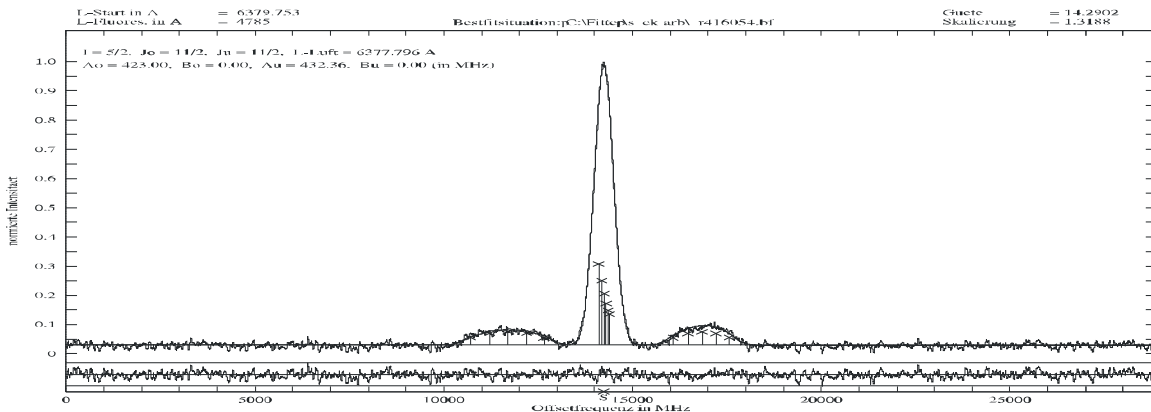
Figure 7.38: Fitting of line at 6377.79 Å for the determination of lower level

Newly found lower is introduced in classification program which generates a transition list showing transitions from this lower level to different upper levels. To confirm the existence of lower level further excitations need to be performed involving the newly found lower level and a known upper level. The transition list of the newly found lower level displays a combination with already known upper level 33870.18 cm^{-1}, even parity,

J = 13/2, 590.48 MHz at the line 5770.966 Å. FT-Spectra of the line shows almost nothing, nevertheless laser excitation of this line was performed.

The monochromator wavelength is set to the strongest fluorescence wavelength of the upper level 33870.18 cm^{-1}, i.e. at 3222 Å. Hyperfine structure of the line at the preset fluorescence wavelength is recorded (see figure 7.39) which at first inspection agrees with the predicted hyperfine pattern in the classification program.
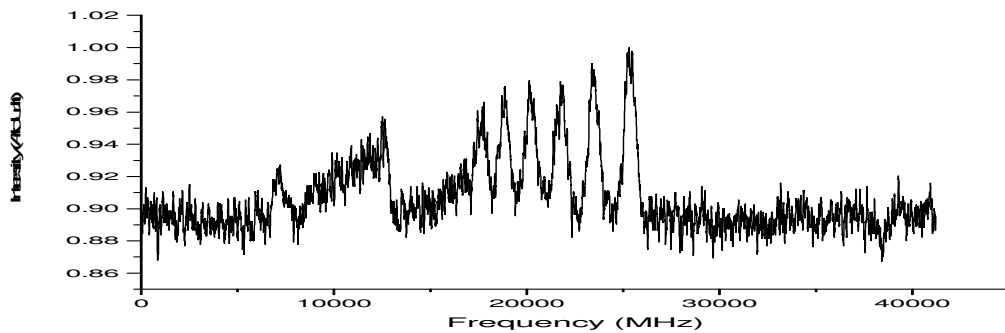
Figure 7.39: Hyperfine structure of the line at 5770.966 Å (second structure at higher frequency)

The structure appearing at the longer wavelength side is a transition to another upper level which lies in the scan range of laser and has by accident nearly the same fluorescence wavelength.

In figure 7.39 the hfs appearing on the shorter wavelength side is fitted keeping fix both the J and A values of lower and upper levels which gave a reliable fitting situation as shown in figure 7.40. This confirms the existence of lower level. Further confirmation of the lower level is performed at the line 6761.50 Å. Table 7.6 list all the observed fluorescence lower levels combining with upper level 32221.927 cm^{-1}.
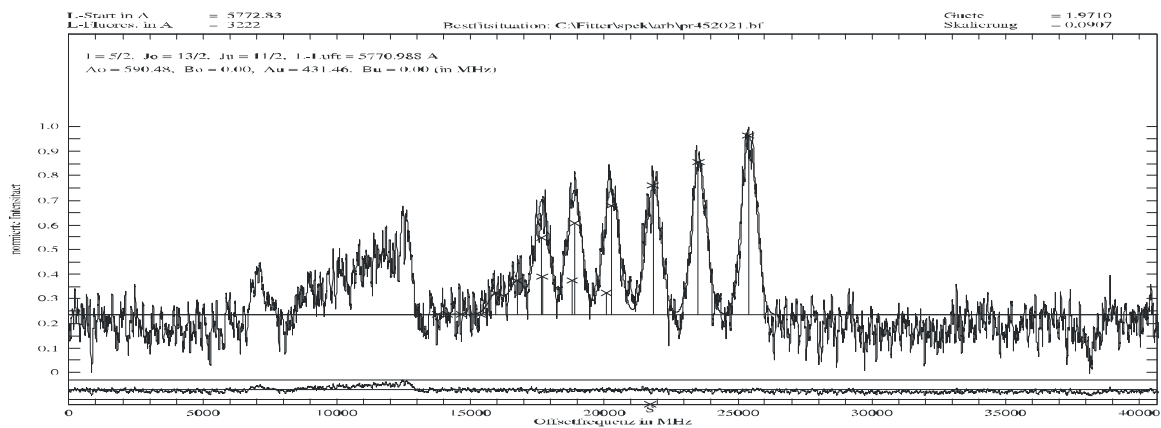
Figure 7.40: Best fit situation of the hyperfine pattern recorded at 5770.966 Å

Table 7.6: Fluorescence lines explained by the new Pr I level 32221.927 cm^{-1}, J = 11/2 even parity and A = 423(1) MHz

Fluorescence Wavelength λ_{air} (Å)	Lower level				
	Energy cm^{-1}	J	Parity	A (MHz)	B (MHz)
3403.257	2846.744	13/2	o	613.240	-12.850
4415.313	9579.832	9/2	o	788.8(4)	-
4785.133	11329.71	9/2	o	530	-
4943.026	11997.05	11/2	o	585.6	-
5811.063	15018.14	13/2	o	108(3)	-
5924.462	15347.433	13/2	o	674(2)	-
6241.623	16204.883	13/2	o	732.6	-
6377.796	16546.863	11/2	o	431.46	-
6915.358	17765.348	13/2	o	490(3)	-

7.2.7 Discovery of $28430.41^{o}_{9/2}$ level via Laser Excitation of Line 5895.27Å

The line in FT-Spectra at 5895.27 Å has a good S/N ratio with resolved hyperfine components and has a relative intensity of 5 (see figure 7.40). Line was not classified since none of the listed suggestions in classification program is in conformity with the FT-Spectra.
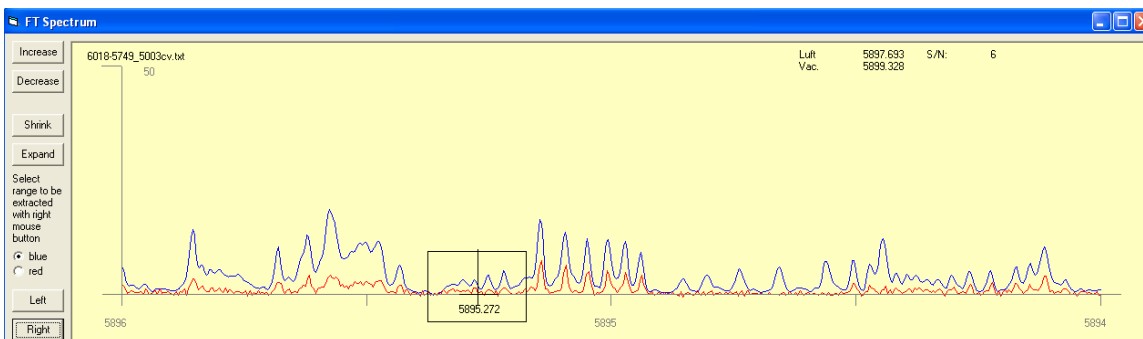
Figure 7.40: FT-Spectra of the line at 5895.27 Å

For laser excitation at 5895.27 Å a LIF signal is observed on fluorescence wavelengths 4603 Å, 4166 Å, 4243 Å and 4423 Å with strongest signal appearing on 4603 Å. LIF signal is then recorded on all observed fluorescence lines by scanning the laser frequency which gives similar hyperfine patterns as shown in figure 7.41. After inspecting the recorded structure it is clear that lower level has less splitting compared to the upper level since the off-diagonal components are not resolved from the diagonal components. It can also be inferred that A constant of upper level is greater than that of the lower level.
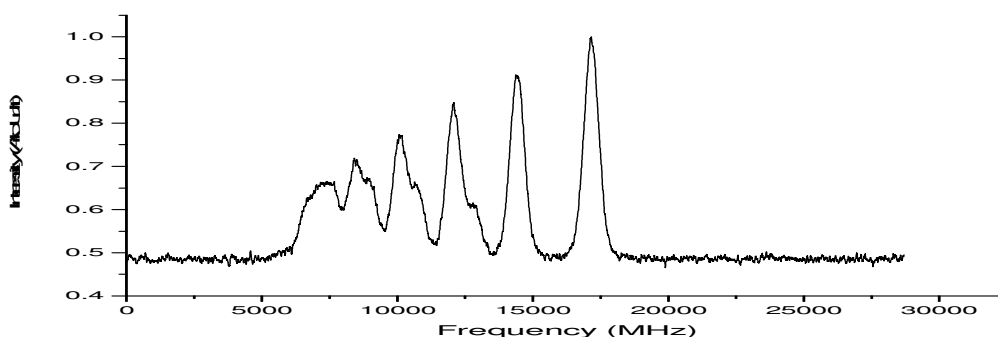
Figure 7.41: Hyperfine structure of line at 5895.27 Å

Recorded structure is fitted best with values $J_o = 9/2 – J_u = 7/2$, $A_o = 629.42$ MHz and $A_u = 271.39$ MHz (see figure 7.42). Using these results and assuming that upper level is unknown a known lower level is searched in the data base. A lower level with level energy 11472.35 cm^{-1}, even parity, $J = 7/2$ and $A = 272.9$ MHz is found. Assuming this as the lower level of excitation the recorded structure is again fitted keeping fix the A value of lower level as $A = 272.9$ MHz. The energy of new upper level is determined by using the center of gravity wave number of the line 16958.051 cm^{-1} and the wave number

of lower level 11472.35 cm^{-1}. This gives **28430.41 cm^{-1}, odd parity, J = 9/2 and A = 630.76 MHz.** Transition list generated by classification program, when the new level is introduced, explained all the observed fluorescence wavelengths. Also line from FT-Spectra could be confirmed.
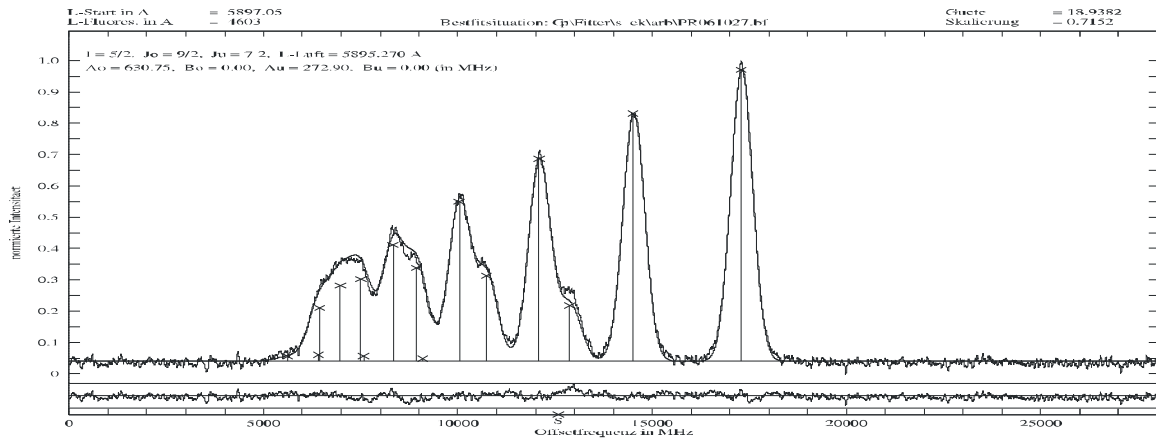
Figure 7.42: Best fit situation of the recorded line at 5895.27 Å

To further confirm the existence of new level and its energy a second excitation is performed at the 5796.83 Å where the new upper level combines with 11184.41 cm^{-1}, even parity, J = 9/2, A = 692.1(4) MHz, B = 14(28). This line in FT-Spectra (see figure 7.43) shows a blend situation and maybe several other lines are also present in close proximity of each other. The line profile seen in FT-Spectra is then the result of convolution of hyperfine structures of all lines.
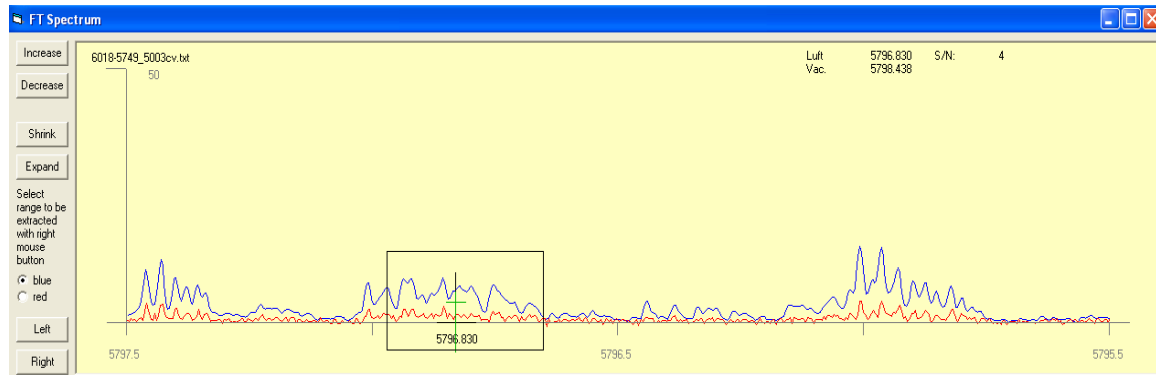
Figure 7.43: FT-Spectra of line at 5796.83 Å

Laser excitation of the line 5796.83 Å is performed which revealed a hyperfine structure as shown in figure 7.44. The recorded hyperfine structure of the line is in good agreement with the predicted hyperfine pattern as seen figure 7.45. Table 7.7 lists all the observed fluorescence lower levels combining with the new upper level 28430.41 cm^{-1}.
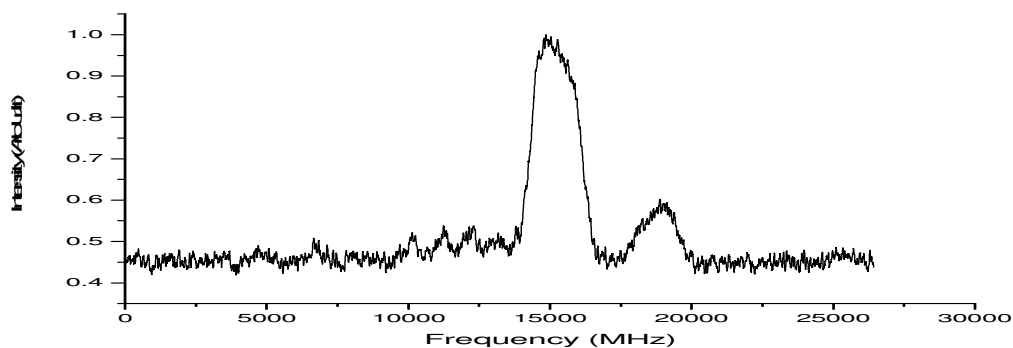
Figure 7.44: Hyperfine pattern of the line 5796.83 Å
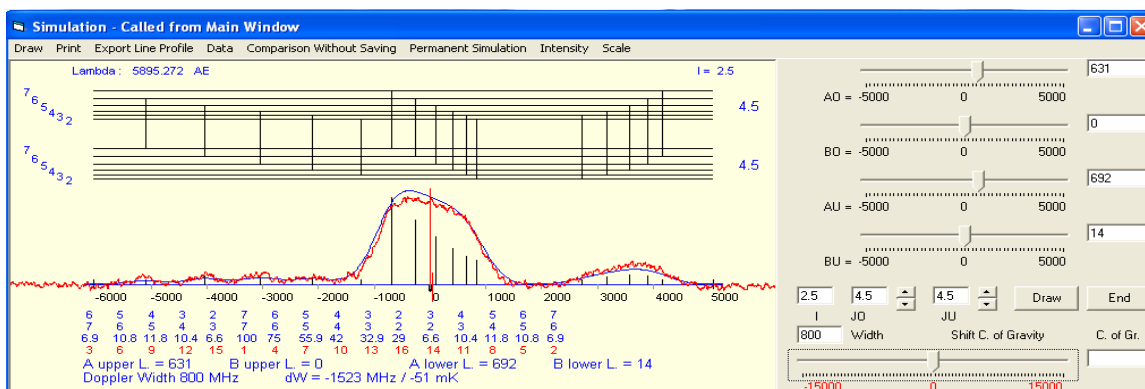
Figure 7.45: Comparison of the line profile with theoretical prediction of line at 5796.83 Å

Table 7.7: Fluorescence lines explained by the new Pr I level 28430.41 cm^{-1}, J = 9/2, odd parity and A = 630.76 MHz

Fluorescence	Lower level				
Wavelength λ_{air} (Å)	Energy cm^{-1}	J	Parity	A (MHz)	B (MHz)
4165.813	4432.24	9/2	e	929(1)	-92(7)
4242.591	4866.53	11/2	e	867.997	-50.319
4422.071	5822.905	9/2	e	861.3(5)	-
4603.568	6714.199	11/2	e	474.692	-29.633

7.2.8 Discovery of $29087.674^{e}_{7/2}$ level via Laser Excitation of Line 5759.76 Å

The level with energy 29087.665 cm^{-1} was discovered by the laser excitation of an unclassified line in FT-Spectra at 5759.75 Å. The line in FT-Spectra appears in a blend situation and has a relative intensity of 7 (see figure 7.46).
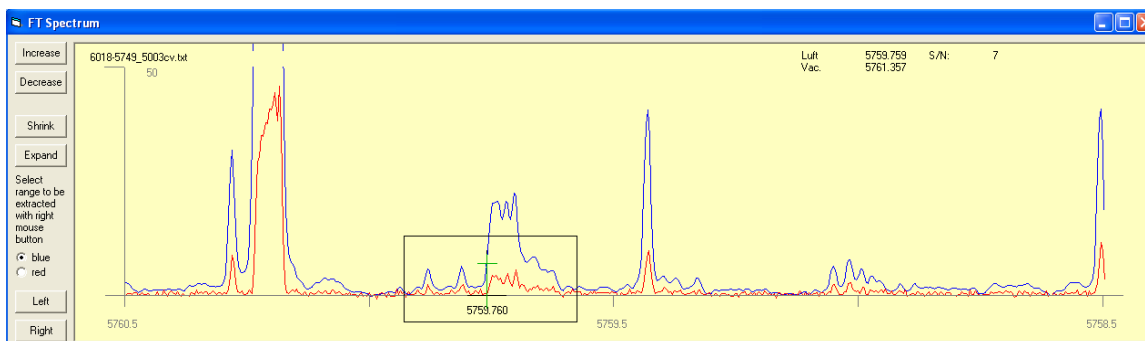
Figure 7.46: FT-Spectra of line at 5759.75Å

Initially at the excitation wavelength 5759.75 Å a LIF signal is observed on fluorescence wavelengths 5169 Å, 5507 Å, 5887 Å, 5947 Å and 6145 Å, with the strongest appearing on 5169 Å. The LIF signal is then recorded on all observed fluorescence wavelengths by scanning the laser frequency. A similar hyperfine pattern as seen in figure 7.47 is observed at all lines. From the appearance of relative intensities of the hyperfine components and the separation between them a transition with low angular momentum values of lower and upper levels is suggested. Spacing and intensity of diagonal hyperfine components is degraded towards shorter wavelength quite sharply. The resolved off-diagonal components indicate that one of the involved levels has a large splitting, meaning large value of hyperfine interaction A constant of the level.
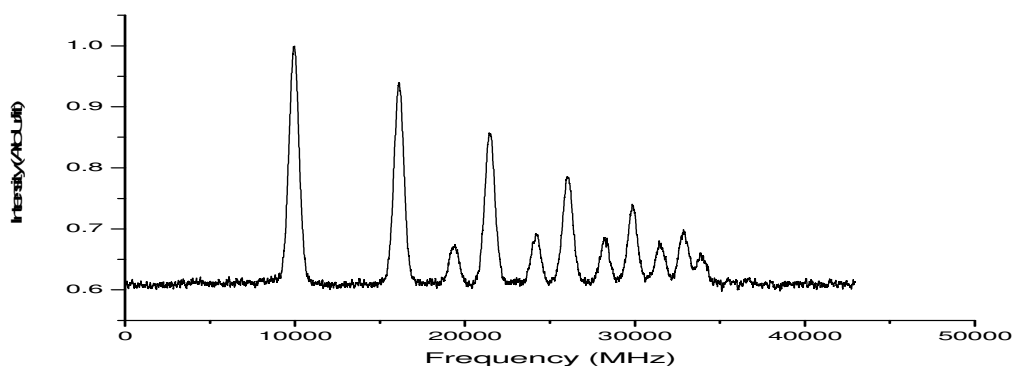
Figure 7.47: Recorded hyperfine pattern of the line at 5759.75 Å

The best fit situation of the recorded structure (see figure 7.48) is obtained on values $J_o = 7/2 - J_u = 9/2$, $A_o = 548.91$ MHz and $A_u = 1365.44$ MHz. Assuming an unknown upper level, an already known lower level is searched based on the best fit parameters. A lower level is found with level energy 11730.6 cm^{-1}, odd parity, J = 9/2 and A = 1365(5) MHz.

Assuming this as a lower level in the observed transition, the recorded structure is again fitted with A = 1365(5) MHz of the lower level being fixed.
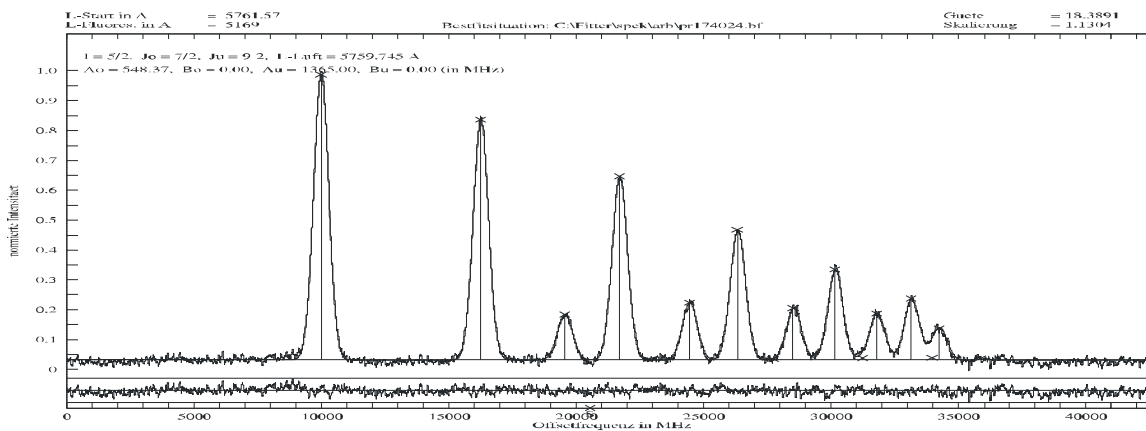
Figure 7.48: Best fit situation of line at 5759.75 Å

The energy of the proposed new upper level is found by adding the center of gravity wave number of the line i.e. 17357.065 cm^{-1} to the wave number of the lower level i.e. 11730.6 cm^{-1}. The new level is **29087.665 cm^{-1}, even parity, J = 7/2, A = 548.37 MHz.** The newly found level is introduced in the classification program which generates a transition list explaining all the observed fluorescence lines. To further consolidate the existence and energy of the newly found upper level a second laser excitation is performed at the line 5947.29 Å, which is found in the transition list of the new upper level and is identified as a transition to lower level 12277.947 cm^{-1}, odd parity, J = 7/3 and a very large hyperfine constant A = 1760(4) MHz. In FT-Spectra (see figure 7.49) this line has a good S/N ratio and its hyperfine components are partially resolved. Several other lines are also present in the close neighborhood of this line but by overlapping the line profile from FT-Spectra over the predicted hyperfine structure of the line confirms the transition.
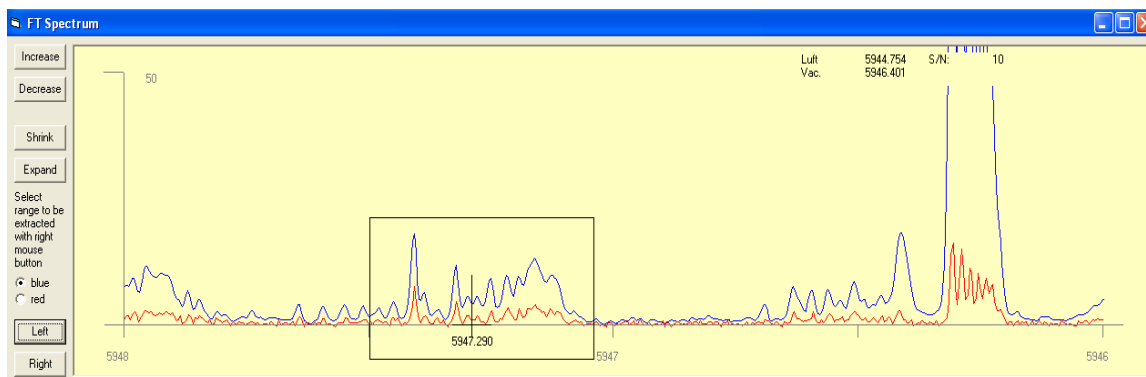
Figure 7.49: FT-Spectra of line at 5947.29 Å

LIF signal is observed on all previously found fluorescence lines and hyperfine structure as shown in figure 7.50 is recorded on 5169 Å as fluorescence wavelength.
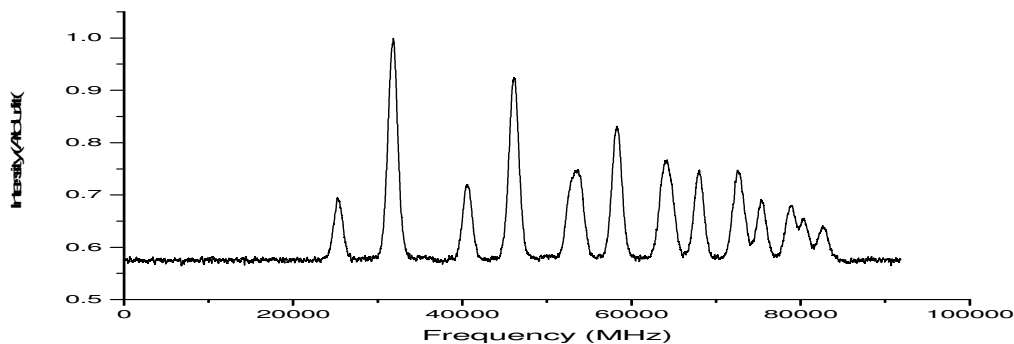
Figure 7.50: Recorded hyperfine pattern of the line at 5947.29 Å

As is clear from the recorded line profile the lower level has a very large splitting compared to the splitting of upper level and this gives it a large width. The recorded structure is in excellent agreement (see figure 7.51) with the prediction as well as with FT-Spectrum. Level energy is again computed and is improved to a value **29087.674 cm^{-1}**. Table 7.8 lists all the observed fluorescence lower levels combining with the new upper level 29087.674 cm^{-1}.
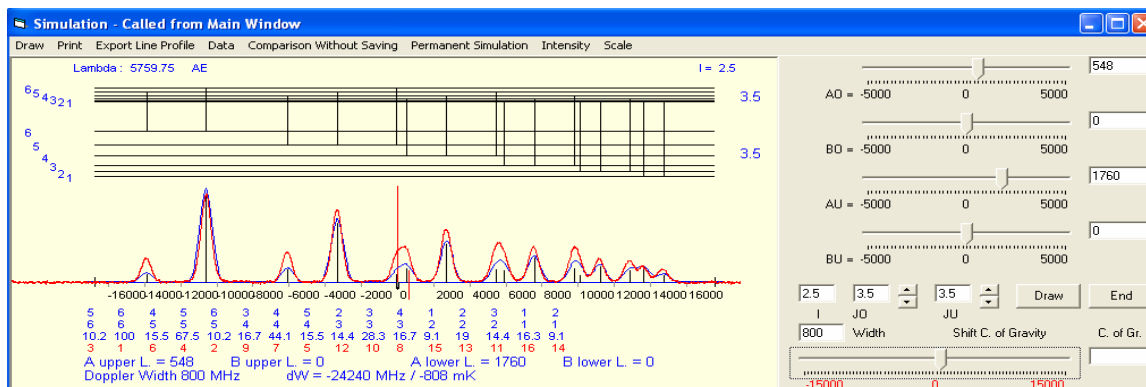
Figure 7.51: Comparison of the recorded line profile with the prediction of the line at 5947.29 Å

As seen in figure 7.51 the normal theoretical intensities (blue curve) of the off-diagonal components are lower as compared to the experimental line profile (red curve). This might be due to saturation effects (section 7.1).

Table 7.8: Fluorescence lines explained by the new Pr I level 29087.674 cm^{-1}, J = 7/2, even parity and A = 548.37 MHz.

Fluorescence Wavelength λ_{air} (Å)	Lower level				
	Energy (cm^{-1})	J	Parity	A (MHz)	B (MHz)
5168.562	9745.313	5/2	o	626.4(3)	5(3)
5507.809	10936.67	9/2	o	929.6(5)	0.3(2)
5888.049	12108.819	5/2	o	1275	-
5947.291	12277.947	7/2	o	1760(4)	-
6145.871	12821.083	9/2	o	1127(3)	-

7.2.9 Discovery of $29324.49^e_{5/2}$ level via Laser Excitation of Line 5768.17 Å

In FT-Spectra the line at 5768.17 Å appears in a blend of several lines without any clear identifiable hyperfine pattern, although S/N ratio of the lines is not so bad (see figure 7.52). Therefore for the classification of lines it is inevitable to investigate the lines by laser excitation.
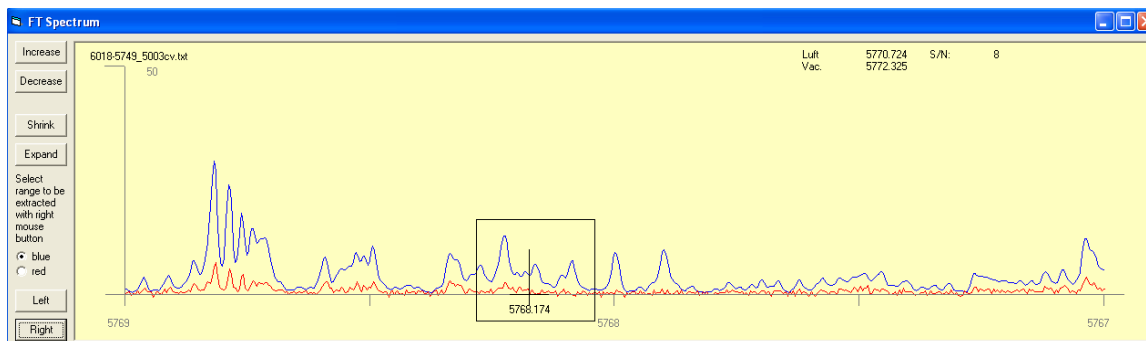
Figure 7.52: FT-Spectra of line at 5768.17 Å

At the excitation wavelength LIF signal is observed on fluorescence wavelengths 4915 Å, 5297 Å, 5578 Å, the strongest one being at 4915 Å. LIF signal was then recorded on all fluorescence wavelengths by scanning the laser frequency of course, only one of the line within the marked region in the FT-Spectra (see figure 7.52) is thus excited. Hyperfine structure recorded on all fluorescence wavelengths show similar hyperfine pattern as shown in figure 7.53. The diagonal components are not fully resolved with all off-diagonal components lying beneath them. This can be interpreted as a transition involving lower and upper levels having small splitting with the upper level more splitted as compared to the lower level. Furthermore from the spacing between few resolved diagonal components a small angular momentum values can be suggested with $\Delta J = +1$.
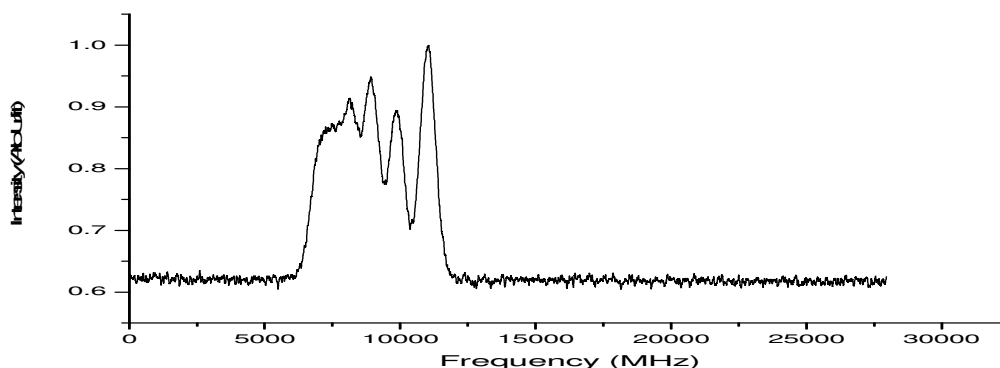
Figure 7.53: Recorded hyperfine structure of line at 5768.17 Å

None of the suggestions list for the line matches with the recorded hyperfine pattern neither in terms of shape nor in terms positions. It was conclude that a new lower/upper level is involved in the excitation of this line. With these pre-fitting assumptions the

recorded structure is fitted and a best fit is obtained for values J_o = 5/2 - J_u = 3/2, A_o = 422.85 MHz and A_u = 232.38 MHz (see figure 7.54).
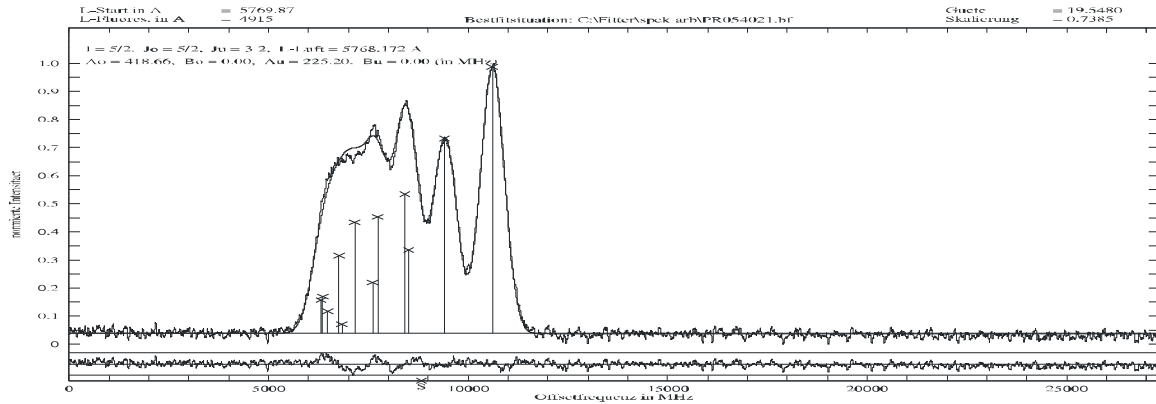
Figure 7.54: Best fit situation of the recorded hfs of the line at 5768.17 Å

Initially assuming a new upper level, a known lower level is searched in the data base of known levels. A level is found with level parameters as 11992.85 cm^{-1}, odd parity, J = 3/2 and A = 225.2 MHz. Assuming this as a lower level in the excitation of line, the recorded structure is again fitted, A = 225.2 MHz of lower level being fixed. The energy of upper level is determined by adding the center of gravity wave number of the excitation line i.e. 17331.708 cm^{-1} and lower level wave number i.e. 11992.85 cm^{-1}. This gives an upper level as **29324.558 cm^{-1}, even parity, J = 5/2 and A = 418.66 MHz.** After introducing the newly found level the transition list generated by the classification program explained all the observed fluorescence lines.

In order to confirm the existence of newly found upper level a second excitation to upper level from some other known level is performed. In the transition list of the upper level a line at 5807.051 Å shows up, which is visible in FT-Spectra and seems to have a good agreement of the pattern with the hyperfine structure predicted. So in order to confirm the upper level a laser excitation is performed at this line. LIF signal is seen on all previously observed fluorescence wavelengths and hyperfine structure is recorded on the strongest fluorescence line i.e. at 4915 Å. The comparison of the recorded line profile with the predicted hf pattern gives an excellent agreement in terms of component positions and theoretical intensities as shown in figure 7.55. This confirms the existence of the new upper level.

In contrast to first excitation to upper level the second excitation show a comparatively wide hyperfine structure. This can be interpreted by a large splitting of lower level involved in the excitation of line at 5807.051 Å, this means that the width of the structure is dictated by the level with larger splitting. Level energy is corrected to **29324.461 cm^{-1}** by FT-Spectra at the line 5578.365 Å. Table 7.9 list lower levels explained by newly found upper level for observed fluorescence lines.
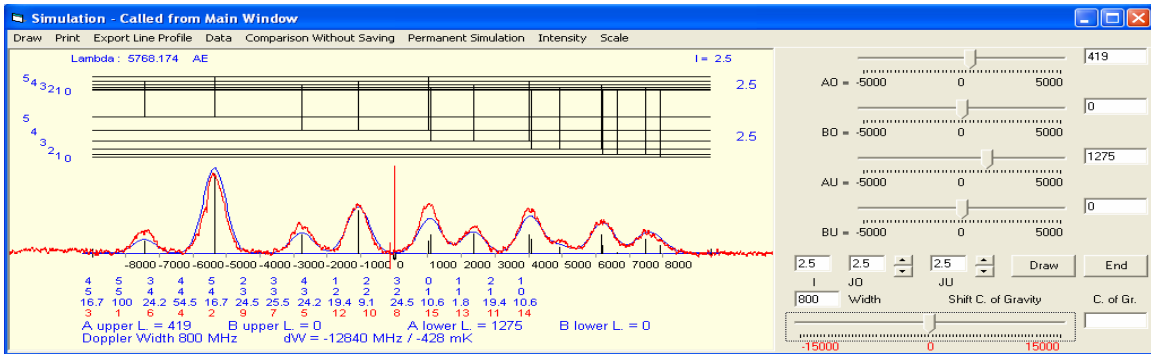
Figure 7.55: Comparison of the recorded line profile with the predicted hf pattern of line 5807.051 Å

Table 7.9: Fluorescence lines explained by the new Pr I level 29324.461 cm^{-1}, J = 5/2, even parity and A = 418(3) MHz.

Fluorescence Wavelength λ_{air} (Å)	Lower level				
	Energy (cm^{-1})	J	Parity	A (MHz)	B (MHz)
4915.521	8986.444	3/2	o	1029	-
5296.666	10449.941	7/2	o	541	-
5578.365	11403.067	7/2	o	1142	-
5807.051	12108.819	5/2	o	1275	-

7.2.10 Discovery of $\mathbf{28146.157}^{e}_{3/2}$ level via Laser Excitation of Line 6188.97 Å

The line at 6188.97 Å in FT-Spectra is an unclassified line with good S/N ratio (see figure 7.56) and could not be classified by any of the transitions listed for this line. The line profile in FT-Spectra suggests a transition involving pair of levels with low angular momentum values. In any case a laser excitation of the line is performed by tuning the laser wavelength to the highest peak and searching for fluorescence wavelengths.
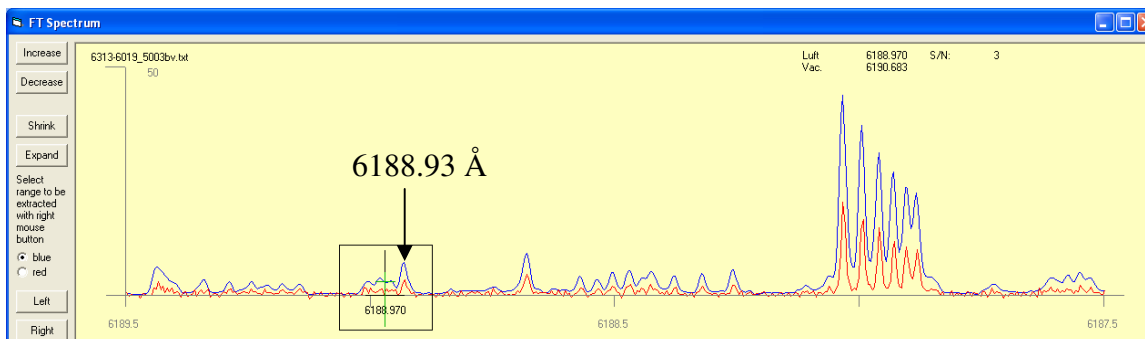
Figure 7.56: FT-Spectra of the line at 6188.97 Å

At the excitation wavelength 6188.93 Å two fluorescence wavelengths were observed 5217 Å, 5880 Å. LIF signal is then recorded on both fluorescence wavelengths by scanning the laser frequency. The strongest LIF signal is seen on 5217 Å. The recorded line profile reveals a similar shape as seen in FT-Spectra, see figure 7.57. Since none of the listed transition for line matches in terms of position or shape it is quite evident that either both or one of the levels involved in the excitation is new.
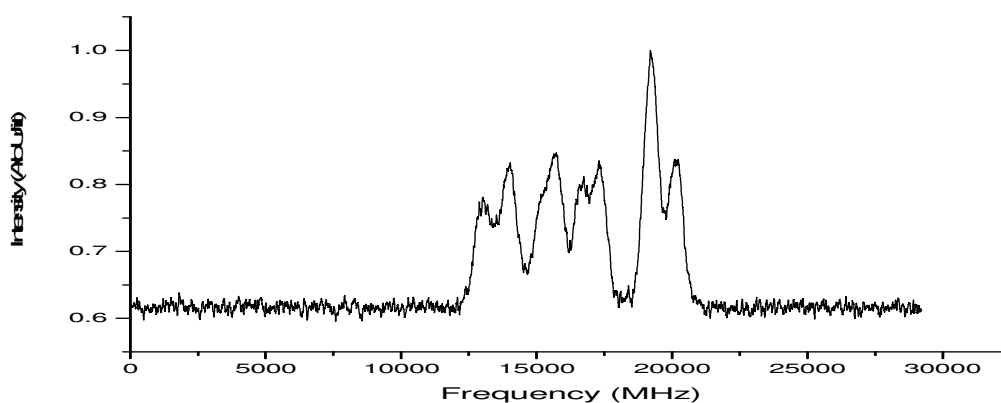
Figure 7.57: Recorded hyperfine structure of the line at 6188.97 Å

After careful inspection of the recorded line profile one can guess a transition involving low angular momentum values possibly $J_o = 3/2$ - $J_u = 3/2$, since the diagonal components appear to be less in number and the off-diagonal components are distributed around diagonal components. The recorded structure is fitted and a best fit (see figure 7.58)

situation is observed with values $J_o = 3/2 - J_u = 3/2$, $A_o = 872.93$ MHz and $A_u = 227.99$ MHz.
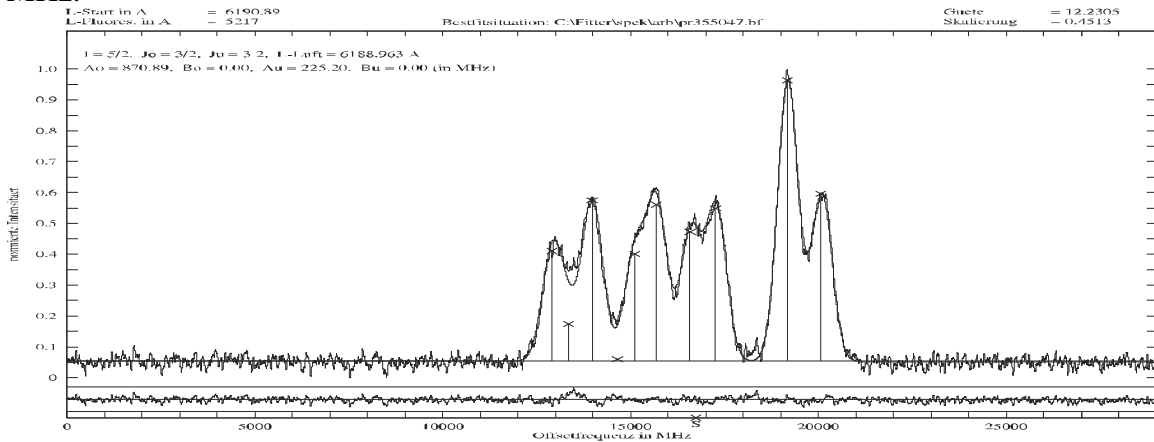
Figure 7.58: Best fit of line at 6188.97 Å

The best fit values indicate that for both lower and upper levels $J = 3/2$. In this case $J < I$ is valid which means the fine structure levels are splitted into $2J + 1$ hyperfine structure levels, i.e. 4 hfs sublevels for both upper and lower levels with quantum numbers $F = 4$, 3, 2, 1 ($|J + I|$ to $|J - I|$). The diagonal components are due to transitions between F-levels with $\Delta F = 0$ and off-diagonal components are due to $\Delta F = \pm 1$. This can be seen in figure 7.59 which also show the comparison between recorded line profile and simulation, using the hyperfine structure constants determined by the fit and theoretical intensity ratios.
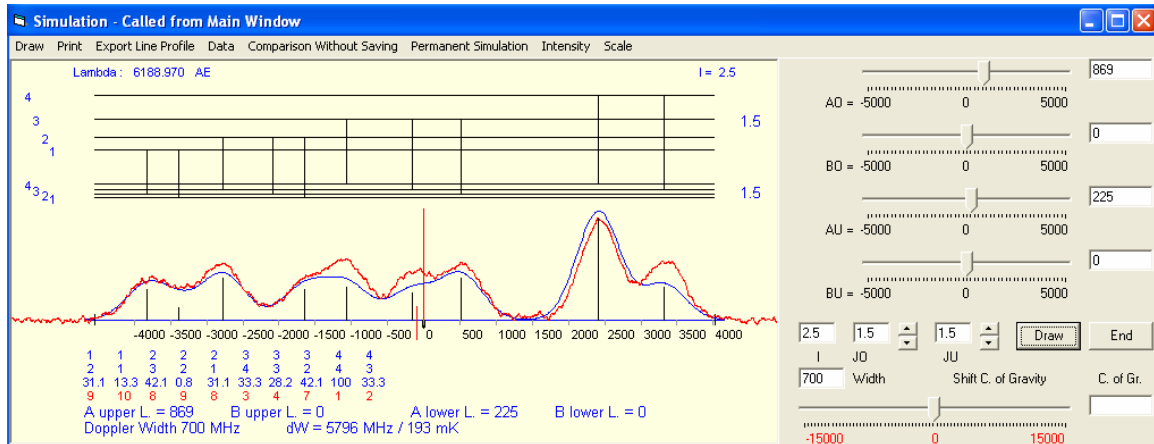
Figure 7.59: Comparison of recorded line profile at 6188.97 Å with simulation of transition

Assuming that an unknown upper level is involved in the excitation of this line a known lower level with suitable J and A is searched in the data base. A level with energy 11992.85 cm^{-1}, odd parity, $J = 3/2$ and $A = 225.2$ MHz is found. Assuming this as the lower level of excitation, the recorded structure is again fitted with A constant of lower level as 225.2 MHz being fixed. The energy of the upper level is determined using the center of gravity wave number of excitation line and wave number of lower level. The

246

energy of new level determined is **28146.157 cm⁻¹, even parity, J = 3/2 and A = 869.10 MHz.** The level is introduced into our level data base and a transition list is generated by classification program which explained all the observed fluorescence lines. The newly found upper level is then confirmed by second laser excitation at the line 5879.15 Å present in the transition list of upper level. The recorded structure for second excitation is in good agreement in terms of shape and positions of hfs components with the predicted pattern as shown in figure 7.60. Table 7.10 list lower levels for observed fluorescence lines explained by the newly found upper level.
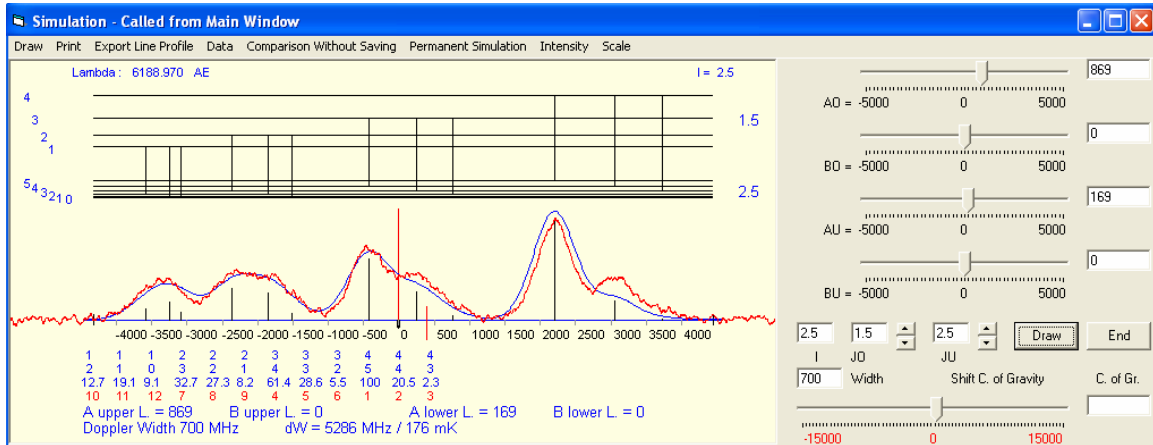
Figure 7.60: Comparison of the recorded line of at 5879.15 Å with predicted hyperfine structure of the line

Table 7.10: Fluorescence lines explained by the new Pr I level 28146.157 cm⁻¹, J = 3/2, even parity and A = 869.10 MHz

Fluorescence Wavelength λ_{air} (Å)	Lower level				
	Energy (cm⁻¹)	J	Parity	A (MHz)	B (MHz)
5217.832	8986.444	3/2	o	1029	-
5879.14	11141.581	5/2	o	169(2)	-

7.2.11 Discovery of $28455.478^e_{1/2}$ level via Laser Excitation of Line 6072.68 Å

A new level with energy 28455.478 cm^{-1} having a very low angular momentum quantum number was discovered while attempting to classify a line at 6072.756 Å using an already known level. The line at 6072.756 Å has good resolved structure was easily classified. While searching for fluorescence wavelengths from already known upper level belonging to this line, a fluorescence wavelength 5134 Å was observed when exciting at a wavelength just under 5th diagonal component of the already known transition i.e. at 6072.68 Å (see figure 7.61).
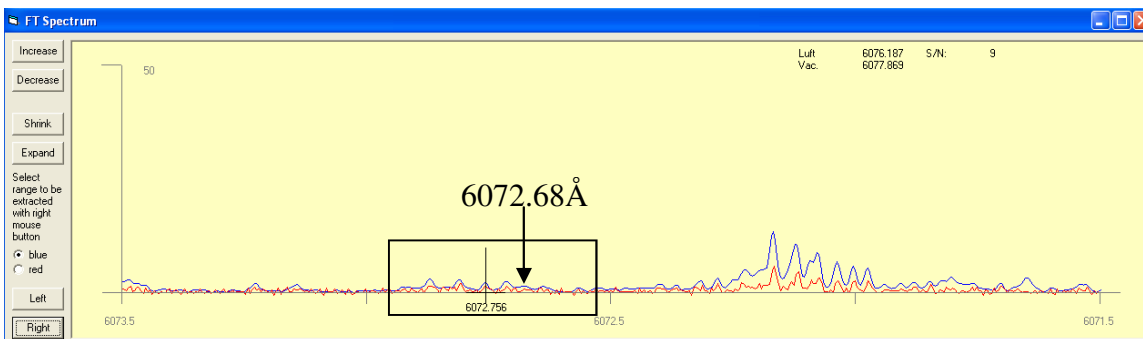
Figure 7.61: FT-Spectra of line at 6072.68 Å

LIF signal is recorded at fluorescence wavelength 5134 Å by scanning the laser frequency as shown in figure 7.62. In order to be certain that while recording the hyperfine structure there are no mode hops three times the LIF signal at the same fluorescence wavelength was recorded.
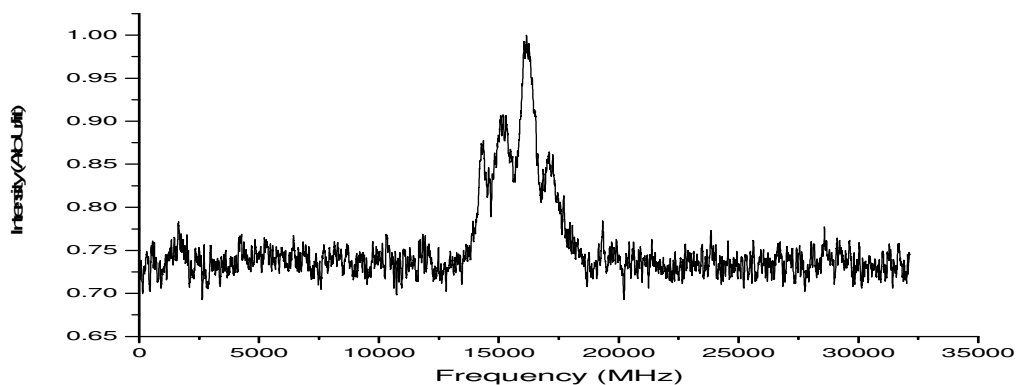
Figure 7.62: Recorded hyperfine structure of line at 6072.68 Å

Although the S/N ratio of the recorded structure is not so good, the structure was considered to be a transition between a pair of levels with very low angular momenta. One can fit the structure after trying different pairs of J-values. The recorded structure is

fitted with best fit is obtained for values $J_o = 1/2 - J_u = 3/2$, $A_o = 929.70$ MHz and $A_u = 227.50$ MHz (see figure 7.63).
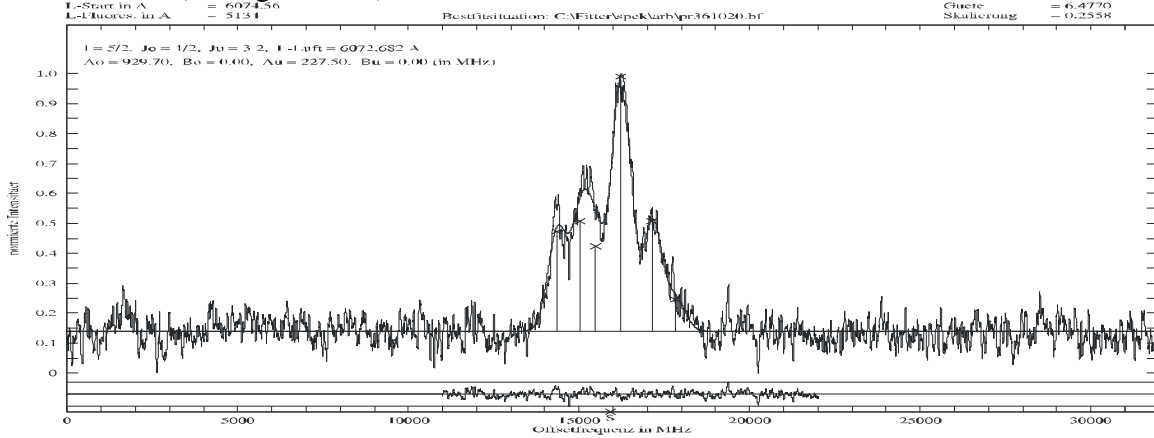
Figure 7.63: Best fit situation of recorded hyperfine structure of line 6072.68 Å

Best fit values indicates again a situation where $J < I$ with upper fine structure level splitted into 2 hfs sublevels and lower fine structure level into 4 hfs sublevels i.e. ($J_o + 1/2$) $F_o = 3, 2$ and ($J_u + 3/2$) $F_u = 4, 3, 2, 1$. Diagonal components are due to transitions for which $\Delta F = -1$ (3 – 4 and 2 – 3) whereas off-diagonal components are due to transitions for which $\Delta F = 0, +1$. This can be seen in figure 7.64 which shows the comparison between recorded line profile and simulation using the hyperfine structure constants determined by the fit and theoretical intensity ratios.
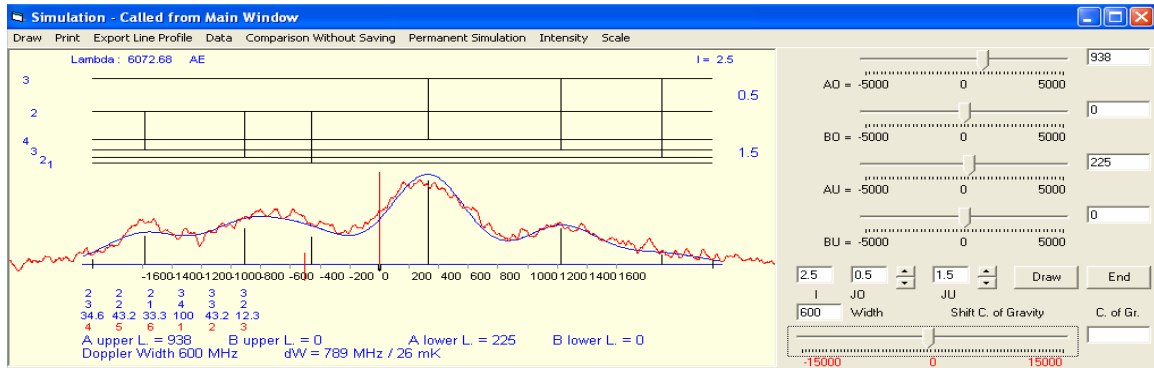
Figure 7.64: Hyperfine structure of the line at 6072.68 Å showing also hfs energy levels

Assuming an unknown upper level in the excitation of the line, a lower level with determined J and A values is searched in the data base of known levels. A lower level with energy 11992.85 cm^{-1}, odd parity, J = 3/2 and A = 225.2 MHz is found. Recorded structure is again fitted keeping A-value of the lower level being fixed. The energy of the upper level is determined which comes out to be **28455.478 cm^{-1}, even party, J = 1/2 and A = 938.31 MHz.** Newly found level is introduced in the data base and a transition list is generated by classification program which explained the observed fluorescence line at 5134 Å as seen in the comparison between predicted hyperfine structure and FT-Spectrum of the line (see figure 7.65). At this line the combination is

28455.478 cm^{-1}, e, J = 1/2, A = 938.31 MHz - 8986.444 cm^{-1}, o, J = 3/2, A = 1029MHz

This confirms the existence of new upper level with quite low angular momentum. The experimental confirmation can be done by laser excitation of line at 5134.947 Å which at present is not possible.
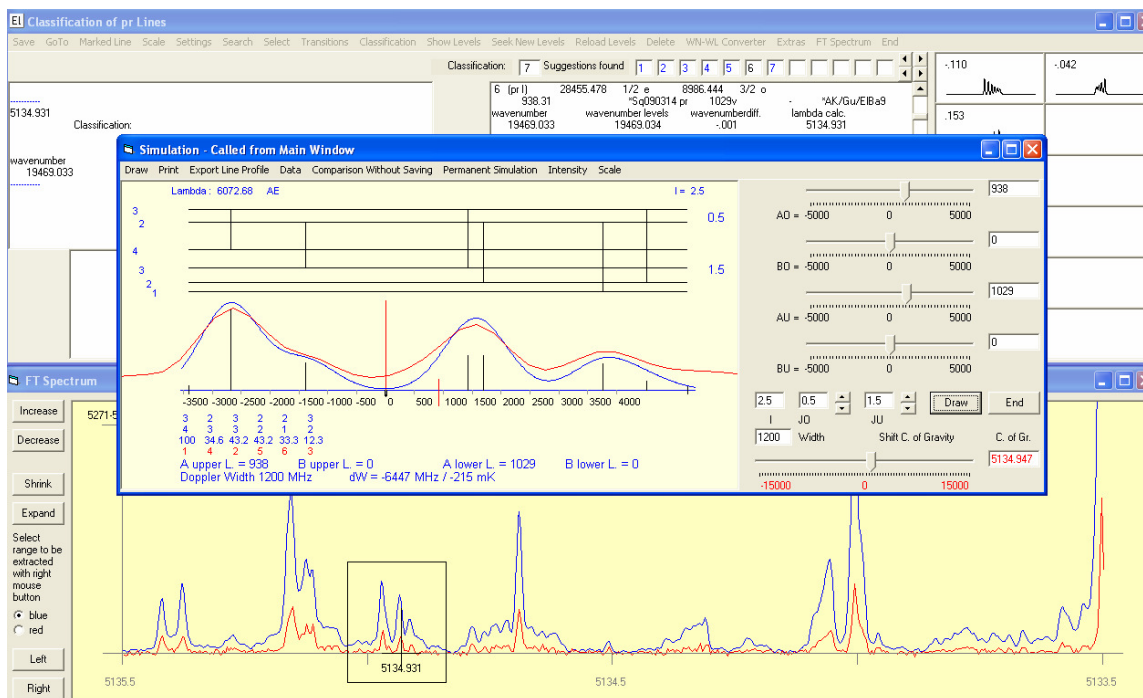
Figure 7.65: Comparison of line at 5134 Å in FT-Spectra with theoretically predicted hyperfine structure

7.2.12 Blend Situation and Discovery of New Pr-I levels $33870.18^e_{13/2}$ and $14821.55^e_{11/2}$

As remarked earlier that due to high line density in praseodymium blend situations are quite common and are often observed while investigating its spectra. One such situation was observed while investigating the spectral region 5695.96 Å to 5695.42 Å i.e. the scan width of our laser. The blend situation observed is the result of convolution of two hyperfine structures recorded on same fluorescence wavelength. FT-Spectra in the spectral region from 5695.96 Å to 5695.42 Å is shown in figure 7.66.
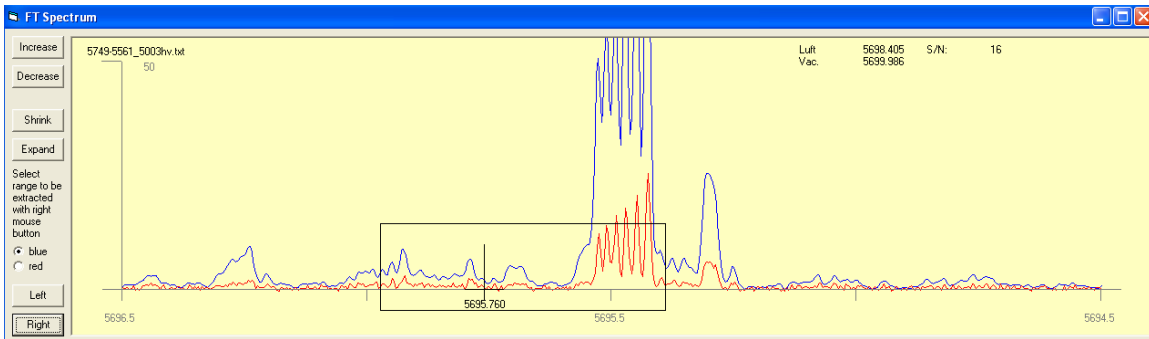
Figure 7.66: FT-Spectra in the region 5695.96 Å to 5695.42 Å

In an attempt to classify the line at 5695.69 Å the laser wavelength is tuned to this value and fluorescence signals were search by scanning the monochromator. At the excitation wavelength 5695.67 Å very strong LIF signals were observed on 6 fluorescence wavelengths i.e. 3223 Å, 4749 Å, 4846 Å, 4905 Å, 5595 Å and 5977 Å. In order to ascertain that fluorescence lines observed belong to one or more upper levels, the recording of hyperfine structure on all observed fluorescence wavelengths is required. Since 3223 Å lies in UV, therefore a structure with good S/N ratio is expected. Therefore LIF signal at this fluorescence wavelength is recorded (see figure 7.67) while scanning the laser wavelength starting from 5695.99 Å.
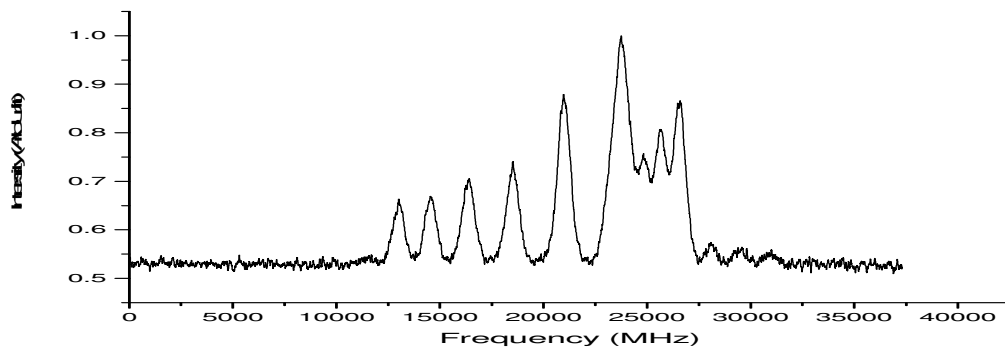
Figure 7.67: Blend situation observed in laser excitation scan range 5695.96 Å to 5695.42 Å, while detecting the LIF signal at 3223 Å

251

One of the structures is clearly seen at higher frequency side and other lying on the lower side with their respective hyperfine components merged together. Interpretation of such a situation can be done in a number of ways. Within the scan width of the laser either a single upper level is excited from two very closely lying lower levels or two independent pairs of levels are excited, and by accident both upper levels at nearly the same fluorescence wavelength. In order to separate the two structures, one need to search fluorescence wavelengths which are specific to one or the other upper level. This can be done by tuning the laser to an excitation wavelength of one of the peaks of one structure which does not mix with the other structure. Fluorescence wavelengths at excitation wavelength 5695.67 Å, which is the strongest diagonal component of structure lying on higher frequency side have already been searched and found. Therefore the laser is now tuned to an excitation wavelength 5695.77 Å which is the position of third strongest diagonal component of the structure appearing at the lower frequency side and LIF signal is searched by scanning the monochromator. Unfortunately the only fluorescence wavelength which could be observed for this structure was already observed i.e. 3223 Å. The reason may be that the upper level involved in this structure has either only two decay channels i.e. to the same lower level and to a very low lying lower level or it may have fluorescence channels lying close to the laser wavelength which is unidentifiable, or in IR region where our monochromator is insensitive.

In any case the LIF signal is recorded on all previously observed fluorescence wavelengths by scanning the laser frequency. On fluorescence channels 4749 Å, 4846 Å, 4905 Å, 5595 Å and 5977 Å the structure at higher frequency side is completely separated from the other structure with strongest signal observed at 4905 Å as shown in figure 7.68.
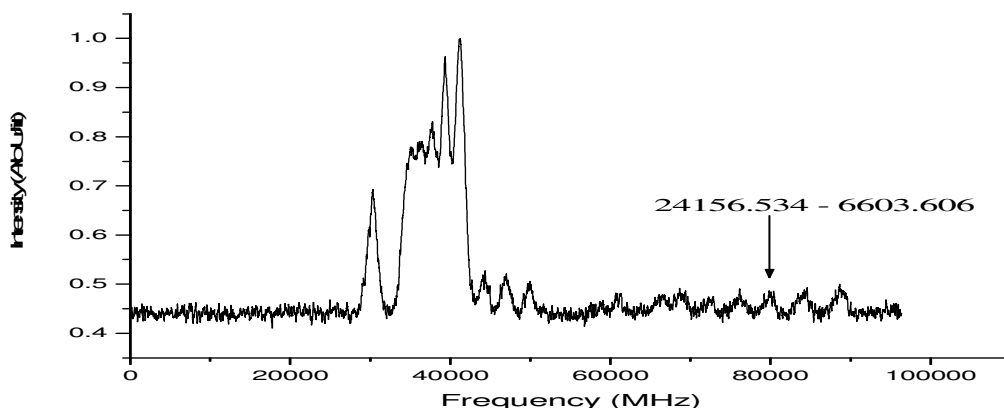
Figure 7.68: Recorded hyperfine structure of the line with start wavelength 5695.99 Å at fluorescence wavelength 4905 Å

The structure appearing on the higher frequency side in figure 7.68 is identified as a known transition between $24156.534^{o}_{15/2} - 6603.606^{e}_{13/2}$, which lie in the scan width of the laser and has a center of gravity wavelength 5695.473 Å. This was further confirmed by recording its LIF signal at fluorescence wavelengths 3223 Å and 5045 Å and scanning the laser wavelength from 5695.70 Å. Although these fluorescence wavelengths do not exist in the transition list of the upper level so they can be explained as indirect

fluorescence in the form of collisional coupling i.e. excited upper level releases its energy by colliding with another atom in the ensemble.

The recorded hyperfine structure in figure 7.68 is fitted and a best fit (see figure 7.69) is obtained at values $J_o = 11/2 - J_u = 11/2$, $A_o = 649.90$ MHz, $A_u = 536.97$ MHz.
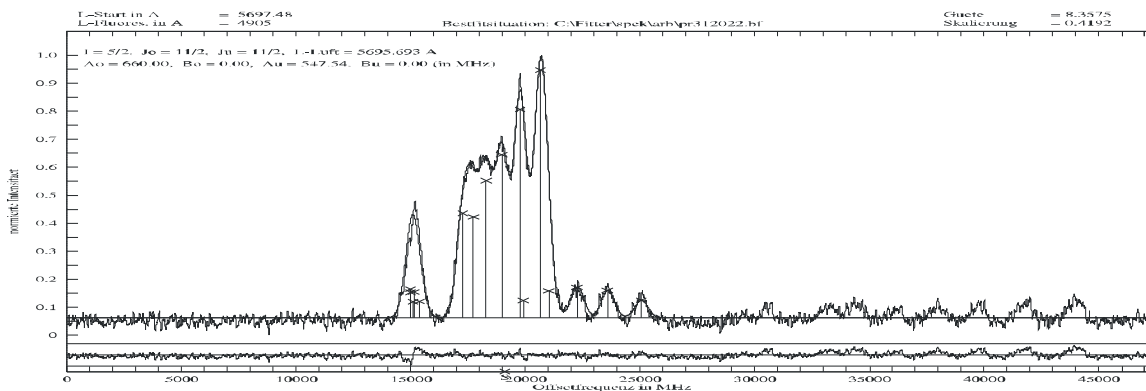
Figure 7.69: Best fit situation of line excited at 5695.69 Å

In order to identify the transition, as usual it is first assumed that the upper level is unknown and a known lower level is searched in the data base of known levels based on fitting parameters. The lower levels with suitable A and J values did lead to calculated upper levels which did not explain any of the fluorescence wavelengths. In the next step, assuming a known upper level, this level is searched based on best fit values. An upper level 32373.82 cm^{-1}, even parity, J = 11/2 and A = 660 MHz was found which explained all the observed fluorescence wavelengths. This implies that a new lower level is involved in the excitation of this line at 5695.69 Å. Recorded structure is again fitted now keeping A value of upper level being fixed, this gives $A_u = 547.54$ MHz. Now the lower level is determined by subtracting the center of gravity wave number 17552.256 cm^{-1} of the line from the energy of the upper level. So the new lower level is **14821.551 cm^{-1}, odd parity, J = 11/2 and A = 547.54 MHz.** Introducing the new level in the classification program a transition list is generated. In order to confirm the newly found lower level a second excitation from the lower level to a known upper level is performed.

In order to separate the structure at the lower frequency side the width of entrance and exit slit of the monochromator is reduced and adjusting fluorescence wavelength as good as possible by tuning the laser frequency to one of the peaks which is not mixing with the other structure. The line is then again excited by scanning the laser wavelength starting at 5695.96 Å and recording its hyperfine structure at fluorescence wavelength 3223 Å. Now the recorded structure is almost separated but recorded with decreased intensity and thus lower S/N ratio (see figure 7.70). Recorded structure is fitted (figure 7.71) with values $J_o = 13/2 - J_u = 13/2$, $A_o = 587.55$ MHz and $A_u = 277.81$ MHz. In the usual manner a known lower level is searched using best fit values which resulted in a lower level 16318.145 cm^{-1}, odd parity, J = 13/2 and A = 280.8(8) MHz. Recorded structure is again fitted by keeping fix the A value of lower level. Assumed new level is **33870.18 cm^{-1}, even parity, J = 13/2 and A = 590.48 MHz** which is determined by center of gravity wave

number of line and energy of the known lower level. After introducing a transition list is generated by classification which explained the single observed fluorescence line.
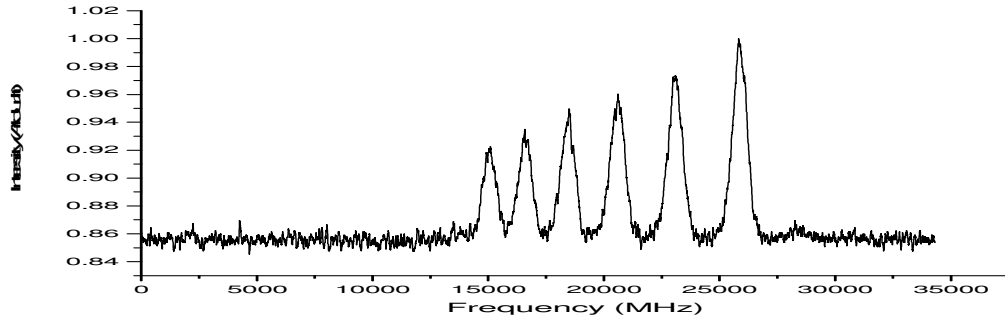
Figure 7.70: Recorded hyperfine structure of the line at 5695.77 Å
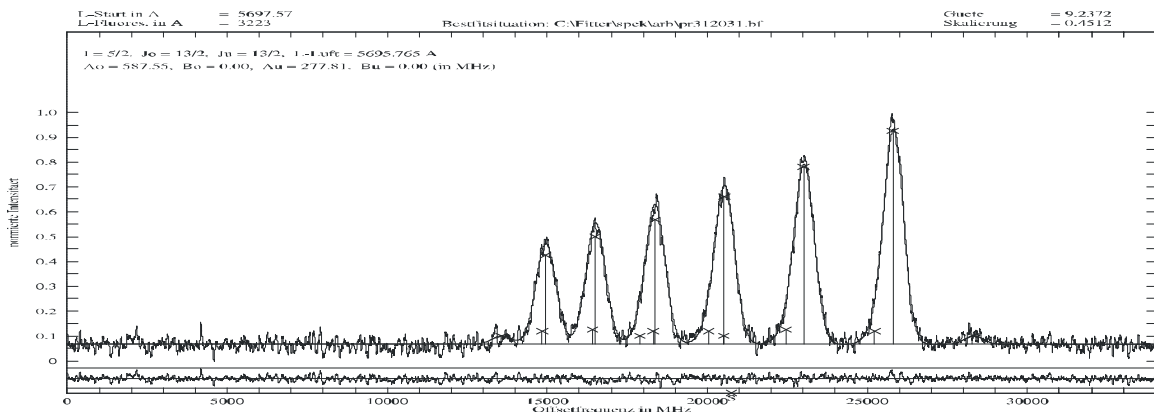
Figure 7.71: Best fit situation of line recorded at 5695.77 Å

The newly found upper level $33870.18^{e}_{13/2}$ is confirmed by further two excitations, one at the line 5770.99 Å and the other at 5651.36 Å, with improvement in the value of the hyperfine constant i.e. A = 593.6 MHz. The comparison of the recorded hyperfine patterns of lines with predicted patterns gave satisfactory result as shown in figures 7.72 and 7.73.
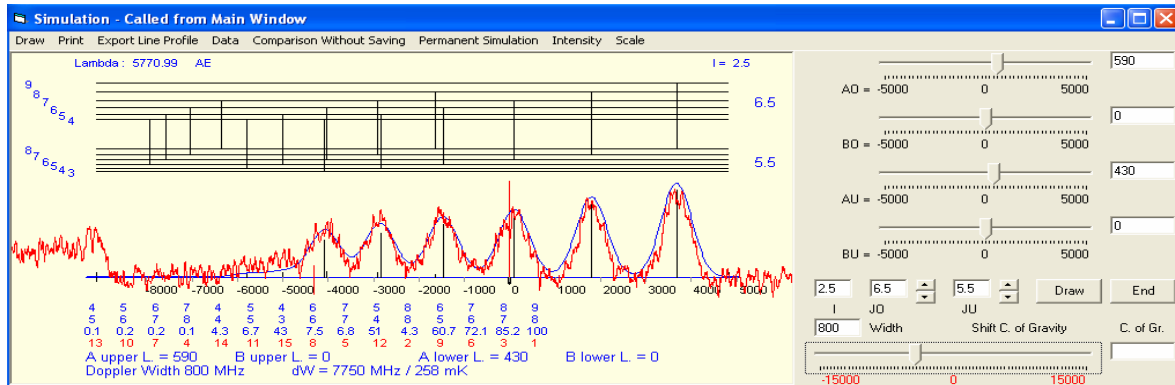
Figure 7.72: Comparison of recorded line profile with predicted pattern at 5770.99 Å
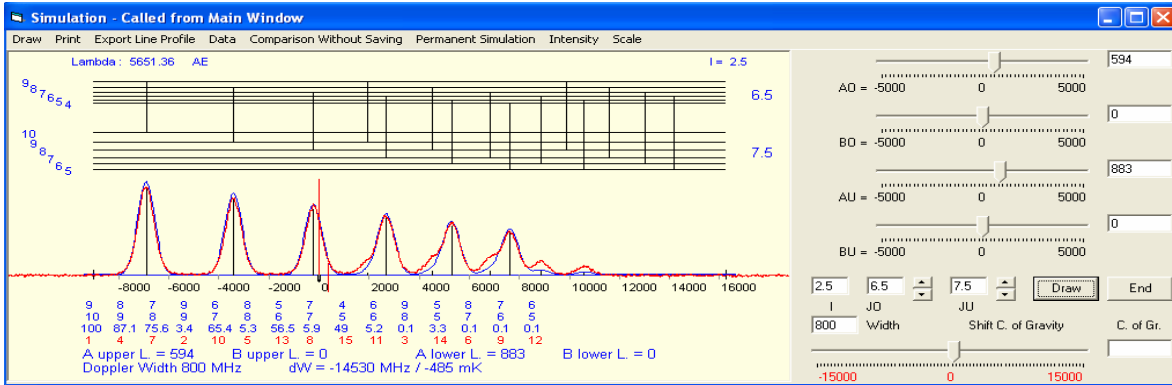
Figure 7.73: Comparison of recorded line profile with predicted pattern at 5651.36 Å

The lower level $\mathbf{14821.551^o_{11/2}}$ was confirmed at three other lines 6160.52 Å, 5998.465 Å and 5807.95 Å corresponding to three already confirmed known upper levels (see figures 7.74, 7.75 and 7.76). Table 7.11 list the combining upper levels with 14821.551 cm^{-1}.
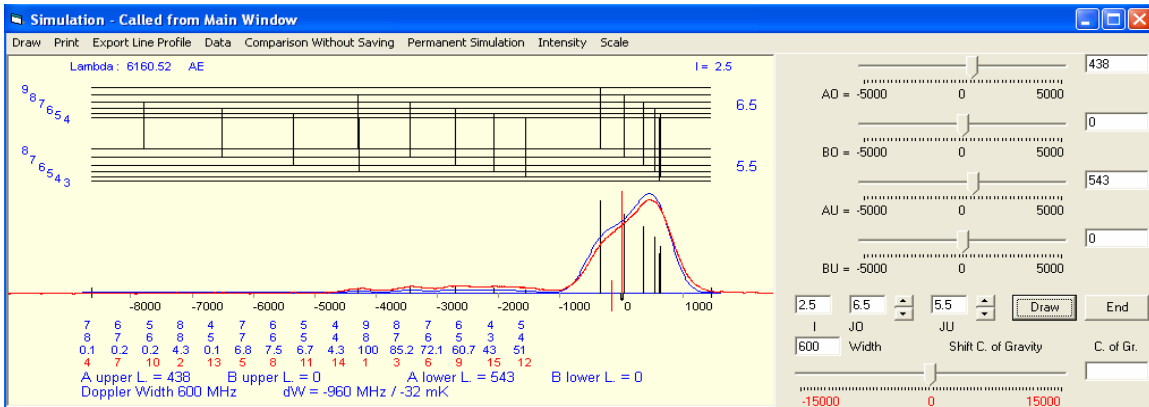
Figure 7.74: Comparison of recorded line profile with the predicted pattern at 6160.52 Å
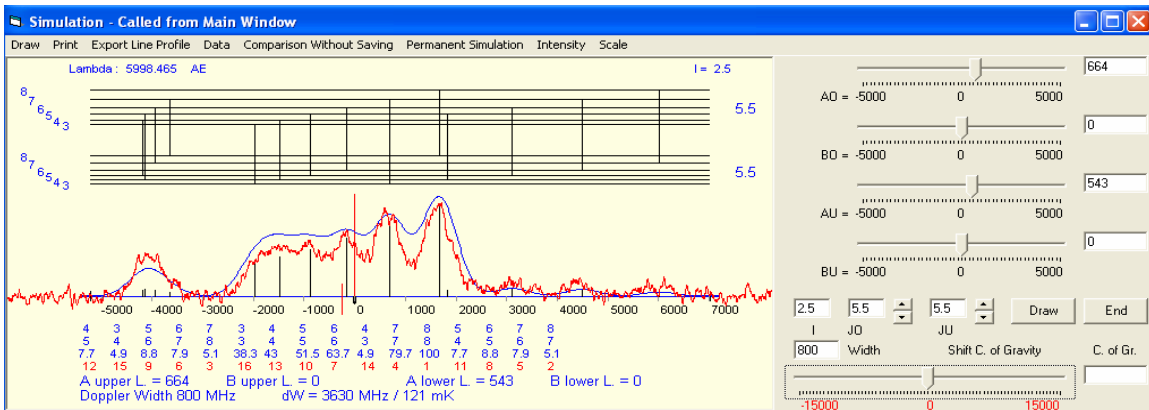
Figure 7.75: Comparison of recorded line profile with the predicted pattern at 5998.465 Å
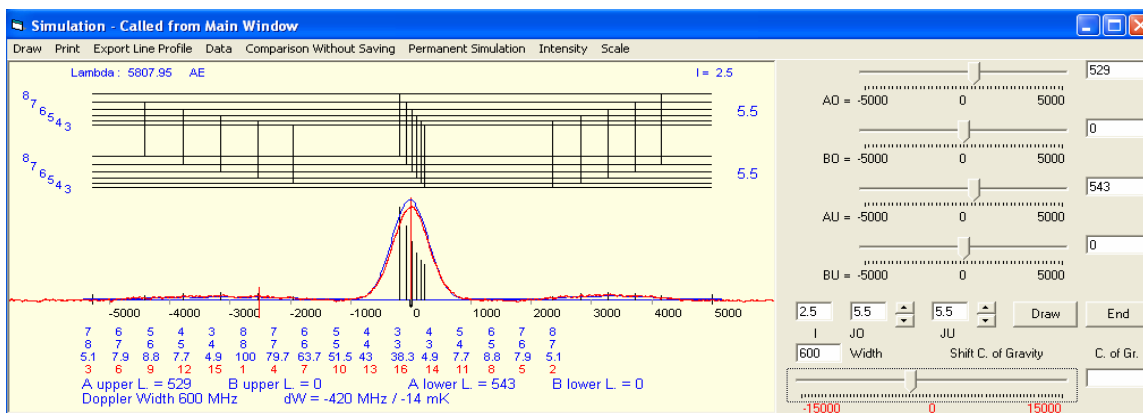
Figure 7.76: Comparison of recorded line profile with the predicted pattern at 5807.95 Å

Table 7.11: List of upper levels combining with Pr I lower level 14821.551 cm^{-1}, J = 11/2, odd parity and A = 547.54 MHz

Excitation wavelength λ_{air} Å	Upper Level					
	Energy (cm^{-1})	J	Parity	A (MHz)	B (MHz)	Fluorescence Wavelengths λ_{air} (Å)
6160.52	31049.456	13/2	e	438.18	-	3370, 5198, 5247, 5310, 5717.97, 6044.55
5998.465	31487.868	11/2	e	664	-	5896.87, 5514.99
5807.95	32034.687	11/2	e	529.31	-	3261, 4827, 4988, 5258, 5776.82, 5875.00

It is interesting to note in this example that both excitation and fluorescence blend situations are observed. At the lines 5695.69 Å and 5695.77 Å two pairs of lower and upper levels are combining and both the upper levels 32373.82 cm^{-1} and 33870.18 cm^{-1} have a common fluorescence line which decay to a level 1376.605 cm^{-1}. The level scheme is shown in figure 7.77.
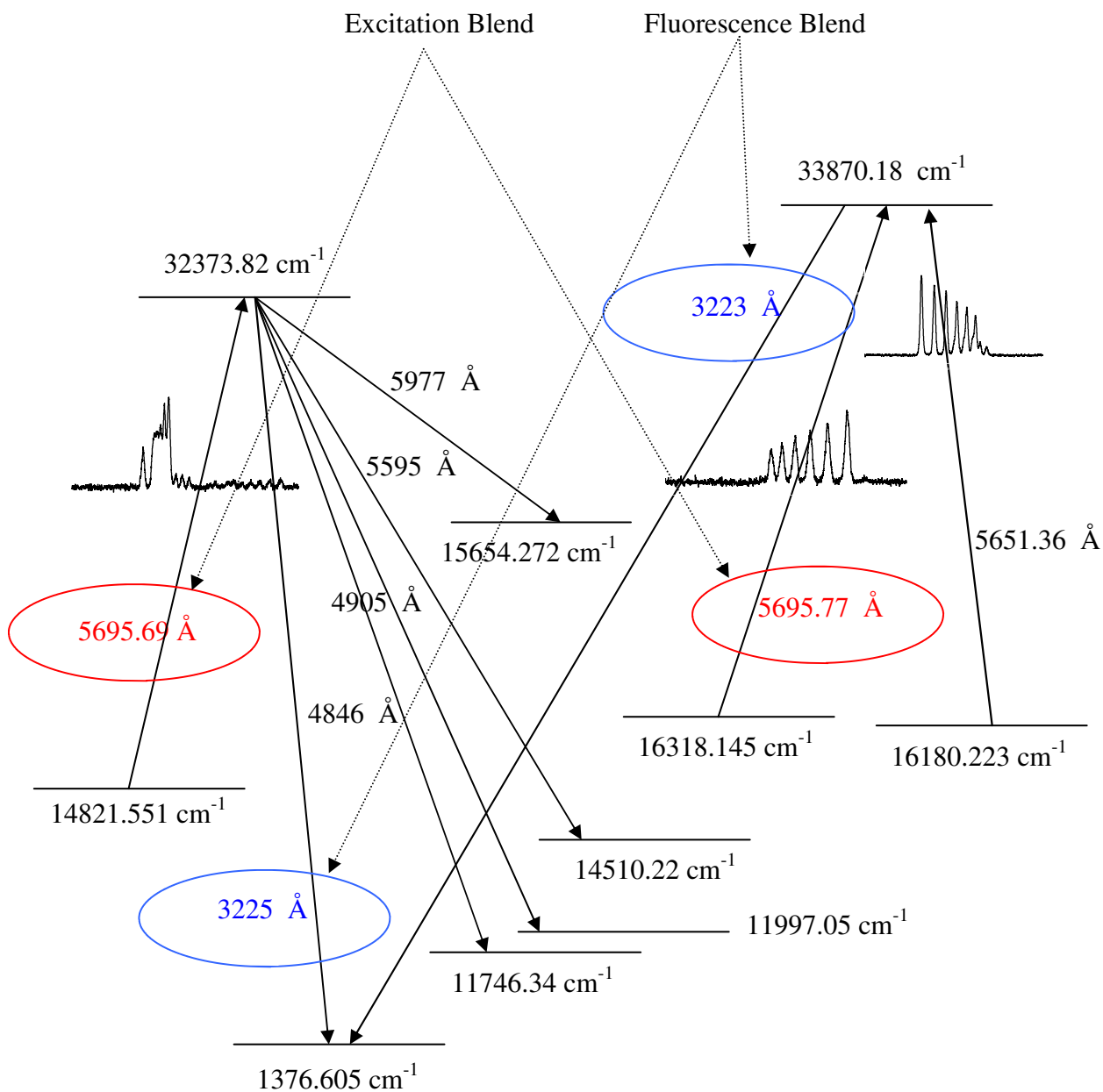
Figure 7.77: Level scheme for lines at 5695.69 Å and 5695.77 Å, showing excitation and fluorescence blend situation.

7.2.13 Discovery of Pr-II Energy Levels 12431.442_4^o and 29901.18_5^e

The region around 5722.61 Å in FT-Spectra (see figure 7.78) has a good S/N ratio and appears to be a blend containing more than one line. In order to identify all the involved transitions laser excitation must be performed by tuning laser frequency to each of the components appearing the FT-Spectra and searching for fluorescence channels.
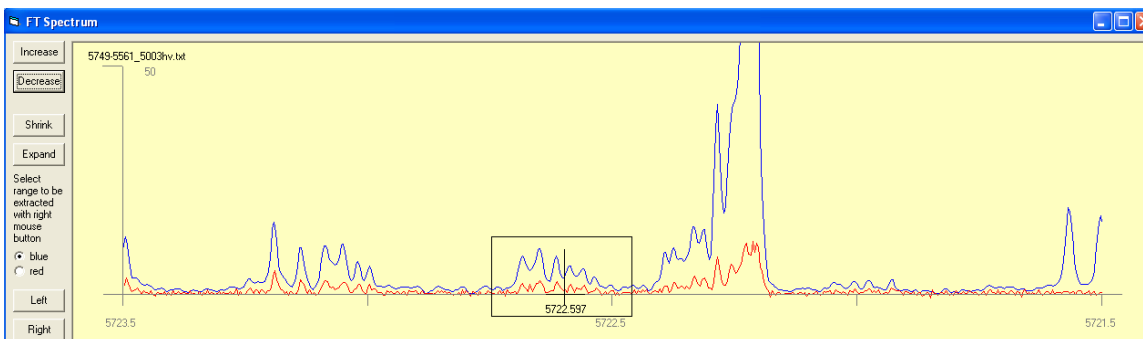
Figure 7.78: FT-Spectra of the line at 5722.59 Å

Laser wavelength is set to a value 5722.55 and for LIF signal fluorescence channels are searched by tuning the transmission wavelength of the monochromator. A number of fluorescence channels were found. At each channel the excited transitions are then recorded by scanning the laser frequency. Comparing all the recorded transitions with the suggestions listed in classification program enabled almost all to be identified as belonging to already known transitions, except the transition recorded at fluorescence channel 3773 Å. Since the decay channels lies in the UV therefore the recorded hyperfine structure has exceptionally good S/N ratio, see figure 7.79. No other fluorescence channel could be observed having a similar hyperfine structure.
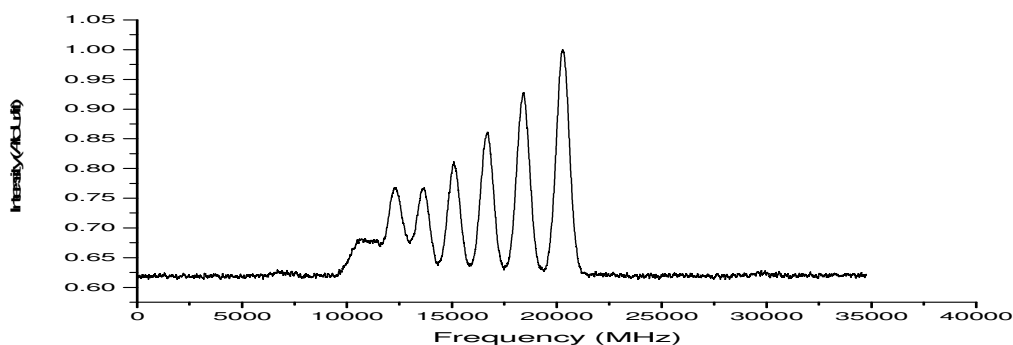
Figure 7.79: Hyperfine structure recorded at excitation line 5722.61 Å

Recorded structure suggest a transition between two levels with $\Delta J = +1$ and $A_o > A_u$. Therefore taking into account this interpretation the recorded structure is fitted using different combinations of J and A values and a best fit (see figure 7.80) is obtained on

ionic J values i.e. $J_o = 5 - J_u = 4$, $A_o = 1002.92$ MHz and $A_u = 863.63$ MHz with a quality factor of 31.
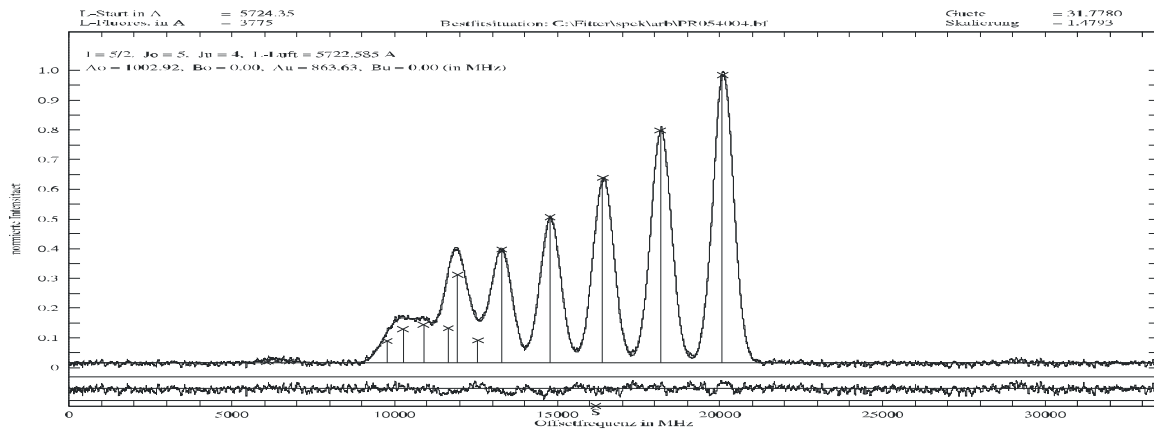
Figure 7.80: Best fit of the line recorded at 5722.61 Å

Assuming an unknown upper level, a lower ionic level is searched with comparable J and A values but none such lower ionic level was found. Now in the reverse order i.e. assuming an unknown lower level, an upper ionic level is searched. Unfortunately, again none of the levels matched the fitted criteria. After further analysis by using neutral atom J values, which did not give good fitting quality factors, it was concluded that both the lower and upper levels in the excited ionic transition are unknown. Fluorescence information might be helpful in situations like these, although it would be much more beneficial if more than one fluorescence channels were observed. In any case, the exact fluorescence wavelength is measured i.e. 3772.65 Å and a line is inserted in the classification program having this value of wavelength. The nearest prominent hyperfine pattern (see figure 7.81) appears in FT-Spectra at roughly center of gravity wavelength 3772.80 Å. It is assumed that this is the observed fluorescence line. Now using classification program the line profile at 3772.80 Å from FT-Spectra is simulated using J and A values of upper level as determined by the fit of the recorded line at 5722.61 Å, i.e. $J_o = 5$ and $A_o = 1002.92$ MHz and only varying the A value for lower level with $J_u = 4$ and 6.
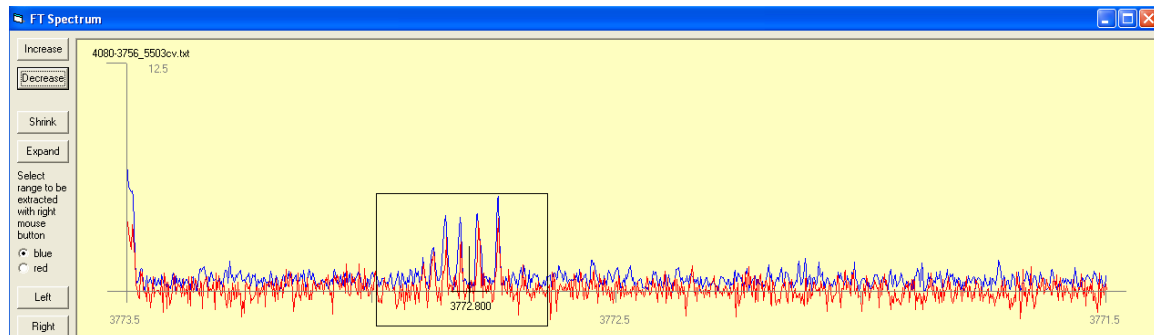
Figure 7.81: FT-Spectra of line at 3772.80 Å

The best simulation result is obtained on values $J_o = 5$ - $J_u = 6$, $A_o = 1003$ MHz and $A_u = -140$ MHz as shown in figure 7.82 below.
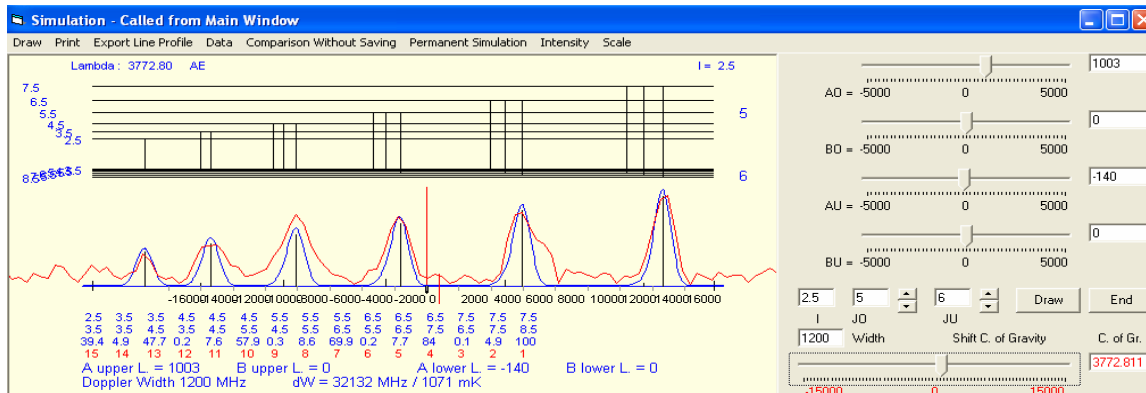
Figure 7.82: Simulation of line profile from FT-Spectra at 3772.80 Å

With the assumption that upper level is unknown in the transition at the line 3772.80 Å, a known very low lying ionic lower level is found in the data base of energy levels i.e. 3403.21 cm^{-1}, odd parity, J = 6 and A = -140.2 MHz. Assuming this level as combining with the unknown upper level, the energy of upper level is determined by adding the rough estimated center of gravity wave number from FT-Spectra and the energy of the probable lower level. The probable new upper level **29901.18 cm^{-1}, even parity, J = 5 and A = 1003 MHz** is inserted in the data base and a transition list is generated by the classification program but no other line except 3772.80 Å appear to be explained from FT-Spectra**.** Nevertheless, the lower level in the excited transition of the line 5722.61 Å is determined by subtracting the center of gravity wave number calculated by the fitter program from the energy of the probable new upper level which gives a new lower level i.e. **12431.442 cm^{-1}, odd parity, J = 4 and A = 860.73 MHz** which is also inserted in the classification program. In order to confirm the existence of these levels further excitations to/from these newly found levels is required.

In an attempt to confirm the lower level a line present in its transition list i.e. 5908.69 Å in FT-Spectra is excited. This line is explained as a transition from newly found lower level to already known level **29350.99 cm^{-1}, even parity, $J_o = 5$ and $A_o = $ 490.6 MHz** which was determined by A. Ginibre [20]. Laser is tuned to the excitation wavelength 5908.70 Å i.e. the position of highest hfs component and a strong LIF signal is observed when the monochromator is tuned to 3852 Å which is the strongest fluorescence line from the upper level. Hyperfine structure is then recorded by scanning the laser frequency. An excellent fit with a quality factor of 41 is obtained of the recorded hyperfine structure based on previous J and A values. Another excitation from lower level is performed at 6687.52 Å. Again good fit quality is obtained for the recorded hyperfine structure with a small improvement in the A constant of Ginibre's [20] upper level. Comparisons between the recorded line profiles and the predicted hyperfine patterns for the two lines are shown in figures 7.83 and 7.84. These two excitations give sufficient proof of the existence of the lower level. Energies of the lower level and of the upper level which was found by the original excitation of line at 5722.61 Å are now

corrected i.e. **12431.364   cm⁻¹ and 29901.053 cm⁻¹** respectively. Figure 7.85 show the levels scheme of the levels involved in the discovery of these two levels.
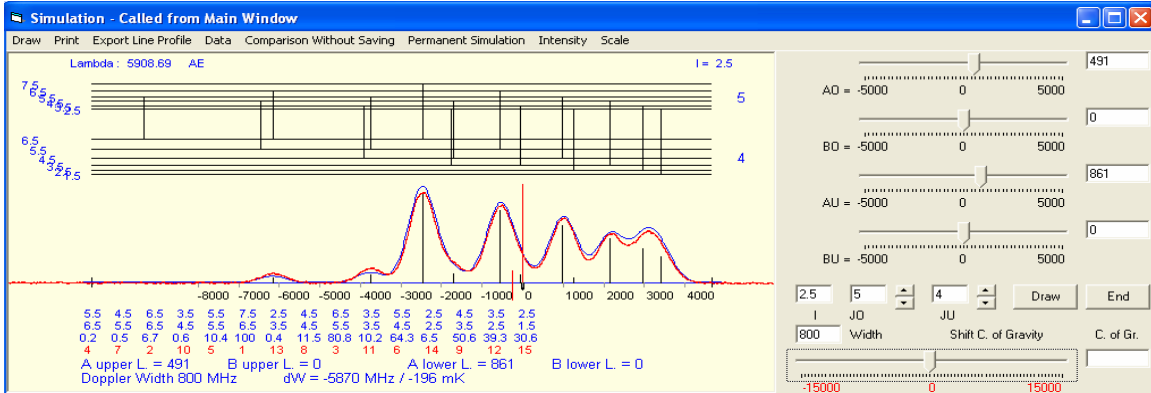
Figure 7.83: Comparison of the recorded line profile with the predicted hyperfine pattern at 5908.70 Å
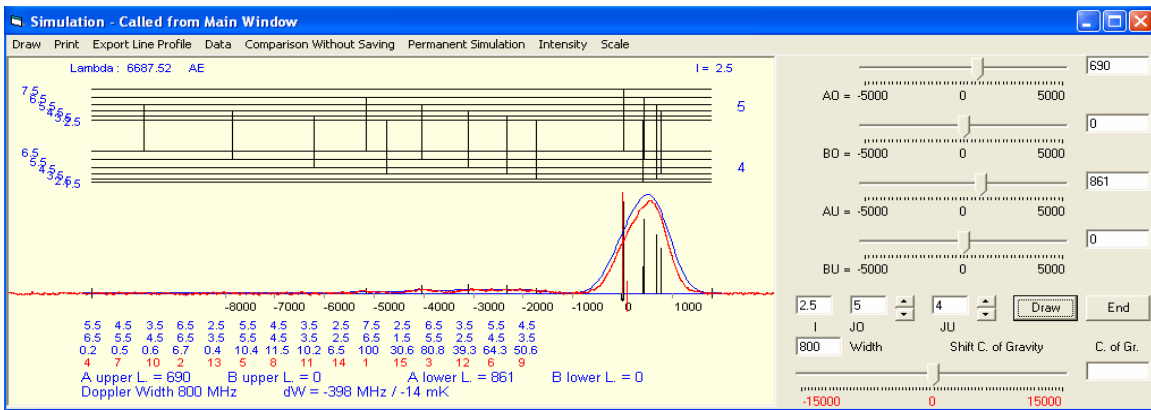
Figure 7.84: Comparison of the recorded line profile with the predicted hyperfine pattern at 6687.52 Å

Figure 7.85: Level scheme for the levels involved in the excitation of line 5722.61 Å

Table 7.12: Newly discovered **Pr-I levels** in **even configuration** combining with known lower levels. (Underlined fluorescence channel indicates recorded LIF signal with best S/N ratio corresponding to file number mentioned in comments column).

New Even parity Upper level				Excitation Wavelength λ_{air} (Å)	Fluorescence Channels λ_{air} (Å)	File numbers, Comments
Energy (cm^{-1})	J	A (MHz)	B (MHz)			
28455.478	1/2	938(9)	-	6072.68	(5134.95)	pr361018
27411.277	3/2	196(3)	-	6144.70 6483.95	6535, 5425 5425	Pr389048 Pr389049
27539.142	3/2	968(1)	-	6096.78 5618.36	5387, 5618, 6478, 6432 6095	pr358058 pr474017
27806.714	3/2	873(5)	-	5998.89 6368.55	5535, 6321, 6369 5998	pr391037 pr486032
28146.157	3/2	873(4)	-	6188.97 5879.15	5217, 5880 5217	pr355047 pr473008
28917.934	3/2	538(1)	-	5623.89 5906.75	5015, 5214 5214	pr498032 pr507056
29520.256	3/2	23.9(5)	-	5703.79	(4868.68)	pr504067
22959.94	5/2	1241	-	7154.431	(7154.431) (8650.483)	FT-Fitted
26801.197	5/2	1051(1)	-	6384.09 6492.50	5611.78, 6384, 6492 6384	pr399005 pr468022
28188.013	5/2	882(1)	-	5864.70 5701.64 5956.03 6283.57	5207, 6217, 6282 5207 5207, 6282 5207	pr130052 pr505004 pr505053 pr291027 pr450009
28561.383	5/2	807(2)	-	5826.46 5739.03 6691.63	5107, 5311, 5581, 6140 5107 5107	pr100012 pr483001 pr407025
29039.26	5/2	529(2)	-	5668.59 4985.54 5864.74	4987 5670 4987	Pr117011 pr505035 Pr206003 Pr505001
29257.387	5/2	515(3)	-	5599.33 5829.85	4840, 4932, 5125, 5317, 5831 5599	pr496003 pr500011
29324.461	5/2	418(3)	-	5768.21 5807.09	5578, 5297, 4918 4918	pr498014 pr498017
29530.791	5/2	757(2)	-	5738.30 6283.85	5239, 5297, 5515, 6020 6284 5738	pr351017 pr450006
29731.99	5/2	777(2)	-	5672.77 5635.67 6205.38	4821, 5001, 5377 4821 5635	pr154034, pr505032 pr306045 pr389006
29868.643	5/2	805(1)	-	6303.67 5898.32	5151, 5340, 5592 5592	pr431052 pr476013
30273.089	5/2	838.5(5)	-	6003.74 6130.11	4869 4869	pr316027 pr491029
30717.623	5/2	588.7(10)	-	5616.91	4766, 5846	Pr302018

				5847.58	4766	Pr473024
31035.306	5/2	773(2)	-	5740.95 5856.41	4696, 4878, 5519 4878	pr314003 pr478025
25305.74	7/2	754	-	7190.879	(7190.879), 6357.18 5861.563	FT-Fitted
25558.27	7/2	702.9(2)	-	5776.04 6707.66	3910, 5820, 6256 5820	pr336012 pr479021
26578.511	7/2	782(2)	-	6198.46 6391.34	5454, 6476 5454	pr389037 pr429006
26750.221	7/2	759(1)	-	6210.96 6404.96	5405 5405	pr361022 pr414041 pr444027
28049.33	7/2	631(1)	-	5842.01 5912.83	3564, 6564, 6607, 6814 3564	pr341054 pr505011 pr473035
29087.634	7/2	549(2)	-	5759.76 5947.28	5170, 5507, 5887, 5947 6145 5170	pr174024 pr498009 pr285050 pr504002
29799.529	7/2	681(3)	-	5651.12 6078.99	5888, 5167, 5435, 6079 5888	pr300048 pr394022
29917.719	7/2	719(2)	-	5881.28 5667.45 5847.48 6000.16	4955, 5594 4955 4955 4955	pr097017 pr128028 pr505039 pr348044 pr505008 pr391026
30281.88	7/2	684(1)	-	6000.50 5757.88	4829, 5273, 5725 4829	pr285017 pr351004 pr505019
30522.946	7/2	594(1)	-	5679.03 5831.59	4771.19 4771.19	pr310035 pr478020
30730.364	7/2	655(1)	-	5843.27 6172.67	3252, 4765, 4929, 5352 6172 5844	pr349004 pr505058 pr392037
31083.278	7/2	566(2)	-1.45	5725.18 5839.96 5647.03	4649, 4845 4845 4845	pr048005 pr341007 pr505015 pr474044
31237.02	7/2	397(1)	-	5598.41 5802.96	4616, 5802, 5985 4616	Pr496054 Pr500012
17534.157	9/2	675(1)	-	5701.57	4952, 4938, 4736, 4744 5133	Excitation from ground, all indirect fluorescence channels decay possibly via Self-absorption pr108012 pr323012 (optoG) pr506048 Level was

						confirmed at 6086.90 Å combining with a level 33958.403 cm⁻¹
21729.54	9/2	414.1(5)	-	4911.94	(4911.94), (4600.741), (8848.835)	FT-Fitted
23661.972	9/2	541.19(5)	-	6742.78 6486.72	<u>4485</u> <u>4485</u>	pr424022 pr480024
23891.53	9/2	635.3(5)	-	6391.54 6639.98	<u>4184</u> <u>4184</u>	pr398021 pr493004
25812.15	9/2	788(1)	-	6720.62 5638.04	<u>4092</u> <u>4092</u>	pr424011 pr475013
26298.385	9/2	755(2)	-	6390.35 6507.92	<u>5487</u> <u>5487</u>	pr398026 pr419033
26842.453	9/2	757(1)	-	6175.58 6475.15	<u>5550</u>, 5329, 3724, 6090 6285, 6474, 6615, 6758 <u>5550</u>	pr355050 pr480013
27304.431	9/2	690(1)	-	6004.23 5925.10 6287.02 6419.16	<u>5414</u>, 5246, 6108, 6285 6621, 6421, 5926 <u>5414</u> <u>5414</u> <u>5414</u>	pr316006 pr327098 pr404010 pr414006
28210.613	9/2	743(2)	-	6066.28 5948.01	3545, 5948, 6186, 6245 6496, <u>6520</u> 6186	pr358077 pr473038
28297.925	9/2	764(2)	-	6152.91 6637.69 6692.76	5756, <u>5889</u>, 6690, 6992 <u>5889</u> <u>5889</u>	pr355094 pr397021 pr407022
28705.998	9/2	857(3)	-	5750.96 5626.10	5476, 6002, 6057, <u>6293</u> <u>6293</u>	pr125018 pr506026 pr148015 pr506059
28807.347	9/2	712(2)	-	5965.87 5854.32 5717.63	<u>5440</u> <u>5440</u> <u>5965</u>	pr273009 pr293011 pr344028
28976.248	9/2	439(1)	-	5986.98 5662.95	3450, 3624, 5390, 5662 <u>6510</u> <u>6510</u>	pr332050 pr474054
29198.871	9/2	653(3)	-	5829.647 5723.08 6125.33	5095, <u>5592</u>, 5723, 5908 <u>5592</u> <u>5908</u>	pr130069 pr506003 pr132007 pr506030 pr377040
29250.135	9/2	586(2)	-	5812.28 5601.62	5082, 5313, <u>3418</u> <u>3418</u>	pr062004 pr484014 pr502011
29340.502	9/2	529(2)	-	6087.96 6207.91 6614.39	4877, 5059, <u>5548</u>, 5559 <u>5548</u>	pr368040 pr380030 pr434003

					5549	
30257.922	9/2	770(2)	-	6235.93 6150.02	<u>4835</u>, 5560, 5916 <u>4835</u>	pr383038 pr386016
30389.64	9/2	746(1)	-	5868.38 5961.97 5708.76	5013, 5519, <u>5708</u>	pr269014 pr288050 pr506018 pr320035 pr506044
30814.475	9/2	637(2)	-	6350.33 5734.11	<u>3244</u>, 5734 <u>3244</u>	pr422008 pr450022 pr471034
30938.77	9/2	634.6(5)	-	6094.26 5981.88 5772.96	<u>4880</u>, 5685, 5773, 5905 5982 <u>4880</u> <u>4880</u>	pr394035 pr394042 pr449039
30966.07	9/2	595(1)	-	5676.31 5972.09	<u>4873</u> <u>4873</u>	pr309005 pr506051 pr477003
31041.905	9/2	570(1)	-	5654.09 5945.19	<u>4854</u>, 5071 <u>4854</u>	pr300027 pr503027
31362.774	9/2	621(1)	-	6010.16 6043.86	<u>4588</u>, 4989, 5162, 5555 6261, f6499 <u>4588</u>	pr368053 pr372031
31410.496	9/2	739.7(10)	-	5742.84 5923.91 5992.97	<u>4768</u>, 5925, 5992 <u>4768</u> <u>4768</u>	pr314018 pr329016 pr327084
31639.28	9/2	683(2)	-	5668.339 5670.58 5911.88	5312,5339, 5469, <u>5549</u> <u>5550</u> <u>5550</u>	pr142024 pr143003 pr506055 pr263052 pr506021
32209.15	9/2	543(4)	-	5833.54 5779.21	<u>4788</u>, 5172, 5303, 5559 <u>4788</u>	pr318000 pr318006
23272.407	11/2	493(4)	-	6654.96 6580.61	4296, <u>4566</u> <u>4566</u>	pr440060 pr479053
23680.085	11/2	664.9(2)	-	6479.12 6408.63 6734.56	4221, 4482, <u>4799</u>, 7142 <u>4799</u> <u>6477</u>	pr401016 pr479065 pr479058
24772.03	11/2	716.2(4)	-	6273.11 6050.90	<u>4559</u>, 5989, 6050, 6272 <u>6272</u>	pr381002 pr383011
25564.412	11/2	587(1)	-	6597.25 5774.01	<u>3910</u> <u>3910</u>	pr440050 pr510036
25683.831	11/2	825(3)	-	5933.62 6554.66 6545.66	<u>4377</u> <u>4377</u> <u>4377</u>	pr285044 pr400036 pr420017
25900.916	11/2	624(1)	-	5858.13 6462.67	6164, <u>6461</u>, 6856 <u>5858</u>	pr258004 pr468013
26843.924	11/2	623(2)	-	6440.89 6614.86	<u>3725</u> <u>3725</u>	pr375036 pr434002
27516.452	11/2	585(2)	13.82	5851.57	3634, 5322, 6029, 6338 <u>6528</u>	pr088007

				5844.42 6029.77 6528.97 6339.36	6528 6528 6029 6528	pr115001 pr349034 pr368003 pr465016 pr442023
28403.321	11/2	415.3(10)	-	6178.29 5996.20	5311, 5996, 6645 6645	pr364041 pr477017
28728.842	11/2	708(1)	-	6056.45 5881.37	3481, 5221, 5460, 5883 6496 6055	pr364001 pr473016
29248.613	11/2	714(2)	-	5706.84 5812.77 6085.63	3418, 5577, 6107, 6555 3418 3418	pr146006 pr340022 pr395013
29524.718	11/2	493(1)	-	6192.18 6175.40	3387, 3553, 5012, 5230 5368, 6536, f6890 3387	pr355035 pr355057
29632.809	11/2	577(1)	-	5741.998 6488.95	5946, 6143, 6488 5741	pr231072 pr468017
29857.89	11/2	627(2)	-	5868.09 5668.71 6059.89	3348, 5515, 5668, 6059 5515 5515	pr113023 pr117005 pr364008
30998.18	11/2	591(1)	-	5880.00 6063.41	4667, 5325, 5668, 5961 6073 3375	pr332073 pr374004
31408.036	11/2	572(1)	-11.20	5818.503 5743.64	3500, 4980, 5394 4980	pr021015 pr029004
31980.532	11/2	588(1)	-	5722.41 5794.94 6123.41	5002 5002 5002	pr090016 pr095004 pr350007 pr389017
32034.687	11/2	529(1)	-	5875.01 5776.82 5807.95	3261, 4827, 4988, 5258 3261 3261	pr082037 pr087006 pr478029
32221.927	11/2	423(1)	-	6377.79 5924.47 5811.06	3405, 4415, 4785, 4942 5812, 5924, 6242, 6915 4785 4785	pr416054 pr449012 pr449016
32496.297	11/2	469(4)	-	5656.22 5719.84 5737.41	3212 3212 3212	pr119049 pr508022 pr509056
32671.946	11/2	530(1)	-	6071.05 5988.28 5770.54	4684, 4835, 5675, 5786 5875, 5988 4835 4835	pr391009 pr391013 pr454015
32891.402	11/2	399(1)	-	5799.82 5593.36	4635, 4784 , 5437, 5593 4784	pr455012 pr495079
32989.103	11/2	478(1)	-	5682.49 5956.36	4763, 4616, 5956 4763	pr009013 pr508002 pr508011

25801.393	13/2	697(2)	-35.68	6202.84 6188.50	4666, 5892, 6495	pr361027 pr366037
26028.258	13/2	556(2)	-	6116.74 6401.30 6409.92	4617, 6116	pr358102 pr394050 pr399011 pr399014
27166.353	13/2	863.8(2)	-	5718.60 6059.89	<u>4385</u> <u>4385</u>	pr104024 pr455039
28608.812	13/2	676(1)	-	5952.80 6556.30 6094.20	<u>5572</u>, 6093, 6405 <u>5572</u> <u>5572</u>	pr286002 pr400033 pr394028
29187.599	13/2	570(1)	-	5754.46 5731.95 6399.41	3795, 5400, <u>5887</u>, 6130 6308 <u>5887</u> <u>5887</u>	pr127016 pr128004 pr458036 pr398006
30484.724	13/2	635(1)	-	5908.82 5829.69 5677.97	<u>3434</u>, 5354 <u>5354</u> <u>3434</u>	pr112008 pr113000 pr309019
30834.815	13/2	667.8(5)	-	5713.05 5939.24 6390.98	3393, 4899, 5255, 5567 5938, 6020, <u>6125</u>, 6207 6390, 6477 <u>6125</u> <u>6125</u>	pr159012 pr329018 pr468010
31012.746	13/2	687(1)	-36.49	5874.98 5730.03 6381.84	3374, 4865, <u>5729</u> <u>3374</u> <u>5875</u>	pr082022 pr087011 pr403033
31304.011	13/2	623(1)	-	5952.93 5853.91	5177, 5460, <u>5562</u> <u>5562</u>	pr286008 pr293026
31483.15	13/2	603(1)	-	5716.9 6136.65 6071.8 5890.14	6071, <u>6136</u> <u>5716</u> <u>5716</u> <u>6136</u>	pr104011 pr450013 pr356059 pr391017 pr466011
31642.946	13/2	518.7(3)	-	5835.14 6076.71 6568.20	<u>3304</u>, 4919, 5090, 5329 5364, 5530, 6076, 6136 6568 <u>3304</u> <u>3304</u>	pr231041 pr391042 pr447005
31729.933	13/2	432.8(5)	-	5639.36 5711.51 6045.09 6429.62	3292, <u>5065</u>, 6044 <u>5065</u> <u>5065</u> <u>5065</u>	pr116036 pr129003 pr393001 pr417025
31798.949	13/2	556(1)	-	5617.48 6019.97 6501.61	4985, 5414, 5484, 5957 6019, 6095	pr302047 pr327010 pr464009
32049.991	13/2	521.2(5)	-	5785.29 5771.70 5930.22 6583.66	3425, <u>4985</u> <u>4985</u> <u>4985</u> <u>4985</u>	pr065008 pr507013 pr507010 pr264021 pr433003
32445.251	13/2	665(2)	-	5847.09	<u>4889</u>, 5656, 5954, 6071 6155	pr057030

				5864.80	<u>5656</u>	pr090027
				5794.43	<u>5656</u>	pr336059
32608.084	13/2	628(1)	-	6085.51	3360, 5100, 5811,	pr395008
				5741.86	5896 5590	pr457018
				5896.74		pr457024
				5809.30		pr457020
32773.833	13/2	834(1)	-	5686.13	<u>3185</u>, 4427, 4471	pr165002
					4885, 5158, 5476,	
					5541, 5560 5953	
				5952.02	<u>3185</u>	pr329022
33040.589	13/2	503(2)	-	5666.82	<u>4751</u>, 5471	pr173007
				5675.64	<u>4751</u>	pr350037
						pr173008
33531.213	13/2	529(1)	-	5769.96	3258, 3430, 4870,	pr452043
					5329 5514, 5593	
				5807.83		pr478028
33870.18	13/2	592(1)	-	5695.76	<u>3223</u>, 4570, 5352	pr312031
				5770.99	<u>3223</u>	pr452021
				5651.36	<u>3223</u>	pr502029
28071.547	15/2	580(1)	-	5761.72	5470, 5660, <u>6132</u>,	pr336040
					6149 6634, 6758	
				5660.71	<u>6132</u>	pr336047
				6130.54	<u>6634</u>	pr473029
						pr377000
28200.351	15/2	590(1)	-	6082.48	4195, 5620, 5720,	pr358045
					<u>6256</u> 6578, 6726	
				6256.78	<u>6726</u>	pr381045
28805.33	15/2	505(1)	-	5866.55	5217, <u>5528</u>, 6029,	pr097042
					6326 6440, 6559	
				6028.53	<u>6440</u>	pr391022
				6326.06	<u>5528</u>	pr442008
29033.86	15/2	410(2)	-	5782.92	<u>3817</u>, 5459	pr128024
				5788.91	<u>3817</u>	pr129004
				6235.85	<u>3817</u>	pr383036
29642.982	15/2	502(1)	-	6532.96	5593, 5735, <u>6131</u>,	pr407001
					6390 6837	
				6389.25	<u>6131</u>	pr463005
29678.099	15/2	698(2)	-	6117.43	5578, 6519, 6590,	pr358016
				5727.11		pr478003
30453.594	15/2	490.1(5)	-	5840.29	3835, 6075, <u>6204</u>	pr341023
				6074.52	<u>6204</u>	pr364030
				6204.28	<u>3835</u>	pr380013
				6755.19	<u>6204</u>	pr425009
30781.638	15/2	510.7(5)	-	5622.87	3786, 4971, 5256,	pr146043
					<u>5730</u> 6080, 6341	
				5730.46	<u>3786</u>	pr323031
31070.645	15/2	551(2)	-	6227.83	3542, 3747, 5191,	pr380034
					5533 5855, <u>6295</u>,	
				6036.83	6380, 6485	pr383017
				6296.08	<u>6295</u>	pr431059
				6379.24	<u>5533</u>	pr416050
					<u>6295</u>	
31349.288	15/2	609(1)	-	5761.03	6122, 6187, <u>6269</u>	pr174032
				6187.48	<u>6122</u>	pr366027
				6267.84	<u>6122</u>	pr482027

31402.843	15/2	630(1)	-	5918.26 6166.71	<u>6167</u> <u>5918</u>	pr021001 pr020000 pr020004 pr369059
31619.982	15/2	520(2)	-	5785.51 5672.50 6085.53	<u>3474</u>, 5452, 5538 <u>3474</u> <u>3474</u>	pr119010 pr148014 pr395003
31688.137	15/2	737.30(6)	-	6137.39 6117.99 6060.38	<u>3467</u>, 5432 <u>3467</u> <u>3467</u>	pr392002 pr392012 pr392007
31744.873	15/2	696.5(5)	-	6116.09 6039.54	3460, 5414, 5633, 5800 5947, 6040, 6478	pr358024 pr393006
31756.217	15/2	476.6(4)	-	5628.98 5885.33	<u>3457</u>, 5000, 5427, 5496 <u>5628</u>	pr146026 pr474002
32166.51	15/2	510(1)	-	5889.51 5962.23 5746.48	3411, 4899, 5293, 5374 5502, 5308, 5662, 5747 6309	pr269039 pr288028 pr320030
32206.775	15/2	552(1)	-	6572.22 5875.65	3406, <u>5281</u>, 5876, 5948 6291 <u>5281</u>	pr105009 pr444002 pr264014
32486.782	15/2	552(1)	-	5780.51 6183.09	<u>3372</u>, 4820, 4836, 5205 6182 <u>3372</u>	pr014028 pr264024 pr366024
32658.325	15/2	531(1)	-	5801.58 5723.77	<u>3353</u>, 5157, 6118 <u>3353</u>	Pr108046 pr449004
32784.03	15/2	501(1)	-	6338.87 5682.86 5836.21	3340, 5473, <u>6021</u> <u>6021</u> <u>6021</u>	pr422045 pr475020 pr475021
33129.815	15/2	519(1)	-	5898.20 6506.73	5320, <u>5445</u>, 6117, 6507 <u>5320</u>	pr259021 pr464016
33415.62	15/2	493(1)	-	6387.90 5808.78	3445, <u>5241</u>, 5415 <u>5241</u>	pr416030 pr475027
33783.23	15/2	465(2)	-	5881.27 5955.05	3232, <u>3401</u>, 5445, 5514 <u>3232</u>	pr097011 pr503043
34000.64	15/2	460.5(3)	-	5807.05 5617.78 6124.23	<u>3375</u>, 5083, 5359, 6156 <u>3375</u> <u>3375</u>	pr111013 pr471024 pr302073 pr387008
34204.135	15/2	442.6(5)	-	6092.38 6048.79 6081.51	<u>5553</u>, 5316, 5387, 6049 <u>5553</u> <u>5553</u>	pr358033 pr358090 pr361048
35146.332	15/2	551.2(4)	-	5722.56 6315.25 5761.58	<u>6316</u> <u>5723</u> <u>6316</u>	pr050041 pr472009 pr468003 pr478014
27466.81	17/2	584(2)	-	5951.49	6367, <u>6385</u>	pr285052

				5969.76	6367	pr386028
28622.60	17/2	419(1)	-	5930.13 6400.06	5034, 5507, 6515 5930	pr286019 pr444031
28918.012	17/2	468(1)	-	6393.09 6511.81 6281.27	4073, 5829, 5880, 6281 6512 6281 6512	pr398017 pr419043 pr404007
29070.702	17/2	440(1)	-	6221.58 6199.75	4049, 5775, 6447, 6786 6990 6786	pr361033 pr389028
29322.753	17/2	423(2)	-	5742.37 5710.07	5229, 6103, 6672 6672	pr231080 pr347002
30560.925	17/2	452(1)	34.94	5785.34 5693.56	5319, 5361, 5675, 5693 5883 5883	pr052007 pr109019
30981.156	17/2	793(2)	-	6233.74 6007.61	5543, 6332, 6416, 6755 5543	pr383053 pr383055
31437.408	17/2	485(2)	-	6153.93 6233.34 6061.30	3695, 5405, 5997, 6007 6060, 6232, 6823, 6930 5405 6232	pr355084 pr361045 pr361053
31629.427	17/2	563(1)	-	6082.04 6159.59	3669, 3735, 4270, 4865 5350 5940, 5990, 6151 6082	pr353043 pr386026
31801.97	17/2	503(1)	-	6399.56 5725.21 5880.00	3645, 5725, 5880, 6656 6752 6397 6398	pr398004 pr471029 pr473004
32137.057	17/2	453(2)	-	5756.28 5766.35 5814.65 6546.12 6511.91	5207, 5618, 5974, 6512 5618 5618 5756 5617	pr043000 pr116006 pr472028 pr116007 pr465025 pr480000
32472.35	17/2	489(1)	-	5785.35 5855.49	3558, 5209, 5515, 5856 6459 3558	pr063030 pr325040 pr447049 pr325024 pr472003
32744.355	17/2	668(1)	-	6035.47 6347.89	3525, 5560, 6349 6036	pr395016 pr422023
33009.799	17/2	584(2)	-	5676.72 6161.56	5067, 5353, 5940 5940	pr300013 pr371029
33657.329	17/2	460(1)	-	6000.07 5953.48	3414, 5175, 5300, 6303 3414	pr332027 pr477008
34704.94	17/2	446.3(5)	-	5870.89 6166.51	6165 5870	pr089030 pr387002
32041.836	19/2	388(2)	-	5847.02 5798.20	5235 5235	pr041012 pr507032 pr041054 pr507044

29606.273	21/2	424(1)	-	6000.46 6751.97	<u>6751</u> 6751	pr285000 pr487015
30275.01	21/2	381	-	5854.44 5768.86 6460.20	5589, 5768, <u>6458</u> <u>6458</u> <u>5768</u>	pr086053 pr476006 pr087000 pr087001 pr476005 pr419053 pr431025
29011.215	23/2	356(2)	-	6322.36	<u>5565</u>	pr397009

Table 7.13: Newly discovered **Pr-I levels** in **odd configuration** combining with known lower levels. (Underlined fluorescence channel indicates fluorescence wavelength for recorded file mentioned in comments column).

New odd parity Upper level				Excitation Wavelength λ_{air} (Å)	Fluorescence Channels λ_{air} (Å)	File numbers Comments
Energy (cm^{-1})	J	A (MHz)	B (MHz)			
23055.74	3/2	-280.2(3)	-	6021.01	5359 (Collisional coupling) (8549.079) (8762.212) (8933.483) (9084.914) (9264.54)	pr368065
25849.518	3/2	876(1)	-	5842.21 6655.71	4992, <u>5154</u>, 6194, 6655 6780 <u>5154</u>	pr292003 pr479013
25899.43	3/2	1262(1)	-	6175.41	5825, <u>5140</u>, 6152, (7014)	pr364038
27496.712	3/2	1415(1)		6044.32 6100.04	4750, <u>5330</u> <u>5330</u>	pr372035 pr491021
28338.91	3/2	1154.5(3)	-	5801.81 5888.67	<u>4567</u> <u>4567</u>	pr036027 pr483039
28656.732	3/2	1060(1)	-	5780.42 5877.13	<u>4503</u>	pr037029 pr498034 pr039021 pr498023
29119.95	3/2	744(1)	-	5721.30 5866.43	4410, <u>5150</u> <u>5150</u>	pr092020 pr097036
29627.43	3/2	-4(2)	-	5757.93 5643.02	5687, <u>6032</u> <u>6032</u>	pr039051 pr165026 pr165027
29687.263	3/2	603(1)	-	5677.44 6037.13	4302, <u>5004</u> <u>4302</u>	pr146010 pr505042 pr396007
32777.119	3/2	535(1)	-	6087.67 5980.19 5916.72	<u>5250</u>, 5414 <u>5250</u> <u>5250</u>	pr368034 pr491035 pr503047 pr503051
22175.22	5/2	1077.01	-	(6358.19)	(6392) (9170.962) (9740.325)	FT-fitted
22678.79	5/2	580(1)	-	(8436.638)	6160.88	FT-fitted
22944.93	5/2	710(1)	-	6092.40 6695.26	<u>6695</u> <u>6092</u>	pr358030 pr479005
24947.255	5/2	1109(1)	-	6561.33 6651.96	<u>5405</u>, 6167 <u>5405</u>	pr397017 pr440066
26345.227	5/2	1178.66	-	6009.91	<u>5024</u>, 5046 (5024) (5046)	pr368048
26415.38	5/2	583(1)	-	(5028.83) 6414.12	(5028.83) 5028, <u>5318</u>	 Pr431033
26831.815	5/2	670(1)	-	5839.11 6462.34	<u>4925</u>, 5526, 6461 <u>4925</u>	pr057013 pr480019
27290.98	5/2	929.6(5)	-	5754.53 5847.64	<u>5185</u>, 5388 <u>5185</u>	pr095024 pr475029
27323.158	5/2	906.5(4)	-	5674.32 5656.74 6061.12	<u>4790</u> <u>4790</u> <u>4790</u>	pr174011 pr498047 pr296019 pr498051 pr394061
27816.365	5/2	1172(2)	-	5673.27 5885.11	4949, <u>5049</u>, 5241, 4696 (5521) <u>5049</u>	pr154022 pr511028 pr510040

28999.54	5/2	920(1)	-	5898.75 5994.41 5768.48	<u>4450</u>, 4675 <u>4450</u> <u>4450</u>	pr097020 pr317023 pr320024
29180.30	5/2	996(1)	-	5701.61 5845.73	4636, <u>5189</u> <u>5189</u>	pr108019 pr505048 pr204027
29573.267	5/2	811.7(5)	-12.30	5704.91 5714.46	4323, <u>4340</u>, 4554, 4636 4798, 5032, 5925 <u>4340</u>	pr032022 pr504073 pr244048 pr504071
29685.664	5/2	827.1(5)	-	5857.32 5958.35	4303, <u>4318</u>, 5380 <u>4318</u>	pr258028 pr477020
30101.32	5/2	943(1)	-	5745.52 5814.27 5857.28	<u>4447</u>, 4890, 5539 <u>4447</u> <u>4447</u>	pr050029 pr061018 pr348078
30149.869	5/2	966(1)	-	5873.10 5797.92	<u>5009</u>, 5249, 5606 <u>5009</u>	pr103013 pr321014
30376.498	5/2	889(1)	-	5722.74 5764.38 5764.17	4837, <u>5115</u>, 5288 <u>5115</u> <u>5115</u>	pr049019 pr119002 pr499054 pr499054
30512.676	5/2	996(1)	-	5678.48 5612.82 5750.55	4154, <u>4367</u>, 5613, 5750 <u>4154</u> <u>4367</u>	pr169020 pr170008 pr498059 pr498005
31043.994	5/2	982.4(5)	-	5754.20 5777.29	4079, 4687, <u>5079</u> <u>5079</u>	pr095029 pr098028
31142.074	5/2	814(1)	-	5695.86	5029, <u>5234</u>, 5311, 5397	pr312016
32068.921	5/2	644(1)	-34.21	5895.20 5859.28	3917, 4088, 4993, 5099 <u>5251</u> <u>5251</u>	pr086034 pr097005
32501.249	5/2	703(6)	-	5840.26 5859.40	4854, 5159, 5181, 5239 <u>5246</u> <u>5246</u>	pr341013 pr503040
32558.096	5/2	405(1)	-	5695.97 5937.54	<u>3828</u>, 5311 <u>3828</u>	pr312006 pr477021
32800.814	5/2	707(1)	-	5697.49 5815.16	3795, <u>4155</u>, 4645, 4785 5081 <u>4155</u>	pr227069 pr476012
19002.86	7/2	796.98	-	(8018.79)	(9096.88)	FT-Fitted
20329.65	7/2	683.22	-	(7247.498)	(7203.753)	FT-Fitted
21094.562	7/2	753(1)	-	5999.90 6546.28	4732, <u>6545</u> 4732	pr332015 pr434028
22301.146	7/2	750(1)	-	6307.68 5594.76	<u>5594</u>, 6808, 7320.064 <u>7322</u>	pr431000 pr499023
22964.64	7/2	1108(1)	-	(6826.672) 6686.44	6054, 6686 , 6826 7539 <u>6826</u>	Ft-Fitted pr479008
23064.427	7/2	754.2(6)	-	6048.36 6017.86	<u>5365</u> <u>5365</u>	pr371001 pr371016
23446.85	7/2	634.85	-	7389.668	(5882.44) (5911.581) (7274.903) (7278.023)	FT-Fitted
23611.86	7/2	269.87	-	(7188.585)	(8402.013) (9804.991) (9842.137)	FT-Fitted

					(9975.801)	
23901.383	7/2	640(1)	-	5729.21	5756, 6139	pr332001
				5756.84	Optogalvanic	pr332004
26574.579	7/2	1008(1)	-	5722.66	4968	pr092030
				5926.11	4968	pr098035
26746.925	7/2	690.8(5)	-	5666.75	3617, 4480, 5337	pr170017
				6099.54	4480	pr491039
26795.389	7/2	650(1)	-	6524.32	4470, 4766, 5215 5324	pr436033
				6599.23	4470	pr447022
27369.327	7/2	1013(1)	-	5728.69	4359, 4639, 5340, 5475, 5877	pr129015
				5876.36	4359	pr276076
28680.02	7/2	901(1)	-	5869.07	4746, 4840, 5107	pr113020
				5743.60	4746	pr114001
29478.545	7/2	776.1(5)	-	5745.55	4573, 4907, 4661 5387 5443	pr053020 pr498035
				5895.00	4573	pr111030 pr498029
30269.667	7/2	678(1)	-	5672.94	5145, 5237, 5488	pr154045
				5674.42	5237	pr174012
30718.587	7/2	793(2)	-	5652.65	4758, 4805, 4910, 5216	pr500022
				5836.70	4805	pr509025
31156.257	7/2	785(5)	-	5696.24	4988, 5098, 5402	pr049041
				5913.13	5098	pr061004 pr507047
				5738.63	5098	pr507019
31402.388	7/2	684(1)	-	5673.46	3708, 4484, 5077, 5171	pr169016
31439.705	7/2	720.8(5)	-	5674.69	3702, 4000, 4475, 5024, 5164, 5321, 5347, 5457, 5545, 5861	pr310002
				5838.15	3702	pr325021
				5794.35	4001	pr332012
				5815.61	5321	pr506000
32301.78	7/2	710(2)	-	5780.41	3774, 4242, 4717,	pr015038
				5783.80	5302	pr032009 pr507016
32524.685	7/2	811(1)	-	5742.00	4839, 4995, 5241, 5355, 5391	pr314010
				5949.37	5241	pr503011
33813.296	7/2	646(4)	-	5771.12	3401, 3655, 4149 4365, 4686, 5093 5265, 5318	pr452023
				5792.5	3401	pr509039
20736.35	9/2	615(1)	-	6299.53	6131, 6931 (7039.934) (7129.608)	pr486001
				6131.74	6931	pr491024
21724.16	9/2	1135.05	-	(7752.781)	(7086.874)	FT-Fitted
22036.64	9/2	579(1)	-	6449.39	5195, 5835 (6601.586) (7128.904) (7288.542) (7569.336)	pr397039
				5822.46	6448	pr473026

22561.013	9/2	926(1)	-	6690.02	<u>6240</u>, 6380, 6872	pr407029
				6238.38	<u>6689</u>	pr485005
24071.325	9/2	746.7(5)	-	5701.06	<u>4695</u>, 5093, 5206, 6077	pr215008
				6075.92	<u>5701</u>	pr386006
25178.609	9/2	839.6(2)	-	5829.52	4819, 4857, <u>4922</u>, 5157, 5362, 5693, 6047, 6456, 6485, 5406	pr215073
				6046.18	<u>4922</u>	pr378017
				5692.79	<u>4922</u>	pr471031
				6744.91	<u>5830</u>	pr424032
25209.246	9/2	878(1)	-	5819.14	4912, <u>5157</u>, 5352, 6272	pr209012
				5682.88	<u>5157</u>	pr310000
26547.124	9/2	794(1)	-	5925.31	4610, <u>4823</u>, 4995, 5085	pr273002
				5731.68	<u>4823</u>	pr323040 pr351005
				6507.47	<u>4823</u>	pr419030
27979.218	9/2	590.1(5)	-	5621.32	4246, <u>4324</u>, 4661, 5085	pr148035
				6525.26	<u>5085</u>	pr436026
28381.982	9/2	621(1)	0.52	5719.91	4431, 4614, 5064, 5186, 5415	pr048034 pr506037
				6393.77		pr416018
28430.448	9/2	630(1)	-	5895.27	4166, 4243, 4423, <u>4603</u>, 4803, 4901 4971, 5531	pr061026 pr498024
				5796.83	<u>4166</u>	pr111027
				5704.09	<u>4603</u>	pr498043
28445.99	9/2	771.2(5)	-	5678.78	<u>4515</u>, 4636, 4800, 4895, 5213	pr310023
				6030.93	<u>4515</u>	pr368017
28936.947	9/2	723.25	-	5789.39	<u>4971</u>, 5139, 5188 5380	pr039025
				5804.33	<u>4971</u>	pr061003
29700.919	9/2	833(1)	-	5818.70	4025, 4185, <u>4315</u> 4348, 4527, 4743 4791, 4994, 5486 5509	pr343003
				5852.09	<u>4315</u>	pr348072
				5998.88	<u>4025</u>	pr391032
30100.133	9/2	742.7(5)	-	5857.47	3962, <u>4275</u>, 4308 4954, 5314, 5367 5437, 5485, 5545	pr258020
				5729.58	<u>4275</u>	pr452016
30230.959	9/2	850(1)	-	5895.16	4096, 4252, 5156, 5272, <u>5351</u>	pr061032
				5887.57	<u>5351</u>	pr114002
30718.272	9/2	694(1)	-	5842.02	3802.975 3867.065 4096.194 4134.325 4626.122 4405.96 <u>4707.414</u> 4757.091 4871.284 5029.340 5141.723 5215.016 5652.831 5790.634	pr292011

				5652.74	4707.414	pr500019
30822.637	9/2	678(1)	-	5696.42	3788, 3998, 4604 4638, 5023	pr312041
				5743.26	3788	pr314024
31098.427	9/2	796.4(4)	-	5773.06	3748, 4070, 4951 5218	pr039008 pr507007
				5659.04	3748	pr050001
				5710.06	3748	pr050002 pr507050
				5653.67	3748	pr119043
31323.207	9/2	697(1)	-	5833.76	4987, 5158, 5260	pr130064
				5685.55	4987	pr132006
31737.15	9/2	722(1)	-	5716.70	3718, 3966, 4415 4797, 4415	pr104016
				5801.58	4797	pr130027
31935.661	9/2	876.2(5)	-	5822.04	5108	pr483045
				6054.59	5108	pr333007
32203.997	9/2	733.1(5)	-	5731.15	3789, 4066, 4680 4698, 5275, 5309	pr148007
				5744.48	4066	pr458021
32786.668	9/2	670(1)	-	5588.49	3526, 3776, 4289, 4885, 5314	pr495053
				5805.81	3526	pr509023
32862.471	9/2	628(8)	-	5677.54	3517, 3698, 3797, 4026, 4834, 5263	pr146014 pr509055
				5706.30	3797	pr510062
33932.119	9/2	655(1)	-	5865.44	3387, 4595, 4874, 5214	pr077024
				5731.80	3387	pr092041
35690.284	9/2	630(1)	-	5668.61	3560, 3615, 3761 3847	pr142008
				5712.35	3615	pr159002
				5842.22	3560	pr292008
24691.482	11/2	749.7(5)	-	5999.95	5043, 4935	pr332018
				6229.72	6000	pr384008
25824.059	11/2	588(1)	-	5819.03	4673, 4999, 5202, 5280	pr343013
				6463.46	5200	pr480018
25934.267	11/2	472.0(5)	-	6070.03	4971, 5171, 4742, 4648, 5095, 5252	pr391001
				6077.07	4971	pr391039
28041.373	11/2	760.5(5)	-	5812.36	4601, 4687, 4898, 4976, 5279 5443, 5654	pr060006
				5833.65	5279	pr098044
				5653.07	5279	pr117032
				5674.55	4976	pr310016
28234.154	11/2	685(1)	9.69	5863.56	4200, 4278, 5331 5591	pr087027
				5897.63	4278	pr098040
				6051.23	4278	pr327031
29096.777	11/2	713(1)	-	5750.98	4054, 4299, 4445, 4657, 4746, 5001, 5042, 5095, 5337 5354, 5582, 5872, 5910, 5930, 6505	pr227014

				5870.72	5001	pr267033
29506.393	11/2	765.4(5)	-	5933.77	4057, 4654, 4988, 5374	pr285043
				6525.60	4057	pr436018
29822.717	11/2	690(1)	-	5822.12	4825.442	pr035033
				5777.73	4825.442	pr036003
				5824.43	4825.442	pr036009
				5854.33	4825.442	pr036010
29907.511	11/2	760(1)	-	6009.80	3992, 4152, 4237, 4343, 4890, 5113, 5260, 5420, 5445, 5605, 5620, 5794	pr368044
				5619.75	4237	pr474020
30411.709	11/2	802(2)	-	5629.01	3846, 3912, 4218, 4249, 4466, 4692, 5012, 5346	pr159021
				5659.14	3846	pr510019
30726.49	11/2	687(1)	-	5839.23	4390, 4658, 4702 5218	pr057004
				6041.32	4702	pr396014
31022.55	11/2	670(1)	-	5780.40	4637, 4966, 5108, 5175 5403	pr014049
				5665.57	5108	pr032015
				6199.91	5177	pr389033
31165.58	11/2	667(1)	-	5764.39	3739, 4306, 4610 4830, 5074	pr108038
				6000.57	3739	pr285009
31728.479	11/2	757(2)	-	5893.14	3858	pr269044
				5857.33	3858	pr503039
				5804.44	3858	pr510052
32006.781	11/2	621(1)	-	5884.18	3684, 4740, 4890	pr035002
				5712.11	3684	pr036024
				5700.76	4890	pr215020
				5843.25	4890	pr349008
32065.871	11/2	667(1)	-	5681.03	3675	pr309045
				5851.68		pr348048
33601.891	11/2	635(1)	-	5715.01	3702, 3895, 4312, 4405, 4911	pr325038
				5998.62	3702	pr369043
34132.030	11/2	603(3)	-	5666.85	3830, 3994	pr170032
				5828.28	3830	pr510044
				5797.46	3830	pr510048
35089.326	11/2	626.6(5)	-	5694.73	3416, 3683	pr109023 pr119029
				5799.56	3683	pr455005
36435.073	11/2	663(1)	-	5865.30	4969, 4760	pr077030
				5876.68	4760	pr087025
22150.902	13/2	322(1)	-	5783.97	6476, 6552	pr332005
				6552.15	5784	pr400042
24528.937	13/2	856.9(5)	-	6551.19	5085, 5668, 5915	pr434020
				5668.64	6551	pr141044 pr474059
				6730.39	5668	pr487003
25312.109	13/2	654.2(5)	-25.78	5898.70	4888, 5261, 5343, 5375, 5427, 5653, 6064, 6714	pr097030
				6065.14	4888	pr381000

26322.034	13/2	853.3(5)	-	5862.32	4659	pr037024
				5714.86	4659	pr109011
				5694.33	4659	pr109013
26645.154	13/2	762.6(5)	-	5825.41	4915	pr023012
				5753.33	4915	pr109009
27037.09	13/2	782.1(5)	-	5626.43	4892, 5151, 5491, 5688, 6196	pr148026
				5689.10	5151	pr154001
				6033.20	5151	pr396021
				6419.12	5490	pr399023
				6460.55	5150	pr464019
29243.515	13/2	638.1(5)	2.17	5858.95	4882, 5267, 5567, 5667	pr068028 pr507041
				5779.05	4882	pr077037 pr507003
				5811.79	4882	pr077039 pr507026
				5837.71	5267	pr077041 pr507209
29646.804	13/2	695(1)	-	5723.61	4607, 4951, 5022, 5316	pr104046
				5884.75	5022	pr474008
30209.73	13/2	830(1)	-	5821.14	4661, 5063, 5961	pr504013
				5961.14	4661	pr507054 pr508006
31621.349	13/2	648.6(5)	-	5745.50	3736, 4723, 4983, 5127	pr046029
				5125.91	3736	pr350044
31772.27	13/2	582(1)	-	5731.02	3716, 4484, 4536	pr323030
				6095.88	3716	pr491038
32013.352	13/2	650.7(5)	-	5652.91	3682, 3888, 4869, 5057, 5467	pr119033 pr121004 pr348076
				5710.01	4869	
				5851.99	3682	
33219.27	13/2	671(1)	-	5745.54	3757, 4897, 5415	pr047007
				5766.68	3757	pr483048
33333.411	13/2	612(1)	52.12	5808.23	3740, 4191, 4156 3781	pr119025
				5790.97	3740	pr509059
33371.42	13/2	574.2(5)	-	5723.66	3734	pr104035 pr506063
				5705.87	3734	pr506066
				5680.60	3734	pr117014
33423.923	13/2	570(1)	-	5864.70	3727, 4175, 5119	pr130054 pr507065
				5843.79	3727	pr349038
33504.56	13/2	693(1)	-	5751.05	3757, 4162, 4339, 4703, 4829	pr126010
				5673.25	4829	pr154024
33600.395	13/2	663(1)	-	5719.51	3665, 3704, 4682	pr169036
				5776.74	3663	pr510057
33789.685	13/2	635.1(5)	-	5721.46	3637, 3677, 4286, 5072, 5340, 5363, 5548	pr042018
				5765.95	3677	pr043003
26759.707	15/2	745(1)	-	5780.34	5315, 5556	pr016008
				5875.78	5554	pr483036
27328.744	15/2	567(1)	-0.07	5859.28	5159, 5270	pr087038 pr507068
				5685.62	5159	pr095007
				5693.69	5159	pr095008 pr507078
28153.81	15/2	574.2(4)	-	6234.34	5050, 5349	pr383041

				6025.68	<u>5349</u>	pr386015
30670.518	15/2	665(1)	-	5704.90	<u>4784</u>, 4963	pr035005
				5801.73	4784	pr471015
31373.316	15/2	604(1)	-19.48	5865.14	4036, 4797, <u>5084</u>, 5582, 5721	pr077013 pr507062
				5914.37	<u>5084</u>	pr263025 pr507059
31453.211	15/2	536.5(3)	-	5756.90	4408, <u>4609</u>, 4765	pr054024
				5801.60	<u>4610</u>	pr108047 pr449007
				5694.71	<u>4611</u>	pr109022
				5616.85	<u>4609</u>	pr302016
				5737.47	<u>4609</u>	pr351011
32303.266	15/2	473.5(4)	-	5754.35	4592, 4854, <u>5127</u>, 5528	pr095019 pr507075
				5802.24	<u>5127</u>	pr097002 pr507071
33281.212	15/2	656(1)	-	5679.09	3747, 3945, 4394, 4706, 4722, 5090, 5344, <u>5517</u>	pr309033
				6502.97	<u>3747</u>	pr419016
35652.887	15/2	475(1)	-	5668.58	3441, 3857, <u>5353</u>	pr476034
				5844.85	<u>5353</u>	pr509034
28182.321	17/2	615.5(5)	-	5643.18	<u>5430</u>, 6275, 6501	pr165032
				6501.06	<u>5644</u>	pr419005
28861.373	17/2	450.5(5)	-	5752.83	<u>5229</u>, 5434, 5645	pr123012
				6199.95	<u>5229</u>	pr389024
30852.689	17/2	579(1)	-17.62	5803.58	<u>4736</u>, 4920, 5562	pr035027
				6040.71	<u>5804</u>	pr389022
				6011.08	<u>5804</u>	pr368061
31761.614	17/2	513(1)	-	5887.44	4710, <u>4850</u>, 4986	pr080002
				5726.23	<u>4986</u>	pr087013
32508.36	17/2	430.3(5)	-	5639.41	4140, 4209, <u>5242</u> 5410, 5491	pr116028
				5687.22	<u>5242</u>	pr128044
33673.106	17/2	490(1)	3.45	5872.95	4790, 4986, <u>5655</u>, 6089	pr092004
				5752.57	<u>5655</u>	pr095002
33759.957	17/2	439.03	-	5874.80	4755, <u>4965</u>, 5212	pr035017 pr0351718 pr495030
				5843.14	<u>4965</u>	pr495035
34028.046	17/2	526(1)	-	5687.77	<u>3897</u>	pr048015 pr457036
				5637.41	<u>3897</u>	pr117001
34190.37	17/2	535(1)	-	6358.19	<u>3870</u>, 3932, 4675, 5096, 5441, 5585, 5699	pr480012
				5699.76	5441	pr482004
34894.326	17/2	571.2(5)	-	5745.56	3768, <u>3827</u>	pr046044
				5724.37	<u>3827</u>	pr050011
27674.59	19/2	471.3(5)	-	5831.81	<u>5583</u>	pr209034
				6050.44	<u>5583</u>	pr372050
29541.534	19/2	459(1)	-	5607.86	5258, 5435, <u>5949</u>, 6281	pr148040
				5949.01	<u>5607</u>	pr286017
				5923.76	<u>5607</u>	pr340040
30678.74	19/2	478.5(5)	-	6004.35	<u>5269</u>	pr316013
				6659.09	<u>5269</u>	pr479020

34145.321	19/2	446(1)	-	6004.02 5744.72	4232, 4455, 4669, <u>4872</u>, 5461 <u>4872</u>	pr316021 pr458024
35296.312	19/2	573(1)	-	6066.28 5615.82	4037, 4700, <u>5386</u>, 5615 <u>5388</u>	pr358085 pr474012
36096.508	19/2	580(1)	-	5785.37 5642.99	<u>3911</u> <u>3911</u>	pr065033 pr308006
28667.067	21/2	407(1)	-15.56	5707.62 6247.39 6646.94	<u>6247</u>, 6647 <u>5707</u> <u>5707</u>	pr091016 pr498038 pr482011 pr495016

Table 7.14: Newly discovered **Pr-I levels** in **even and odd configurations** combining with known upper levels. (Underlined fluorescence channel indicates fluorescence wavelength for recorded file mentioned in comments column).

New lower level				Excitation Wavelength λ_{air} (Å)	Fluorescence Channels λ_{air} (Å)	File numbers Comments
Energy (cm^{-1})	J	A (MHz)	B (MHz)			
Even Configuration						
14877.858	3/2	1214(1)	-	5770.30	3895, 4959, 5213, 5263, 5330	pr452031 (32203.17cm^{-1})
				6326.59	4127, 4766	pr486017 (30679.611 cm^{-1})
Odd Configuration						
14821.551	11/2	542(1)	-	5695.69	3226, 4846, 4905, 5595, 5977	pr312029 (32373.82 cm^{-1})
				6160.52	3370, 5198, 5247, 5310	pr355076 pr344013 (31049.456 cm^{-1})
				5998.47	5513	pr369039 (31487.868 cm^{-1})
				5807.95	3261, 4827, 4988, 5258	pr478029 (32034.687 cm^{-1})
15654.272	13/2	577(1)	-	6158.33	3442, 3635, 5249, 5294, 5371, 5696, 5752, 6063, 6376, 6423	pr361041 (31887.961 cm^{-1})
				6123.41	5002	pr389017 (31980.532 cm^{-1})
				6207.98	5059, 5426, 5630	pr380024 (31758.102 cm^{-1})
				5979.36	4906, 3227	pr394016 (32373.82 cm^{-1})
17676.482	17/2	856(1)	-	6125.36	3375, 5206, 5374, 5880, 6170, 6447	pr355108 (33997.543 cm^{-1})
				6197.14	5415, 5430, 5506	pr369011 (33808.373 cm^{-1})
17794.723	15/2	220(1)	-	6170.06	3375, 5206, 5374 5880, 6125, 6447	pr355061 (33997.543 cm^{-1})
				5761.58	6316	pr478014 (35146.332 cm^{-1})

Table 7.15: Newly discovered **Pr-II levels** in **even and odd configurations** combining with known lower or upper levels. (Underlined fluorescence channel indicates fluorescence wavelength for recorded file mentioned in comments column).

New level				Excitation Wavelength λ_{air} (Å)	Fluorescence Channels λ_{air} (Å)	File numbers Comments
Energy (cm^{-1})	J	A (MHz)	B (MHz)			
Even Configuration						
29901.053	5	1000(1)	-	5722.61	<u>3773</u> (3772.811)	pr054009 pr502025 Confirmed from FT-Spectra at 3772.811 Å
Odd Configuration						
10769.52	3	1154(2)	-	5785.29 5903.10	<u>3801</u>, 3623, 4852, 4987, 7602	pr052001(3)
12431.364	4	860(1)	-	5722.61 5908.69 6687.53	<u>3773</u> <u>3852</u> <u>3885</u>	pr054009 pr502025 pr112001 pr410041

7.3 Laser excitation of lines connecting known pair of levels

Ginibre [12, 13] while investigating the spectra of praseodymium I and II calculated large number of energy levels both in even and odd configurations. Since during this investigation laser excitation was not performed, therefore the data lack the useful information concerning the excitation wavelengths and the fluorescence lines as decay channels from the upper level and so a proper identification of fluorescence lower levels is not possible. This data is beneficial in the classification of spectral lines. Further more in some cases the values of hyperfine constants are not precise this is obvious from comparisons with FT-Spectra or the J-value of a level differs by 1 unit. Apart from the discovery of new levels the dissertation also includes the excitation of these lines involving pair of levels and searching for fluorescence channels from the upper level. Table 7.16 and 7.17 lists the investigated Pr-I and Pr-II lines respectively.

Table 7.16: Laser excitation of **Pr-I lines** with already known pair of levels.

Level					Excitation λ_{air} (Å)	Fluorescence Channels λ_{air} (Å)	File numbers Comments
Energy (cm^{-1})	J	P	A (MHz)	B (MHz)			
25503.39	3/2	o	999(5)	-	6306.05 6330.26	5249 5249	pr397002 pr422054
25423.52	7/2	e	1220.75 (100)	-105(5)	5821.3	6768, 6900, 6990	
23280.083	9/2	o	863.4	-	6548.27	5304	pr434034
25209.246	9/2	o	875.4	-	5819.14	5157, 5352, 4912, 6272	pr209012
23576.782	9/2	o	477.39	-	5866.51 6423.45	6778 5866	pr098010 pr450002
17125.27	9/2	e	614.0(3)	-4(4)	5837.74	4950 (Self absorption)	pr461007
23818.558	9/2	e	848.01	-	6421.48	4455	pr399025
24441.776	9/2	e	908.7(1)	-	6174.32	4090, 4335, 6111, 6408	pr361005
23976.01	9/2	e	890.3	-	6289.31	4697	pr431064
17405.424	11/2	e	740.94	-38.59	5743.74	6236, 6866 Self Abs. 5227, 5132, 5051, 5017, 4950, 4936, 4714	pr483016
17577.836	11/2	e	964.03	-	5687.40	6169 Self Abs. 4736, 4807, 4853, 4880, 4941,4952, 5015 5044, 5134, 5171 5459	pr128042
24590.79	11/2	e	914.1	-	6345.28	6055	pr442025
25209.67	11/2	o	736.87	-19.93	5686.86	5157	pr048025
25280.374	11/2	o	912(1)	-	5795.13	4896, 5435, 6010, 6078	pr350014
26357.20	11/2	e	746.51	-	5672.58	4002	pr148013
24307.505	11/2	e	730(1)	-	6419.14	6228	pr399024
27725.404	11/2	e	636.58	-	5773.86	5540, 6093, 6377,	pr320007

						5954 5530	
2846.744	13/2	o	613.240	-12.850	5889.77	<u>5043</u>	pr457029
20290.608	13/2	e	902.32	-	6283.81	<u>5285</u>	pr450005
22719.327	13/2	o	903.7	-	5599.80	<u>6625</u>	pr496043
22974.563	13/2	o	623.52		6000.26	<u>6147</u>	pr332038
24116.062	13/2	o	736.86	-	5615.52 5744.92	<u>4693</u>, 4741, 4977, 4938, 5045, 5616, 5193, 6065, 6184, 6491 <u>5193</u>	pr302036 pr483004
24267.84	13/2	e	847	-	6175.94	6477, <u>5045</u>	pr364036
24390.112	13/2	o	951.80	-3.05	5713.65 5655.85	<u>5120</u>, 5530 <u>5120</u>	
25454.38	13/2	e	775.9	-	6339.33	<u>5978</u>	pr442018
25587.88	13/2	e	749.97	10.07	5931.52 5967.62	<u>4714</u> <u>4714</u>	pr077003 pr287000
25840.14	13/2	e	654.6(3)	-4(9)	5844.04	<u>4659</u>	pr349032
26107.237	13/2	e	791.11	-63.70	5754.20	4042, 4601, 6087, 6368, <u>6377</u>, 6961	pr095034
27991.773	13/2	o	763.68	-	5705.72	<u>5397</u>, 5218	pr050015
28032.99	13/2	e	502.7	-	5757.54 5982.57	3751, <u>5437</u>, 5981 <u>3751</u>	pr374056
26258.60	13/2	e	655.06	-	6031.73	<u>4569</u>	pr368022
24928.881	13/2	o	758.5(3)	-35(7)	5779.16	<u>5369</u>	pr318010
24634.79	15/2	e	435.8	-62	6287.05	<u>4936</u>	pr431008
26553.42	15/2	o	738.0	-	5850.10	<u>5955</u>	pr111024
26654.42	15/2	e	535.4	-	5878.11 6154.55	<u>4487</u> <u>4487</u>	pr113008 pr371038
26710.25	15/2	e	466.4	-	5871.72	<u>4189</u>	pr267019
24754.55	15/2	e	627.7(6)	-	6617.34	<u>6239</u>	pr105018
25781.45	15/2	e	640.45	-	6196.14	4359, <u>6503</u>, 7122, 7157	pr355025
26333.179	15/2	e	547.2(3)	-	6403.24	<u>5992</u>	pr416001
26121.226	17/2	o	771.0	-	5760.21	<u>5629</u>	pr320000
30010.489	17/2	e	426.15	-	5858.33	<u>5524</u>	pr258041
28046.975	17/2	o	599.6	-	5686.86	<u>5078</u>	pr048027
27275.681	17/2	o	566.3	-	5702.83	<u>5400</u>	pr351020
26998.598	17/2	e	500(1)	-	6141.49	<u>7287</u>	pr355000
25114.50	17/2	o	699.5	-	6515.32	<u>5970</u>	pr419051
28423.32	17/2	e	487(1)	-	6601.93	<u>6001</u>	pr438001
27068.72	19/2	o	578.1(2)	-39(8)	5779.28	<u>4872</u>	pr318011
28964.055	19/2	e	380.26	-13.97	5812.41	<u>6241</u>	pr060014
27027.92	19/2	o	792(1)	-54(10)	5792.94 6296.91	<u>6060</u>, 6296, 6528 <u>5793</u>	pr350001 pr431056

Table 7.17: Laser excitation of **Pr-II lines** with already known pair of levels.

Energy (cm⁻¹)	J	P	A (MHz)	B (MHz)	Excitation λ_air (Å)	Fluorescence Channels λ_air (Å)	File numbers Comments
9044.98	3	o	934(1)	-	5818.57	4084	pr021032
					6087.51	3925	pr368029
25578.52	3	e	1032.5 (10)	-	5719.62	3907, 5514, 5605, 6012	pr169040
24755.016	4	e	602.63	-	5773.16	4037, 4111, 4344, 4838	pr320013
26226.52	4	e	680.5(5)	-	5818.57	3812, 4084, 5515, 5626	pr021032
					5933.78	3876	pr285036
					5847.06	3876	pr507037
28049.92	4	e	612.9	-	5785.29	3801	pr052001
25467.56	4	e	726.7(10)	-	6087.51	3925	pr368029
442.067	5	o	1913.5	-18	6049.39	6566	pr392033 pr392034 (pr392334)
9378.54	5	o	615(1)	-	5933.78	4084	pr285035
25499.57	5	e	633.06	-	5868.80	3989	pr269021
26707.328	5	e	516.26	-	5769.10	4005	pr095010
26973.49	5	e	611.6	-	5681.88	3947	pr121001
27198.24	5	e	599.6	-	5695.89	3927	pr312012
27380.45	5	e	690.31	-	6687.53	3885	pr410041
29350.99	5	e	490.6	-	5908.69	3852	pr112001
9646.62	6	o	616.2	-	5695.89	3927	pr312012
10729.72	6	o	529.71	-	5785.38	4062	pr325039
26961.96	6	e	609.7	-	5685.60	3951	pr208009
					5904.47	3951	pr261049
27604.94	6	e	581.1	-	5731.87	3852, 4062	pr092036
28508.79	6	e	636.5	-	5623.04	3918, 3981	pr146035
28009.80	7	e	554.13	-	5785.38	4062	pr325039
29723.97	8	e	518.02	-	5719.08	4056	pr169041

7.4 Classification of lines using known or unknown levels via Laser excitation

As remarked earlier the spectral line density in praseodymium is very high with a huge number of lines yet to be classified. Most often the Fourier Transform (F.T.) recordings show either convolution of more than one line or hyperfine patterns of lines which are only partially resolved showing no off-diagonal components. So in order to classify such lines it becomes necessary to do their laser excitation and record LIF signal. As for instance one such segment i.e. from 5600.00 Å to 5598.934 Å was experimentally investigated and 10 lines were classified using new and already known pair of levels. Hundreds of lines have been classified in this manner, some of them are presented in table 7.18.

Table 7.18: List of lines classified using known or unknown levels

Excitation wavelength λ_{air} (Å)	J-Values		Level Energies (cm^{-1})	
	Even	Odd	Even	Odd
4985.54	5/2	3/2	29039.208	8986.444
5125.91	13/2	13/2	12118.06	31621.349
5588.49	9/2	9/2	14897.77	32786.668
5593.36	11/2	13/2	32891.402	15018.14
5594.76	9/2	7/2	4432.24	22301.146
5598.41	7/2	9/2	31237.02	13379.78
5599.33	5/2	7/2	29257.387	11403.067
5601.62	9/2	7/2	29250.135	11403.067
5607.86	17/2	19/2	11714.38	29541.534
5612.82	3/2	5/2	12701.269	30512.676
5615.82	17/2	19/2	17494.42	35296.312
5616.85	13/2	15/2	13654.547	31453.211
5616.91	5/2	7/2	30717.623	12919.185
5617.48	13/2	11/2	31798.949	14002.323
5617.78	15/2	13/2	34000.64	16204.883
5618.36	3/2	5/2	27539.142	9745.313
5619.75	13/2	11/2	12118.06	29907.511
5621.32	7/2	9/2	10194.74	27979.218
5622.87	15/2	15/2	30781.638	13002.05
5623.89	3/2	5/2	28917.934	11141.581
5626.10	9/2	9/2	28705.998	10936.67
5626.43	11/2	13/2	9268.741	27037.09
5628.98	15/2	13/2	31756.217	13996.091
5629.01	9/2	11/2	12651.578	30411.709
5635.67	5/2	3/2	29731.99	11992.85
5637.42	15/2	17/2	16294.4	34028.046
5638.04	9/2	11/2	25812.15	8080.44
5639.36	13/2	11/2	31729.933	14002.323

5639.41	15/2	17/2	14780.939	32508.36
5642.99	17/2	19/2	18380.34	36096.508
5643.021	3/2	3/2	11911.437	29627.43
5643.18	15/2	17/2	10466.73	28182.321
5647.03	7/2	9/2	31083.278	13379.78
5651.12	7/2	5/2	12108.819	29799.529
5651.36	13/2	15/2	33870.18	16180.223
5652.65	7/2	9/2	13032.665	30718.272
5652.74	7/2	7/2	13032.665	30718.587
5652.91	13/2	13/2	14328.241	32013.352
5653.07	9/2	11/2	10356.71	28041.373
5653.68	7/2	9/2	13415.769	31098.427
5654.09	9/2	11/2	31041.905	13360.529
5656.22	11/2	11/2	32496.297	14821.551
5656.74	3/2	5/2	9650.06	27323.158
5659.04	9/2	9/2	13432.49	31098.427
5659.14	9/2	11/2	12746.08	30411.709
5660.71	15/2	13/2	28071.547	10410.76
5662.95	9/2	11/2	28976.248	11322.42
5665.57	11/2	11/2	13376.992	31022.55
5666.75	9/2	7/2	9105.035	26746.925
5666.82	13/2	15/2	33040.589	15399.08
5666.85	9/2	11/2	16490.447	34132.03
5667.45	7/2	7/2	29917.719	12277.947
5668.34	9/2	11/2	31639.28	14002.323
5668.58	13/2	15/2	18016.641	35652.887
5668.59	5/2	7/2	29039.208	11403.067
5668.61	9/2	9/2	18054.202	35690.284
5668.64	11/2	13/2	6892.949	24528.937
5668.71	11/2	13/2	29857.89	12222.1
5670.59	9/2	7/2	31639.28	14009.252
5672.77	5/2	5/2	29731.99	12108.819
5672.94	5/2	7/2	12647.027	30269.667
5673.25	11/2	13/2	15882.93	33504.56
5673.27	7/2	5/2	10194.74	27816.365
5674.32	7/2	5/2	9704.75	27323.158
5674.42	9/2	7/2	12651.578	30269.667
5674.54	13/2	11/2	10423.68	28041.373
5674.69	9/2	7/2	13822.5	31439.705
5675.64	13/2	13/2	33040.589	15426.41
5676.31	9/2	9/2	30966.07	13353.89
5676.72	17/2	15/2	33009.799	15399.08
5677.44	5/2	3/2	12078.583	29687.263
5677.54	7/2	9/2	15254.089	32862.471

5677.97	13/2	11/2	30484.724	12877.67
5678.48	5/2	5/2	12907.042	30512.676
5678.78	11/2	9/2	10841.482	28445.99
5679.03	7/2	7/2	30522.946	12919.185
5679.09	13/2	15/2	15677.65	33281.212
5680.60	13/2	13/2	15772.56	33371.42
5681.03	9/2	11/2	14468.31	32065.871
5682.49	11/2	9/2	32989.103	15396.075
5682.88	7/2	9/2	7617.455	25209.246
5685.62	15/2	15/2	9745.42	27328.744
5687.22	15/2	17/2	14929.926	32508.36
5687.77	15/2	17/2	16451.35	34028.046
5689.10	13/2	13/2	9464.46	27037.09
5692.79	7/2	9/2	7617.455	25178.609
5693.56	17/2	15/2	30560.925	13002.05
5693.69	17/2	15/2	9770.33	27328.744
5694.33	15/2	13/2	8765.556	26322.034
5694.71	13/2	15/2	13897.891	31453.211
5694.73	9/2	11/2	17534.157	35089.326
5695.69	11/2	11/2	32373.82	14821.551
5695.76	13/2	13/2	33870.18	16318.145
5695.97	5/2	5/2	15006.707	32558.096
5696.24	9/2	7/2	13605.68	31156.257
5696.42	9/2	9/2	13272.62	30822.637
5697.49	7/2	5/2	15254.089	32800.814
5699.76	15/2	17/2	16650.62	34190.37
5700.76	13/2	11/2	14470.06	32006.781
5701.06	7/2	9/2	6535.587	24071.325
5701.58	9/2	9/2	0	17534.157
5701.61	5/2	5/2	11646.26	29180.3
5701.640	11/2	13/2	16778.51	34312.458
5701.64	5/2	7/2	28188.037	10654.11
5703.79	3/2	3/2	29520.196	11992.85
5704.09	11/2	9/2	10904.07	28430.448
5704.90	13/2	15/2	13146.6	30670.518
5704.91	7/2	5/2	12049.463	29573.267
5705.87	13/2	13/2	15850.49	33371.42
5706.30	9/2	9/2	15342.79	32862.471
5706.84	11/2	9/2	29248.613	11730.6
5707.62	19/2	21/2	11151.49	28667.334
5708.77	9/2	11/2	30389.64	12877.67
5710.01	11/2	13/2	14505.09	32013.352
5710.06	7/2	9/2	13590.35	31098.427
5710.07	17/2	15/2	29322.753	11814.66

5711.51	13/2	11/2	31729.933	14226.248
5712.35	9/2	9/2	18189.22	35690.284
5713.05	13/2	13/2	30834.815	13335.895
5714.46	5/2	5/2	12078.583	29573.267
5714.86	11/2	13/2	8829.078	26322.034
5715.01	9/2	11/2	16108.959	33601.891
5716.70	7/2	9/2	14249.395	31737.15
5716.9	13/2	13/2	31483.15	13996.091
5717.63	9/2	11/2	28807.347	11322.42
5718.60	13/2	13/2	27166.353	9684.19
5719.51	11/2	13/2	16121.23	33600.395
5719.84	11/2	13/2	32496.297	15018.14
5719.91	11/2	9/2	10904.07	28381.982
5721.30	5/2	3/2	11646.26	29119.95
5721.46	11/2	13/2	16316.5	33789.685
5722.41	11/2	13/2	31980.532	14510.22
5722.56	15/2	17/2	35146.332	17676.482
5722.66	9/2	7/2	9105.035	26574.579
5722.72	5/2	5/2	12907.042	30376.498
5723.11	9/2	9/2	29198.871	11730.6
5723.61	11/2	13/2	12180.13	29646.804
5723.66	11/2	13.2	15904.93	33371.42
5724.37	15/2	17/2	17429.98	34894.326
5725.18	7/2	7/2	31083.278	13621.414
5725.21	17/2	17/2	31801.97	14340.21
5726.23	17/2	17/2	14302.923	31761.614
5727.11	15/2	13/2	29678.099	12222.1
5728.69	7/2	7/2	9918.17	27369.327
5729.21	5/2	7/2	6451.823	23901.383
5729.58	9/2	9/2	12651.578	30100.133
5730.46	15/2	13/2	30781.638	13335.895
5731.02	13/2	13/2	14328.241	31772.27
5731.15	11/2	9/2	14760.32	32203.997
5731.68	9/2	9/2	9105.035	26547.124
5731.80	9/2	9/2	16490.447	33932.119
5731.95	13/2	13/2	29187.599	11746.34
5734.11	9/2	9/2	30814.475	13379.78
5737.41	11/2	9/2	32496.297	15071.648
5737.47	17/2	15/2	14028.75	31453.211
5738.30	5/2	5/2	29530.791	12108.819
5738.63	5/2	7/2	13735.262	31156.257
5738.85	11/2	11/2	17405.54	34825.79
5739.03	5/2	5/2	28561.383	11141.581
5740.95	5/2	7/2	31035.306	13621.414

5741.99	11/2	13/2	29632.809	12222.1
5742.00	5/2	7/2	15113.984	32524.685
5742.37	17/2	19/2	29322.753	11913.16
5742.84	9/2	11/2	31410.496	14002.323
5743.26	7/2	9/2	13415.769	30822.637
5743.60	7/2	7/2	11274.18	28680.02
5743.64	11/2	11/2	31408.036	14002.323
5744.48	11/2	9/2	14800.7	32203.997
5744.72	17/2	19/2	16742.603	34145.321
5745.50	15/2	13/2	14221.304	31621.349
5745.52	3/2	5/2	12701.269	30101.32
5745.54	15/2	13/2	15819.324	33219.114
5745.55	5/2	7/2	12078.583	29478.545
5745.56	17/2	17/2	17494.42	34894.326
5746.48	15/2	15/2	32166.51	14769.55
5750.98	9/2	11/2	28705.998	11322.42
5750.98	9/2	11/2	11713.22	29096.777
5751.05	11/2	13/2	16121.23	33504.56
5752.57	15/2	17/2	16294.4	33673.106
5752.83	15/2	17/2	11483.45	28861.373
5753.33	11/2	13/2	9268.741	26645.154
5754.20	13/2	13/2	26107.237	8733.45
5754.20	5/2	5/2	13670.188	31043.994
5754.35	15/2	15/2	14929.926	32303.266
5754.46	13/2	15/2	29187.599	11814.66
5754.53	7/2	5/2	9918.17	27290.98
5756.28	17/2	15/2	32137.057	14769.55
5756.84	7/2	7/2	6535.587	23901.383
5756.90	13/2	15/2	14087.57	31453.211
5757.88	7/2	7/2	30281.88	12919.185
5757.93	3/2	1/2	12264.888	29627.43
5759.76	7/2	9/2	29087.634	11730.6
5761.58	15/2	15/2	35146.332	17794.723
5761.72	15/2	17/2	28071.547	10720.4
5764.38	3/2	5/2	13033.479	30376.498
5764.39	9/2	11/2	13822.5	31165.58
5765.95	15/2	13/2	16451.35	33789.685
5766.35	17/2	19/2	32137.057	14799.88
5766.68	11/2	13/2	15882.93	33219.114
5768.21	5/2	3/2	29324.461	11992.85
5768.48	7/2	5/2	11668.787	28999.54
5768.86	21/2	19/2	30275.01	12945.51
5769.96	13/2	13/2	33531.213	16204.883
5770.30	3/2	5/2	14877.858	32203.17

5770.54	11/2	13/2	32671.946	15347.433
5770.99	13/2	11/2	33870.18	16546.863
5771.12	9/2	7/2	16490.447	33813.296
5771.70	13/2	11/2	32049.991	14728.898
5772.96	9/2	7/2	30938.77	13621.414
5773.06	7/2	9/2	13781.35	31098.427
5773.86	11/2	13/2	27725.404	10410.76
5774.01	11/2	9/2	25564.412	8250.17
5776.04	7/2	9/2	25558.27	8250.17
5776.74	15/2	13/2	16294.4	33600.395
5777.29	7/2	5/2	13739.706	31043.994
5777.73	9/2	11/2	12519.718	29822.717
5779.05	11/2	13/2	11944.2	29243.315
5779.18	13/2	13/2	7630.147	24928.881
5779.18	13/2	13/2	7630.147	24928.881
5779.21	9/2	9/2	32209.15	14910.533
5780.34	13/2	15/2	9464.46	26759.707
5780.40	11/2	11/2	13727.48	31022.55
5780.41	5/2	7/2	15006.707	32301.78
5780.42	3/2	3/2	11361.817	28656.732
5782.92	15/2	13/2	29033.86	11746.34
5783.80	9/2	7/2	15016.889	32301.78
5783.97	11/2	13/2	4866.53	22150.902
5785.29	13/2	15/2	32049.991	14769.55
5785.34	17/2	17/2	30560.925	13280.44
5785.37	17/2	19/2	18816.311	36096.508
5785.51	15/2	17/2	31619.982	14340.21
5788.91	15/2	17/2	29033.86	11764.25
5789.39	7/2	9/2	11668.787	28936.947
5790.97	13/2	13/2	16069.9	33333.411
5792.5	9/2	7/2	16554.331	33813.296
5792.94	17/2	19/2	9770.33	27027.92
5794.35	9/2	7/2	14186.36	31439.705
5794.94	11/2	11/2	31980.532	14728.898
5796.83	9/2	9/2	11184.41	28430.448
5797.46	9/2	11/2	16887.83	34132.03
5797.92	5/2	5/2	12907.042	30149.869
5798.20	19/2	19/2	32041.836	14799.88
5799.56	13/2	11/2	17851.441	35089.326
5799.82	11/2	13/2	32891.402	15654.272
5801.58	15/2	13/2	32658.325	15426.41
5801.58	11/2	9/2	14505.09	31737.15
5801.60	15/2	15/2	14221.304	31453.211
5801.73	15/2	15/2	13439.04	30670.518

5801.81	5/2	3/2	11107.69	28338.91
5802.24	13/2	15/2	15073.268	32303.266
5802.96	7/2	7/2	31237.02	14009.252
5803.58	19/2	17/2	13626.72	30852.689
5804.33	9/2	9/2	11713.22	28936.947
5805.81	11/2	9/2	15567.28	32786.668
5807.09	5/2	5/2	29324.461	12108.819
5807.12	15/2	15/2	34000.64	16784.817
5807.95	11/2	11/2	32034.548	14821.551
5807.97	7/2	9/2	28149.612	10936.67
5808.23	11/2	13/2	16121.23	33333.411
5809.30	13/2	15/2	32608.084	15399.08
5811.06	11/2	13/2	32221.927	15018.14
5811.79	13/2	13/2	12041.67	29243.315
5812.28	9/2	9/2	29250.135	12049.95
5812.36	11/2	11/2	10841.482	28041.373
5812.77	11/2	9/2	29248.613	12049.95
5814.27	5/2	5/2	12907.042	30101.32
5814.65	17/2	17/2	32137.057	14943.85
5815.16	5/2	5/2	15609.117	32800.814
5815.16	5/2	5/2	15609.117	32800.814
5815.61	7/2	7/2	14249.395	31439.705
5818.70	9/2	9/2	12519.718	29700.919
5819.03	9/2	11/2	8643.839	25824.059
5819.14	9/2	9/2	8029.29	25209.246
5821.14	11/2	13/2	13035.73	30209.73
5822.04	9/2	9/2	14764.29	31935.661
5822.12	9/2	11/2	12651.578	29822.717
5822.46	11/2	9/2	4866.53	22036.64
5824.43	11/2	11/2	12658.427	29822.717
5825.41	11/2	13/2	9483.54	26645.154
5826.46	5/2	7/2	28561.383	11403.067
5828.28	13/2	11/2	16979.03	34132.03
5829.52	9/2	9/2	8029.29	25178.609
5829.65	9/2	9/2	29198.871	12049.95
5829.69	13/2	13/2	30484.724	13335.895
5829.71	15/2	15/2	18466.97	35615.714
5829.85	5/2	5/2	29257.387	12108.819
5831.59	7/2	9/2	30522.946	13379.78
5831.81	17/2	19/2	10532.001	27674.59
5833.54	9/2	9/2	32209.15	15071.648
5833.76	9/2	9/2	14186.36	31323.207
5835.14	13/2	13/2	31642.946	14510.22
5836.23	15/2	13/2	32784.03	15654.272

5836.70	7/2	7/2	13590.35	30718.587
5837.71	13/2	13/2	12118.06	29243.315
5838.15	5/2	7/2	14315.726	31439.705
5839.11	5/2	5/2	9710.64	26831.815
5839.23	9/2	11/2	13605.68	30726.49
5839.98	7/2	5/2	31083.278	13964.63
5840.26	5/2	5/2	15383.441	32501.249
5840.29	15/2	13/2	30453.594	13335.895
5840.39	13/2	15/2	17667.851	34785.249
5842.01	7/2	9/2	28049.33	10936.67
5842.02	9/2	9/2	13605.68	30718.272
5842.21	5/2	3/2	8737.448	25849.518
5843.14	15/2	17/2	16650.62	33759.957
5843.25	9/2	11/2	14897.77	32006.781
5843.27	7/2	7/2	30730.364	13621.414
5843.79	11/2	13/2	16316.5	33423.923
5843.79	11/2	13/2	16316.5	33423.923
5844.42	11/2	13/2	27516.452	10410.76
5844.85	15/2	15/2	18548.54	35652.887
5845.73	5/2	5/2	12078.583	29180.3
5847.02	19/2	17/2	32041.836	14943.85
5847.48	7/2	9/2	29917.719	12821.083
5847.64	7/2	5/2	10194.74	27290.98
5851.57	11/2	11/2	27516.452	10431.72
5851.68	11/2	11/2	14981.51	32065.871
5851.99	15/2	13/2	14929.926	32013.352
5852.09	7/2	9/2	12617.767	29700.919
5854.33	9/2	9/2	28807.347	11730.6
5854.33	9/2	11/2	12746.08	29822.717
5854.44	21/2	21/2	30275.01	13198.7
5855.49	17/2	15/2	32472.35	15399.08
5855.49	17/2	15/2	32472.35	15399.08
5856.41	5/2	5/2	31035.306	13964.63
5857.11	13/2	15/2	26715.373	9646.85
5857.28	3/2	5/2	13033.479	30101.32
5857.32	7/2	5/2	12617.767	29685.664
5857.47	7/2	9/2	13032.665	30100.133
5858.13	11/2	11/2	25900.916	8835.38
5858.95	11/2	13/2	12180.13	29243.315
5859.28	13/2	15/2	10266.51	27328.744
5859.28	5/2	5/2	15006.707	32068.921
5859.40	7/2	5/2	15439.446	32501.249
5862.35	11/2	13/2	9268.741	26322.034
5863.56	9/2	11/2	11184.41	28234.154

5864.70	5/2	5/2	28188.037	11141.581
5864.74	5/2	3/2	29039.208	11992.85
5864.80	13/2	15/2	32445.251	15399.08
5865.17	13/2	15/2	14328.241	31373.316
5865.30	13/2	11/2	19390.38	36435.073
5865.44	9/2	9/2	16887.83	33932.119
5866.43	5/2	3/2	12078.583	29119.95
5866.55	15/2	17/2	28805.33	11764.25
5868.09	11/2	9/2	29857.89	12821.083
5868.38	9/2	9/2	30389.64	13353.89
5869.07	5/2	7/2	11646.26	28680.02
5869.95	13/2	13/2	26715.373	9684.19
5870.89	17/2	17/2	34704.94	17676.482
5871.01	9/2	11/2	5822.905	22851.014
5872.95	15/2	17/2	16650.62	33673.106
5873.10	5/2	5/2	13127.787	30149.869
5874.80	17/2	17/2	16742.603	33759.957
5875.01	11/2	13/2	32034.548	15018.14
5875.78	15/2	15/2	9745.42	26759.707
5876.36	9/2	7/2	10356.71	27369.327
5876.68	13/2	11/2	19423.46	36435.073
5877.13	5/2	3/2	11646.26	28656.732
5879.15	3/2	5/2	28146.157	11141.581
5880.00	11/2	13/2	30998.18	13996.091
5880.00	17/2	19/2	31801.97	14799.88
5881.27	15/2	15/2	33783.23	16784.817
5881.29	7/2	7/2	29917.538	12919.185
5881.37	11/2	9/2	28728.842	11730.6
5882.44	5/2	7/2	6451.823	23446.85
5884.18	9/2	11/2	15016.889	32006.781
5884.75	11/2	13/2	12658.427	29646.804
5885.11	5/2	5/2	10828.988	27816.365
5885.33	15/2	15/2	31756.217	14769.55
5887.44	15/2	17/2	14780.939	31761.614
5887.51	5/2	3/2	12647.027	29627.43
5887.57	11/2	9/2	13250.69	30230.959
5888.67	3/2	3/2	11361.817	28338.91
5893.14	9/2	11/2	14764.29	31728.479
5895.00	9/2	7/2	12519.718	29478.545
5895.20	7/2	5/2	15110.661	32068.921
5895.27	7/2	9/2	11472.35	28430.448
5896.74	13/2	13/2	32608.084	15654.272
5897.63	11/2	11/2	11282.87	28234.154
5898.20	15/2	15/2	33129.815	16180.223

5898.32	5/2	7/2	29868.643	12919.185
5898.70	15/2	13/2	8363.916	25312.109
5898.75	3/2	5/2	12051.532	28999.54
5906.75	3/2	3/2	28917.934	11992.85
5908.82	13/2	15/2	30484.724	13565.52
5911.90	9/2	11/2	31639.28	14728.898
5912.83	7/2	5/2	28049.33	11141.581
5913.13	7/2	7/2	14249.395	31156.257
5914.37	13/2	15/2	14470.06	31373.316
5923.76	21/2	19/2	12665.074	29541.534
5923.91	9/2	9/2	31410.496	14534.423
5924.47	11/2	13/2	32221.927	15347.433
5925.10	9/2	11/2	27304.431	10431.72
5925.31	11/2	9/2	9675.04	26547.124
5926.11	7/2	7/2	9704.75	26574.579
5930.13	17/2	17/2	28622.6	11764.25
5933.62	11/2	11/2	25683.831	8835.38
5933.77	11/2	11/2	12658.427	29506.393
5937.54	5/2	5/2	15720.838	32558.096
5939.24	13/2	11/2	30834.815	14002.323
5945.19	9/2	11/2	31041.905	14226.248
5947.28	7/2	7/2	29087.634	12277.947
5948.01	9/2	7/2	28210.613	11403.067
5949.01	17/2	19/2	12736.67	29541.534
5949.37	5/2	7/2	15720.838	32524.685
5951.49	17/2	15/2	27466.81	10668.96
5952.02	13/2	11/2	32773.833	15977.6
5952.80	13/2	15/2	28608.812	11814.66
5952.93	13/2	13/2	31304.011	14510.22
5953.48	17/2	15/2	33657.329	16865.077
5955.05	15/2	17/2	33783.23	16995.46
5956.03	5/2	7/2	28188.037	11403.067
5956.36	11/2	13/2	32989.103	16204.883
5958.35	5/2	5/2	12907.042	29685.664
5961.14	15/2	13/2	13439.04	30209.73
5961.97	9/2	7/2	30389.64	13621.414
5962.23	15/2	15/2	32166.51	15399.08
5965.87	9/2	9/2	28807.347	12049.95
5969.77	17/2	17/2	27466.81	10720.4
5972.09	9/2	11/2	30966.07	14226.248
5979.36	11/2	13/2	32373.82	15654.272
5980.19	3/2	5/2	16059.899	32777.119
5981.88	9/2	11/2	30938.77	14226.248
5986.98	9/2	7/2	28976.248	12277.947

5992.97	9/2	11/2	31410.496	14728.898
5994.41	7/2	5/2	12321.925	28999.54
5996.20	11/2	9/2	28403.321	11730.6
5998.62	11/2	11/2	16935.88	33601.891
5998.88	11/2	9/2	13035.73	29700.919
5998.89	3/2	5/2	27806.714	11141.581
5999.90	9/2	7/2	4432.24	21094.562
5999.95	9/2	11/2	8029.29	24691.482
6000.07	17/2	17/2	33657.329	16995.46
6000.16	7/2	5/2	29917.719	13256.067
6000.46	21/2	19/2	29606.273	12945.51
6000.50	7/2	7/2	30281.88	13621.414
6000.57	11/2	11/2	14505.09	31165.58
6003.74	5/2	7/2	30273.089	13621.414
6004.02	17/2	19/2	17494.42	34145.321
6004.23	9/2	7/2	27304.431	10654.11
6004.35	17/2	19/2	14028.75	30678.74
6007.61	7/2	9/2	26578.511	10936.67
6009.80	9/2	11/2	13272.62	29907.511
6009.91	5/2	5/2	9710.64	26345.227
6010.16	9/2	11/2	31362.774	14728.898
6011.08	15/2	17/2	14221.304	30852.689
6021.01	5/2	3/2	6451.823	23055.74
6025.68	13/2	15/2	11562.79	28153.81
6028.53	15/2	13/2	28805.33	12222.1
6029.77	11/2	9/2	27516.452	10936.67
6030.93	7/2	9/2	11869.331	28445.99
6033.20	15/2	13/2	10466.73	27037.09
6035.47	17/2	15/2	32744.355	16180.223
6036.83	15/2	13/2	31070.645	14510.22
6037.13	5/2	3/2	13127.787	29687.263
6040.71	17/2	17/2	14302.923	30852.689
6041.32	11/2	11/2	14178.38	30726.49
6043.86	9/2	11/2	31362.774	14821.551
6044.32	1/2	3/2	10956.833	27496.712
6046.18	9/2	9/2	8643.839	25178.609
6048.36	7/2	7/2	6535.587	23064.427
6048.79	15/2	17/2	34204.135	17676.482
6050.44	19/2	19/2	11151.49	27674.59
6050.90	11/2	9/2	24772.03	8250.17
6051.23	9/2	11/2	11713.22	28234.154
6056.45	11/2	13/2	28728.842	12222.1
6059.89	11/2	11/2	29857.89	13360.529
6059.89	13/2	15/2	27166.353	10668.96

6061.12	5/2	5/2	10828.988	27323.158
6061.30	17/2	17/2	31437.408	14943.85
6065.14	11/2	13/2	8829.078	25312.139
6066.28	9/2	9/2	28210.613	11730.6
6066.28	17/2	19/2	18816.311	35296.312
6070.03	13/2	11/2	9464.45	25934.267
6071.05	11/2	13/2	32671.946	16204.883
6071.8	13/2	13/2	31483.15	15018.14
6072.68	1/2	3/2	28455.478	11992.85
6074.53	15/2	13/2	30453.594	13996.091
6075.92	7/2	9/2	7617.455	24071.325
6077.07	11/2	11/2	9483.54	25934.267
6078.99	7/2	9/2	29799.529	13353.89
6081.51	15/2	13/2	34204.135	17765.348
6082.48	15/2	17/2	28200.351	11764.25
6085.51	13/2	15/2	32608.084	16180.223
6085.63	11/2	9/2	29248.613	12821.083
6087.32	13/2	13/2	26107.237	9684.19
6087.67	3/2	3/2	16355.022	32777.119
6087.96	9/2	7/2	29340.502	12919.185
6092.38	15/2	15/2	34204.135	17794.723
6092.40	7/2	5/2	6535.587	22944.93
6094.26	9/2	9/2	30938.77	14534.423
6095.88	13/2	13/2	15372.3	31772.27
6096.78	3/2	5/2	27539.142	11141.581
6099.54	9/2	7/2	10356.71	26746.925
6116.09	15/2	15/2	31744.873	15399.08
6116.74	13/2	13/2	26028.258	9684.19
6117.43	15/2	13/2	29678.099	13335.895
6117.99	15/2	13/2	31688.137	15347.433
6123.41	11/2	13/2	31980.532	15654.272
6123.41	11/2	13/2	31980.532	15654.272
6124.23	15/2	17/2	34000.64	17676.482
6125.33	9/2	11/2	29198.871	12877.67
6125.36	17/2	17/2	33997.543	17676.482
6130.11	5/2	5/2	30273.089	13964.63
6130.54	15/2	17/2	28071.547	11764.25
6131.74	9/2	9/2	4432.24	20736.35
6137.39	15/2	15/2	31688.137	15399.08
6144.70	3/2	5/2	27411.277	11141.581
6150.02	9/2	11/2	30257.922	14002.323
6152.91	9/2	9/2	28297.925	12049.95
6153.93	17/2	15/2	31437.408	15399.08
6158.33	15/2	13/2	31887.961	15654.272

6159.59	17/2	15/2	31629.427	15399.08
6160.52	13/2	11/2	31049.456	14821.551
6161.56	17/2	15/2	33009.799	16784.817
6166.51	17/2	17/2	34704.94	18492.797
6170.06	17/2	15/2	33997.543	17794.723
6172.67	7/2	9/2	30730.364	14534.423
6175.40	11/2	13/2	29524.718	13335.895
6175.41	5/2	3/2	9710.64	25899.43
6175.58	9/2	7/2	26842.453	10654.11
6178.29	11/2	13/2	28403.321	12222.1
6188.50	13/2	15/2	25801.393	9646.85
6188.97	3/2	3/2	28146.157	11992.85
6192.18	11/2	9/2	29524.718	13379.78
6198.46	7/2	7/2	26578.511	10449.941
6199.75	17/2	19/2	29070.702	12945.51
6199.91	9/2	11/2	14897.77	31022.55
6199.95	17/2	17/2	12736.67	28861.373
6202.84	13/2	13/2	25801.393	9684.19
6204.28	15/2	17/2	30453.594	14340.21
6205.38	5/2	7/2	29731.99	13621.414
6207.91	9/2	7/2	29340.502	13236.599
6207.98	13/2	13/2	31758.102	15654.272
6210.96	7/2	7/2	26750.221	10654.11
6221.58	17/2	15/2	29070.702	13002.05
6227.83	15/2	13/2	31070.645	15018.14
6229.72	9/2	11/2	8643.839	24691.482
6233.34	17/2	15/2	31437.408	15399.08
6233.74	17/2	17/2	30981.156	14943.85
6234.34	13/2	15/2	12118.06	28153.81
6235.85	15/2	15/2	29033.86	13002.05
6235.93	9/2	11/2	30257.922	14226.248
6238.38	7/2	9/2	6535.587	22561.013
6247.39	21/2	21/2	12665.074	28667.067
6256.78	15/2	13/2	28200.351	12222.1
6267.84	15/2	15/2	31349.288	15399.08
6267.84	15/2	15/2	31349.288	15399.08
6273.11	11/2	11/2	24772.03	8835.38
6281.27	17/2	15/2	28918.012	13002.05
6283.57	5/2	7/2	28188.037	12277.947
6283.85	5/2	7/2	29530.791	13621.414
6287.02	9/2	7/2	27304.431	11403.067
6289.31	9/2	11/2	23976.01	8080.44
6296.91	19/2	19/2	11151.49	27027.92
6299.53	11/2	9/2	4866.53	20736.35

6303.67	5/2	7/2	29868.643	14009.252
6306.05	3/2	3/2	9650.06	25503.39
6307.68	5/2	7/2	6451.823	22301.146
6315.25	15/2	13/2	35146.332	19315.962
6326.06	15/2	15/2	28805.33	13002.05
6326.59	3/2	5/2	14877.858	30679.611
6330.26	5/2	3/2	9710.64	25503.39
6338.87	15/2	15/2	32784.03	17012.703
6339.36	11/2	13/2	27516.452	11746.34
6347.89	17/2	17/2	32744.355	16995.46
6350.33	9/2	9/2	30814.475	15071.648
6358.19	5/2	5/2	6451.823	22175.22
6358.19	15/2	17/2	18466.97	34190.37
6368.55	3/2	5/2	27806.714	12108.819
6377.79	11/2	11/2	32221.927	16546.863
6384.09	5/2	5/2	26801.197	11141.581
6387.90	15/2	13/2	33415.62	17765.348
6389.25	15/2	13/2	29642.982	13996.091
6390.35	9/2	7/2	26298.385	10654.11
6391.34	7/2	9/2	26578.511	10936.67
6391.54	9/2	7/2	28210.613	12569.6
6393.09	17/2	17/2	28918.012	13280.44
6393.77	9/2	9/2	28381.982	12746.08
6399.41	15/2	13/2	29187.599	13565.52
6399.56	17/2	15/2	31801.97	16180.223
6400.06	17/2	15/2	28622.6	13002.05
6401.30	13/2	13/2	26028.258	10410.76
6404.96	7/2	5/2	26750.221	11141.581
6408.63	11/2	11/2	23680.085	8080.44
6409.92	13/2	11/2	26028.258	10431.72
6414.12	5/2	5/2	10828.988	26415.38
6419.12	13/2	13/2	11462.858	27037.09
6419.16	9/2	9/2	27304.431	11730.6
6440.89	11/2	11/2	26843.924	11322.42
6449.39	7/2	9/2	6535.587	22036.64
6460.20	21/2	19/2	30275.01	14799.88
6460.55	13/2	13/2	11562.79	27037.09
6462.34	3/2	5/2	11361.817	26831.815
6462.67	11/2	11/2	25900.916	10431.72
6463.46	9/2	11/2	10356.71	25824.059
6475.15	9/2	7/2	26842.453	11403.067
6479.12	11/2	9/2	23680.085	8250.17
6483.95	3/2	3/2	27411.277	11992.85
6486.72	9/2	9/2	23661.972	8250.17

6488.95	11/2	11/2	29632.809	14226.248
6492.50	5/2	7/2	26801.197	11403.067
6501.06	15/2	17/2	12804.49	28182.321
6501.61	13/2	11/2	31798.949	16422.282
6502.97	15/2	15/2	17907.819	33281.212
6506.73	15/2	13/2	33129.815	17765.348
6507.47	9/2	9/2	11184.41	26547.124
6507.92	9/2	9/2	26298.385	10936.67
6511.81	17/2	15/2	28918.012	13565.52
6511.91	17/2	15/2	32137.057	16784.817
6515.32	17/2	17/2	9770.33	25114.5
6524.32	7/2	7/2	11472.35	26795.389
6525.26	11/2	9/2	12658.427	27979.218
6525.60	9/2	11/2	14186.36	29506.393
6528.97	11/2	11/2	27516.452	12204.304
6532.96	15/2	17/2	29642.982	14340.21
6545.66	11/2	13/2	25683.831	10410.76
6546.12	17/2	15/2	32137.057	16865.077
6546.28	9/2	7/2	5822.905	21094.562
6551.19	11/2	13/2	9268.741	24528.937
6552.15	11/2	13/2	6892.949	22150.902
6556.30	13/2	11/2	28608.812	13360.529
6561.33	5/2	5/2	9710.64	24947.255
6568.20	13/2	11/2	31642.946	16422.282
6572.22	15/2	17/2	32206.775	16995.46
6580.61	11/2	11/2	23272.407	8080.44
6597.25	11/2	13/2	25564.412	10410.76
6599.23	5/2	7/2	11646.26	26795.389
6614.19	15/2	15/2	13439.04	28553.89
6614.86	11/2	9/2	26843.924	11730.6
6637.69	9/2	7/2	28297.925	13236.599
6639.98	9/2	11/2	23891.53	8835.38
6646.94	19/2	21/2	13626.72	28667.067
6651.96	7/2	5/2	9918.17	24947.255
6654.96	11/2	9/2	23272.407	8250.17
6655.71	5/2	3/2	10828.988	25849.518
6659.09	17/2	19/2	15665.829	30678.74
6686.44	7/2	7/2	8013.104	22964.64
6690.02	7/2	9/2	7617.455	22561.013
6692.76	9/2	11/2	28297.925	13360.529
6695.26	7/2	5/2	8013.104	22944.93
6707.66	7/2	7/2	25558.27	10654.11
6720.62	9/2	9/2	25812.15	10936.67
6730.39	11/2	13/2	9675.04	24528.937

6734.56	11/2	11/2	23680.085	8835.38
6742.78	9/2	11/2	23661.972	8835.38
6744.91	9/2	9/2	10356.71	25178.609
6751.97	21/2	19/2	29606.273	14799.88
6755.19	15/2	13/2	30453.594	15654.272

Chapter 8

Conclusion

This thesis is aimed to experimentally investigate the spectral lines of praseodymium atoms and ions using Laser Induced Fluorescence (LIF) Spectroscopy in a hollow cathode discharge lamp. To reduce Doppler broadening the atoms and ions in ground and excited states are cooled by liquid nitrogen. By continuous scanning the laser wavelength hyperfine levels of fine structure levels are excited, resulting in a hyperfine structure pattern for the combining fine structure levels. The hyperfine structure of fine structure levels arises due to the electric and magnetic interactions between spinning and orbiting electrons and the spinning nucleus.

The major portion of thesis is dedicated to searching for new atomic and ionic fine structure levels of praseodymium both in even and odd configurations. More than 300 new up to now unknown fine structure levels were discovered ranging in total orbital angular momentum quantum number from 1/2 to 21/2. These levels are confirmed by more than one laser excitation or by FT-Spectra.

Due to very high level density in praseodymium it is highly probable that two or more levels with $\Delta J = 0$ or 1 lie very close to each other resulting in an interaction which may cause that one level perturbs the other one and vice versa. This perturbation may be noticed in a shift of the positions of the F-sublevels and also cause a deviation from the normal intensity rules. This means that transition probabilities from such closely lying levels to other levels are affected causing a change in the relative intensities of the hyperfine components from normal intensities. One such anomaly was recorded where anomalous intensity distribution of hyperfine components was observed. The anomaly is explained as a transition containing three closely spaced lower set of levels which are always excited simultaneously to a single upper level in the same scan range of laser. The interaction between these triplet levels is observed to be quite strong, as evident from large number of transitions (up till now around 44 transitions) from level triplet to known or unknown upper levels. Almost in all these transitions from level triplet the relative intensities of hyperfine components show a deviation from normal intensity rules. Nevertheless in all the excited transitions deviation from interval rule was never observed.

Furthermore, level energies and hyperfine interaction constants A and B of a large number of already known levels were also corrected via laser excitation. Part of the investigations was also dedicated to classifying new and already known lines in praseodymium.

This scientific endeavor is a small step towards understanding the interactions and their nature which occur inside an atom.

Chapter 9
Bibliography

9.1 Literature Consulted

- Cowan R.D., "The Theory of Atomic Structure and Spectra", University of California Press, Berkely 1981.

- Sobel'mann, I. I. "An Introduction to the Theory of Atomic Spectra", Pergamon Press 1972

- Kuhn, H. G., "Atomic Spectra" Longmans, Green & CO. LTD. 1969.

- Demtröder, W., "Laser Spectroscopy", Springer (1982)

- White, H. E., "Introduction to atomic spectra", McGraw Hill (1934)

- Sobel'mann, I. I., Vanshtein, L. A., Yukov, E. A., "Excitation of atoms and broadenings of spectral lines" springer (1981)

- G. K. Woodgate, "Elementary Atomic Structure", Second Edition Oxford Science Publications (2000)

9.2 References

[01] White. H. E. Phys. Rev. **34**, 1397-1403 (1929)

[02] Rosen. N., Harrison. G. R., and McNally, Jr. J. R., Phys. Rev. **60**, 722 (1941)

[03] Lew. H. Phys. Rev. **89**, 530 (1953)

[04] Brix. P., Phys. Rev. **89**, 1245 (1953)

[05] Baker. J. M. and Bleaney. B, Proc. Phys. Soc. London, Sect. **A 68**, 936 (1955)

[06] Murakawa, K., J. Phys. Soc. Japan **15**, 2306 (1960)

[07] Judd. B. R. Lindgren. I., Phys. Rev. **122**, 1802 (1961)

[08] Wybourne. B. G., J. Chem. Phys. **37**, 1807 (1962)

[09] Amado. Y. C., Phys. Rev. **126**, 1004-1008 (1962)

[10] Spector, N., J. Opt. Soc. Am. **54**, 1359 (1964)

[11] Reader. J., and Sugar. J., Phys. Rev. 137, 784 (1965)

[12] A. Ginibre Physica Scripta. Vol. **23**, 260-267, 1981

[13] Macfarlane. R. M., Burum. D. P., and Shelby. R. M., Phys. Rev. Lett. **49**, 636 (1982)

[14] Cheng K T and Childs W. J., Phys. Rev. A **31** 2775 (1985)

[15] M.N. Reddy and G.N. Rao Physica **C 150** (1988) 457-464

[16] A. Ginibre – Emery, Thèse Université de Paris-Sud, Centre d'Orsay, 1988

[17] A. Krzykowski, B. Furmann, D. Stefanska, A. Jarosz, A. Kajoch, Optics Communications **140** (1997) 216-219.

[18] J.Ruczkowski, E. Stachowska, M. Elantkowska, G. H. Guthohrlein and J. Dembczynski, Physica Scripta. Vol. **68**, 133-140, 2003.

[19] B. Furmann, A. Krzykowski, D. Stefanska and J. Dembczynski, Phys. Scr. **74** (2006) 658-669.

[20] Ginibre, A. Physica Scripta **39**, 694-709 (1989)

[21] Ginibre, A. Physica Scripta **39**, 710-721 (1989)

[22] Iimura. H. Nakahara. Y., Ichikawa. S. , Kotani. K., Wakasugi. M., and Horiguchi. T., J. Phys. Soc. Jpn. **59**, 4208 (1990)

[23] Kim M. K.and Kachru. R., Phys. Rev. **B 44**, 9826 (1991)

[24] Iimura. H., Nakahara. Y., Ichikawa. S., Kubota. M., and Horiguchi. T., Phys. Rev. C **50**, 661 (1994)

[25] Maosheng. L., et al, Phys. Rev. **A 62**, 052504 (2000)

[26] S. Ivarsson, U. Litzen and G. M. Wahlgren, Physica Scripta. Vol. **64**, 455-461, (2001)

[27] B. Furmann, D. Stefanska, E. Stachowska, J.Ruczkowski, and and J. Dembczynski, Eur. Phys. J. D. **17**, 275-284 (2001)

[28] Ma Hong-Liang, Chin. Phys. Soc. Vol. 11 No. 9, September 2002

[29] B. Furmann, D. Stefanska, J. Dembczynski and E. Stachowska, At. Data and Nuclear Data Tables 93 (2007) 127-137 Elsevier Inc.

[30] P. A. Franken, A. E. Hill, C. W. Peters, and G. Weinreich, Phys. Rev. Lett. **7**, 118(1961)

[31] M. Bass, P. A. Franken, A. E. Hill, C. W. Peters, and G. Weinreich, Phys. Rev. Lett. **8**, 18(1962)

[32] R. W. Terhune, P. D. Maker, and C. M. Savage, Phys. Rev. Lett. **8**, 404(1962).

[33] M. Bass, P. A. Fraken, J. F. Ward, and G. Weinreich, Phys. Rev. Lett. **9**, 446(1962).

[34] K. E. Neihuhr, Appl. Phys. Lett. **2**, 136(1963).

[35] A. W. Smith and N. Braslou, J. Appl. Phys. **34**, 2105(1963).

[36] C. C. Wang and G. W. Racette, Appl. Phys. Lett. **6**, 169(1965).

[37] J. A. Giordmaine and R. C. Miller, Phys. Rev. Lett. **14**, 973(1965).

[38] J. A. Armstrong, N. Bloembergen, J. Ducuing, and P. S. Pershan, Phys. Rev. **127**, 1918(1962).

[39] E. J. Woodbury and W. K. Ng, Proc. IRE. **50**, 2367(1962).

[40] G. Eckhardt, R. W. Hellwarth, F. J. McClung, S. E. Schwarz, D. Weiner, and E. J. Woodbury, Phys. Rev. Lett. **9**, 455(1962).

[41] R. Y. Chiao, C. H. Townes, and B. P. Stoicheff, Phys. Rev. Lett. **12**, 592(1964).

[42] R. Y. Chiao, E. Garmire, and C. H. Townes, Phys. Rev. Lett. **13**, 479(1964) [Erratum, **14**, 1056(1965).

[43] G. A. Askar'yan, Sov. Phys. JETP, **15**, 1088(1962).

[44] F. Shimizu, Phys. Rev. Lett. **19**, 1097(1967).

[45] A. C. Cheung, D. M. Rank, R. Y. Chiao, and C. H. Townes, Phys. Rev. Lett. **20**, 786(1968).

[46] T. K. Gustafson, J. P. Taran, H. A. Haus, J. R. Lifsitz, and P. L. Kelley, Phys. Rev. **177**, 306(1969).

[47] M . M. T. Loy and Y. R. Shen, Phys. Rev. Lett. **22**, 994(1969).

[48] R. Polloni, C. A. Sacchi, and O. Svelto, Phys. Rev. Lett. **23**, 690(1969).

[49] N. A. Kurnit, I. D. Abella, and S. R. Hartmann, Phys. Rev. Lett. **13**, 567(1964).

[50] S. L. McCall and E. L. Hahn, Bull. Am. Phys. Soc. **10**, 1189(1965).

[51] S. L. McCall and E. L. Hahn, Phys. Rev. Lett. **18**, 908(1967).

[52] C. L. Tang and B. D. Silverman, in Physics of Quantum Electronics, eds. P. L. Kelley, B. Lax, and P. E. Tannenwald (McGraw-Hill, New York, 1966), pp. 280-293.

[53] G. B. Hocker and C. L. Tang, Phys. Rev. lett. **21**, 591(1968).

[54] A. L. Schawlow and C. H. Townes, Phys. Rev. **112**, 1940(1958).

[55] N. G. Basov and A. M. Prokhrov, Usp. Fiz. Nauk. **57**, 485(1955); J. P. Gordon, H. J. Zeiger, and C. H. Townes, Phys. Rev. **99**, 1264(1955).

[56] P. P. Sorokin, J. J. Luzzi, J. R. Lankard, and G. D. Pettit, IBM Journal, **8**, 182(1964).

[57] G. Bret and F. Cires, Appl. Phys. Lett. **4**, 175(1964).

[58] P. Kafalos, J. I. Masters, and E. M. E. Murray, J. Appl. Phys. **35**, 2349(1964).

[59] B. H. Soffer, J. Appl. Phys. **35**, 2551(1964).

[60] M. Göppert-Mayer, Ann. Physik, **9**, 273(1931).

[61] W. Kaiser and C. G. B. Garrett, Phys. Rev. Lett. **7**, 229(1961).

[62] J. F. Porter, Jr., Phys. Rev. Lett. **7**, 414(1961).

[63] P.D. Marker and R.W. Terhune, Phys. Rev. **137**, A801(1965)

[64] Eli Yablonovitch, N. Bloembergen, and J. J. Wynne, Phys. Rev. **B3**, 2060(1971)

[65] M. D. Levenson, C. Flytzanis, and N. Bloembergen, Phys. Rev. **B6,** 3962(1972)

[66] J. J. Wynne, Phys. Rev. Lett. **29**, 650(1972)

[67] T. W. Hänsch, M. D. Levenson, and A. L. Schawlow, Phys. Rev. Lett. **26**, 946(1971).

[68] T. W. Hänsch, I. S. Shahin, and A. L. Schawlow, Phys. Rev . Lett. **27**, 707(1971).

[69] L. S. Vasilenko, V. P. Chebotaev, and A. V. Shishaev, JETP Lett. **12**, 113(1970).

[70] D. Pritchard, J. Apt. and T. W. Ducas, Phys. Rev. Lett. **32**, 641(1974).

[71] F. Biraben, B. Cagnac, and G. Grynberg, Phys. Rev. Lett. **32**, 643(1974).

[72] M. D. Levenson and N. Bloembergen, Phys. Rev. Lett. **32**, 645(1974).

[73] T. W. Hänsch, K. C. Harvey, G. Meisel, and A. L. Schawlow, Opt. Commun. **11**, 50(1974).

[74] W. J. Jones and B. P. Stoicheff, Phys. Rev. Lett. **13**, 657(1964).

[75] R. A. McLaren and B. P. Stoicheff, Appl. Phys. Lett. **16**, 140(1970).

[76] R. R. Alfano and S. L. Shapiro, Chem. Phys. Lett. **8**, 631(1971).

[77] I. Reinhold and M. Maier, Opt. Commun. **5**, 31(1972).

[78] A. Owyoung and E. D. Jones, Opt. Lett. **1**, 152(1977).

[79] B. F. Levine, C. V. Shank, and J. P. Heritage, IEEE J. Quantum Electron. QE-**15**, 1418(1979).

[80] D. Heiman, R. W. Hellwarth, M. D. Levenson, and G. Martin, Phys. Rev. Lett. **36**, 189(1976).

[81] P. F. Liao, and G. C. Bjorklund, Phys. Rev. Lett. **36**, 584(1976).

[82] C. Wieman and T. W. Hänsch, Phys. Rev. Lett. **36**, 1170(1976).

[83] J. J. Song, G. L. Eesley, and M. D. Levenson, Appl. Phys. Lett. **29**, 567(1976).

[84] R. Teets, R. Feiberg, T. W. Hänsch, and A. L. Schawlow, Phys. Rev. Lett. **37**, 683(1976).

[85] B. Ya. Zel'dovich, V. I. Popovichev, V. V. Ragul'skii, and F. S. Faizullov, JETP Lett. **15**, 109(1972).

[86] O. Yu. Nosach, V. I. Popovichev, V. V. Ragul'skii, and F. S. Faizullov, JETP Lett. **16**, 435(1972).

[87] A. Yariv, Appl. Phys. Lett. **28**, 88(1976); J. Opt. Soc. Am. **66**, 301(1976); Opt. Commun. **21**, 49(1977).

[88] R. W. Hellwarth, J Opt. Soc. Am. **67**, 1(1977).

[89] P. V. Avizonis, F. A. Hopf, W. D. Bomberger, S. F. Jacobs, A. Tomita, and K. H. Womack, Appl. Phys. Lett. **31**, 435(1977).

[90] D. M. Bloom and G. C. Bjorklund, Appl. Phys. Lett. **31**, 592(1977).

[91] A. Szöke, V. Daneu, J. Goldhar, and N. A. Kurnit, Appl. Phys. Lett. **15**, 376(1969).

[92] S. L. McCall, H. M. Gibbs, and T. N. C. Venkatesan, J. Opt. Soc. Am. **65**, 1184(1975).

[93] H. M. Gibbs, S. L. MaCall, and T. N. C. Venkatesan, J. Opt. Soc. Am. **36**, 1135(1976).

[94] P. W. Smith and E. H. Turner, Appl. Phys. Lett. **30**, 280(1977).

[95] H. N. Russell and F. A. Saunders, Astrophys. J. **61**, 38 (1925)

[96] Cowan R.D., "The Theory of Atomic Structure and Spectra", University of California Press, Berkely 1981

[97] Burger and Dorgela, Zeits. Für Phys. **23**, 258 (1924); Ornstein and Burger, ibid. **24**, 41 (1924)

[98] M. D. Levenson, A. L. Schawlow, Phys. Rev. Lett. **A 6,** 10(1972).

[99] T. W. Hänsch, I. S. Shahin, and A. L. Schawlow, Phys. Rev . Lett. **27**, 707(1971).

[100] C. Borde, Acad. Sci. **B** 271, 371 (1970).

[101] D. A. Jackson and H. Kuhn, Proc. Roy. Soc. **A154,** 679, (1936)

[102] S. Ezekiel and R. Weiss, "Laser Induced Fluorescence in a Molecular Beam of Iodine", Physical Review Letters, January 15, 1968

[103] P. F. Liao, and G. C. Bjorklund, Phys. Rev. Lett. **36**, 584(1976).

[104] C. Wieman and T. W. Hänsch, Phys. Rev. Lett. **36**, 1170(1976).

[105] R. Frisch, Z. Phys. 86, 42 (1933)

[106] A. Ashkin, Phys. Rev. Lett., **25**, 1321 (1970)

[107] Jacquinot, P. et al., Opt. Comm. **8**, 163 (1973)

[108] Rabi. I. I. et al., Phys. Rev., **53**, 318 (1938)

[109] Rabi. I. I., Phys. Rev., **87**, 379 (1952)

[110] Marrus, R. McColn, D., Phys. Rev. Lett. **15**, 813 (1965)

[111] W. Demtröder, Laser Spectroscopy Basic Concepts and Instrumentation, Springer-Verlag Berlin Heidelberg New york 1982

[112] F. M. Penning; Physica **8**, 137 (1928)

[113] R. B. Green, R. A. Keller, G.G. Luther, P.K. Schenck and J.C. Travis; Applied Phys. Lett. **29**, 727 (1976).

[114] King, D. Schenck, P. K., Smith, K. C., and Travis, J. C. Appl. Opt. **16**, 2617 (1977)

[115] Grandin, J. F., Husson, X. J. Phys. **B 14**, 433 (1981)

[116] Caesar, T., and Huelly, J. L., J. Phys. **C 44**, 216 (1983)

[117] Skolnick, M. L., IEEE J. Quantum Electron. **6**, 139 (1970)

[118] Thomason, W. H., Elbers, D. C., Rev. Sci. Instrum. **46**, 409, (1975)

[119] Schüler, H., Z. Phys. **35**, 323 (1926)

[120] Schüler, H., Z. Phys. **59**, 149 (1930)

[121] Paschen, F., Ann. Phys. **18**, 867 (1933)

[122] Feldmann, D. Opt. Comm. **29**, 67 (1979)

[123] Miyazaki, K. et al. Phys. Rev. **A 28**, 2229 (1983)

[124] Behrens, H. O., Guthohrlein. G. H., J. Phys. **C7-44**, 149 (1983)

[125] Behrens, H. O., Guthohrlein. G. H., Kasper, A., J. Phys. **C7-44**, 239 (1983)

[126] B. Gamper, Diploma Thesis, Graz University of Technology, Graz 2007

[127] L. Windholz, G.H. Guthhrlein, Physica Scripta **T105**, 55-60 (2003)

[128] R. Peck, K. Reeder, J. Opt. Soc. Am. **62**, 958 (1972)

[129] Ritz, W. Astrophys. J. **28**, 237 (1908).

[130] Quiering, T., Universitat der Bundeswehr, Hamburg,: diploma thesis (1984).

[131] Böklen, K.D., Bossert T., Foerster W.: Z. Physik **A 274**, 195 (1975)

[132] Childs. W.J. and L. S. Goodman L. S.: Phys. Rev. **A 24**, 1342 (1981)

[133] Kuhn, H. G., Atomic Spectra Longmans, Green & CO. LTD. 1969.